

**Multimodality Imaging and Clinical Implications of  
Bioresorbable Scaffolds in Complex Coronary Artery Disease**

**Takashi Muramatsu**

Financial support by Erasmus University Rotterdam, Fujita Health University, and Abbott Vascular Japan for the publication of this thesis is gratefully acknowledged.

ISBN: 978-94-6169-671-7

**Multimodality Imaging and Clinical Implications of  
Bioresorbable Scaffolds in Complex Coronary Artery Disease**

**Multimodale beeldvorming en klinische implicaties van  
bioresorbeerbare scaffolds bij complexe coronaire hartziektes**

**Thesis**

to obtain the degree of Doctor from the Erasmus University Rotterdam  
by command of the rector magnificus

Prof. dr. H.A.P.Pols

and in accordance with the decision of the Doctorate Board

The public defense shall be held on  
Friday the 22<sup>nd</sup> May 2015 at 11:30 o'clock

by

Takashi Muramatsu  
born in Nagoya, Japan



## **DOCTORAL COMMITTEE**

### **Promotor**

Prof. dr. P.W.J.C. Serruys

### **Co-promotor**

Dr. Y. Onuma

### **The inner doctoral committee**

Prof. dr. Y. Ozaki

Prof. dr. R.J. van Geuns

Dr. K. Nieman

### **The plenary doctoral committee**

Prof. dr. P.J. de Feyter

Prof. dr. K. Kozuma

Dr. H.M. Garcia-Garcia

*To my beloved wife*



## TABLE OF CONTENTS

### Introduction

#### Chapter 1: From Metallic Stents to Bioresorbable Scaffolds: A Change in the Paradigm of Coronary Interventions.

##### 1.1 A history of progress in coronary interventions

Progress in treatment by percutaneous coronary intervention: The stent of the future.

*Rev Esp Cardiol.* 2013;66:483-96.

Muramatsu T, Onuma Y, Zhang Y, Bourantas CV, Kharlamov A, Diletti R, Farooq V, Gogas BD, Garg S, García-García HM, Ozaki Y, Serruys PW.

[Review, Impact Factor (2013): 3.342]

##### 1.2 Igaki-Tamai stent

Long-term (>10 years) clinical outcomes of first-in-man biodegradable poly-l-lactic acid coronary stents: Igaki-Tamai stents.

*Circulation.* 2012;125:2343-53.

Nishio S, Kosuga K, Igaki K, Okada M, Kyo E, Tsuji T, Takeuchi E, Inuzuka Y, Takeda S, Hata T, Takeuchi Y, Kawada Y, Harita T, Seki J, Akamatsu S, Hasegawa S, Bruining N, Brugaletta S, de Winter S, Muramatsu T, Onuma Y, Serruys PW, Ikeguchi S.

[Original research paper, Impact Factor (2012): 15.202]

##### 1.3 Magnesium alloy

Bioresorbable drug-eluting magnesium-alloy scaffold for treatment of coronary artery disease.

*Int J Mol Sci.* 2013;14:24492-500.

Campos CM, Muramatsu T, Iqbal J, Zhang YJ, Onuma Y, Garcia-Garcia HM, Haude M, Lemos PA, Warnack B, Serruys PW.

[Review, Impact Factor (2013): 2.339]

## Chapter 2: Methodology and Clinical Applications of Multimodality Imaging

### 2.1 Overview of methodologies and parameters to evaluate BRS

Assessing bioresorbable coronary devices: Methods and parameters.

*JACC Cardiovasc Imaging*. 2014;7:1400-11.

García-García HM, Serruys PW, Campos CM, Muramatsu T, Nakatani S, Zhang YJ, Onuma Y, Stone GW.

[Review, Impact Factor (2013): 6.986]

### 2.2 Quantitative coronary angiography

Comparison of acute gain and late lumen loss after PCI with bioresorbable vascular scaffolds versus everolimus-eluting stents: An exploratory observational study prior to a randomised trial.

*Eurointervention*. 2014;10:672-80.

Zhang YJ, Bourantas CV, Muramatsu T, Iqbal J, Farooq V, Diletti R, Campos CM, Onuma Y, García-García HM, Serruys PW.

[Original research paper, Impact Factor (2013): 3.758]

### 2.3 Reproducibility of IVUS-GS and IVUS-VH analyses

Reproducibility of intravascular ultrasound radiofrequency data analysis (Virtual Histology) with a 45 MHz rotational imaging catheter in ex vivo human coronary arteries.

*J Cardiol*. 2015;65:134-42.

Muramatsu T, García-García HM, Brugaletta S, Heo JH, Onuma Y, Fedewa RJ, Nair A, Ozaki Y, Serruys PW.

[Original research paper, Impact Factor (2013): 2.566]

### 2.4 Palpography

Implications of a bioresorbable vascular scaffold implantation on vessel wall strain of the treated and the adjacent segments.

*Int J Cardiovasc Imaging*. 2014;30:477-84.

Bourantas CV, García-García HM, Campos CA, Zhang YJ, Muramatsu T, Morel MA, Nakatani S, Gao X, Cho YK, Isibashi Y, Gijsen FJ, Onuma Y, Serruys PW.

[Original research paper, Impact Factor (2013): 2.322]

### **2.5 Optical coherence tomography: coronary evaginations**

Coronary evaginations are associated with positive vessel remodeling and are nearly absent following implantation of newer-generation drug-eluting stents: An optical coherence tomography and intravascular ultrasound study.

*Eur Heart J.* 2014;35:795-807.

Radu MD, Räber L, Kalesan B, Muramatsu T, Kelbæk H, Heo JH, Jørgensen E, Helqvist S, Farooq V, Brugaletta S, Garcia-Garcia HM, Jüni P, Saunamäki K, Windecker S, Serruys PW.

[Original research paper, Impact Factor (2013): 14.723]

### **2.6 MSCT assessment of coronary plaque evolution after the BVS implantation**

Impact of everolimus-eluting bioresorbable scaffold in coronary atherosclerosis (Submitted)

Campos CM, Garcia-Garcia HM, Muramatsu T, de Araújo Gonçalves P, Onuma Y, Dudek D, Thuesen L, Webster M, Nieman K, Ormiston JA, Serruys PW.

[Original research paper]

### **2.7 Longitudinal follow-up of the Absorb BVS with multimodality imaging**

Dynamics of vessel wall changes following the implantation of the Absorb everolimus-eluting bioresorbable vascular scaffold: A multi-imaging modality study at 6, 12, 24 and 36 months.

*Eurointervention.* 2014;9:1271-84.

Serruys PW, Onuma Y, Garcia-Garcia HM, Muramatsu T, van Geuns RJ, de Bruyne B, Dudek D, Thuesen L, Smits PC, Chevalier B, McClean D, Koolen J, Windecker S, Whitbourn R, Meredith I, Dorange C, Veldhof S, Hebert KM, Rapoza R, Ormiston JA.

[Original research paper, Impact Factor (2013): 3.758]

## **Chapter 3: Anatomical and Functional Lesion Assessment with Three Dimensional Imaging Techniques**

### **3.1 Validation of 3D-QCA in bifurcation phantom model**

Advanced three-dimensional quantitative coronary angiographic assessment of bifurcation lesions: methodology and phantom validation.

*Eurointervention.* 2013;8:1451-60.

Girasis C, Schuurbijs JCH, Muramatsu T, Aben JP, Onuma Y, Soekhradj S, Morel MA, van Geuns RJ, Wentzel JJ, Serruys PW.  
[Original research paper, Impact Factor (2013): 3.758]

### **3.2 Virtual functional assessment of coronary artery lesions with 3D-QCA**

Fast virtual functional assessment of intermediate coronary lesions using routine angiographic data and blood flow simulation in humans: Comparison with pressure wire-fractional flow reserve.

*Eurointervention*. 2014;10:574-83.

Papafaklis MI, Muramatsu T\*, Ishibashi Y, Lakkas LS, Nakatani S, Bourantas CV, Ligthart JM Onuma Y, Echavarría-Pinto M, Tzirka G, Kotsia A, Nikas DN, Mogabgab O, van Geuns RJ, Naka KK, Fotiadis DI, Brilakis ES, García-García HM, Escaned J, Zijlstra F, Michalis LK, Serruys PW.

\* Equally contributed to the first author

[Original research paper, Impact Factor (2013): 3.758]

### **3.3 Comparison between 2D- and 3D-QCA in bifurcation lesions**

Comparison between two-dimensional and three-dimensional quantitative coronary angiography bifurcation analyses for the assessment of bifurcation lesions: A sub-analysis of the TRYTON pivotal IDE coronary bifurcation trial.

*Catheter Cardiovasc Interv*. 2015 (Epub ahead of print)

Muramatsu T, Grundeken MJ, Ishibashi Y, Nakatani S, Campos CA, Morel MA, Jonker H, Girasis C, de Winter RJ, Wykrzykowska JJ, García-García HM, Leon MB, Serruys PW, Onuma Y.

[Original research paper, Impact Factor (2013): 2.396]

### **3.4 Three-dimensional OCT assessment of bioresorbable magnesium alloy in bifurcation**

Serial 2-Dimensional and 3-Dimensional optical coherence tomography assessment of overhanging struts of drug-eluting absorbable metal scaffold. "DREAMS" for jailed side branch?

*JACC Cardiovasc Interv*. 2014;7:575-6.

Muramatsu T, García-García HM, Serruys PW, Waksman R, Verheye S.

[Case report, Impact Factor (2013): 7.440]

## Chapter 4: Light-based Imaging Assessment for Acute Myocardial Infarction and Clinical Implications of Bioresorbable Scaffolds

### 4.1 Methodology to quantify in-stent structures with OFDI

Quantitative optical frequency domain imaging assessment of in-stent structures in patients with ST-segment elevation myocardial infarction: Impact of imaging sampling rate.

*Circ J.* 2012;76:2822-31.

Muramatsu T, Garcia-Garcia HM, Lee IS, Bruining N, Onuma Y, Serruys PW.

[Original research paper, Impact Factor (2012): 3.578]

### 4.2 Morphologic assessment of thrombus with three-dimensional approach

Thrombotic arch in ST-segment elevation myocardial infarction: Comparison between 2-dimensional and 3-dimensional optical frequency domain imaging.

*Eur Heart J.* 2012;33:1510.

Muramatsu T, Serruys PW, Onuma Y.

[Case report, Impact Factor (2012): 14.097]

### 4.3 Impact of thrombus aspiration on OFDI measurements and clinical outcomes in STEMI patients

Short- and mid-term results of the randomized TROFI trial.

Muramatsu T, Onuma Y, Garcia-Garcia HM, Serruys PW.

[This chapter merged two papers; Onuma Y, et al. *Eur Heart J.* 2013;34:1050-60. and Garcia-Garcia HM, et al. *Eur Heart J Cardiovasc Imaging.* 2014;15:987-95.]

### 4.4 Early clinical experience of polylactide bioresorbable scaffold for STEMI and NSTEMI in the Thoraxcenter

Early and late optical coherence tomography findings following everolimus-eluting bioresorbable vascular scaffold implantation in myocardial infarction: a preliminary report.

*Hellenic J Cardiol.* 2015;56:125-35.

Karanasos A, Muramatsu T, Diletti R, Nauta S, Onuma Y, Lenzen M, Nakatani S, van Mieghem NM, Schultz C, de Jaegere PP, Serruys PW, Zijlstra F, Regar E, van Geuns RJ.

[Original research paper, Impact Factor (2013): 0.785]

#### **4.5 Short-term outcomes of STEMI patients treated with the Absorb BVS**

Everolimus-eluting bioresorbable vascular scaffolds for treatment of patients presenting with ST-segment elevation myocardial infarction: BVS STEMI first study.

*Eur Heart J.* 2014;35:777-86.

Diletti R, Karanasos A, Muramatsu T, Nakatani S, van Mieghem NM, Onuma Y, Nauta ST, Ishibashi Y, Lenzen MJ, Ligthart J, Schultz C, Regar E, de Jaegere PP, Serruys PW, Zijlstra F, van Geuns RJ.

[Original research paper, Impact Factor (2013): 14.723]

### **Chapter 5: Lessons Learned from Early BVS Studies and Clinical Implications for Complex Subsets of Lesions or Patients**

#### **5.1 Scaffold thrombosis and scaffold dislodgement**

Lessons learned from acute and late scaffold failures in the ABSORB EXTEND trial.

*Eurointervention.* 2014;10:449-57.

Ishibashi Y, Onuma Y, Muramatsu T, Nakatani S, Iqbal J, Garcia-Garcia HM, Bartorelli AL, Whitbourn R, Abizaid A, Serruys PW.

[Original research paper, Impact Factor (2013): 3.758]

#### **5.2 Scaffold restenosis**

Early (before 6 months), late (6-12 months) and very late (after 12 months) angiographic scaffold restenosis in the ABSORB Cohort B trial.

*Eurointervention.* 2014 (Epub ahead of print)

Nakatani S, Onuma Y, Ishibashi Y, Muramatsu T, Iqbal J, Zhang YJ, van Geuns RJ, Ormiston JA, Serruys PW; on behalf of the ABSORB Cohort B investigators.

[Original research paper, Impact Factor (2013): 3.758]

#### **5.3 Acute disruption and late discontinuities**

Incidence and imaging outcomes of acute scaffold disruption and late structural discontinuity after implantation of the Absorb everolimus-eluting fully bioresorbable vascular scaffold: Optical coherence tomography assessment in the ABSORB Cohort B trial.

*JACC Cardiovasc Interv.* 2014;7:1400-11.

Onuma Y, Serruys PW, Muramatsu T, Nakatani S, van Geuns RJ, de Bruyne B,

Dudek D, Thuesen L, Smits PC, Chevalier B, McClean D, Koolen J, Windecker S, Whitbourn R, Meredith IT, García-García HM, Veldhof S, Rapoza R, Ormiston JA.  
[Original research paper, Impact Factor (2013): 7.440]

#### **5.4 Absorb BVS in diabetic patients**

One-year clinical outcomes of diabetic patients treated with the everolimus-eluting bioresorbable vascular scaffolds: A pooled analysis from the ABSORB Cohort B and the ABSORB EXTEND trials.

*JACC Cardiovasc Interv.* 2014;7:482-93.

Muramatsu T, Onuma Y, van Geuns RJ, Chevalier B, Patel T, Seth A, Diletti R, García-García HM, Dorange C, Veldhof S, Cheong WF, Ozaki Y, Whitbourn R, Bartorelli A, Stone GW, Abizaid A, Serruys PW.

[Original research paper, Impact Factor (2013): 7.440]

#### **5.5 Clinical use of the Absorb BVS in true bifurcation lesion**

Complex bifurcation percutaneous coronary intervention with the Absorb bioresorbable vascular scaffold.

*Eurointervention.* 2013;9:888.

Džavík V, Muramatsu T, Crooks N, Nakatani S, Onuma Y.

[Case report, Impact Factor (2013): 3.758]

#### **5.6 Side branch occlusion and peri-procedural myocardial infarction**

Incidence and short-term clinical outcomes of small side branch occlusion after implantation of an everolimus-eluting bioresorbable vascular scaffold: An interim report of 435 patients in the ABSORB-EXTEND single-arm trial in comparison with an everolimus-eluting metallic stent in the SPIRIT first and II trials.

*JACC Cardiovasc Interv.* 2013;6:247-57.

Muramatsu T, Onuma Y, García-García HM, Farooq V, Bourantas CV, Morel MA, Li X, Veldhof S, Bartorelli A, Whitbourn R, Abizaid A, Serruys PW.

[Original research paper, Impact Factor (2013): 7.440]

#### **5.7 Peri-procedural myocardial infarction in a randomized controlled trial**

Incidence and potential mechanism(s) of post-procedural rise of cardiac enzyme in patients with coronary artery narrowing after implantation of an everolimus eluting bioresorbable vascular scaffold or everolimus eluting metallic stent.

(Submitted)

Ishibashi Y, [Muramatsu T](#), Cho YK, Nakatani S, Grundeken MJ, Garcia-Garcia HM, van Boven AJ, Piek JJ, Sabaté M, Kelbæk H, Baumbach A, McClean D, de Sousa Almeida M, Wasungu L, Miquel-Hebert K, Chevalier B, Onuma Y, Serruys PW.

[Original research paper]

### **5.8 Preventive passivation of high-risk plaques by BRS technologies**

Early detection and invasive passivation of future culprit lesions: A future potential or an unrealistic pursuit of Chimeras?

*Am Heart J.* 2013;165:869-81.

Bourantas CV, Garcia-Garcia CV, Diletti R, [Muramatsu T](#), Serruys PW.

[Review, Impact Factor (2013): 4.696]

## **Chapter 6: Future Perspectives**

Freeing the vessel from metallic cage: what can we achieve with bioresorbable vascular scaffolds?

*Cardiovasc Interv and Ther.* 2012;27:141-54.

Onuma Y, [Muramatsu T](#), Kharlamov A, Serruys PW.

[Review]

## **Summary and Conclusions (Samenvatting en Conclusies)**

### **Acknowledgements**

### **Curriculum Vitae**

### **List of Publications**

# Introduction





## INTRODUCTION

It has been nearly 4 decades since Dr. Andreas Grüntzig introduced the first balloon angioplasty in 1977. Undoubtedly that was the beginning of history of percutaneous coronary interventions (PCI). Balloon angioplasty had been accepted as an alternative treatment for obstructive coronary artery diseases (CAD) to surgery. Conversely, this technique also brought pitfalls such as elastic recoil and vessel closure during the procedure, as well as constrictive remodeling and restenosis even after successful procedure.

Coronary stents were first developed in the mid 1980s to overcome the aforementioned limitations of balloon angioplasty. In the 1990s, this technology became widely accepted as a promising treatment strategy for patients with CAD after the landmark BENESTENT trial, which demonstrated the superiority of bare metal stent (BMS) over balloon angioplasty. Although coronary stenting improved both angiographic results and clinical outcomes, neointimal hyperplasia and consequent in-stent restenosis still continued to be major limitations of this technology. In order to minimize neointimal hyperplasia and thereby reducing repeat revascularisation, drug-eluting stents (DES) were developed. Early pivotal randomised trials of the first generation DES showed excellent results in reducing the incidence of in-stent restenosis, so that they rapidly replaced BMS. In 2006, safety concerns were raised with the DES following the reports linking their use to an increased risk of stent thrombosis. First generation DES, with permanent polymers, have been associated with delayed endothelialisation, endothelial dysfunction, and local hypersensitivity reactions, resulting in an increased risk of stent thrombosis and the need for prolongation of dual antiplatelet therapy. Second generation DES, with thinner struts and more biocompatible polymers, have considerably improved their safety profile. However, concerns still persist over the presence of durable polymers, as evidence from animal and human studies suggested that some durable polymers may cause persistent arterial wall inflammation and delayed vascular healing, both of which may have a potential role in precipitating stent thrombosis and delayed in-stent restenosis, namely late catch-up phenomenon. Newer generation DES, coated with biodegradable polymers, offer the attractive combination of controlled drug elution in parallel with biodegradation of the polymer into inert monomers. After the completion of biodegradation, only a “BMS” remains, thereby reducing the

long-term risks associated with the presence of a permanent polymer. An extension of this concept has driven the development of polymer-free DES or those with novel polymer coatings.

Fully bioresorbable scaffolds (BRS) are a novel therapeutic approach as they provide transient vessel support in contrast to the permanent caging caused by metallic stents. The concept of BRS technology was introduced in 1980s, but this technology initially failed to develop because of inability to manufacture an ideal polymer that could limit inflammation and restenosis. In 1998, a Japanese interventional cardiologist Dr. Hideo Tamai implanted the “Igaki-Tamai” PLLA stent for the first time in human coronary arteries. Despite the lack of drug-elution, the “Igaki-Tamai” stent has shown acceptable long-term (>10 years) clinical safety and efficacy in their first-in-man trial, proving a concept of the BRS technology. More interestingly, in contrast to the metallic prosthesis, autopsy specimens showed healing with thickened neointima at the previously stented segment, without any inflammatory cell infiltration or foreign body reactions. In 2006, the fully bioresorbable everolimus-eluting poly(lactide) scaffold, namely the Absorb BVS, was introduced. This novel technology has been extensively investigated in the ABSORB Clinical Program, in that the first-in-man ABSORB Cohort B trial using the current generation BVS showed excellent results in terms of safety and efficacy. Since September 2012, this device has been widely used in the clinical setting.

The aims of this thesis are 1) to understand the concept, mechanical properties, methodologies for multimodality imaging assessment, and clinical performance of the fully bioresorbable everolimus-eluting poly(lactide) scaffold; 2) to investigate advanced three-dimensional imaging techniques for anatomical and functional lesion assessment; 3) to discuss the methodology of light-based imaging assessment for STEMI patients; and finally 4) to explore the clinical implications in more complex subsets of lesions/patients and future therapeutic potentials of this technology.

# Chapter 1

## From Metallic Stents to Bioresorbable Scaffolds: A Change in the Paradigm of Coronary Interventions

### 1.1 A history of progress in coronary interventions

Progress in treatment by percutaneous coronary intervention:  
the stent of the future.

*Rev Esp Cardiol.* 2013;66:483-96.

[Review, Impact Factor (2013): 3.342]

Muramatsu T, Onuma Y, Zhang Y, Bourantas CV, Kharlamov A, Diletti R, Farooq V, Gogas BD, Garg S, García-García HM, Ozaki Y, Serruys PW.





## Progress in Treatment by Percutaneous Coronary Intervention: The Stent of the Future

Takashi Muramatsu,<sup>a</sup> Yoshinobu Onuma,<sup>a</sup> Yao-Jun Zhang,<sup>a</sup> Christos V. Bourantas,<sup>a</sup>  
Alexander Kharlamov,<sup>a</sup> Roberto Diletti,<sup>a</sup> Vasim Farooq,<sup>a</sup> Bill D. Gogas,<sup>b</sup> Scot Garg,<sup>c</sup>  
Hector M. García-García,<sup>a</sup> Yukio Ozaki,<sup>d</sup> and Patrick W. Serruys<sup>a,\*</sup>

<sup>a</sup>Thoraxcenter, Erasmus Medical Center, Rotterdam, The Netherlands

<sup>b</sup>Department of Interventional Cardiology, Andreas Gruentzig Cardiovascular Center, Emory University School of Medicine, Atlanta, Georgia, United States

<sup>c</sup>Department of Cardiology, East Lancashire, NHS Trust, Lancashire, United Kingdom

<sup>d</sup>Department of Cardiology, Fujita Health University, Toyoake, Japan

### Article history:

Available online 4 May 2013

### Keywords:

Bioresorbable scaffold  
Coronary artery disease  
Drug-eluting stent  
Vascular reparative therapy

### ABSTRACT

First generation drug-eluting stents have considerably reduced in-stent restenosis and broadened the applications of percutaneous coronary interventions for the treatment of coronary artery disease. The polymer is an integral part of drug-eluting stents in that, it controls the release of an antiproliferative drug. The main safety concern of first generation drug-eluting stents with permanent polymers—stent thrombosis—has been caused by local hypersensitivity, delayed vessel healing, and endothelial dysfunction. This has prompted the development of newer generation drug-eluting stents with biodegradable polymers or even polymer-free drug-eluting stents. Recent clinical trials have shown the safety and efficacy of drug-eluting stents with biodegradable polymer, with proven reductions in very late stent thrombosis as compared to first generation drug-eluting stents. However, the concept of using a permanent metallic prosthesis implies major drawbacks, such as the presence of a foreign material within the native coronary artery that causes vascular inflammation and neoatherosclerosis, and also impedes the restoration of the vasomotor function of the stented segment. Bioresorbable scaffolds have been introduced to overcome these limitations, since they provide temporary scaffolding and then disappear, liberating the treated vessel from its cage. This update article presents the current status of these new technologies and highlights their future perspectives in interventional cardiology.

© 2012 Sociedad Española de Cardiología. Published by Elsevier España, S.L. All rights reserved.

### Avances en el tratamiento mediante intervención coronaria percutánea: el *stent* del futuro

### RESUMEN

Los *stents* liberadores de fármacos de primera generación han reducido considerablemente las reestenosis en el *stent* y han ampliado las aplicaciones de las intervenciones coronarias percutáneas en el tratamiento de la enfermedad coronaria. El polímero es parte integrante de los *stents* liberadores de fármacos, ya que controla la liberación de un fármaco antiproliferativo. La principal preocupación respecto a los *stents* liberadores de fármacos de primera generación con polímeros permanentes—la trombosis del *stent*—se ha debido a la hipersensibilidad local, la cicatrización tardía del vaso y la disfunción endotelial. Esto ha llevado al desarrollo de *stents* liberadores de fármacos de nueva generación con polímeros biodegradables o incluso sin polímero. En ensayos clínicos recientes se ha observado la seguridad y la eficacia de los *stents* liberadores de fármacos con polímero biodegradable, que han mostrado una reducción demostrada de la trombosis de *stent* muy tardía, comparados con los de primera generación. Sin embargo, el concepto de utilizar prótesis metálicas permanentes tiene importantes inconvenientes, como la presencia de un cuerpo extraño en el interior de la arteria coronaria nativa, que causa inflamación vascular y neoaterosclerosis e impide también el restablecimiento de la función vasomotora del segmento tratado con el *stent*. Para superar esas limitaciones, se han introducido las estructuras de base bioabsorbible, que proporcionan un almacén temporal y luego al desaparecer liberan el vaso tratado de la jaula que le imponían. En este artículo de puesta al día se presenta el estado actual de estas nuevas tecnologías y se resaltan sus perspectivas futuras en cardiología intervencionista.

© 2012 Sociedad Española de Cardiología. Publicado por Elsevier España, S.L. Todos los derechos reservados.

\* Corresponding author: Department of Interventional Cardiology, Thoraxcenter, Erasmus Medical Center, Ba583, Dr. Molewaterplein 40, 3015 GD, Rotterdam, The Netherlands.

E-mail address: p.w.j.c.serruys@erasmusmc.nl (P.W. Serruys).

## Abbreviations

BMS: bare metal stent  
BRS: bioresorbable scaffold  
DES: drug-eluting stent  
LLL: late lumen loss  
MACE: major adverse cardiac events  
MI: myocardial infarction  
SES: sirolimus-eluting stent  
ST: stent thrombosis

## INTRODUCTION

Coronary stents were first developed in the mid 1980s to overcome the inherent limitations of balloon angioplasty, including elastic recoil and vessel closure in the acute phase, as well as constrictive remodeling and restenosis in the late phase.<sup>1–3</sup> In the 1990s, this technology became widely accepted as a promising treatment strategy for patients with coronary artery disease after the landmark Belgian Netherlands Stent trial, which demonstrated the superiority of the bare metal stent (BMS) over balloon angioplasty.<sup>4</sup> Although coronary stenting improved angiographic results and clinical outcomes, neointimal hyperplasia and restenosis continued to be major limitations of this technology.<sup>5</sup> In order to minimize neointimal hyperplasia and thereby reduce repeat revascularization, drug-eluting stents (DES) were developed. Early pivotal trials of the first generation DES showed excellent results with respect to the reduction of in-stent restenosis, such that they rapidly replaced BMS.<sup>6,7</sup> In the year 2006, safety concerns were raised with DES following reports linking their use to an increased risk of stent thrombosis (ST).<sup>8,9</sup> First generation DES, with permanent polymers, have been associated with delayed endothelialization, endothelial dysfunction, and local hypersensitivity reactions, resulting in an increased risk of ST and the need for prolongation of dual antiplatelet therapy.<sup>10,11</sup>

Newer generation DES, with thinner struts and more biocompatible polymers, have considerably improved their safety profile.<sup>12–15</sup> However, concerns still persist over the presence of durable polymers, as evidence from animal and human studies still suggest that these durable polymers may cause persistent arterial wall inflammation and delayed vascular healing, both of which may subsequently have a potential role in precipitating ST and delayed in-stent restenosis (ie, late catch-up phenomenon).<sup>16</sup> Newer generation DES, coated with biodegradable polymers, offer the attractive combination of controlled drug elution in parallel with biodegradation of the polymer into inert monomers. After the completion of biodegradation, only a “BMS” remains, thereby reducing the long-term risks associated with the presence of a permanent polymer.<sup>17</sup> An extension of this concept has brought the development of newer DES that are completely free of polymer, or come with novel coatings. In addition, bioresorbable metallic (ie, magnesium) and polymeric scaffolds have been developed, which initially safeguard the patency of the treated vessel and then disappear. The aim of this article is to review new stent technologies that are currently undergoing clinical investigation and discuss their future perspectives in interventional cardiology.

## NEW GENERATION METALLIC DRUG ELUTING STENT

### Drug Eluting Stent With Biodegradable Polymers

Biodegradable polymeric coatings facilitate drug delivery to the vessel wall and are then resorbed without any long-term sequelae.

Since their introduction in the year 2004,<sup>18</sup> many DES with biodegradable polymers have been developed, particularly after it was hypothesized that this technology would potentially reduce the risk of very late ST (VLST), an adverse event which has been associated with durable-polymer DES. The randomized ISAR-TEST 4 trial was conducted to test the noninferiority of a biodegradable-polymer rapamycin-eluting stent (RES; Yukon Choice PC, Translumina; Hechingen, Germany) to a durable-polymer DES (ie, the first generation Cypher sirolimus-eluting stent [SES] or the second generation Xience V everolimus-eluting stent [EES]), with respect to clinical outcomes. A total of 2603 patients were enrolled in the trial. At 3-year follow-up, there were no significant differences in a composite of cardiac death, target-vessel myocardial infarction (MI), and target lesion revascularization (TLR) (RES 20.1% vs DES 20.9%,  $P=.59$ ), as well as the incidence of definite/probable ST (RES 1.4% vs DES 1.9%,  $P=.51$ ).<sup>19</sup> Longer-term clinical follow-up is required to evaluate the potential superiority of RES over the traditional DES in reducing the risk of VLST.

### Biolimus-eluting Stent With Biodegradable Polymer

Biolimus A9 is a semisynthetic limus-drug designed for stent application which has a similar potency to sirolimus, but is 10 times more lipophilic. It is immersed at a concentration of 15.6  $\mu\text{g}/\text{mm}$  into a polylactic acid biodegradable polymer that covers the abluminal stent surface. Polylactic acid is coreleased with biolimus and completely metabolized into carbon dioxide and water over 6 months to 9 months. The stainless steel stent platform has a strut thickness of 112  $\mu\text{m}$ , with a quadrature link design. Currently, the stent platforms utilizing this technology are the BioMatrix Flex (Biosensors Inc.; Singapore), NOBORI (Terumo Corp.; Tokyo, Japan), and Axxess (Biosensors Inc.).

In the LEADERS trial, the BioMatrix stent was shown to be noninferior to the first generation durable-polymer Cypher SES, with respect to a composite end point of cardiac death, MI, and ischemia-driven target vessel revascularization at 12-month follow-up (BioMatrix 10.6% vs Cypher 12.0%,  $P=.37$ ).<sup>20</sup> This noninferiority has recently been confirmed at 5-year follow-up.<sup>21</sup> Importantly, the BioMatrix stent showed a significantly lower incidence of definite VLST at 5-year follow-up (hazard ratio=0.26 [0.10–0.68]). A pooled data analysis of the randomized ISAR-TEST 3, ISAR-TEST 4, and LEADERS trials also showed that the DES with biodegradable polymers were associated with a lower risk of VLST as well as MI compared to the Cypher SES.<sup>22</sup> The LEADERS trial not only provided the first evidence of improved clinical outcomes compared to the first generation DES, but is also the proof of concept in terms of biodegradable-polymer DES.

### Everolimus-eluting Stent With Biodegradable Polymer: SYNERGY Stent

The SYNERGY stent (Boston Scientific; Natick, Massachusetts, United States) consists of a thin-strut (74  $\mu\text{m}$ ), platinum-chromium platform that delivers everolimus from a bioabsorbable polylactide-co-glycolide polymer applied to the abluminal surface. In the randomized, EVOLVE trial, the safety and efficacy of 2 dose formulations (standard dose [SD], 113  $\mu\text{g}/20\text{mm}$ , and half dose [HD], 56  $\mu\text{g}/20\text{mm}$ ) of the SYNERGY stent were compared to the durable-polymer PROMUS Element EES (Boston Scientific).<sup>23</sup> A total of 291 patients were randomly assigned in a 1:1:1 ratio to SYNERGY, SYNERGY HD, and EES. The primary clinical endpoint was the 30-day rate of target lesion failure (TLF), defined as a composite of cardiac death, MI related to the target vessel, and TLR. TLF occurred in 3.1%, 1.1%, and 0% of patients in the SYNERGY, SYNERGY HD, and EES groups, respectively. The 6-month in-stent

**Table 1**  
Overview of Drug-eluting Stents With a Biodegradable Polymer Under Clinical Investigation or Already Available Outside the United States

Drug-eluting stent manufacturer	Drug, dosage	Stent platform	Stent/coating thickness, $\mu\text{m}$	Polymer	Biodegradation of polymer, months	Drug release kinetics, % (days)	Study no. of patients	Angiographic follow-up, months	In-stent late loss, mm	Binary restenosis, %	Current status
BioMatrix Flex (Biosensors)	Biolimus A9 (15.6 $\mu\text{g}/\text{mm}$ )	SS	112/10	Abuminal PLA	6-9	45 (30)	LEADERS (857)	9	0.13	20.9	CE approved
NOBORI (Terumo)	Biolimus A9 (15.6 $\mu\text{g}/\text{mm}$ )	SS	112/10	Abuminal PLA	6-9	45 (30)	NOBORI I (153)	9	0.11	0.7	CE approved
Access (Biosensors)	Biolimus A9 (22 $\mu\text{g}/\text{mm}$ )	Nitinol	152/15	Abuminal PLA	6-9	45 (30)	DIVERGE (302)	9	MB, 0.29; SB, 0.29	MB, 2.3; SB, 4.8	CE approved
Supralimus (Shahjahanand Medical)	Sirolimus (1.25 $\mu\text{g}/19 \text{ mm}$ )	SS	80/4-5	PLLA-PLGA - PCL-PVP	7	100 (48)	SERIES I (100)	6	0.09	0.0	CE approved
Infinium (Shahjahanand Medical)	Paclitaxel (122 $\mu\text{g}/19 \text{ mm}$ )	SS	80/4-5	PLLA-PLGA - PCL-PVP	7	50 (9-11)	SIMPLE II (111)	9	0.54	8.3	CE approved
BioMime (Meril Life Science)	Sirolimus (1.25 $\mu\text{g}/\text{mm}^2$ )	Co-Cr	65/2	PLLA+PLGA	N/A	100 (30)	MERIT II (242)	8	0.11	5.0	CE approved
Ostro (Biotronik)	Sirolimus (1.4 $\mu\text{g}/\text{mm}^2$ )	Co-Cr	60/7	PLLA with silicon carbide layer	N/A	50 (30)	BIOFLOW I (30)	9	0.05	0.0	CE approved
DESyne BD (Elvir Medical)	Novolimus (65 $\mu\text{g}/14 \text{ mm}$ )	Co-Cr	81/<3	Abuminal PLA	6-9	90 (90)	EXCELLA BD (115)	6	0.12	0.0	CE approved
SYNERGY (Boston Scientific)	Everolimus (SD, 113 $\mu\text{g}/20 \text{ mm}$ ; HD, 56 $\mu\text{g}/20 \text{ mm}$ )	Pt-Cr	71/3	Abuminal PLGA rollcoat	3	50 (60)	EVOLVE (SD 92; HD, 99)	6	SD, 0.10; HD, 0.13	SD, 2.3; HD, 1.1	CE approved
MiStent (Micell)	Sirolimus (N/A)	Co-Cr	64/3-5 (luminal), 10-15 (abuminal)	PLGA	3	50 (30)	DISSOLVE II (121)	9	0.27	4.9	CE approval submitted
Excel (JW Medical Systems)	Sirolimus (195-376 $\mu\text{g}/\text{stent}$ )	SS	119/15	PLLA	6-9	N/A	Registry (2077)	6	0.21	3.8	Ongoing evaluation
Firehawk (MicroPort Medical)	Sirolimus (3 $\mu\text{g}/\text{mm}$ )	Co-Cr	N/A	Abuminal PDLLA (groove-filled)	9	90 (90)	TARGET I (199)	9	0.13	1.0	Ongoing evaluation
NOYA (Medfavour Beijing Medical)	Sirolimus (8.8 $\mu\text{g}/\text{mm}$ )	Co-Cr	81/6	PDLLA	N/A	80 (30)	NOYA I (150)	9	0.11	4.2	Ongoing evaluation
Inspiron (Screech)	Sirolimus (56 $\mu\text{g}/13 \text{ mm}$ )	Co-Cr	75/5	Abuminal PLLA+PLGA	6-9	80 (30)	INSPIRON I (38)	6	0.22	3.9	Ongoing evaluation
Thivoil (Esen Technologies)	Sirolimus (8 $\mu\text{g}/\text{mm}$ )	Co-Cr	80/6	PLGA	3-6	80 (38)	I-LOWE-T (168)	8	0.25	5.7	Ongoing evaluation
BuMA (StroMed)	Sirolimus (1.4 $\mu\text{g}/\text{mm}^2$ )	SS	100	PLGA	N/A	100 (30)	PANDA-1 (113)	9	0.24	N/A	Ongoing evaluation
Svelte (Svelte)	Sirolimus (130 $\mu\text{g}/18 \text{ mm}$ )	Co-Cr	81/6	Amino acid-based carrier coating	12	N/A	DIRECT FIM (30)	6	0.15	N/A	Ongoing evaluation

CE, Conformité Européenne; Co-Cr, cobalt-chromium; HD, half dose; MB, main branch; N/A, not applicable; PCL, poly-L-lactide-co- $\epsilon$ -caprolactone; PDLLA, poly-D, L-lactic acid; PLLA, poly-lactide; PLGA, poly-lactide-co-glycolide; PLLA, poly-L-lactic acid; Pt-Cr, platinum-chromium; PVP, poly-vinyl-pyrrolidone; SB, side branch; SD, standard dose; SS, stainless steel.

late lumen loss (LLL) was 0.10 mm for SYNERGY, 0.13 mm for SYNERGY HD, and 0.15 mm for EES ( $P_{\text{noninferiority}} < .001$ ). There were no ST events in any group at up to 6-month follow-up. Recently, the SYNERGY stent acquired the *Conformité Européenne* (CE) mark approval; a pivotal EVOLVE II trial aiming a head-to-head comparison of 12-month TLF with SYNERGY (842 patients) and EES (842 patients) is currently ongoing.

#### Other Drug Eluting Stents With Biodegradable Polymers

Currently, many DES with biodegradable polymers are commercially available or under clinical investigation (Table 1). Preliminary studies have shown comparable results at 6 months to 9 months to that of aforementioned DES with biodegradable polymers. Although biodegradable polymers appear to have become a promising drug-delivery technology in the newer generation DES platform, there are issues remaining to be addressed before their widespread clinical application.<sup>24</sup> Further research is needed in order to optimize the composition and release kinetics of these polymers.

#### Porous Polymer-free Drug Eluting Stent

The next major step forward may be metallic stent structures which allow for appropriate drug-elution kinetics without the use of polymers. Several devices have been designed to test this approach by incorporating drugs into a microporous or nanoporous surface of the stent (Table 2). The efficacy of a polymer-free SES (SES-PF; Yukon Choice, Translumina) was investigated in the ISAR-TEST 3 trial.<sup>25,26</sup> The SES-PF (201 patients) was compared to a SES with a biodegradable polymer (202 patients, SES-BP; Yukon Coice PC, Translumina) and a SES with a permanent polymer (202 patients, SES-PP; Cypher, Cordis; Miami Lakes, Florida, United States). At 2 years, there were no significant differences in death, MI (SES-PF 6.5%, SES-BP 5.9%, and SES-PP 6.4%), TLR (SES-PF 13.4%, SES-BP 8.4%, and SES-PP 10.4%), and definite/probable ST (SES-PF 1.0%, SES-BP 0.5%, and SES-PP 1.0%). Patients undergoing paired angiography at 6 months to 8 months and at 2 years (302 patients), demonstrated a lower delayed LLL in the SES-PF (-0.01 mm) group, as compared to both the SES-BP (0.17 mm) and the SES-PP (0.16 mm) ( $P < .001$ ) groups. The absence of delayed LLL in the SES-PF group may indicate a lower propensity for stent-vessel wall interactions, owing to less inflammatory or hypersensitive reactions. Recently, the 5-year clinical outcomes in the ISAR-TEST trial have been reported.<sup>27</sup> There were no statistically significant differences in ST events between SES-PF and the first generation TAXUS paclitaxel-eluting stent (PES) (SES-PF 0.5% vs PES 1.6%,  $P = .32$ ). Extended follow-up data may further support the durability, safety, and efficacy of the SES-PF.

#### BioFreedom Stent

The BioFreedom stent (Biosensors Inc.), is a 316L stainless steel, polymer-free stent that is coated with biolimus A9 (Fig. 1). Preclinical studies have reported lower injury scores; lower numbers of struts with fibrin, granulomas, and giant cells; significantly lower percentage of diameter stenosis; and greater endothelialization with the BioFreedom stent at 180-day follow-up as compared to the Cypher SES.<sup>28</sup> The first-in-man (FIM) trial enrolled 182 patients who were randomized to receive either BioFreedom with SD sirolimus (15.6  $\mu\text{g}/\text{mm}$ ), BioFreedom with low dose (LD) sirolimus (7.8  $\mu\text{g}/\text{mm}$ ), or TAXUS Liberté PES. At 12 months, the in-stent LLL was 0.17 mm in the BioFreedom SD

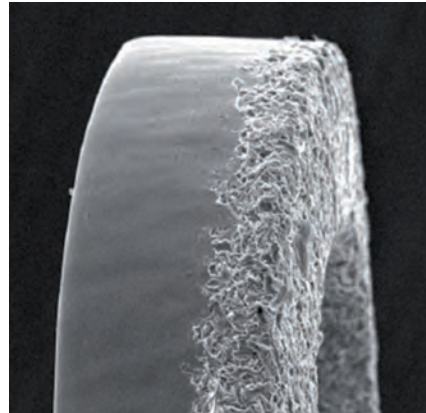


**Figure 1.** The surface of the polymer-free BioFreedom stent. A scanning electron microscopy image shows the micropores impregnated with biolimus A9 only in the albuminal side of the strut.

arm ( $P < .0001$  vs PES), 0.22 mm in the BioFreedom LD arm ( $P = .21$  vs PES), and 0.35 mm in the PES arm. There were no ST events and no differences in major adverse cardiac events (MACE) including all-cause death, MI, and emergent bypass surgery or TLR at up to 36 months (BioFreedom SD 11.9%; BioFreedom LD 18.1%, and PES 10.0%).<sup>29</sup> Currently, a randomized LEADERS FREE trial has been planned to examine the noninferiority (a composite of cardiac death, MI, and ST) and superiority (clinically driven TLR) of the BioFreedom stent to BMS in >2400 elderly patients with dual antiplatelet therapy for 1 month after stent implantation.

#### VESTAsync Stent

The VESTAsync stent (MIV Therapeutics; Atlanta, Georgia, United States) combines a stainless steel platform with a nanoporous, hydroxyapatite (biocompatible crystalline derivative of calcium phosphate) surface coating that is impregnated with 55  $\mu\text{g}$  of sirolimus mixture (Fig. 2). It is expected that sirolimus will be completely released within the first 3 months after the implantation, and that the hydroxyapatite will be stable over 4 months. The safety and efficacy of the VESTAsync stent was evaluated in the VESTAsync I FIM trial. A total of 15 patients with single de novo coronary artery lesions were enrolled. In-stent LLL was 0.36 mm at 9 months, with no MACE reported at up to 1-year follow-up.<sup>30</sup> Recently a randomized VESTAsync II trial has been reported.<sup>31</sup> The patients treated with the VESTAsync stent (50 patients) showed a significantly lower in-stent LLL compared to those treated with BMS (25 patients) at 8 months (VESTAsync 0.39 mm vs BMS 0.74 mm,  $P = .03$ ). No evidence of ST was reported at up to 2-year follow-up.

#### Nano<sup>+</sup> Stent

The Nano<sup>+</sup> stent (Lepu Medical; Beijing, China) is a stainless steel, polymer-free stent with a nanoporous surface coated with

**Table 2**  
Overview of Polymer-free and Novel-coating Drug-eluting Stents Under Clinical Investigation or Already Available Outside the United States

Drug-eluting stent, manufacturer	Drug, dosage	Stent platform	Stent thickness, $\mu\text{m}$	Surface modification	Drug release kinetics	Study no. of patients	Angiographic follow-up, months	In-stent late loss, mm	Binary restenosis, %	Current status
<i>Porous polymer-free DES</i>										
Yukon Choice (Translumina)	Sirolimus (11.7–21.9 $\mu\text{g}$ )	SS	87	Abtimalinal microporous surface	100%, 25 days	ISAR-TEST 1 (225)	9	0.48	14.2	CE approved
BioFreedom (Biosensors)	Biolimus A9 (SD, 15.6 $\mu\text{g}/\text{mm}^2$ ; HD, 7.8 $\mu\text{g}/\text{mm}^2$ )	SS	119	Abtimalinal microporous surface	90%, 50 h	FIM (SD, 31; HD, 35)	12	SD, 0.17; HD, 0.22	N/A	CE approval submitted
VESTAsync (MIV Therapeutics)	Sirolimus (55 $\mu\text{g}$ )	SS	65	Nanoporous surface with hydroxyapatite	100%, 90 days	VESTAsync II (15)	8	0.39	0	Ongoing evaluation
Nano <sup>®</sup> (Lepu Medical)	Sirolimus (2.2 $\mu\text{g}/\text{mm}^2$ )	SS	100	Abtimalinal nanoporous surface	80%, 30 days	N/A	N/A	N/A	N/A	Ongoing evaluation
<i>DES with other technologies</i>										
Cres8 (CID)	Sirolimus (0.9 $\mu\text{g}/\text{mm}^2$ )	Co-Cr	80	Abtimalinal reservoirs	100%, 90 days	NEXT-Cres8 (162)	6	0.14	3.2	CE approved
Combo (OrbusNeich Medical)	EPC-sirolimus (5 $\mu\text{g}/\text{mm}^2$ )	SS	100/3-5	Abtimalinal biodegradable polymer and luminal CD34 antibody layer	N/A	REMEDEE (124)	9	0.39	8.3	Ongoing evaluation
FOCUS np (Envision Scientific)	Sirolimus (108 $\mu\text{g}/16\text{mm}$ )	Co-Cr	73	Abtimalinal coating with encapsulated drug by nanoparticles	100%, 28 days	N/A	N/A	N/A	N/A	Ongoing evaluation

CE, Conformité Européenne; Co-Cr, cobalt-chromium; SD, standard dose; DES, drug-eluting stent; EPC, endothelial progenitor cell (capture technology); HD, half dose; N/A, not applicable; SS, stainless steel.

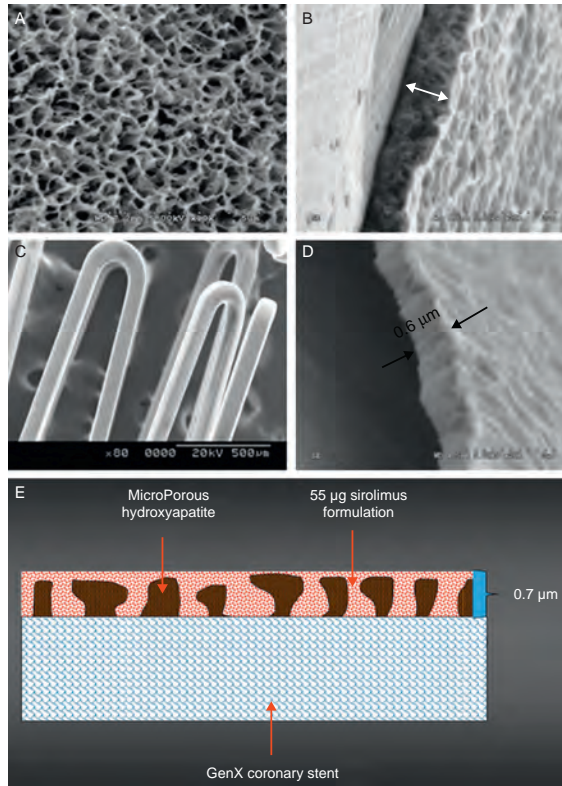


**Figure 2.** The polymer-free VESTAync sirolimus-eluting stent system. The scanning electron microscopy images of microporous hydroxyapatite coating (A), cross section of the hydroxyapatite coating (B), final coating including the hydroxyapatite filled with sirolimus formulation (C), and cross section of the final coating (D). A schematic representation of the surface coating (E).

sirolimus ( $2.2 \mu\text{g}/\text{mm}^2$ ). The average diameter of the pores is approximately  $400 \text{ nm}$  and almost  $80\%$  of the drug is programmed to be released within 30 days. The Bicare stent is another nanopore-based polymer-free DES, which uses both sirolimus and probucol. These 2 stents have a similar design, the only difference between the Bicare stent and the Nano<sup>®</sup> stent being the drug type. Thirty patients with de novo lesions were enrolled in the Bicare FIM trial.<sup>32</sup> In-stent LLL was  $0.14 \text{ mm}$  and the rate of tissue coverage of the struts was  $98.3\%$  determined by optical coherence tomography (OCT) at 4 months.<sup>32</sup> Similarly, the ISAR-TEST 5 trial demonstrated the noninferiority of polymer-free sirolimus and probucol-eluting stents (Yukon Choice, Translumina) over the second generation durable-polymer resolute zotarolimus-eluting stents (Medtronic Cardiovascular; Santa Clara, California, United States) in terms of MACE and ST at 1-year follow-up.<sup>33</sup> A post-market study of the Nano<sup>®</sup> stent is currently ongoing in China, and another trial aiming the CE mark approval has been planned in Europe.

## Drug Eluting Stent With Other Technologies

### Cre8 Stent

The Cre8 stent (CID; Saluggia, Italy) is a polymer-free stent that is integrally coated with an ultra-thin ( $0.3 \mu\text{m}$ ) passive carbon coating (i-Carbofilm, CID). The amphiphilic formulation, constituted by sirolimus ( $0.9 \mu\text{g}/\text{mm}^2$ ) with an excipient composed of a long-chain fatty acid mixture to modulate the drug release, is loaded into abluminal reservoirs. Complete release of sirolimus is expected within the first 3 months after stent deployment. A total of 323 patients were randomized to receive either Cre8 (162 patients) or TAXUS Liberté PES (161 patients) in the NEXT FIM trial.<sup>34</sup> The primary endpoint was in-stent LLL at 6 months, and was significantly lower in the Cre8 group (Cre8  $0.14 \text{ mm}$  vs PES  $0.34 \text{ mm}$ ,  $P < .0001$ ). A cumulative incidence of MACE including cardiac death, MI, and TLR in the Cre8 group was  $6.7\%$  at 2 years,

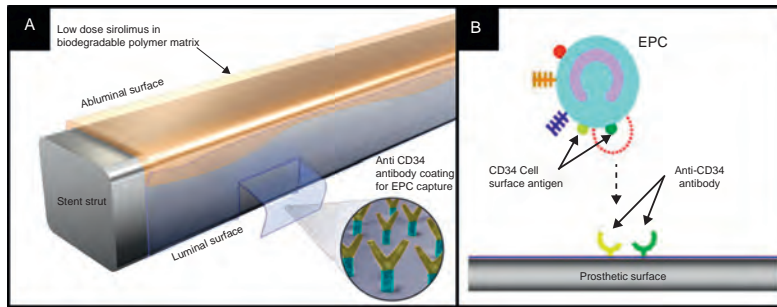


**Figure 3.** The Combo dual therapy stent system. A: The Combo stent consists of an abluminal biodegradable polymer matrix with a sirolimus and a luminal CD-34 antibody layer. B: A schematic representation of the endothelial progenitor cells capture technology. The CD-34 antigens on the surface of the endothelial progenitor cells attach to the anti-CD-34 antibodies on the stent's surface, promoting endothelialization. EPC, endothelial progenitor cells.

showing no differences compared to PES (7.1%). Only 1 case of definite late ST was observed in each group at up to 2-year follow-up.<sup>35</sup> An all-comers registry (1000 patients) is currently ongoing and is expected to complete enrollment of patients by early 2013.

#### Combo Stent

The Combo stent (OrbusNeich Medical; Hong Kong, China) applies the endothelial progenitor cell capture technology to enhance vessel healing (ie, immobile CD34 antibodies on the luminal surface of the strut), incorporating abluminal LD sirolimus and a biodegradable polymer into the current DES technology (Fig. 3). Data from OCT and histology at 28 days in a porcine model indicated that this hybrid stent promotes endothelialization, and reduces neointimal formation and inflammation when compared to the Cypher SES and the first generation Genous endothelial progenitor cell stent.<sup>36</sup> The REMEDEE FIM trial randomized 180 patients to treatment with either the Combo stent (124 patients) or the TAXUS Liberté PES (59 patients). The in-stent LLL at 9 months was 0.39 mm in the Combo group and 0.44 mm in the PES group ( $P_{\text{noninferiority}} = .0012$ ). Binary restenosis was observed in 8.3% patients in the Combo group and in 13.5% patients in the PES group ( $P = .30$ ). No cases of ST were reported in both groups at up to 9-months follow-up.<sup>37</sup> Further investigation is required to determine the prohealing effect and clinical efficacy of this device.

#### FOCUS *np* Stent

The FOCUS *np* stent (Envision; Surat, India) platform has a novel carrier; a phospholipid 2-layer nanoparticle that encapsulates sirolimus (Fig. 4). The encapsulated sirolimus is coated on the surface of the stent and the balloon (108  $\mu\text{g}$  of sirolimus on a  $3.0 \times 16.0$  mm system). Sirolimus is programmed to be completely released within 28 days, however, the tissue concentration of sirolimus peaks within the first 24 h. A preclinical study with the FOCUS *np* stent showed similar LLL and inflammation scores to that seen in the Cypher SES at 28 days and at 90 days. A FIM trial will be completed in early 2013.<sup>38</sup>

#### BIORESORBABLE SCAFFOLDS

Fully bioresorbable scaffolds (BRS) are a novel approach as they provide transient vessel support in contrast to the

permanent caging caused by metallic stents. The concept of BRS was introduced by Stack et al. in the year 1988.<sup>39</sup> Zidar and colleagues first implanted BRS made of poly-L-lactic acid (PLLA) into canine femoral arteries.<sup>40</sup> Despite significant scaffold degradation with low-grade vascular inflammation at 9-month follow-up, this technology failed to develop because of the inability to manufacture an ideal polymer that could limit inflammation and restenosis.<sup>41,42</sup> In the year 2000, Tamai and colleagues reported their FIM experience with BRS implantation for the treatment of human coronary arteries.<sup>43</sup> This "Igaki-Tamai" PLLA stent had a unique zigzag helical coil design, with a strut thickness of 170  $\mu\text{m}$ . This system was self-expanding but also required balloon inflation with heated contrast for expansion. The FIM study of the Igaki-Tamai stent (15 patients) demonstrated no MACE or ST events within 30 days, and 1 repeat percutaneous coronary intervention at 6-month follow-up. Our group reported the findings of OCT at 10 years after Igaki-Tamai stent implantation, showing absence of visible struts, with endoluminal lining of the vessel wall.<sup>44</sup> Recently, Nishio et al. reported >10-year clinical outcomes of the first 50 patients treated with Igaki-Tamai stents. Autopsy specimens showed interesting histological findings, that indicated healing with thickened neointima at the previously stented segment, without inflammatory cell infiltration or foreign body reactions. As measured by quantitative coronary angiography, LLL decreased from 0.91 mm at 6 months to 0.59 mm at 3 years, whilst intravascular ultrasound (IVUS) showed an increased external elastic lamina area (15.0  $\text{mm}^2$  postprocedurally and 16.9  $\text{mm}^2$  at 3 years). These findings suggest that the artery restored its capability to respond to expansive remodeling and late lumen enlargement once the scaffold degraded.

Currently, numerous BRS are being tested in clinical or preclinical studies. An overview of this technology has been shown in Table 3 and Figure 5.

#### Absorbable Magnesium Stent

Magnesium (Mg) is the fourth commonest cation within the human body. It is essential for the synthesis of over 300 enzymes, and is a cofactor for ATPase. A high dose infusion of Mg can cause vasodilatation and the development of collaterals during ischaemia. The degradation of Mg produces an electronegative charge that results in the stent being hypothrombogenic.<sup>45</sup>

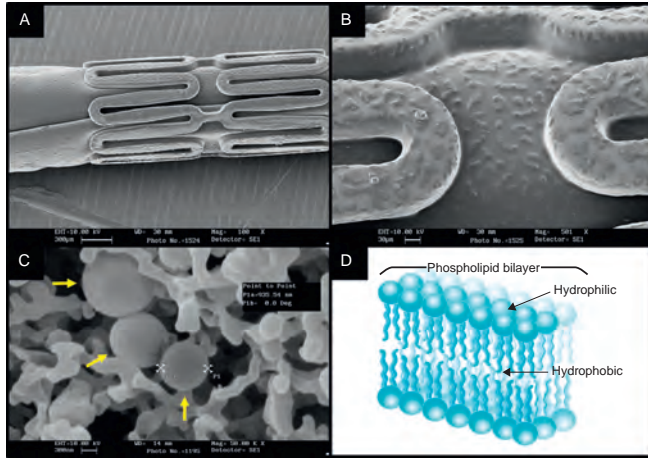


**Figure 4.** The nanocarrier-based FOCUS np sirolimus-eluting stent. The scanning electron microscopy (SEM) images of the crimped stent (A) and the magnified surface of the strut and balloon (B) coated with encapsulated sirolimus (C, yellow arrows). The nanocarrier consists of a lipid bilayer with a hydrophilic head and two lipophilic/hydrophobic tails (D), and the drug is released on pH change.

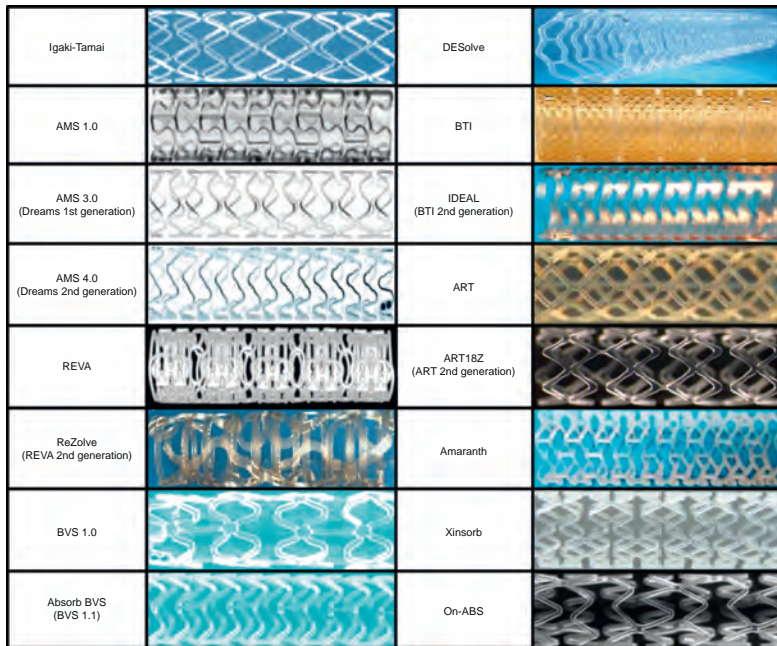


**Figure 5.** Bioresorbable scaffolds under clinical or preclinical investigation.

**Table 3**  
Overview of Bioresorbable Scaffolds Under Current Pre-clinical or Clinical Investigation

Bioresorbable scaffold, manufacturer	Strut material	Coating material	Drug	Radio-opacity	Strut thickness, $\mu\text{m}$	Crossing profile, mm	Stent-to-artery coverage, %	Duration of radial support	Resorption time, months	Angiographic late loss, mm (months)	Target lesion revascularization rate, % (months)	Current status
Isaki-Tamai (Kyoto Medical)	PLLA	None	None	Gold markers	170	N/A	24	6 months	24	0.48 (6)	6.7 (6)	CE approved (PAD)
AMS-1.0 (Biotronik)	Mg	None	None	None	165	1.2	10	Days or weeks	<4	1.08 (4)	45 (12)	FIM completed
AMS-3.0 (Biotronik)	Mg	None	Pacitaxel	None	125	N/A (6 Fr compatible)	N/A	Weeks	>4	0.64 (6) 0.52 (12)	4.3 (6) 4.7 (12)	FIM (BIOSOLVE-I) completed
AMS-4.0 (Biotronik)	Mg	PLLA	Sirolimus	Metallic markers	N/A	N/A (6 Fr compatible)	N/A	N/A	N/A	N/A	N/A	Used in BIOSOLVE-I
BVS 1.0 (Abbott Vascular)	PLLA	PDLLA	Everolimus	Platinum markers	157	1.4	26	Weeks	24	0.44 (6)	0.0 (60)	FIM completed
Absorb BVS 1.1 (Abbott Vascular)	PLLA	PDLLA	Everolimus	Platinum markers	157	1.4	26	6 months	24	0.19 (6) 0.27 (12)	3.6 (12)	CE approved
REVA (REVA Medical)	Poly-tyrosine-derived polycarbonate polymer	None	None	Scaffold itself	200	1.7	55	3-6 months	24	1.81 (6)	67 (12)	FIM completed
ReZolve (REVA Medical)	Poly-tyrosine-derived polycarbonate polymer	None	Sirolimus	Scaffold itself	114-228	1.5	N/A	4-6 months	24	N/A	N/A	FIM planned in 2013
DESolve (Elxir Medical)	PLLA	PLLA	Mvolimus	Metallic markers	150	1.5	N/A	N/A	12-24	0.19 (8)	6.7 (12)	FIM completed
IDEAL BioStent (Xenogenics)	polymer salicylate+ linker	Salicylate	Sirolimus	None	175	1.5-1.7	57	3 months	>12	N/A	N/A	FIM completed
ARTIBZ (Arterial Remodeling Technologies)	PDLLA	None	None	None	170	N/A (6 Fr compatible)	<25	3-6 months	18	None	None	FIM initiated
Xinorb (Huaan Biotechnology)	PLLA+PCL+PLGA	None	Sirolimus	Metallic markers	160	N/A	N/A	N/A	N/A	None	None	Pre-clinical underway
Amaranth PLLA (Amaranth Medical)	PLLA	None	None	None	150-200	N/A (6 Fr compatible)	N/A	3-6 months	N/A	None	None	FIM initiated
On-ABS (ObusNtech Medical)	PLLA+PCL+PDLLA	None	EPC+ sirolimus	None	150	N/A	N/A	N/A	N/A	None	None	Pre-clinical underway

CE, Conformité Européenne; EPC, endothelial progenitor cell (capture technology); FIM, first-in-man; Mg, magnesium; N/A, not applicable; PAD, peripheral artery disease; PCL, poly-L-lactide-co- $\epsilon$ -caprolactone; PDLLA, poly-D, L-lactic acid; PLGA, poly-lactide-co-glycolide; PLLA, poly-L-lactic acid.

The first generation absorbable metallic stent (AMS-1, Biotronik; Berlin, Germany) was composed of 93% Mg and 7% rare earth metals. In the porcine model, the AMS-1 was shown to be rapidly endothelialized, and largely degraded into inorganic salts at 60 days, with little associated inflammatory response.<sup>46</sup> The PROGRESS AMS trial was a single-arm FIM study, which assessed the efficacy and safety of this stent in 63 patients with single de novo lesions.<sup>47</sup> No evidence of death, MI, or ST was reported at up to 12-month follow-up. Disappointingly, the TLR rate was 23.8% at 4 months and 45% at 12 months. The in-stent LLL was 1.08 mm and the vasodilator function, after the nitroglycerin administration, appeared to be restored in the stented segment at 4-month angiographic follow-up.<sup>48</sup> IVUS data suggested that the increased LLL was attributed to an increased neointimal formation and insufficient radial strength of the Mg alloy, due to rapid stent degradation resulting in vessel recoil. Consequently, new stents have been developed, namely AMS-2 and AMS-3. The AMS-2 stent was designed to address excessive vessel recoil seen with AMS-1. It provided prolonged mechanical integrity by using a different Mg alloy, which not only had a higher collapse pressure, but also a slower degradation time. In addition, the strut thickness was reduced from 165  $\mu\text{m}$  to 125  $\mu\text{m}$ , and the cross-sectional shape of the strut altered from rectangular to square. These modifications facilitated prolonged mechanical integrity, improved radial strength, and resulted in reduced neointimal proliferation in animal studies. The AMS-3 stent (ie, drug-eluting AMS [DREAMS]) was designed to incorporate a bioresorbable matrix for the controlled release of paclitaxel with the AMS-2 platform. This device was evaluated in the BIOSOLVE-I trial (46 patients), and demonstrated an in-stent LLL of 0.64 mm at 6 months and 0.52 mm at 12 months. The rate of TLF was 7.0% at up to 12-month follow-up, due to 2 clinically driven TLRs and 1 periprocedural MI.<sup>49</sup> The second generation DREAMS has a modified stent platform and sirolimus as its antiproliferative drug. The BIOSOLVE-II study aimed to assess the safety and efficacy of this device will be initiated in the year 2013.

#### Everolimus-eluting Poly-L-lactic Acid Scaffold: Absorb BVS

The backbone of Absorb BVS (Abbott Vascular; Santa Clara, California, United States) is made of PLLA. The coating consists of poly-D, L-lactide (PDLLA), which is a random copolymer of D-lactic acid and L-lactic acid with lower crystallinity than the backbone PLLA. The PDLLA coating controls the release of the antiproliferative drug everolimus. The first generation Absorb BVS (1.0) was tested in 30 patients who were enrolled in the ABSORB FIM (cohort A) trial. Multiple modality imaging was assessed in this trial, and the results can be summarized as follows: a) partial bioresorption of the polymeric struts; b) late lumen enlargement between 6 months and 2 years; c) restoration of vasomotion and endothelial function at 2 years; d) sustained scaffolding of plaque deformability documented with palpography, and e) feasibility of noninvasive imaging with multislice computed tomography.<sup>50,51</sup> Five-year clinical follow-up is available in 29 patients.<sup>52</sup> Only 1 patient experienced a non-Q wave MI related to the treatment of a non-flow-limiting stenosis at 46 days after Absorb BVS implantation. There were no ST events in the entire period and no MACE between 6 months and 5 years, resulting in an overall MACE rate of 3.4% at 5 years. Late scaffold shrinkage was the primary reason for an increased in-stent LLL (0.44 mm) at 6 months. Lumen area was reduced by 16.6%, whilst the late recoil was 11.7%.<sup>53</sup> In order to enhance the radial strength of the struts and to reduce late recoil, the strut design and the manufacturing process of the polymer were modified in the second generation Absorb BVS (1.1). Firstly, the new design had in-phase zigzag hoops linked by bridges that allowed for a more uniform strut distribution. This new scaffold

design reduced maximum circular unsupported surface area that provided for more uniform vessel wall support and drug delivery. Secondly, a modified manufacturing process resulted in a slower hydrolysis (in vivo degradation) rate of the polymer, thus allowing for prolongation of its mechanical integrity.<sup>54</sup>

The Absorb BVS 1.1 was evaluated in 101 patients in the ABSORB cohort B trial. This cohort was divided in 2 subgroups: the first group (B1) underwent invasive imaging with quantitative coronary angiography, IVUS, and OCT postprocedurally, at 6 months, and at 24 months; whereas the second group (B2) underwent invasive imaging postprocedurally, at 12 months, and at 36 months. In the entire cohort B population, the overall MACE rate was 9.0%, including 3 non-Q wave MIs and 6 ischemia-driven TLRs, without cardiac death during the 2-year follow-up. There were no possible, probable, or definite scaffold thromboses despite dual antiplatelet therapy rates of 97% at 6 months, 81.2% at 12 months, and 24.8% at 24 months.

For the cohort B1 population, serial multimodality imaging results are currently available.<sup>55</sup> Serial angiographic analyses showed that in-scaffold LLL of 0.16 mm at 6 months increased to 0.27 mm at 2 years. Notably, serial IVUS analyses demonstrated that the mean lumen area increased, whereas the minimum lumen area remained stable between 6 months and 2 years (Fig. 6). Percentage hypercholechoenic area, a more sensitive parameter to measure degradation of polymeric material, decreased from 25.3% postprocedurally to 20.4% at 6 months and to 13.8% at 2 years. Similar to IVUS, serial OCT investigation confirmed the progressive increase in mean scaffold area from 7.47  $\text{mm}^2$  postprocedurally, to 7.70  $\text{mm}^2$  at 6 months, and 8.24  $\text{mm}^2$  at 24 months.

The promising results of Absorb BVS constitute the proof of concept that this device can adequately revascularize coronary vessels and prevent restenosis. The Absorb BVS acquired the CE mark approval in January 2011, and since September 2012 it is commercially available in different diameters (2.5 mm, 3.0 mm, and 3.5 mm) and lengths (12 mm, 18 mm, and 28 mm). This device is now being evaluated in the ABSORB-EXTEND registry (~800 patients). A pivotal, randomized trial (ABSORB II), comparing Absorb BVS with Xience Prime EES (Abbott Vascular) in 500 patients, is simultaneously ongoing in Europe.

#### Tyrosine Polycarbonate Stent

The REVA stent (REVA Medical, San Diego, California, United States) consists of a tyrosine-derived poly carbonate that degrades into water, carbon dioxide, and ethanol. In addition to its radio-opacity, the REVA stent also has a unique "slide and lock" design that provides flexibility. This design maintains the acute lumen gain following stent deployment, and provides additional support to the scaffold during vessel remodeling. The RESORB FIM trial enrolled 27 patients. The in-stent LLL was disappointingly high (1.81 mm) and IVUS data showed no vessel recoil as indicated by external elastic lamina area (15.5  $\text{mm}^2$  postprocedurally and 15.3  $\text{mm}^2$  at 6 months). There was a high rate of TLR (66.7%) between 4 months and 6 months, mostly due to excessive neointimal hyperplasia.<sup>56</sup> The second generation ReZolve stent had a more robust polymer, a "spiral" slide and lock system, and a coating of sirolimus. Furthermore, the ReZolve2 stent had a smaller profile (1.52 mm) and achieved approximately 30% increase in radial strength. The safety and efficacy of the ReZolve or ReZolve2 stent is currently under investigation in the RESTORE study (50 patients) that was initiated in December 2011. Preliminary data (26 patients) showed that technical success rate was 85%, due to the delivery failure seen in 4 patients. Two cases with TLR as a primary endpoint were reported at 6-months follow-up.<sup>57</sup>

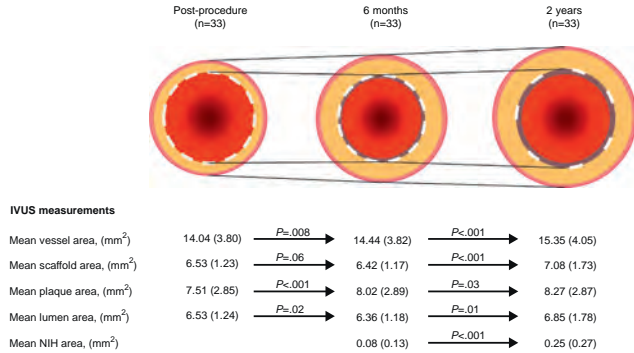


**Figure 6.** Serial changes in intravascular ultrasound measurements over postprocedure, 6 months, and 2 years after Absorb BVS implantation. NIH, neointimal hyperplasia. IVUS, intravascular ultrasound.

### Myolimus-eluting Poly-L-Lactic Acid Scaffold: DESolve

DESolve BRS (Elixir Medical; Sunnyvale, California, United States) has a similar PLLA backbone to the Absorb BVS, but it is coated with myolimus (3 µg/mm), an mTOR inhibitor macrocyclic lactone, and a sirolimus analogue. Sufficient radial strength was achieved over 3 months and the bioresorption of the scaffold was observed between 1 year and 2 years. The DESolve-I FIM trial (16 patients) demonstrated that the rate of acute recoil was 6.4%, and in-scaffold LLL was 0.19 mm at 6 months.<sup>58</sup> In IVUS investigation, the respective mean scaffold area and lumen area was 5.35 mm<sup>2</sup> and 5.35 mm<sup>2</sup> postprocedurally, and 5.61 mm<sup>2</sup> and 5.10 mm<sup>2</sup> at 6 months (P=no significant). OCT revealed that 98.7% of the struts were covered at 6 months. All patients were clinically followed up to 1 year, and 3 patients experienced MACE including 1 cardiac death, 1 target vessel MI, and 1 TLR. There were no patients with the evidence of ST. The DESolve Nx trial is currently enrolling 120 patients treated with the next generation DESolve Nx stent with novolimus (5 µg/mm), which is an active metabolite of sirolimus.<sup>59</sup>

### Poly Salicylic Acid Stent: IDEAL

The IDEAL BRS (Xenogenics Corp.; Canton, Massachusetts, United States) has 2 components: the backbone and the drug layer. The backbone of the device is made of polylactide anhydride mixed with a polymer of salicylic acid and sebacic acid linker. The drug layer consists of salicylate that controls the release of the antiproliferative drug sirolimus. The presence of salicylic acid provides the device with anti-inflammatory properties, which have been confirmed in preclinical studies.<sup>60</sup> The IDEAL BRS was tested in a small number of humans (11 patients) in 2008. Although this study has not been fully reported, there was insufficient neointimal suppression and a reduction in lumen area due to inadequate drug dosing and rapid release of the sirolimus.<sup>61</sup> The second generation IDEAL BioStent has a higher drug dose, slower drug-release kinetics, and a smaller system profile. The device is currently undergoing preclinical evaluation.

### Arterial Remodeling Technologies Bioresorbable Scaffold

The ART BRS (Arterial Remodeling Technologies; Noisy le Roi, France) is manufactured from a PLLA amorphous polymer

without an antiproliferative drug. This device is 6 Fr compatible, and provides transient scaffolding for 5 months to 7 months. Full resorption occurs within 18 months. The performance of the ART BRS was compared with the BMS in rabbit and porcine models, and no MACE was reported. The acute recoil was comparable to BMS. Interestingly, angiographic analyses demonstrated the phenomenon of late lumen enlargement, as well as increased external elastic lamina area detected by IVUS at 9 months. Based on the results of preclinical studies, the ARTDIVA FIM trial has already commenced and is recruiting patients at 5 sites in France. It aims to evaluate clinical outcomes at 6 months.<sup>62</sup>

### Xinsorb Bioresorbable Scaffold

The Xinsorb BRS (Huaan Biotechnology; Laiwu, China) is a fully bioresorbable sirolimus-loaded scaffold that consists of PLLA, polylactide-co-glycolide, and poly-L-lactide-co-ε-caprolactone. An experimental study evaluated the feasibility of Xinsorb BRS in comparison with the Excel DES (JW Medical; Shandong, China). Sixteen Xinsorb scaffolds and 16 Excel stents were implanted in the coronary arteries of porcine models.<sup>63</sup> In vitro drug-elution kinetics indicated that 78% of sirolimus was released from Xinsorb BRS within the first 14 days. Histomorphometry demonstrated a significantly lower percentage diameter restenosis in the Xinsorb BRS compared to the Excel DES (18.6% vs 21.4% at 30 days and 24.5% vs 27.7% at 90 days, respectively). In addition, the struts of the Xinsorb BRS were completely covered by neointima at 90 days.<sup>64</sup> Although these preliminary results are encouraging, further extensive preclinical studies are necessary to investigate the safety and efficacy of this device. The company is expecting to organize a FIM trial in the year 2013.

### Other Bioresorbable Scaffolds

The Amaranth PLLA scaffold (Amaranth Medical; Mountain View, California, United States) and the On-ABS (OrbusNeich, Hong Kong, China) are currently under preclinical evaluation. In addition, there are several other devices that are still under development. These include the Sahajanand BRS (Sahajanand Medical Technologies; Surat, India), the Avatar BRS (S3 V; Hyderabad, India), the MeRes BRS (Meril Life Sciences; Vapi, Gujarat, India), and the Zorion BRS (Zorion Medical; Indianapolis, Indiana, United States).

	BA	BMS	DES	VRT
Acute occlusion	-	+	+	+
Acute ST	N/A	-/+	+	+
Subacute ST	N/A	+	+	+
Acute recoil	-	+	+	+
Constrictive remodelling	-	+	+	+
Neointimal hyperplasia	-	-	+	+
Expansive remodelling	+	-	-	+
Late luminal enlargement	+	-	-	+
Late or very late ST	N/A	-	-	+/?

**Figure 7.** Schematic illustration presenting the evolution of percutaneous coronary interventions. BA, balloon angioplasty; BMS, bare metal stents; DES, drug-eluting metallic stents; N/A, not applicable because of the absence of stent; ST, stent thrombosis; VRT, vascular reparative therapy. "+" implies prevented or not restricted, whilst "-" implies not prevented or restricted. Modified with permission from Serruys et al.<sup>67</sup>

## FUTURE PERSPECTIVES

The new enemy in the DES era—ST—has accelerated technological evolution in interventional cardiology. Newer generation DES, with biodegradable polymers, have shown an impressive reduction in VLST, contributing to improved long-term outcomes, as compared to first generation DES. The polymer-free DES or BRS are relatively new technologies, with many trials still in progress. The currently available angiographic, intravascular imaging, and clinical data, suggest acceptable safety and efficacy of these new technologies. However, it remains unclear as to whether biodegradable-polymer DES or polymer-free DES can minimize late ST events, particularly as these late events have also been observed in patients receiving BMS.<sup>65,66</sup> Furthermore, considering the fatal consequences of ST, focus should be maintained on the eradication, rather than the minimization of this serious complication. There is a fundamental difference in concept between the DES and the BRS technologies, with the latter having a capability of liberating the vessel from a permanent metallic cage. Therefore, BRS technology has a theoretical advantage in reducing ST by means of endoluminal prosthesis elimination. BRS also facilitates the restoration of vasomotor function, which indirectly results in the completeness of vessel healing. The entire process of this treatment has been hence named as vascular reparative therapy (Fig. 7).<sup>67</sup>

One possible fate of the stenotic lesion treated with metallic stents is the development of in-stent neointimal tissue (even seen with DES), where the antiproliferative drug slows down or postpones the phenomenon. This neointimal tissue may in turn become atherosclerotic, degenerate to a vulnerable plaque, and finally rupture inside the cage of the stent (ie, neoatherosclerosis).<sup>68,69</sup> A stiff metallic stent can also alter vessel geometry and biomechanics, which may result in long-term flow disturbances and chronic irritation, in addition to the risk of late strut fractures, which potentially contribute to restenosis and adverse clinical events.<sup>70,71</sup> From a physiological perspective, the absence of a rigid metallic cage facilitates the restoration of vasomotor function,

adaptive shear stress, and late luminal enlargement. After bioresorption, there would be no triggers for thrombosis, such as uncovered struts or durable polymers. The absence of foreign materials may also reduce concerns about future treatment options, such as precluding bypass-graft surgery, and the requirements for long-term dual antiplatelet therapy with a potential reduction in associated bleeding complications. Since BRS have only been evaluated in limited patients with noncomplex lesions, the feasibility of these devices in complex lesions requires further clinical evaluation. In addition, future investigations are required to establish if BRS technology is superior to permanent metallic DES.

## CONCLUSIONS

Newer metallic DES technology has proven to decrease the risk of revascularization and ST events. The optimal design, however, of scaffolds, polymers, antiproliferative drugs and their degradation/release kinetics is still under investigation. BRS technology is anticipated not only to eliminate the risk of VLST, but also to contribute to the restoration of physiological function of treated vessels. Although further technical development and clinical evaluation are required before BRS can be accepted as the ultimate device for the treatment of coronary artery disease, this new technology looks promising and could be the next revolution in interventional cardiology.

## CONFLICTS OF INTEREST

None declared.

## REFERENCES

1. Gruntzig AR, Senning A, Siegenthaler WE. Nonoperative dilatation of coronary-artery stenosis: percutaneous transluminal coronary angioplasty. *N Engl J Med.* 1979;301:61–8.

2. Sigwart U, Puel J, Mirkovitch V, Joffre F, Kappenberger L. Intravascular stents to prevent occlusion and restenosis after transluminal angioplasty. *N Engl J Med.* 1987;316:701-6.
3. Sigwart U, Urban P, Golf S, Kaufmann U, Imbert C, Fischer A, et al. Emergency stenting for acute occlusion after coronary balloon angioplasty. *Circulation.* 1988;78(5 Pt 1):1121-7.
4. Serruys PW, De Jaegere P, Kiemeneij F, Macaya C, Rutsch W, Heyndrickx G, et al. A comparison of balloon-expandable-stent implantation with balloon angioplasty in patients with coronary artery disease. Benestent Study Group. *N Engl J Med.* 1994;331:489-95.
5. Hoffmann R, Mintz GS, Dussault GR, Popma JJ, Pichard AD, Satler LF, et al. Patterns and mechanisms of in-stent restenosis: A serial intravascular ultrasound study. *Circulation.* 1996;94:1247-54.
6. Morice MC, Serruys PW, Sousa JE, Fajadet J, Ban Hayashi E, Perin M, et al. A randomized comparison of a sirolimus-eluting stent with a standard stent for coronary revascularization. *N Engl J Med.* 2002;346:1773-80.
7. Stone GW, Ellis SG, Cox DA, Hermiller J, O'Shaughnessy C, Mann JT, et al. A polymer-based, paclitaxel-eluting stent in patients with coronary artery disease. *N Engl J Med.* 2004;350:221-31.
8. Nordmann AJ, Briel M, Bucher HC. Mortality in randomized controlled trials comparing drug-eluting vs. bare metal stents in coronary artery disease: a meta-analysis. *Eur Heart J.* 2006;27:2784-814.
9. Camenzind E, Steg PG, Wijns W. Stent thrombosis late after implantation of first-generation drug-eluting stents: a cause for concern. *Circulation.* 2007;115:1440-55, discussion 55.
10. Joner M, Finn AV, Farb A, Mont EK, Kolodgie FD, Ladich E, et al. Pathology of drug-eluting stents in humans: delayed healing and late thrombotic risk. *J Am Coll Cardiol.* 2006;48:193-202.
11. Virmani R, Guagliumi G, Farb A, Musumeci G, Grieco N, Motta T, et al. Localized hypersensitivity and late coronary thrombosis secondary to a sirolimus-eluting stent: should we be cautious? *Circulation.* 2004;109:701-5.
12. Rasmussen K, Maeng M, Kalltoft A, Thyssen P, Kelbaek H, Tilsted HH, et al. Efficacy and safety of zotarolimus-eluting and sirolimus-eluting coronary stents in routine clinical care (SORT OUT III): a randomised controlled superiority trial. *Lancet.* 2010;375:1090-9.
13. Stone GW, Rizvi A, Newman W, Mastali K, Wang JC, Caputo R, et al. Everolimus-eluting versus paclitaxel-eluting stents in coronary artery disease. *N Engl J Med.* 2010;362:1663-74.
14. Kedhi E, Joesoef KS, McFadden E, Wassing J, Van Mieghem C, Goedhart D, et al. Second-generation everolimus-eluting and paclitaxel-eluting stents in real-life practice (COMPARE): a randomised trial. *Lancet.* 2010;375:201-9.
15. Stefanini GG, Kalesan B, Serruys PW, Heg D, Buszman P, Linke A, et al. Long-term clinical outcomes of biodegradable polymer biolimus-eluting stents versus flexible polymer sirolimus-eluting stents in patients with coronary artery disease (LEADERS): 4 year follow-up of a randomised non-inferiority trial. *Lancet.* 2011;378:1940-8.
16. Finn AV, Nakazawa G, Joner M, Kolodgie FD, Mont EK, Gold HK, et al. Vascular responses to drug eluting stents: importance of delayed healing. *Arterioscler Thromb Vasc Biol.* 2007;27:1500-10.
17. De la Torre Hernandez JM, Windecker S. Trombosis muy tardía con nuevos stents farmacocativos: ¿ha dejado de ser un asunto relevante? *Rev Esp Cardiol.* 2012;65:595-8.
18. Grube E, Sonoda S, Ikeno F, Honda Y, Kar S, Chan C, et al. Six- and twelve-month results from first human experience using everolimus-eluting stents with bioabsorbable polymer. *Circulation.* 2004;109:2168-71.
19. Byrne RA, Kastrati A, Massberg S, Wiecekorek A, Laugwitz KL, Hadamitzky M, et al. Biodegradable polymer versus permanent polymer drug-eluting stents and everolimus- versus sirolimus-eluting stents in patients with coronary artery disease: 3-year outcomes from a randomized clinical trial. *J Am Coll Cardiol.* 2011;58:1325-31.
20. Windecker S, Serruys PW, Wandel S, Buszman P, Trznadel S, Linke A, et al. Biolimus-eluting stent with biodegradable polymer versus sirolimus-eluting stent with durable polymer for coronary revascularisation (LEADERS): a randomised non-inferiority trial. *Lancet.* 2008;372:1163-73.
21. Serruys PW, Buszman P, Linke A, Ischinger T, Antoni D, Klaus V, et al. TCT-44 LEADERS: 5-year follow-up from a prospective, randomized trial of biolimus A9-eluting stents with a biodegradable polymer vs. sirolimus-eluting stents with a durable polymer- final report of the LEADERS study. *J Am Coll Cardiol.* 2012;60:B13-4.
22. Stefanini GG, Byrne RA, Serruys PW, De Waha A, Meier B, Massberg S, et al. Biodegradable polymer drug-eluting stents reduce the risk of stent thrombosis at 4 years in patients undergoing percutaneous coronary intervention: a pooled analysis of individual patient data from the ISAR-TEST 3, ISAR-TEST 4, and LEADERS randomized trials. *Eur Heart J.* 2012;33:1214-22.
23. Meredith IT, Verheye S, Dubois CL, Dens J, Fajadet J, Carrie D, et al. Primary endpoint results of the EVOLVE trial: a randomized evaluation of a novel bioabsorbable polymer-coated, everolimus-eluting coronary stent. *J Am Coll Cardiol.* 2012;59:1362-70.
24. Farooq V, Gogas BD, Serruys PW. Restenosis: delineating the numerous causes of drug-eluting stent restenosis. *Circ Cardiovasc Interv.* 2011;4:195-205.
25. Mehilji J, Byrne RA, Wiecekorek A, Iijima R, Schulz S, Bruskina O, et al. Randomized trial of three rapamycin-eluting stents with different coating strategies for the reduction of coronary restenosis. *Eur Heart J.* 2008;29:1975-82.
26. Byrne RA, Kufner S, Tiroch K, Massberg S, Laugwitz KL, Birkmeier A, et al. Randomised trial of three rapamycin-eluting stents with different coating strategies for the reduction of coronary restenosis: 2-year follow-up results. *Heart.* 2009;95:1489-94.
27. King L, Byrne RA, Mehilji J, Schomig A, Kastrati A, Pache J. Five-year clinical outcomes of a polymer-free sirolimus-eluting stent versus a permanent polymer paclitaxel-eluting stent: final results of the intracoronary stenting and angiographic restenosis-test equivalence between two drug-eluting stents (ISAR-TEST) trial. *Catheter Cardiovasc Interv.* 2013;81:E23-8.
28. Tada N, Virmani R, Grant G, Bartlett L, Black A, Clavijo C, et al. Polymer-free biolimus a9-coated stent demonstrates more sustained intimal inhibition, improved healing, and reduced inflammation compared with a polymer-coated sirolimus-eluting cypher stent in a porcine model. *Circ Cardiovasc Interv.* 2010;3:174-83.
29. Grube E, Mueller R, Schuler G, Hauptmann KE, Schofer J. TCT-46: Comparison of polymer-free BioFreedom stents with durable polymer Taxus Liberté stents: 3-year results from the BioFreedom first-in-man trial. *J Am Coll Cardiol.* 2012;60:B14.
30. Costa Jr JR, Abizaid A, Costa R, Feres F, Tanajura LF, Maldonado G, et al. 1-year results of the hydroxyapatite polymer-free sirolimus-eluting stent in the treatment of single de novo coronary lesions: the VESTASYN C trial. *JACC Cardiovasc Interv.* 2009;2:422-7.
31. Costa Jr JR. VESTASync (MIV Therapeutics) program update. *Transcatheter Cardiovascular Therapeutics.* 2012.
32. Yu M, Xu B, Wu Y, Yan H, Chen J, Qian J, et al. TCT-229: First report of a novel polymer-free dual-drug eluting stent in de novo coronary artery disease: results of the first in man BICARE trial. *J Am Coll Cardiol.* 2011;58(20S1):B62.
33. Massberg S, Byrne RA, Kastrati A, Schulz S, Pache J, Hausleiter J, et al. Polymer-free sirolimus- and probucol-eluting versus new generation zotarolimus-eluting stents in coronary artery disease: the intracoronary stenting and angiographic results: test efficacy of sirolimus- and probucol-eluting versus zotarolimus-eluting stents (ISAR-TEST 5) trial. *Circulation.* 2011;124:624-32.
34. Carrie D, Berland J, Verheye S, Hauptmann KE, Vrolix M, Violini R, et al. A multicenter randomized trial comparing amphilimus with paclitaxel-eluting stents in de novo native coronary artery lesions. *J Am Coll Cardiol.* 2012;59:1371-6.
35. Carrie D. Cre8 program update. *Transcatheter Cardiovascular Therapeutics.* 2012.
36. Aoki J, Serruys PW, Van Beusekom H, Ong AT, McFadden EP, Sianos G, et al. Endothelial progenitor cell capture by stents coated with antibody against CD34: the HEALING-FIM (healthy endothelial accelerated lining inhibits neointimal growth-first in man) registry. *J Am Coll Cardiol.* 2005;45:1574-9.
37. Haude M. REMEDEE COMBO program update. *Transcatheter Cardiovascular Therapeutics.* 2012.
38. Seth A. Nanoparticle based stents FOCUSnp program update. *Transcatheter Cardiovascular Therapeutics.* 2012.
39. Stack RS, Calif RM, Phillips HR, Pryor DB, Quigley PJ, Bauman RP, et al. Interventional cardiac catheterization at Duke Medical Center. *Am J Cardiol.* 1988;62(10 Pt 2):F3-24.
40. Zidar J, Lincoff A, Stack R. Biodegradable stents. In: Topol EJ, editor. *Textbook of interventional cardiology.* 2nd ed. Philadelphia: Saunders; 1994. p. 787-802.
41. Waksman R. The disappearing stent: when plastic replaces metal. *Circulation.* 2012;125:2291-4.
42. Van der Giessen WJ, Lincoff AM, Schwartz RS, Van Beusekom HM, Serruys PW, Holmes Jr DR, et al. Marked inflammatory sequelae to implantation of biodegradable and nonbiodegradable polymers in porcine coronary arteries. *Circulation.* 1996;94:1690-7.
43. Tamai H, Igaki K, Kyo E, Kosuga K, Kawashima A, Matsui S, et al. Initial and 6-month results of biodegradable poly-L-lactic acid coronary stents in humans. *Circulation.* 2000;102:399-404.
44. Onuma Y, Garg S, Okamura T, Lighthart J, Van Geuns RJ, De Feyter PJ, et al. Ten-year follow-up of the IGAKI-TAMAI stent. A posthumous tribute to the scientific work of Dr. Hideo Tamai EuroIntervention. 2009;5 Suppl. F:F109-11.
45. Heublein B, Rohde R, Kaese V, Niemeier M, Hartung W, Haverich A. Biocorrosion of magnesium alloys: a new principle in cardiovascular implant technology? *Heart.* 2003;89:651-6.
46. Waksman R, Pakala R, Kuchulakanti PK, Baffour R, Hellings D, Seabron R, et al. Safety and efficacy of bioabsorbable magnesium alloy stents in porcine coronary arteries. *Catheter Cardiovasc Interv.* 2006;68:607-17, discussion 18-9.
47. Erbel R, Di Mario C, Bartunek J, Bonnier J, De Bruyne B, Eberli FR, et al. Temporary scaffolding of coronary arteries with bioabsorbable magnesium stents: a prospective, non-randomised multicentre trial. *Lancet.* 2007;369:1869-75.
48. Ghimire G, Spiro J, Kharbanda R, Roughton M, Barlis P, Mason M, et al. Initial evidence for the return of coronary vasoactivity following the absorption of bioabsorbable magnesium alloy coronary stents. *EuroIntervention.* 2009;4:481-4.
49. Haude M, Erbel R, Erne P, Verheye S, Degen H, Böse D, et al. Safety and performance of the drug-eluting absorbable metal scaffold (DREAMS) in patients with de-novo coronary lesions: 12 month results of the prospective, multicentre, first-in-man BIOSOLVE-1 trial. *Lancet.* 2013;12:61765-6. <http://dx.doi.org/10.1016/S0140-6736>.
50. Ormiston JA, Serruys PW, Regar E, Dudek D, Thuesen L, Webster MW, et al. A bioabsorbable everolimus-eluting coronary stent system for patients with single de-novo coronary artery lesions (ABSORB): a prospective open-label trial. *Lancet.* 2008;371:899-907.

51. Serruys PW, Ormiston JA, Onuma Y, Regar E, Gonzalo N, Garcia-Garcia HM, et al. A bioabsorbable everolimus-eluting coronary stent system (ABSORB): 2-year outcomes and results from multiple imaging methods. *Lancet*. 2009;373:897–910.
52. Onuma Y, Nieman K, Webster M, Thuesen L, Dudek D, Ormiston JA, et al. TCT-37: Five-year clinical outcomes and non-invasive angiographic imaging results with functional assessment after bioresorbable everolimus-eluting scaffold implantation in patients with de novo coronary artery disease. *J Am Coll Cardiol*. 2012;60:B11.
53. Tanimoto S, Bruining N, Van Domburg RT, Rotger D, Radeva P, Ligthart JM, et al. Late stent recoil of the bioabsorbable everolimus-eluting coronary stent and its relationship with plaque morphology. *J Am Coll Cardiol*. 2008;52:1616–20.
54. Serruys PW, Onuma Y, Dudek D, Smits PC, Koolen J, Chevalier B, et al. Evaluation of the second generation of a bioresorbable everolimus-eluting vascular scaffold for the treatment of de novo coronary artery stenosis: 12-month clinical and imaging outcomes. *J Am Coll Cardiol*. 2011;58:1578–88.
55. Ormiston JA, Serruys PW, Onuma Y, Van Geuns RJ, De Bruyne B, Dudek D, et al. First serial assessment at 6 months and 2 years of the second generation of absorb everolimus-eluting bioresorbable vascular scaffold: a multi-imaging modality study. *Circ Cardiovasc Interv*. 2012;5:620–32.
56. Grube E. Bioabsorbable stent. The Boston Scientific and REVA technology. *EuroPCR*. 2009. Barcelona; 2009.
57. Costa RA. REVA ReZolve clinical program update. *Transcatheter Cardiovascular Therapeutics*. 2012.
58. Yan J, Bhat VD. Elixir Medical's bioresorbable drug eluting stent (BDES) programme: an overview. *EuroIntervention*. 2009;5 Suppl. F:80–2.
59. Verheyne S. First-in-man results with a myolimus-eluting bioresorbable PLLA-based vascular scaffold. *Transcatheter Cardiovascular Therapeutics*. 2012.
60. Jabara R, Chronos N, Robinson K. Novel bioabsorbable salicylate-based polymer as a drug-eluting stent coating. *Catheter Cardiovasc Interv*. 2008;72:186–94.
61. Jabara R, Chronos N, Robinson K. Novel fully bioabsorbable salicylate-based sirolimus-eluting stent. *EuroIntervention*. 2009;5 Suppl. F:F58–64.
62. Fajadet J. The AKI stent: design and early first-in-man experiences. *Transcatheter Cardiovascular Therapeutics*. 2012.
63. Shen L, Wang Q, Wu Y, Xie J, Zhang F, Ge L, et al. Preliminary evaluation of fully bioabsorbable PLLA sirolimus eluting stents in a porcine model. *Chin J Intervent Cardiol*. 2009;19:301–5.
64. Shen L, Wang Q, Wu Y, Xie J, Ge J. Short-term effects of sirolimus eluting fully bioabsorbable polymeric coronary stents in a porcine model. *Transcatheter Cardiovascular Therapeutics*. 2011.
65. Daemen J, Wenaweser P, Tsuchida K, Abrecht L, Vaina S, Morger C, et al. Early and late coronary stent thrombosis of sirolimus-eluting and paclitaxel-eluting stents in routine clinical practice: data from a large two-institutional cohort study. *Lancet*. 2007;369:667–78.
66. Stettler C, Wandel S, Allemann S, Kastrati A, Morice MC, Schomig A, et al. Outcomes associated with drug-eluting and bare-metal stents: a collaborative network meta-analysis. *Lancet*. 2007;370:937–48.
67. Serruys PW, Garcia-Garcia HM, Onuma Y. From metallic cages to transient bioresorbable scaffolds: change in paradigm of coronary revascularization in the upcoming decade? *Eur Heart J*. 2012;33:16–25.
68. Ramcharitar S, Garcia-Garcia HM, Nakazawa G, Kukreja N, Ligthart J, Virmani R, et al. Ultrasonic and pathological evidence of a neo-intimal plaque rupture in patients with bare metal stents. *EuroIntervention*. 2007;3:290–1.
69. Nakazawa G, Otsuka F, Nakano M, Vorupahi M, Yazdani SK, Ladic E, et al. The pathology of neointimal hyperplasia in human coronary implants bare-metal and drug-eluting stents. *J Am Coll Cardiol*. 2011;57:1314–22.
70. Wentzel JJ, Whelan DM, Van der Giessen WJ, Van Beusekom HM, Andharyswara I, Serruys PW, et al. Coronary stent implantation changes 3-D vessel geometry and 3-D shear stress distribution. *J Biomech*. 2000;33:1287–95.
71. Wentzel JJ, Gijzen FJ, Schuurbiens JC, Van der Steen AF, Serruys PW. The influence of shear stress on in-stent restenosis and thrombosis. *EuroIntervention*. 2008;4 Suppl. C:C27–32.

## 1.2 Igaki-Tamai stent

Long-term (>10 years) clinical outcomes of first-in-man biodegradable poly-l-lactic acid coronary stents: Igaki-Tamai stents.

*Circulation*. 2012;125:2343-53.

[Original research paper, Impact Factor (2012): 15.202]

Nishio S, Kosuga K, Igaki K, Okada M, Kyo E, Tsuji T, Takeuchi E, Inuzuka Y, Takeda S, Hata T, Takeuchi Y, Kawada Y, Harita T, Seki J, Akamatsu S, Hasegawa S, Bruining N, Brugaletta S, de Winter S, Muramatsu T, Onuma Y, Serruys PW, Ikeguchi S.





# Long-Term (>10 Years) Clinical Outcomes of First-in-Human Biodegradable Poly-L-Lactic Acid Coronary Stents Igaki-Tamai Stents

Soji Nishio, MD; Kunihiko Kosuga, MD, PhD, FJCC; Keiji Igaki, PhD; Masaharu Okada, MD, PhD; Eisho Kyo, MD; Takafumi Tsuji, MD; Eiji Takeuchi, MD, PhD; Yasutaka Inuzuka, MD, PhD; Shinsaku Takeda, MD; Tatsuhiko Hata, MD, PhD; Yuzo Takeuchi, MD, PhD; Yoshitaka Kawada, MD; Takeshi Harita, MD; Junya Seki, MD; Shunji Akamatsu, ME; Shinichi Hasegawa, ME; Nico Bruining, PhD; Salvatore Brugaletta, MD; Sebastiaan de Winter, BSc; Takashi Muramatsu, MD; Yoshinobu Onuma, MD; Patrick W. Serruys, MD, PhD; Shigeru Ikeguchi, MD, PhD

**Background**—The purpose of this study was to evaluate the long-term safety of the Igaki-Tamai stent, the first-in-human fully biodegradable coronary stent made of poly-L-lactic acid.

**Methods and Results**—Between September 1998 and April 2000, 50 patients with 63 lesions were treated electively with 84 Igaki-Tamai stents. Overall clinical follow-up (>10 years) of major adverse cardiac events and rates of scaffold thrombosis was analyzed together with the results of angiography and intravascular ultrasound. Major adverse cardiac events included all-cause death, nonfatal myocardial infarction, and target lesion revascularization/target vessel revascularization. During the overall clinical follow-up period ( $121 \pm 17$  months), 2 patients were lost to follow-up. There were 1 cardiac death, 6 noncardiac deaths, and 4 myocardial infarctions. Survival rates free of all-cause death, cardiac death, and major adverse cardiac events at 10 years were 87%, 98%, and 50%, respectively. The cumulative rates of target lesion revascularization (target vessel revascularization) were 16% (16%) at 1 year, 18% (22%) at 5 years, and 28% (38%) at 10 years. Two definite scaffold thromboses (1 subacute, 1 very late) were recorded. The latter case was related to a sirolimus-eluting stent, which was implanted for a lesion proximal to an Igaki-Tamai stent. From the analysis of intravascular ultrasound data, the stent struts mostly disappeared within 3 years. The external elastic membrane area and stent area did not change.

**Conclusion**—Acceptable major adverse cardiac events and scaffold thrombosis rates without stent recoil and vessel remodeling suggested the long-term safety of the Igaki-Tamai stent. (*Circulation*. 2012;125:2343-2352.)

**Key Words:** angioplasty ■ coronary artery disease ■ polymers ■ prognosis ■ stents

In the 1990s, the biocompatibility of poly-L-lactic acid (PLLA) was controversial. Zidar et al<sup>1</sup> reported a minimal inflammatory reaction and minimal neointimal hyperplasia with the use of PLLA stents in canine femoral arteries. On the other hand, Van der Giessen et al<sup>2</sup> reported a marked inflammatory response after the implantation of 5 different polymer stents, including lactic acid, in a porcine coronary model. Finally, a decade ago, the concept of a biodegradable stent came to fruition as the first biodegradable stents were used in the clinical setting. Dr Keiji Igaki, an engineer, and Dr Hideo Tamai, an interventional cardiologist who passed away on February 10, 2009, invented the first-in-human fully biode-

gradable stent (Igaki-Tamai stent) made of PLLA.<sup>3</sup> At that time, 50 patients were treated with Igaki-Tamai stents in Japan, and 15 patients were treated with these stents outside of Japan (Italy, Netherlands, Germany, and Korea).

### Editorial see p 2291 Clinical Perspective on p 2352

Despite the promising initial and 6-month results,<sup>3</sup> the arrival of drug-eluting stents diverted attention from biodegradable stents. Drug-eluting stents significantly reduced in-stent restenosis rates and target lesion revascularization (TLR) rates compared with bare metal stents.<sup>4</sup> However,

Received October 11, 2010; accepted March 2, 2012.

From the Department of Cardiology, Shiga Medical Center for Adults, Shiga, Japan (S.N., K.K., M.O., Y.I., S.T., T.H., Y.T., Y.K., T.H., J.S., S.A., S.H., S.I.); Kyoto Medical Planning Co, Ltd, Kyoto, Japan (K.I.); Kusatsu Heart Center, Shiga, Japan (E.K., T.T.); Department of Pathology, Shiga Medical Center for Adults, Shiga, Japan (E.T.); and Thoraxcenter, Erasmus Medical Center, Rotterdam, the Netherlands (N.B., S.B., S.d.W., T.M., Y.O., P.W.S.).

Correspondence to Kunihiko Kosuga, MD, PhD, FJCC, Department of Cardiology, Shiga Medical Center for Adults, 5-4-30, Moriyama, Moriyama City, Shiga, 524-8524 Japan. E-mail JCH02462@nifty.com

© 2012 American Heart Association, Inc.

*Circulation* is available at <http://circ.ahajournals.org>

DOI: 10.1161/CIRCULATIONAHA.110.000901

safety issues with drug-eluting stents, especially very late stent thrombosis (VLST), have become an increasingly reported problem,<sup>2-7</sup> and recently, increasing attention has been paid to fully biodegradable coronary stents. So far, initial and midterm results are available for 2 biodegradable stents: the bioabsorbable magnesium (AMS) stent (BIOTRONIK, Berlin, Germany),<sup>8</sup> and the bioresorbable everolimus-eluting PLLA (BVS) scaffold (Abbott Vascular, Santa Clara, CA).<sup>9,10</sup> Moreover, the Igaki-Tamai stent, sold under the trade name REMEDY, is now clinically available for peripheral artery disease in Europe. However, further work is required to determine the long-term safety of these stents. Before putting the biodegradable drug-eluting PLLA stent into routine clinical practice, we need to confirm that PLLA does not cause any critical adverse events during the whole process of biodegradation. The purpose of this study was to assess the long-term safety of Igaki-Tamai stents in human coronary arteries.

## Methods

### Study Design and Study Cohort

We undertook a single-arm, single-center, observational prospective study that enrolled 50 patients treated with 84 Igaki-Tamai stents. The patients were eligible if they had stable ischemic heart disease with a lesion that could be treated by implantation of the Igaki-Tamai stent. The study was approved by the hospital ethics committee of Shiga Medical Center for Adults. Written informed consent was obtained from all patients (according to the Helsinki Declaration). The indications for stent implantation were the prevention of restenosis in a de novo lesion, restenosis of a major coronary artery after plain balloon angioplasty, and suboptimal results after plain balloon angioplasty. All patients were selected electively. Exclusion criteria were acute coronary syndrome, lesions located in the left main trunk, and chronic total occlusion. In this study, we followed up this cohort for >10 years to assess the long-term safety of Igaki-Tamai stents.

### Igaki-Tamai Stent

The Igaki-Tamai stent (Kyoto Medical Planning Co, Ltd, Kyoto, Japan) is the first fully biodegradable stent implanted in human coronary arteries (Figure 1). The properties of the stent have been described previously.<sup>3</sup> Briefly, the stent is composed of a non-drug-eluting, high-molecular-weight PLLA monofilament (183 kDa) with a zigzag helical coil design. PLLA is a biodegradable, thermoplastic, aliphatic polyester that is degraded to lactic acid and finally metabolized to carbon dioxide and water. The stent strut thickness is 0.17 mm (0.007 in); its diameter is 3.0, 3.5, and 4.0 mm; and its length is 12 mm. The stent structures are not radiopaque, and each end of the stent has implanted radiopaque gold markers.

The stent was deployed with a balloon-expandable 5F covered sheath system through an 8F guiding catheter. The balloon inflation was performed through heated contrasts of 80° with 30-second inflation at 6 to 14 atm. The stent has a self-expanding capability, and dilatation continues until equilibrium is attained between the circumferential elastic resistance of the arterial wall and the dilating force of the PLLA stent.

### Procedures

All patients received 10 000 U intravenous heparin at the beginning of the procedure. Before stents were implanted, the lesions were dilated by an optimally sized balloon or debulked by directional atherectomy or rotational atherectomy if needed. The stent size was decided by intravascular ultrasound (IVUS) studies, and multiple stentings were performed, depending on lesion length, to cover the entire lesion. The stent was deployed by balloon inflation. Postdilatation was performed if needed. All patients were required to receive

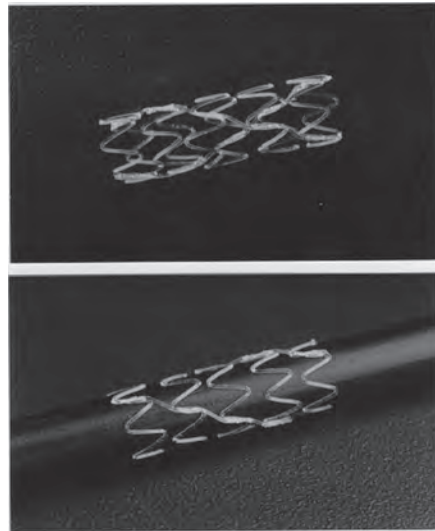


Figure 1. The Igaki-Tamai stent.

aspirin (81 mg/d) for at least 6 months and ticlopidine (200 mg/d) for 1 month, which is the usual dose in Japan.

### In-Hospital Results and Clinical Follow-Up

The baseline characteristics of patients and lesions and in-hospital outcomes were obtained by a review of the medical records, procedural reports, and coronary angiograms. Clinical follow-up data were obtained by either telephone interviews or reviews of medical records. The occurrence of major adverse cardiac events (MACEs) and definite/probable scaffold thrombosis was recorded. MACEs included cardiac death, noncardiac death, nonfatal myocardial infarction (MI), TLR, and target vessel revascularization (TVR).

Cardiac death included any death with a cardiac cause (eg, MI, congestive heart failure, low-output failure, fatal arrhythmia), un witnessed death, and death of unknown cause. Noncardiac death included any death not covered by cardiac death. MI was defined as the presence of at least two of the following: ischemic symptoms, elevation in cardiac enzymes (creatine kinase and its MB isoenzyme) at least twice their upper normal limits, and new ECG changes compatible with MI. MI was classified as lesion-related MI and non-lesion-related MI by ECG and coronary angiography. Scaffold thrombosis (definite, probable, and possible) was defined according to Academic Research Consortium criteria.<sup>11</sup> Even if the implanted PLLA stent was considered completely biodegraded and thrombus was observed in the scaffolded lesion, it was considered scaffold thrombosis. TLR was defined as any repeat percutaneous coronary intervention of the target lesion or bypass graft surgery for restenosis or other complications. The target lesion was defined as the treated segment from 5 mm proximal to the stent to 5 mm distal to the stent. TVR was defined as any repeat percutaneous coronary intervention or coronary artery bypass graft surgery of the target vessel.

### Quantitative Coronary Angiography and IVUS Analyses

Scheduled follow-up coronary angiography and IVUS were performed before, immediately after, 1 day after, and 6 months after the procedures. At the beginning of this study, we thought that the PLLA stent would have disappeared within 6 months. However, the PLLA

stent did not disappear at 6 months of follow-up, and we recommended that all patients undergo angiography at 1 and/or 2 years of follow-up. After 2 years of follow-up, additional angiography and IVUS were performed on the basis of clinical indications as determined by the attending physicians.

Quantitative coronary angiography was analyzed with the Cardiovascular Measurement System (Medis Medical Imaging Systems, Leiden, the Netherlands). The procedure was considered successful if residual stenosis <50% with Thrombolysis in Myocardial Infarction grade 3 flow was achieved. Late loss was defined as the difference between minimal lumen diameter (MLD) after the procedure and at follow-up.

The IVUS system (CVIS, Boston Scientific Corp, Natick, MA) was used with an automated pullback at 0.5 mm/s. The image processing was performed by the echoPlaque software (INDEC Medical Systems, Santa Clara, CA). The external elastic membrane (EEM) area, the stent area, the minimal lumen area (MLA), and the projected MLD were measured. The EEM area and the stent area were measured every 1 mm, and the results were averaged. To assess the interobserver agreement, all IVUS images were measured by 2 observers, and the correlation coefficient for measurements between the 2 observers was 0.988 ( $P<0.001$ ). To assess the intraobserver variability, 20 randomly selected IVUS images were remeasured, and the correlation coefficient for repeated measurements was 0.970 ( $P<0.001$ ).

### IVUS Echogenicity Analysis

Before quantitative IVUS echogenicity analysis was performed, the IVUS data were retrospectively ECG gated by the previously validated Intelligate method.<sup>12-15</sup> Of note, a low frame rate does not allow accurate detection of near end-diastolic frames and cannot be processed by the Intelligate algorithm. Therefore, IVUS data acquired with a 30-MHz catheter and attached to a Clearview console were retrospectively corrected before further analyses. The postprocedural and follow-up IVUS images were analyzed side by side through a comparison of the matched segments, as previously described.<sup>16</sup> The lumen, scaffold, and EEM contours were detected with the CURAD Vessel Analysis software (Curad BV, Wijk bij Duurstede, the Netherlands),<sup>17</sup> and these contours were subsequently used to perform the echogenicity analysis.

Fully automated quantitative echogenicity analysis software, previously developed in house and validated, was used to quantify the hyperechogenicity changes in the scaffolded segment, as previously shown in the ABSORB trials.<sup>18,19</sup> In brief, the mean gray value of the adventitia was used to classify tissue components as either hypoechoic or hyperechoic. The adventitia was defined as a layer extending from 0.2 to 0.5 mm outside the EEM. To avoid artifacts, tissue within acoustic shadowed areas was excluded and very high gray-level pixels were identified as upper tissue.<sup>19</sup> After the tissue identification process, the relative fraction of hypoechoic versus hyperechoic tissue volumes was calculated for the entire scaffolded segment. At the various follow-up time points, the echogenicity was calculated between the stent and the EEM contours as previously described.<sup>18</sup> The software calculated the echogenicity as a volume and percentage for each scaffolded segment (setting hypoechoicity and hyperechoicity to 100%).

### Statistical Analysis

Continuous variables were expressed as mean $\pm$ SD. Paired comparisons of serial observations over time in the same lesions were performed by a Wilcoxon signed-rank test. Values of  $P<0.05$  were considered significant. The time (days) to a MACE was calculated from the procedure date (if there were multiple procedure dates, the first was used). Kaplan-Meier life-table analysis was used to estimate cumulative event-free survival.

## Results

### Baseline Characteristics of Patients and Lesions

Between September 1998 and April 2000, 50 patients with 63 lesions were treated electively with 84 biodegradable Igaki-

**Table 1. Baseline Patient Characteristics (n=50)**

Male, n (%)	44 (88)
Age, y	61 $\pm$ 11
>65 y, n (%)	19 (38)
Diabetes mellitus, n (%)	20 (40)
Hypertension, n (%)	36 (72)
Hypercholesterolemia, n (%)	21 (42)
History of smoking, n (%)	29 (58)
History of MI, n (%)	18 (36)
Prior PCI, n (%)	19 (38)
Prior CABG, n (%)	1 (2)
CCS class 3 or 4, n (%)	19 (38)
No. of diseased vessels, n (%)	
1	19 (38)
2	25 (50)
3	6 (12)
No. of lesions treated with Igaki-Tamai stents, n (%)	
1	41 (84)
2	5 (8)
3	4 (8)

MI indicates myocardial infarction; PCI, percutaneous coronary intervention; CABG, coronary artery bypass grafting; and CCS, Canadian Cardiovascular Society.

Tamai stents during 57 procedures at our institution. Baseline patient clinical characteristics are shown in Table 1. Subjects included 44 men and 6 women with a mean age of 61 $\pm$ 11 years. Lesion characteristics are shown in Table 2. All target lesions were American Heart Association/American College of Cardiology type B or C. Debulking before stenting was performed in 16 procedures (2 rotational atherectomy and 14 directional atherectomy). All stents were successfully delivered, and angiographic success was achieved in all procedures.

### In-Hospital Outcomes

There were no in-hospital MACEs except for 1 case of subacute scaffold thrombosis. This occurred in a patient who was taken off antiplatelet therapy secondary to an acute hemorrhagic gastric ulcer. Neither ticlopidine nor heparin was administered after gastric bleeding, and subacute scaffold thrombosis occurred on postoperative day 5. Although percutaneous coronary intervention was immediately performed, this patient suffered a nonfatal lesion-related MI.

### Long-Term Clinical Outcomes

The mean clinical follow-up period was 121 $\pm$ 17 months (maximum, 136 months), and the clinical follow-up rate was 100% at 4 years, 98% at 7 years, and 96% at 10 years. One patient was lost to follow-up at 4 years and 1 at 7 years. Kaplan-Meier event-free analysis of all-cause death, cardiac death, and MACEs is shown in Figure 2. At the 10-year follow-up, 87% (95% confidence interval [CI], 77-97) of patients were free from all-cause death. Moreover, 98% (95% CI, 94-100) of patients were free from cardiac death, and 50% (95% CI, 36-64) of patients were free from MACEs.

**Table 2. Lesion Characteristics**

	Single Stenting	Multiple Stenting	Total
Lesions, n	45	18	63
De novo	42	17	59
Restenosis after POBA	3	1	4
Lesion length, mm	11.7±3.6	18.1±7.3	13.5±5.7
Reference diameter, mm	2.99±0.45	2.84±0.46	2.95±0.46
Target lesion, n (%)			
LAD	20	8	28 (45)
LCx	12	7	19 (30)
RCA	13	3	16 (25)
AHA/ACC classification, n (%)			
Type A	0	0	0
Type B1	16	0	16 (25)
Type B2	34	2	36 (57)
Type C	2	9	11 (18)
Debulking before stenting, n (%)			
Rotablater	1	1	2 (3)
DCA	10	4	14 (22)
Stents, n	45	39	84
3.0 mm	4	6	10 (12)
3.5 mm	26	26	52 (62)
4.0 mm	15	7	22 (26)

POBA indicates plain old balloon angioplasty; LAD, left anterior descending coronary artery; LCx, left circumflex coronary artery; RCA, right coronary artery; AHA/ACC, American Heart Association/American College of Cardiology; and DCA, directional coronary atherectomy.

All MACEs that occurred during the follow-up period are shown in Table 3.

One patient died of unknown causes at 57 months, and 6 other deaths were due to noncardiac causes. One lesion-related MI and 2 non-lesion-related MIs were recorded.

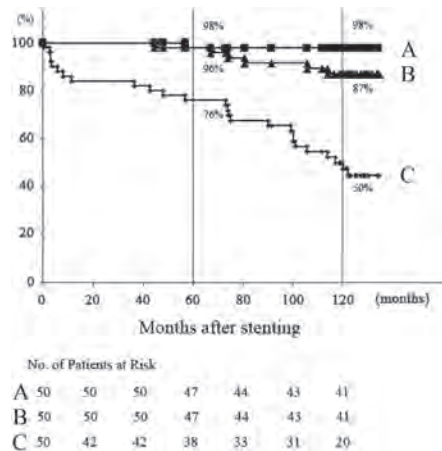


**Figure 2.** Kaplan-Meier curves showing survival rates free of (A) cardiac death, (B) death, and (C) major cardiac adverse events.

**Table 3. Cumulative Rates of Major Adverse Cardiac Events During the 10-Year Follow-Up (n=50)**

	In-Hospital, n (%)	Long-Term, n (%)	Total, n (%)
Cardiac deaths	0	1 (2)	1 (2)
Noncardiac death	0	6 (12)	6 (12)
Stroke	...	2 (4)	2 (4)
Lung cancer	...	2 (4)	2 (4)
Pneumonia	...	1 (2)	1 (2)
COPD	...	1 (2)	1 (2)
Nonfatal MI			
Lesion-related MI	1 (2)	1 (2)	2 (4)
Non-lesion-related MI	0	2 (4)	2 (4)
Scaffold thrombosis (definite/probable)			
Acute	1 (2)	0	1 (2)
Subacute	0	0	0
Late	0	0	0
Very late	0	1 (2)	1 (2)
TLR			
PCI	1 (2)	13 (26)	14 (28)
CABG	0	0	0
TVR			
PCI	1 (2)	20 (40)	21 (42)
CABG	0	0	0

COPD indicates chronic obstructive pulmonary disease; MI, myocardial infarction; TLR, target lesion revascularization; PCI, percutaneous coronary intervention; CABG, coronary artery bypass grafting; and TVR, target vessel revascularization.

The 10-year cumulative TLR and TVR rates are shown in Figure 3. The cumulative rates of TLR per patient were 16% (95% CI, 6–26) at both 1 and 3 years, 18% (95% CI, 7–29) at 5 years, and 28% (95% CI, 15–40) at 10 years. The cumulative rates of TVR per patient were 16% (95% CI, 6–26) at both 1 and 3 years, 22% (95% CI, 11–33) at 5 years, and 38% (95% CI, 24–52) at 10 years. There were 14 TLRs within 10 years, and the TLR rate was 33% (6 of 18) for lesions treated with multiple stenting and 18% (8 of 45) for lesions treated with single stenting.

According to Academic Research Consortium criteria, 1 case of definite very late scaffold thrombosis was recorded

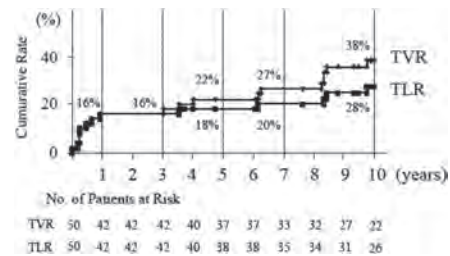


**Figure 3.** Cumulative rates of target lesion revascularization (TLR) and target vessel revascularization (TVR) per patient.

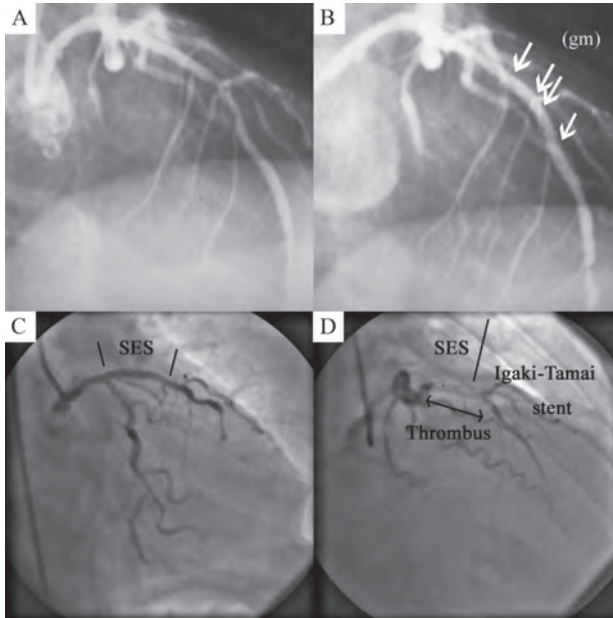


**Figure 4.** Coronary angiogram of a patient with definite scaffold thrombosis at 10 years. **A**, The index lesion. **B**, Two Igaki-Tamai stents were implanted in the left anterior descending artery (November 1999). Gold markers (gm) are shown. **C**, A sirolimus-eluting stent (SES) was implanted in a new lesion just proximal to the lesion where the Igaki-Tamai stents had been implanted (September 2006). **D**, Very late scaffold thrombosis of the left anterior descending artery (December 2009). The stent struts of the Igaki-Tamai stents were not detected by intravascular ultrasound.

during the 10-year follow up period, which occurred in the same patient who had the previously mentioned lesion-related MI. This very late scaffold thrombosis occurred 10 years after implantation of Igaki-Tamai stents, but the patient also had a sirolimus-eluting stent (SES) implanted. Two Igaki-Tamai stents were implanted in the left anterior descending coronary artery in 1999. However, an SES was implanted in a new lesion just proximal to the Igaki-Tamai stents in 2006. In 2009, the patient was admitted to the hospital with acute coronary syndrome. The coronary angiogram of this case is shown in Figure 4. It demonstrated a massive thrombus in the SES and a small amount of thrombus in the proximal portion of the lesion where the Igaki-Tamai stents had been implanted (ie, the thrombus was distributed mainly within the SES). After thrombus aspiration, IVUS images showed that the Igaki-Tamai stent struts had disappeared. Residual thrombus was observed in the SES, and additional balloon angioplasty was needed for this lesion. On the other hand, residual thrombus was not observed in the lesion where the Igaki-Tamai stent had been implanted, and additional balloon angioplasty was not needed for this lesion.

#### Antiplatelet Therapy

Although the scheduled duration of dual antiplatelet therapy (DAPT) was 1 month, the actual duration of DAPT was selected by the attending physicians. Of 50 patients, data were obtained in 48 patients on the prescription of DAPT in the first 3 years after PLLA implantation. The duration of DAPT was 1 month in 18 patients (36%), 2 to 3 months in 15

patients (30%), 4 to 12 months in 10 patients (20%), and 13 to 36 months in 5 patients (10%). Within 3 years after PLLA implantation, DAPT was restarted in 4 patients because of implantation of additional metallic stents or cerebral infarction.

#### Angiographic Results

Angiographic follow-up was performed 95% of the lesions at 6 months, 89% of the lesions at 1 year, 43% of the lesions at 5 years, and 20% of the lesions at 10 years. Changes in MLD and percent diameter stenosis of all available lesions except post-TLR lesions determined by quantitative coronary angiography are shown in Table 4. In this unpaired comparison, the mean MLD decreased to  $1.76 \pm 0.74$  mm at 6 months, with improvement at 3 years. Serial changes in the MLD and percent diameter stenosis of 18 lesions without TLRs are also shown in Figure 5A. In these 18 lesions, angiography and IVUS were performed during the first 3 years. In this paired comparison, the mean MLD decreased to  $2.08 \pm 0.63$  mm at 6 months. After this time point, MLD improvement was observed, but the changes were not statistically significant ( $P=0.12$ , 6 months versus 3 years).

#### IVUS Analysis

Quantitative IVUS analysis of all available lesions except post-TLR lesions is shown in Table 5. In this unpaired comparison, the MLA decreased to  $3.64 \pm 1.68$  mm<sup>2</sup> at 6 months. However, after this time point, MLA improvement was observed. Serial changes in the cross-sectional areas of

**Table 4. Quantitative Coronary Angiographic Analysis of All Available Lesions Except Post-Target Lesion Revascularization Lesions (Unpaired)**

	RVD, mm	MLD, mm	%DS	Late Loss, mm
Before the procedure (n=63 lesions)	2.95±0.46	0.91±0.39	69±13	...
After the procedure (n=63 lesions)	3.04±0.44	2.68±0.43	12±8	...
At 1 d (n=63 lesions)	3.09±0.48	2.70±0.46	12±10	...
At 6 mo (n=60 lesions)	2.80±0.45	1.76±0.74	38±22	0.91±0.69
At 1 y (n=46 lesions)	2.82±0.46	2.01±0.54	29±13	0.67±0.45
At 2 y (n=38 lesions)	2.81±0.49	2.08±0.47	26±12	0.61±0.43
At 3 y (n=25 lesions)	3.02±0.49	2.22±0.56	25±18	0.59±0.50

RVD indicates reference vessel diameter; MLD, minimal lumen diameter; and %DS, percent diameter stenosis.

18 lesions without TLRs are also shown in Figure 5B. In this paired comparison, the MLA decreased to  $4.23 \pm 1.82 \text{ mm}^2$  at 6 months. After this time point, MLA improvement was observed ( $P=0.028$ , 6 months versus 3 years). The changes in the EEM and stent areas did not become significant until 3 years.

Serial IVUS findings of a representative case are shown in Figure 6A. Between poststenting and the 6-month follow-up, there were almost no changes in the number of stent struts. However, at 12 and 24 months, the number of the struts was decreased; finally, at 36 months, most of the struts had

visually disappeared. After 36 months, we had the chance to see the IVUS images in a small number of patients (4 lesions at 42 months, 2 lesions at 48 months, and 3 lesions at 54 months). The stent struts of the Igaki-Tamai stent had also visually disappeared.

**IVUS Echogenicity Analysis**

The complete serial IVUS data (before, after, and at 6 months, 1 year, 2 years, and 3 years) on 13 lesions treated with a single stent and without TLR were analyzed for the echogenicity analysis. There was a significant increase in hyperechogenicity of the scaffolded segment after stent implantation ( $P=0.018$ ). A significant reduction in hyperechogenicity was detected beginning at 12 months, with a value of hyperechogenicity at 36 months comparable to the pre-stent implantation values (Figure 6B).

**Histological Analysis**

The stent strut was histologically examined in 1 case during the follow-up period. After 42 months of follow-up, directional atherectomy was performed to excise a lesion that was previously stented (Figure 7). Piecemeal fragments of artery wall were obtained. These specimens demonstrated intimal thickening composed of completed fibrosis with scant fibroblasts with few inflammatory cells. They also disclosed the remnants of polymeric struts. Around the remnants of polymeric struts, there was almost no inflammatory cell infiltration or foreign body reaction. Thrombus also was not observed. Alcian blue staining and periodic acid–Schiff staining are shown in Figure 7. The space previously occupied by PLLA was stained by Alcian blue.

**Discussion**

The motivation for developing biodegradable stents has been to overcome the limitations of metallic stents. Metallic stents have a potential risk of stent thrombosis, can be an obstacle to surgical revascularization, and can be an impairment to noninvasive imaging such as multislice computed tomography. The development of stent malapposition in cases of plaque shrinkage/positive vessel remodeling can also occur. Currently, drug-eluting stents are the treatment of choice for coronary artery stenosis; however, VLST has become an important safety issue. Several mechanisms of VLST have been proposed, including delayed endothelialization, chronic inflammation of arteries, hypersensitivity reactions (eosinophilic infiltration),<sup>20</sup> and incomplete stent apposition with vessel remodeling.<sup>21</sup> All of these problems with metallic stents can be solved with the use of fully biodegradable stents because there are no foreign materials after PLLA degradation. Therefore, many cardiologists and engineers have recently focused their attentions on the development of a fully biodegradable stent.

In our study, there was a high survival rate free of cardiac death (98% at 10 years), demonstrating the long-term safety of this stent. During the 10 years of follow-up, only 1 cardiac death was recorded at 57 months. Although many noncardiac death cases were reported in this study, they have no relation to the Igaki-Tamai stents.

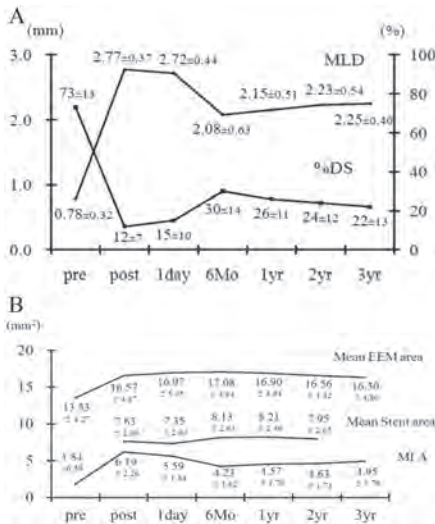


**Figure 5. A.** Serial changes in minimal lumen diameter (MLD) and percent diameter stenosis (%DS) of 18 lesions without target lesion revascularizations. **B.** Changes in cross-sectional areas of 18 serial lesions without target lesion revascularizations. EEM indicates external elastic membrane; MLA, minimal lumen area.

**Table 5. Quantitative Intravascular Ultrasound Analysis of All Available Lesions Except Post–Target Lesion Revascularization Lesions (Unpaired)**

	Mean EEM Area, mm <sup>2</sup>	Mean Stent Area, mm <sup>2</sup>	MLA, mm <sup>2</sup>	Neointimal Area, mm <sup>2</sup>	Projected MLD, mm
Before the procedure (n=59 lesions)	12.79±4.22	...	1.96±0.97	...	1.42±0.36
After the procedure (n=62 lesions)	14.61±4.54	6.72±2.21	5.44±1.89	...	2.69±0.45
At 1 d (n=62 lesions)	15.02±4.87	6.49±2.24	5.06±1.81	...	2.64±0.47
At 6 mo (n=53 lesions)	15.37±4.92	7.23±2.44	3.64±1.68	2.26±0.74	1.87±0.52
At 1 y (n=44 lesions)	15.97±4.81	7.57±2.61	4.06±1.61	2.20±1.10	1.99±0.42
At 2 y (n=38 lesions)	14.95±4.08	7.05±2.38	4.15±1.49	1.56±0.77	2.06±0.42
At 3 y (n=24 lesions)	16.85±5.42	...	5.18±2.09	...	2.22±0.49

EEM indicates external elastic membrane; MLA, minimal lumen area; and MLD, minimal lumen diameter.

MACE-free survival rates continued to decrease during follow-up (50% at 10 years), mainly as a result of the increase in TLR and TVR rates. During the process of biodegradation (1–3 years), TLR and TVR reached a near plateau, suggesting that the process of PLLA biodegradation does not correlate with increased risk of clinical events. There is the possibility that if the Igaki-Tamai stent becomes drug eluting, the TLR rates could be improved. At 5 years, the TLR rate was 18%, which is comparable to results of permanent bare metal stents.<sup>22,23</sup> After 5 years, TLR rates progressively increased up to 28% at 10 years. This increase in TLR rates in this study during the long-term follow-up is difficult to evaluate, and there are few reports about long-term (5–10-year) clinical and angiographic outcomes. Kimura and colleagues<sup>23</sup> reported on the long-term (7–11 year) clinical and angiographic data of Palmaz-Schatz stents, and MACE-free rates continued to decrease during the follow-up period (37% at 8 years), which was similar to that of our study. Although late revascularization was due predominantly to progressive disease at nontarget sites, a significant decrease in MLD was observed from 6 months to late follow-up, and Kimura and colleagues concluded that progressive luminal narrowing beyond 4 years

after coronary stent placement was common. Their findings are consistent with the increase in TLR/TVR rates in our study.

We have previously reported 14 cases that highlight the histological findings of new in-stent lesions developing beyond 5 years,<sup>24</sup> and in that study, new atherosclerotic progression occurred inside the metallic stent. This might also suggest that the new atherosclerotic progression was a possible cause of the increase in TLR rates after 5 years in our study.

Unpaired quantitative coronary angiography and quantitative analysis of IVUS showed that MLD and MLA decreased at 6 months, just as with metallic stents, with improvement at 3 years (Tables 4 and 5). This phenomenon was also observed in the paired analysis of 18 lesions without TLRs, but the improvement at 3 years was not statistically significant (Figure 5). On the other hand, the stent area and EEM area did not change over time, suggesting that stent recoil and vessel remodeling did not occur during biodegradation. The absorption of the polymeric struts with plaque regression might contribute to the improvement of MLA over time.

In this cohort, the duration of DAPT was <3 months in 66% of patients. Two definite scaffold thrombosis cases were

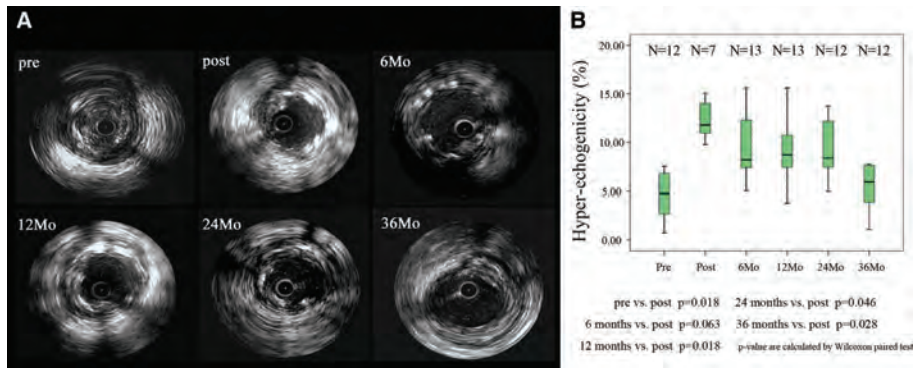


**Figure 6.** Changes in intravascular ultrasound (IVUS) echogenicity overtime. **A**, Serial IVUS findings of a representative case. After stent implantation, there is an increase in hyper-echogenicity with the stent struts visible, which progressively disappear at longer follow-up. **B**, The hyper-echogenicity of the 13 lesions analyzed is plotted. At 3 years, the hyper-echogenicity is close to the value observed before the procedure.

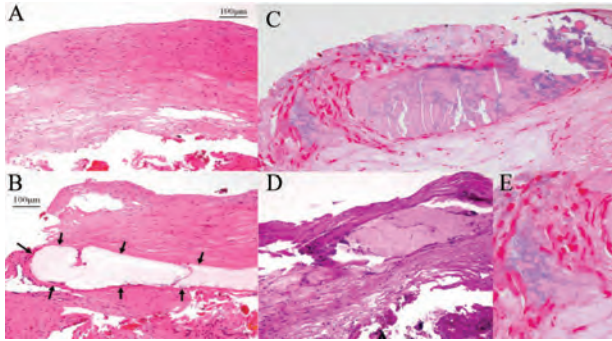


**Figure 7.** Histological features of specimens excised by directional atherectomy (42 months after the implantation of Igaki-Tamai stent). **A**, Resected intima with fibrous thickening without inflammatory cell infiltration. The upper side is the luminal surface (hematoxylin and eosin stain). **B**, Remnants of polymeric struts are observed in a deeper layer of thickened intima (arrows). Note the minimal inflammation around the remnants (hematoxylin and eosin stain). The space previously occupied by poly-*l*-lactic acid was stained by Alcian blue (**C**), but not by periodic acid-Schiff (**D**). **E**, Magnified Alcian blue staining.

reported during the follow-up, but only 1 case was associated with the Igaki-Tamai stent. This patient had subacute scaffold thrombosis at day 5 that was due to cessation of antiplatelet therapy after acute hemorrhagic gastric ulcer. This was the first reported case of PLLA scaffold thrombosis in humans, which indicated that even though the stent material is not metallic, antiplatelet therapy is mandatory. The other case was that of a very late scaffold thrombosis at 10 years, which is explained entirely by VLST secondary to an SES. VLST might rarely occur after PLLA stent deployment because the struts disappear within 3 years, and stent thrombosis theoretically does not occur after strut degradation.

One major concern about PLLA stents has been whether stent degradation occurs in a reasonable time period. Previous bench work showed that degradation of polymers results in different acoustic properties of the material and that this process is detected by IVUS as diminishing gray-level intensities of the struts over time.<sup>10,18,25</sup> IVUS-derived quantitative echogenicity has previously been shown to be valuable in monitoring the degradation and bioresorption processes of polymeric scaffolds made of poly-lactide.<sup>18</sup> In the ABSORB trials testing the ABSORB BVS, which is made of poly-lactide, the quantitative differential echogenicity applied to monitor in vivo changes of the scaffold showed, for example, that at the expected time of total degradation and bioresorption ( $\approx 2$  years), the acoustic signals exhibited only little evidence of polymer residues.<sup>10,18</sup> In the present analysis, the average hyperechogenicity significantly increased after stent implantation, compatible with the introduction of polymeric material in the coronary segment<sup>26</sup>; a subsequent decrease was then detected up to 3 years, when the hyperechogenicity was close to that observed before the procedure (Figure 6B), suggesting that the Igaki-Tamai stent required 3 years to disappear from human coronary arteries. This finding may support a different degradation time between the Igaki-Tamai stent and the ABSORB BVS, which can be explained by the differences in the manufacturing process of the PLLA influencing the acoustic properties detected by the echogenicity analysis.<sup>25</sup> Of note, whereas the Igaki-Tamai stent consists totally of PLLA (molecular weight, 183 KDa), the BVS consists of PLLA (molecular weight is confidential) for the backbone and a copolymer of D- and L-lactic acid (PDLLA)

for the coating, which includes everolimus. Because PDLLA has lower crystallinity than PLLA, PDLLA degrades faster than PLLA.<sup>27</sup>

Although we only used the IVUS system in this study, other modalities such as optical coherence tomography may be useful for acquiring more information. Onuma and colleagues<sup>28</sup> reported optical coherence tomography images at 10-year follow-up of the Igaki-Tamai stent. The stent struts were not visible, and the endoluminal lining of the vessel was circular and smooth by optical coherence tomography in their study, which may further support the full degradation of the Igaki-Tamai stent.

Chronic inflammation, triggered by permanent polymers, may contribute to the increased risk of VLST and restenosis in drug-eluting stents.<sup>20</sup> Therefore, histological analysis of the PLLA stent struts in a chronic phase is of great significance, and we had the opportunity to examine the histology in 1 case (Figure 7). As mentioned previously, the remnants of polymeric struts were disclosed, complete endothelialization was observed, thrombus was not detected, and active inflammation was not observed around the strut remnants. Although the disappearance of PLLA could not be verified, Alcian blue staining on histological examination suggested that the strut remnants were filled with proteoglycan. These histological findings were compatible with the preclinical porcine studies of the ABSORB BVS.<sup>10</sup>

There are still some deficits of this stent prototype that need to be improved, especially the system for stent deployment. In this initial cohort, we used contrast media heated to 80° to achieve adequate stent expansion, which might have affected the TLR rates. Moreover, because this stent has a self-expanding capability, a 5F covered sheath system was necessary. However, with the development of new technology, the Igaki-Tamai stent can now be implanted with normal contrast media. The cumbersome delivery system has also been improved. Currently, the Igaki-Tamai stent can be implanted in vitro through a 6F guiding catheter without a covered sheath system, but this catheter is not yet commercially available.

Our study has several limitations. This was an observational, single-center, nonrandomized study. There was no clinical events committee in this study; however, the data

were analyzed independently from Dr Igaki, who had provided the Igaki-Tamai stents. The clinical follow-up period of 10 years was not planned at the beginning of this study, and late angiography and IVUS were not dictated by the protocol but rather were based on clinical indications. There were no independent core laboratories. Because of the small number of patients in our cohort, it is difficult to comment on events that have a low incidence, especially scaffold thrombosis. Because the significance level was not adjusted for multiple tests, the rates of type I error may be high. Angiography and IVUS follow-up studies were performed in a relatively small percent of patients, so there is the potential for bias.

### Conclusions

Acceptable MACE rates similar to those of bare metal stents and scaffold thrombosis rates without stent recoil and vessel remodeling suggested the long-term safety of the Igaki-Tamai stent. In IVUS analysis, the stent struts mostly disappeared within 3 years. Although the mechanism of vessel healing in a chronic phase may not be the same between Igaki-Tamai stents and bioabsorbable drug-eluting PLLA stents, our study is essential in paving the way for a bioabsorbable drug-eluting PLLA stent, especially from the standpoint of long-term safety.

### Acknowledgments

We are indebted to the Department of Cardiovascular Medicine, Kyoto University, Kyoto, Japan, for offering the clinical information.

### Disclosures

Kyoto Medical Planning Co. Ltd. has commercialized this technology. Dr Igaki is the inventor and developer of the Igaki-Tamai stent. In this study, the data were analyzed independently from Dr Igaki. The other authors report no conflicts.

### References

- Zidar J, Lincoff A, Stack R. Biodegradable stents. In: Topol EJ, ed. *Textbook of Interventional Cardiology*. 2nd ed. Philadelphia, PA: Saunders; 1994:787–802.
- Van der Giessen WJ, Lincoff AM, Schwartz RS, van Beusekom HM, Serruys PW, Holmes DR Jr, Ellis SG, Topol EJ. Marked inflammatory sequelae to implantation of biodegradable and nonbiodegradable polymers in porcine coronary arteries. *Circulation*. 1996;94:1690–1697.
- Tamai H, Igaki K, Kyo E, Kosuga K, Kawashima A, Matsui S, Komori H, Tsuji T, Motohara S, Uehata H. Initial and 6-month results of biodegradable poly-L-lactic acid coronary stents in humans. *Circulation*. 2000;102:399–404.
- Morice MC, Serruys PW, Sousa JE, Fajadet J, Ban Hayashi E, Perin M, Colombo A, Schuler G, Barragan P, Guagliumi G, Molnar F, Falotico R; RAVEL Study Group. A randomized comparison of a sirolimus-eluting stent with a standard stent for coronary revascularization. *N Engl J Med*. 2002;346:1773–1780.
- Wenaweser P, Daemen J, Zwahlen M, van Domburg R, Jüni P, Vaina S, Hellige G, Tsuchida K, Morger C, Boersma E, Kukreja N, Meier B, Serruys PW, Windecker S. Incidence and correlates of drug-eluting stent thrombosis in routine clinical practice: 4-year results from a large 2-institutional cohort study. *J Am Coll Cardiol*. 2008;52:1134–1140.
- Daemen J, Wenaweser P, Tsuchida K, Abrecht L, Vaina S, Morger C, Kukreja N, Jüni P, Sianos G, Hellige G, van Domburg RT, Hess OM, Boersma E, Meier B, Windecker S, Serruys PW. Early and late coronary stent thrombosis of sirolimus-eluting and paclitaxel-eluting stents in routine clinical practice: data from a large two-institutional cohort study. *Lancet*. 2007;369:667–678.
- Kimura T, Morimoto T, Nakagawa Y, Tamura T, Kadota K, Yasumoto H, Nishikawa H, Hiasa Y, Muramatsu T, Meguro T, Inoue N, Honda H, Hayashi Y, Miyazaki S, Oshima S, Honda T, Shiode N, Namura M, Sone T, Nobuyoshi M, Kita T, Mitsudo K; J-Cypher Registry Investigators. Antiplatelet therapy and stent thrombosis after sirolimus-eluting stent implantation. *Circulation*. 2009;119:987–995.
- Erbel R, Di Mario C, Bartunek J, Bonnier J, de Bruyne B, Eberli FR, Erne P, Haude M, Heublein B, Horrigan M, Ilesley C, Böse D, Koolen J, Lüscher TF, Weisman N, Waksman R; PROGRESS-AMS (Clinical Performance and Angiographic Results of Coronary Stenting with Absorbable Metal Stents) Investigators. Temporary scaffolding of coronary arteries with bioabsorbable magnesium stents: a prospective, non-randomised multicentre trial. *Lancet*. 2007;369:1869–1875.
- Ormiston JA, Serruys PW, Regar E, Dudek D, Thuesen L, Webster MW, Onuma Y, Garcia-Garcia HM, McGreevy R, Veldhof S. A bioabsorbable everolimus-eluting coronary stent system for patients with single de-novo coronary artery lesions (ABSORB): a prospective open-label trial. *Lancet*. 2008;371:899–907.
- Serruys PW, Ormiston JA, Onuma Y, Regar E, Gonzalo N, Garcia-Garcia HM, Nieman K, Bruining N, Dorange C, Miquel-Hébert K, Veldhof S, Webster M, Thuesen L, Dudek D. A bioabsorbable everolimus-eluting coronary stent system (ABSORB): 2-year outcomes and results from multiple imaging methods. *Lancet*. 2009;373:897–910.
- Cutlip DE, Windecker S, Mehran R, Boam A, Cohen DJ, van Es GA, Steg PG, Morel MA, Mauri L, Vranckx P, McFadden E, Lansky A, Hamon M, Krucoff MW, Serruys PW; Academic Research Consortium. Clinical end points in coronary stent trials: a case for standardized definitions. *Circulation*. 2007;115:2344–2351.
- Rodriguez-Granillo GA, McFadden EP, Aoki J, van Mieghem CA, Regar E, Bruining N, Serruys PW. In vivo variability in quantitative coronary ultrasound and tissue characterization measurements with mechanical and phased-array catheters. *Int J Cardiovasc Imaging*. 2006;22:47–53.
- De Winter SA, Hamers R, Degerterkin M, Tanabe K, Lemos PA, Serruys PW, Roelandt JR, Bruining N. Retrospective image-based gating of intracoronary ultrasound images for improved quantitative analysis: the Intelligate method. *Catheter Cardiovasc Interv*. 2004;61:84–94.
- Bruining N, van Birgelen C, de Feyter PJ, Ligthart J, Li W, Serruys PW, Roelandt JR. ECG-gated versus nongated three-dimensional intracoronary ultrasound analysis: implications for volumetric measurements. *Cathet Cardiovasc Diagn*. 1998;43:254–260.
- van Birgelen C, Mintz GS, Nicosia A, Foley DP, van der Giessen WJ, Bruining N, Airlian SG, Roelandt JR, de Feyter PJ, Serruys PW. Electrocardiogram-gated intravascular ultrasound image acquisition after coronary stent deployment facilitates on-line three-dimensional reconstruction and automated lumen quantification. *J Am Coll Cardiol*. 1997;30:436–443.
- Tanimoto S, Bruining N, van Domburg RT, Rotger D, Radeva P, Ligthart JM, Serruys PW. Late stent recoil of the bioabsorbable everolimus-eluting coronary stent and its relationship with plaque morphology. *J Am Coll Cardiol*. 2008;52:1616–1620.
- Hamers R, Bruining N, Knook M, Sabate M. A novel approach to quantitative analysis of intravascular ultrasound images. *Computers Cardiol*. 2008;28:589–592.
- Bruining N, de Winter S, Roelandt JR, Regar E, Heller I, van Domburg RT, Hamers R, Onuma Y, Dudek D, Webster MW, Thuesen L, Ormiston JA, Cheong WF, Miquel-Hébert K, Veldhof S, Serruys PW. Monitoring in vivo absorption of a drug-eluting bioabsorbable stent with intravascular ultrasound-derived parameters: a feasibility study. *J Am Coll Cardiol Cardiovasc Interv*. 2010;3:449–456.
- Bruining N, Verheyte S, Knaepen M, Somers P, Roelandt JR, Regar E, Heller I, de Winter S, Ligthart J, Van Langenhove G, de Feyter PJ, Serruys PW, Hamers R. Three-dimensional and quantitative analysis of atherosclerotic plaque composition by automated differential echogenicity. *Catheter Cardiovasc Interv*. 2007;70:968–978.
- Joner M, Finn AV, Farb A, Mont EK, Kolodgie FD, Ladich E, Kutys R, Skorija K, Gold HK, Virmani R. Pathology of drug-eluting stents in humans: delayed healing and late thrombotic risk. *J Am Coll Cardiol*. 2006;48:193–202.
- Cook S, Wenaweser P, Togni M, Billinger M, Morger C, Seiler C, Vogel R, Hess O, Meier B, Windecker S. Incomplete stent apposition and very late stent thrombosis after drug-eluting stent implantation. *Circulation*. 2007;115:2426–2434.
- Kiemeneij F, Serruys PW, Macaya C, Rutsch W, Heyndrickx G, Albertsson P, Fajadet J, Legrand V, Materne P, Belardi J, Sigwart U, Colombo A, Goy JJ, Disco CM, Morel MA. Continued benefit of coronary stenting versus balloon angioplasty: five-year clinical follow-up of the Benestent-I trial. *J Am Coll Cardiol*. 2001;37:1598–1603.
- Kimura T, Abe K, Shizuta S, Odashiro K, Yoshida Y, Sakai K, Kaitani K, Inoue K, Nakagawa Y, Yokoi H, Iwabuchi M, Hamasaki N, Nosaka H, Nobuyoshi M. Long-term clinical and angiographic follow-up after coronary stent placement in native coronary arteries. *Circulation*. 2002;105:2986–2991.

24. Hasegawa K, Tamai H, Kyo E, Kosuga K, Ikeguchi S, Hata T, Okada M, Fujita S, Tsuji T, Takeda S, Fukuhara R, Kikuta Y, Motohara S, Ono K, Takeuchi E. Histopathological findings of new in-stent lesions developed beyond five years. *Catheter Cardiovasc Interv*. 2006;68:554–558.
25. Parker NG, Mather ML, Morgan SP, Povey MJ. Longitudinal acoustic properties of poly(lactic acid) and poly(lactic-co-glycolic acid). *Biomed Mater*. 2010;5:055004.
26. Garcia-Garcia HM, Gonzalo N, Pawar R, Kukreja N, Dudek D, Thuesen L, Ormiston JA, Regar E, Serruys PW. Assessment of the absorption process following bioabsorbable everolimus-eluting stent implantation: temporal changes in strain values and tissue composition using intravascular ultrasound radiofrequency data analysis: a substudy of the ABSORB clinical trial. *EuroIntervention*. 2009;4:443–448.
27. Oberhauser JP, Hossainy S, Rapoza R. Design principles and performance of bioresorbable polymeric vascular scaffolds. *EuroIntervention*. 2009;5:F15–F22.
28. Onuma Y, Grag S, Okamura T, Ligthart J, van Geuns RJ, de Feyter PJ, Serruys PW, Tamai H. Ten-year follow-up of the IGAKI-TAMAI stent. *EuroIntervention Suppl*. 2009;5:F109–F111.

### CLINICAL PERSPECTIVE

The Igaki-Tamai stent is the first-in-man fully biodegradable coronary stent made of poly-L-lactic acid (PLLA). In the present study, there was a high survival rate free of cardiac death (98% at 10 years) demonstrating the long-term safety of this stent. In the intravascular ultrasound echogenicity analysis, the Igaki-Tamai stent required 3 years to disappear from human coronary arteries. During the process of biodegradation (1–3 years), target lesion revascularization and target vessel revascularization reached a near plateau, suggesting that the process of PLLA biodegradation does not correlate with increased risk of clinical events. Although the mechanism of vessel healing in a chronic phase may not be the same between Igaki-Tamai stents and bioabsorbable drug-eluting PLLA stents, our study is essential in paving the way for a bioabsorbable drug-eluting PLLA stent, especially from the standpoint of long-term safety.

### 1.3 Magnesium alloy

Bioresorbable drug-eluting magnesium-alloy scaffold for treatment of coronary artery disease.

*Int J Mol Sci.* 2013;14:24492-500.

[Review, Impact Factor (2013): 2.339]

Campos CM, Muramatsu T, Iqbal J, Zhang YJ, Onuma Y, Garcia-Garcia HM, Haude M, Lemos PA, Warnack B, Serruys PW.





Review

## Bioresorbable Drug-Eluting Magnesium-Alloy Scaffold for Treatment of Coronary Artery Disease

Carlos M. Campos<sup>1,2</sup>, Takashi Muramatsu<sup>1,3</sup>, Javaid Iqbal<sup>1</sup>, Ya-Jun Zhang<sup>1</sup>, Yoshinobu Onuma<sup>1</sup>, Hector M. Garcia-Garcia<sup>1</sup>, Michael Haude<sup>5</sup>, Pedro A. Lemos<sup>2</sup>, Boris Warnack<sup>6</sup> and Patrick W. Serruys<sup>1,4,\*</sup>

<sup>1</sup> Department of Interventional Cardiology, Erasmus University Medical Centre, Thoraxcenter, Rotterdam 3015 GD, The Netherlands; E-Mails: carloscampos1@gmail.com (C.M.C.); takam0401@gmail.com (T.M.); j.iqbal@sheffield.ac.uk (J.I.); 13770668667@139.com (Y.-J.Z.); yoshinobuonuma@gmail.com (Y.O.); HGarcia@cardialysis.nl (H.M.G.-G.)

<sup>2</sup> Heart Institute (InCor), University of São Paulo Medical School, Sao Paulo 05403-000, Brazil; E-Mail: pedro.lemos@incor.usp.br

<sup>3</sup> Department of Cardiology, Fujita Health University Hospital, Tokyo 470-1192, Japan

<sup>4</sup> Department of Cardiology, Imperial College London, London SW7 2AZ, UK

<sup>5</sup> Städtische Kliniken Neuss, Lukaskrankenhaus GmbH, Neuss 41464, Germany; E-Mail: michael.haude@uni-due.de

<sup>6</sup> BIOTRONIK AG, Bülach CH-8180, Switzerland; E-Mail: boris.warnack@biotronik.com

\* Author to whom correspondence should be addressed; E-Mail: p.w.j.c.serruys@erasmusmc.nl.

Received: 21 October 2013; in revised form: 3 December 2013 / Accepted: 12 December 2013 / Published: 16 December 2013

---

**Abstract:** The introduction of metallic drug-eluting stents has reduced the risk of restenosis and widened the indications of percutaneous coronary intervention in treatment of coronary artery disease. However, this medical device can induce hypersensitive reaction that interferes with the endothelialization and healing process resulting in late persistent or acquired malapposition of the permanent metallic implant. Delayed endothelialization and malapposition may lead to late and very late stent thrombosis. Bioresorbable scaffolds (BRS) have been introduced to potentially overcome these limitations, as they provide temporary scaffolding and then disappear, liberating the treated vessel from its cage. Magnesium is an essential mineral needed for a variety of physiological functions in the human body and its bioresorbable alloy has the strength-to-weight ratio comparable with that of strong aluminum alloys and alloy steels. The aim of this review is to present the new developments in Magnesium BRS

technology, to describe its clinical application and to discuss the future prospects of this innovative therapy.

**Keywords:** bioresorbable scaffold; drug-eluting stent; bioabsorbable; biodegradable; coronary artery disease; magnesium

---

## 1. Introduction

The percutaneous treatment of coronary artery disease consists of catheter-based techniques to enlarge lumen of an artery narrowed by an atherosclerotic lesion. The development of this method began in 1977 with balloon angioplasty, which consisted of a mechanical dilatation of the atherosclerotic lesion with the hazard of thrombosis and vascular occlusions due to a combination of elastic recoil and vessel wall dissections (medial and/or intimal) [1]. Furthermore, proliferative neointima and constrictive remodeling could abrogate the transient therapeutic benefit of the dilatation of the stenosis [2]. In 1986, the introduction of metallic stents offered a mechanical solution to the dissection, elastic recoil and constrictive remodeling [3–5]. However, the implantation of these bare metal stents still caused neointimal proliferation leading to in-stent restenosis [6]. A decade later, in 1999, coating and elution of cytostatic and cytotoxic drugs reduced, if not eliminated, the exuberant in-stent neointima in response to the implantation of a foreign body [7–9]. However, this medical device created new enemies: hypersensitive reaction mediated by eosinophils, lack of endothelialization and late persistent or acquired struts malapposition, which are source of late and very late stent thrombosis [10–12].

Considering these historical limitations, the next step in the evolution of percutaneous coronary intervention (PCI) was to create a device capable of dilating the coronary obstruction, providing vascular supports for dissections, preventing elastic recoil and constrictive remodeling, inhibiting neointimal hyperplasia and disappearing “after the job was done”.

Over the last 10 years, considerable efforts have been made to develop fully bioresorbable devices, called bioresorbable scaffolds (BRS). BRS technology has gradually matured, and there are numerous devices available, which are currently undergoing preclinical or clinical testing, and magnesium is an attractive alloy for this concept. The aim of this review is to describe the current concept, the mechanism of absorption and the data available on magnesium-based BRS.

## 2. Potential Benefits of a Transient Scaffold

PCI with BRS has potential advantages over the current generation of metallic bare-metal stent (BMS)/drug-eluting stent (DES) technology. Physiologically, the absence of a rigid metallic cage can facilitate the restoration of the vessel vasomotor tone, adaptive shear stress, late luminal enlargement, and late expansive remodeling. After bioresorption, there would be potentially no triggers for thrombosis, such as uncovered stent struts, durable polymer or remnant drug, with potential reductions in adverse events such as stent/scaffold thrombosis. The absence of foreign material may also reduce the requirement for long-term dual antiplatelet therapy and associated bleeding complications.

In the long term, BRS should not hamper future treatment options such as PCI, coronary artery bypass graft, or pharmacological plaque regression [13].

### 3. Magnesium as a Component for BRS

Magnesium is an essential mineral needed for a variety of physiological functions in the human body. The usual daily magnesium intake with a western diet is sufficient to avoid deficiency but seems not to be high enough to establish high normal serum magnesium concentrations that are protective against various diseases. The extracellular magnesium concentration is primarily regulated by the kidney and redundant magnesium cations can be harmlessly and efficiently excreted in the urine [14]. Combining its rapid corrosion with a controlled degradation process through Zinc and Manganese alloying, purification and anodization, magnesium has been developed into a bioresorbable and biocompatible implant material [15].

Although magnesium is available commercially with high degree of purity (exceeding 99.8%), it has low strength and rapid corrosion in unalloyed form. Therefore, it is commonly used in its alloy form, which is possible with a wide variety of elements [15,16].

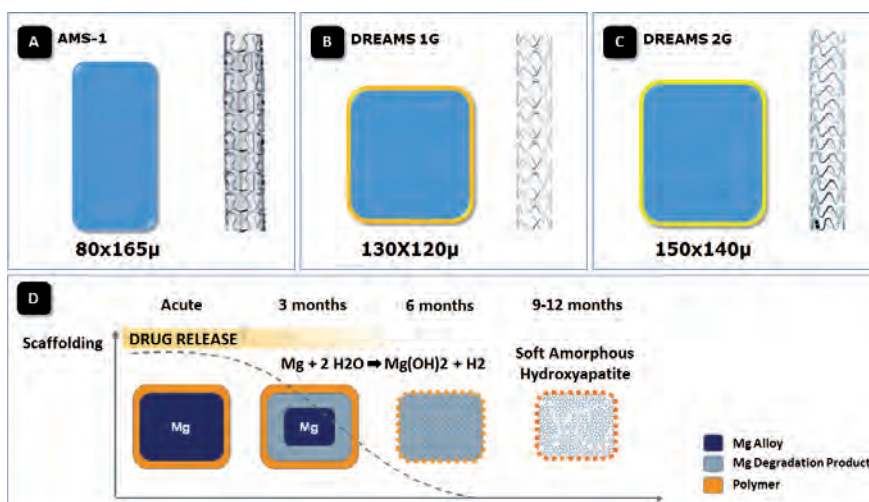
Although Magnesium is the lightest structural metal, the strength-to-weight ratio of precipitation-hardened magnesium alloys is comparable with that of strong aluminum alloys and alloy steels [16]. Consequently, a magnesium BRS has potential to provide a high radial strength for dilating atherosclerotic narrowing and, hence, higher acute gain of coronary lumen. Another virtue of magnesium as an endoprosthesis is its electrochemical properties. Devices with negatively charged surfaces are less thrombogenic than those with positive surfaces. Magnesium is more electronegative than other metals used for implants and has shown anti-thrombogenic properties *in vivo* [17–21].

### 4. The First Generation Magnesium BRS

The first generation of bioabsorbable metal scaffolds (AMS-1; Biotronik AG, Bülach, Switzerland) was made from a WE43 alloy, composed of 93% Mg and 7% rare earth elements (Figure 1). The AMS-1 was a tubular, slotted, balloon-expandable scaffold sculpted by laser from a tube of a bioabsorbable magnesium alloy without drug-elution. The mechanical characteristics of the magnesium scaffolds were similar to stainless steel stents, including low elastic recoil (less than 8%), high collapse pressure (0.8 bar), and minimum amount of shortening after inflation (less than 5%) [22].

In porcine coronary arteries, the histologic evaluation of AMS-1 showed that none of the arteries analyzed had incomplete stent apposition, excess of intimal thickening at the stent edges or intraluminal thrombus. The neointimal tissue proliferation was significantly less in the stented segments of the magnesium alloy scaffold as compared to a control group of stainless steel stents. The reduction of neointima formation was not translated to larger vessel lumen and the overall stented segment was significantly smaller when compared to the stainless steel stent. This can result from underexpansion of the stent at deployment, early or late recoil, or all of the above. Although statistically not significant, the extent of fibrin deposition and inflammation for stented segments of stainless steel stents were slightly higher in the group treated with stainless steel stents than those treated with magnesium BRS. The AMS-1 was largely bioabsorbed into inorganic ions within 60 days of implantation [23].

**Figure 1.** (A) Schematic cross-sectional profile of magnesium scaffolds struts of (A) uncoated, non-eluting, AMS-1 with  $80 \times 165 \mu$ ; (B) DREAMS 1st Generation (DREAMS 1G) with  $130 \times 120 \mu$  struts and (C) DREAMS 2nd generation (2G) with  $150 \times 140 \mu$  struts. The poly(lactide-co-glycolide)-coating with paclitaxel elution of the DREAMS 1G scaffold is indicated by the thin light orange layer. The PLA-coating with sirolimus elution of the DREAMS 2G scaffold is indicated by the thin dark orange layer; and (D) Schematic representation of the resorption process in the drug-eluting absorbable magnesium scaffold. The release of the anti-proliferative drug occurs within the first 3 months after device implantation. Hydrolysis of the scaffold affects the radial strength of the scaffold, resulting in a gradual resorption of the device into a soft amorphous hydroxyapatite at 9 months follow-up. AMS-1, first-generation bare absorbable metal scaffold; DREAMS, Drug-Eluting Absorbable Metal Scaffold.



The AMS-1 was evaluated in a prospective, non-randomized, multicenter, clinical trial ( $n = 63$ ). There were no safety concerns regarding deaths, myocardial infarction, or scaffold thrombosis. However, the long-term patency rates were lower than expected. The in-scaffold late lumen loss (LLL) was  $1.08 \pm 0.49$  mm. The LLL was a combined effect of a decrease in external elastic membrane area (representing 42% of LLL), decrease in scaffold area (18% of LLL) and neointima formation (40% of LLL). Thus, the main mechanism of restenosis (60% of LLL) was a faster than expected scaffold degradation with an early loss of radial force and consequent vessel recoil. The ischemia-driven target lesion revascularization rate was 23.8% after 4 months, and the overall target lesion revascularization rate was 45% at 1 year [22,24–26].

## 5. The Paclitaxel-Eluting Absorbable Metal Scaffold (DREAMS)

To prolong vessel scaffolding AMS-1 was redesigned (Figure 1). The balloon-expandable DREAMS scaffold (Biotronik AG, Bülach, Switzerland) used a refined, slower-resorbable WE43 alloy with 6-crown 3-link design and with a higher collapse pressure than AMS-1 (1.5 vs. 0.8 bar). The cross-sectional profile of scaffold struts in DREAMS was redesigned to be square-shaped, as opposed to the rectangular shape in AMS-1. In a porcine coronary model, the scaffold degradation showed a preferential cellularization at the lateral sides of the struts and a square shape slowed the resorption process compared to the first generation magnesium AMS-1 [27]. Thereby, strut thickness was reduced from 165 to 120  $\mu\text{m}$ . To reduce neointimal growth the DREAMS was coated with a 1  $\mu\text{m}$  bioresorbable poly(lactide-*co*-glycolide) polymer matrix (PLGA) containing the antiproliferative drug paclitaxel (0.07  $\mu\text{g}/\text{mm}^2$ ) [27].

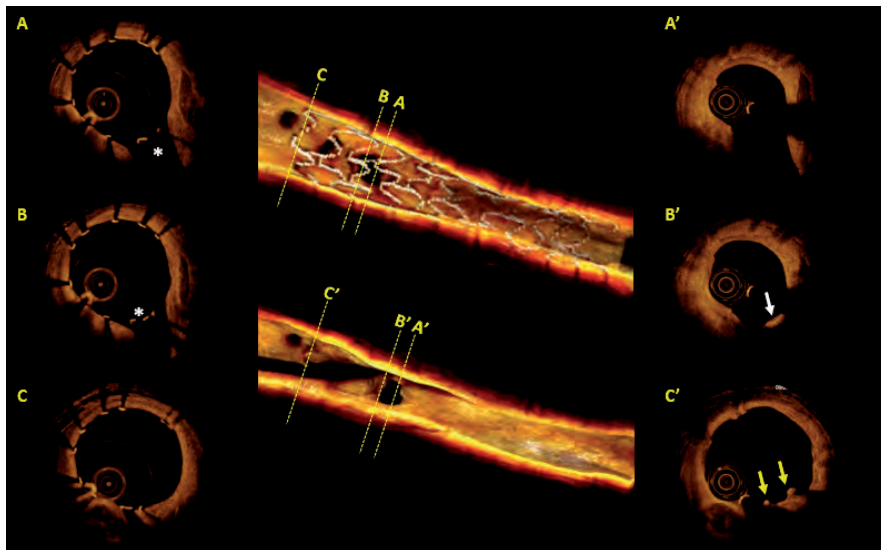
The first *in vivo* evaluation of DREAMS used a porcine model and evaluated the best lactide to glycolide ratio for the PLGA polymer formulation. This formulation regulates the resorption rate of the drug-carrying PLGA polymer and, therefore, the release of paclitaxel. Seventy-three magnesium scaffolds (ratio of lactide to glycolide of 50/50 in 25 scaffolds, 85/15 with high molecular weight of PLGA in 24, 85/15 with low molecular weight of PLGA in 24) and 36 control stents (18 TAXUS Liberté, 18 eucaTAX) were implanted. The best-performing magnesium scaffold—85/15 with high molecular weight—was equivalent to TAXUS Liberté and superior to eucaTAX regarding late luminal loss, intimal area, fibrin score, and endothelialization. Intimal inflammation score was higher in 85/15H than in the control scaffolds at 28 days, but was similar at 90 and 180 days. Endothelialization was nearly completed within 90 days in all devices [27].

The Figure 1 describes the dynamics and byproducts of magnesium scaffold resorption at 28, 90 and 180 days. Two phases of the resorption process of magnesium alloy were identified. First, a Mg-rich compound containing a large amount of oxygen is formed, possibly representing a mixture of Mg hydroxide and Mg carbonate. Several weeks later, these compounds convert to amorphous calcium phosphate, filling exactly the voids previously occupied by the dissolved scaffold struts. Measured at 28 days, the average *in vivo* degradation rates for the three DREAMS versions ranged from 0.036–0.072  $\text{mg}/(\text{cm}^2 \text{ day})$  [27].

The first-in-man BIOSOLVE-I trial assessed the safety and performance of this first generation drug-eluting magnesium-based BRS in 46 patients with 47 lesions at five European centers. During the procedure, all devices were successfully delivered. The in-scaffold late lumen loss was reduced at 6 months ( $0.65 \pm 0.5 \text{ mm}$ ) and at 12 months ( $0.52 \pm 0.39 \text{ mm}$ ) compared to  $1.08 \pm 0.49 \text{ mm}$  of the prior generation bare AMS-1 magnesium scaffold. However, the late lumen loss with DREAMS still did not match the excellent results of currently available drug-eluting stents.

In the BIOSOLVE-I trial, data for serial OCT were available for only seven patients with 5791 assessable struts. At 6 month follow-up, 97.2% (95%  $\text{CI}_{96.7-97.6}$ ) of the struts were apposed and at 12 months 99.8% (95%  $\text{CI}_{99.6-99.9}$ ) of the struts were apposed with only 0.1% (0.03–0.3) persistent incomplete strut apposition and 0.1% (0.03–0.3) late acquired incomplete strut apposition. An illustrative case of DREAMS BRS with OCT images is shown in Figure 2. At 12 months, three of 43 (7%, 95%  $\text{CI}_{1.7-19.3}$ ) patients had target lesion failure with no cardiac death or scaffold thrombosis [28].

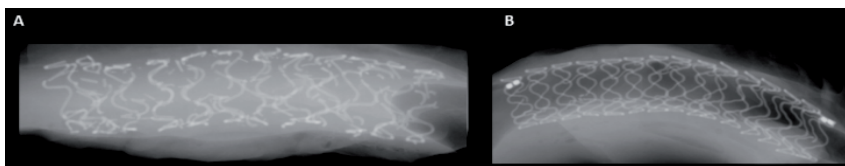
**Figure 2.** Post-implantation and 12-month follow-up optical coherence tomography (OCT; LightLab Imaging, Westford, MA, USA) of a percutaneous coronary intervention of the left anterior descending coronary artery, whereby a  $3.25 \times 16$  mm paclitaxel-eluting absorbable metal scaffold (DREAMS 1G; Biotronik, Bülach, Switzerland) was implanted. Post-procedurally a side branch was jailed by the struts of DREAMS 1G (Panels A and B). At 12 months follow-up, OCT showed a smooth luminal surface with moderate neointimal hyperplasia in the scaffolded segment. Just few remnants of struts were still visible with shadows (panel C', yellow arrows). The struts overhanging a side branch ostium were partially replaced by a neointimal membranous bridge (panel B', white arrow), while three-dimensional OCT revealed unobstructed and widely opened ostium of side branch.



## 6. The Sirolimus-Eluting Absorbable Metal Scaffold (DREAMS 2nd Generation)

DREAMS was further modified to create the next generation: the DREAMS 2nd generation (DREAMS 2G, Figure 1) which is made of a WE43 alloy with 6-crown 2-link design and a strut thickness of  $150 \mu\text{m}$  with radiopaque markers at both ends (made from tantalum) resulting in slower dismantling and resorption rate (Figure 3). The distal markers were added to make scaffold implantation and possible post-dilation more precise. To further reduce the neointima formation, the DREAMS 2G was coated with a bioresorbable polylactic acid polymer ( $7 \mu\text{m}$ ) featuring sirolimus at a dose of  $1.4 \mu\text{g}/\text{mm}^2$ —known to have more potent antiproliferative effect than paclitaxel [29–31]. DREAMS 2G has completed preclinical assessment and is currently being evaluated in BIOSOLVE-II trial.

**Figure 3.** High-resolution faxitron evaluation from a porcine coronary model after 90 days of implantation. At this time point, faster dismantling rate and resorption of the scaffold DREAMS 1G (A) than its latest development, the DREAMS 2G (B) could be detected.



## 7. Conclusions

BRS is a relatively new technology introduced to address the limitations of the traditional metallic stents. BRS will usher the practitioner in a new era of treatment of coronary lesions, as they provide temporary vessel scaffolding and then disappear, thereby allowing for the restoration of the vessel wall physiology and vasomotion. Magnesium alloy has a great potential since it is a metal with high radial strength and less thrombogenic electrochemical properties than most metals used for implants. Evidence from studies of the DREAMS 1st generation indicates that it has improved the drawbacks of the first generation bare AMS-1 (e.g., rapid bioresorption and device shrinkage). The DREAMS 2nd generation has completed its preclinical assessment and the experimental data suggest that it may be able to compete with the drug-eluting metallic stents in terms of safety and efficacy. BIOSOLVE-II trial will test the real potential of this technology.

## Conflicts of Interest

B Warnack is a full-time employee of BIOTRONIK AG., M Haude received grants from BIOTRONIK AG and serves as an advisor for BIOTRONIK AG. All other authors have no conflict of interest and did not receive grants or financial support from industry or from any other source to prepare this manuscript.

## References

1. Gruntzig, A. Transluminal dilatation of coronary-artery stenosis. *Lancet* **1978**, *1*, 263.
2. Ormiston, J.A.; Stewart, F.M.; Roche, A.H.; Webber, B.J.; Whitlock, R.M.; Webster, M.W. Late regression of the dilated site after coronary angioplasty: A 5-year quantitative angiographic study. *Circulation* **1997**, *96*, 468–474.
3. Sigwart, U.; Puel, J.; Mirkovitch, V.; Joffe, F.; Kappenberger, L. Intravascular stents to prevent occlusion and restenosis after transluminal angioplasty. *N. Engl. J. Med.* **1987**, *316*, 701–706.
4. Roubin, G.S.; Cannon, A.D.; Agrawal, S.K.; Macander, P.J.; Dean, L.S.; Baxley, W.A.; Breland, J. Intracoronary stenting for acute and threatened closure complicating percutaneous transluminal coronary angioplasty. *Circulation* **1992**, *85*, 916–927.
5. Schatz, R.A.; Baim, D.S.; Leon, M.; Ellis, S.G.; Goldberg, S.; Hirshfeld, J.W.; Cleman, M.W.; Cabin, H.S.; Walker, C.; Stagg, J.; *et al.* Clinical experience with the Palmaz-Schatz coronary stent. Initial results of a multicenter study. *Circulation* **1991**, *83*, 148–161.

6. Serruys, P.W.; Keane, D. The bailout stent. Is a friend in need always a friend indeed? *Circulation* **1993**, *88*, 2455–2457.
7. Sousa, J.E.; Costa, M.A.; Abizaid, A.; Abizaid, A.S.; Feres, F.; Pinto, I.M.; Seixas, A.C.; Staico, R.; Mattos, L.A.; Sousa, A.G.; *et al.* Lack of neointimal proliferation after implantation of sirolimus-coated stents in human coronary arteries: A quantitative coronary angiography and three-dimensional intravascular ultrasound study. *Circulation* **2001**, *103*, 192–195.
8. Rensing, B.J.; Vos, J.; Smits, P.C.; Foley, D.P.; van den Brand, M.J.; van der Giessen, W.J.; de Feijter, P.J.; Serruys, P.W. Coronary restenosis elimination with a sirolimus eluting stent: First European human experience with 6-month angiographic and intravascular ultrasonic follow-up. *Eur. Heart J.* **2001**, *22*, 2125–2130.
9. Morice, M.C.; Serruys, P.W.; Sousa, J.E.; Fajadet, J.; Ban Hayashi, E.; Perin, M.; Colombo, A.; Schuler, G.; Barragan, P.; Guagliumi, G.; *et al.* A randomized comparison of a sirolimus-eluting stent with a standard stent for coronary revascularization. *N. Engl. J. Med.* **2002**, *346*, 1773–1780.
10. Finn, A.V.; Joner, M.; Nakazawa, G.; Kolodgie, F.; Newell, J.; John, M.C.; Gold, H.K.; Virmani, R. Pathological correlates of late drug-eluting stent thrombosis: Strut coverage as a marker of endothelialization. *Circulation* **2007**, *115*, 2435–2441.
11. Joner, M.; Finn, A.V.; Farb, A.; Mont, E.K.; Kolodgie, F.D.; Ladich, E.; Kutys, R.; Skorija, K.; Gold, H.K.; Virmani, R. Pathology of drug-eluting stents in humans: Delayed healing and late thrombotic risk. *J. Am. Coll. Cardiol.* **2006**, *48*, 193–202.
12. Cook, S.; Ladich, E.; Nakazawa, G.; Eshtehardi, P.; Neidhart, M.; Vogel, R.; Togni, M.; Wenaweser, P.; Billinger, M.; Seiler, C.; *et al.* Correlation of intravascular ultrasound findings with histopathological analysis of thrombus aspirates in patients with very late drug-eluting stent thrombosis. *Circulation* **2009**, *120*, 391–399.
13. Serruys, P.W.; Garcia-Garcia, H.M.; Onuma, Y. From metallic cages to transient bioresorbable scaffolds: Change in paradigm of coronary revascularization in the upcoming decade? *Eur. Heart J.* **2012**, *33*, 16b–25b.
14. Vormann, J. Magnesium: Nutrition and metabolism. *Mol. Aspects Med.* **2003**, *24*, 27–37.
15. Song, G. Control of biodegradation of biocompatible magnesium alloy. *Corros. Sci.* **2007**, *49*, 1696–1701.
16. Chawla, S.L.; Gupta, R.K. *Materials Selection for Corrosion Control*; ASM International: Materials Park, OH, USA, 1993.
17. Sawyer, P.N.; Srinivasan, S. The role of electrochemical surface properties in thrombosis at vascular interfaces: Cumulative experience of studies in animals and man. *Bull. N. Y. Acad. Med.* **1972**, *48*, 235–256.
18. Anstall, H.B.; Hayward, G.H.; Huntsman, R.G.; Weitzman, D.; Lehmann, H. The effect of magnesium on blood coagulation in human subjects. *Lancet* **1959**, *1*, 814–815.
19. Rukshin, V.; Shah, P.K.; Cercek, B.; Finkelstein, A.; Tsang, V.; Kaul, S. Comparative antithrombotic effects of magnesium sulfate and the platelet glycoprotein IIb/IIIa inhibitors tirofiban and eptifibatide in a canine model of stent thrombosis. *Circulation* **2002**, *105*, 1970–1975.
20. Rukshin, V.; Azarbal, B.; Shah, P.K.; Tsang, V.T.; Shechter, M.; Finkelstein, A.; Cercek, B.; Kaul, S. Intravenous magnesium in experimental stent thrombosis in swine. *Arterioscler. Thromb. Vasc. Biol.* **2001**, *21*, 1544–1549.

21. Moravej, M.; Mantovani, D. Biodegradable metals for cardiovascular stent application: Interests and new opportunities. *Int. J. Mol. Sci.* **2011**, *12*, 4250–4270.
22. Erbel, R.; di Mario, C.; Bartunek, J.; Bonnier, J.; de Bruyne, B.; Eberli, F.R.; Erne, P.; Haude, M.; Heublein, B.; Horrigan, M.; *et al.* Temporary scaffolding of coronary arteries with bioabsorbable magnesium stents: A prospective, non-randomised multicentre trial. *Lancet* **2007**, *369*, 1869–1875.
23. Waksman, R.; Pakala, R.; Kuchulakanti, P.K.; Baffour, R.; Hellinga, D.; Seabron, R.; Tio, F.O.; Wittchow, E.; Hartwig, S.; Harder, C.; *et al.* Safety and efficacy of bioabsorbable magnesium alloy stents in porcine coronary arteries. *Catheter. Cardiovasc. Interv.* **2006**, *68*, 607–617; discussion 618–609.
24. Bose, D.; Eggebrecht, H.; Haude, M.; Schmermund, A.; Erbel, R. First absorbable metal stent implantation in human coronary arteries. *Am. Heart Hosp. J.* **2006**, *4*, 128–130.
25. Bose, D.; Eggebrecht, H.; Erbel, R. Absorbable metal stent in human coronary arteries: Imaging with intravascular ultrasound. *Heart* **2006**, *92*, 892.
26. Waksman, R.; Erbel, R.; di Mario, C.; Bartunek, J.; de Bruyne, B.; Eberli, F.R.; Erne, P.; Haude, M.; Horrigan, M.; Ilesley, C.; *et al.* Early- and long-term intravascular ultrasound and angiographic findings after bioabsorbable magnesium stent implantation in human coronary arteries. *JACC Cardiovasc. Interv.* **2009**, *2*, 312–320.
27. Wittchow, E.; Adden, N.; Riedmuller, J.; Savard, C.; Waksman, R.; Braune, M. Bioresorbable drug-eluting magnesium-alloy scaffold: Design and feasibility in a porcine coronary model. *EuroIntervention* **2013**, *8*, 1441–1450.
28. Haude, M.; Erbel, R.; Erne, P.; Verheye, S.; Degen, H.; Böse, D.; Vermeersch, P.; Wijnbergen, I.; Weissman, N.; Prati, F.; *et al.* Safety and performance of the drug-eluting absorbable metal scaffold (DREAMS) in patients with *de novo* coronary lesions: 12 month results of the prospective, multicentre, first-in-man BIOSOLVE-I trial. *Lancet* **2013**, *381*, 836–844.
29. Colmenarez, H.; Fernandez, C.; Escaned, J. Impact of technological developments in drug-eluting stents on patient-focused outcomes: A pooled direct and indirect comparison of randomised trials comparing first- and second-generation drug-eluting stents. *EuroIntervention* **2013**, in press.
30. Abizaid, A.; Ormiston, J.A.; Fajadet, J.; Mauri, L.; Schofer, J.; Verheye, S.; Dens, J.; Thuesen, L.; Macours, N.; Qureshi, A.C.; *et al.* Two-year follow-up of the NEVO RES-ELUTION I (NEVO RES-I) trial: A randomised, multicentre comparison of the NEVO sirolimus-eluting coronary stent with the TAXUS Liberté paclitaxel-eluting stent in *de novo* native coronary artery lesions. *EuroIntervention* **2013**, *9*, 721.
31. Kollum, M.; Heitzer, T.; Schmoor, C.; Brunner, M.; Witzenbichler, B.; Wiemer, M.; Hoffmann, R.; Gutleben, K.J.; Schultheiss, H.P.; Horstkotte, D.; *et al.* Intra-individual head-to-head comparison of Sirolimus(R)- and Paclitaxel(R)-eluting stents for coronary revascularization. A randomized, multi-center trial. *Int. J. Cardiol.* **2013**, *167*, 1552–1559.

© 2013 by the authors; licensee MDPI, Basel, Switzerland. This article is an open access article distributed under the terms and conditions of the Creative Commons Attribution license (<http://creativecommons.org/licenses/by/3.0/>).



# Chapter 2

## Methodology and Clinical Applications of Multimodality Imaging

### 2.1 Overview of methodologies and parameters to evaluate BRS

Assessing bioresorbable coronary devices: methods and parameters.

*JACC Cardiovasc Imaging*. 2014;7:1400-11.

[Review, Impact Factor (2013): 6.986]

Garcia-Garcia HM, Serruys PW, Campos CM, Muramatsu T, Nakatani S, Zhang YJ, Onuma Y, Stone GW.





# Assessing Bioresorbable Coronary Devices



## Methods and Parameters

Hector M. Garcia-Garcia, MD, PhD,\* Patrick W. Serruys, MD, PhD,\* Carlos M. Campos, MD,†  
Takashi Muramatsu, MD, PhD,\* Shimpei Nakatani, MD,\* Yao-Jun Zhang, MD, PhD,\* Yoshinobu Onuma, MD, PhD,\*  
Gregg W. Stone, MD, PhD‡

### ABSTRACT

Bioresorbable vascular scaffolds (BRS) represent a novel approach to provide transient vessel support to drug-delivery capability without the long-term limitations of metallic drug-eluting stents (DES). The technology has the potential to overcome many of the safety concerns associated with metallic DES and possibly even convey further clinical benefit. In particular, the BRS are designed to provide short-term lumen support, and after being completely bioresorbed, eliminate the permanent caging typical of metallic DES. However, this technology has required new imaging modalities and methodologies for its assessment because the design, degradation rate, loss of mechanical property, and drug deliverability may affect its safety and efficacy. We provide an overview of all existing methods for assessing bioresorbable devices, from noninvasive to invasive, from light to sound based, and from morphological to functional parameters. (J Am Coll Cardiol Img 2014;7:1130-48) © 2014 by the American College of Cardiology Foundation.

The clinical introduction of bioresorbable scaffolds (BRS) resulted in a revolutionary change in the application of local coronary therapies. These devices have the unique ability to provide a temporary scaffold that is necessary to maintain the patency of the vessel after intervention, releasing antiproliferative drugs. The BRS then gradually degrade, liberating the vessel from its cage and permitting the restoration of vascular physiology and integrity (1,2).

Percutaneous coronary intervention with BRS has potential advantages over the current use of metallic stents because after resorption, there should be no trigger for thrombosis, thereby reducing stent/scaffold thrombosis. The lack of foreign material may also reduce the requirements for long-term dual antiplatelet therapy and its correlated bleeding

complications. The absence of a rigid metallic cage can facilitate restoration of the vessel vasomotor tone, adaptive shear stress, late luminal enlargement, and late expansive remodeling. In the long term, BRS may allow a percutaneous/surgical revascularization of the treated segment or pharmacologically induced plaque regression, whereas traditional stents often preclude this option. For clinical follow-up, BRS enable noninvasive evaluation by multislice coronary tomography (MSCT), enabling visualization of the vascular lumen in the treated segment without the blooming effect observed with metallic stents.

Over the last 10 years, considerable effort has been put forth to develop new fully bioresorbable devices. BRS technology has gradually matured, and there are numerous devices available for preclinical or clinical evaluation (Table 1). However, this

From the \*Thoraxcenter, Erasmus, Rotterdam, the Netherlands; †Heart Institute (InCor), University of São Paulo Medical School, São Paulo, Brazil; and the ‡Columbia University Medical Center and Cardiovascular Research Foundation, New York, New York. Dr. Stone has served as a consultant to Reva Medical. All other authors have reported that they have no relationships relevant to the content of this paper to disclose.

Manuscript received April 24, 2014; revised manuscript received June 11, 2014; accepted June 26, 2014.

technology has required new imaging modalities and methodology for the assessment of BRS because their design, degradation rate, loss of mechanical properties, coating, and drug deliverability may affect safety and efficacy (Table 2). This review describes the imaging methods for BRS, compares BRS with metallic stents, and describes the clinical relevance of BRS.

### INVASIVE QUANTITATIVE CORONARY ANGIOGRAPHY

Invasive quantitative coronary angiography (QCA) remains one of the most commonly used methods for the assessment of lumen parameters for BRS. Coronary restenosis is influenced by both acute gain provided by the intervention and the subsequent late lumen loss (Figure 1). Considering the variety of BRS under development, clear understanding of the coronary restenotic mechanics is needed.

SEE PAGE 1149

In each patient, the treated segment (in-scaffold) and the peri-scaffold segments (defined by a length of 5 mm proximal and distal to the scaffold edge—in-segment) should be analyzed by QCA in paired matched angiographic views after the procedure and at follow-up. Because these devices are radiolucent, the only visible structures for QCA analysis are the

metallic markers at the proximal and distal ends of the device (Figure 2).

The following QCA parameters are computed: minimal luminal diameter (MLD), reference vessel diameter obtained by an interpolated method, late loss, and binary restenosis.

#### LATE LOSS AND/OR LATE LUMINAL GAIN.

Late loss and/or late luminal gain are defined as the difference between MLD at post-procedure minus MLD at follow-up. For lumen diameter reduction, this will be a positive number; for late increase in lumen size, this will be a negative number. Figure 1 summarizes the lumen size changes of current BRS tested in clinical scenarios. Please note the unique effect of *all* BRS, which is the late increase in lumen size (late gain). This luminal gain starts when BRS start to lose their mechanical integrity (Table 3).

**ACUTE RECOIL.** For acute recoil assessment, 2 specific views are analyzed. One is an image of complete expansion of the last balloon (either the device delivery balloon or the post-dilation balloon) at the highest pressure. The other is a cine frame immediately after the last balloon deflation and the subsequent nitrate injection. These 2 images should be analyzed in the same angiographic projection selected to minimize foreshortening.

### ABBREVIATIONS AND ACRONYMS

- BRS** = bioresorbable scaffolds
- FF** = fibrofatty
- FRR** = fractional flow reserve
- ISA** = incomplete scaffold apposition
- IVUS** = intravascular ultrasound
- MLD** = minimal lumen diameter
- MPS** = metallic platform stents
- MSCT** = multislice coronary tomography
- OCT** = optical coherence tomography
- QCA** = quantitative coronary angiography
- VH** = virtual histology

**TABLE 1** Bioresorbable Scaffolds: Materials and Current Development

Company	Product	Material	Development	Pre-Clinical	Clinical	Post-Clinical
Abbott Laboratories	Absorb	PLLA/PDLLA	✓	✓	✓	✓
Elixir	DESolve	PLLA/PDLLA	✓	✓	✓	✓
Meril	MeRes	PLLA	✓	✓	✓	
Amaranth Medical	FORTITUDE	PLLA	✓	✓	✓	
ART/Terumo	ART18Z	PDLLA	✓	✓	✓	
Biotronik	DREAMS	Magnesium + PLLA	✓	✓	✓	
Huaan	XINSORB	PLA/PCL/PGA	✓	✓	✓	
Kyoto Medical	IGAKI-TAMAI	PLLA	✓	✓	✓	
Xenogenics	Ideal BioStent	Polyanhydride (ASA/adipic acid anhydride)	✓	✓	✓	
Arterius	ReBioStent	Bioresorbable polymer	✓	✓		
Cardionovum	ReNATURAL	Metal	✓	✓		
Medtronic	Mg Spiral	Magnesium	✓	✓		
OrbusNeich	On-AVS	PLLA/PDLA/TMC/eCAP	✓	✓		
Reva	Fantom	Tyrosine polycarbonate	✓	✓		
S3V	Avatar	Not available	✓	✓		
Zorion Medical	ZMED	Magnesium + polymer	✓	✓		
LifeTech	Lifetech Iron Stent	Iron	✓	✓		
Boston Scientific	BSC BRS	Magnesium	✓	✓		
Sahajanand	Sahajanand BRS	PLLA?	✓			

ASA = salicylic acid; BRS = bioresorbable scaffolds; PCL = polycaprolactone; PDLA = poly-D-lactide; PDLLA = poly(L-lactide-co-D,L-lactide); PGA = polyglycolic acid; PLA = poly(lactic acid); PLLA = poly-L-lactide; TMC = trimethylene carbonate.

**TABLE 2 Mechanical Properties and Degradation Rate of Different Material Candidates for Bioresorbable Coronary Scaffolds**

Material	Tensile Strength, MPa	Elongation, %	Degradation Time
Poly(L-lactide)	60-70	2-6	24 months*
Poly(DL-lactide)	45-55	2-6	12-16 months*
Poly(glycolide)	90-110	1-2	6-12 months*
50/50 DL-lactide/glycolide	40-50	1-4	1-2 months*
82/18 L-lactide/glycolide	60-70	2-6	12-18 months*
70/30L-lactide/ $\epsilon$ -prolactone	18-22	>100	12-24 months*
Pure Fe	200	40	0.19 mm/year
Fe-35Mn alloy	430	30	0.44 mm/year
WE43 alloy	280	2	1.35 mm/year

\*Degradation time depends on geometry (44,45).  
MPa = megapascals.

Acute stent/scaffold recoil is calculated as follows.

- When a stent/scaffold delivery balloon was used for stent/scaffold expansion, acute absolute stent/scaffold recoil is defined as the difference between the mean diameter of the stent/scaffold delivery balloon at the highest pressure at implantation of stent/scaffold (X) and mean luminal diameter of stented/scaffolded segment after implantation (Y). Absolute acute stent/scaffold recoil is calculated as  $X - Y$ , whereas relative acute stent/scaffold recoil is defined as  $(X - Y)/X$  and is expressed as a percentage.
- When a post-dilation balloon was used in the procedure, acute absolute recoil is defined as the difference between the mean diameter of the post-dilation balloon at the highest pressure in the post-dilated segment ( $X_o$ ) and mean luminal diameter after post-dilation ( $Y_o$ ). Relative acute recoil is defined as  $(X_o - Y_o)/X_o$  and is expressed as a percentage.

The same methodology was used throughout the ABSORB Cohort A and Cohort B trials. The absolute acute recoil in Absorb BVS 1.1 (Abbott Laboratories, Abbott Park, Illinois) was  $0.19 \pm 0.18$  mm ( $6.7 \pm 6.4\%$ ), which was not statistically different than that in BVS 1.0 ( $0.20 \pm 0.21$  mm;  $6.9 \pm 7.0\%$ ) or the metallic everolimus-eluting stent ( $0.13 \pm 0.21$  mm;  $4.3 \pm 7.1\%$ ). In multivariable models of the 3 pooled populations, the balloon/artery ratio was an independent predictor of acute recoil, whereas the type of device (scaffold or stent) was not (3). The DESolve Nx BRS (Elixir Medical, Sunnyvale, California) and the ART stent (ART,

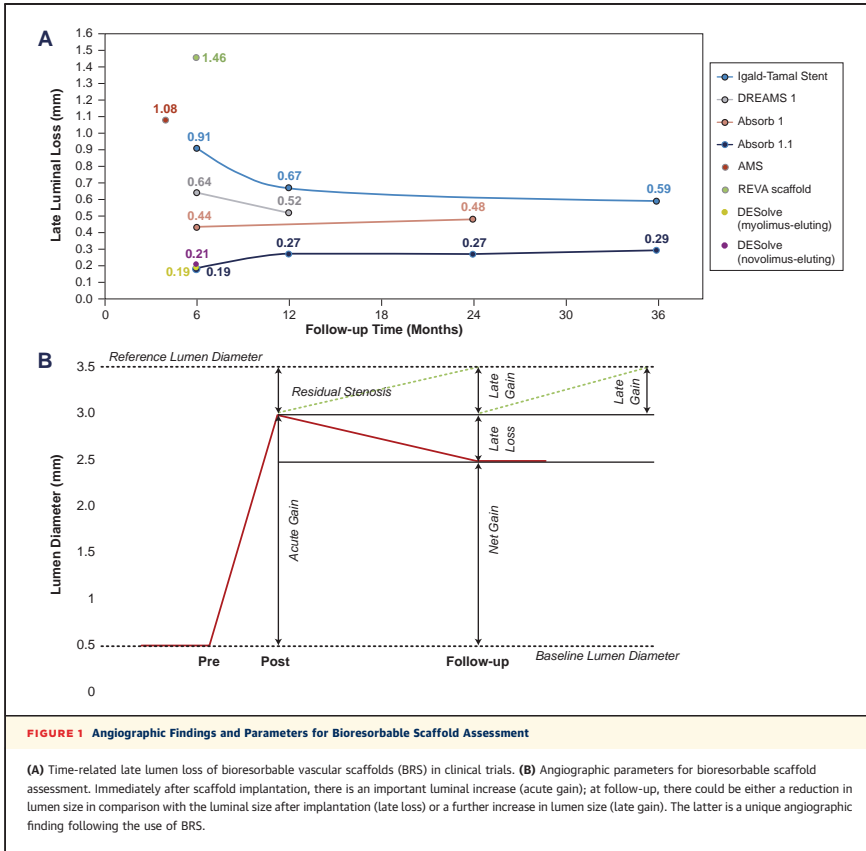
Noisy le Roi, France) have acute recoils of  $6.4 \pm 4.6\%$  (4) and  $4.0\%$  (data on file, ART), respectively.

**CONFORMABILITY.** Coronary geometry changes after stenting might result in wall shear stress changes and adverse events. These changes in 3-dimensional (3D) vessel geometry are associated with decreased and increased shear stress zones close to the stent edges. These changes were found to be related to the asymmetrical patterns of in-stent restenosis (5). Angiographically, the geometric changes can be assessed by measuring the curvature and angulation. “Curvature” is defined as the infinitesimal rate of change in the tangent vector at each point of the center line. This measurement has a reciprocal relationship with the radius of the perfect circle defined by the curve at each point. The curvature value is calculated as  $1/\text{radius}$  of the circle in  $\text{cm}^{-1}$  (6). “Angulation” is defined as the angle in degrees that the tip of an intracoronary guidewire would need to reach the distal part of a coronary bend (Figure 3) (6).

For the Absorb scaffold, from post-implantation to follow-up, curvature increased by  $8.4\%$  ( $p < 0.01$ ) with BRS and decreased  $1.9\%$  ( $p = 0.54$ ) with the metallic platform stents (MPS) ( $p = 0.01$ ). Angulation increased  $11.3\%$  with BRS ( $p < 0.01$ ) and  $3.8\%$  with MPS ( $p = 0.01$ );  $p < 0.01$ . From pre-implantation to follow-up, the artery curvature decreased  $3.4\%$  with BRS ( $p = 0.05$ ) and the artery angulation decreased  $3.9\%$  ( $p = 0.16$ ), whereas MPS presented with  $26.1\%$  decrease in curvature ( $p < 0.01$ ) and  $26.9\%$  decrease in angulation ( $p < 0.01$ ) (both  $p < 0.01$  for the comparison between BRS and MPS) (7). For drug-eluting absorbable magnesium scaffolds (DREAMS), the vessel curvature decreased  $40.5\%$  post-implantation ( $p < 0.01$ ), but the difference between baseline and 12-month follow-up was reduced to  $7.4\%$  ( $p = 0.03$ ) (8). This means that the BRS tended to restore the coronary configuration and systolodiastolic movements to those seen before implantation, whereas the coronary geometry remained similar to that seen after implantation with MPS.

**VASOMOTION.** Vasomotor testing, using nitroglycerin, methylergometrine (endothelium-independent vasoconstrictor), and acetylcholine (Ach) (endothelium-dependent vasoactive agent), can be performed at various time points.

Vasomotion of the scaffolded segment following intraluminal administration of Ach suggests that: 1) the scaffolding function of the struts has completely disappeared and the so-called scaffolded segment can now exhibit vasomotion; 2) the endothelial lining (coverage) is coalescent; 3) the ciliary function of the endothelial cell is functional; and



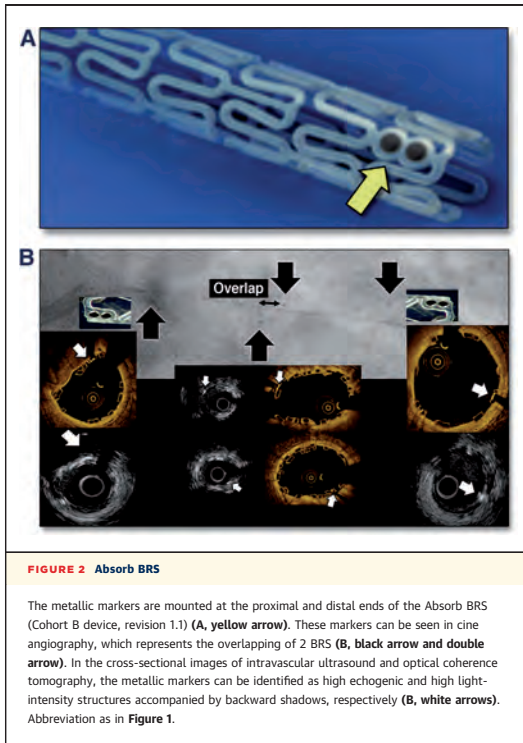
4) the biochemical process through which nitric oxide is released properly works. A positive Ach test with vasodilation of the scaffold is indirect proof that the endothelium is functional (9).

Mean lumen diameters in the scaffolded proximal and distal segments are measured by QCA after a baseline infusion of saline and subselective intracoronary administration of Ach, infused through a microcatheter at increasing doses up to a maximum of  $10^{-6}$  M. In particular, a 2-min selective infusion of Ach ( $10^{-8}$ ,  $10^{-7}$ , and  $10^{-6}$  mol/l) is administered with a washout period of at least 5 min between each dose (10). Nitrate (200  $\mu$ g) is administered following Ach. Vasoconstriction to Ach is defined as

a 3% change in the mean lumen diameter, beyond the variability of the method of analysis, after infusion of the maximal dose of Ach ( $10^{-6}$  M), as previously shown.

In the Absorb scaffold, patients at 24 months (n = 8) exhibited, on average, a significant increase in the mean lumen diameter after Ach administration compared with patients at 12 months [+6.16 (-1.07, +13.14) vs. -6.41% (-11.74, -1.17); p = 0.006] (11).

The timing of restored vasomotion after BRS is also a surrogate for loss of structural integrity of the device and an indication when the vessel may respond to normal and exercise-induced changes in coronary blood flow and pressure. For the Absorb scaffold, the



time seems to be 12 months; for the DREAMS scaffold, the time seems to be 6 months (8).

#### NONINVASIVE QCA BY MSCT

Unlike any other metallic prosthesis, polymeric BRS allow in-scaffold assessment of the coronary lumen because the struts are radiolucent; the exception is BRS made of tyrosine polycarbonate and iron, which are radiopaque. Similarly to coronary angiography, the only recognizable structures are the metallic markers at both ends of the devices (Figure 4). BRS technologies use radiopaque markers that are made of platinum, gold, or tantalum. These materials should not interfere with angiographic assessments.

**LATE LOSS/LATE LUMINAL GAIN.** As mentioned previously, MSCT provides QCA-like parameters, and the same definitions are used.

**CONFORMABILITY.** In MSCT, the center line of the vessels can be precisely determined and both curvature and angulation can be easily computed (Figure 5). We compute the radius of the circumscribed circle through 3 sequential center-line coordinates. The curvature at  $P_i$  is defined as the inverse of the radius of the circumscribed circle around the 3 coordinates ( $P_a$ ,  $P_i$ , and  $P_b$ ), where  $P_a$  and  $P_b$  are equally distant from  $P_i$  over a 4-mm moving window at 0.1-mm intervals along the coronary center line (12). Different than the curvature measured in a fixed 2D projection in angiography, this curvature assessment in MSCT can be performed in a 3D reconstructed image.

**NONINVASIVE FRACTIONAL FLOW RESERVE.** Computational fluid dynamics, as applied to MSCT images, is a novel method that enables prediction of blood flow and pressure fields in coronary arteries and calculation of lesion-specific fractional flow reserve (FFR) (13-15). The FFR is computed from commonly acquired MSCT scans ( $FFR_{CT}$ ) without any modification of MSCT protocols, additional image acquisition, or administration of medications.

The  $FFR_{CT}$  technology is based on 3 key principles. The first is that coronary supply meets myocardial demand at rest (total resting coronary flow is relative to ventricular mass). The second is that resistance of the microcirculation at rest is inversely but not linearly proportional to the size of the feeding vessel. The third principle is that microcirculation reacts predictably to maximal hyperemic conditions in patients with normal coronary flow. On the basis of these principles, a lumped parameter model representing the resistance to flow during simulated hyperemia is applied to each coronary branch of the segmented MSCT model. The  $FFR_{CT}$  is modeled for conditions of adenosine-induced hyperemia; an  $FFR_{CT} \leq 0.80$  is considered diagnostic of lesion-specific ischemia (Figures 6A and 6B) (16).

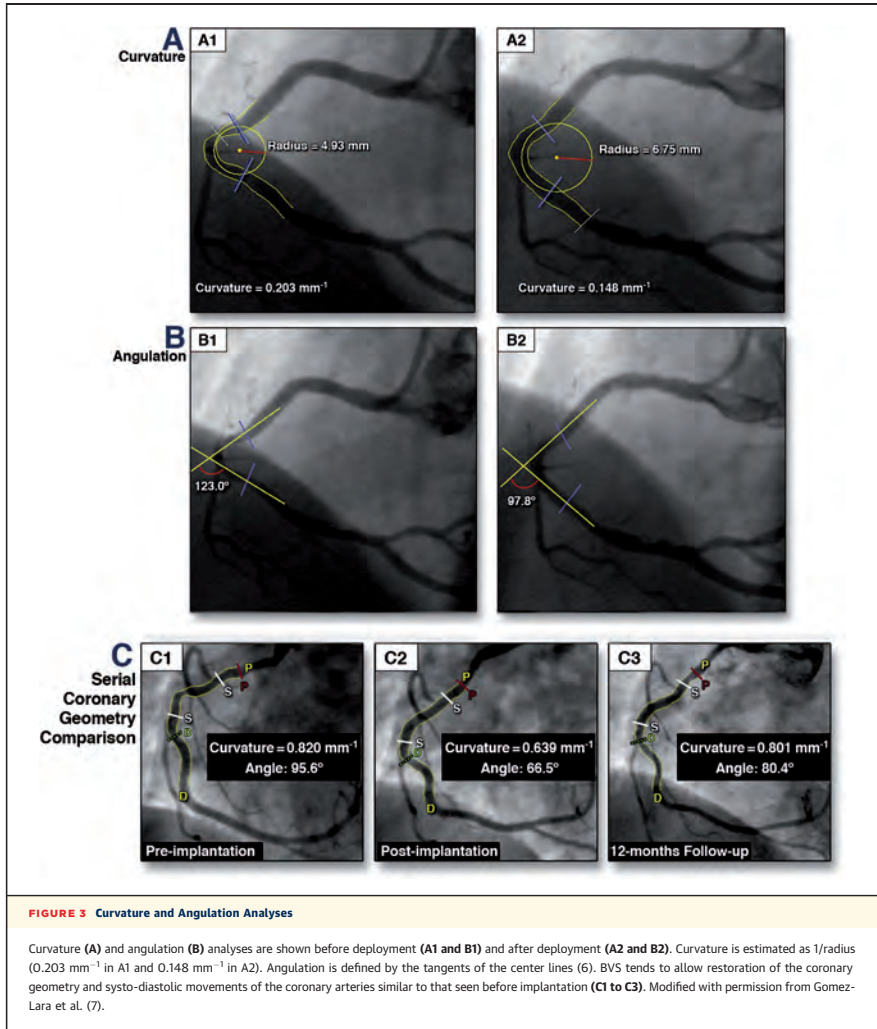
#### GRAY-SCALE INTRAVASCULAR ULTRASOUND

Treated coronary vessels are examined after the procedure and at follow-up with intravascular ultrasound (IVUS) catheters. The scaffolded segment and its 5-mm distal and proximal segments are also examined. The vessel area, scaffold area, lumen area, intrascaffold neointimal area, and luminal area stenosis are measured with a computer-based contour detection program.

**PERCENTAGE OF LUMEN AREA STENOSIS.** The percentage of lumen area stenosis is calculated as

TABLE 3 Definitions and Formulas of Parameters for Assessment of BRS			
Parameter	Imaging Modality	Formula	Definition and Notes
Late loss/late luminal gain	Angiography (QCA)/MSCT	MLD (post-procedure) - MLD (follow-up)	For a lumen diameter reduction, this will be a positive number; for a late increase in lumen size, this will be a negative number
Acute recoil	Angiography (QCA)/MSCT	1. Without post-dilation: mean diameter (delivery balloon at the highest pressure) - mean luminal diameter (after implantation) 2. With post-dilation: mean diameter (post-dilation balloon at the highest pressure) - mean luminal diameter (after post-dilation)	Two specific views need to be analyzed: one is an image of complete expansion of the last balloon (either the device delivery balloon or the post-dilation balloon) at the highest pressure and the other is a cine frame immediately after the last balloon deflation and subsequent nitrate injection; these 2 images are analyzed in the same angiographic projection selected to minimize foreshortening
Curvature	Angiography (QCA)/MSCT	$1/\rho$ (cm <sup>-1</sup> )	Defined as the infinitesimal rate of change in the tangent vector at each point of the center line; this measurement has a reciprocal relationship with the radius of the perfect circle defined by the curve at each point
Angulation	Angiography (QCA)/MSCT		Defined as the angle in degrees that the tip of an intracoronary guidewire would need to reach the distal part of a coronary bend
Vasomotion	Angiography (QCA)	1. Vasoconstriction: $\Delta$ mean lumen diameter (post-pre) $\leq -3\%$ 2. Vasodilation: $\Delta$ mean lumen diameter (post-pre) $\geq 3\%$	Vasoconstriction/vasodilation are defined as at least 3% change in the mean lumen diameter after infusion of the maximal dose of Ach/ nitrates, respectively
Noninvasive fractional flow reserve (FFR <sub>CT</sub> )	MSCT		Computed by a dedicated program; FFR <sub>CT</sub> was modeled after conditions of adenosine-induced hyperemia; FFR <sub>CT</sub> $\leq 0.80$ is considered diagnostic of lesion-specific ischemia
Lumen area stenosis	Gray-scale IVUS/OCT	$(\text{Mean lumen area} - \text{minimum lumen area}) / \text{mean lumen area} \times 100$	
Eccentricity index	Gray-scale IVUS/OCT	Minimum scaffold diameter/maximum scaffold diameter in a frame	The average of all eccentricity indexes of each frame within a scaffolded segment is calculated
Symmetry index	Gray-scale IVUS/OCT	$(\text{Minimum scaffold diameter} - \text{maximum scaffold diameter}) / \text{maximum scaffold diameter}$ within a scaffolded segment	The maximum and the minimum stent/scaffold diameters in this calculation are possibly located in 2 different frames over the length of the device implanted
Neointima hyperplasia area	Gray-scale IVUS	Scaffold area - lumen area	Applicable in frames where all struts are apposed
Percentage area obstruction	Gray-scale IVUS	Neointima hyperplasia area/scaffold area $\times 100$	
Late recoil	Gray-scale IVUS/OCT	Scaffold area at post-procedure - scaffold area at follow-up	
Incomplete apposition/late incomplete apposition	Gray-scale IVUS/OCT		Defined as 1 or more scaffold struts separated from the vessel wall; acquired late incomplete apposition is defined as incomplete apposition at follow-up that is not present after the procedure
Compositional area	Virtual histology		Necrotic core, dense calcium, fibrofatty, and fibrous areas are analyzed; polymeric struts are usually recognized as dense calcium
Compositional area	iMap		Fibrotic, lipidic, necrotic, and calcified tissues are analyzed
Compositional area	IB-IVUS		Lipid, fibrous, dense fibrous, and calcified tissues are analyzed
Strain value	Palpography		Radiofrequency data obtained at different pressure levels are compared to determine local tissue deformation; strain value is normalized to a pressure difference of 2.5 mm Hg per frame, which allows the construction of a "strain" image in which hard (low strain/compliance) and soft (high strain/compliance) values range between 0% and 2%
Scaffold area	OCT		At baseline, the scaffold area is measured by joining the middle point of the black core abluminal side of the apposed struts or the abluminal edge of the frame borders of malapposed struts; at follow-up, the back (abluminal) side of the central black core has been used to delimit the scaffold area
Blood flow area	OCT	$(\text{Scaffold area} + \text{ISA area}) - (\text{intraluminal strut areas} + \text{prolapse area} + \text{intraluminal defect})$	
Neointimal hyperplasia area	OCT	1. When all struts are apposed: scaffold area - (lumen area + black box area) 2. When malapposed struts: (scaffold area + ISA area + malapposed strut with surrounding tissues) - (lumen area + strut area)	Note the difference in methodology versus that of gray-scale IVUS
Thickness of tissue coverage	OCT	Distance between the abluminal site of the strut and the lumen - strut thickness	

Ach = acetylcholine; ISA = incomplete stent apposition; IB = integrated backscattered; IVUS = intravascular ultrasound; MLD = minimal lumen diameter; MSCT = multislice coronary tomography; OCT = optical coherence tomography; QCA = quantitative coronary angiography; other abbreviation as in Table 1.



100 times the mean lumen cross-sectional area minus the minimal lumen area divided by the mean lumen cross-sectional area within the scaffolded segment.

**ECCENTRICITY AND SYMMETRY.** The eccentricity and symmetry, easily detectable by IVUS, have

previously been demonstrated to be related to either favorable or adverse clinical outcomes (17,18). With the transition from a metallic stent to a polymeric bioresorbable platform, re-evaluation of these geometric parameters is required at short- and long-term follow-ups.

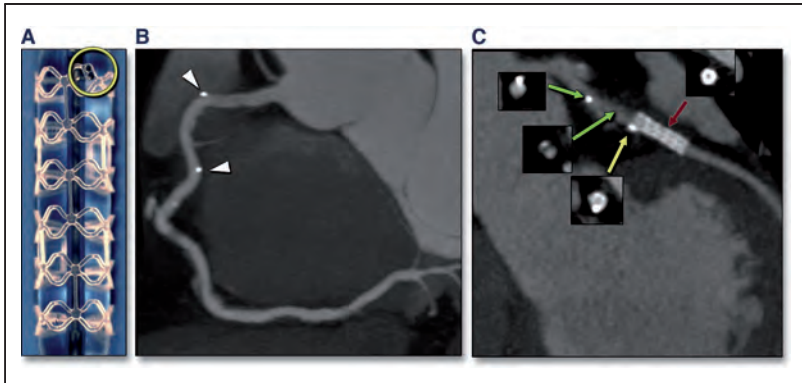


**FIGURE 4** Multislice Coronary Tomography

Multislice coronary tomography (MSCT) shows the radio-opaque markers visible in the scaffolded vessel (A). The radio-opaque markers appear much larger (arrows) than the actual size because of an artefact (i.e., blooming effect) due to partial volume averaging which is typical of highly radio-opaque objects that are imaged by MSCT (B). (C) shows a comparison of lumen assessment by MSCT for a bioresorbable scaffold (green arrows), an overlap scaffold-metallic stent (yellow arrow), and a metallic stent (red arrow).

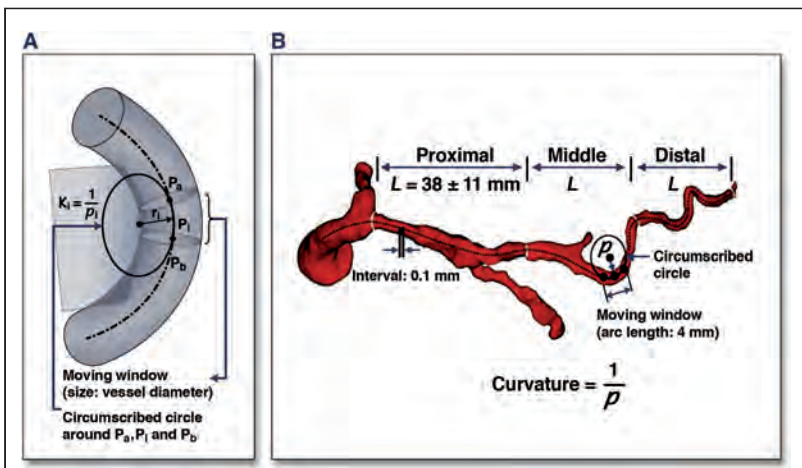
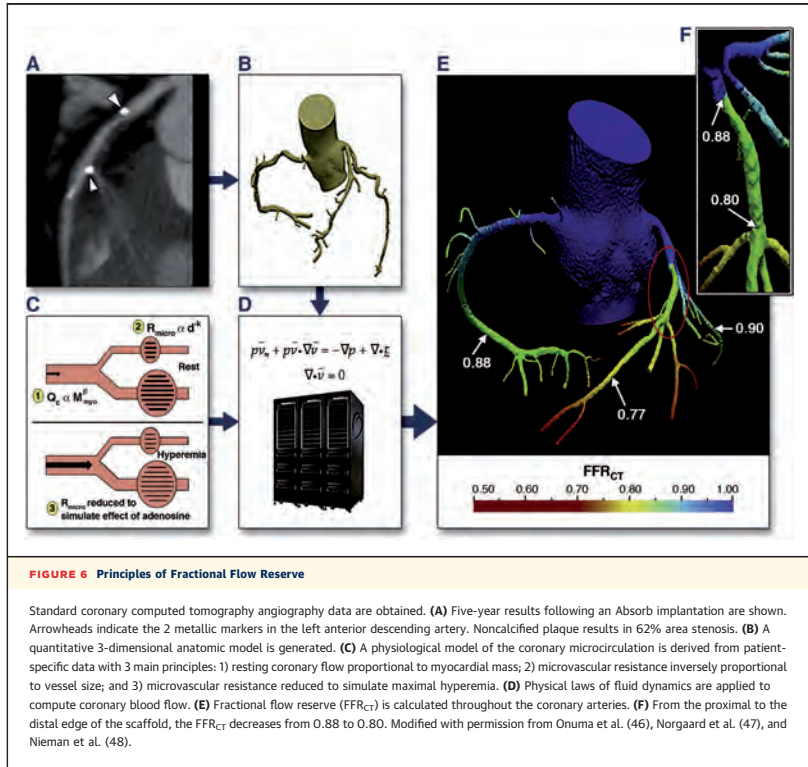


**FIGURE 5** Curvature

(A) Method to calculate vessel curvature. A window size of the vessel diameter was moved down along the center-line path incrementally to identify 3 adjacent points on the center-line path for the curvature calculation. In MSCT, curvature is computed as the inverse of the radius of a circumscribed circle over a 4-mm moving window at 0.1-mm intervals along the left anterior descending artery center line (B). Modified with permission from Choi et al. (12).



Eccentricity index is defined as the ratio of the minimum and maximum diameters in each frame; thereafter, the average of all eccentricity indexes is calculated. Symmetry index is calculated as (maximum stent/scaffold diameter in a single frame – minimum stent/scaffold diameter in a single frame) divided by the maximum stent/scaffold diameter. Note that the maximum and minimum stent/scaffold diameters in this calculation are possibly located in 2 different frames over the length of the device implanted (Figure 7).

**NEOINTIMA HYPERPLASIA.** Assessment of the neointima hyperplasia by IVUS is in principle similar to the methodology used for metallic devices. Neointimal hyperplasia area is defined as scaffold area minus lumen area if all struts are apposed. Percentage

volume obstruction is defined as neointima hyperplasia volume divided by scaffold volume.

**LATE RECOIL.** Although “late recoil” has been used frequently in interventional cardiology to describe the constrictive remodeling of the external elastic membrane area, here it relates more specifically to the area reduction of the scaffolded segment, a phenomenon not previously observed in metallic stents. Attributed to the early alteration of the mechanical integrity of the scaffold, this phenomenon can be controlled by polymer processing.

Late absolute stent recoil is defined as stent area at post-procedure (X) – stent area at follow-up (Y). Late percent stent recoil was defined as  $(X - Y)/X \times 100$ .

The assessment of late recoil helped to clarify the reasons for the suboptimal performance of the

first-generation magnesium scaffold. For the AMS-1 (Biotronik, Bülach, Switzerland), this parameter was responsible for 42% of luminal obstruction due to its rapid scaffold degradation and led to its design modification (19,20).

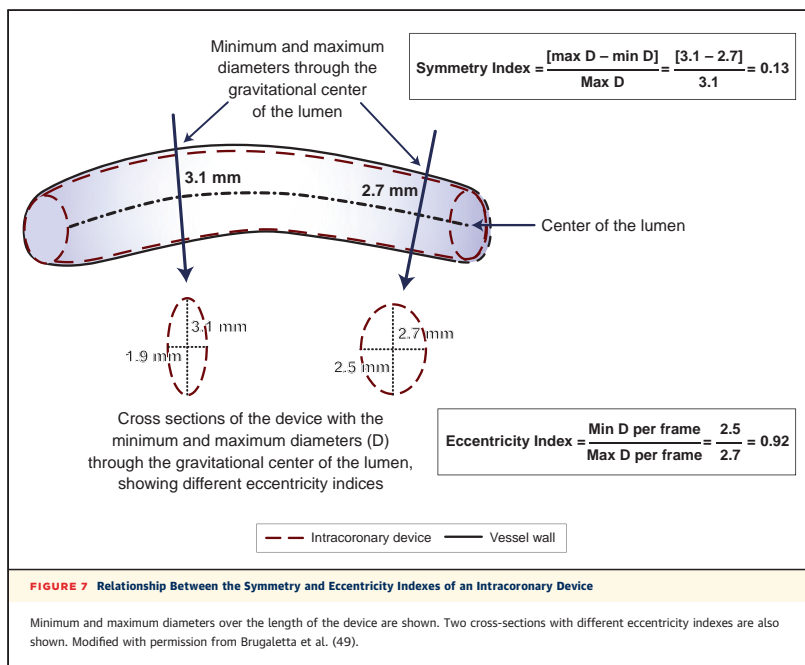
Late absolute and percent recoil of the Absorb BVS 1.0 was  $0.65 \pm 1.71 \text{ mm}^2$  (95% confidence interval:  $0.49$  to  $0.80 \text{ mm}^2$ ) and  $7.60 \pm 23.3\%$  (95% confidence interval:  $5.52\%$  to  $9.68\%$ ) (21). With the newer iteration of the device, BVS 1.1, the mean scaffold area increased from baseline to 3 years by IVUS ( $6.3$  to  $7.1 \text{ mm}^2$ ) and by optical coherence tomography (OCT) ( $7.8$  to  $8.6 \text{ mm}^2$ ) (22). Similarly, the DESolve Nx BRS showed an increase in mean scaffold area by IVUS ( $5.4$  to  $5.6 \text{ mm}^2$ ) and OCT ( $6.6$  to  $6.8 \text{ mm}^2$ ) (4).

**INCOMPLETE APPPOSITION.** Incomplete apposition is defined as 1 or more scaffold struts separated from the vessel wall; acquired late incomplete apposition is defined as incomplete apposition at follow-up that is not present after the procedure.

With BVS 1.1 at baseline, 4 patients showed incomplete stent apposition (ISA). One ISA persisted

at follow-up, and 3 ISAs resolved. At 6 months' follow-up, 3 patients developed a late acquired ISA (23). In the other group followed up to 1 year, at baseline, there were 5 patients with ISA and at follow-up there were only 4 (24). At 2 years, incomplete apposition by IVUS was only observed in 2 patients. At 3 years, 3 patients presented late acquired malapposition (22). The DESolve Nx BRS resulted in only 1 patient with malapposition at 6 months by OCT (4).

**EDGE EFFECTS.** The edge effect was first introduced in the era of endovascular brachytherapy using radioactive stents of various activity levels to describe tissue proliferation at the nonirradiated proximal and distal edges and resulted in the failure of this invasive treatment. The advent of first- and second-generation drug-eluting stents (DES) reduced in-stent restenosis to approximately 5% to 10% depending on the lesion subset and type of DES. When in-segment restenosis (stent and 5-mm proximal and distal margins) occurred, it was most commonly focal and located at the proximal edge.



The ABSORB Cohort B trial enrolled 101 patients and was divided into B1 (n = 45) and B2 (n = 56) subgroups. The adjacent (5-mm) proximal and distal vessel segments to the implanted Absorb BVS were investigated at either 6 months (B1) or 1 year (B2) with intravascular ultrasound-virtual histology (IVUS-VH) imaging.

At the 5-mm proximal edge, the only significant change was modest constrictive remodeling at 6 months (change in vessel cross-sectional area:  $-1.80\%$  [ $-3.18\%$ ;  $1.30\%$ ];  $p < 0.05$ ), with a tendency to regress at 1 year (change in vessel cross-sectional area:  $-1.53\%$  [ $-7.74\%$ ;  $2.48\%$ ];  $p = 0.06$ ). The relative changes in the fibrotic and fibrofatty (FF) tissue areas at this segment were not statistically significant at either time point. At the 5-mm distal edge, a significant increase in the FF tissue areas of  $43.32\%$  ( $-19.90\%$ ;  $244.28\%$ ;  $p < 0.05$ ) 1 year post-implantation was evident. Changes were also observed in dense calcium areas, which need to be interpreted with caution. The polymeric struts are detected as “pseudo” dense calcium structures with the IVUS-VH imaging modality, and the edges of the polymeric scaffold are not sharply demarcated because the vessel surrounding the imaging device are affected by the “to and fro” motion of the cardiac

contraction, causing a longitudinal displacement of the IVUS catheter relative to the arterial wall (25).

#### VIRTUAL HISTOLOGY

Ultrasound backscattered signals are acquired using either a 20-MHz (electronic) or 45-MHz (mechanical) IVUS catheter. Backscattering of radiofrequency signals provides information on vessel wall tissue composition. Four tissue components (necrotic core [red], dense calcium [white], fibrous, [green], and FF [light green]) are identified with autoregressive classification systems and expressed as percentages per cross-section (necrotic core, dense calcium, FF, and fibrous) (26). In each cross-section, polymeric scaffold struts are detected as areas of apparent dense calcium and necrotic core resulting from the strong backscattering properties of the polymer. We use the change in quantitative analyses of these areas between implantation and follow-up as a surrogate assessment of the chemical and structural alterations of the polymeric struts (Figure 8). The recent analysis of the ABSORB Cohort B study showed that the mean dense calcium areas were  $29.84 \text{ mm}^2$  (post-implantation),  $28.16 \text{ mm}^2$  (6 months),  $24.25 \text{ mm}^2$  (1 year),  $27.74 \text{ mm}^2$  (2 years), and  $21.52 \text{ mm}^2$  (3-year

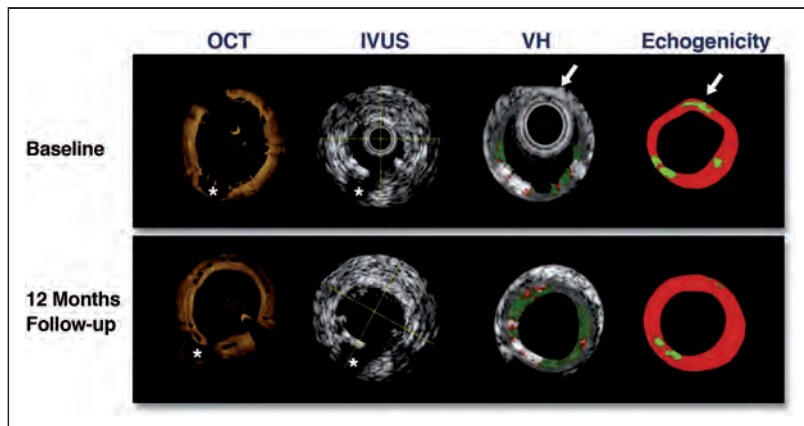


**FIGURE 8** Comparison Between Imaging Techniques in Detecting the Degradation Parameters in Matched Frames

After implantation, the polymeric struts are seen as open boxes in optical coherence tomography (OCT), whereas they are white structures in gray-scale intravascular ultrasound (IVUS) (at 4 and 7 to 8 o'clock). The color-coded virtual histology (VH) image depicts them in white (dense calcium), whereas echogenicity shows them in green (hyperechogenic). Note that at follow-up, OCT shows all struts integrated (covered with tissue) into the vessel wall. Gray-scale IVUS shows that the strut at 4 o'clock is less apparent, whereas the corresponding ones in VH and echogenicity are also not detected. These latter observations reflect some biodegradation.

follow-up). The average necrotic core areas, at the same aforementioned time points, were 31.31 mm<sup>2</sup>, 30.11 mm<sup>2</sup>, 30 mm<sup>2</sup>, 31.67 mm<sup>2</sup>, and 26.49 mm<sup>2</sup>, respectively. The sharp decrease in dense calcium and necrotic core areas between 24 and 36 months may also reflect the end of the inflammatory process, with regression of the plaque behind the struts (22).

In addition, the other critical observation with IVUS between the 6-month and 2-year follow-ups was a late luminal enlargement (10.9%) with significant plaque media reduction (12.7%) and without significant change in the vessel wall area (27). It is still unknown whether this “plaque media regression” on IVUS is a true atherosclerotic regression, with change in vessel wall composition and plaque morphology (from thin-cap atheroma to thick-cap atheroma) or a pseudo-regression due to bioabsorption of the polymeric struts. True atherosclerotic regression could only be hypothesized based on animal and in vitro experiments showing that mammalian target of rapamycin can trigger a complex chain of biological reactions that lead finally to activation of genes related to autophagy of macrophages. Systemic application of everolimus decreased atherosclerotic plaque formation in low-density lipoprotein receptor knockout mice (28).

#### IMAP

Ultrasound backscattered signals are acquired using a 40-MHz mechanically rotating IVUS catheter. iMap is another radiofrequency-based processing method for coronary plaque tissue characterization (29). iMap uses a pattern recognition algorithm on the spectra that were obtained from a fast Fourier transformation and a histology-derived database (29). The color code for tissue types is different than that for IVUS-VH. iMap depicts fibrotic (light green), lipidic (yellow), necrotic (pink), and calcified (blue) tissues, whereas IVUS-VH depicts fibrous (green), FF (yellow-green), necrotic core (red), and dense calcium (white) tissues (30). Although iMap has been validated for characterization of stents/scaffolds, we have observed that it detects polymeric struts as calcified tissue (Figure 9); however, it misses some of the polymeric struts, which makes this technology not suitable to serially follow the absorption process of these polymeric scaffolds.

#### INTEGRATED BACKSCATTERED IVUS

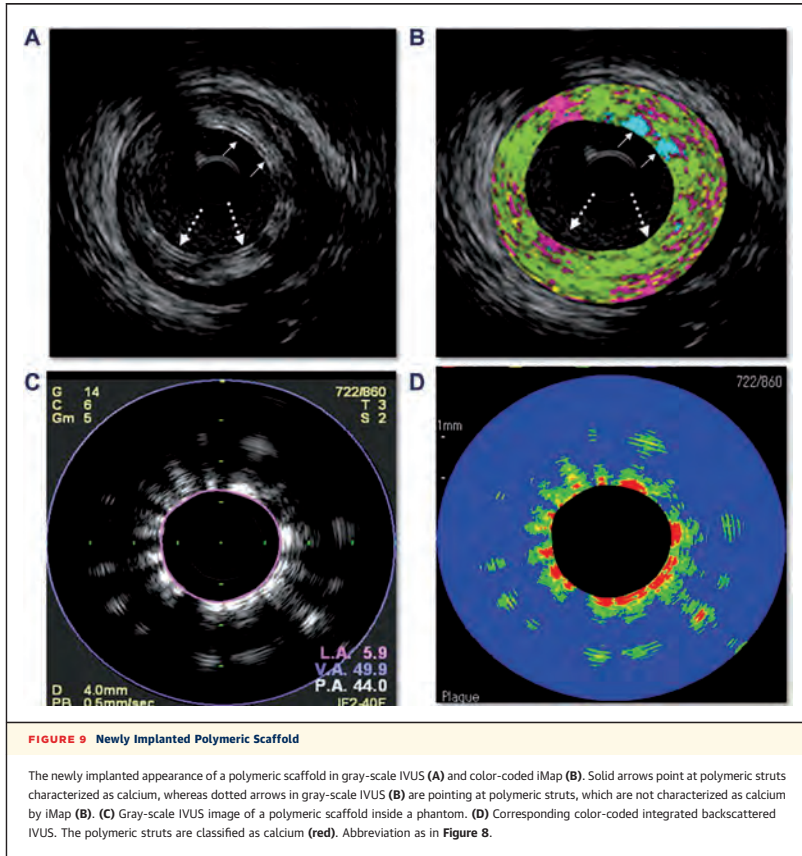
Ultrasound backscattered signals are acquired using a 40-MHz mechanically rotating IVUS catheter. Integrated backscattered values for each tissue

component were calculated as an average power using a fast Fourier transformation, measured in decibels, of the frequency component of the back-scattered signal from a small volume of tissue. With predefined ranges of integrated backscattered values, each plaque component is characterized as lipid (blue), fibrous (green), dense fibrous (yellow), or calcified (red) tissue (Figure 9) (31,32).

#### PALPOGRAPHY

Percutaneous implantation of metallic prostheses has been used to alleviate flow-limiting lesions by overstretching the plaque and the underlying vessel wall. From a mechanical perspective, this treatment may locally stiffen the artery, reducing its compliance and creating a mismatch in compliance with respect to the segments contiguous to the implanted device (5). This mismatch may eventually provoke flow disturbances and wall shear stress alterations, with subsequent blood stasis. The wall shear stress distribution in a stented artery has been reported as a determinant factor for cellular growth and thrombus formation. The Absorb everolimus-eluting BVS theoretically has many advantages compared with rigid metallic stents. In particular, because the scaffold is made completely of polylactide, it does not have the same stiffness as metal, thereby having the potential to overcome in part the problems related to local stiffening of the artery and compliance mismatch associated with MPS. In addition, the mismatch in compliance after scaffold implantation may potentially disappear in the long term once the scaffold is completely bioabsorbed.

IVUS palpography is a technique that allows for the assessment of local mechanical tissue properties. The underlying principle is that at defined pressure, differences in soft-tissue (e.g., lipid-rich) components deform more than hard-tissue components (e.g., fibrous calcified) (33). In coronary arteries, the tissue of interest is the vessel wall, whereas the blood pressure, with its physiological changes during the heart cycle, is used as the excitation force. Radiofrequency data obtained at different pressure levels are compared to determine local tissue deformation. The strain value is normalized to a pressure difference of 2.5 mm Hg per frame; this allows the construction of a “strain” image in which hard (low strain/compliance) and soft (high strain/compliance) values range between 0% and 2%. In post-mortem coronary arteries, the sensitivity and specificity of palpography to detect high strain values have previously been reported as 88% and 89%, respectively (34).



Local strain is calculated from the gated radio-frequency traces using cross-correlation analyses, displayed and color-coded from blue (for 0% strain) to yellow (for 2% strain) via red, as previously described.

Strain values were assigned a Rotterdam classification (ROC) score ranging from I to IV (ROC I 0 to 0.5%; ROC II 0.6% to <0.9%; ROC III 0.9% to 1.2%; and ROC IV >1.2%). A region was defined as a high-strain spot when it had high strain (ROC III to IV) that spanned an arc of at least 12° at the surface of a plaque (identified on the IVUS recording) adjacent to low-strain regions (<0.5%), as previously reported (33). The highest value of strain in the cross-section

was taken as the strain level of the spot. The compliance of each segment is calculated per segment (proximal edge, scaffold segment, and distal edge) and defined as the mean of the maximum strain values per cross-section in ROC I/II/III/IV spots, expressed as ROC/mm.

#### ECHOGENICITY

Echogenicity uses the gray-scale IVUS data to further evaluate the distribution of the gray values within a specific coronary segment. The mean gray value of the adventitia is used to classify tissue components as either hypoechoic or

hyperechogenic (Figure 8). The adventitia surrounding the coronary artery is defined as a layer extending from 0.2 to 0.5 mm outside the external elastic membrane. To avoid artifacts, tissue within acoustic shadowed areas is excluded and very high gray-level pixels are identified as upper tissue. After the tissue identification process, the relative fraction of hypoechogenic versus hyperechogenic tissue volumes is calculated for the entire scaffolded segment. The software calculates the echogenicity as a volume and percentage for each scaffolded segment (setting hypoechogenicity and hyperechogenicity to 100%). The percent differential echogenicity was calculated for each scaffolded coronary segment, as follows (35,36).

$$\% \text{DifferentialEchogenicity} = \frac{(\% \text{Hyper6M} - \% \text{HyperPre}) - (\% \text{HyperPost} - \% \text{HyperPre})}{(\% \text{HyperPost} - \% \text{HyperPre})} \cdot 100\%$$

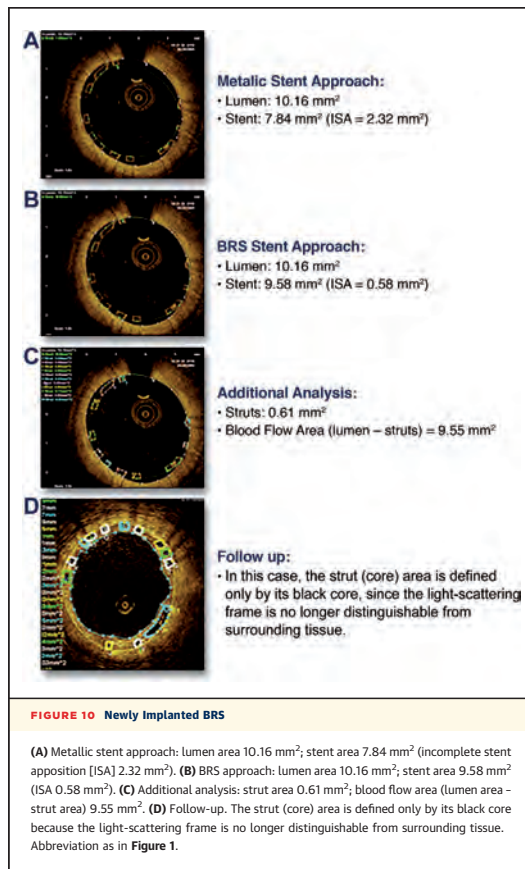
Echogenicity parameters have been shown to be able to detect temporal changes in the gray-level intensities for Absorb and DREAMS, being putatively correlated to scaffold degradation over time (8,35).

#### OPTICAL COHERENCE TOMOGRAPHY

The BVS presents important differences with respect to metallic stents when imaged by OCT. The optically translucent polymeric struts appear as black central cores framed by light-scattering borders that do not shadow the vessel wall and allow complete imaging of the strut thickness. The main quantitative measurements (strut core area, strut area, lumen area, scaffold area, ISA area, and neointimal area) require different analysis rules than the metallic stents (Figure 10).

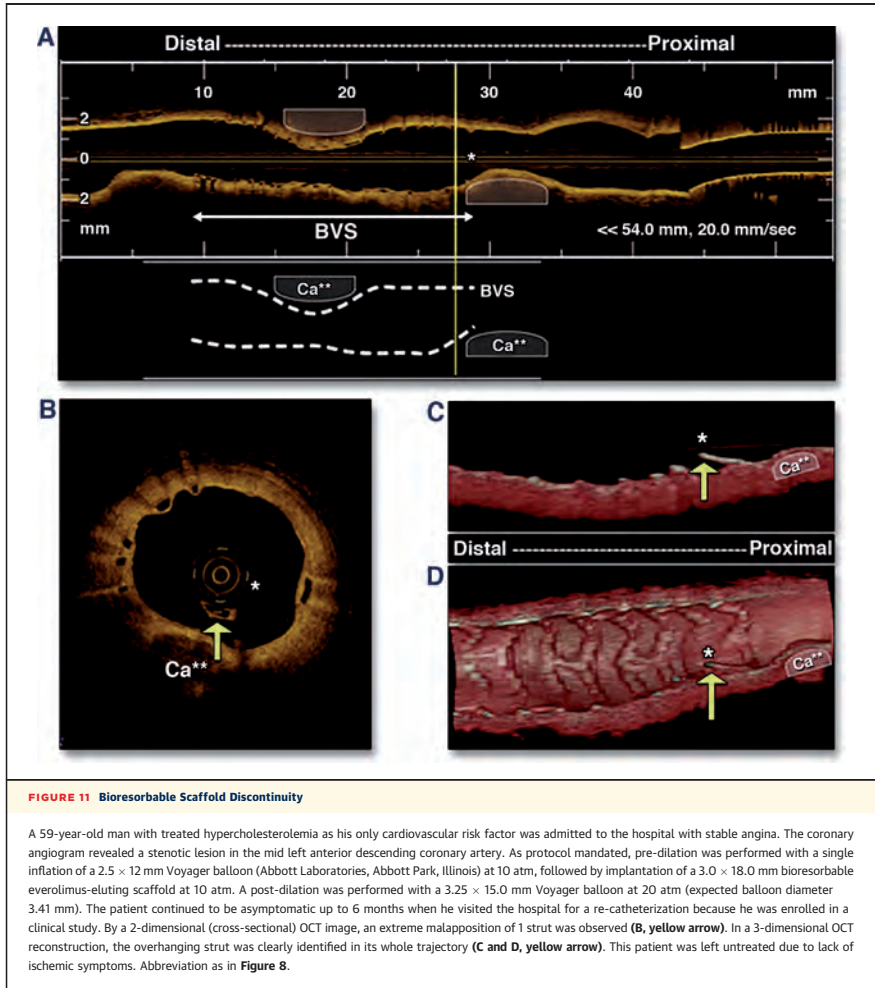
Qualitatively, the diagnosis of acute strut fracture resulting from balloon overdistension or late structural strut discontinuity can be established if 2 struts overhang each other in the same angular sector of the lumen perimeter, with or without malapposition, or if isolated struts are located more or less at the center of the vessel without obvious connection to other surrounding struts in 2D OCT. For confirmation of the diagnosis, it is helpful to perform 3D OCT reconstruction of the disrupted strut. A case description of strut fracture is shown in Figure 11.

At baseline, the strut area is imaged as a central black core and a light-scattering frame border. However, at follow-up, embedding, coverage, and thickening of the frame borders, with apparent reduction of the central core, render the analysis of the struts



more complex. At this time point, the strut (core) area is defined only by its black core because the light-scattering frame is no longer distinguishable from surrounding tissue. At follow-up, the strut area starts to gain some tissue filling that can be seen as “white core” (Figure 12).

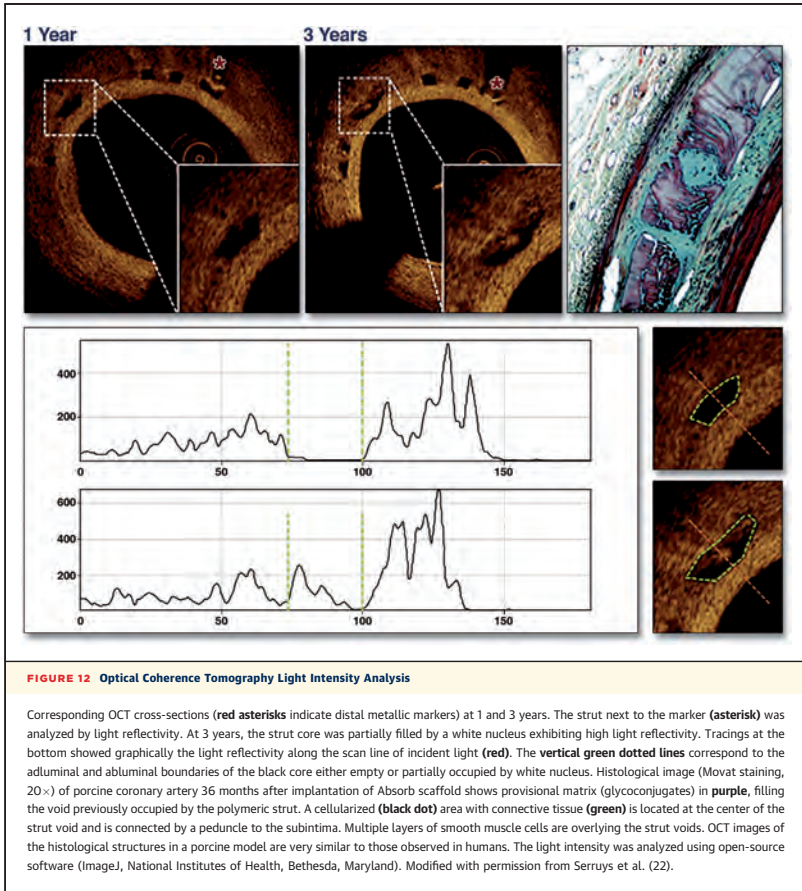
The lumen and scaffold contours are obtained with a semiautomated detection algorithm available in many offline software packages, and additional manual corrections are performed if necessary. At baseline, because the polymeric struts are translucent, the vessel wall lumen area can be imaged and delineated at the back (abluminal) side of the struts. At follow-up, the luminal area is drawn by



semiautomatic detection, following the endoluminal contour of the neointima between and on top of the apposed struts. For malapposed struts, the endoluminal contour of the vessel wall behind the malapposed struts is used.

At baseline, the scaffold area is measured by joining the middle point of the black core abluminal side of the apposed struts or the abluminal edge of

the frame borders of malapposed struts. The scaffold area is identical to the lumen area in the absence of ISA and prolapse. At follow-up, the back (abluminal) side of the central black core is used to delimit the scaffold area. Three different situations deserve special consideration. First, incomplete strut apposition is defined as a clear separation between the back (abluminal) side of the strut and the vessel wall. For



malapposed struts, incomplete strut apposition area is delineated by the abluminal side of the frame border of the malapposed strut (covered or uncovered) and the endoluminal contour of the vessel wall. Second, in prolapse protruding between struts into the lumen at baseline, the prolapse area can be estimated between the prolapsed contour (lumen contour) and the scaffold area. Third, an intraluminal defect free from the vessel wall (e.g., thrombus) is also quantified as an area. According to these findings, the flow area is defined as (scaffold area + ISA area) - (intraluminal strut areas + prolapse area + intraluminal defect).

Neointimal hyperplasia area is defined as (scaffold area - [lumen area + black box area]) if all struts are apposed (Figure 10D), whereas it is calculated as ([scaffold area + ISA area + malapposed strut with surrounding tissues] - [Lumen area + strut area]) for malapposed struts.

The thickness of the coverage is measured in every strut between the abluminal site of the strut core and the lumen. Because the strut thickness is 150  $\mu\text{m}$ , the strut is considered covered whenever the thickness of the coverage is above this threshold value. This method may slightly underestimate the thickness of the coverage because it does not take into account

changes in the size of the strut core over time. Consequently, the percentage of uncovered struts may be slightly overestimated.

This OCT Healing Score is a weighted index that combines the following parameters (37):

1. Presence of intrastent structure (ISS) is assigned a weight of “4.”
2. Presence of both malapposed and uncovered struts (%MU) is assigned a weight of “3.”
3. Presence of uncovered struts alone (%U) is assigned a weight of “2.”
4. Presence of malapposition alone (%M) is assigned a weight of “1.”

$$\text{Neointimal Healing Score} = (\text{ISS} \times 4) + (\%MU \times 3) + (\%U \times 2) + (\%M \times 1)$$

**LESSONS FROM OCT FOR BRS RESORPTION.** OCT may not be sensitive enough to assess the resorption process of the polymer, but it provides critical information on the integration of the polymer into the vessel wall. At the beginning, the absence of strut footprints on OCT was interpreted as a sign of complete bioresorption, but now we know that the preserved box appearance with optical translucency is compatible with complete polymer dissolution (38). The DESolve Nx BRS showed significant reduction in the number of struts with the black box appearance at 6 months (4).

**TWO-DIMENSIONAL VERSUS 3-DIMENSIONAL OCT.** Three-dimensional OCT provides much more useful information at bifurcations and overlapping segments than 2D OCT. Indeed, 3D OCT enables a detailed assessment of both the longitudinal and cross-sectional relationship between the jailed side branches orifice and the overhanging struts (39). Serial 3D OCT also provides information about anatomic modifications such as the presence of neointimal bridges, which usually appear as an extension of the pre-existing carina. From the quantitative point of view, using 3D OCT reconstructed models, one can assess the changes over time in the number of compartments and their geometric areas.

Three-dimensional OCT offers a unique opportunity to observe the modifications of the shape of the struts after side branch dilation.

In the overlapping regions, 2D OCT helps to identify single or stacked struts (inner vs. outer) and stacked strut clusters (Figure 2). Lumen area is drawn in nonoverlapping segments, and the following considerations should be made for the scaffold area: it is drawn from the abluminal side of the black core area

of the outermost strut or stacked strut cluster (where all of the struts appose the vessel endothelium) apposing the vessel wall. Where there does not appear to be any apposition of a single strut or stacked strut cluster to the vessel endothelium, the contour of the scaffold area continues to follow the outermost (most abluminal) scaffold strut or stacked strut cluster. Three-dimensional OCT of overlapping regions also helps us to assess the type of overlapping: interdigitating struts versus complete overlap (40,41).

#### AGREEMENT OF QCA, IVUS, AND OCT FOR ASSESSMENT OF BRS

---

For scaffold length measurement, QCA has shown a typical systematic bias: variable underestimation of length but consistent underestimation of the same magnitude at the index procedure and at follow-up, eventually due to the effect of foreshortening. OCT is the most accurate technique for measuring scaffold length, whereas solid-state IVUS presents a random error, mostly due to lack of smooth and continuous pullback; therefore, volumetric analysis is not reliable. There is poor agreement for minimal lumen area estimation between all of the imaging modalities studied, including IVUS-OCT; hence, their values are not interchangeable (42).

IVUS, due to its limited resolution, is unable to detect incomplete malapposition and struts at side branches compared with OCT. IVUS also has poor reproducibility for the assessment of these 2 variables, whereas OCT has excellent assessment (43).

#### CONCLUSIONS

---

The upcoming bioresorbable era requires new imaging modalities, parameters, and methodologies for the longitudinal assessment of BRS. One of the manifested characteristics of BRS is bioresorption of the polymeric struts into the arterial wall. Although proper validation with VH, echogenicity, and palpography to evaluate this phenomenon has been lacking, other observations with OCT and histology have demonstrated convincing results. We introduced a detailed description of the parameters and methodologies for the assessment of BRS that should be needed in the future longitudinal studies.

**REPRINT REQUESTS AND CORRESPONDENCE:** Dr. Hector M. Garcia-Garcia, Thoraxcenter—Erasmus Medical Center, z120 Dr Molerwaterplein 40, 3015 GD Rotterdam, the Netherlands. E-mail: hect2701@gmail.com OR h.garciagarcia@erasmusmc.nl.

## REFERENCES

- Serruys PW, Garcia-Garcia HM, Onuma Y. From metallic cages to transient bioresorbable scaffolds: change in paradigm of coronary revascularization in the upcoming decade? *Eur Heart J* 2012;33:16-25b.
- Waksman R. Biodegradable stents: they do their job and disappear. *J Invasive Cardiol* 2006;18:70-4.
- Onuma Y, Serruys PW, Gomez J, et al. Comparison of in vivo acute stent recoil between the bioresorbable everolimus-eluting coronary scaffolds (revision 1.0 and 1.1) and the metallic everolimus-eluting stent. *Catheter Cardiovasc Interv* 2011;78:3-12.
- Verheye S, Ormiston JA, Stewart J, et al. A next-generation bioresorbable coronary scaffold system: from bench to first clinical evaluation: 6- and 12-month clinical and multimodality imaging results. *J Am Coll Cardiol Interv* 2014;7:89-99.
- Wentzel JJ, Whelan DM, van der Giessen WJ, et al. Coronary stent implantation changes 3-D vessel geometry and 3-D shear stress distribution. *J Biomech* 2000;33:1287-95.
- Gomez-Lara J, Garcia-Garcia HM, Onuma Y, et al. A comparison of the conformability of everolimus-eluting bioresorbable vascular scaffolds to metal platform coronary stents. *J Am Coll Cardiol Interv* 2010;3:1190-8.
- Gomez-Lara J, Brugaletta S, Farooq V, et al. Angiographic geometric changes of the lumen arterial wall after bioresorbable vascular scaffolds and metallic platform stents at 1-year follow-up. *J Am Coll Cardiol Interv* 2011;4:789-99.
- Waksman R, Prati F, Bruining N, et al. Serial observation of drug-eluting absorbable metal scaffold: multi-imaging modality assessment. *Circ Cardiovasc Interv* 2013;6:644-53.
- Holzmann S. Endothelium-induced relaxation by acetylcholine associated with larger rises in cyclic GMP in coronary arterial strips. *J Cyclic Nucleotide Res* 1982;8:409-19.
- Hofma SH, van der Giessen WJ, van Dalen BM, et al. Indication of long-term endothelial dysfunction after sirolimus-eluting stent implantation. *Eur Heart J* 2006;27:166-70.
- Brugaletta S, Heo JH, Garcia-Garcia HM, et al. Endothelial-dependent vasomotion in a coronary segment treated by ABSORB everolimus-eluting bioresorbable vascular scaffold system is related to plaque composition at the time of bioresorption of the polymer: indirect finding of vascular reparative therapy? *Eur Heart J* 2012;33:1325-33.
- Choi G, Cheng CP, Wilson NM, Taylor CA. Methods for quantifying three-dimensional deformation of arteries due to pulsatile and nonpulsatile forces: implications for the design of stents and stent grafts. *Ann Biomed Eng* 2009;37:14-33.
- Kim HJ, Jansen KE, Taylor CA. Incorporating autoregulatory mechanisms of the cardiovascular system in three-dimensional finite element models of arterial blood flow. *Ann Biomed Eng* 2010;38:2314-30.
- Kim HJ, Vignon-Clementel IE, Coogan JS, Figueroa CA, Jansen KE, Taylor CA. Patient-specific modeling of blood flow and pressure in human coronary arteries. *Ann Biomed Eng* 2010;38:1995-2009.
- Serruys PW, Girasis C, Papadopoulou SL, Onuma Y. Non-invasive fractional flow reserve: scientific basis, methods and perspectives. *Euro-Intervention* 2012;8:511-9.
- Koo BK, Erglis A, Doh JH, et al. Diagnosis of ischemia-causing coronary stenoses by noninvasive fractional flow reserve computed from coronary computed tomographic angiograms. Results from the prospective multicenter DISCOVER-FLOW (Diagnosis of Ischemia-Causing Stenoses Obtained Via Noninvasive Fractional Flow Reserve) study. *J Am Coll Cardiol* 2011;58:1989-97.
- de Jaegere P, Mudra H, Figulla H, et al. Intravascular ultrasound-guided optimized stent deployment. Immediate and 6 months clinical and angiographic results from the Multicenter Ultrasound Stenting in Coronaries Study (MUSIC Study). *Eur Heart J* 1998;19:1214-23.
- Otake H, Shite J, Ako J, et al. Local determinants of thrombus formation following sirolimus-eluting stent implantation assessed by optical coherence tomography. *J Am Coll Cardiol Interv* 2009;2:459-66.
- Erbel R, Di Mario C, Bartunek J, et al. Temporary scaffolding of coronary arteries with bioabsorbable magnesium stents: a prospective, non-randomised multicentre trial. *Lancet* 2007;369:1869-75.
- Campos CM, Muramatsu T, Iqbal J, et al. Bioresorbable drug-eluting magnesium-alloy scaffold for treatment of coronary artery disease. *Int J Mol Sci* 2013;14:24492-500.
- Tanimoto S, Bruining N, van Domburg RT, et al. Late stent recoil of the bioabsorbable everolimus-eluting coronary stent and its relationship with plaque morphology. *J Am Coll Cardiol* 2008;52:1616-20.
- Serruys PW, Onuma Y, Garcia-Garcia HM, et al. Dynamics of vessel wall changes following the implantation of the Absorb everolimus-eluting bioresorbable vascular scaffold: a multi-imaging modality study at 6, 12, 24 and 36 months. *EuroIntervention* 2014;9:1271-84.
- Serruys PW, Onuma Y, Ormiston JA, et al. Evaluation of the second generation of a bioresorbable everolimus drug-eluting vascular scaffold for treatment of de novo coronary artery stenosis: six-month clinical and imaging outcomes. *Circulation* 2010;122:2301-12.
- Serruys PW, Onuma Y, Dudek D, et al. Evaluation of the second generation of a bioresorbable everolimus-eluting vascular scaffold for the treatment of de novo coronary artery stenosis: 12-month clinical and imaging outcomes. *J Am Coll Cardiol* 2011;58:1578-88.
- Gogas BD, Serruys PW, Diletti R, et al. Vascular response of the segments adjacent to the proximal and distal edges of the ABSORB everolimus-eluting bioresorbable vascular scaffold: 6-month and 1-year follow-up assessment: a virtual histology intravascular ultrasound study from the first-in-man ABSORB Cohort B Trial. *J Am Coll Cardiol Interv* 2012;5:656-65.
- Nair A, Margolis MP, Kuban BD, Vince DG. Automated coronary plaque characterisation with intravascular ultrasound backscatter: ex vivo validation. *EuroIntervention* 2007;3:113-20.
- Ormiston JA, Serruys PW, Onuma Y, et al. First serial assessment at 6 months and 2 years of the second generation of absorb everolimus-eluting bioresorbable vascular scaffold: a multi-imaging modality study. *Circ Cardiovasc Interv* 2012;5:620-32.
- Mueller MA, Beutner F, Teupser D, Ceglarek U, Thery J. Prevention of atherosclerosis by the mTOR inhibitor everolimus in LDLR<sup>-/-</sup> mice despite severe hypercholesterolemia. *Atherosclerosis* 2008;198:39-48.
- Sathyanarayana S, Carlier S, Li W, Thomas L. Characterisation of atherosclerotic plaque by spectral similarity of radiofrequency intravascular ultrasound signals. *EuroIntervention* 2009;5:133-9.
- Garcia-Garcia HM, Gogas BD, Serruys PW, Bruining N. IVUS-based imaging modalities for tissue characterization: similarities and differences. *Int J Cardiovasc Imaging* 2011;27:215-24.
- Okubo M, Kawasaki M, Ishihara Y, et al. Development of integrated backscatter intravascular ultrasound for tissue characterization of coronary plaques. *Ultrasound Med Biol* 2008;34:655-63.
- Okubo M, Kawasaki M, Ishihara Y, et al. Tissue characterization of coronary plaques: comparison of integrated backscatter intravascular ultrasound with virtual histology intravascular ultrasound. *Circ J* 2008;72:1631-9.
- Schaar JA, Regar E, Mastik F, et al. Incidence of high-strain patterns in human coronary arteries: assessment with three-dimensional intravascular palpography and correlation with clinical presentation. *Circulation* 2004;109:2716-9.
- Schaar JA, De Korte CL, Mastik F, et al. Characterizing vulnerable plaque features with intravascular elastography. *Circulation* 2003;108:2636-41.
- Bruining N, de Winter S, Roelandt JR, et al. Monitoring in vivo absorption of a drug-eluting bioabsorbable stent with intravascular ultrasound-derived parameters: a feasibility study. *J Am Coll Cardiol Interv* 2010;3:449-56.
- Bruining N, Verheye S, Knaapen M, et al. Three-dimensional and quantitative analysis of atherosclerotic plaque composition by automated differential echogenicity. *Catheter Cardiovasc Interv* 2007;70:968-78.
- Garcia-Garcia HM, Muramatsu T, Nakatani S, et al. Serial optical frequency domain imaging in STEMI patients: the follow-up report of TROFI study. *Eur Heart J Cardiovasc Imaging* 2014;15:987-95.
- Onuma Y, Serruys PW, Perkins LE, et al. Intracoronary optical coherence tomography and histology at 1 month and 2, 3, and 4 years after

- implantation of everolimus-eluting bioresorbable vascular scaffolds in a porcine coronary artery model: an attempt to decipher the human optical coherence tomography images in the ABSORB trial. *Circulation* 2010;122:2288-300.
39. Okamura T, Onuma Y, Garcia-Garcia HM, et al. 3-Dimensional optical coherence tomography assessment of jailed side branches by bioresorbable vascular scaffolds: a proposal for classification. *J Am Coll Cardiol Interv* 2010;3:836-44.
40. Farooq V, Onuma Y, Radu M, et al. Optical coherence tomography (OCT) of overlapping bioresorbable scaffolds: from benchwork to clinical application. *EuroIntervention* 2011;7:386-99.
41. Farooq V, Serruys PW, Heo JH, et al. Intracoronary optical coherence tomography and histology of overlapping everolimus-eluting bioresorbable vascular scaffolds in a porcine coronary artery model: the potential implications for clinical practice. *J Am Coll Cardiol Interv* 2013;6:523-32.
42. Gutierrez-Chico JL, Serruys PW, Girasis C, et al. Quantitative multi-modality imaging analysis of a fully bioresorbable stent: a head-to-head comparison between QCA, IVUS and OCT. *Int J Cardiovasc Imaging* 2012;28:467-78.
43. Gomez-Lara J, Brugaletta S, Diletti R, et al. Agreement and reproducibility of gray-scale intravascular ultrasound and optical coherence tomography for the analysis of the bioresorbable vascular scaffold. *Catheter Cardiovasc Interv* 2012;79:890-902.
44. Moravej M, Mantovani D. Biodegradable metals for cardiovascular stent application: interests and new opportunities. *Int J Mol Sci* 2011;12:4250-70.
45. van Alst M, Eenink MJ, Krufft MA, van Tuil R. ABC's of bioabsorption: application of lactide based polymers in fully resorbable cardiovascular stents. *EuroIntervention* 2009;5 Suppl F: F23-7.
46. Onuma Y, Dudek D, Thuesen L, et al. Five-year clinical and functional multislice computed tomography angiographic results after coronary implantation of the fully resorbable polymeric everolimus-eluting scaffold in patients with de novo coronary artery disease: the ABSORB Cohort A trial. *J Am Coll Cardiol Interv* 2013;6:999-1009.
47. Nørgaard BL, Leipsic J, Gaur S, et al. Diagnostic performance of noninvasive fractional flow reserve derived from coronary computed tomography angiography in suspected coronary artery disease: the NXT trial (Analysis of Coronary Blood Flow Using CT Angiography: Next Steps). *J Am Coll Cardiol* 2014;63:1145-55.
48. Nieman K, Serruys PW, Onuma Y, et al. Multislice computed tomography angiography for noninvasive assessment of the 18-month performance of a novel radiolucent bioresorbable vascular scaffolding device: the ABSORB trial (a clinical evaluation of the bioabsorbable everolimus eluting coronary stent system in the treatment of patients with de novo native coronary artery lesions). *J Am Coll Cardiol* 2013;62:1813-4.
49. Brugaletta S, Gomez-Lara J, Diletti R, et al. Comparison of in vivo eccentricity and symmetry indices between metallic stents and bioresorbable vascular scaffolds: insights from the ABSORB and SPIRIT trials. *Catheter Cardiovasc Interv* 2012;79:219-28.

---

**KEY WORDS** bioresorbable scaffolds, coronary, imaging, intravascular ultrasound, multislice computed tomography, optical coherence tomography



## 2.2 Quantitative coronary angiography

Comparison of acute gain and late lumen loss after PCI with bioresorbable vascular scaffolds versus everolimus-eluting stents: an exploratory observational study prior to a randomised trial.

*Eurointervention.* 2014;10:672-80.

[Original research paper, Impact Factor (2013): 3.758]

Zhang YJ, Bourantas CV, Muramatsu T, Iqbal J, Farooq V, Diletti R, Campos CA, Onuma Y, Garcia-Garcia HM, Serruys PW.





# Comparison of acute gain and late lumen loss after PCI with bioresorbable vascular scaffolds versus everolimus-eluting stents: an exploratory observational study prior to a randomised trial

Yao-Jun Zhang<sup>1,2</sup>, MD, PhD; Christos V. Bourantas<sup>1</sup>, MD, PhD; Takashi Muramatsu<sup>1</sup>, MD, PhD; Javaid Iqbal<sup>1</sup>, MRCP, PhD; Vasim Farooq<sup>1</sup>, MBChB, MRCP; Roberto Diletti<sup>1</sup>, MD; Carlos A.M. Campos<sup>1,3</sup>, MD; Yoshinobu Onuma<sup>1</sup>, MD; Hector M. Garcia-Garcia<sup>1</sup>, MD, PhD; Patrick W. Serruys<sup>1\*</sup>, MD, PhD

1. Thoraxcenter, Erasmus Medical Center, Rotterdam, The Netherlands; 2. Department of Cardiology, Nanjing First Hospital, Nanjing Medical University, Nanjing, China; 3. Heart Institute (InCor), University of São Paulo Medical School, Sao Paulo, Brazil

GUEST EDITOR: Andreas Baumbach, MD; Division of Cardiology, Bristol Heart Institute, Bristol, United Kingdom

This paper also includes accompanying supplementary data published online at: [http://www.pcronline.com/eurointervention/77th\\_issue/118](http://www.pcronline.com/eurointervention/77th_issue/118)

## KEYWORDS

- acute gain
- bioresorbable vascular scaffold
- everolimus-eluting stent
- late lumen loss
- minimal lumen area

## Abstract

**Aims:** The study sought to compare the acute gain and two-year follow-up late lumen loss (LLL) between the Absorb bioresorbable vascular scaffold (BVS) and the analogous everolimus-eluting metallic stent (EES).

**Methods and results:** The current analysis included all the patients recruited in the ABSORB Cohort B and SPIRIT II trials implanted with a single 3.0×18 mm device (Absorb BVS or EES) who underwent serial angiographic examinations at baseline and at two-year follow-up. The acute gain was defined as the difference between post- and preprocedural minimal lumen diameter (MLD). The in-stent/scaffold LLL was calculated as the difference in stent/scaffold segment between the post-procedural MLD and follow-up MLD. Thirty-three patients (33 lesions) implanted with the Absorb BVS, and 26 patients (28 lesions) implanted with the EES were studied. The acute gain was similar in the Absorb BVS group (1.23±0.38 mm) compared to the EES group (1.32±0.26 mm, p=0.29). The in-stent/scaffold LLL at two-year follow-up in the Absorb BVS group (0.26±0.19 mm) was also similar compared to the EES group (0.22±0.22 mm, p=0.29). Although the two groups had similar two-year clinical outcomes (major adverse cardiac events: Absorb BVS: 6.1% vs. EES: 0.0%), patients treated with the Absorb BVS exhibited a significantly lower two-year in-stent/scaffold MLD compared to the EES (2.02±0.26 mm vs. 2.22±0.34 mm, p=0.01).

**Conclusions:** Although BVS and EES demonstrated similar two-year clinical outcomes, patients treated with the Absorb BVS exhibited a significantly lower two-year in-stent/scaffold MLD compared to patients treated with the EES. Appropriately powered randomised trials are necessary to confirm these exploratory results and evaluate their prognostic and clinical significance.

\*Corresponding author: Interventional Cardiology Department, Erasmus MC, 's Gravendijkwal 230, 3015 CE Rotterdam, The Netherlands. E-mail: [p.w.j.c.serruys@erasmusmc.nl](mailto:p.w.j.c.serruys@erasmusmc.nl)

© Europa Digital & Publishing 2014. All rights reserved.

SUBMITTED ON 22/08/2013 - REVISION RECEIVED ON 22/10/2013 - ACCEPTED ON 20/11/2013

## Introduction

Coronary metallic stents have been widely used as the standard endoluminal device for the treatment of patients with coronary artery disease (CAD)<sup>1</sup>. The introduction of drug-eluting stents (DES) has markedly reduced the risk of restenosis, particularly in complex anatomical cases and high-risk patients<sup>2</sup>. Recent advances in stent technology, with the introduction of biocompatible or biodegradable polymers, have minimised the risk of complications, in particular stent thrombosis, evident with the first-generation DES<sup>3,4</sup>. Despite these improvements, newer-generation DES have not managed to address all the limitations of coronary stents, such as the risk of neoatherosclerosis, preclusion of late lumen enlargement and the lack of reactive vasomotion<sup>5</sup>. Furthermore, the risk of stent thrombosis and its clinical sequelae, although substantially reduced in incidence with newer-generation DES, still remains.

Bioresorbable scaffolds were introduced to overcome the above-mentioned drawbacks, as they potentially have the ability to restore the patency of the vessel and then gradually disappear, thus allowing the artery to maintain its physiological integrity and responsiveness<sup>6</sup>. Today, more than 14 bioresorbable scaffolds are either being investigated in clinical trials or undergoing preclinical evaluation<sup>7</sup>. Three biodegradable scaffolds currently have Conformité Européenne (CE) mark approval: the Igaki-Tamai<sup>®</sup> (Kyoto Medical Planning Co., Ltd, Kyoto, Japan) scaffold for the treatment of peripheral vascular disease, the DESolve<sup>®</sup> scaffold (Elixir Medical Corporation, Sunnyvale, CA, USA), and the Absorb bioresorbable vascular scaffold (BVS; Abbott Vascular, Santa Clara, CA, USA) for the treatment of CAD. The latter consists of a poly-L-lactic acid (PLLA) backbone, coated with a bioresorbable polymer that contains and controls the release of the antiproliferative drug everolimus<sup>8</sup>. The differential mechanical properties of PLLA, compared to conventional metallic stents, are likely to affect device expansion and recoil during implantation. Furthermore, a higher acute gain post device implantation, and a relatively lower late lumen loss (LLL) at follow-up, have been shown to be predictors of a more favourable long-term prognosis<sup>9,10</sup>. The purpose of this study was to compare the post device implantation acute gain, and the two-year LLL, in patients treated with the Absorb BVS and the analogous metallic platform drug-eluting stent (XIENCE V; Abbott Vascular, Santa Clara, CA, USA).

## Methods

### STUDY DESIGN AND POPULATION

The present study represents a pooled patient analysis of the ABSORB Cohort B and the SPIRIT II clinical trials, recruiting patients treated with a single 3.0×18 mm device, who underwent angiographic examination at baseline and at two-year follow-up. The patients recruited in this analysis had different baseline and angiographic characteristics, and therefore a further analysis was conducted after matching the two populations for the following variables: diabetes mellitus, reference vessel diameter (RVD), preprocedural minimal lumen diameter (MLD), and lesion length.

### ABSORB COHORT B

The ABSORB Cohort B (a clinical evaluation of the bioresorbable everolimus-eluting coronary stent system in the treatment of patients with *de novo* native coronary artery lesions) trial is a non-randomised, multicentre, single-arm study (ClinicalTrials.gov NCT00856856). All patients over the age of 18 years with evidence of myocardial ischaemia were suitable for inclusion. The treated lesions were native *de novo* stenoses with an estimated diameter of 3.0 mm, a length <14 mm, and a percentage diameter stenosis (DS) of >50% and <100%. One hundred and one patients (102 lesions) treated with an Absorb BVS device were enrolled and divided into two groups (Cohort B1 and B2). Patients enrolled in Cohort B1 (n=45) underwent quantitative coronary angiography (QCA) and intravascular ultrasound (IVUS) examinations at baseline, six months and two years. Patients enrolled in Cohort B2 (n=56) underwent the same invasive tests, at baseline, one year, and three years (study ongoing).

### SPIRIT II

SPIRIT II was a multicentre, randomised two-arm trial, which recruited 300 patients with *de novo* lesions (ClinicalTrials.gov NCT00180310). Study patients were randomised in a 3:1 ratio to either everolimus-eluting (EES, n=233) or paclitaxel-eluting (n=77) stents<sup>11</sup>. The study had similar clinical inclusion criteria to the ABSORB Cohort B trial. The treated *de novo* lesions had an RVD 2.25–4.25 mm, and a percentage DS >50% and <100%. Angiographic follow-up was performed in all patients at six months. One hundred and fifty-two patients (113 patients in EES group) underwent angiographic and/or IVUS examinations at two years.

### QUANTITATIVE CORONARY ANALYSIS ASSESSMENT

QCA analyses were undertaken in corresponding end-diastolic angiographic frames acquired pre and post device implantation, and at two-year follow-up<sup>12</sup>. The following measurements were obtained: lesion length, MLD, RVD derived by an interpolated method, in-stent/scaffold acute gain, LLL, net gain, percentage DS and minimum lumen area (MLA). The in-stent/scaffold acute gain was defined as the difference between pre- and post-procedural MLD. The LLL was defined as the difference between post-procedural and follow-up MLD. The net gain was defined as the sum of the offsetting effects of the acute gain and LLL. Two different MLA metrics, based on video-densitometry (VID) and edge-detection (ED) techniques, were analysed<sup>13,14</sup>. The basic principles of the video-densitometric technique have been described previously<sup>14</sup>. This technique is a non-geometric approach to the analysis of coronary angiography, based on the relationship between the attenuating power of the lumen filled with contrast medium and the x-ray image intensifier. An absolute reference for densitometric area is calculated using the diameter measurements obtained from the edge-detection technique, assuming circular vessel geometry in a user-defined reference segment outside the stenosis.

## INTRAVASCULAR ULTRASOUND GREYSCALE ANALYSIS

IVUS examinations were undertaken post-procedurally and at two-year follow-up, either with a mechanical (Atlantis; Boston Scientific, Natick, MA, USA) or a phased array (Eagle Eye; Volcano Corp., Rancho Cordova, CA, USA) catheter<sup>12</sup>. The following metrics were calculated: mean lumen area, minimum lumen area (MLA), mean scaffold/stent area, mean neointimal hyperplasia (NIH) area, and mean vessel area. In addition, the “projected MLD” was used to assess the lumen diameter, estimated by rotating the object representing the lumen around the centre of gravity three times in 30° steps. For each rotation, the projection distances on the x and y axes were calculated and compared with the previous diameter<sup>15</sup>.

## CLINICAL ENDPOINTS

Composite ischaemia-driven major adverse cardiac events (MACE) included cardiac death, any myocardial infarction (MI), and ischaemia-driven target lesion revascularisation (ID-TLR). The ID-TLR was defined as a QCA percentage DS of ≥50%, with symptoms of ischaemia, or DS ≥70% at the time of scheduled or unscheduled angiography. An event was classified as non-Q-wave MI only if there was an elevation of creatinine kinase (CK) levels ≥2 times the upper limit of normal, with an elevated CK-MB. All events were adjudicated by an independent clinical events committee.

## STATISTICAL ANALYSIS

Continuous variables are presented as mean±standard deviation (SD). Binary variables are presented as counts and percentages. The p-value was calculated using the Mann-Whitney U test (two-sided) if the variable was continuous. Fisher’s exact test was used if the variable was categorical. Matching was processed at the lesion level using the optimal method minimising the overall distance. The distance between cases and controls,  $D_{ij}$ , is defined as the weighted sum of the absolute differences between the case and control matching factors, i.e., where  $W_k$ =the weight assigned to matching factor k and  $X_{ik}$ =the value of variable X(k) for subject i.

$$D_{ij} = W_k \sum_{k=1}^p |X_{ik} - X_{jk}|$$

Variables used for the matching were standardised variables and equally weighted for this analysis. Statistical significance was assumed at p<0.05. All statistical analyses were performed with SAS 9.1.3 (SAS Institute Inc., Cary, NC, USA).

## Results

### BASELINE CHARACTERISTICS

A flow chart summarising patient selection is shown in **Figure 1**. In total, 59 patients (61 lesions) were included in the final analysis. Thirty-three patients (33 lesions) were implanted with 3.0×18 mm Absorb BVS, and 26 patients (28 lesions) with 3.0×18 mm EES. No significant differences in a history of diabetes mellitus (p=1.00), hypertension (p=1.00), or hypercholesterolaemia (p=0.27) were

evident between the two groups. Patients treated with an EES were more likely to have two-vessel CAD (p=0.01) and to have presented with unstable angina (p=0.03) (**Table 1**).

**Table 1. Baseline clinical characteristics.**

	BVS (N <sub>i</sub> =33, N <sub>j</sub> =33)	EES (N <sub>i</sub> =26, N <sub>j</sub> =28)	p-value
Age (years)	64.06±9.51	62.42±13.70	0.79
Male	78.8%	76.9%	1.00
Diabetes mellitus	15.2%	15.4%	1.00
Hypertension	48.5%	46.2%	1.00
Hypercholesterolaemia	90.9%	80.0%	0.27
Current smoker	15.2%	30.8%	0.21
Family history of CAD	45.5%	52.2%	0.79
Prior MI	39.4%	28.0%	0.41
History of PCI	12.1%	3.9%	0.37
Stable angina	75.8%	50.0%	0.06
Unstable angina	12.1%	38.5%	0.03
Silent ischaemia	0.0%	3.9%	0.44

Data are mean±SD or %. BVS: bioresorbable vascular scaffold; CAD: coronary artery disease; EES: everolimus-eluting stent; MI: myocardial infarction; N<sub>i</sub>: number of lesions; N<sub>j</sub>: number of patients; PCI: percutaneous coronary intervention

### ANGIOGRAPHIC CHARACTERISTICS

The preprocedural angiographic characteristics were similar in the BVS and EES groups (**Table 2**). The majority of treated stenoses were type B lesions (AHA/ACC classification, BVS: 94.0%, EES: 100.0%)<sup>16</sup>. No statistically significant differences were evident between the BVS and EES groups for DS, MLD and RVD. The percentage of post-dilatation (63.64% vs. 46.43%, p=0.20), and the maximum pressure of post-dilatation (17.29±6.92 atm vs. 16.15±3.87 atm, p=0.71) were comparable between the BVS and EES groups.

### ACUTE GAIN, LLL AND OTHER ANGIOGRAPHIC MEASUREMENTS

The results of the QCA analysis are shown in **Table 3**. There was a similar acute gain in the BVS group (BVS: 1.23±0.38 mm, EES: 1.32±0.26 mm, p=0.29) (**Figure 2**). The post-procedural in-stent/scaffold MLD in the BVS group was similar compared to the EES group (BVS: 2.28±0.27 mm, EES: 2.44±0.26 mm, p=0.02). The two-year in-stent/scaffold LLL in the Absorb BVS group was similar compared to the EES group (BVS: 0.26±0.19 mm vs. EES: 0.22±0.22 mm, p=0.29). However, the two-year in-stent/scaffold MLD was significantly lower in the Absorb BVS compared to the EES (2.02±0.26 mm vs. 2.22±0.34 mm, p=0.02). Notably, the reported net gain did not differ statistically between the two groups at two-year follow-up (0.97±0.40 mm vs. 1.10±0.35 mm, p=0.22).

### INTRAVASCULAR ULTRASOUND ANALYSIS

Thirty patients (30 lesions) from the Absorb BVS group and 22 patients (24 lesions) from the EES group had IVUS examinations

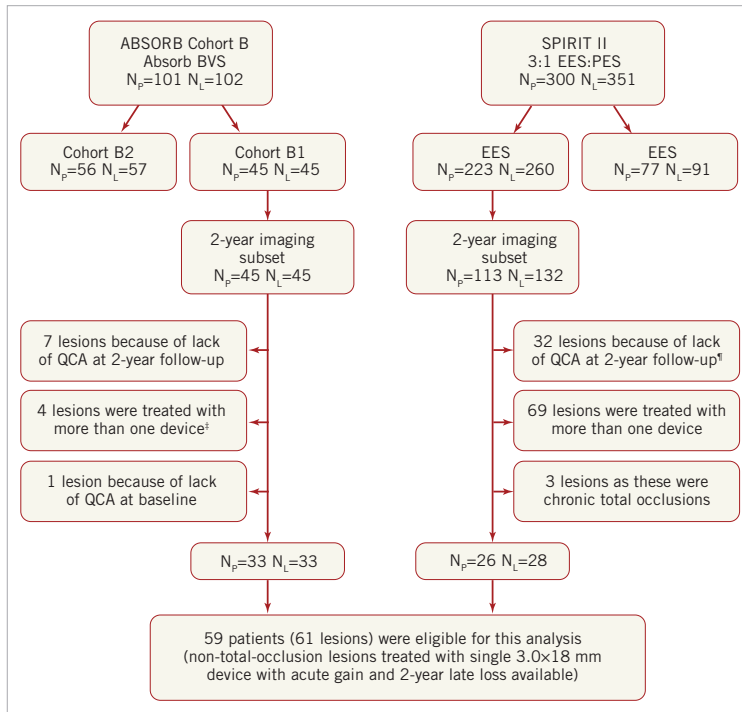


**Figure 1.** Flow chart of patient selection. 4 patients refused, 2 patients were not suitable for angiographic follow-up while in 1 case post-nitrate angiographic images were not available for QCA analysis. \*18 patients (21 lesions) refused follow-up coronary angiography; 2 patients were deemed unsuitable for invasive follow-up, 5 were withdrawn from the study, 3 died from non-cardiac death and in 1 case the QCA was not feasible. †3 patients had additional bail-out stenting and 1 patient was not included, who received 1 non-study stent in the target vessel during procedure. BVS: bioresorbable vascular scaffold; EES: everolimus-eluting stent; N<sub>l</sub>: number of lesions; N<sub>p</sub>: number of patients; PES: paclitaxel-eluting stent; QCA: quantitative coronary angiography

post device implantation. IVUS assessments were undertaken in 32 patients (32 lesions) treated with an Absorb BVS, and in 20 patients (21 lesions) implanted with an EES, at two-year follow-up. The mean vessel area, mean lumen area, MLA, and stent/scaffold areas, post procedure and at follow-up were similar between the two groups (Figure 3, Table 4). In addition, there were no significant differences between the two groups in the mean NIH area at follow-up ( $0.26 \pm 0.28 \text{ mm}^2$  vs.  $0.27 \pm 0.37 \text{ mm}^2$ ,  $p=0.59$ ). The IVUS-derived “projected MLD” was significantly lower in the BVS group compared to the EES group (post procedure:  $2.34 \pm 0.29 \text{ mm}$  vs.  $2.49 \pm 0.26 \text{ mm}$ ,  $p=0.04$ ; two-year follow-up:  $2.30 \pm 0.27 \text{ mm}$  vs.  $2.48 \pm 0.26 \text{ mm}$ ,  $p=0.03$ , respectively).

#### FURTHER ANALYSIS AFTER MATCHING

After matching, 28 patients with 28 lesions in the BVS group, and 26 patients with 28 lesions in the EES group were analysed. The

main results of the QCA and IVUS analyses are shown in Table 5 and Table 6. The evaluation of the acute gain and LLL by QCA showed a trend in the same direction as seen in the entire population. At two-year follow-up, angiographic in-stent/scaffold MLD by QCA and projected MLD by IVUS remained statistically lower in the BVS group than in the EES group ( $p=0.01$ ,  $p=0.01$ , respectively).

#### CLINICAL OUTCOMES

During two-year follow-up, two patients developed ID-TLR in the Absorb group. One patient had in-scaffold restenosis (ISR) at 168 days of follow-up, showing a Type 1B ISR at the proximal edge of the scaffold (QCA MLD: 0.89 mm, %DS: 63.5%, in-scaffold LLL: 0.50 mm); the other patient had ISR at 383 days of follow-up, also showing a Type 1B ISR in the segment proximal to

**Table 2. Baseline angiographic characteristics post device implantation.**

		BVS (N <sub>p</sub> =33, N <sub>l</sub> =33)	EES (N <sub>p</sub> =26, N <sub>l</sub> =28)	p-value
Angulation*		3.0%	10.7%	0.32
Calcification (heavy or moderate)		18.2%	35.7%	0.15
Eccentricity		97.0%	100.0%	1.00
AHA/ACC lesion classification	A	3.0%	0.0%	1.00
	B1	48.5%	17.9%	0.02
	B2	45.5%	82.1%	<0.01
	C	3.0%	0.0%	1.00
Target vessel	LAD	39.4%	46.4%	0.61
	LCX	27.3%	25.0%	1.00
	RCA	33.3%	28.6%	0.78
Lesion length (mm)		10.12±4.15	11.83±4.20	0.12
Diameter stenosis (%)		58.97±12.54	57.74±8.41	0.46
Pre-procedure MLD (mm)		1.05±0.34	1.12±0.26	0.20
Reference vessel diameter (mm)		2.59±0.46	2.66±0.36	0.35
Post-dilatation rate		63.6%	46.4%	0.20
Balloon diameter (mm)		3.24±0.27	3.31±0.25	0.47
Maximum pressure (atm)		17.29±6.92	16.15±3.87	0.71

Data are mean±SD or %. \*angulation was defined as angulated segment >45 degrees according to the ACC/AHA lesion classification. LAD: left anterior descending; LCX: left circumflex coronary artery; MLD: minimum lumen diameter; N<sub>p</sub>: number of patients; N<sub>l</sub>: number of lesions; RCA: right coronary artery

the scaffold (QCA MLD: 0.90 mm, %DS: 67.0%, in-scaffold LLL: 1.20 mm). Two patients in the Absorb BVS group but no patients in the EES group experienced non-Q-wave MI at two-year follow-up. No death was reported in either the Absorb BVS or the EES group.

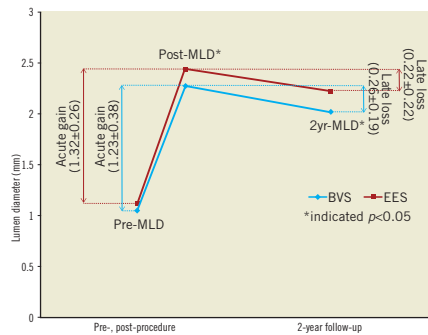


**Figure 2. Schematic representation of the QCA-derived measurements pre- and post-procedure, and at two-year follow-up.** BVS: bioresorbable vascular scaffold; EES: everolimus-eluting stent; MLD: minimum lumen diameter; Post: post-procedure; Pre: pre-procedure

**Table 3. Quantitative coronary angiographic (QCA) analyses.**

	BVS (N <sub>p</sub> =33, N <sub>l</sub> =33)	EES (N <sub>p</sub> =26, N <sub>l</sub> =28)	p-value
Acute gain (mm)	1.23±0.38	1.32±0.26	0.29
Post in-stent/scaffold MLD (mm)	2.28±0.27	2.44±0.26	0.02
2yr in-stent/scaffold MLD (mm)	2.02±0.26	2.22±0.34	0.01
2yr in-stent/scaffold DS (%)	20.85±7.02	15.24±9.35	<0.01
2yr in-stent/scaffold LLL (mm)	0.26±0.19	0.22±0.22	0.29
2yr net gain (mm)	0.97±0.40	1.10±0.35	0.22
Post-MLA derived from VID (mm <sup>2</sup> )	5.26±1.58	5.70±1.50	0.31
2yr MLA derived from VID (mm <sup>2</sup> )	4.48±1.30	4.95±1.94	0.46
Post-MLA derived from ED (mm <sup>2</sup> )	4.35±1.29	4.57±1.18	0.38
2yr MLA derived from ED (mm <sup>2</sup> )	3.53±1.13	4.23±1.69	0.14

Data are mean±SD. 2yr: 2-year follow-up; BVS: bioresorbable vascular scaffold; DS: diameter stenosis; ED: edge detection; EES: everolimus-eluting stent; LLL: late lumen loss; MLA: minimum lumen area; MLD: minimal lumen diameter; N<sub>p</sub>: number of patients; N<sub>l</sub>: number of lesions; Post: post-procedure; VID: video-densitometry

**Table 4. Comparison of IVUS measurements between the BVS and the EES groups at baseline and two-year follow-up.**

	BVS Post: N <sub>p</sub> =30, N <sub>l</sub> =30 2yr: N <sub>p</sub> =32, N <sub>l</sub> =32	EES Post: N <sub>p</sub> =22, N <sub>l</sub> =24 2yr: N <sub>p</sub> =20, N <sub>l</sub> =21	p-value
Post-projected MLD (mm)	2.34±0.29	2.49±0.26	0.04
2yr projected MLD (mm)	2.30±0.27	2.48±0.26	0.03
Post-mean VA (mm <sup>2</sup> )	14.47±3.97	13.71±2.54	0.48
2yr mean VA (mm <sup>2</sup> )	15.32±3.78	14.02±2.52	0.40
Post-mean LA (mm <sup>2</sup> )	6.61±1.14	6.68±1.03	0.84
2yr mean LA (mm <sup>2</sup> )	6.76±1.38	6.61±1.05	0.74
Post-MLA (mm <sup>2</sup> )	5.51±0.99	5.59±0.98	0.62
2yr MLA (mm <sup>2</sup> )	5.07±1.08	5.44±1.03	0.12
Post-stent/scaffold area (mm <sup>2</sup> )	6.60±1.13	6.68±1.03	0.79
2yr stent/scaffold area (mm <sup>2</sup> )	6.99±1.36	6.89±0.96	0.95
2yr NIH area (mm <sup>2</sup> )	0.26±0.28	0.27±0.37	0.59

Data are mean±SD. 2yr: 2-year follow-up; BVS: bioresorbable vascular scaffold; EES: everolimus-eluting stent; LA: lumen area; MLA: minimum lumen area; MLD: minimum lumen diameter; NIH: neointimal hyperplasia; N<sub>p</sub>: number of patients; N<sub>l</sub>: number of lesions; Post: post-procedure; VA: vessel area

## Discussion

The main findings of the study are that: 1) there was similar acute gain in patients implanted with an Absorb BVS, but the difference between the two groups did not reach statistical significance; 2) the two-year follow-up in-stent/scaffold LLL in the Absorb BVS was also similar compared to the EES; 3) although the two groups had similar two-year clinical outcomes, patients treated with the Absorb BVS exhibited a significantly lower two-year in-stent/scaffold MLD compared to the EES.

## COMPARISON OF ACUTE GAIN BETWEEN THE ABSORB BVS AND EES

QCA has been extensively used to study the performance of new endovascular treatments. The immediate benefit of a coronary

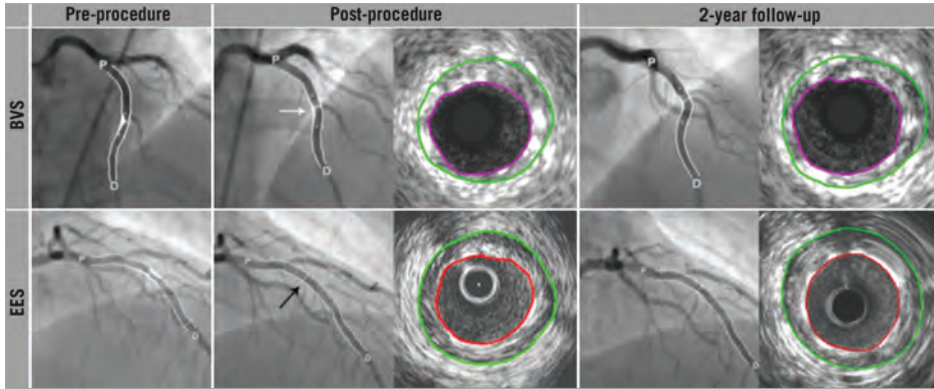


**Figure 3.** Serial cineangiograms pre-procedurally, post-procedurally and at two-year follow-up, for the Absorb BVS and the EES. From left to right in the upper panels, coronary angiograms of a mid-left anterior descending (LAD) coronary lesion treated with Absorb BVS, pre-procedurally, post-procedurally, and at 2-year follow-up, and corresponding IVUS cross-sectional views for the projected MLD. Post-procedurally, the scaffold was insufficiently expanded (white arrow) and consequently associated with a lower acute gain. In the lower panels, from left to right, angiogram of a mid-LAD coronary lesion treated with an EES, pre-procedurally, post-procedurally, and at 2-year follow-up, and corresponding IVUS cross-sectional views for the projected MLD. Post-procedurally, the EES was well expanded with a consequent greater acute gain (black arrow). BVS: bioresorbable vascular scaffold; D: distal; EES: everolimus-eluting stent; IVUS: intravascular ultrasound; P: proximal; QCA: quantitative coronary angiography

intervention, as expressed by the acute gain, has historically been used as a surrogate endpoint to compare plain old balloon angioplasty, rotational atherectomy, and bare metal stents (BMS)<sup>7</sup>. In the BMS era, it was shown that increased acute gain and a larger post-procedural MLD were predictors of a more favourable prognosis, thus suggesting device post-dilation to be of significant clinical value<sup>18</sup>. This effect appeared to be maintained in the DES era<sup>9</sup>. Specifically,

**Table 5. Quantitative coronary angiographic (QCA) analyses (matching on diabetes, reference vessel diameter, preprocedural minimum lumen diameter, lesion length).**

	BVS (N <sub>p</sub> =28, N <sub>l</sub> =28)	EES (N <sub>p</sub> =26, N <sub>l</sub> =28)	p-value
Acute gain (mm)	1.22±0.38	1.32±0.26	0.24
Post-in-stent MLD (mm)	2.27±0.27	2.44±0.26	0.02
2yr in-stent/scaffold MLD (mm)	2.00±0.25	2.22±0.34	0.01
2yr in-stent/scaffold DS (%)	20.83±6.92	15.24±9.35	0.01
2yr in-stent/scaffold LLL (mm)	0.28±0.18	0.22±0.22	0.28
2yr net gain (mm)	0.94±0.41	1.10±0.35	0.12
Post-MLA derived from VID (mm <sup>2</sup> )	5.20±1.54	5.70±1.50	0.23
2yr MLA derived from VID (mm <sup>2</sup> )	4.30±1.12	4.95±1.94	0.29
Post-MLA derived from ED (mm <sup>2</sup> )	4.37±1.31	4.57±1.18	0.39
2yr MLA derived from ED (mm <sup>2</sup> )	3.42±1.02	4.23±1.69	0.09

Data are mean±SD. 2yr: 2-year follow-up; BVS: bioresorbable vascular scaffold; DS: diameter stenosis; ED: edge detection; EES: everolimus-eluting stent; LLL: late lumen loss; MLA: minimum lumen area; MLD: minimal lumen diameter; N<sub>p</sub>: number of patients; N<sub>l</sub>: number of lesions; Post: post-procedure; VID: video-densitometry

in a substudy of the STLLR (Stent deployment Techniques on clinical outcomes of patients treated with the Cypher™ stent) trial, it was demonstrated that a lower acute gain, after implantation of a sirolimus-eluting stent, was the only predictor of TLR<sup>9</sup>.

**Table 6. Comparison of IVUS measurements between the BVS and the EES groups at baseline and two-year follow-up (matching on diabetes, reference vessel diameter, preprocedural minimum lumen diameter, lesion length).**

	BVS Post: N <sub>p</sub> =25, N <sub>l</sub> =25 2yr: N <sub>p</sub> =27, N <sub>l</sub> =27	EES Post: N <sub>p</sub> =22, N <sub>l</sub> =24 2yr: N <sub>p</sub> =20, N <sub>l</sub> =21	p-value
Post-projected MLD (mm)	2.29±0.23	2.49±0.26	0.01
2yr projected MLD (mm)	2.25±0.25	2.48±0.26	0.01
Post-mean VA (mm <sup>2</sup> )	14.45±3.86	13.71±2.54	0.43
2yr mean VA (mm <sup>2</sup> )	15.09±3.58	14.02±2.52	0.23
Post-mean LA (mm <sup>2</sup> )	6.48±0.90	6.68±1.03	0.48
2yr mean LA (mm <sup>2</sup> )	6.58±1.27	6.61±1.05	0.92
Post-MLA (mm <sup>2</sup> )	5.35±0.78	5.59±0.98	0.35
2yr MLA (mm <sup>2</sup> )	4.92±1.01	5.44±1.03	0.08
Post-stent/scaffold area (mm <sup>2</sup> )	6.47±0.89	6.68±1.03	0.44
2yr stent/scaffold area (mm <sup>2</sup> )	6.83±1.26	6.89±0.96	0.86
2yr NIH area (mm <sup>2</sup> )	0.26±0.28	0.27±0.37	0.92

Data are mean±SD. 2yr: 2-year follow-up; BVS: bioresorbable vascular scaffold; EES: everolimus-eluting stent; LA: lumen area; MLA: minimum lumen area; MLD: minimum lumen diameter; NIH: neointimal hyperplasia; N<sub>p</sub>: number of patients; N<sub>l</sub>: number of lesions; Post: post-procedure; VA: vessel area

In the present study, the acute gain associated with the Absorb BVS was demonstrated to be numerically lower compared to the EES. However, this difference did not reach statistical significance, probably secondary to the relatively small number of patients. Conversely, bench studies have demonstrated that the two devices have comparable radial strength, and exhibit a similar acute recoil post implantation<sup>19</sup>. The numerically higher acute gain associated with the EES may be secondary to the higher size of post-dilation balloon during device deployment, which is not recommended in the Absorb BVS because of the limited distensibility of the Absorb BVS, and the risk of inducing acute strut fracture if dilated beyond its design limits<sup>19</sup>. However, the percentage of post-dilatation used and maximum pressure of post-dilatation in the BVS group are higher than seen in the EES group, though they did not differ significantly between the Absorb BVS and EES groups (**Table 2**). In addition, the different strut thicknesses of these two devices may also influence the acute gain; the advent of optical coherence tomography with a high resolution imaging technique is expected to provide a precise assessment of this parameter.

#### COMPARISON OF LLL BETWEEN THE ABSORB BVS AND EES

The in-stent/scaffold LLL constitutes a traditional measure to evaluate in-stent/scaffold restenosis, and to examine the long-term efficacy of DES<sup>20</sup>. Numerous studies have shown that LLL is a predictor of future cardiovascular events, and it has been used as a surrogate endpoint to compare different devices<sup>10</sup>. In permanent metallic stent platforms, the LLL is solely due to neointimal proliferation, and thus the LLL provides an indirect angiographic evaluation of the vessel wall response to the endovascular device<sup>21</sup>. In contrast, the LLL in the Absorb BVS depends not only on neointimal formation, but also on the late scaffold expansion, which may potentially occur as early as one year post device implantation<sup>22</sup>. Although the current analysis demonstrated no differences between the LLL in the EES and the Absorb BVS, the patients implanted with an Absorb BVS had a smaller MLD at two-year follow-up. This finding may be attributed to the smaller MLD reported post-Absorb BVS implantation.

#### COMPARISONS OF THE MEASUREMENTS DERIVED FROM QCA AND IVUS

Notably, the significant differences in the QCA-derived MLD between the BVS and EES groups were confirmed by the IVUS-derived projected MLDs post procedure and at two-year follow-up. Moreover, the MLA derived from two different QCA methods (VID and ED) demonstrated consistent, non-significant differences between the QCA and IVUS analyses post procedure and at two years. Several reasons may be involved in this paradox between the MLA and MLD in the two groups. It should be noted that a few patients did not undergo IVUS examinations post-procedurally (three in the Absorb BVS and four in the EES group) and at two-year follow-up (one in the Absorb BVS and seven in the EES group). Furthermore, the two devices have different mechanical properties (e.g., conformability and flexibility) which potentially affected their expansion pattern, with the Absorb BVS shown to

have a more eccentric expansion when compared to the metallic EES<sup>23</sup>. An asymmetric expansion of the Absorb BVS is likely to have been underestimated by the QCA, since this MLD is based on the analysis of two-dimensional images. Moreover, different patterns of restenosis were possibly involved after implantation of an Absorb BVS or an EES, something which should be investigated in the near future<sup>24</sup>. Therefore, it may be argued that, in patients treated with an Absorb BVS, the operator should assess the results of QCA with caution and, in cases of scaffold underexpansion, should consider further evaluation of its deployment, either with intravascular imaging modalities or with three-dimensional QCA, before attempting post-dilatation.

#### Clinical relevance

Traditionally, metallic stent implantation is associated with an increased incidence of post-procedural chest pain (PPCP) compared with angioplasty<sup>25</sup>. The majority of PPCP after stenting is identified as non-ischaeamic and argued to be benign<sup>26</sup>. However, a study from Kini et al showed that non-ischaeamic PPCP was probably induced by micromyonecrosis and vessel stretching after stent implantation, and patients with PPCP had a significantly higher restenosis rate compared with no PPCP at nine-month follow-up<sup>27</sup>. The aetiology of non-ischaeamic PPCP has been attributed to oversizing stents and high inflation pressures. A higher stent-to-vessel ratio together with a raised inflation pressure may achieve a larger post-procedure MLD, but also results in irritation of sensory nerves located in the adventitia, causes deep adventitia injury, and increases the incidence of PPCP<sup>28</sup>. In our study, the patients had a significantly lower post-procedure MLD in the Absorb BVS group than that seen in the XIENCE V group ( $2.28 \pm 0.27$  mm vs.  $2.44 \pm 0.26$  mm,  $p=0.02$ ), which could be accounted for in the Absorb BVS group by less continuous stretching of the treated vessel segment. However, the exact prevalence of PPCP after Absorb BVS implantation and its correlation with clinical events at follow-up require further investigation.

Recently, the concept of a “bioresorbable scaffold” has been highlighted<sup>29</sup>. The feasibility of this concept was proven in the early 1990s and, over the last 20 years, a considerable effort has been made to develop new fully bioresorbable scaffolds<sup>6</sup>. Strikingly however, as previously discussed, the reported numerically lower acute gain and higher late loss in the Absorb BVS group potentially resulted in a significantly different MLD post procedure and at two-year follow-up compared to the analogous metallic drug-eluting stent. The findings of this observational study were hypothesis-generating and initiated prior to a randomised trial which is necessary to confirm these exploratory results as well as to evaluate their prognostic and clinical significance.

#### Limitations

A considerable limitation of the present study is that the Absorb BVS and EES groups had different baseline characteristics, which may have affected the reported outcomes. In order to address this pitfall, we conducted a separate analysis after matching patients (**Online Table 1, Online Table 2**), based on the history of diabetes

and on angiographic variables including RVD, pre-procedure MLD and lesion length. The repeated analysis demonstrated similar results. Most of the stenoses treated by the two devices were simple lesions and hence the reported findings cannot be extrapolated to the general population. A further precise assessment regarding QCA-derived variables between these two devices, to be conducted by adjusting procedural and lesion characteristics, is warranted. Moreover, further evaluation is also required in larger populations and in complex lesions, in order to examine the differences in the QCA measurements between the two devices and their prognostic implications.

## Conclusions

Patients implanted with an Absorb BVS appear to exhibit similar acute gain and in-stent/scaffold LLL compared to those treated with the analogous EES. Although the two groups had similar two-year clinical outcomes, patients treated with the Absorb BVS exhibited a significantly lower two-year in-stent/scaffold MLD compared to the EES group. Appropriately powered randomised trials are required to assess the reported results and to evaluate the impact of QCA-derived metrics on clinical outcomes.

### Impact on daily practice

A higher acute gain post-stent implantation, and a relatively lower late lumen loss (LLL) at follow-up have been shown to be predictors of a more favourable long-term prognosis. The comparable acute gain and two-year LLL between the Absorb BVS and EES are for the first time reported in this study. However, the numerically lower acute gain and higher late loss in the Absorb BVS group potentially resulted in a significantly different MLD post-procedure and at two-year follow-up, compared with the EES group.

## Guest Editor

This paper was guest edited by Andreas Baumbach, MD, Division of Cardiology, Bristol Heart Institute, Bristol, United Kingdom.

## Funding

This study was sponsored by Abbott Vascular, Santa Clara, CA, USA.

## Conflict of interest statement

The authors have no conflicts of interest to declare. The Guest Editor has received research support from Abbott Vascular.

## References

1. Brophy JM, Belisle P, Joseph L. Evidence for use of coronary stents. A hierarchical bayesian meta-analysis. *Ann Intern Med.* 2003;138:777-86.
2. Serruys PW, Silber S, Garg S, van Geuns RJ, Richardt G, Buszman PE, Kelbaek H, van Boven AJ, Hofma SH, Linke A, Klauss V, Wijns W, Macaya C, Garot P, DiMario C, Manoharan G, Kornowski R, Ischinger T, Bartorelli A, Ronden J, Bressers M,

Gobbens P, Negoita M, van Leeuwen F, Windecker S. Comparison of zotarolimus-eluting and everolimus-eluting coronary stents. *N Engl J Med.* 2010;363:136-46.

3. Baber U, Mehran R, Sharma SK, Brar S, Yu J, Suh JW, Kim HS, Park SJ, Kastrati A, de Waha A, Krishnan P, Moreno P, Sweeny J, Kim MC, Suleman J, Pyo R, Wiley J, Kovacic J, Kini AS, Dangas GD. Impact of the everolimus-eluting stent on stent thrombosis: a meta-analysis of 13 randomized trials. *J Am Coll Cardiol.* 2011;58:1569-77.
4. Mauri L, Hsieh WH, Massaro JM, Ho KK, D'Agostino R, Cutlip DE. Stent thrombosis in randomized clinical trials of drug-eluting stents. *N Engl J Med.* 2007;356:1020-9.
5. Bourantas CV, Onuma Y, Farooq V, Zhang Y, Garcia-Garcia HM, Serruys PW. Bioresorbable scaffolds: current knowledge, potentialities and limitations experienced during their first clinical applications. *Int J Cardiol.* 2013;167:11-21.
6. Onuma Y, Serruys PW. Bioresorbable scaffold: the advent of a new era in percutaneous coronary and peripheral revascularization. *Circulation.* 2011;123:779-97.
7. Zhang Y, Bourantas CV, Farooq V, Muramatsu T, Diletti R, Onuma Y, Garcia-Garcia HM, Serruys PW. Bioresorbable scaffolds in the treatment of coronary artery disease. *Med Devices (Auckl).* 2013;6:37-48.
8. Onuma Y, Piazza N, Ormiston JA, Serruys PW. Everolimus-eluting bioabsorbable stent--Abbot Vascular programme. *EuroIntervention.* 2009;5:F98-102.
9. Tahara S, Bezerra HG, Kyono H, Carrigan T, Mehanna E, Wang W, Costa MA. Impact of acute gain on clinical outcomes of patients treated with sirolimus-eluting stent. A sub-analysis study from the STLLR trial. *Circ J.* 2011;75:2113-9.
10. Mauri L, Orav EJ, Kuntz RE. Late loss in lumen diameter and binary restenosis for drug-eluting stent comparison. *Circulation.* 2005;111:3435-42.
11. Ruygrok PN, Desaga M, Van Den Branden F, Rasmussen K, Suryapranata H, Dorange C, Veldhof S, Serruys PW. One year clinical follow-up of the XIENCE V Everolimus-eluting stent system in the treatment of patients with de novo native coronary artery lesions: the SPIRIT II study. *EuroIntervention.* 2007;3:315-20.
12. Ormiston JA, Serruys PW, Onuma Y, van Geuns RJ, de Bruyne B, Dudek D, Thuesen L, Smits PC, Chevalier B, McClean D, Koolen J, Windecker S, Whitbourn R, Meredith I, Dorange C, Veldhof S, Hebert KM, Rapoza R, Garcia-Garcia HM. First serial assessment at 6 months and 2 years of the second generation of absorb everolimus-eluting bioresorbable vascular scaffold: a multi-imaging modality study. *Circ Cardiovasc Interv.* 2012;5:620-32.
13. von Birgelen C, Umans VA, Di Mario C, Keane D, Gil R, Prati F, de Feyter P, Serruys PW. Mechanism of high-speed rotational atherectomy and adjunctive balloon angioplasty revisited by quantitative coronary angiography: edge detection versus videodensitometry. *Am Heart J.* 1995;130:405-12.
14. Serruys PW, Reiber JH, Wijns W, van den Brand M, Kooijman CJ, ten Katen HJ, Hugenholtz PG. Assessment of percutaneous transluminal coronary angioplasty by quantitative coronary

angiography: diameter versus densitometric area measurements. *Am J Cardiol.* 1984;54:482-8.

15. Tsuchida K, Serruys PW, Bruining N, Dudek D, Drzewiecki J, Banning AP, Zmudka K, Schiele F, Zhou Z, Rademaker TA, van Es GA, Koglin J, Russell ME, Colombo A. Two-year serial coronary angiographic and intravascular ultrasound analysis of in-stent angiographic late lumen loss and ultrasonic neointimal volume from the TAXUS II trial. *Am J Cardiol.* 2007;99:607-15.

16. Bonow RO, Masoudi FA, Rumsfeld JS, DeLong E, Estes NA 3rd, Goff DC Jr, Grady K, Green LA, Loth AR, Peterson ED, Pina IL, Radford MJ, Shahian DM. ACC/AHA classification of care metrics: performance measures and quality metrics: a report of the American College of Cardiology/American Heart Association Task Force on Performance Measures. *J Am Coll Cardiol.* 2008;52:2113-7.

17. Ozaki Y, Lemos PA, Yamaguchi T, Suzuki T, Nakamura M, Ismail TF, Kitayama M, Nishikawa H, Kato O, Serruys PW. A quantitative coronary angiography-matched comparison between a prospective randomised multicentre cutting balloon angioplasty and bare metal stent trial (REDUCE III) and the Rapamycin-Eluting Stent Evaluation At Rotterdam Cardiology Hospital (RESEARCH) study. *EuroIntervention.* 2010;6:400-6.

18. Kuntz RE, Safian RD, Carrozza JP, Fishman RF, Mansour M, Baim DS. The importance of acute luminal diameter in determining restenosis after coronary atherectomy or stenting. *Circulation.* 1992;86:1827-35.

19. Onuma Y, Serruys PW, Gomez J, de Bruyne B, Dudek D, Thuesen L, Smits P, Chevalier B, McClean D, Koolen J, Windecker S, Whitbourn R, Meredith I, Garcia-Garcia H, Ormiston JA. Comparison of in vivo acute stent recoil between the bioresorbable everolimus-eluting coronary scaffolds (revision 1.0 and 1.1) and the metallic everolimus-eluting stent. *Catheter Cardiovasc Interv.* 2011;78:3-12.

20. Mauri L, Orav EJ, Candia SC, Cutlip DE, Kuntz RE. Robustness of late lumen loss in discriminating drug-eluting stents across variable observational and randomized trials. *Circulation.* 2005;112:2833-9.

21. Pocock SJ, Lansky AJ, Mehran R, Popma JJ, Fahy MP, Na Y, Dangas G, Moses JW, Pucelikova T, Kandzari DE, Ellis SG, Leon MB, Stone GW. Angiographic surrogate end points in drug-eluting stent trials: a systematic evaluation based on individual patient data from 11 randomized, controlled trials. *J Am Coll Cardiol.* 2008;51:23-32.

22. Brugaletta S, Heo JH, Garcia-Garcia HM, Farooq V, van Geuns RJ, de Bruyne B, Dudek D, Smits PC, Koolen J, McClean D,

Dorange C, Veldhof S, Rapoza R, Onuma Y, Bruining N, Ormiston JA, Serruys PW. Endothelial-dependent vasomotion in a coronary segment treated by ABSORB everolimus-eluting bioresorbable vascular scaffold system is related to plaque composition at the time of bioreabsorption of the polymer: indirect finding of vascular reparative therapy. *Eur Heart J.* 2012;33:1325-33.

23. Brugaletta S, Gomez-Lara J, Diletti R, Farooq V, van Geuns RJ, de Bruyne B, Dudek D, Garcia-Garcia HM, Ormiston JA, Serruys PW. Comparison of in vivo eccentricity and symmetry indices between metallic stents and bioresorbable vascular scaffolds: insights from the ABSORB and SPIRIT trials. *Catheter Cardiovasc Interv.* 2012;79:219-28.

24. Tsuchida K, Serruys PW, Bruining N, Dudek D, Drzewiecki J, Banning AP, Zmudka K, Schiele F, Zhou Z, Rademaker TA, van Es GA, Koglin J, Russell ME, Colombo A. Two-year serial coronary angiographic and intravascular ultrasound analysis of in-stent angiographic late lumen loss and ultrasonic neointimal volume from the TAXUS II trial. *Am J Cardiol.* 2007;99:607-15.

25. Jeremias A, Kutscher S, Haude M, Heinen D, Holtmann G, Senf W, Erbel R. Nonischemic chest pain induced by coronary interventions: a prospective study comparing coronary angioplasty and stent implantation. *Circulation.* 1998;98:2656-8.

26. Gruettner J, Henzler T, Sueselbeck T, Fink C, Borggrefe M, Walter T. Clinical assessment of chest pain and guidelines for imaging. *Eur J Radiol.* 2012;81:3663-8.

27. Kini AS, Lee P, Mitre CA, Duffy ME, Sharma SK. Postprocedure chest pain after coronary stenting: implications on clinical restenosis. *J Am Coll Cardiol.* 2003;41:33-8.

28. Gallagher R, Lynch F, Paul G, Petkovski D, Kandl B, Lang S, Thomas N, Fildes J, James B, Love F. Chest symptoms following coronary stenting in the first 10 weeks of recovery. *Eur J Cardiovasc Nurs.* 2008;7:73-9.

29. Bourantas CV, Zhang Y, Farooq V, Garcia-Garcia HM, Onuma Y, Serruys PW. Bioresorbable scaffolds: current evidence and ongoing clinical trials. *Curr Cardiol Rep.* 2012;14:626-34.

## Online data supplement

**Online Table 1.** Baseline clinical characteristics (matching on diabetes, reference vessel diameter, preprocedural minimum lumen diameter, lesion length).

**Online Table 2.** Baseline angiographic characteristics post device implantation (matching on diabetes, reference vessel diameter, preprocedural minimum lumen diameter, lesion length).

## Online data supplement

**Online Table 1. Baseline clinical characteristics (matching on diabetes, reference vessel diameter, preprocedural minimum lumen diameter, lesion length).**

	BVS (N <sub>p</sub> =28, N <sub>l</sub> =28)	EES (N <sub>p</sub> =26, N <sub>l</sub> =28)	p-value	
Age (years)	63.93±9.44	62.42±13.70	0.64	
Male	78.57%	76.92%	1.00	
Diabetes mellitus	14.29%	15.38%	1.00	
Hypertension	50.00%	46.15%	0.79	
Hypercholesterolaemia	89.29%	80.00%	0.45	
Current smoker	14.29%	30.77%	0.20	
Family history of CAD	42.86%	52.17%	0.58	
Prior MI	75.00%	28.00%	0.57	
History of PCI	14.29%	3.85%	0.35	
Stable angina	75.00%	50.00%	0.09	
Unstable angina	10.71%	38.46%	0.03	
Silent ischaemia	0.00%	3.85%	0.48	
Number of diseased vessels	One vessel	85.71%	61.54%	0.06
	Two vessels	3.57%	34.62%	<0.01
	Three or more vessels	10.71%	3.85%	0.61

Data are mean±SD or %. BVS: bioresorbable vascular scaffold; CAD: coronary artery disease; EES: everolimus-eluting stent; MI: myocardial infarction; N<sub>p</sub>: number of patients; N<sub>l</sub>: number of lesions; PCI: percutaneous coronary intervention

**Online Table 2. Baseline angiographic characteristics post device implantation (matching on diabetes, reference vessel diameter, preprocedural minimum lumen diameter, lesion length).**

	BVS (N <sub>p</sub> =28, N <sub>l</sub> =28)	EES (N <sub>p</sub> =26, N <sub>l</sub> =28)	p-value	
Angulation	0.00%	10.71%	0.24	
Calcification (heavy or moderate)	21.43%	35.71%	0.38	
Eccentricity	100.00%	100.00%	NA	
AHA/ACC lesion classification	A	0.00%	0.00%	NA
	B1	46.43%	17.86%	0.04
	B2	50.00%	82.14%	0.02
	C	3.57%	0.00%	1.00
Target vessel	LAD	35.71%	46.43%	0.59
	LCX	28.57%	25.00%	1.00
	RCA	35.71%	28.57%	0.78
Lesion length (mm)	10.21±4.05	11.83±4.20	0.15	
Diameter stenosis (%)	58.93±11.79	57.74±8.41	0.67	
Pre-procedure MLD (mm)	1.06±0.34 (28)	1.12±0.26	0.43	
Reference vessel diameter (mm)	2.58±0.39	2.66±0.36	0.45	
Post-dilatation rate	57.1%	46.4%	0.59	
Balloon diameter (mm)	3.20±0.28	3.31±0.25	0.32	
Maximum pressure (atm)	17.56±7.26	16.15±3.87	0.67	

Data are mean±SD or %. LAD: left anterior descending artery; LCX: left circumflex coronary artery; MLD: minimum lumen diameter; N<sub>p</sub>: number of patients; N<sub>l</sub>: number of lesions; RCA: right coronary artery

### 2.3 Reproducibility of IVUS-GS and IVUS-VH analyses

Reproducibility of intravascular ultrasound radiofrequency data analysis (Virtual Histology) with a 45 MHz rotational imaging catheter in ex vivo human coronary arteries.

*J Cardiol.* 2015;65:134-42.

[Original research paper, Impact Factor (2013): 2.566]

Muramatsu T, García-García HM, Brugaletta S, Heo JH, Onuma Y, Fedewa RJ, Nair A, Ozaki Y, Serruys PW.





# Reproducibility of intravascular ultrasound radiofrequency data analysis (virtual histology) with a 45-MHz rotational imaging catheter in ex vivo human coronary arteries



Takashi Muramatsu (MD, PhD)<sup>a,b</sup>, Hector M. García-García (MD, PhD)<sup>a,c,\*</sup>,  
Salvatore Brugaletta (MD, PhD)<sup>d</sup>, Jung Ho Heo (MD)<sup>e</sup>, Yoshinobu Onuma (MD, PhD)<sup>a</sup>,  
Russell J. Fedewa (PhD)<sup>f</sup>, Anuja Nair (PhD)<sup>g</sup>, Yukio Ozaki (MD, PhD)<sup>b,\*\*</sup>,  
Patrick W. Serruys (MD, PhD)<sup>a</sup>

<sup>a</sup>Thoraxcenter, Erasmus Medical Center, Rotterdam, The Netherlands

<sup>b</sup>Department of Cardiology, Fujita Health University Hospital, Toyoake, Japan

<sup>c</sup>Cardialysis B.V., Rotterdam, The Netherlands

<sup>d</sup>Department of Cardiology, Thorax Institute, Hospital Clinic, Barcelona, Spain

<sup>e</sup>Division of Cardiology, Department of Internal Medicine, Kosin University Gospel Hospital, Busan, South Korea

<sup>f</sup>Biomedical Engineering Department, Cleveland Clinic, Cleveland, OH, USA

<sup>g</sup>Volcano Corporation, Rancho Cordova, CA, USA

## ARTICLE INFO

### Article history:

Received 24 March 2014

Received in revised form 1 May 2014

Accepted 7 May 2014

Available online 18 September 2014

### Keywords:

Intravascular ultrasound

Virtual histology

Reproducibility

Ex vivo

Coronary artery disease

## ABSTRACT

**Background:** Despite the frequent use of spectral analysis of intravascular ultrasound radiofrequency data (VH<sup>®</sup> IVUS) in clinical studies, the assessment for reproducibility using this with high frequency IVUS remains unexplored.

**Purpose:** The aim of this study was to examine the reproducibility of VH IVUS using 45-MHz rotational IVUS in ex vivo human coronary arteries.

**Methods:** Data were collected using 45-MHz VH IVUS (Revolution<sup>®</sup>, Volcano Corporation, San Diego, CA, USA) via a series of pullbacks from eight human coronary artery specimens. Imaging data were analyzed by two independent observers. Intraobserver and interobserver reproducibility were assessed using five pullbacks from five vessels. The intercatheter reproducibility was assessed using three different catheters in each of the five vessels. The intracatheter reproducibility was assessed between the two sequential pullbacks from each of the 15 catheters used in the intercatheter assessment.

**Results:** Geometrical measurements consistently showed low variability (relative difference <10%) and excellent intraclass correlation coefficients (ICCs), ranging from 0.88 to 1.00. With respect to the compositional measurements, the relative differences were predominantly higher than those of geometrical measurements. In particular, fibrous-fatty area showed a higher relative difference (17.5% in intercatheter assessment) compared to fibrous, necrotic core, and dense calcium areas (6.5%, 8.4%, and 6.4%, respectively). However, each compositional measurement also showed acceptable reproducibility (ICCs ranging from 0.82 to 1.00).

**Conclusions:** The 45-MHz rotational VH IVUS technology had acceptable reproducibility with respect to geometrical and compositional assessments in ex vivo human coronary arteries. These data are crucial when designing future longitudinal studies addressing geometrical measurements and plaque characterization by 45-MHz VH IVUS.

© 2014 Japanese College of Cardiology. Published by Elsevier Ltd. All rights reserved.

\* Corresponding author at: Thoraxcenter, Erasmus Medical Center, z120, Dr Molerwaterplein 40, 3015 GD Rotterdam, The Netherlands. Tel.: +31 10 206 28 28; fax: +31 10 206 28 44.

\*\* Co-corresponding author at: Department of Cardiology, Fujita Health University Hospital, 1-98, Dengaku, Kutsukake, Toyoake 470-1192, Japan. Tel.: +81 562 93 2312; fax: +81 562 93 2315.

E-mail addresses: hgarcia@cardialysis.nl (H.M. García-García), ozakiyuk@fujita-hu.ac.jp (Y. Ozaki).

<http://dx.doi.org/10.1016/j.jicc.2014.05.004>

0914-5087/© 2014 Japanese College of Cardiology. Published by Elsevier Ltd. All rights reserved.

## Introduction

Intravascular ultrasound (IVUS) facilitates the assessment of extent, distribution, severity, and morphology in human atherosclerotic coronary arteries [1–3]. In the field of interventional cardiology, IVUS has been used not only for therapeutic decision making [4,5], but also for clinical research evaluating serial changes in atherosclerotic coronary plaque size and composition [6–10]. The spectral analysis of IVUS radiofrequency data (VH<sup>®</sup> IVUS) facilitates plaque characterization. This VH IVUS technology (Volcano Corporation, San Diego, CA, USA) classifies plaque components as fibrous, fibrous-fatty, necrotic core, or dense calcium [11,12]. The predictive accuracy of the 20-MHz VH IVUS technology was previously examined by direct comparison with pathohistology of ex vivo (97%) and in vivo (95%) human coronary arteries [12,13]. These studies illustrated the clinical significance of VH IVUS images to assess the distribution of the tissue components within the plaque [14]. Indeed, distributions of these components might reflect the clinical characteristics of patients [15] and were also associated with cardiovascular risk score [16]. A previous clinical trial demonstrated that the presence of a thin-cap fibroatheroma detected by VH IVUS was an independent predictor of future cardiac events [17]. It should also be noted that, in the IBIS-2 study, an Lp-PLA<sub>2</sub> inhibitor darapladib (GlaxoSmithKline, Philadelphia, PA, USA) was studied with regard to its capabilities to modify plaque components. One of the key findings was that Lp-PLA<sub>2</sub> inhibition with darapladib interferes with necrotic core expansion as assessed by VH IVUS [18]. This study highlighted the potential of VH IVUS to detect changes in plaque that are related to the mechanism of action of the investigational drugs. Since the fate of coronary plaques is related to their histological composition [19], valid plaque characterization could provide clinically relevant information and become a therapeutic target for future studies regarding pharmacological intervention [7–9,18] and bioresorbable scaffold implantation [20,21].

The first commercially available VH IVUS system was developed with 20-MHz solid-state array IVUS. A new-generation 45-MHz rotational VH IVUS has been developed and produces better resolution images that might improve plaque characterization. However, there have been no published data in terms of reproducibility that is crucial for longitudinal studies. Therefore, the aim of this study was to assess the reproducibility of geometrical and compositional measurements using 45-MHz rotational VH IVUS in ex vivo human coronary arteries.

## Methods

### *Samples and imaging procedure*

A total of nine harvested specimens of human coronary arteries were used for this study. The mean age of the donors was 61.3 years, and all coronary artery specimens showed severe atherosclerotic plaque. The specimens were pinned on a custom-made room-temperature-vulcanizing silicone elastomer using needles in a dissecting tray filled with saline during imaging. The elastomer has acoustic impedance comparable to water in order to minimize ultrasonic artifacts within the IVUS image. A 3.2-French, 45-MHz rotational IVUS catheter (Revolution<sup>®</sup>, Volcano Corporation) was inserted from the ostium to the distal end of the specimen. IVUS data were acquired with a pullback speed of 0.5 mm/s. An electrocardiogram simulator (430B ECG simulator, Medi Cal Instruments, Inc., Lewis Center, OH, USA) was used to trigger the VH IVUS data acquisition at a frequency of 60 beats per minute.

### *45-MHz VH IVUS data analysis*

The IVUS data were recorded with a commercially available IVUS console that was enabled for 45-MHz ultrasound backscatter data acquisition (s5 Imaging System, Volcano Corporation). In each pullback, the region of interest (ROI) was defined using distal and proximal side branches. The same side branches were used as anatomical landmarks for each pullback data within a given vessel. Contour detection of vessel lumen and media–adventitia interface was independently performed by two experienced IVUS analysts. QIvus Version 2.1 software (Medis, Leiden, The Netherlands) was used for the off-line contour detection, and the virtual histology (VH) images were processed with the contours using the VH OEM Version 2.0.2 software (Volcano Corporation) that was modified specifically to assess tissue characterization in ex vivo data in the absence of blood attenuation.

### *Reproducibility assessment*

In this study, we assessed the intraobserver, interobserver, intracatheter, and intercatheter reproducibility. Among the nine vessels (i.e., coronary artery specimens); one vessel was excluded from the current analysis because of poor specimen quality due to severe damage. For the assessment of intraobserver reproducibility, five pullbacks from five vessels were randomly selected and analyzed twice at an interval of 2 weeks by the same observer (i.e., agreement between 1st and 2nd analyses). For the assessment of interobserver reproducibility, the same five pullbacks as used for the intraobserver assessment were analyzed by two independent analysts (i.e., agreement between observer 1 and observer 2). In addition, five vessels were evaluated by three catheters each with two sequential pullbacks per catheter, leading to the capability of multiple assessments: intracatheter reproducibility comparing two sequential pullbacks with 15 catheters (i.e., agreement between 1st and 2nd pullbacks), and intercatheter reproducibility comparing the first pullback of catheter 1, catheter 2, and catheter 3 in each vessel (i.e., agreement among three catheters).

We applied the frame-level analysis for the assessment of intraobserver and interobserver reproducibility because all the same frames (i.e., crosssections) should be analyzed, while the segment-level analysis was applied for the assessment of intracatheter and intercatheter reproducibility because the analyzed crosssections could be different between the pullbacks even after matching the segments with the landmark side branches. Each component of geometrical and compositional measurements was compared under the aforementioned conditions.

### *Statistical analysis*

Descriptive variables are presented as means  $\pm$  standard deviations (SDs). The reproducibility with corresponding 95% confidence intervals (CIs) was determined using intraclass correlation coefficients (ICCs). Bland–Altman plots were generated to estimate the limit of agreement (LOA) defined as the mean difference of measurements between the two conditions  $\pm$  2 SD [22]. Statistical analysis was performed with PASW 18 software (SPSS Inc., Chicago, IL, USA).

## Results

### *Intraobserver agreement*

The mean length of ROI was  $20.5 \pm 4.1$  mm for the five pullbacks. Geometrical and compositional data of the matched frames are shown in Table 1. The relative intraobserver differences in geometrical measurements were negligible. Of note, the relative

**Table 1**

Geometrical and compositional measurements of the same frames with two subsequent analyses (intraobserver agreement).

Variables	1st analysis	2nd analysis	Difference		LOA <sup>a</sup>		ICC (95% CI)
			Absolute	Relative (%)	Lower	Upper	
<b>Geometrical data</b>							
Lumen CSA (mm <sup>2</sup> )	6.77 ± 1.94	6.74 ± 1.95	0.03 ± 0.51	0.4	-1.05	1.00	0.98 (0.98-0.99)
Lumen minimum diameter (mm)	2.48 ± 0.46	2.47 ± 0.46	0.02 ± 0.16	0.7	-0.33	0.30	0.97 (0.96-0.98)
Lumen maximum diameter (mm)	3.39 ± 0.56	3.38 ± 0.55	0.01 ± 0.15	0.3	-0.31	0.28	0.98 (0.98-0.99)
Lumen mean diameter (mm)	2.88 ± 0.44	2.87 ± 0.44	0.01 ± 0.12	0.2	-0.24	0.22	0.98 (0.98-0.99)
Vessel CSA (mm <sup>2</sup> )	17.49 ± 3.99	17.79 ± 3.99	0.31 ± 0.60	1.7	-0.90	1.51	0.99 (0.99-1.00)
Vessel minimum diameter (mm)	4.45 ± 0.57	4.48 ± 0.57	0.02 ± 0.11	0.5	-0.19	0.23	0.99 (0.99-0.99)
Vessel maximum diameter (mm)	4.93 ± 0.55	4.99 ± 0.57	0.06 ± 0.13	1.3	-0.20	0.33	0.98 (0.98-0.99)
Vessel mean diameter (mm)	4.68 ± 0.55	4.72 ± 0.55	0.04 ± 0.09	0.9	-0.14	0.22	0.99 (0.99-0.99)
Plaque area (mm <sup>2</sup> )	10.72 ± 3.42	11.05 ± 3.46	0.33 ± 0.76	3.1	-1.19	1.85	0.99 (0.98-0.99)
Plaque burden (%)	60.81 ± 9.76	61.59 ± 9.72	0.78 ± 3.50	1.3	-6.22	7.78	0.97 (0.95-0.97)
<b>Compositional data</b>							
Fibrous area (mm <sup>2</sup> )	2.81 ± 1.57	2.88 ± 1.56	0.07 ± 0.24	2.3	-0.41	0.54	0.99 (0.99-1.00)
Fibrous tissue (%)	38.75 ± 15.87	38.50 ± 15.87	0.25 ± 2.92	0.6	-6.09	5.59	0.99 (0.99-0.99)
Fibrous-fatty area (mm <sup>2</sup> )	2.87 ± 2.22	3.03 ± 2.29	0.16 ± 0.48	5.5	-0.80	1.11	0.99 (0.98-0.99)
Fibrous-fatty tissue (%)	36.09 ± 17.36	36.60 ± 17.28	0.51 ± 4.48	1.4	-8.45	9.48	0.98 (0.98-0.99)
Necrotic core area (mm <sup>2</sup> )	1.15 ± 0.66	1.21 ± 0.68	0.06 ± 0.15	5.1	-0.24	0.35	0.99 (0.98-0.99)
Necrotic core tissue (%)	17.12 ± 8.95	17.08 ± 8.54	0.04 ± 2.25	0.2	-4.53	4.45	0.98 (0.98-0.99)
Dense calcium area (mm <sup>2</sup> )	0.52 ± 0.48	0.54 ± 0.49	0.02 ± 0.08	3.2	-0.14	0.17	0.99 (0.99-1.00)
Dense calcium tissue (%)	8.04 ± 7.05	7.82 ± 6.76	0.22 ± 1.57	2.8	-3.37	2.92	0.99 (0.98-0.99)

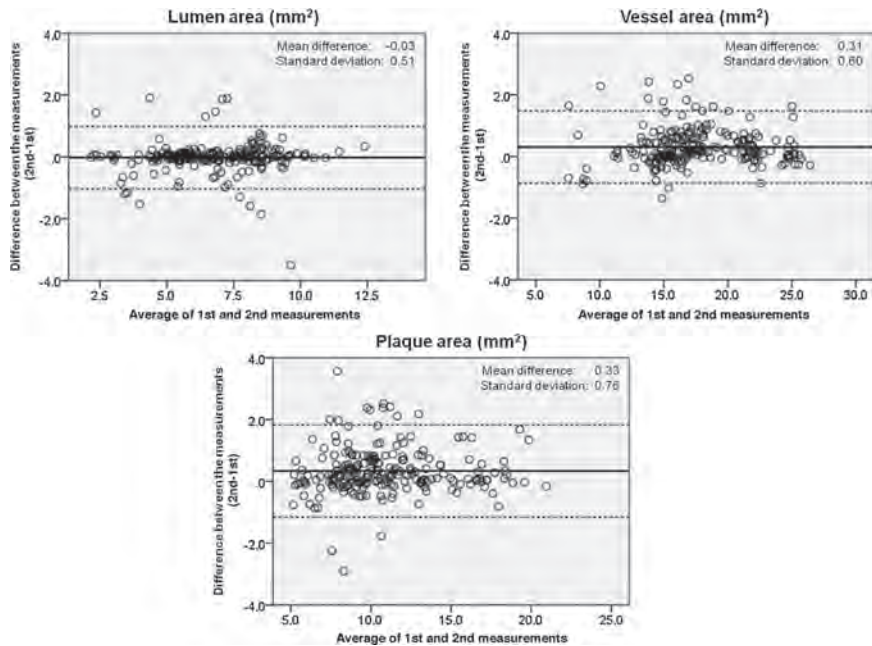
N = 5 pullbacks with 210 frames.

CSA, cross-sectional area; LOA, limit of agreement; ICC, intraclass correlation coefficient.

<sup>a</sup> LOA was defined as mean ± 2 SD of absolute difference by Bland-Altman method.

differences in plaque area and plaque burden were 3.1% and 1.3%, respectively. Although compositional measurements showed slightly greater relative differences than geometrical measurements, the relative differences were consistently less than 10%, with the greatest

relative difference of 5.5% for fibrous-fatty area. The ICCs showed excellent reproducibility and Bland-Altman plots showed narrow LOAs in both geometrical (Fig. 1) and compositional (Fig. 2) measurements. The LOAs for lumen, vessel, and plaque areas were

**Fig. 1.** Bland-Altman plots depicting the intraobserver agreement for geometrical measurements.

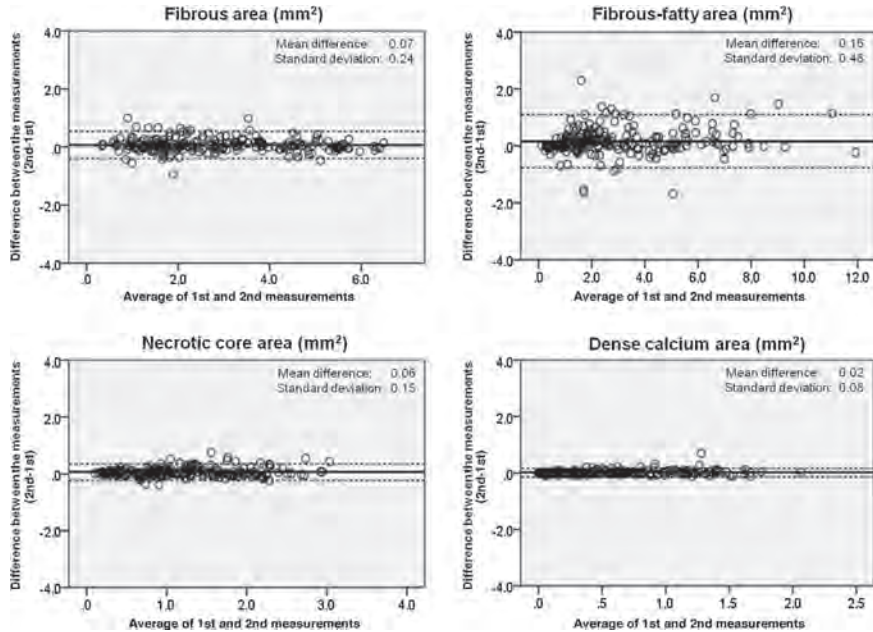


Fig. 2. Bland-Altman plots depicting the intraobserver agreement for compositional measurements.

1.00,  $-1.05 \text{ mm}^2$ ; 1.51,  $-0.90 \text{ mm}^2$ ; and 1.85,  $-1.19 \text{ mm}^2$ , respectively. The LOAs for the area measurements of fibrous, fibrous-fatty, necrotic core, and dense calcium were  $0.54, -0.41 \text{ mm}^2$ ;  $1.11, -0.80 \text{ mm}^2$ ;  $0.35, -0.24 \text{ mm}^2$ ; and  $0.17, -0.14 \text{ mm}^2$ , respectively.

#### Interobserver agreement

Geometrical and compositional data of the matched frames are shown in Table 2. The relative interobserver differences

**Table 2**  
Geometrical and compositional measurements of the same frames by two observers (interobserver agreement).

Variables	Observer 1	Observer 2	Difference		LOA <sup>a</sup>		ICC (95% CI)
			Absolute	Relative (%)	Lower	Upper	
<b>Geometrical data</b>							
Lumen CSA (mm <sup>2</sup> )	6.77 ± 1.94	7.01 ± 1.90	0.24 ± 0.54	3.6	-0.84	1.32	0.98 (0.97-0.98)
Lumen minimum diameter (mm)	2.48 ± 0.46	2.55 ± 0.42	0.07 ± 0.16	2.7	-0.25	0.38	0.96 (0.95-0.97)
Lumen maximum diameter (mm)	3.39 ± 0.56	3.40 ± 0.54	0.01 ± 0.18	0.2	-0.35	0.37	0.97 (0.96-0.98)
Lumen mean diameter (mm)	2.88 ± 0.44	2.94 ± 0.41	0.06 ± 0.13	2.1	-0.19	0.31	0.97 (0.96-0.98)
Vessel CSA (mm <sup>2</sup> )	17.49 ± 3.99	17.51 ± 4.04	0.03 ± 1.05	0.2	-2.08	2.14	0.98 (0.98-0.99)
Vessel minimum diameter (mm)	4.45 ± 0.57	4.43 ± 0.56	0.02 ± 0.18	0.5	-0.38	0.34	0.97 (0.97-0.98)
Vessel maximum diameter (mm)	4.93 ± 0.55	4.96 ± 0.57	0.03 ± 0.19	0.6	-0.35	0.41	0.97 (0.96-0.98)
Vessel mean diameter (mm)	4.68 ± 0.55	4.69 ± 0.55	0.00 ± 0.15	0.0	-0.29	0.30	0.98 (0.98-0.99)
Plaque area (mm <sup>2</sup> )	10.72 ± 3.42	10.51 ± 3.56	0.21 ± 1.19	2.0	-2.60	2.17	0.97 (0.96-0.98)
Plaque burden (%)	60.81 ± 9.76	59.14 ± 10.06	1.67 ± 4.35	2.8	-10.37	7.02	0.94 (0.92-0.96)
<b>Compositional data</b>							
Fibrous area (mm <sup>2</sup> )	2.81 ± 1.57	2.67 ± 1.52	0.14 ± 0.34	5.0	-0.83	0.55	0.99 (0.98-0.99)
Fibrous tissue (%)	38.75 ± 15.87	38.43 ± 16.19	0.33 ± 3.31	0.8	-6.94	6.29	0.99 (0.99-0.99)
Fibrous-fatty area (mm <sup>2</sup> )	2.87 ± 2.22	2.92 ± 2.29	0.05 ± 0.76	1.7	-1.47	1.56	0.97 (0.96-0.98)
Fibrous-fatty tissue (%)	36.09 ± 17.36	37.26 ± 18.36	1.16 ± 5.35	3.2	-9.53	11.86	0.98 (0.97-0.98)
Necrotic core area (mm <sup>2</sup> )	1.15 ± 0.66	1.08 ± 0.66	0.07 ± 0.19	6.1	-0.46	0.32	0.98 (0.97-0.98)
Necrotic core tissue (%)	17.12 ± 8.95	16.41 ± 8.66	0.71 ± 2.56	4.1	-5.84	4.42	0.98 (0.97-0.98)
Dense calcium area (mm <sup>2</sup> )	0.52 ± 0.48	0.51 ± 0.47	0.02 ± 0.10	3.2	-0.21	0.18	0.99 (0.99-0.99)
Dense calcium tissue (%)	8.04 ± 7.05	7.91 ± 6.79	0.13 ± 2.10	1.6	-4.34	4.08	0.98 (0.97-0.98)
N = 5 pullbacks with 210 frames in each observer.							
CSA, cross-sectional area; LOA, limit of agreement; ICC, intraclass correlation coefficient.							
<sup>a</sup> LOA was defined as mean ± 2 SD of absolute difference by Bland-Altman method.							

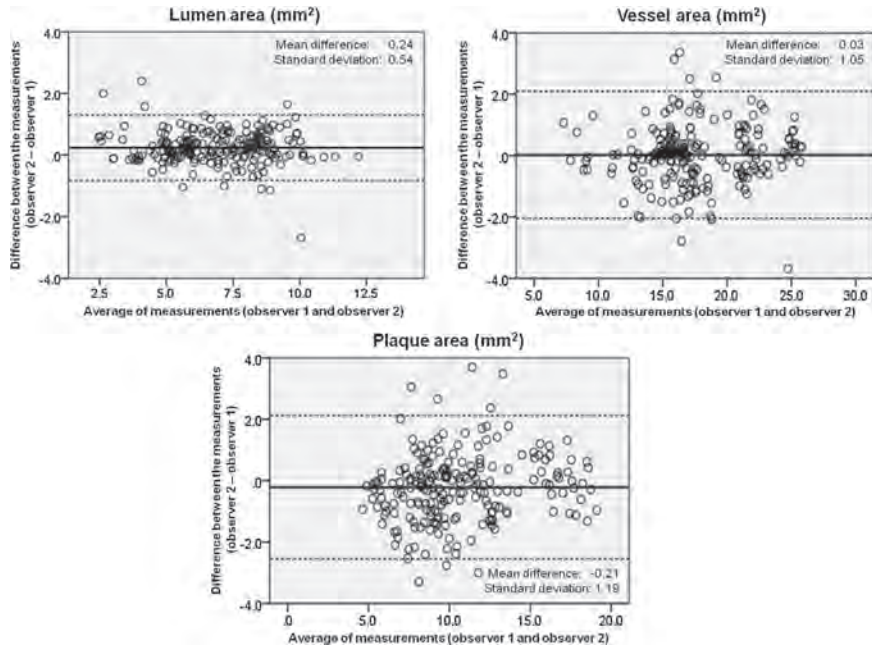


Fig. 3. Bland-Altman plots depicting the interobserver agreement for geometrical measurements.

in geometrical measurements were also negligible and those of plaque area and plaque burden were 2.0% and 2.8%, respectively. With respect to compositional measurements, the relative differences were consistently less than 10% and ICCs showed excellent reproducibility. Bland-Altman plots showed narrow LOAs in both geometrical (Fig. 3) and compositional (Fig. 4) measurements. The LOAs for lumen, vessel, and plaque areas were 1.32,  $-0.84 \text{ mm}^2$ ; 2.14,  $-2.08 \text{ mm}^2$ ; and 2.17,  $-2.60 \text{ mm}^2$ , respectively. The LOAs for the area measurements of fibrous, fibrous-fatty, necrotic core, and dense calcium were 0.55,  $-0.83 \text{ mm}^2$ ; 1.56,  $-1.47 \text{ mm}^2$ ; 0.32,  $-0.46 \text{ mm}^2$ ; and 0.18,  $-0.21 \text{ mm}^2$ , respectively.

#### Intracatheter agreement

Geometrical and compositional data of the matched ROI are shown in Table 3. A total of 15 catheters were used for the present data analysis. The relative intracatheter differences were less than 5% in both geometrical and compositional measurements. ICCs predominantly showed excellent reproducibility except for the proportional measurement of fibrous-fatty plaque, although the coefficient was 0.84. The LOAs for lumen, vessel, and plaque areas were 0.44,  $-0.50 \text{ mm}^2$ ; 1.05,  $-0.77 \text{ mm}^2$ ; and 1.23,  $-0.89 \text{ mm}^2$ , respectively. The LOAs for the area measurements of fibrous, fibrous-fatty, necrotic core, and dense calcium were 0.30,  $-0.21 \text{ mm}^2$ ; 1.10,  $-0.88 \text{ mm}^2$ ; 0.22,  $-0.20 \text{ mm}^2$ ; and 0.16,  $-0.18 \text{ mm}^2$ , respectively.

#### Intercatheter agreement

Geometrical and compositional data of the matched ROI are shown in Table 4. With respect to geometrical measurements, the mean relative differences were less than 10% and ICCs showed good agreement, ranging from 0.88 to 1.00. Although fibrous-fatty area showed greater variability than the other compositional measurements (average relative difference, 17.5%), ICCs showed good reproducibility, ranging from 0.82 to 1.00. Considering the average plaque area ( $10.9 \text{ mm}^2$ ), however, the average of absolute difference in fibrous-fatty area was numerically small ( $0.46 \text{ mm}^2$ ).

#### Discussion

Gray-scale IVUS has been employed as a gold standard of geometrical assessment of coronary plaque [23]. VH IVUS was introduced as a complementary technology that provides an accurate compositional assessment of plaque [11-13]. Several previous studies employed the 20-MHz VH IVUS technology to evaluate the temporal changes in plaque composition after pharmacological intervention [7-9,18] or bioresorbable scaffold implantation [20,24]. The VH IVUS algorithm was recently developed for a 45-MHz rotational IVUS catheter. The higher frequency of the 45-MHz rotational catheter provides the potential for improved VH IVUS with the cost of increased attenuation and reduced imaging field-of-view in comparison with the 20-MHz solid-state array IVUS. Understanding the reproducibility of the

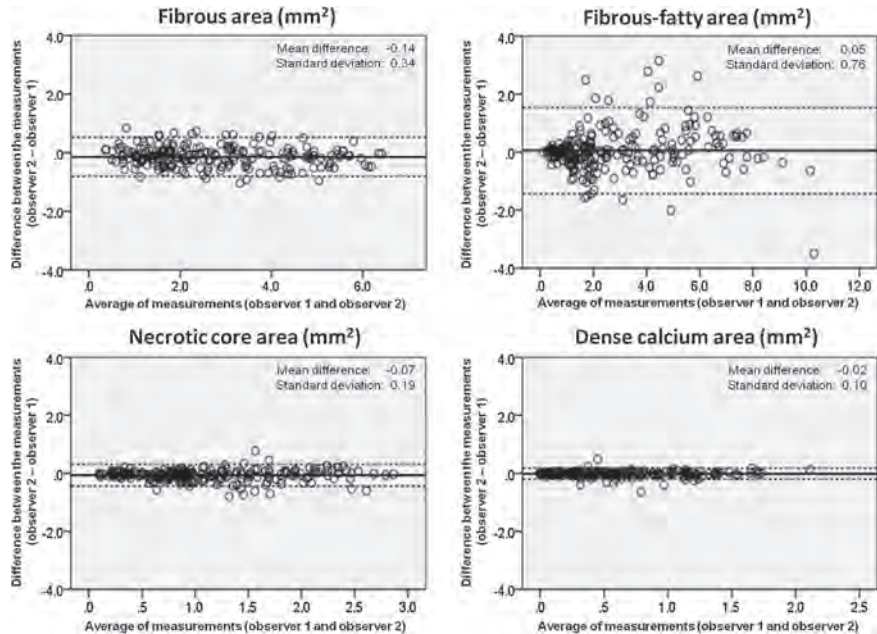


Fig. 4. Bland-Altman plots depicting the interobserver agreement for compositional measurements.

45-MHz VH IVUS algorithm is critical to create a foundation on which to design future longitudinal studies.

In this study, a narrow range of agreement was demonstrated by the Bland-Altman plots. The relative differences of geometrical

measurements were predominantly less than 3% and ICCs were high. It should be noted that plaque burden, which is one of the most commonly used primary endpoints in IVUS studies evaluating plaque progression/regression, showed excellent

**Table 3**  
Geometrical and compositional measurements of the matched ROI with two subsequent pullbacks (intracatheter agreement).

Variables	1st pullback	2nd pullback	Difference		LOA <sup>a</sup>		ICC (95% CI)
			Absolute	Relative (%)	Lower	Upper	
<b>Geometrical data</b>							
Lumen CSA (mm <sup>2</sup> )	6.74 ± 0.86	6.70 ± 0.71	0.03 ± 0.23	0.47	-0.50	0.44	0.98 (0.94-0.99)
Lumen minimum diameter (mm)	2.50 ± 0.20	2.51 ± 0.17	0.004 ± 0.071	0.14	-0.14	0.15	0.96 (0.90-0.99)
Lumen maximum diameter (mm)	3.32 ± 0.19	3.31 ± 0.15	0.01 ± 0.05	0.24	-0.10	0.08	0.98 (0.95-0.99)
Lumen mean diameter (mm)	2.88 ± 0.19	2.88 ± 0.16	0.004 ± 0.050	0.13	-0.10	0.10	0.98 (0.95-0.99)
Vessel CSA (mm <sup>2</sup> )	17.55 ± 3.20	17.69 ± 2.98	0.14 ± 0.46	0.80	-0.77	1.05	0.99 (0.98-1.00)
Vessel minimum diameter (mm)	4.42 ± 0.46	4.44 ± 0.44	0.02 ± 0.05	0.56	-0.08	0.13	1.00 (0.99-1.00)
Vessel maximum diameter (mm)	4.98 ± 0.41	5.00 ± 0.37	0.02 ± 0.08	0.38	-0.14	0.18	0.99 (0.97-1.00)
Vessel mean diameter (mm)	4.69 ± 0.43	4.71 ± 0.41	0.02 ± 0.06	0.49	-0.09	0.14	1.00 (0.99-1.00)
Plaque area (mm <sup>2</sup> )	10.81 ± 2.98	10.98 ± 2.72	0.17 ± 0.53	1.59	-0.89	1.23	0.99 (0.97-1.00)
Plaque burden (%)	60.92 ± 6.01	61.65 ± 5.39	0.73 ± 1.30	1.19	-1.87	3.32	0.98 (0.95-0.99)
<b>Compositional data</b>							
Fibrous area (mm <sup>2</sup> )	2.38 ± 0.95	2.43 ± 0.93	0.04 ± 0.13	1.86	-0.21	0.30	1.00 (0.99-1.00)
Fibrous tissue (%)	33.48 ± 7.98	33.62 ± 8.57	0.14 ± 1.65	0.40	-3.16	3.43	0.99 (0.97-1.00)
Fibrous-fatty area (mm <sup>2</sup> )	2.62 ± 1.14	2.73 ± 1.09	0.11 ± 0.49	4.25	-0.88	1.10	0.95 (0.85-0.98)
Fibrous-fatty tissue (%)	33.95 ± 4.38	34.44 ± 5.49	0.48 ± 3.74	1.42	-7.01	7.97	0.84 (0.54-0.95)
Necrotic core area (mm <sup>2</sup> )	1.56 ± 0.62	1.57 ± 0.56	0.01 ± 0.11	0.65	-0.20	0.22	0.99 (0.98-1.00)
Necrotic core tissue (%)	20.68 ± 3.02	20.49 ± 2.95	0.19 ± 1.60	0.91	-3.38	3.01	0.93 (0.79-0.98)
Dense calcium area (mm <sup>2</sup> )	0.88 ± 0.44	0.87 ± 0.43	0.01 ± 0.09	0.86	-0.18	0.16	0.99 (0.97-1.00)
Dense calcium tissue (%)	11.73 ± 5.02	11.45 ± 5.35	0.27 ± 1.31	2.34	-2.89	2.34	0.98 (0.96-1.00)

N = 15 catheters sequentially pulled back in five vessels.  
 CSA, cross-sectional area; LOA, limit of agreement; ICC, intraclass correlation coefficient.  
<sup>a</sup> LOA was defined as mean ± 2 SD of absolute difference by Bland-Altman method.

**Table 4** Geometrical and compositional measurements of the matched ROI with three subsequent catheters (intercatheter agreement).

Variables	Catheter 1		Catheter 2		Catheter 3		Δcatheter 2 – catheter 1		Relative (%)		Δcatheter 3 – catheter 2		Relative (%)		Absolute		Relative (%)		Overall mean		ICC (95% CI)	
	Absolute	Relative (%)	Absolute	Relative (%)	Absolute	Relative (%)	Absolute	Relative (%)	Absolute	Relative (%)	Absolute	Relative (%)	Absolute	Relative (%)	Absolute	Relative (%)	Absolute	Relative (%)	Absolute	Relative (%)	Absolute	Relative (%)
<b>Geometrical data</b>																						
Lumen CSA (mm <sup>2</sup> )	7.07 ± 1.19	6.60 ± 0.67	6.57 ± 0.60	0.57 ± 0.40	7.6	0.32 ± 0.18	4.8	0.59 ± 0.74	8.7	0.49	7.0	0.88 (0.45–0.99)										
Lumen min diameter (mm)	2.60 ± 0.28	2.47 ± 0.17	2.47 ± 0.13	0.13 ± 0.11	4.7	0.06 ± 0.04	2.4	0.14 ± 0.17	5.6	0.11	4.3	0.88 (0.47–0.99)										
Lumen max diameter (mm)	3.36 ± 0.25	3.29 ± 0.14	3.31 ± 0.17	0.11 ± 0.06	3.3	0.07 ± 0.03	2.2	0.11 ± 0.10	3.4	0.10	3.0	0.92 (0.66–0.99)										
Lumen mean diameter (mm)	2.96 ± 0.27	2.85 ± 0.16	2.85 ± 0.14	0.12 ± 0.08	4.0	0.07 ± 0.03	2.4	0.12 ± 0.15	4.3	0.11	3.6	0.90 (0.55–0.99)										
Vessel CSA (mm <sup>2</sup> )	17.62 ± 3.43	17.79 ± 3.33	17.53 ± 3.52	0.57 ± 0.28	3.5	0.78 ± 0.28	4.6	0.61 ± 0.66	3.5	0.65	3.9	0.99 (0.96–1.00)										
Vessel min diameter (mm)	4.44 ± 0.51	4.46 ± 0.47	4.40 ± 0.51	0.07 ± 0.04	1.6	0.08 ± 0.05	1.8	0.08 ± 0.05	1.8	0.07	1.7	1.00 (0.98–1.00)										
Vessel max diameter (mm)	4.99 ± 0.44	5.00 ± 0.40	4.99 ± 0.47	0.08 ± 0.05	1.6	0.12 ± 0.07	2.4	0.11 ± 0.11	2.1	0.10	2.0	0.99 (0.94–1.00)										
Vessel mean diameter (mm)	4.70 ± 0.47	4.72 ± 0.43	4.69 ± 0.48	0.07 ± 0.05	1.6	0.10 ± 0.05	2.2	0.08 ± 0.09	1.8	0.08	1.9	0.99 (0.96–1.00)										
Plaque area (mm <sup>2</sup> )	10.54 ± 3.18	11.19 ± 3.29	10.96 ± 3.17	0.65 ± 0.25	6.5	0.62 ± 0.26	5.6	0.62 ± 0.45	3.90	0.57	5.4	0.99 (0.97–1.00)										
Plaque burden (mm <sup>2</sup> )	59.39 ± 7.51	61.89 ± 5.89	61.90 ± 5.78	2.50 ± 2.09	4.6	0.95 ± 0.63	1.6	2.73 ± 2.81	4.6	2.06	3.6	0.97 (0.85–1.00)										
<b>Compositional data</b>																						
Fibrous area (mm <sup>2</sup> )	2.41 ± 1.15	2.43 ± 1.03	2.39 ± 0.88	0.11 ± 0.08	5.0	0.15 ± 0.11	6.4	0.20 ± 0.21	7.9	0.15	6.5	0.89 (0.97–1.00)										
Fibrous tissue (%)	34.35 ± 8.48	32.81 ± 8.50	33.76 ± 9.01	1.49 ± 1.20	4.3	1.48 ± 0.97	4.4	1.78 ± 1.56	5.4	1.37	4.7	0.89 (0.96–1.00)										
Fibrous-fatty area (mm <sup>2</sup> )	2.35 ± 1.04	2.29 ± 1.36	2.27 ± 1.26	0.39 ± 0.32	25.7	0.38 ± 0.23	13.4	0.40 ± 0.27	13.3	0.46	17.3	0.97 (0.85–1.00)										
Fibrous-fatty tissue (%)	34.1 ± 0.7	32.8 ± 0.52	34.7 ± 0.6	0.08 ± 0.09	9.7	0.10 ± 0.1	12	0.12 ± 0.08	8.8	0.10	8.3	0.92 (0.97–1.00)										
Necrotic core area (mm <sup>2</sup> )	1.57 ± 0.65	1.55 ± 0.65	1.61 ± 0.66	0.08 ± 0.09	9.7	0.10 ± 0.1	7.1	0.16 ± 0.16	8.1	0.10	8.4	0.92 (0.97–1.00)										
Necrotic core tissue (%)	21.30 ± 2.24	19.46 ± 3.89	20.97 ± 2.79	2.19 ± 1.93	10.9	1.84 ± 1.14	11.0	0.56 ± 0.74	3.1	1.53	8.3	0.91 (0.61–0.98)										
Dense calcium area (mm <sup>2</sup> )	0.87 ± 0.47	0.90 ± 0.48	0.85 ± 0.44	0.04 ± 0.03	8.0	0.06 ± 0.02	8.4	0.03 ± 0.03	2.9	0.04	6.4	1.00 (0.99–1.00)										
Dense calcium tissue (%)	12.34 ± 5.99	11.27 ± 5.77	10.95 ± 4.43	1.07 ± 0.76	9.7	1.54 ± 0.76	15.6	1.42 ± 1.75	11.1	1.34	12.1	0.98 (0.92–1.00)										

N=15 catheters (5 pairs of 3 catheters) evaluated in five vessels. CSA, cross-sectional area; ICC, interclass correlation coefficient.

reproducibility in any settings of assessment (ICC ranging from 0.94 to 0.98).

Although compositional measurements generally resulted in greater relative differences, indicating greater variability, than those of geometrical measurements, the reproducibility was generally acceptable (ICC ranged from 0.82 to 1.00). These results are in line with the previous studies evaluating the reproducibility of 20-MHz VH IVUS and 40-MHz iMAP catheter [25,26]. Another key observation is that necrotic core measurements showed only slight variability and excellent reproducibility. This result is of great importance since necrotic core has been considered the most clinically relevant plaque component in predicting adverse cardiovascular events [17] and has the potential to be a key focus of longitudinal studies [27].

In contrast, area (mm<sup>2</sup>) and proportional (%) estimates of fibrous-fatty plaque generally demonstrated greater variability and lower reproducibility compared to the other plaque components. A major limitation of radiofrequency (RF)-based plaque characterization is the technical problem with respect to acoustic shadowed area. In severely calcified lesions, RF signals are more likely to contain noise because of reflection by thick layers of calcification. This phenomenon leads to potential biases as follows: (1) an observer-related bias as the acoustic shadow often makes vessel boundaries (i.e., media-*adventitia* interface) invisible that potentially results in miscalculation of vessel area; (2) a software-related bias as the signal processing algorithm does not take the shadowed area into account and will automatically assign the pixels in these regions to the other components within their database based on the noise [28]. Indeed, our sample coronary arteries appeared to be more severely diseased with higher compositions of necrotic core and dense calcium compared to those in the previous reproducibility studies of plaque characterization techniques [25,26]. An example of intracatheter reproducibility assessment in severely calcified lesion is shown in Fig. 5. ROI was perfectly matched between the two sequential pullbacks detecting the morphology of calcification and a landmark side branch (yellow asterisk). Generally these two pullbacks looked similar in terms of plaque distributions in both segment-level analysis (area charts) and frame-level analysis (lower images as shown in Frame 33). In the matched frames with severe calcification, however, vessel boundaries were invisible and resulted in an apparently different contour detection of vessel area between the two pullbacks (middle images as shown in Frame 22). Plaque behind the calcification was generally characterized as fibrous-fatty tissue, and consequently plaque area and fibrous-fatty area showed the differences between the two pullbacks in this sampled frame. Therefore, our result is not surprising since saline and the shadowed regions behind dense calcium both will generally be classified as fibrous-fatty due to the higher attenuation of 45-MHz VH IVUS. Inclusion of saline area inside the lumen or beyond the vessel when evaluating severely calcified regions will also result in a disproportionate increase in fibrous-fatty tissue as compared to the other plaque components. A previous histological study demonstrated that 83% of coronary lesions behind severely calcified lesions had an extensive necrotic tissue containing large numbers of cholesterol crystals and microcalcifications [29]. Careful attention should thus be required to interpret the plaque composition in severely calcified lesions.

The precise contour detection has an essential role in the reproducibility of VH IVUS measurements for either 20-MHz or 45-MHz catheters. Despite the potential error of imaging analysis as previously mentioned, ICCs showed excellent reproducibility and relative differences of measurements were predominantly less than the commonly accepted threshold (10%) in the present study.

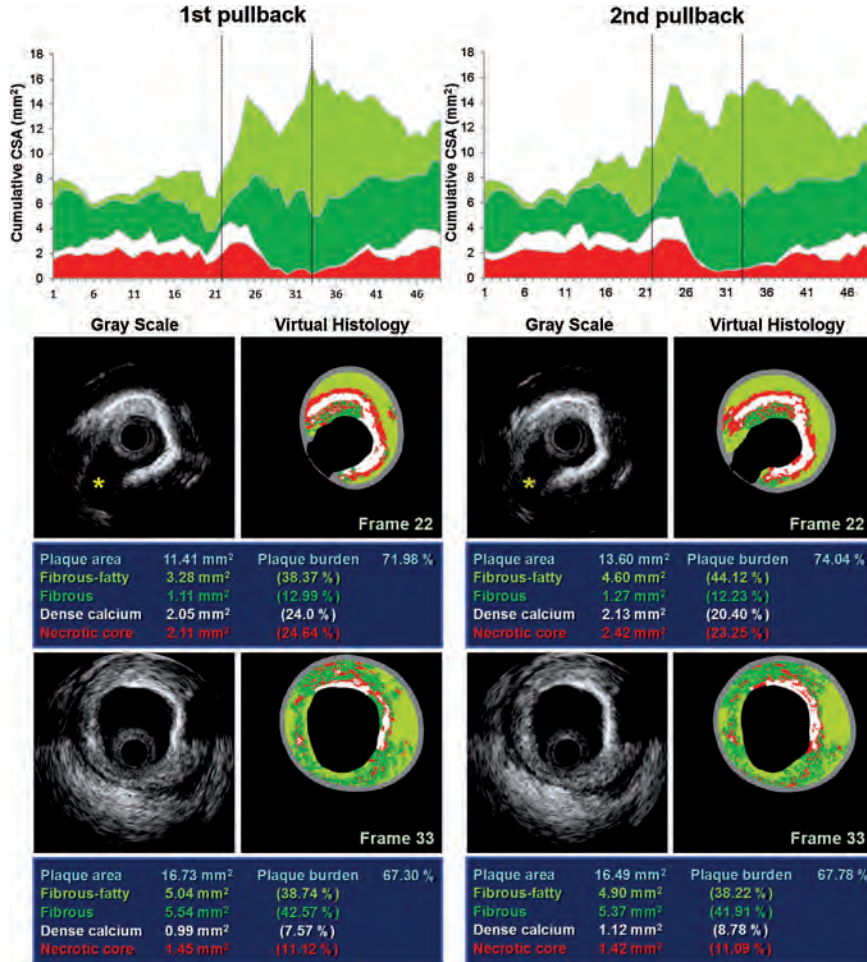


**Fig. 5.** An example of intracatheter reproducibility assessment in a severely calcified vessel. Sequential plotting of a matched region of interest (ROI) interrogated with two pullbacks using the same catheter (intracatheter reproducibility assessment). The mean cross-sectional area (CSA) (y-axis) of each plaque component is color coded (necrotic core, red; dense calcium, white; fibrous, green; and fibrous-fatty, greenish-yellow). This figure shows the impact of severe calcification on the assessments for geometrical and compositional measurements.

Our results could provide important information in order to perform more precise power calculations for future longitudinal studies.

#### Study limitations

The present study was conducted with a small number of samples because of the ex vivo nature of the study. In addition, we did not validate the accuracy of measurement using

pathohistology data as the reference and gold standard of plaque characterization.

#### Conclusions

In the present ex vivo study, geometrical and compositional assessments using 45-MHz rotational VH IVUS showed good agreement and acceptable reproducibility. Our results may provide important information when designing future clinical studies.

## Conflict of interest

Dr. Nair is a full employee of Volcano Corporation, and the rest of the authors have nothing to disclose regarding the contents relevant to this paper.

## References

- [1] Kimura BJ, Russo RJ, Bhargava V, McDaniel MB, Peterson KL, DeMaria AN. Atheroma morphology and distribution in proximal left anterior descending coronary artery: in vivo observations. *J Am Coll Cardiol* 1996;27:825–31.
- [2] Smits PC, Pasterkamp G, Quarles van Ufford MA, Eefting FD, Stella PR, de Jaegere PP, Borst C. Coronary artery disease: arterial remodelling and clinical presentation. *Heart* 1999;82:461–4.
- [3] Jeremias A, Huegel H, Lee DP, Hassan A, Wolf A, Yeung AC, Yock PG, Fitzgerald PJ. Spatial orientation of atherosclerotic plaque in non-branching coronary artery segments. *Atherosclerosis* 2000;152:209–15.
- [4] de Jaegere P, Mudra H, Figulla H, Almagor Y, Doucet S, Penn I, Colombo A, Hamm C, Bartorelli A, Rothman M, Nobuyoshi M, Yamaguchi T, Voudris V, DiMario C, Makovski S, et al. Intravascular ultrasound-guided optimized stent deployment. Immediate and 6 months clinical and angiographic results from the Multicenter Ultrasound Stenting in Coronaries Study (MUSIC Study). *Eur Heart J* 1998;19:1214–23.
- [5] Fitzgerald PJ, Oshima A, Hayase M, Metz JA, Bailey SR, Baim DS, Cleman MW, Deutsch E, Diver DJ, Leon MB, Moses JW, Osterle SN, Overlie PA, Pepine CJ, Safian RD, et al. Final results of the Can Routine Ultrasound Influence Stent Expansion (CRUISE) study. *Circulation* 2000;102:523–30.
- [6] Fang JC, Kinlay S, Beltrame J, Hikiti H, Wainstein M, Behrendt D, Suh J, Frei B, Mudge GH, Selwyn AP, Ganz P. Effect of vitamins C and E on progression of transplant-associated arteriosclerosis: a randomised trial. *Lancet* 2002;359:1108–13.
- [7] Nissen SE, Tsumoda T, Tuzcu EM, Schoenhagen P, Cooper CJ, Yasin M, Eaton GM, Lauer MA, Sheldon WS, Grines CL, Halpern S, Crowe T, Blankenship JC, Kerensky R. Effect of recombinant apoA-I Milano on coronary atherosclerosis in patients with acute coronary syndromes: a randomized controlled trial. *JAMA* 2003;290:2292–300.
- [8] Nissen SE, Tuzcu EM, Schoenhagen P, Brown BG, Ganz P, Vogel RA, Crowe T, Howard G, Cooper CJ, Brodie B, Grines CL, DeMaria AN, REVERSAL Investigators. Effect of intensive compared with moderate lipid-lowering therapy on progression of coronary atherosclerosis: a randomized controlled trial. *JAMA* 2004;291:1071–80.
- [9] Nissen SE, Nicholls SJ, Sipahi I, Libby P, Raichlen JS, Ballantyne CM, Davignon J, Erbel R, Fruchart JC, Tardif JC, Schoenhagen P, Crowe T, Cain V, Wolski K, Goormastic M, et al. Effect of very high-intensity statin therapy on regression of coronary atherosclerosis: the ASTEROID trial. *JAMA* 2006;295:1556–65.
- [10] Araki T, Nakamura M, Utsunomiya M, Sugi K. Visualization of coronary plaque in type 2 diabetes mellitus patients using a new 40 MHz intravascular ultrasound imaging system. *J Cardiol* 2012;59:42–9.
- [11] Nair A, Kuban BD, Tuzcu EM, Schoenhagen P, Nissen SE, Vince DG. Coronary plaque classification with intravascular ultrasound radiofrequency data analysis. *Circulation* 2002;106:2200–6.
- [12] Nair A, Margolis MP, Kuban BD, Vince DG. Automated coronary plaque characterisation with intravascular ultrasound backscatter: ex vivo validation. *EuroIntervention* 2007;3:113–20.
- [13] Nasu K, Tsuchikane E, Katoh O, Vince DG, Virmani R, Surmely JF, Murata A, Takeda Y, Ito T, Ehara M, Matsubara T, Terashima M, Suzuki T. Accuracy of in vivo coronary plaque morphology assessment: a validation study of in vivo virtual histology compared with in vitro histopathology. *J Am Coll Cardiol* 2006;47:2405–12.
- [14] Garcia-Garcia HM, Mintz GS, Lerman A, Vince DG, Margolis MP, van Es GA, Morel MA, Nair A, Virmani R, Burke AP, Stone GW, Serruys PW. Tissue characterisation using intravascular radiofrequency data analysis: recommendations for acquisition, analysis, interpretation and reporting. *EuroIntervention* 2009;5:177–89.
- [15] Garcia-Garcia HM, Serruys PW, Mintz GS, Saito S, Klaus V, Margolis P, Carlier S, Goedhard D, Schwartz R. Synergistic effect of cardiovascular risk factors on necrotic core in coronary arteries: a report from the global intravascular radiofrequency data analysis registry. *JACC Cardiovasc Imaging* 2009;2:629–36.
- [16] Marso SP, Frutkin AD, Mehta SK, House JA, McCrory JR, Klaus V, Lerman A, Leon MB, Nair A, Margolis P, Erbel R, Nasu K, Schiele F, Margolis J. Intravascular ultrasound measures of coronary atherosclerosis are associated with the Framingham risk score: an analysis from a global IVUS registry. *EuroIntervention* 2009;5:212–8.
- [17] Stone GW, Maehara A, Lansky AJ, de Bruyne B, Cristea E, Mintz GS, Mehran R, McPherson J, Farhat N, Marso SP, Parisse H, Templin B, White R, Zhang Z, Serruys PW, et al. A prospective natural-history study of coronary atherosclerosis. *N Engl J Med* 2011;364:226–35.
- [18] Serruys PW, Garcia-Garcia HM, Buzsman P, Erne P, Verheye S, Aschermann M, Duckers H, Bleie O, Dudek D, Botker HE, von Birgelen C, D'Amico D, Hutchinson T, Zambanini A, Mastik F, et al. Effects of the direct lipoprotein-associated phospholipase A2 inhibitor darapladib on human coronary atherosclerotic plaque. *Circulation* 2008;118:1172–82.
- [19] Davies MJ, Richardson PD, Woolf N, Katz DR, Mann J. Risk of thrombosis in human atherosclerotic plaques: role of extracellular lipid, macrophage, and smooth muscle cell content. *Br Heart J* 1993;69:377–81.
- [20] Serruys PW, Ormiston JA, Onuma Y, Regar E, Gonzalo N, Garcia-Garcia HM, Nieman K, Brauning N, Dorange C, Miquel-Hebert K, Veldhof S, Webster M, Thuesen L, Dudek D. A bioabsorbable everolimus-eluting coronary stent system (ABSORB): 2-year outcomes and results from multiple imaging methods. *Lancet* 2009;373:897–910.
- [21] Diletti R, Serruys PW, Faraouq V, Sudhir K, Dorange C, Miquel-Hebert K, Veldhof S, Rapoza R, Onuma Y, Garcia-Garcia HM, Chevalier B, ABSORB II randomized controlled trial: a clinical evaluation to compare the safety, efficacy, and performance of the Absorb everolimus-eluting bioresorbable vascular scaffold system against the XIENCE everolimus-eluting coronary stent system in the treatment of subjects with ischemic heart disease caused by de novo native coronary artery lesions: rationale and study design. *Am Heart J* 2012;164: 654–63.
- [22] Bland JM, Altman DG. Statistical methods for assessing agreement between two methods of clinical measurement. *Lancet* 1986;1:307–10.
- [23] Mintz GS, Nissen SE, Anderson WD, Bailey SR, Erbel R, Fitzgerald PJ, Pinto FJ, Rosenfield K, Siegel RJ, Tuzcu EM, Yock PG. American College of Cardiology Clinical Expert Consensus Document on Standards for Acquisition, Measurement and Reporting of Intravascular Ultrasound Studies (IVUS). A report of the American College of Cardiology Task Force on Clinical Expert Consensus Documents. *J Am Coll Cardiol* 2001;37:1478–92.
- [24] Garcia-Garcia HM, Gonzalo N, Pawar R, Kukreja N, Dudek D, Thuesen L, Ormiston JA, Regar E, Serruys PW. Assessment of the absorption process following bioabsorbable everolimus-eluting stent implantation: temporal changes in strain values and tissue composition using intravascular ultrasound radiofrequency data analysis. A substudy of the ABSORB clinical trial. *EuroIntervention* 2009;4:443–8.
- [25] Rodriguez-Granillo GA, Vaina S, Garcia-Garcia HM, Valgimigli M, Duckers E, van Geuns RJ, Regar E, van der Giessen WJ, Bressers M, Goedhard D, Morel MA, de Feyter PJ, Serruys PW. Reproducibility of intravascular ultrasound radiofrequency data analysis: implications for the design of longitudinal studies. *Int J Cardiovasc Imaging* 2006;22:621–31.
- [26] Heo JH, Brugaletta S, Garcia-Garcia HM, Gomez-Lara J, Ligthart JM, Witberg K, Magro M, Shin ES, Serruys PW. Reproducibility of intravascular ultrasound iMAP for radiofrequency data analysis: implications for design of longitudinal studies. *Catheter Cardiovasc Interv* 2011. <http://dx.doi.org/10.1002/ccd.23335>. Nov 22 [Epub ahead of print].
- [27] Rodriguez-Granillo GA, Aoki J, Ong AT, Valgimigli M, Van Mieghem CA, Regar E, McFadden E, De Feyter P, Serruys PW. Methodological considerations and approach to cross-technique comparisons using in vivo coronary plaque characterization based on intravascular ultrasound radiofrequency data analysis: insights from the Integrated Biomarker and Imaging Study (IBIS). *Int J Cardiovasc Intervent* 2005;7:52–8.
- [28] Garcia-Garcia HM, Gogas BD, Serruys PW, Bruining N. IVUS-based imaging modalities for tissue characterization: similarities and differences. *Int J Cardiovasc Imaging* 2011;27:215–24.
- [29] Kume T, Okura H, Kawamoto T, Akasaka T, Toyota E, Neishi Y, Watanabe N, Sukmawan R, Yamada R, Sadahira Y, Yoshida K. Assessment of the histological characteristics of coronary arterial plaque with severe calcification. *Circ J* 2007;71:643–7.



## 2.4 Palpography

Implications of a bioresorbable vascular scaffold implantation on vessel wall strain of the treated and the adjacent segments.

*Int J Cardiovasc Imaging.* 2014;30:477-84.

[Original research paper, Impact Factor (2013): 2.322]

Bourantas CV, Garcia-Garcia HM, Campos CA, Zhang YJ, Muramatsu T, Morel MA, Nakatani S, Gao X, Cho YK, Isibashi Y, Gijssen FJ, Onuma Y, Serruys PW.





# Implications of a bioresorbable vascular scaffold implantation on vessel wall strain of the treated and the adjacent segments

Christos V. Bourantas · Hector M. Garcia-Garcia · Carlos A. M. Campos · Yao-Jun Zhang · Takashi Muramatsu · Marie-Angèle Morel · Shimpei Nakatani · Xingyu Gao · Yun-Kyeong Cho · Yuki Isibashi · Frank J. H. Gijsen · Yoshinobu Onuma · Patrick W. Serruys

Received: 26 September 2013 / Accepted: 15 January 2014  
© Springer Science+Business Media Dordrecht 2014

**Abstract** *Background* Metallic stents change permanently the mechanical properties of the vessel wall. However little is known about the implications of bioresorbable vascular scaffolds (BVS) on the vessel wall strain. *Methods* Patients ( $n = 53$ ) implanted with an Absorb BVS that had palpographic evaluation at any time point [before device implantation, immediate after treatment, at short-term (6–12 months) or mid-term follow-up (24–36 months)] were included in the current analysis. The palpographic data were used to estimate the mean of the maximum strain values and the obtained measurements were classified using the Rotterdam classification (ROC) score and expressed as ROC/mm. *Results* Scaffold implantation led to a significant decrease of the vessel wall strain in the treated segment [0.35 (0.20, 0.38) vs. 0.19 (0.09, 0.29);  $P = 0.005$ ] but it did not affect the proximal and distal edge. In patients who had serial palpographic examination the vessel wall strain continued to decrease in the scaffolded segment at short-term [0.20 (0.12, 0.29) vs. 0.14 (0.08, 0.20);  $P = 0.048$ ] and mid-term follow-up [0.20

(0.12, 0.29) vs. 0.15 (0.10, 0.19),  $P = 0.024$ ]. No changes were noted with time in the mechanical properties of the vessel wall at the proximal and distal edge. *Conclusions* Absorb BVS implantation results in a permanent alteration of the mechanical properties of the vessel wall in the treated segment. Long term follow-up data are needed in order to examine the clinical implications of these findings.

**Keywords** Bioresorbable vascular scaffold · Palpography · Vessel wall strain

## Introduction

Vessel wall mechanical behavior appears to be associated with the compositional characteristics of the plaque and predict future cardiovascular events [1–4]. Several studies have shown that pharmaceutical or an interventional treatment can influence the mechanical properties of the vessel wall by altering its constituents [5–9]. Following an endoluminal device implantation (i.e., a metallic stent or a bioresorbable scaffold) the local vessel wall strain of the implanted segment is reduced and this has been attributed to the increased stiffness of the deployed device [5, 6, 9].

Recently we have reported the results of the palpographic analysis performed in segments implanted with the updated revision of the Absorb bioresorbable vascular scaffold (BVS) 1.1 [6]. We found that the vessel wall strain is reduced in the scaffolded segments immediately after device deployment but there are no further changes in the mechanical properties of the vessel wall between post-scaffold implantation and at short-term follow-up (i.e., at 6–12 months). The present analysis aims to investigate the mid-term implications (i.e., at 24–36 months) of the Absorb BVS 1.1 on the vessel wall strain.

---

On behalf of the Absorb Cohort B Investigators.

---

**Electronic supplementary material** The online version of this article (doi:10.1007/s10554-014-0373-4) contains supplementary material, which is available to authorized users.

---

C. V. Bourantas · H. M. Garcia-Garcia · C. A. M. Campos · Y.-J. Zhang · T. Muramatsu · M.-A. Morel · S. Nakatani · Y.-K. Cho · Y. Isibashi · F. J. H. Gijsen · Y. Onuma · P. W. Serruys (✉)  
Interventional Cardiology Department, Thoraxcenter, Erasmus Medical Center, 's-Gravendijkwal 230, 3015, CE, Rotterdam, The Netherlands  
e-mail: p.w.j.c.serruys@erasmusmc.nl

X. Gao  
Abbott Vascular, Santa Clara, CA, USA

## Methods

### Included patients and study design

The ABSORB Cohort B trial (A Clinical Evaluation of the Bioabsorbable Everolimus Eluting Coronary Stent System for the Treatment of Patients with de Novo Native Coronary Artery Lesions) was a prospective multicenter single-arm study designed to investigate the safety and efficacy of the Absorb BVS 1.1 (Abbott Vascular, Santa Clara, CA, USA) [10]. One hundred one patients were included in this study and were divided in two groups (B1 and B2). The first group had invasive imaging evaluation [i.e., coronary angiography, grayscale intravascular ultrasound (IVUS), IVUS virtual histology, palpographic and optical coherence tomographic imaging] at baseline, 6 months and 2 years follow-up; while the second group had the abovementioned invasive tests at baseline, 1 year and at 3 years follow-up. Optical coherence tomographic (OCT) examination was optional and was not performed in all the studied patients. The current analysis included only the patients who had a palpographic assessment at least at one time point. The Absorb Cohort B study was sponsored and financially supported by Abbott Vascular.

The Absorb BVS 1.1 used in the ABSORB Cohort B trial, is a fully bioresorbable device with dimensions  $3.0 \times 18$  mm. The composition of the device consists of poly-L-lactide (PLLA) that is covered by an thin layer of an amorphous matrix of poly-D,L-lactide (PDLLA) which contains and controls the release of the anti-proliferative drug everolimus (concentration:  $100 \mu\text{g}/\text{cm}^2$ ). The Absorb BVS 1.1 has an in-phase zigzag hoops linked with bridges design that provides the device increased radial strength and eliminates the risk of late scaffold recoil, while the polymer of this revision has been processed in such a way so as to have a delayed degradation (by approximately 18 months comparing to the 1st revision).

The palpographic sub-study of the ABSORB Cohort B trial had pre-specified hypotheses. In particular the investigators expected that the delayed degradation in Absorb BVS 1.1 would result: either (1) in a delayed restoration of the normal, pre-scaffold implantation, strain, or (2) it would allow the built up of neointima tissue that would permanently alter the mechanical properties of the vessel wall.

### IVUS acquisition and analysis

Intravascular ultrasound imaging was performed in the treated artery using an Eagle Eye 20 MHz imaging catheter (acquisition frame rate 30 frames/s, Volcano Corp, Rancho Cordova, CA, USA) that was withdrawn with the use of an automated pull-back device at a speed of 0.5 mm/s. During

IVUS examination the electrocardiogram and the aortic pressure were recorded.

The radiofrequency IVUS imaging data were acquired using a custom design workstation and were transferred to an independent clinical research organization (Cardialysis, Rotterdam, the Netherlands) for offline analysis. For each studied artery the IVUS images portraying the 5 mm proximal, the scaffolded, and the 5 mm distal segment were analyzed. The local strain was estimated from the radiofrequency IVUS data using cross correlation analysis according to a previously described methodology [11]. The measured strain values were displayed in spread-out vessel plots using a color coded map with the blue indicating low strain values and the red/yellow a high strain (range 0–2 %) [11].

The strain values were classified according to the Rotterdam classification (ROC) score to four classes (ROC I: 0–0.5 %, ROC II: 0.6–0.9 %, ROC III: 0.9–<1.2 % and ROC IV: >1.2 %). A cross section was considered to have high strain when the measured strain was classified as ROC III–IV in an arc of  $>12^\circ$ . For each cross section the highest strain value was recorded and considered as the strain of this section. The mean of the maximum strain values measured in each segment was determined and used to characterize the strain of the segment. Results are presented as ROC/mm (Fig. 1).

### Statistics

Continuous variables depending on their distribution are presented as mean  $\pm$  standard deviation or as median with 25th and 75th percentiles, as indicated in the tables. Categorical variables are presented as absolute values and percentages. Because of the small number of patients who had palpographic evaluation at different time points we merged the data from Cohort B1 and B2 and present our results at 4 time points: at baseline pre-scaffold implantation, immediately after scaffold implantation, at short-term (6–12 months), and at mid-term follow-up (24–36 months). Comparison between the two cohorts was done by *t* test and Chi square test, or Fisher's exact test when Cochran's rule is not met.

Changes in the strain values between two different time points were evaluated by means of paired Wilcoxon signed rank test. A P value  $<0.05$  (two-tailed) was considered statistically significant. Data analysis was performed using the SAS statistical computer package (SAS 9.2, SAS Institute Inc., Cary, NC, USA).

## Results

### Studied population

Fifty-three from the 101 patients who were enrolled in the Absorb Cohort B study had palpographic evaluation at

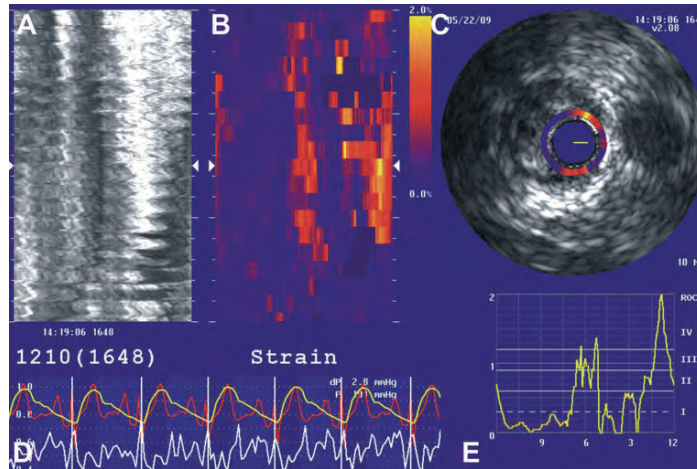


**Fig. 1** Snapshot showing the palpographic evaluation of a lesion before scaffold implantation. Panel A shows a longitudinal IVUS cross-section of the studied segment while panel B a spread out plot of the measured vessel wall strain (the blue color indicates low strain and the red/yellow high strain values). An IVUS cross section with the estimated strain at the superficial plaque shown in color coding is

portrayed in panel C. Panel D shows the electrocardiogram, the measured strain, and the blood pressure changes during the cardiac cycle throughout the pull-back of the catheter, whereas panel E displays the strain values measured in the cross-section shown in panel C. High strain was noted at 1 and 6 o'clock

least at one time point and included in this analysis. The baseline characteristics of the studied population are shown in Table 1. The patients that were enrolled in the Absorb Cohort B1 group did not smoke and were more likely to suffer from hypercholesterolemia and be admitted with stable angina symptoms comparing to the subjects included in the Absorb Cohort B2 group but otherwise there were not significant differences in the baseline demographics and angiographic characteristics between the two groups.

#### Palpographic evaluation

Only 14 patients had palpographic evaluation before scaffold implantation, 44 patients had this investigation immediate after device deployment, 41 at short-term, and 36 at mid-term follow-up. Twenty patients had serial palpographic examination at the three time points (i.e., at baseline immediate after scaffold deployment, at short-term and mid-term follow-up).

For the entire study population ( $n = 53$  patients) the strain values did not change immediate after scaffold deployment at the proximal and distal edge (Table 2). On the other hand in the treated segment the strain decreased significantly after device deployment. The vessel wall strain estimated at the proximal edge at the two follow-up time points was not different from the vessel wall strain before scaffold

deployment ( $P = 0.814$  for the short-term follow-up and  $P = 0.162$  for the mid-term follow-up). However, when we compared the follow-up values at the proximal edge with the strain measured immediately after scaffold deployment we found statistical significant differences (Table 2). At the distal edge the strain values did not change with time.

The strain values in the scaffolded segment at the two follow-up time points were considerably lower comparing to baseline before device implantation ( $P = 0.002$  for the short-term and  $P = 0.001$  for the mid-term follow-up) but they were not different from these measured immediately after scaffold deployment.

When we included in our analysis only the segments ( $n = 20$  patients) that had serial palpographic examination (i.e., at baseline immediate after device deployment, at short-term, and at mid-term follow-up) we found that the strain of the proximal edge and distal edge did not change with time (Table 3; Fig. 2). On the other hand in the scaffolded segment the strain values were significantly decreased at short- and mid-term follow-up comparing to baseline.

#### Discussion

In this study we examined for the first time the implications of the second revision Absorb BVS on the mechanical

**Table 1** Baseline demographics, angiographic characteristics and medications of the studied population

Patients' demographics	Absorb Cohort B N = 53	Absorb Cohort B1 N = 20	Absorb Cohort B2 N = 33	P
Age (years)	61.28 ± 8.41	63.84 ± 8.87	59.72 ± 7.85	0.096
Male	71.7 % (38/53)	75.0 % (15/20)	69.7 % (23/33)	0.678
Hypertension	67.3 % (35/52)	60.0 % (12/20)	71.9 % (23/32)	0.374
Hypercholesterolemia	83.0 % (44/53)	100.0 % (20/20)	72.7 % (24/33)	0.010
Diabetes	18.9 % (10/53)	15.0 % (3/20)	21.2 % (7/33)	0.725
Current smoking	15.1 % (8/53)	0.0 % (0/20)	24.2 % (8/33)	0.019
Prior PCI	22.6 % (12/53)	25.0 % (5/20)	21.2 % (7/33)	0.748
Stable angina	73.6 % (39/53)	90.0 % (18/20)	63.6 % (21/33)	0.035
Unstable angina	9.4 % (5/53)	5.0 % (1/20)	12.1 % (4/33)	0.639
Silent ischemia	1.9 % (1/53)	0.0 % (0/20)	3.0 % (1/33)	1.000
<i>Treated vessel</i>				
Left anterior descending	47.2 % (25/53)	45.0 % (9/20)	48.5 % (16/33)	0.805
Left circumflex	24.5 % (13/53)	25.0 % (5/20)	24.2 % (8/33)	1.000
Right coronary artery	28.3 % (15/53)	30.0 % (6/20)	27.3 % (9/33)	0.831
<i>QCA analysis pre-treatment</i>				
RVD (mm)	2.61 ± 0.34	2.60 ± 0.44	2.61 ± 0.28	0.949
MLD (mm)	1.04 ± 0.27	0.99 ± 0.31	1.07 ± 0.23	0.365
Diameter stenosis (%)	59.80 ± 9.96	61.25 ± 12.74	58.94 ± 7.98	0.482
<i>Medications</i>				
β-blockers	73.6 % (39)	65.0 % (13)	78.8 % (26)	0.270
RAAS inhibitors	69.8 % (37)	65.0 % (13)	72.7 % (24)	0.443
Statins	94.3 % (50)	100.0 % (20)	90.9 % (30)	0.165

PCI percutaneous coronary intervention, QCA quantitative coronary angiography, RVD reference vessel diameter, MLD minimum luminal diameter, RAAS renin angiotensin aldosterone system

**Table 2** Strain values at the proximal edge, the scaffolded segment and the distal edge before device implantation, immediately after device deployment, at short-term follow-up and at mid-term follow-up

	Pre-scaffold implantation (n = 14)	Post-scaffold implantation (n = 44)	$P_1$	Short term follow- up (n = 41)	Mid-term follow- up (n = 36)	$P_2$	$P_3$	$P_4$
Proximal edge	0.19 (0.13, 0.36) (12)	0.23 (0.10, 0.35) (29)	0.793	0.17 (0.12, 0.31) (28)	0.15 (0.07, 0.20) (19)	0.989	0.022	0.043
Scaffolded segment	0.35 (0.20, 0.38) (14)	0.19 (0.09, 0.29) (44)	0.001	0.16 (0.12, 0.22) (41)	0.15 (0.10, 0.20) (36)	0.391	0.064	0.410
Distal edge	0.14 (0.08, 0.31) (9)	0.15 (0.06, 0.28) (28)	0.739	0.10 (0.04, 0.26) (29)	0.19 (0.11, 0.26) (25)	0.675	0.771	0.445

$P_1$  denotes the significance of difference between the strain values estimated before and immediate after device implantation;  $P_2$  the significance of difference between the strain values at post-scaffold implantation and at short-term follow-up;  $P_3$  the significance of difference between the strain values at post-scaffold implantation and at mid-term follow-up; and  $P_4$  the significance of differences of the strain values at the two follow-up time points

The number in the parenthesis at the left side of each column indicates the number of segments analyzed at each time point

properties of the vessel wall. We found that in contrast to the first generation which has a transient effect on vessel wall strain, the updated revision Absorb BVS 1.1 causes a permanent decrease of the strain values at the treated segment without affecting the mechanical properties of the proximal and distal edge [5, 6].

The reduction of the vessel wall strain noted immediately after Absorb BVS 1.0 or after Absorb BVS 1.1

deployment has been attributed to the shielding effect of the device, and to fact that the foreign material is likely to interfere with the palpographic estimations due to the artifactual acoustic properties of the struts [5, 6, 12]. In the first revision Absorb BVS the change in the strain values at the treated vessel was temporary as at 6 months and 24 months follow-up the measured strain was increased and approached the strain estimated before device

**Table 3** Strain values at the proximal edge, the scaffolded segment and the distal edge before device implantation, immediately after device deployment, at short-term and at mid-term follow-up in

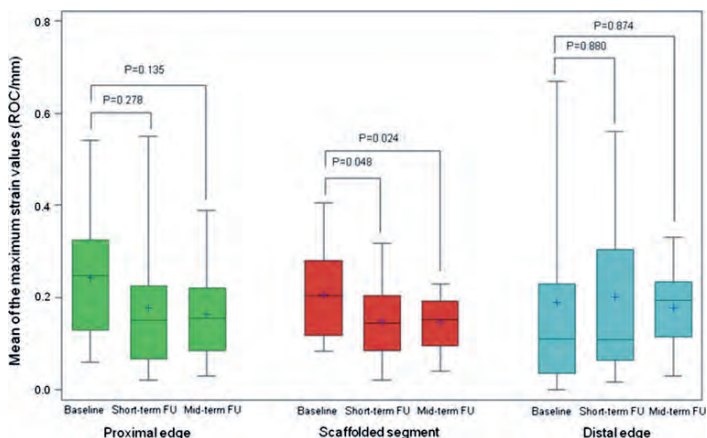
patients who had serial palpographic examination immediate after scaffold implantation and at the two follow-up time points

	Post-scaffold implantation (n = 20)	Short term follow-up (n = 20)	Mid-term follow-up (n = 20)	$P_1$	$P_2$	$P_3$
Proximal edge	0.25 (0.13, 0.33) (12)	0.15 (0.07, 0.23) (12)	0.16 (0.09, 0.22) (12)	0.278	0.135	0.817
Scaffolded segment	0.20 (0.12, 0.29) (20)	0.14 (0.08, 0.20) (20)	0.15 (0.10, 0.19) (20)	0.048	0.024	0.922
Distal edge	0.11 (0.04, 0.23) (12)	0.11 (0.06, 0.31) (12)	0.20 (0.11, 0.24) (12)	0.880	0.874	0.692

$P_1$  denotes the significance of difference between the strain values at post-scaffold implantation and at short-term follow-up;  $P_2$  the significance of difference between the strain values at post-scaffold implantation and at mid-term follow-up; and  $P_3$  the significance of differences of the strain values at the two follow-up time points

The number in the parenthesis at the left side of each column indicates the number of segments analyzed at each time point

**Fig. 2** Changes in vessel wall strain (ROC/mm) at the proximal edge the scaffolded segment and the distal edge in patients who had serial palpographic examination immediately after scaffold implantation at short-term and mid-term follow-up. ROC Rotterdam classification



implantation [5, 6]. These findings were attributed to the resorption process which was completed at 2 years follow-up but also to the late recoil noted in the first revision [13, 14]. The latter argument is highlighted by the findings of Tanimoto et al. [13] who showed that late scaffold recoil is more intense at 6 months follow-up in the high-strain fibro-necrotic plaques; thus it can be speculated that the late recoil of the scaffold over these plaques may allow restoration of their mechanical properties contributing to the increased strain values noted at 6 and 24 months follow-up.

On the other hand in the second revision Absorb BVS the polymer has been processed in such a way so as its degradation to delay by approximately 18 months comparing to the first revision and the scaffold has a different design which provides the device with a better radial support [14]. These modifications prolong the mechanical integrity of the scaffold resulting in a delayed restoration of vessel vasomotion at 12 months follow-up, and eliminate the risk of late recoil [15].

Furthermore, we have recently demonstrated that in Absorb BVS 1.1 a thick layer of neointimal tissue develops (mean thickness 210–220  $\mu\text{m}$  at short-term follow-up) that covers the entire circumference of the vessel shielding the underlying plaque [16]. Histology studies in porcine models have shown that the neointima tissue consists of smooth muscles cells and fibrous tissue and thus the superficial plaque is anticipated to exhibit low strain values in a palpographic examination [2, 3, 17]. Indeed the strain values reported in our analysis at short- and mid-term follow-up are close to the strain measured in fibrotic plaques by Korte et al. [3] using elastography in pig models. It appears that the second revision Absorb BVS 1.1 modifies permanent the mechanical properties of the superficial plaque by altering its phenotype to a more stable form (Fig. 3). Our findings indicate that in contrast to the metallic stents, which are anticipated to have a similar effect on the mechanical properties of the vessel wall, in bioresorbable scaffolds minor changes in their design are

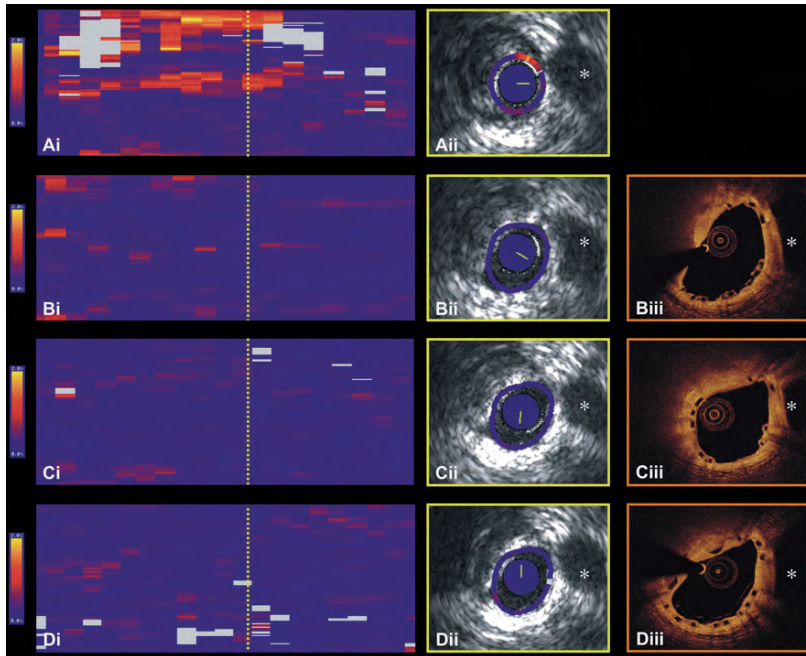


**Fig. 3** Spread out plot of the vessel wall strain at baseline before Absorb BVS implantation (Ai), immediate after scaffold deployment (Bi), at short-term (Ci), and mid-term follow-up (Di). The *blue color* indicates low strain values where the *red/yellow* a high strain. It is apparent that the incidence of the high strain values decreased immediate after scaffold deployment and it is even lower at short- and mid-term follow-up. Panels Aii, Bii, Cii and Dii portray corresponding IVUS cross-sections acquired at baseline before and immediate after scaffold deployment, at short-term, and at mid-term follow-up respectively. The position of these frames in the spread-out vessel plots is indicated with a *yellow line*. High strain values are noted at the shoulders of an echolucent plaque before scaffold implantation

(Aii), however immediate after device deployment the strain values are low in the entire circumference of the lumen (Bii). OCT imaging performed after scaffold deployment this time point (Biii) indicates the presence of a lipid rich plaque (the correspondence between IVUS and OCT is shown with an *asterisk*). The strain values remain low at short- and mid-term follow-up in the IVUS cross-section (panels Cii and Dii respectively). OCT performed at the follow-up time points shows that neointima tissue has been developed that sealed the underlying plaque. The mean thickness of the neointima tissue is measured 150  $\mu\text{m}$  at short-term and 220  $\mu\text{m}$  at mid-term follow-up (Supplementary figure)

likely to have detrimental implications on vessel wall strain. Thus the results of this analysis cannot be extrapolated to other scaffolds even to these with a similar design and composition.

The effect of the decreased strain on vessel wall pathophysiology is yet unknown. Several studies have demonstrated that the ability of the vessel wall to expand as a response to a pulsatile cyclic strain has an athero-protective role as it stimulates eNOS gene regulation, promotes prostacyclin synthesis and maintains the contractile phenotype of the smooth muscles cells [18–20]. However, plaques exhibiting low strain such as the pathological

intimal thickening appear stable and rarely cause future events, while the plaques that demonstrate a high strain are associated with increased vulnerability [1, 4, 21]. Therefore it can be argued that the low strain estimated in stable plaques is sufficient for the stimulation of the pulsatile cyclic strain-dependent athero-protective mechanisms and for triggering the necessary mechanotransduction and pathophysiological pathways that prevent plaque progression. In Absorb BVS this argument is supported by histology studies showing that in scaffolded segments the smooth muscles cells maintain their benign contractile phenotype, and by clinical reports demonstrating

restoration of the endothelial dependent vasomotion at 1 year follow-up, suggesting a functionally normal endothelium that is capable to respond to chemical and mechanical stimuli [15, 22].

Although palpography appears unable to predict the natural history of a high risk plaque there is robust evidence to support that the mechanical properties of the vessel wall provide useful prognostic information since patients with high strain plaques are more likely to experience acute coronary events comparing to those with low strain lesions [1, 4]. Furthermore, the Integrated Biomarkers and Imaging Studies I and II have shown that an aggressive pharmaceutical treatment reduces local strain values, whereas the vShield Evaluated at Cardiac hospital in Rotterdam for Investigation and Treatment of TCFA (SECRITT) trial that implemented a self-expanding stent to seal high risk plaques have demonstrated a significant decrease of the strain values immediate after device deployment [7–9]. Our results are similar to what has been reported to metallic stents, showing that Absorb BVS 1.1 implantation changes permanently the mechanical properties of the vessel wall and stabilizes the plaque. However, further palpographic data after the full resorption of the BVS are needed to confirm this statement and further research and robust data from randomized control trials are required before advocating the use of these devices for the invasive sealing of vulnerable, prone-to-rupture plaques [16, 23, 24].

#### Limitations

A major limitation of the current study is the fact that a considerable number of patients did not have serial palpographic examination. Thus, we included all the data that were available from each patient acknowledging the fact that missing examinations can affect the reported results. To confirm the findings of our initial analysis we also performed a sub-analysis including the patients who had truly serial examinations. Although the number of patients in the sub-analysis was small the agreement noted between the results of the initial analysis and the sub-analysis with regards the scaffolded segment allows us to report these findings with some certainty. Another limitation of our analysis was the lack of a control group with serial palpographic examination that would allow us to compare the reported changes in the vessel wall stain in the scaffolded segments with these in native untreated arteries.

Unfortunately OCT was an optional examination in the ABSORB Cohort B study and thus only very few patients ( $n = 4$ ) had serial palpographic and OCT assessment. Thus we were unable to combine these data and examine the association between the changes in the measured strain at

follow-up and the neointimal thickness as well as the effect of the different plaque characteristics (i.e., composition of the plaque, thickness of the fibrous tissue over calcific and lipid tissue, extent of the lipid and calcific tissue, plaque burden and eccentricity) on this relation [25, 26].

#### Conclusions

This study for the first time investigated the mid-term implications of the second revision Absorb BVS on the mechanical properties of the plaque. We found that in contrast to the first revision where the strain values of the treated segment change temporarily, in the second revision the strain of the vessel wall gradually decreases with time. Long-term clinical follow-up data and evidence from randomized studies are required in order to examine the clinical implications of these findings.

**Acknowledgments** Christos V. Bourantas is funded by the Hellenic Heart Foundation.

**Conflict of interest** Xingyu Gao is employee of Abbott Vascular. None of the other authors have any conflict of interest to declare.

#### References

1. Schaar JA, Regar E, Mastik F et al (2004) Incidence of high-strain patterns in human coronary arteries: assessment with three-dimensional intravascular palpography and correlation with clinical presentation. *Circulation* 109(22):2716–2719
2. Schaar JA, De Korte CL, Mastik F et al (2003) Characterizing vulnerable plaque features with intravascular elastography. *Circulation* 108(21):2636–2641
3. de Korte CL, Siervogel MJ, Mastik F et al (2002) Identification of atherosclerotic plaque components with intravascular ultrasound elastography in vivo: a Yucatan pig study. *Circulation* 105(14):1627–1630
4. Brugaletta S, Garcia-Garcia HM, Serruys PW et al (2012) Relationship between palpography and virtual histology in patients with acute coronary syndromes. *JACC Cardiovasc Imaging* 5(3Suppl):S19–S27
5. Serruys PW, Ormiston JA, Onuma Y et al (2009) Abioabsorbable everolimus-eluting coronary stent system (ABSORB): 2-year outcomes and results from multiple imaging methods. *Lancet* 373(9667):897–910
6. Brugaletta S, Gogas BD, Garcia-Garcia HM et al (2012) Vascular compliance changes of the coronary vessel wall after bioresorbable vascular scaffold implantation in the treated and adjacent segments. *Circ J* 76(7):1616–1623
7. Van Mieghem CA, McFadden EP, de Feyter PJ et al (2006) Noninvasive detection of subclinical coronary atherosclerosis coupled with assessment of changes in plaque characteristics using novel invasive imaging modalities: the integrated biomarker and imaging study (IBIS). *J Am Coll Cardiol* 47(6):1134–1142
8. Serruys PW, Garcia-Garcia HM, Buszman P et al (2008) Effects of the direct lipoprotein-associated phospholipase A(2) inhibitor

- darapladib on human coronary atherosclerotic plaque. *Circulation* 118(11):1172–1182
9. Wyrzykowska JJ, Diletti R, Gutierrez-Chico JL et al (2012) Plaque sealing and passivation with a mechanical self-expanding low outward force nitinol vShield device for the treatment of IVUS and OCT-derived thin cap fibroatheromas (TCFAs) in native coronary arteries: report of the pilot study vShield Evaluated at Cardiac hospital in Rotterdam for Investigation and Treatment of TCFA (SECRITT). *EuroIntervention* 8(8):945–954
  10. Serruys PW, Onuma Y, Ormiston JA et al (2010) Evaluation of the second generation of a bioresorbable everolimus drug-eluting vascular scaffold for treatment of de novo coronary artery stenosis: six-month clinical and imaging outcomes. *Circulation* 122(22):2301–2312
  11. Schaar JA, van der Steen AF, Mastik F et al (2006) Intravascular palpography for vulnerable plaque assessment. *J Am Coll Cardiol* 47(8 Suppl):C86–C91
  12. Garcia-Garcia HM, Gonzalo N, Pawar R et al (2009) Assessment of the absorption process following bioabsorbable everolimus-eluting stent implantation: temporal changes in strain values and tissue composition using intravascular ultrasound radiofrequency data analysis. A substudy of the ABSORB clinical trial. *EuroIntervention* 4(4):443–448
  13. Tanimoto S, Bruining N, van Domburg RT (2008) Late stent recoil of the bioabsorbable everolimus-eluting coronary stent and its relationship with plaque morphology. *J Am Coll Cardiol* 52(20):1616–1620
  14. Gomez-Lara J, Brugaletta S, Diletti R et al (2011) A comparative assessment by optical coherence tomography of the performance of the first and second generation of the everolimus-eluting bioresorbable vascular scaffolds. *Eur Heart J* 32(3):294–304
  15. Serruys PW, Onuma Y, Dudek D et al (2011) Evaluation of the second generation of a bioresorbable everolimus-eluting vascular scaffold for the treatment of de novo coronary artery stenosis: 12-month clinical and imaging outcomes. *J Am Coll Cardiol* 58(15):1578–1588
  16. Brugaletta S, Radu MD, Garcia-Garcia HM et al (2012) Circumferential evaluation of the neointima by optical coherence tomography after ABSORB bioresorbable vascular scaffold implantation: can the scaffold cap the plaque? *Atherosclerosis* 221(1):106–112
  17. Onuma Y, Serruys PW, Perkins LE et al (2010) Intracoronary optical coherence tomography and histology at 1 month and 2, 3, and 4 years after implantation of everolimus-eluting bioresorbable vascular scaffolds in a porcine coronary artery model: an attempt to decipher the human optical coherence tomography images in the ABSORB trial. *Circulation* 122(22):2288–2300
  18. Peng X, Haldar S, Deshpande S et al (2003) Wall stiffness suppresses Akt/eNOS and cytoprotection in pulse-perfused endothelium. *Hypertension* 41(2):378–381
  19. Gupta V, Grande-Allen KJ (2006) Effects of static and cyclic loading in regulating extracellular matrix synthesis by cardiovascular cells. *Cardiovasc Res* 72(3):375–383
  20. Schad JF, Meltzer KR, Hicks MR et al (2011) Cyclic strain upregulates VEGF and attenuates proliferation of vascular smooth muscle cells. *Vasc Cell* 3:21
  21. Stone GW, Maehara A, Lansky AJ et al (2011) A prospective natural-history study of coronary atherosclerosis. *N Engl J Med* 364(3):226–235
  22. Serruys PW, Garcia-Garcia HM, Onuma Y (2012) From metallic cages to transient bioresorbable scaffolds: change in paradigm of coronary revascularization in the upcoming decade? *Eur Heart J* 33(1):16–25
  23. Bourantas CV, Farooq V, Zhang Y, et al. (2013) Circumferential distribution of the neointima at 6 months and 2 years follow-up after a bioresorbable vascular scaffold implantation. A substudy of the ABSORB Cohort B Clinical Trial *EuroIntervention* (In press)
  24. Stone GW (2013) Rationale and design of PROSPECT II. 11 Vulnerable Plaque Meeting, Paris, France, 23–26 June 2013
  25. Imoto K, Hiro T, Fujii T et al (2005) Longitudinal structural determinants of atherosclerotic plaque vulnerability: a computational analysis of stress distribution using vessel models and three-dimensional intravascular ultrasound imaging. *J Am Coll Cardiol* 46(8):1507–1515
  26. Kumar RK, Balakrishnan KR (2005) Influence of lumen shape and vessel geometry on plaque stresses: possible role in the increased vulnerability of a remodelled vessel and the “shoulder” of a plaque. *Heart* 91(11):1459–1465

## 2.5 Optical coherence tomography: coronary evaginations

Coronary evaginations are associated with positive vessel remodeling and are nearly absent following implantation of newer-generation drug-eluting stents: An optical coherence tomography and intravascular ultrasound study.

*Eur Heart J.* 2014;35:795-807.

[Original research paper, Impact Factor (2013): 14.723]

Radu MD, Räber L, Kalesan B, Muramatsu T, Kelbæk H, Heo JH, Jørgensen E, Helqvist S, Farooq V, Brugaletta S, Garcia-Garcia HM, Jüni P, Saunamäki K, Windecker S, Serruys PW.





# Coronary evaginations are associated with positive vessel remodelling and are nearly absent following implantation of newer-generation drug-eluting stents: an optical coherence tomography and intravascular ultrasound study

Maria D. Radu<sup>1,2†</sup>, Lorenz Räber<sup>1,3†</sup>, Bindu Kalesan<sup>4</sup>, Takashi Muramatsu<sup>1</sup>, Henning Kelbæk<sup>2</sup>, Jungho Heo<sup>1</sup>, Erik Jørgensen<sup>2</sup>, Steffen Helqvist<sup>2</sup>, Vasim Farooq<sup>1</sup>, Salvatore Brugaletta<sup>1</sup>, Hector M. Garcia-Garcia<sup>5</sup>, Peter Jüni<sup>4</sup>, Kari Saunamäki<sup>2</sup>, Stephan Windecker<sup>3</sup>, and Patrick W. Serruys<sup>1\*</sup>

<sup>1</sup>Thoraxcenter, Erasmus University Medical Centre, Ba583a, 's-Gravendijkwal 230, 3015 CE Rotterdam, Netherlands; <sup>2</sup>Rigshospitalet, Copenhagen University Hospital, Copenhagen, Denmark; <sup>3</sup>Department of Cardiology, Bern University Hospital, Bern, Switzerland; <sup>4</sup>Institute of Social and Preventive Medicine, Bern University, Bern, Switzerland; and <sup>5</sup>Cardialysis BV, Rotterdam, Netherlands

Received 16 August 2012; revised 11 June 2013; accepted 6 August 2013; online publish-ahead-of-print 16 October 2013

## Objectives

The purpose of this study was to assess the occurrence, predictors, and mechanisms of optical coherence tomography (OCT)-detected coronary evaginations following drug-eluting stent (DES) implantation.

## Background

Angiographic ectasias and aneurysms in stented segments have been associated with a risk of late stent thrombosis. Using OCT, some stented segments show coronary evaginations reminiscent of ectasias.

## Methods

Evaginations were defined as outward bulges in the luminal contour between struts. They were considered major evaginations (MEs) when extending  $\geq 3$  mm along the vessel length, with a depth  $\geq 10\%$  of the stent diameter. A total of 228 patients who had sirolimus (SES)-, paclitaxel-, biolimus-, everolimus (EES)-, or zotarolimus (ZES)-eluting stents implanted in 254 lesions, were analysed after 1, 2, or 5 years; and serial assessment using OCT and intravascular ultrasound (IVUS) was performed post-intervention and after 1 year in 42 patients.

## Results

Major evaginations occurred frequently at all time points in SES (~26%) and were rarely seen in EES (3%) and ZES (2%,  $P = 0.003$ ). Sirolimus-eluting stent implantation was the strongest independent predictor of ME [adjusted OR (95% CI) 9.1 (1.1–77.4),  $P = 0.008$ ]. Malapposed and uncovered struts were more common in lesions with vs. without ME (77 vs. 25%,  $P < 0.001$  and 95 vs. 20%,  $P < 0.001$ , respectively) as was thrombus [49 vs. 14%, OR 7.3 (95% CI: 1.7–31.2),  $P = 0.007$ ]. Post-intervention intra-stent dissection and protrusion of the vessel wall into the lumen were associated with an increased risk of evagination at follow-up [OR (95% CI): 2.9 (1.8–4.9),  $P < 0.001$  and 3.3 (1.6–6.9),  $P = 0.001$ , respectively]. In paired IVUS analyses, lesions with ME showed a larger increase in the external elastic membrane area (20% area change) compared with lesions without ME (5% area change,  $P < 0.001$ ).

## Conclusion

Optical coherence tomography-detected MEs are a specific morphological footprint of early-generation SES and are nearly absent in newer-generation ZES and EES. Evaginations appear to be related to vessel injury at baseline; are associated with positive vessel remodelling; and correlate with uncoverage, malapposition, and thrombus at follow-up.

## Keywords

Optical coherence tomography • Intravascular ultrasound • Coronary evaginations • Early-generation drug-eluting stents • Newer-generation drug-eluting stents • Positive remodelling • Malapposition • Uncovered stent struts

<sup>†</sup>M.D.R. and L.R. contributed equally to this work.

\*Corresponding author. Tel: +31 104635260, Fax: +31 104369154, Email: p.w.j.c.serruys@erasmusmc.nl

Published on behalf of the European Society of Cardiology. All rights reserved. © The Author 2013. For permissions please email: journals.permissions@oup.com

## Introduction

Early-generation drug-eluting stents (DESs) have been associated with an increased risk of very late stent thrombosis (ST) due to delayed arterial healing with evidence of prolonged inflammation, resulting in incomplete endothelialization and acquired malapposition.<sup>1,2</sup> Owing to an ultrahigh resolution (10  $\mu\text{m}$ ), optical coherence tomography (OCT) allows an *in vivo* histology-like evaluation of coronary arteries and implanted devices, including the identification of uncovered and malapposed struts.<sup>3,4</sup> Using OCT, it has been observed that some stented segments show outward vessel bulging—coronary evaginations—of the luminal contour between struts during the follow-up.<sup>5,6</sup> Three-dimensional (3D) visualization of these segments suggests an ectatic appearance of the vessel wall reminiscent of that seen in angiographic ectasias and aneurysms, which were previously shown to be associated with cardiovascular adverse events.<sup>7,8</sup> Although both drugs and polymers of DES have been suspected as culprits for these changes, the specific mechanisms of the luminal enlargement remain unknown and can only be determined with serial invasive assessment. At present, there are no data on the occurrence, predictors, and mechanisms of OCT-detected coronary evaginations following implantation of early- and newer-generation DES. The objectives of the present study were therefore to assess evaginations using OCT at follow-up in a large cohort of patients; and to investigate the underlying mechanism by serial investigations with OCT and intravascular ultrasound (IVUS) in a subset of patients.

## Methods

### Study population

The pooled analysis included OCT acquisitions from the LEADERS-, RESOLUTE-, and SIRTAX-LATE OCT substudies, and from the Copenhagen OCT registry, employing the following stents: Cypher Select<sup>®</sup> (Cordis, Johnson and Johnson, Warren, NJ, USA); Taxus Express<sup>®</sup> (Boston Scientific, Natick, MA, USA); Endeavor Resolute<sup>®</sup> (Medtronic, Inc., Santa Rosa, CA, USA); Xience V<sup>®</sup> (Abbott Vascular, Santa Clara, CA, USA); and Biomatrix<sup>®</sup> (Biosensors, Inc., Newport Beach, CA, USA).

The design and eligibility criteria for LEADERS-, RESOLUTE-, and SIRTAX-LATE OCT substudies are described in detail elsewhere.<sup>6,9,10</sup> The Copenhagen OCT registry was a single-centre prospective non-randomized evaluation of strut coverage and apposition at 12-month follow-up in relation to apposition at baseline, using the Cypher Select<sup>®</sup>, Taxus Express<sup>®</sup>, and Endeavor Resolute<sup>®</sup> stents. Patients were eligible if they had  $\geq 1$  lesion with  $>50\%$  diameter stenosis in a native coronary artery, with a reference vessel diameter between 2.25 and 4.0 mm. Exclusion criteria were ST-segment elevation myocardial infarction (MI), left ventricular ejection fraction  $<30\%$ , renal insufficiency (creatinine  $>133 \mu\text{mol/L}$ ), and lesion location in the left main stem or bypass graft. Optical coherence tomography and IVUS were performed after a satisfactory angiographic result, defined as a residual diameter stenosis  $<20\%$  and thrombus in MI flow grade 3, and imaging with both modalities was repeated at 1-year follow-up. A total of 56 consecutive patients were included at baseline out of which eight withdrew consent for follow-up, and two were excluded due to system failure or insufficient quality for analysis. Figure 1 shows an overview of the number of patients, lesions, and stent types included in each cohort, and the time point of OCT acquisition.

Out of the 46 patients with 48 lesions from the Copenhagen OCT registry, 43 patients with 45 lesions were available with complete serial OCT assessment at baseline and follow-up. Out of these, 40 patients with 42 lesions had a serial IVUS assessment. All studies were conducted in accordance with the Declaration of Helsinki and approved by the ethical committees of the involved centres. All patients provided written informed consent prior to the enrolment.

### Optical coherence tomography and intravascular ultrasound acquisitions

Optical coherence tomography-images were acquired with commercially available time-domain M2 and M3 systems; and the frequency-domain C7 system from LightLab/St Jude (Westford, MA, USA) at a frame rate of 15.6, 20, and 100 frames/s; and a pullback speed of 1, 3, and 10 mm/s; with the M2, M3, and C7, respectively. Acquisition with occlusive (M2) and non-occlusive (M3 and C7) techniques was described previously.<sup>11</sup> Intravascular ultrasound images were acquired with the Atlantis SR Pro 40 MHz catheter and iLab system (Boston Scientific, Natick, MA, USA) at a frame rate of 30 frames/s and pullback speed of 0.5 mm/s, according

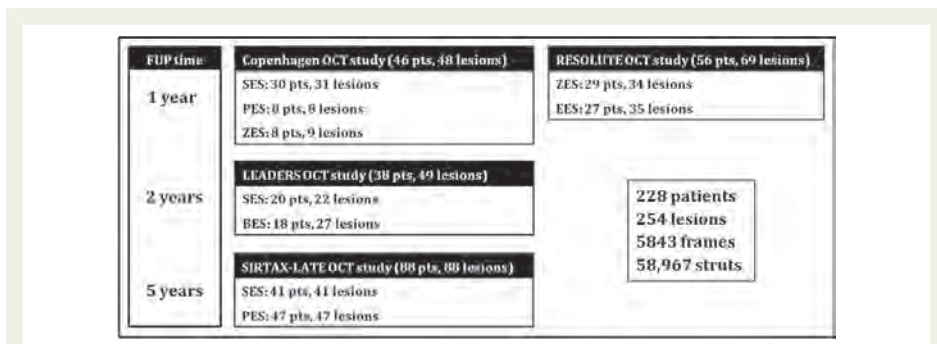


**Figure 1** Overview of the optical coherence tomography data used for the pooled analysis. FUP, follow-up; SES, sirolimus-eluting stent; PES, paclitaxel-eluting stent; ZES, zotarolimus-eluting stent; EES, everolimus-eluting stent; BES, biolimus-eluting stent.

to accepted standards. As for serial investigations, the same imaging systems were used at baseline and follow-up.

### Optical coherence tomography image analysis

The region of interest included the stented segments which were analysed systematically at 1 mm intervals according to corelab standards (Cardialysis, BV, Rotterdam, The Netherlands). The methodology is

shown in Figure 2A. The lumen- and stent area were assessed as previously reported.<sup>12</sup> Malapposition was considered to be present when the distance from the endoluminal strut border to the lumen contour was larger than the sum of strut metal + polymer thickness, resulting in cut-offs of  $\geq 160 \mu\text{m}$  for Cypher,  $\geq 160 \mu\text{m}$  for Taxus Express,  $\geq 100 \mu\text{m}$  for Endeavor Resolute,  $\geq 90 \mu\text{m}$  for Xience V, and  $\geq 130 \mu\text{m}$  for the Biomatrix stent.<sup>10,12,13</sup> In case of malapposition, the incomplete

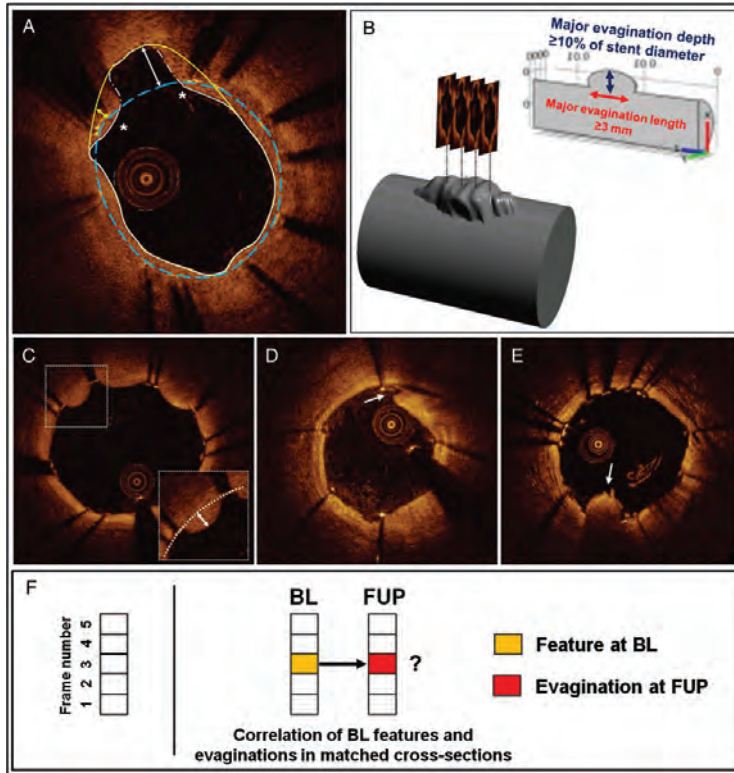


**Figure 2** Overview of optical coherence tomography image analysis. (A) Frame-level analysis included the assessment of the stent area (blue-broken trace) and lumen area (white trace). Evaginations were defined as bulges in the luminal contour between struts with a maximum depth (white double-headed arrow) exceeding the actual strut thickness. Evagination areas were delineated by the stent contour towards the centre of the lumen and the lumen contour in the opposite direction (broken trace along the luminal contour at 11 o'clock). Struts projecting into the lumen without separation from the vessel wall were defined as protruding when the distance (yellow double-headed arrow) from the stent area trace to a 'lumen help line' (yellow trace extrapolated between deepest point of evaginations and lumen contour) exceeded the actual strut thickness. (B) A three-dimensional reconstruction of an evagination. Evaginations were considered major when extending  $\geq 3$  mm longitudinally, with a depth  $\geq 10\%$  of the stent diameter. Prolapse (C) was defined as convex-shaped tissue projecting into the lumen between struts without disruption of the luminal continuity, and registered only when the distance from the stent area trace (white-dotted line) to the maximum point of prolapse was  $\geq 150 \mu\text{m}$ . Intra-stent dissections (D) were defined as disruptions of the luminal vessel contour within the stented segment, whereas tissue protrusion (E) was defined as a mass with an irregular surface attached to the vessel wall or struts and protruding into the lumen. Various features at baseline (i.e. prolapse, intra-stent dissection, tissue protrusion, and malapposed struts) were cross-correlated with the presence of evaginations in matched cross-sections at follow-up (F).

stent apposition (ISA) area was measured. Struts projecting into the lumen without obvious separation from the vessel wall were labelled protruding when the distance from the strut marker to a 'lumen help line' exceeded that of the actual strut thickness, using the same cut-offs as for malapposition.<sup>5,6</sup> The 'lumen help line' was drawn by extrapolating a trace line between the deepest points in evagination/s and the luminal vessel contour laterally. Struts within overlapped segments and those overlying side branch ostia were excluded from the analysis. Struts were considered uncovered if any part of the strut was visibly exposed to the lumen, and covered if a layer of tissue was identified above the struts.<sup>3</sup>

A coronary evagination (Figure 2A) was defined as the presence of an outward bulge in the luminal vessel contour between apposed struts with a maximum depth of the bulge exceeding that of the actual strut thickness, as measured semi-automatically from the deepest point in the bulge to the stent area trace using the thickness-ruler function.<sup>5</sup> The same cut-offs as for malapposition were used. For each evagination, we assessed the evagination area defined as the area limited by the stent contour towards the centre of the lumen and the lumen

contour in the opposite direction. Imaging of evaginations with both time- and Fourier-domain OCT systems was performed in a few cases, excluding any influence of OCT system on the appearance of evaginations.

Evaginations may extend over several consecutive cross-sections, giving the vessel an ectatic appearance by 3D reconstruction (Figure 2B). Thus, evaginations can be characterized both at the 2D cross-sectional level, and along the length of the stented segment. We assessed the presence of major evagination (ME), defined as the occurrence of cross-sectional evagination in  $\geq 3$  adjacent frames (i.e. minimum 3 mm of length) with a minimal evagination depth of 10% of the nominal stent diameter. Evagination areas of the various cross-sections belonging to a ME were assumed to be constant 0.5 mm proximal and distal to the analysed cross-section in order to calculate evagination volumes for each 1 mm segment. If evaginations were present in adjacent cross-sections, they were assumed to be in a continuum, and their volumes were summed up to calculate the total evagination volume. In addition, we assessed the presence of thrombus defined as a mass  $\geq 100 \mu\text{m}$  in diameter with an irregular surface attached to the vessel wall or struts and protruding into the lumen.

**Table 1** Baseline demographics and baseline patient and lesion level predictors of major evaginations adjusted for time to follow-up

Characteristics	Entire cohort n (%)	Major evagination at follow-up		Crude OR (95% CI)	P-value	Adj OR (95% CI)	P-value
		Yes, n (%)	No, n (%)				
No. of patients	228	31	197				
Age	60.0 $\pm$ 10.4	59.2 $\pm$ 11.0	60.2 $\pm$ 10.3	1.00 (0.96–1.04)	1.00	1.00 (0.96–1.05)	0.89
Male gender	179 (78.5)	24 (77.2)	155 (78.7)	0.88 (0.35–2.26)	0.78	0.89 (0.33–2.41)	0.82
Hypertension	127 (55.7)	15 (48.4)	112 (56.9)	0.77 (0.35–1.69)	0.52		
Hyperlipidaemia	153 (67.1)	20 (64.5)	133 (67.5)	0.87 (0.38–2.00)	0.74		
Diabetes mellitus	44 (19.3)	4 (12.9)	40 (20.3)	0.58 (0.19–1.80)	0.35		
Current/previous smoker	87 (38.2)	11 (35.5)	76 (38.6)	0.75 (0.33–1.71)	0.49		
Previous MI	58 (25.7)	6 (19.4)	52 (26.7)	0.68 (0.26–1.82)	0.45		
LVEF $\leq$ 50	42 (18.4)	12 (38.7)	30 (15.2)	3.20 (1.32–7.72)	0.01	2.71 (1.03–7.16)	0.044
STEMI	48 (21.1)	9 (29.0)	39 (19.8)	1.89 (0.74–4.82)	0.19	1.48 (0.49–4.44)	0.48
Stent type					0.0055		0.0084
EES (reference)	27 (11.8)	1 (3.2)	26 (13.2)	Reference		Reference	
PES	55 (24.1)	4 (12.9)	51 (25.9)	2.06 (0.19–22.48)		1.96 (0.17–22.53)	
BES	18 (7.9)	2 (6.5)	16 (8.1)	3.26 (0.27–39.38)		3.80 (0.31–46.61)	
ZES	37 (16.2)	1 (3.2)	36 (18.3)	0.72 (0.04–12.08)		0.83 (0.05–14.01)	
SES	91 (40.0)	23 (74.2)	68 (34.5)	8.84 (1.07–72.97)		9.05 (1.06–77.35)	
Multivessel disease	23 (13.4)	3 (10.3)	20 (14.0)	0.61 (0.15–2.57)	0.51		
No. of lesions	254	33	221				
Target vessel					0.15		
Left main (reference)	3 (1.2)	1 (3.1)	2 (0.9)	Reference			
LAD	101 (40.0)	7 (21.9)	94 (43.1)	0.16 (0.01–2.45)	0.19		
Circumflex	57 (22.8)	7 (21.9)	50 (22.9)	0.20 (0.01–3.26)	0.26		
RCA	88 (35.2)	17 (53.1)	71 (32.6)	0.47 (0.03–6.93)	0.58		
Graft	1 (0.4)	0 (0)	1 (0.5)	0.16 (0.01–2.45)	0.19		
Stent diameter <sup>a</sup>	3.0 $\pm$ 0.4	3.1 $\pm$ 0.4	3.0 $\pm$ 0.4	7.05 (0.42–119.3)	0.18		
Total stented length <sup>a</sup>	21.6 $\pm$ 13.9	22.6 $\pm$ 10.4	21.4 $\pm$ 14.3	1.00 (0.91–1.11)	0.96		
Stents per lesion <sup>a</sup>	1.4 $\pm$ 0.7	1.4 $\pm$ 0.8	1.4 $\pm$ 0.7	0.91 (0.07–11.12)	0.94		

<sup>a</sup>Expressed as means  $\pm$  SD.

The Copenhagen OCT registry included OCT examinations at baseline and 1-year follow-up. Cross-sections at baseline and follow-up were matched on the basis of distance from stent borders and the presence of anatomical landmarks such as side branches. This allowed the following serial assessments at the cross-sectional level (Figure 2C–E):

At baseline, we assessed the presence of tissue prolapse, intra-stent dissection and tissue protrusion. *Tissue prolapse* was defined as convex-shaped tissue with a regular surface protruding into the lumen between adjacent struts without disruption of the continuity of the luminal vessel surface.<sup>14</sup> The tissue was considered prolapsing only when the distance from the stent area trace to the maximum point of prolapse was  $\geq 150$   $\mu\text{m}$ , chosen arbitrarily since some degree of prolapse can be seen in most cross-sections. *Intra-stent dissections* were defined as disruptions of the luminal vessel contour within the stented segment, whereas *tissue protrusion* was defined as a mass with an irregular surface attached to the vessel wall or struts and protruding into the lumen. These features as well as the presence of  $\geq 1$  malapposed strut were then correlated with the presence of evagination at the time of serial follow-up, in matched cross-sections (Figure 2F).

### Intravascular ultrasound image analysis

Intravascular ultrasound pullbacks were analysed off-line using the QCU-CMS software (Medis, Leiden, The Netherlands) at standard 1 mm intervals, in the same region of interest as for OCT, following the international consensus.<sup>15</sup> Accordingly, we measured the lumen-, stent-, and external elastic membrane area, the latter referred to as vessel area. The plaque and media (P&M) area was calculated as (vessel area – stent area – lumen area outside the stent), and the plaque burden as (P&M area/vessel area)  $\times$  100. Positive vessel remodelling was defined as an increase in the vessel area from baseline to follow-up.

### Statistical analysis

We used Bayesian hierarchical random-effects model based on Markov chain Monte–Carlo simulation methods<sup>16</sup> with non-informative priors, to compare OCT features such as strut malapposition, protrusion, and coverage between lesions with ME and lesions without. The model included random-effects at the level of cross-sections and lesions, accounting for the correlation of characteristics of cross-sections within lesions, and assigning analytical weights to each lesion depending on the number of struts or cross-sections observed per lesion. Continuous characteristics of lesions such as lumen area and stent area were compared between lesions with vs. without ME using frequentist mixed maximum-likelihood regression models with study cohort, type of stent, patient, and/or lesion as random intercepts. Means and standard deviations were estimated from predicted values. To determine the

association of characteristics of lesions and patients at baseline with the presence or absence of ME at follow-up, we used mixed maximum logistic regression models adjusted for time to follow-up (1, 2, or 5 years) with study cohort, type of stent and lesion specified as random intercepts. The same model was used to analyse stent and lumen area over time as assessed with OCT and IVUS in the Copenhagen OCT registry. Mixed maximum logistic regression models with type of stent, patient, and lesion as random intercepts were used to assess the association of the baseline cross-sectional OCT features intra-stent dissection, strut malapposition, tissue protrusion, and prolapse with cross-sectional evagination at follow-up, with univariable and multivariable mutual adjustments for all four features. Statistical analyses were performed using WinBUGS version 1.4.3 (Imperial College and MRC, UK) and Stata, version 11.0 (StataCorp, College Station, TX, USA).

## Results

### Incidence and extent of evaginations

A total of 228 patients with 254 lesions containing 5843 frames with 58 967 struts were included in the analysis (Figure 1). Overall, 75.8% of patients were male and 19.3% had diabetes (Table 1). The clinical setting at stent implantation was STEMI in 21.1% of cases, and 40.0% of patients received a SES. Overall, a median (IQR) of 19 (15–26) cross-sections and 183 (140–273) struts were analysed per lesion. Out of 254 lesions, 152 (59.8%) had at least one cross-section with evagination, and 33 (13.0%) lesions contained at least one ME. Out of the 33 lesions with ME, 23 had a SES implanted, four a PES, four a BES, one a ZES, and one an EES. The frequency of cross-sectional and ME according to stent type and time point of implantation are shown in Table 2. Both ‘any’ cross-sectional and ME were more frequent in the SES group when compared with the PES-, ZES-, and EES-groups. The frequency of ME was low for lesions treated with ZES and EES at 1 year, and PES at 5 years.

Table 3 shows the mean evagination- and ISA volumes per lesion in lesions with any cross-sectional evagination and lesions with ME according to stent type and time since implantation. Evagination volumes were consistently larger for the SES group when compared with the other stents. Incomplete stent apposition volumes were similarly larger in SES at 2 and 5 years. Evaluating SES alone, there was a trend for an increase in ISA volumes from 1 to 2 to 5 years (all lesions:  $P = 0.024$ ; lesions with any cross-sectional evagination:

**Table 2** Occurrence of cross-sectional and major evaginations stratified by stent type and time to follow-up

Lesions	SES	PES	BES	ZES	EES	P-value
No. of lesions with any evagination/total no. of lesions (%)						
Year 1	22/31 (71)	4/8 (50)		25/43 (58)	13/35 (37)	0.045
Year 2	16/22 (73)		15/27 (56)			0.25
Year 5	29/41 (71)	28/47 (60)				0.37
No. of lesions with major evagination/total no. of lesions (%)						
Year 1	8/31 (26)	1/8 (13)		1/43 (2)	1/35 (3)	0.003
Year 2	4/22 (18)		4/27 (15)			1.00
Year 5	11/41 (27)	3/47 (6)				0.02

**Table 3** Evagination and incomplete stent apposition volumes at the lesion level in lesion with any and major evaginations by stent type and time to follow-up

	SES	PES	BES	ZES	EES	P-value
At Year 1						
Lesions with any evagination						
EV	2.24 ± 1.68 (22)	0.50 ± 0.72 (4)		0.38 ± 1.79 (25)	0.42 ± 1.29 (13)	0.002
ISAV	0.20 ± 2.12 (22)	3.00 ± 0.90 (4)		0.76 ± 2.25 (25)	2.20 ± 1.63 (13)	0.30
Lesions with ME						
EV	24.20 ± 1.77 (8)	5.31 ± 0.59 (1)		4.42 ± 0.59 (1)	10.28 ± 0.59 (1)	0.39
ISAV	0.54 ± 1.64 (8)	12.10 ± 0.58 (1)		0.26 ± 0.58 (1)	6.23 ± 0.58 (1)	<0.001
All lesions						
ISAV	0.14 ± 1.80 (31)	1.51 ± 0.92 (8)		0.57 ± 2.12 (43)	0.92 ± 1.92 (35)	0.17
At Year 2						
Lesions with any evagination						
EV	2.47 ± 2.52 (16)		0.57 ± 2.44 (15)			0.03
ISAV	1.54 ± 3.32 (16)		0.19 ± 3.21 (15)			0.24
Lesions with ME						
EV	30.40 ± 1.30 (4)		4.08 ± 1.19 (4)			0.01
ISAV	5.22 ± 5.15 (4)		0.79 ± 5.15 (4)			0.21
All lesions						
ISAV	1.34 ± 2.69 (22)		0.12 ± 2.98 (27)			0.12
At Year 5						
Lesions with any evagination						
EV	2.54 ± 1.58 (29)	0.72 ± 1.55 (28)				<0.001
ISAV	3.81 ± 6.69 (29)	1.42 ± 6.57 (28)				0.10
Lesions with ME						
EV	11.80 ± 0.59 (11)	4.40 ± 0.25 (3)				0.008
ISAV	7.47 ± 13.52 (11)	1.91 ± 7.06 (3)				0.41
All lesions						
ISAV	2.72 ± 5.49 (41)	1.04 ± 5.88 (47)				0.09

ME, major evagination; EV, evagination volume; ISAV, incomplete stent apposition volume. Volumes are expressed as means ± SD (no. of lesions) mm<sup>3</sup> and predicted from maximum-likelihood models.

$P = 0.016$ ; lesions with ME:  $P = 0.14$ ). The average depths and lengths of cross-sectional and ME are presented in the appendix.

### Predictors of major evaginations

Table 1 presents patient and lesion characteristics and their association with ME. The indication for stent implantation was STEMI in 29.0% of patients with and 19.8% of patients without ME ( $P = 0.19$ ). Left ventricular ejection fraction  $\leq 50\%$  was more frequent in patients with compared with those without ME, and the use of SES emerged as an independent predictor for the presence of ME.

### Pooled optical coherence tomography analysis

The quantitative results of the OCT analysis at the time of follow-up are shown in Table 4. Minimal and average lumen and stent areas were larger in lesions with when compared with those without ME.

Malapposed, protruding, and uncovered struts were more common in lesions with than without ME, and found in 77.2 vs. 24.9% ( $P < 0.001$ ), 97.0 vs. 82.1% ( $P < 0.001$ ), and 94.6 vs. 20.1% ( $P < 0.001$ ) lesions, respectively. Similarly, the proportion of lesions with  $\geq 10\%$  malapposed and uncovered struts was significantly larger in the ME group. The average (means ± SD) thickness of strut coverage was smaller in lesions with MEs compared with those without this feature [ $0.11 \pm 0.29$  vs.  $0.14 \pm 0.23$  mm; difference (95% CI):  $-0.03$  ( $-0.06$  to  $-0.004$ ) mm,  $P = 0.022$ ]. At follow-up, thrombus was more frequent in lesions with 'any' evagination [28.0 vs. 5.9%, OR (95% CI): 6.1 (2.0–17.1),  $P = 0.001$ ] as well as ME [48.5 vs. 14.0%, OR (95% CI): 7.3 (1.7–31.5),  $P = 0.007$ ].

### Serial optical coherence tomography and intravascular ultrasound analyses

Quantitative serial OCT results are shown in Table 5. All lesions with ME were implanted with SES. The stent and lumen areas were larger

**Table 4** Results of follow-up optical coherence tomography analysis

	Major evagination at follow-up		Difference (95% CI)	P-value
	Yes	No		
Lesions analysed, <i>n</i>	33	221		
Frames analysed, <i>n</i>	804	5039		
Struts analysed, <i>n</i>	8385	50,582		
Lumen area, mm <sup>2a</sup>	8.34 ± 5.90	6.44 ± 2.50	1.90 (1.08–2.72)	<0.001
Minimal lumen area, mm <sup>2a</sup>	5.99 ± 5.60	4.88 ± 2.20	1.12 (0.34–1.89)	0.005
Stent area, mm <sup>2a</sup>	8.50 ± 6.10	7.37 ± 3.00	1.13 (0.33–1.93)	0.006
Minimal stent area, mm <sup>2a</sup>	6.71 ± 6.40	5.88 ± 3.70	0.83 (0.03–1.62)	0.04
Strut type, % (95% CrI)				
Malapposed struts <sup>b</sup>				
Malapposed struts per lesion	1.07 (0.41–2.62)	0.11 (0.06–0.17)	0.96 (0.31–2.52)	<0.001
Lesions with ≥ 1	77.20 (52.80–92.80)	24.9 (15.40–34.90)	51.80 (25.40–72.60)	<0.001
Lesions with ≥ 10%	5.53 (0.86–19.30)	0.18 (0.02–1.19)	5.24 (0.70–18.90)	0.001
Protruding struts <sup>b</sup>				
Protruding struts per lesion	3.04 (1.52–5.87)	0.11 (0.06–0.17)	2.92 (1.42–5.77)	<0.001
Lesions with ≥ 1	97.00 (86.70–99.60)	82.1 (72.30–89.60)	14.30 (4.04–23.80)	0.01
Lesions with ≥ 10%	9.34 (2.03–27.10)	4.93 (1.93–10.80)	4.09 (-3.42–21.20)	0.37
Uncovered struts <sup>b</sup>				
Uncovered struts per lesion	3.82 (2.12–6.82)	1.39 (1.06–1.79)	2.43 (0.70–5.46)	0.002
Lesions with ≥ 1	94.60 (81.00–99.10)	20.10 (11.40–30.00)	74.00 (56.00–85.80)	<0.001
Lesions with ≥ 10%	5.59 (0.85–19.30)	<0.01 (<0.01–0.16)	5.57 (0.84–19.30)	<0.001

Lumen and stent areas are expressed as means ± SD.

CrI, credibility interval.

<sup>a</sup>Using traditional mixed maximum-likelihood model.

<sup>b</sup>Using Bayesian hierarchical 2-level logistic regression model.

**Table 5** Quantitative serial optical coherence tomography results of the stented segment

	Major evagination at follow-up		Difference (95% CI)	P-value
	Yes	No		
Patients analysed, <i>n</i>	8	35		
Lesions analysed, <i>n</i>	8	37		
Frames analysed, <i>n</i>	154	705		
SA BL, mm <sup>2</sup>	8.60 ± 1.42	7.14 ± 1.22	1.84 (0.32–3.37)	0.02
SA FUP, mm <sup>2</sup>	9.21 ± 1.59	7.33 ± 1.36	2.28 (0.57–3.98)	0.009
SA change, mm <sup>2</sup>	0.61 ± 0.29	0.20 ± 0.24	0.43 (-0.02–0.88)	0.06
LA BL, mm <sup>2</sup>	8.85 ± 1.11	7.30 ± 0.92	1.89 (0.45–3.33)	0.01
LA FUP, mm <sup>2</sup>	9.03 ± 1.22	6.29 ± 1.01	2.89 (1.27–4.52)	<0.001
LA change, mm <sup>2</sup>	0.17 ± 0.66	-1.00 ± 0.59	0.99 (0.29–1.69)	0.006

Areas are presented as means ± SD.

SA, stent area; LA, lumen area; BL, baseline; FUP, follow-up.

in lesions with when compared with those without ME at both baseline and follow-up, with a significant change in the lumen area at follow-up in both groups [increase in the lumen area in lesions with ME ( $P = 0.01$ ), and decrease in the lumen area in lesions

without ME ( $P < 0.001$ )]. The change in the stent area from baseline to follow-up within the ME group was not significant ( $P = 0.15$ ).

Table 6 shows the association of OCT characteristics recorded at baseline with cross-sectional evagination at follow-up in matched

**Table 6** Assessment of the correlation of baseline optical coherence tomography features and evaginations, in matched cross-sections

	Evagination at follow-up		Crude OR (95% CI)	P-value	Multivariable OR (95% CI)	P-value
	Yes	No				
No. of frames at follow-up	128	713				
Characteristics of cross-section at baseline						
Intra-stent dissection, n (%)	60 (46.9)	159 (21.8)	3.01 (1.81–5.00)	<0.001	2.93 (1.75–4.89)	<0.001
Malapposed strut, n (%)	12 (9.4)	35 (4.8)	1.76 (0.77–4.03)	0.18	1.69 (0.72–3.99)	0.23
Tissue protrusions, n (%)	27 (21.1)	73 (10.0)	3.27 (1.59–6.70)	0.001	3.34 (1.61–6.93)	0.001
Prolapse, n (%)	26 (20.3)	162 (22.2)	1.04 (0.57–1.90)	0.90	1.06 (0.57–1.99)	0.85

Using mixed logistic regression with stent type, patient, and lesion as random intercept.

cross-sections. In both uni- and multivariable analyses, intra-stent dissections, and tissue protrusions at baseline were associated with cross-sectional evagination at follow-up: the odds of evagination at follow-up were increased by about three in the presence of either dissection or tissue protrusion at baseline.

The corresponding serial IVUS analyses are summarized in Table 7. At baseline, the vessel area was larger among lesions with ME. Serial IVUS analysis showed a larger increase in the vessel area and positive remodelling in lesions with ME when compared with those without (21.1 vs. 4.6%,  $P < 0.001$ ), mainly driven by an increase in the P&M area and accompanied by an increase in the lumen area. Again, the stent area appeared to increase between baseline and follow-up in lesions with ME ( $P = 0.84$ ), but not in lesions without [difference in change between groups (95% CI): 0.43 (0.01–0.85) mm<sup>2</sup>,  $P = 0.04$ ].

## Discussion

The present study shows that OCT-detected MEs are specifically related to early-generation SES, and much smaller and in general less frequent in newer-generation DES. The mechanism underlying the pathogenesis of ME was suggestively a positive remodelling. Signs of injury documented immediately after stent implantation were associated with an increased risk of evagination at follow-up.

### Positive remodelling as a cause of coronary evagination

Coronary artery ectasias and aneurysms following DES implantation have generated great interest owing to their association with ST.<sup>7,8,17</sup> These vessel distensions have often been accompanied by ISA, suggesting positive remodelling as the underlying pathomechanism, since regional vessel remodelling was previously identified as a cause of late acquired stent malapposition (LASM).<sup>7,17,18</sup> In the present study, we took advantage of information obtained by OCT on depth, cross-sectional area, and longitudinal extent, to assess evaginations in three dimensions. The association between positive remodelling and ME suggests that positive remodelling is the mechanism underlying the pathogenesis of evaginations.

We observed that ME in general occurred more frequently and appeared to be larger in SES, suggesting these to be a specific

morphological footprint of these early-generation DES. Conversely, MEs were less frequent in PES compared with SES at 5 years—a difference which is confirmatory of the SIRTAX-LATE OCT study. At 1 year, MEs were less frequent in PES compared with SES but were almost absent in newer-generation ZES and EES. No difference, however, was observed between SES and BES at 2 years—something that needs to be interpreted in light of a relatively low sample size of only 18 SES and 18 BES patients at 2 years of follow-up. (Accordingly, it cannot be excluded that this finding could be due to chance. Nevertheless, assessment of evagination volumes showed that these were significantly larger for SES compared with BES, thus being in line with the findings in the other subgroups, particularly the SES vs. ZES and EES, where the sample size was also relatively low.) In a meta-analysis, Hassan *et al.*<sup>19</sup> reported similar findings in terms of IVUS-detected LASM, which were also accompanied by positive vessel remodelling, with the highest incidence in SES followed by PES, and newer-generation ZES and EES. These similarities, together with the observed association of ME with malapposed, protruding, and uncovered struts, suggest that these features may be part of the same disease entity.

Pre-clinical and human autopsy studies previously demonstrated that the inflammatory response following DES implantation strongly relates to the type of stent: SES typically induces granulomatous inflammation with macrophages, giant cells, lymphocytes, and eosinophils; PES exhibits extensive fibrin deposition and medial smooth muscle cell necrosis; ZES and EES show only low levels of inflammation and fibrin deposition.<sup>1,20–22</sup> In addition, SES has been associated with marked adventitial inflammation and fibrosis—findings associated with positive remodelling.<sup>20,23</sup> These results are in line with observations of aneurysmal vessel dilation, stent malapposition, and generalized eosinophilic vasculitis in a case of late ST in a patient with SES.<sup>24</sup> Similarly, the extent of vascular remodelling predominantly after SES implantation correlated with the number of eosinophils harvested from thrombus aspirates in patients with very late ST,<sup>25</sup> supporting the notion that OCT-detected ME represent a pathological vascular reaction particularly related to this stent.

If evaginations and protruding struts are precursors of ISA, a stretch in the P&M may occur during the vessel expansion before complete detachment from the stent. Interestingly, we observed a trend towards a decrease in the size of ME from 1 and 2 to 5-year

**Table 7** Quantitative serial intravascular ultrasound results of the stented segment

	Major evagination at follow-up		Diff (95% CI)	P-value
	Yes	No		
SA BL, mm <sup>2</sup>	8.67 ± 1.94	7.61 ± 1.62	1.31 (−0.43 to 3.05)	0.14
SA FUP, mm <sup>2</sup>	9.18 ± 2.03	7.67 ± 1.68	1.76 (−0.09 to 3.60)	0.06
SA change, mm <sup>2</sup>	0.50 ± 0.31	0.06 ± 0.24	0.43 (0.01 to 0.85)	0.04
LA BL, mm <sup>2</sup>	8.67 ± 1.92	7.59 ± 1.61	1.33 (−0.39 to 3.06)	0.13
LA FUP, mm <sup>2</sup>	9.28 ± 2.00	7.37 ± 1.63	2.10 (0.24 to 3.97)	0.03
LA change, mm <sup>2</sup>	0.59 ± 0.40	−0.22 ± 0.33	0.75 (0.22 to 1.28)	0.006
VA BL, mm <sup>2</sup>	16.53 ± 2.63	13.78 ± 1.99	3.44 (0.62 to 6.25)	0.02
VA FUP, mm <sup>2</sup>	20.06 ± 3.44	14.41 ± 2.76	6.29 (3.00 to 9.59)	<0.001
VA change, mm <sup>2</sup>	3.51 ± 1.19	0.63 ± 1.00	2.84 (1.71 to 3.98)	<0.001
P&M area BL, mm <sup>2</sup>	7.86 ± 1.79	6.14 ± 1.56	2.11 (0.52 to 3.70)	0.009
P&M area FUP, mm <sup>2</sup>	10.78 ± 2.36	7.02 ± 2.06	4.17 (2.08 to 6.27)	<0.001
P&M area change, mm <sup>2</sup>	2.89 ± 0.92	0.87 ± 0.76	2.06 (1.11 to 3.00)	<0.001
PB BL, %	46.82 ± 4.02	44.36 ± 2.95	3.02 (−2.65 to 8.70)	0.30
PB FUP, %	52.78 ± 4.36	48.46 ± 3.15	5.26 (−0.93 to 11.46)	0.10
PB change, %	5.90 ± 1.98	3.95 ± 1.72	2.21 (−0.08 to 4.49)	0.06

Areas are presented as means ± SD.

SA, stent area; LA, lumen area; VA, vessel area; P&M, plaque and media; PB, plaque burden; BL, baseline; FUP, follow-up.

follow-up among SES-stented segments, while there was a trend towards an increase in ISA volume, suggesting that evaginations may transition into ISA. Regarding the large ISA volumes at 1 year in the two cases of PES and ZES with ME, the ISA in the PES represented persistent malapposition, whereas the ISA in ZES was located in the proximity of a large bifurcation and thus likely present at baseline.

The unexpected finding of a larger stent area only in lesions with ME, which was consistent across the pooled analysis as well as the serial independent evaluation with OCT and IVUS, may either be related to the vessel expansion before detachment or due to chance. It is unlikely that a more intense use of nitroglycerine or potentially higher flush rate during OCT acquisition at follow-up when compared with baseline could have induced these findings only in lesions with ME.

### Mechanisms of vessel remodelling

The SES-specific remodelling pattern may be triggered by the polymer rather than the drug. Evidence in favour of this hypothesis is the presence of a focal giant cell reaction surrounding polymer remnants separated from the stent struts,<sup>24</sup> together with observations that durable-polymer SES when compared with polymer-free SES and bare-metal stents are associated with a larger external elastic membrane area.<sup>23</sup> Considering that 80% of sirolimus is released from durable-polymer SES within the first 4 weeks, it seems unlikely that sirolimus itself induces long-term alterations of the vessel wall such as the ME detected up to 5 years in the present study.

The specific mechanisms by which polymers may induce positive remodelling in cases of coronary aneurysms and LASM remain speculative. In relation to SES, it is known that methacrylate may exert a

toxic effect on endothelial cells and leucocytes, and can modulate pro-coagulant activities of monocytes.<sup>26</sup> Exposure to the poly-*n*-butyl-methacrylate polymer can furthermore cause delayed (type IV) hypersensitivity reactions mediated at least in part by accumulated CD4 T-helper cells secreting interleukin (IL)-4 and IL-13.<sup>24</sup> Of note, IL-13 was associated with increased smooth muscle cell contractility in asthma,<sup>27</sup> and can induce alveolar remodelling and emphysema in mice via induction of matrix metalloproteinase (MMP)-9 and MMP-12.<sup>28</sup> Both these MMPs were identified as important factors in the development of abdominal aortic aneurysms in humans by degradation of elastin.<sup>29</sup> At the same time, MMP-12 has been found to be a mediator of the accumulation of macrophages and eosinophils.<sup>28</sup> Similar pathways may be responsible for the remodelling and eosinophilia observed in SES-treated coronary arteries. However, then remains the question why not all patients develop this finding.

To further address this, we compared OCT findings following stent implantation with the presence of evaginations at follow-up in corresponding cross-sections. Accordingly, our study demonstrated that cross-sections exhibiting intra-stent dissections and tissue protrusions at baseline—both representing markers of injury—were associated with an increased risk of evagination at the time of OCT follow-up. (Of note, tissue protrusions were defined as tissue projections with irregular lumen contour and thereby suggestive of either thrombus or tissue disruptions other than intra-stent dissections, whereas tissue prolapses were characterized by an intact lumen contour, suggestive of prolapsing plaque.) This relationship is supported by previous observations relating OCT-detected evaginations and coronary artery aneurysms with vessel wall dissections and deep arterial injury caused by oversized balloons, stents, and atherectomy.<sup>5,30,31</sup> Nevertheless, considering that intra-stent

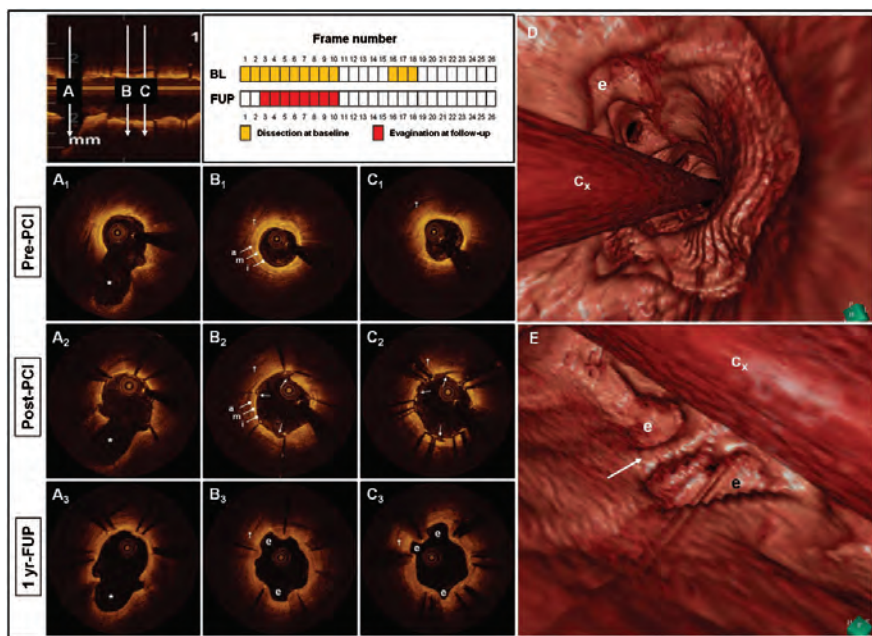


**Figure 3** Co-location of intra-stent dissections post-PCI and evaginations at follow-up. (A–C) Three cross-sections obtained at corresponding sites before (A<sub>1</sub>–C<sub>1</sub>), immediately after (A<sub>2</sub>–C<sub>2</sub>), and at 1 year (A<sub>3</sub>–C<sub>3</sub>) following stent implantation. The large side-branch (\*) in (A<sub>1</sub>)–(A<sub>3</sub>) confirms a good matching, as does the pericardial space (†) and evidence of trilaminar vessel structure (i, intima; m, media; a, adventitia) in (B<sub>1</sub>)–(B<sub>3</sub>) and (C<sub>1</sub>)–(C<sub>3</sub>). In (B<sub>2</sub>) and (C<sub>2</sub>), a large intra-stent dissection extends from 10 to 1 o'clock (white arrows), exposing the underlying adventitia, and a small dissection is seen at 6 o'clock (white arrow). Of note, evaginations (e) are clearly seen at the corresponding sites at follow-up in (B<sub>3</sub>) and (C<sub>3</sub>). The upper middle panel shows a schematic overview of the location of intra-stent dissection at baseline and evagination at follow-up within matched frames. (D) An endoscopic three-dimensional view of the vessel in question, where evaginations (e) create an irregular luminal surface. The optical coherence tomography-catheter (Cx) is located to the left of the 'point of view'. (E) A perpendicular view of the evagination in (B<sub>3</sub>) and (C<sub>3</sub>) at 10 o'clock (white e in (E)), which in the three-dimensional reconstruction is separated from another evagination (black e in (E)) along the vessel segment by a strut (white arrow). The evagination at 12 o'clock in (C<sub>3</sub>) is hidden behind the optical coherence tomography-catheter (Cx) in (E).

dissections were present in 27%, 15%, and 31% of cross-sections in SES, PES and ZES, respectively, it may be argued that the influence of stent type, as compared to that of vessel injury, is relatively greater on the development of ME, which in the serially studied lesions were all present in segments implanted with SES. Although the depth of intra-stent dissections could not be systematically assessed due to the limited tissue penetration of OCT, we did observe 12 cases of evaginations following intra-stent dissections extending into the media and adventitia (Figure 3).

### Potential clinical relevance of coronary evaginations

Features associated with very late ST include uncovered struts, late malapposition, positive remodelling, chronic inflammation as well

as ectasias and aneurysms.<sup>1,2,7,8,17,25,32</sup> We found nearly all these features to be more common in lesions with ME, suggesting that ME may be part of the same pathophysiological entity commonly recognized as inappropriate healing following DES implantation, proposing a possible link with late ST. Moreover, our finding of a greater frequency of thrombus in lesions with 'any' and MEs may be an expression of a potential thrombogenicity of these lesions compared with those without evaginations. Although our pooled study sample included one of the largest OCT cohorts to date, it was too small for a meaningful evaluation of such a relationship, however, two of the patients with ME from the SIRTAX-LATE cohort experienced very late ST at 5 and 12 months following 5-year OCT follow-up. Both of these occurred in SES which had some of the most extensive evagination- and ISA volumes in the entire cohort.<sup>6</sup> Along the same line, Alfonso *et al.*<sup>7</sup> described that among patients with angiographic

coronary artery aneurysms, subsequent ST correlated with a larger vessel and lumen volume by IVUS at the time of imaging. Similarly, Imai *et al.*<sup>8</sup> observed an increased risk of ST and target lesion revascularization in SES with ectasias measuring  $\geq 20\%$  of the stent diameter and extending longitudinally at least the length of the stent diameter, corresponding to an ectasia depth and length of 0.6 mm and 3 mm in a 3 mm stent, respectively—a similar length but twice the depth of the ME definition used in our study. These data suggest that the extent of evagination matters and that clarification of the natural history of evaginations as well as the relationship between the degree of evagination and clinical events merits consideration.

Although first-generation SES are no longer manufactured, they have been implanted in a considerable number of patients worldwide. Recent data from a registry of >12 000 patients, and a meta-analysis including 49 trials, suggest that treatment with newer-generation EES is associated with a lower risk of very late ST when compared with early-generation SES and PES,<sup>33,34</sup> which are additionally associated with a continued risk of very late ST when compared with EES. In this context, it is interesting that the occurrence of evaginations, malapposition, and uncoverage by OCT in the present study, as well as the incidence of IVUS-detected LASM in previous studies,<sup>19</sup> follow a similar pattern. Our findings therefore suggest that evaginations detected with high-resolution OCT may be predictors of late ST particularly in SES, and alongside malapposition and uncoverage provide a possible explanation for differences in late adverse ischaemic events in early- compared with newer-generation DES. Conversely, PES when compared with SES showed fewer ME and only a modest increase when compared with newer-generation DES. Although clinical rates of ST have been comparable between SES and PES, the trigger leading to thrombosis appears to differ<sup>21</sup> in view of substantial differences in the frequency of evaginations. Studies assessing clinical outcomes with OCT and IVUS—particularly with serial imaging—are demanding to perform due to the relatively complex and costly set-ups and the large number of patients required. In view of this, the present study, although relatively small with the 254 imaged lesions, provides important new insights into the utility of OCT for assessing vascular reactions following stent implantation, and suggests that this technology can identify features specific for different stents, which may be useful for improving the prediction of events in the future.

## Limitations

The following shortcomings must be considered when interpreting the results of the present study. First, we pooled data from four separate cohorts with different time to follow-up, out of which one came from a non-randomized registry. Efforts were made to adjust for these issues by using frequentist and Bayesian mixed models accounting for the clustered nature of data. Secondly, we did not assess the type of malapposition at follow-up primarily as our focus was on evaginations, and since the relationship between acquired malapposition and positive remodelling has already been shown.<sup>18</sup> Considering that positive remodelling is a common denominator of evaginations and LASM, it seems reasonable to assume that the majority of malapposed struts at follow-up within lesions with ME were late acquired,

particularly since there was no correlation between malapposed struts at baseline and ME at follow-up. Thirdly, we extrapolated cross-sectional evagination areas 0.5 mm proximal and distal to the frame of interest to estimate the volume of ME, which may both over- and underestimate the size. Separate evaluation of cross-sectional and ME does however not affect the results of the relative occurrence and predictors of evaginations. Whether this is also true for the mechanisms is unknown since serial IVUS was only available for one of the cohorts. In this regard, it cannot be discarded that evaginations at 2 and 5 years may be caused by mechanisms other than remodelling as observed at 1 year. Furthermore, OCT cross-sections were analysed at 1 mm intervals, although the highest sampling density with commercially available new-generation OCT is 0.2 mm. This could potentially give inaccurate estimates of the occurrence and size of cross-sectional and ME. Considering that gold-standard histology typically evaluates entire lesions based on three to five cross-sections—remarkably lower compared with the average 19 cross-sections per lesion assessed in our study—we chose to accept this level of accuracy, as well as the potential imprecision in the selection of corresponding cross-sections at baseline and follow-up, which is inevitably present whenever serial evaluations are performed. Also, although care was taken to obtain as accurate measurements of evagination- and ISA-volumes as possible, the inherent risk of multiplication of small measurement errors cannot be excluded. Finally, even though this study is one of the largest OCT studies to date, the small number of lesions with MEs, especially in the ZES and EES groups at 1 year, nonetheless limits the power of the study.

## Conclusion

Optical coherence tomography-detected MEs are a specific morphological footprint of early-generation SES and are nearly absent in newer-generation ZES and EES. Optical coherence tomography detected intra-stent dissections and tissue protrusions at baseline are associated with an increased risk of evaginations at follow-up. The mechanism underlying the pathogenesis of ME is suggestively a positive remodelling.

## Acknowledgements

We are grateful to Marcel Zwahlen and Thomas Gsponer at the Institute for Social and Preventive Medicine at the University of Bern, Switzerland, for advice on statistical modelling.

## Funding

This work was supported by the following funding: M.D.R. has received research grants from The Heart Centre Rigshospitalet Research Foundation and Copenhagen University. Part of the analysis was funded by intramural grants provided by CTU Bern, Bern University Hospital, the Institute of Social and Preventive Medicine, University of Bern, and a grant to S.W., P.J., L.R. (SPUM) from the Swiss National Science Foundation (Grant 33CM30-124112).

**Conflict of interest:** Dr. S.W. has received consulting and lecture fees from Abbott, Boston Scientific, Biosensors, Cordis, and Medtronic.

## Appendix

### Addendum to the methodology and results

#### Optical coherence tomography and intravascular ultrasound image analysis

The lumen area (LA) was measured using the automatic area trace function. Stent struts were defined as signal-intense spots with dorsal shadowing and a marker was placed at the endoluminal leading edge of the strut, in the mid-point of its axis. The stent area (SA) was measured by connecting the strut markers with a trace line. Strut apposition was assessed for each strut by measuring the distance from the strut marker to the lumen contour semi-automatically using the thickness-ruler function.

For the LEADERS and RESOLUTE trials, lumen and stent area measurements, strut apposition, and strut coverage were assessed by corelab analysts (Cardialysis) blinded to stent type and clinical outcomes. The OCT analyses of the SIRTAX-LATE OCT substudy, the Copenhagen OCT registry, and the assessment of evaginations and protruding struts in all studies were performed by two observers. In case of disagreement, a referee was consulted to a final decision. The time-consuming assessment of evaginations in the LEADERS, RESOLUTE, and Copenhagen cohorts were performed un-blinded, as blinding would have implied a detailed assessment of evaginations using the cut-off of the thinnest stent (Xience, 90  $\mu\text{m}$  or Resolute, 100  $\mu\text{m}$ ), and thus the assessment of a large number of bulges in the thicker stents which would, following un-blinding, not fulfil the definition of evagination. Assessments of OCT cross-sections at

baseline and follow-up were performed independently, without knowledge of the characteristics of matched cross-sections. The same methodology was used throughout all four OCT studies.

Intravascular ultrasound analyses were performed by two observers, and in case of disagreement a referee was consulted to reach a final decision. Baseline IVUS assessment was performed independently of the follow-up evaluation, and without knowledge of the results of the OCT analysis.

#### Details of the Bayesian approach

The proportions of malapposed, protruding, and uncovered struts per lesion were analysed using a model with Bernoulli distribution, while the proportions of lesions with  $\geq 1$  and  $\geq 10\%$  malapposed, protruding, and uncovered struts were analysed using Bayesian hierarchical random-effects model with logit distribution. Estimates were derived from the median of the posterior distribution of the 50 001 to 150 000 iteration, with the initial 50 000 iterations discarded as 'burn-in'. We derived 95% credibility intervals (95% CrI) from the 2.5th and 97.5th percentiles of the posterior distribution, also calculating two-sided *P*-values from the posterior distribution. 95% CrI and *P*-values from posterior distributions can be interpreted similarly to conventional 95% confidence intervals and *P*-values.

#### Additional details on the evagination size

The average depths and lengths of cross-sectional and ME are presented in the appendix table 1 and 2.

**Appendix table 1** Specification of the volume, depth and number of cross-sections spanned for "any" cross-sectional evaginations, by stent type and time to FUP

	SES	PES	BES	ZES	EES	p
<b>At Year 1</b>						
Lesions with any evagination N	22	4		25	13	
EV	2.24 $\pm$ 1.68	0.50 $\pm$ 0.72		0.38 $\pm$ 1.79	0.42 $\pm$ 1.29	0.002
Max depth	0.36 $\pm$ 0.45	0.33 $\pm$ 0.19		0.23 $\pm$ 0.48	0.25 $\pm$ 0.34	0.005
N CS/lesion*	4.02 (2.90–6.68)	2.56 (2.09–3.67)		3.01 (2.34–4.16)	2.26 (1.94–2.88)	0.46
<b>At Year 2</b>						
Lesions with any evagination N	16		15			
EV	2.47 $\pm$ 2.52		0.57 $\pm$ 2.44			0.03
Max depth	0.32 $\pm$ 0.63		0.26 $\pm$ 0.61			0.15
N CS/lesion*	4.41 (3.57–10.96)		2.32 (1.74–8.49)			0.13
<b>At Year 5</b>						
Lesions with any evagination N	29	28				
EV	2.54 $\pm$ 1.58	0.72 $\pm$ 1.55				<0.001
Max depth	0.36 $\pm$ 0.80	0.30 $\pm$ 0.56				0.13
N CS/lesion*	4.44 (3.99–5.92)	2.25 (1.96–2.73)				<0.001

N CS/lesions refers to the number of CSs per lesion with any evagination. Values are presented as means  $\pm$  SD unless otherwise specified. EV, evagination volume; CS, cross-section.

\*Expressed as median (IQR). Volumes are expressed in  $\text{mm}^3$ , and depths in mm.

**Appendix table 2** Specification of the volume, depth and number of cross-sections spanned for major evaginations, by stent type and time to FUP

	SES	PES	BES	ZES	EES	p
<b>At Year 1</b>						
Lesions with ME N	8	1		1	1	
EV	24.20 ± 1.77	5.31 ± 0.59		4.42 ± 0.59	10.28 ± 0.59	0.39
Max depth	0.57 ± 0.50	0.58 ± 0.17		0.75 ± 0.17	0.69 ± 0.17	0.90
N CS/lesion*	9.00 (7.00–11.00)	6.00 (6.00–6.00)		13.00 (13.00–13.00)	11.00 (11.00–11.00)	0.39
<b>At Year 2</b>						
Lesions with ME N	4		4			
EV	30.40 ± 1.30		4.08 ± 1.19			0.01
Max depth	0.49 ± 0.59		0.43 ± 0.54			0.54
N CS/lesion*	19.00 (12.00–28.50)		7.50 (5.50–11.50)			0.02
<b>At Year 5</b>						
Lesions with ME N	11	3				
EV	11.80 ± 0.59	4.40 ± 0.25				0.009
Max depth	0.58 ± 0.55	0.40 ± 0.23				0.18
N CS/lesion*	7.00 (6.00–12.00)	4.00 (2.00–7.00)				0.06

N CS/lesions refers to the number of CSs per lesion with any evagination. Values are presented as means ± SD unless otherwise specified.

ME, major evagination; CS, cross-section.

\*Expressed as median (IQR). Volumes are expressed in mm<sup>3</sup>, and depths in mm.

## References

- Joner M, Finn AV, Farb A, Mont EK, Kolodgie FD, Ladich E, Kutys R, Skorija K, Gold HK, Virmani R. Pathology of drug-eluting stents in humans: delayed healing and late thrombotic risk. *J Am Coll Cardiol* 2006;**48**:193–202.
- Finn AV, Joner M, Nakazawa G, Kolodgie F, Newell J, John MC, Gold HK, Virmani R. Pathological correlates of late drug-eluting stent thrombosis: strut coverage as a marker of endothelialization. *Circulation* 2007;**115**:2435–2441.
- Tearney GJ, Regar E, Akasaka T, Adriaenssens T, Barlis P, Bezerra HG, Bouma B, Bruining N, Cho JM, Chowdhary S, Costa MA, de Silva R, Dijkstra J, Di Mario C, Dudeck D, Falk E, Feldman MD, Fitzgerald P, Garcia H, Gonzalo N, Granada JF, Guagliumi G, Holm NR, Honda Y, Ikano F, Kawasaki M, Kochman J, Koltowski L, Kubo T, Kume T, Kyono H, Lam CC, Lamouche G, Lee DP, Leon MB, Maehara A, Manfrin O, Mintz GS, Mizuno K, Morel MA, Nadkarni S, Okura H, Otake H, Pietrasik A, Prati F, Raber L, Radu MD, Rieber J, Riga M, Rollins A, Rosenberg M, Sirbu V, Serruys PW, Shimada K, Shinkle T, Shite J, Siegel E, Sonada S, Suter M, Takarada S, Tanaka A, Terashima M, Troels T, Uemura S, Ughi GJ, van Beusekom HM, van der Steen AF, van Es GA, van Soest G, Virmani R, Waxman S, Weisman NJ, Weisz G. Consensus standards for acquisition, measurement, and reporting of intravascular optical coherence tomography studies: a report from the international working group for intravascular optical coherence tomography standardization and validation. *J Am Coll Cardiol* 2012;**59**:1058–1072.
- Nakano M, Vorpahl M, Otsuka F, Taniwaki M, Yazdani SK, Finn AV, Ladich ER, Kolodgie FD, Virmani R. Ex vivo assessment of vascular response to coronary stents by optical frequency domain imaging. *JACC Cardiovasc Imaging* 2012;**5**:71–82.
- Radu M, Jorgensen E, Kelbaek H, Helqvist S, Skovgaard L, Saunamaki K. Optical coherence tomography at follow-up after percutaneous coronary intervention: relationship between procedural dissections, stent strut malapposition and stent healing. *EuroIntervention* 2011;**7**:353–361.
- Raber L, Baumgartner S, Garcia-Garcia H, Kalesan B, Justiz P, Pilgrim T, Moschovitis A, Meier B, Serruys P, Juni P, Windecker S. Vascular healing response five years after implantation of first-generation DES. The SIRTAX-LATE optical coherence tomography study. *JACC Cardiovasc Interv*. 2012;**5**:946–57.
- Alfonso F, Perez-Vicayno MJ, Ruiz M, Suarez A, Cazares M, Hernandez R, Escaned J, Banuelos C, Jimenez-Quevedo P, Macaya C. Coronary aneurysms after drug-eluting stent implantation: clinical, angiographic, and intravascular ultrasound findings. *J Am Coll Cardiol* 2009;**53**:2053–2060.
- Imai M, Kadota K, Goto T, Fujii S, Yamamoto H, Fuku Y, Hosogi S, Hirono A, Tanaka H, Tada T, Morimoto T, Shiomi H, Kozuma K, Inoue K, Suzuki N, Kimura T, Mitsudo K. Incidence, risk factors, and clinical sequelae of angiographic peri-stent contrast staining after sirolimus-eluting stent implantation. *Circulation* 2011;**123**:2382–2391.
- Barlis P, Regar E, Serruys PW, Dimopoulos K, van der Giessen WJ, van Geuns RJ, Ferrante G, Wandel S, Windecker S, van Es GA, Eerdmans P, Juni P, di Mario C. An optical coherence tomography study of a biodegradable vs. durable polymer-coated limus-eluting stent: a LEADERS trial sub-study. *Eur Heart J* 2010;**31**:165–176.
- Gutierrez-Chico JL, van Geuns RJ, Regar E, van der Giessen WJ, Kelbaek H, Saunamaki K, Escaned J, Gonzalo N, di Mario C, Borgia F, Nuesch E, Garcia-Garcia HM, Silber S, Windecker S, Serruys PW. Tissue coverage of a hydrophilic polymer-coated zotarolimus-eluting stent vs. a fluoropolymer-coated everolimus-eluting stent at 13-month follow-up: an optical coherence tomography substudy from the RESOLUTE All Comers trial. *Eur Heart J* 2011;**32**:2454–2463.
- Prati F, Cera M, Ramazzotti V, Imola F, Giudice R, Albertucci M. Safety and feasibility of a new non-occlusive technique for facilitated intracoronary optical coherence tomography (OCT) acquisition in various clinical and anatomical scenarios. *EuroIntervention* 2007;**3**:365–370.
- Gonzalo N, Garcia-Garcia HM, Serruys PW, Commissaris KH, Bezerra H, Gobbens P, Costa M, Regar E. Reproducibility of quantitative optical coherence tomography for stent analysis. *EuroIntervention* 2009;**5**:224–232.
- Barlis P, Tanigawa J, Di Mario C. Coronary bioabsorbable magnesium stent: 15-month intravascular ultrasound and optical coherence tomography findings. *Eur Heart J* 2007;**28**:2319.
- Gonzalo N, Serruys PW, Okamura T, Shen ZJ, Onuma Y, Garcia-Garcia HM, Sarno G, Schultz C, van Geuns RJ, Ligthart J, Regar E. Optical coherence tomography assessment of the acute effects of stent implantation on the vessel wall: a systematic quantitative approach. *Heart* 2009;**95**:1913–1919.
- Mintz GS, Nissen SE, Anderson WD, Bailey SR, Erbel R, Fitzgerald PJ, Pinto FJ, Rosenfield K, Siegel RJ, Tuzck EM, Yock PG. American College of Cardiology Clinical Expert Consensus Document on Standards for Acquisition, Measurement and Reporting of Intravascular Ultrasound Studies (IVUS). A report of the American College of Cardiology Task Force on Clinical Expert Consensus Documents. *J Am Coll Cardiol* 2001;**37**:1478–1492.
- Spiegelhalter DJ, Myles JP. *Bayesian Approaches to Clinical Trials and Health Care Evaluation*. Chichester: John Wiley & Sons; 2004.
- Cook S, Wenaweser P, Togni M, Billinger M, Morger C, Seiler C, Vogel R, Hess O, Meier B, Windecker S. Incomplete stent apposition and very late stent thrombosis after drug-eluting stent implantation. *Circulation* 2007;**115**:2426–2434.
- Mintz GS, Shah VM, Weissman NJ. Regional remodeling as the cause of late stent malapposition. *Circulation* 2003;**107**:2660–2663.
- Hassan AK, Berghhean SC, Stijnen T, van der Hoeven BL, Snoep JD, Plevier JW, Schallj MJ, WouterJukema J. Late stent malapposition risk is higher after drug-eluting stent compared with bare-metal stent implantation and associates with late stent thrombosis. *Eur Heart J* 2009;**31**:1172–1180.

20. Wilson GJ, Nakazawa G, Schwartz RS, Huijbregtse B, Poff B, Herbst TJ, Bain DS, Virmani R. Comparison of inflammatory response after implantation of sirolimus- and paclitaxel-eluting stents in porcine coronary arteries. *Circulation* 2009;**120**: 141–149. 141–142.
21. Nakazawa G, Finn AV, Vorpahl M, Ladich ER, Kolodgie FD, Virmani R. Coronary responses and differential mechanisms of late stent thrombosis attributed to first-generation sirolimus- and paclitaxel-eluting stents. *J Am Coll Cardiol* 2011;**57**: 390–398.
22. Otsuka F, Nakano M, Vorpahl M, Yazdani SK, Ladich E, Kolodgie F, Finn AV, Virmani R. Pathology of second- versus first-generation drug-eluting stents in humans: does safety issue still exist?. *Eur Heart J* 2011;**32**(Abstract supplement):82.
23. John MC, Wessely R, Kastrati A, Schomig A, Joner M, Uchihashi M, Crimins J, Lajoie S, Kolodgie FD, Gold HK, Virmani R, Finn AV. Differential healing responses in polymer- and nonpolymer-based sirolimus-eluting stents. *JACC Cardiovasc Interv* 2008;**1**:535–544.
24. Virmani R, Guagliumi G, Farb A, Musumeci G, Grieco N, Motta T, Mihalscik L, Tespili M, Valsecchi O, Kolodgie FD. Localized hypersensitivity and late coronary thrombosis secondary to a sirolimus-eluting stent: should we be cautious?. *Circulation* 2004;**109**:701–705.
25. Cook S, Ladich E, Nakazawa G, Eshtehardi P, Neidhart M, Vogel R, Togni M, Wenaweser P, Billinger M, Seiler C, Gay S, Meier B, Pichler WJ, Juni P, Virmani R, Windecker S. Correlation of intravascular ultrasound findings with histopathological analysis of thrombus aspirates in patients with very late drug-eluting stent thrombosis. *Circulation* 2009;**120**:391–399.
26. Dahl OE, Westvik AB, Kierulf P, Lyberg T. Effect of monomethylmethacrylate on procoagulant activities of human monocytes and umbilical vein endothelial cells *in vitro*. *Thromb Res* 1994;**74**:377–387.
27. Risse PA, Jo T, Suarez F, Hirota N, Tolloczko B, Ferraro P, Grutter P, Martin JG. Interleukin-13 inhibits proliferation and enhances contractility of human airway smooth muscle cells without change in contractile phenotype. *Am J Physiol Lung Cell Mol Physiol* 2011;**300**:L958–L966.
28. Lanone S, Zheng T, Zhu Z, Liu W, Lee CG, Ma B, Chen Q, Homer RJ, Wang J, Rabach LA, Rabach ME, Shipley JM, Shapiro SD, Senior RM, Elias JA. Overlapping and enzyme-specific contributions of matrix metalloproteinases-9 and -12 in IL-13-induced inflammation and remodeling. *J Clin Invest* 2002;**110**:463–474.
29. Curcuj JA, Liao S, Huffman MD, Shapiro SD, Thompson RW. Expression and localization of macrophage elastase (matrix metalloproteinase-12) in abdominal aortic aneurysms. *J Clin Invest* 1998;**102**:1900–1910.
30. Bell MR, Garratt KN, Bresnahan JF, Edwards WD, Holmes DR Jr. Relation of deep arterial resection and coronary artery aneurysms after directional coronary atherectomy. *J Am Coll Cardiol* 1992;**20**:1474–1481.
31. Slota PA, Fischman DL, Savage MP, Rake R, Goldberg S. Frequency and outcome of development of coronary artery aneurysm after intracoronary stent placement and angioplasty. STRESS Trial Investigators. *Am J Cardiol* 1997;**79**:1104–1106.
32. Guagliumi G, Sirbu V, Musumeci G, Gerber R, Biondi-Zoccai G, Ikejima H, Ladich E, Lortkipanidze N, Matiasvili A, Valsecchi O, Virmani R, Stone GW. Examination of the *in vivo* mechanisms of late drug-eluting stent thrombosis: findings from optical coherence tomography and intravascular ultrasound imaging. *JACC Cardiovasc Interv* 2012;**5**:12–20.
33. Räber L, Magro M, Stefanini GG, Kalesan B, van Domburg RT, Onuma Y, Wenaweser P, Daemen J, Meier B, Juni P, Serruys PW, Windecker S. Very late coronary stent thrombosis of a newer-generation everolimus-eluting stent compared with early-generation drug-eluting stents: a prospective cohort study. *Circulation* 2012;**125**:1110–1121.
34. Palmerini T, Biondi-Zoccai G, Della Riva D, Stettler C, Sangiorgi D, D'Ascenzo F, Kimura T, Briguori C, Sabate M, Kim HS, De Waha A, Kedhi E, Smits PC, Kaiser C, Sardella G, Marullo A, Kirtane AJ, Leon MB, Stone GW. Stent thrombosis with drug-eluting and bare-metal stents: evidence from a comprehensive network meta-analysis. *Lancet* 2012;**379**:1393–1402.

## 2.6 MSCT assessment of coronary plaque evolution after the BVS implantation

Impact of everolimus-eluting bioresorbable scaffold in coronary atherosclerosis

(Submitted)

[Original research paper]

Campos CM, Garcia-Garcia HM, [Muramatsu T](#), de Araújo Gonçalves P, Onuma Y, Dudek D, Thuesen L, Webster M, Nieman K, Ormiston JA, Serruys PW.





## Impact of Everolimus-Eluting Bioresorbable Scaffold in Coronary Atherosclerosis

Carlos M. Campos<sup>1,2</sup>, MD; Hector M. Garcia-Garcia MD, MSc, PhD<sup>1\*</sup>; Takashi Muramatsu<sup>1,3</sup>, MD, PhD; Pedro De Araujo Gonçalves<sup>4</sup> MD, PhD; Yoshinobu Onuma<sup>1</sup>, MD, PhD; Dariusz Dudek<sup>5</sup>, MD; Leif Thuesen<sup>6</sup>, MD; Mark WI Webster, MBCHB<sup>7</sup>; Pieter Kitslaai MSc<sup>8,9</sup>; Susan Veldhof<sup>10</sup>; Johan H. C. Reiber, PhD<sup>8,9</sup>; Koen Nieman<sup>1,11</sup>, MD, PHD; John A. Ormiston<sup>7</sup>, MB CHB; Patrick W. Serruys<sup>1,12</sup>, MD, PhD

1. Department Cardiology, Erasmus University Medical Centre, Thoraxcenter, Rotterdam, The Netherlands
2. Heart Institute (InCor), University of São Paulo Medical School, Sao Paulo, Brazil
3. Department of Cardiology, Fujita Health University Hospital, Toyoake, Japan.
4. Hospital de Santa Cruz, Cardiology department, CHLO, Lisbon, Portugal; Hospital da Luz, Cardiovascular center, ESS, Lisbon, Portugal; CEDOC, Chronic Diseases Research Center, FCM-NOVA, Lisbon, Portugal
5. Jagiellonian University, Krakow, Poland
6. Department of Cardiology, Aarhus University Hospital, Skejby, Denmark
7. Auckland City Hospital, Auckland, New Zealand
8. Medis Medical Imaging Systems bv, Leiden, The Netherlands
9. Division of Image Processing, Department of Radiology, Leiden University Medical Center, Leiden, The Netherlands
10. Abbott, Vascular, Diegem, Belgium
11. Department of Radiology, Thoraxcenter, Erasmus Medical Center, Rotterdam, the Netherlands;
12. International Centre for Circulatory Health, NHLI, Imperial College London, London, United Kingdom

---

\*Address for correspondence

Hector M. Garcia-Garcia, MD, MSc, PhD: Thoraxcenter – Erasmus MC  
z120 Dr Molerwaterplein 40  
3015 GD Rotterdam  
The Netherlands  
Tel +31 10 20 62 828  
Fax +31 10 20 62 844  
hect2701@gmail.com

## **Introduction**

The clinical introduction of bioresorbable scaffolds (BRS) was enacted as the fourth revolution in interventional cardiology<sup>1</sup>. These devices have the unique ability to provide a temporary scaffold that is necessary to maintain the patency of the vessel after intervention, and then they gradually permit the restoration of vascular physiology and integrity(1, 2). Among the potential advantages of BRS, the atherosclerotic plaque reduction and late lumen enlargement in the treated regions (3-5) may represent a paradigm shift in the treatment of coronary artery disease (CAD).

Pharmacological therapy has shown that, depending on patient clinical profile, it is possible to promote plaque regression(6-8). Therefore, plaque regression in patients treated with BRS may be related not to the device itself but due to the effect of the pharmacological therapy in a vessel that is free from its internal cage.

The aim of the present study was to perform a within-patient comparison of the natural history of coronary atherosclerosis between segments treated with poly-l-lactide-acid (PLLA) everolimus-eluting bioresorbable scaffold (Absorb BVS first generation, Abbott Vascular, Santa Clara, California) and non-intervened segments in the Absorb Cohort A trial assessed by multislice computed tomography (MSCT).

## **Methods**

### **Study Population**

The design of the Absorb Cohort A trial has been previously described(9). In brief, it is a single-arm, prospective, open-label study, with safety and imaging endpoints. A total of 30 patients were enrolled at 4 participating sites between March and July 2006.

Patients were older than 18 years of age with a diagnosis of stable, unstable, or silent ischemia. All treated lesions (diameter stenosis >50%) were single, de novo in a native coronary artery of 3.0 mm in diameter, suitable for the 12- or 18-mm scaffold. Major exclusion criteria were patients presenting with an acute myocardial infarction (MI), unstable arrhythmias, or a left ventricular ejection fraction <30%, restenotic lesions, lesions located in the left main coronary artery, lesions involving a side branch >2 mm in diameter, and the presence of thrombus or another clinically significant stenosis in the target vessel. The ethics committees approved the protocol at the participating institutions, and the enrolled patients gave written informed consent before inclusion. Clinical endpoints were assessed at 30 days, 6 and 9 months, and 1, 2, 3, 4, and 5 years. Noninvasive MSCT imaging studies were done at 18-month and 5-year follow-up.

### **Study device**

The study device has been described elsewhere(9). Briefly, the polymeric device consists of a backbone of poly-L-lactide (PLLA) coated with poly-D,Llactide (PDLLA) that contains and controls the release of the antiproliferative drug everolimus. Absorb BVS first generation has a crossing profile of 1.4 mm in circumferential hoops of PLLA with struts 150 µm thick either directly joined or linked by straight bridges. Both ends of the scaffold have two adjacent radio-opaque metal markers. The doses of

everolimus on the Absorb BVS 1.0 are 98 µg for a 12 mm scaffold and 153 µg for the 18 mm scaffold.

### **MSCT angiography**

The CT scanners used were 64-slice CT (Brilliance 64, Philips, Best, the Netherlands; CVi, GE Healthcare, Milwaukee, Wisconsin), 256-slice CT (iCT, Philips), 320-slice CT (Aquilion One, Toshiba, Nasu, Japan), 64-slice dualsource CT (Definition, Siemens AG, Forchheim, Germany), and 128-slice dual-source CT (Definition Flash, Siemens). Standard acquisition techniques were used, which included beta-blockers in patients with a fast heart rate, tube settings depending on patient size (80 to 140 kV), and axial scan protocols for patients with lower heart rates to reduce radiation doses, all at the discretion of the individual sites. Images were reconstructed using thin slices (0.5 to 0.67 mm) and medium smooth reconstruction filters, including 1 or more phases of cardiac cycle depending on the scan protocol.

### **MSCT analysis**

The MSCT analysis followed a previously established methodology(10-13). All datasets were transferred to an offline workstation for analysis using a semi-automated plaque analysis software (QAngioCT Research Edition version 2.1, Medis medical imaging systems b.v., Leiden, the Netherlands). The assessment of the inner lumen and outer vessel volumes was performed following a stepwise approach. First, a centreline originating from the ostium was automatically extracted. Straightened multiplanar reformatted images were generated, and the lumen and vessel borders were detected longitudinally in 4 different vessel views by the software. Cross-sectional images of these longitudinal contours were examined at 0.5-mm intervals and, if necessary, adjusted by an experienced observer. The settings for window level and width were fixed at 740 HU and 220 HU, respectively. Gradient magnitude images, which display

the degree of CT attenuation change, were used to facilitate the detection of lumen and vessel wall borders.

Only the major epicardial vessels were considered for analysis using the modified 17-segment American Heart Association model for coronary segment classification (proximal and mid segments of the right, left circumflex and left descending anterior coronary arteries) (14). The scaffolded regions were delimited by the presence of the radiopaque markers. In case of overlapping metallic stents (n=3), the scaffolded regions were assessed up to the regions without stent interference. The present study used as comparator for the scaffolded regions the intra-patient non-intervened native coronary vessels by assessing the first 2 proximal segments, divided in proximal or distal according to established anatomical references (Figure 1) (14).

### **MSCT study imaging endpoints**

Normalization for segment length provides equal weighting of each patient in the calculation of atheroma volume and also for varying segment length between the two scans (10, 15). The following IVUS-like parameters were calculated for the non-intervened and scaffolded segments after normalization:

Percent atheroma volume (PAV):  $[(\text{total vessel volume} - \text{total lumen volume}) / \text{total vessel volume}] * 100\%$

Normalized TAV (TAVnorm):  $[(\text{total vessel volume} - \text{total lumen volume}) / \text{segment length}] * \text{mean segment length in the population}$ .

Normalized Percentage change in TAV (% change in TAV):  $[(\text{TAVnorm at 5 years} - \text{TAVnorm at 18 months}) / \text{TAVnorm at 18 months}] * 100\% \times \text{mean segment length in the population}$

### **Statistical analysis**

Continuous variables are presented as mean $\pm$ SD and median (interquartile range [IQR]), as indicated. Categorical variables are presented as counts and percentages. Continuous variables between the 2 different time points were compared by the paired samples t test. A p value <0.05 was considered significant. Statistical analyses were performed with use of SPSS version 22.0 software (SPSS, Chicago, Illinois).

## Results

Patient demographic characteristics and a flow chart of the present study are shown in Table 1 and Figure 1, respectively. Of the 30 patients enrolled in the Absorb Cohort A trial, 18 underwent serial MSCT at 18-month and 5-year follow-up, and were included in the present analysis. The mean age was  $62 \pm 8$  years old, 67% were male, 6% had diabetes mellitus and 78% had stable angina pectoris. The most frequently treated vessel was the LAD (44%) and the mean lesion length at baseline was  $9.1 \pm 3.6$ mm.

All scaffolds (n=18) were assessable by MSCT at 18-month and 5-year follow-up.

Regarding the non-intervened segments, of 72 possible analysable segments, 1 segment at 18-months was excluded due to motion artefacts (Figure 1). The mean scaffold length was  $11.9 \pm 1.9$ mm and the mean length of the non-intervened segments was  $22.6 \pm 11.7$ mm.

**Matched Segment Serial Comparison.** Between 18-month and 5-year follow-up, scaffolded segments did not show a significant change in any analysed parameters, including mean plaque burden, total atheroma volume, total lumen volume and vessel volume (Table 1; Figure 2). Control segments had a significant temporal increase in atherosclerotic burden as determined by the mean plaque burden (increased in  $2.7 \pm 6.5\%$ ;  $P=0.03$ ) and total atheroma volume (increased in  $8.0 \pm 22.8$ mm<sup>3</sup>;  $P<0.01$ )(Table 1; Figure 2).

**Comparison of natural history of atherosclerosis in scaffolded vs. non-intervened segments.** The change in percent atheroma volume was significantly different between scaffolded regions and non-intervened segments. While in the scaffolded segments the mean plaque burden decreased by  $1.2 \pm 7.7\%$ , in the non-intervened segments it increased by  $2.7 \pm 6.5\%$  ( $P=0.03$ ) (Table 1; Figure 2). There was also a trend to difference in the change of normalized total atheroma volume ( $P=0.10$ ) and % change in

total atheroma volume ( $P=0.09$ ) in favour of scaffolded segments (Table 1, Figures 2 and 3). The change in the vessel volume was only slightly greater in the non-intervened segments ( $P=0.72$ ). Although the difference between groups was not significant, the bigger increase in plaque burden without proportional increase in vessel volume in the non-intervened segment resulted in an opposite change in the lumen volume; while there was a lumen gain (increase of  $3.7\pm 14.4\text{mm}^3$ ) in the scaffold segment, a lumen loss in non-intervened segments (decrease of  $3.4\pm 19.8\text{mm}^3$ ;  $P=0.16$ ) was observed (Table 1, Figure 2).

## Discussion

The main findings of the present study can be summarized as follows: (1) Segments treated with Absorb BVS 1.0 had a stabilization of the atherosclerotic process, without significant paired change in the vessel, lumen and plaque dimensions; (2) non-intervened coronary segments had a significant increase in the plaque volume and percent atheroma volume; (3) the comparison between scaffolded and non-intervened segments showed a significant benefit of the Absorb BVS scaffold in terms of plaque burden.

Coronary atherosclerosis has been challenging medical practice in terms of reversion of its chronic progressive inflammatory process and subsequent symptoms and events(6, 8, 10, 16, 17). As summarized in Table 3, therapeutic interventions may influence progression or regression of coronary artery disease. In addition, many individual factors may influence the coronary plaque modification such as waist circumference, serum CD40L, baseline diastolic blood pressure, gender and the aptitude in improving the lipid profile and C-reactive protein (7, 18-20). The present study, being a matched segment within-patient comparison, for the first time, assessed the long-term evolution of atherosclerosis in segments treated by a scaffold and non-intervened segments. It raises the hypothesis that local therapy with Absorb BVS could add benefit to atherosclerosis regression on top of pharmacological therapy. Importantly, the atherosclerosis progression observed in the non-intervened segments is not at variance with previous data that used the same methodology(10) (Table 3) and did not result in coronary events (4).

The plaque burden reduction in the Absorb BVS–implanted coronary segments has been documented previously (3, 5). The explanation for this finding may come from the ability of mTOR inhibitors to hinder atherosclerotic plaque formation. Rapamycin and

rapalogs are potent inhibitors of vascular smooth muscle cell (SMC) proliferation. mTOR inhibitors have anti-macrophage properties through different mechanisms such as inhibition of monocyte chemoattractant protein-1 (MCP-1) upregulation, impaired recruitment of monocytes to the vessel and downregulation of de novo protein synthesis(21). mTORC inhibition also prevents lipid accumulation in the plaque due to stimulation of cholesterol efflux and downregulation of low-density lipoprotein (LDL) and scavenger receptors(21). It has been hypothesized that everolimus may produce a local autophagic response resulting in degradation and/or efflux of lipids via lipophagy and the loss of macrophages in the plaque (22). Indeed, also in animal studies, systemic administration of rapamycin or everolimus has shown to promote 7-85% plaque reduction(21, 23, 24). However, this process is not fully understood since the Absorb BVS elutes 80% of everolimus within 30 days and the plaque regression in patients treated with Absorb BVS occurs only after 2 years(3, 5).

In addition to the plaque burden reduction, it has been hypothesized that Absorb BVS may seal the thin-cap fibroatheromas (TCFA), which are lipid core plaques covered by a thin fibrous cap (<65  $\mu\text{m}$ ) (25). An optical coherence tomography study has shown that 1-year after Absorb BVS implantation there is formation of symmetric neo-tissue with a mean thickness of 220  $\mu\text{m}$ (25). As the device is completely degraded, this may therefore favour the use of a bioresorbable device for the treatment of TCFA.

Furthermore, pre-clinical studies have demonstrated that the main component of the neointima following Absorb BVS implantation is fibrous tissue, whereas fibrin and granulomatous cells are infrequent at long-term follow-up(26).

Finally, the present manuscript documents the longest non-invasive assessment after Absorb BVS implantation and demonstrates the feasibility of MSCT on following

patients with bioresorbable polymeric devices and quantifying the atherosclerotic burden in all coronary tree.

### **Limitations**

The present study assessed patients in a first-in-humans trial including patients with low clinical and anatomical complexity. Our results should be considered as hypothesis generating given the small sample size herewith described, not permitting a definitive statement that Absorb BVS should be used as a standard therapy for plaque regression. The ongoing Multicentre Prospective Natural History Study Using Multimodality Imaging in Patients With Acute Coronary Syndromes (PROSPECT II trial, ClinicalTrials.gov Identifier: NCT02171065) will examine whether the treatment of lesions with plaque burden  $\geq 70\%$  with the Absorb BVS plus optimal medical therapy safely increases the minimal lumen diameter at 2 years compared with optimal medical treatment alone and may add further evidence in this regard.

**Role of funding source.** The Absorb Cohort A trial was sponsored by Abbott Vascular (Santa Clara, California).

**Conflicts of interest:** Susan Veldhof is full-time employee of Abbott Vascular, Diegem, Belgium. The others authors have no conflict of interest and did not receive grants or financial support from industry or from any other source to prepare this manuscript.

### **References**

1. Serruys PW, Garcia-Garcia HM, Onuma Y. From metallic cages to transient bioresorbable scaffolds: change in paradigm of coronary revascularization in the upcoming decade? *European heart journal*. 2012;33(1):16-25b.
2. Waksman R. Biodegradable stents: they do their job and disappear. *J Invasive Cardiol*. 2006;18(2):70-4.
3. Serruys PW, Onuma Y, Garcia-Garcia HM, Muramatsu T, van Geuns RJ, de Bruyne B, et al. Dynamics of vessel wall changes following the implantation of the Absorb everolimus-eluting bioresorbable vascular scaffold: a multi-imaging modality study at 6, 12, 24 and 36 months. *EuroIntervention : journal of EuroPCR in collaboration with the Working Group on Interventional Cardiology of the European Society of Cardiology*. 2013.
4. Onuma Y, Dudek D, Thuesen L, Webster M, Nieman K, Garcia-Garcia HM, et al. Five-year clinical and functional multislice computed tomography angiographic results after coronary implantation of the fully resorbable polymeric everolimus-eluting scaffold in patients with de novo coronary artery disease: the ABSORB cohort A trial. *JACC Cardiovasc Interv*. 2013;6(10):999-1009.
5. Garcia-Garcia HM, Serruys PW, Campos CM, Onuma Y. Differential impact of five coronary devices on plaque size: Insights from the ABSORB and SPIRIT trials. *Int J Cardiol*. 2014;175(3):441-5.
6. Nicholls SJ, Ballantyne CM, Barter PJ, Chapman MJ, Erbel RM, Libby P, et al. Effect of two intensive statin regimens on progression of coronary disease. *The New England journal of medicine*. 2011;365(22):2078-87.
7. Nicholls SJ, Tuzcu EM, Sipahi I, Grasso AW, Schoenhagen P, Hu T, et al. Statins, high-density lipoprotein cholesterol, and regression of coronary atherosclerosis. *JAMA : the journal of the American Medical Association*. 2007;297(5):499-508.
8. Nissen SE, Tuzcu EM, Schoenhagen P, Brown BG, Ganz P, Vogel RA, et al. Effect of intensive compared with moderate lipid-lowering therapy on progression of coronary atherosclerosis: a randomized controlled trial. *JAMA : the journal of the American Medical Association*. 2004;291(9):1071-80.
9. Ormiston JA, Serruys PW, Regar E, Dudek D, Thuesen L, Webster MW, et al. A bioabsorbable everolimus-eluting coronary stent system for patients with single de-novo coronary artery lesions (ABSORB): a prospective open-label trial. *Lancet*. 2008;371(9616):899-907.
10. Papadopoulou SL, Neefjes LA, Garcia-Garcia HM, Flu WJ, Rossi A, Dharampal AS, et al. Natural history of coronary atherosclerosis by multislice computed tomography. *JACC Cardiovasc Imaging*. 2012;5(3 Suppl):S28-37.
11. Boogers MJ, Broersen A, van Velzen JE, de Graaf FR, El-Naggar HM, Kitslaar PH, et al. Automated quantification of coronary plaque with computed tomography: comparison with intravascular ultrasound using a dedicated registration algorithm for fusion-based quantification. *European heart journal*. 2012;33(8):1007-16.
12. de Graaf MA, Broersen A, Kitslaar PH, Roos CJ, Dijkstra J, Lelieveldt BP, et al. Automatic quantification and characterization of coronary atherosclerosis with computed tomography coronary angiography: cross-correlation with intravascular ultrasound virtual histology. *The international journal of cardiovascular imaging*. 2013;29(5):1177-90.
13. Garcia-Garcia H.M. SPW, Campos C.M., Muramatsu T., Nakatani S., Zhang YJ., Onuma Y., Stone G.W. Assessing Bioresorbable Coronary Devices: Methods and Parameters. *JACC Cardiovasc Imaging*. 2014;7(11):1130-48.
14. Austen WG, Edwards JE, Frye RL, Gensini GG, Gott VL, Griffith LS, et al. A reporting system on patients evaluated for coronary artery disease. Report of the Ad Hoc Committee for Grading of Coronary Artery Disease, Council on Cardiovascular Surgery, American Heart Association. *Circulation*. 1975;51(4 Suppl):5-40.
15. Mintz GS, Garcia-Garcia HM, Nicholls SJ, Weissman NJ, Bruining N, Crowe T, et al. Clinical expert consensus document on standards for acquisition, measurement and reporting

of intravascular ultrasound regression/progression studies. *EuroIntervention : journal of EuroPCR in collaboration with the Working Group on Interventional Cardiology of the European Society of Cardiology*. 2011;6(9):1123-30, 9.

16. Nissen SE, Nicholls SJ, Sipahi I, Libby P, Raichlen JS, Ballantyne CM, et al. Effect of very high-intensity statin therapy on regression of coronary atherosclerosis: the ASTEROID trial. *JAMA : the journal of the American Medical Association*. 2006;295(13):1556-65.

17. Raber L, Taniwaki M, Zaugg S, Kelbaek H, Roffi M, Holmvang L, et al. Effect of high-intensity statin therapy on atherosclerosis in non-infarct-related coronary arteries (IBIS-4): a serial intravascular ultrasonography study. *European heart journal*. 2014.

18. Garcia-Garcia HM, Klauss V, Gonzalo N, Garg S, Onuma Y, Hamm CW, et al. Relationship between cardiovascular risk factors and biomarkers with necrotic core and atheroma size: a serial intravascular ultrasound radiofrequency data analysis. *Int J Cardiovasc Imaging*. 2012;28(4):695-703.

19. Puri R, Nissen SE, Ballantyne CM, Barter PJ, Chapman MJ, Erbel R, et al. Factors underlying regression of coronary atheroma with potent statin therapy. *European heart journal*. 2013;34(24):1818-25.

20. Puri R, Nissen SE, Libby P, Shao M, Ballantyne CM, Barter PJ, et al. C-reactive protein, but not low-density lipoprotein cholesterol levels, associate with coronary atheroma regression and cardiovascular events after maximally intensive statin therapy. *Circulation*. 2013;128(22):2395-403.

21. Martinet W, De Loof H, De Meyer GR. mTOR inhibition: a promising strategy for stabilization of atherosclerotic plaques. *Atherosclerosis*. 2014;233(2):601-7.

22. Croons V, Martinet W, Herman AG, Timmermans JP, De Meyer GR. Selective clearance of macrophages in atherosclerotic plaques by the protein synthesis inhibitor cycloheximide. *The Journal of pharmacology and experimental therapeutics*. 2007;320(3):986-93.

23. Pakala R, Stabile E, Jang GJ, Clavijo L, Waksman R. Rapamycin attenuates atherosclerotic plaque progression in apolipoprotein E knockout mice: inhibitory effect on monocyte chemotaxis. *Journal of cardiovascular pharmacology*. 2005;46(4):481-6.

24. Mueller MA, Beutner F, Teupser D, Ceglarek U, Thiery J. Prevention of atherosclerosis by the mTOR inhibitor everolimus in LDLR<sup>-/-</sup> mice despite severe hypercholesterolemia. *Atherosclerosis*. 2008;198(1):39-48.

25. Brugaletta S, Radu MD, Garcia-Garcia HM, Heo JH, Farooq V, Girasis C, et al. Circumferential evaluation of the neointima by optical coherence tomography after ABSORB bioresorbable vascular scaffold implantation: can the scaffold cap the plaque? *Atherosclerosis*. 2012;221(1):106-12.

26. Onuma Y, Serruys PW, Perkins LE, Okamura T, Gonzalo N, Garcia-Garcia HM, et al. Intracoronary optical coherence tomography and histology at 1 month and 2, 3, and 4 years after implantation of everolimus-eluting bioresorbable vascular scaffolds in a porcine coronary artery model: an attempt to decipher the human optical coherence tomography images in the ABSORB trial. *Circulation*. 2010;122(22):2288-300.

### Figure Legends:

**Figure 1. Flowchart of the 5-Year Serial MSCT Study.** Scaffolded segments (left panel; represented in green) were matched at 18-month and 5-year follow-up for serial comparison. Non-intervened segments delimited by anatomical markers (right panel; represented in blue) were matched at 18-month and 5-year follow-up for serial comparison. One non-intervened segment had motion artifact at 18-months hindering the serial comparison and was excluded.

**Figure 2. MSCT IVUS like parameters.** Scaffold segments did not show significant temporal change in vessel, lumen and plaque volume parameters. The non-intervened segments had an increase in the plaque volume (C), representing a higher percentage of the vessel area (D).

**Figure 3. Percentage change in the atheroma volume in the scaffolded (green) and non-intervened vessels (blue).** Each dot represents one segment. The observed shift to the left in scaffolded regions correspond to a trend towards atherosclerosis regression compared to non-intervened vessels ( $P=0.09$ ).

**Figure 4. (A) Lumen and vessel areas of a scaffold implanted in left anterior descending coronary artery at 18 months (upper panel, left) and 5 years (upper panel, right).** There is an increase in the lumen volume and decrease in the plaque burden (lower panel). **(B) Lumen and vessel areas of the same patient but in the proximal right coronary artery at 18 months (upper panel, left) and 5 years (upper panel, right).** There is an increase in the plaque burden (lower panel) and vessel volume with a slight increase in the lumen volume (lower panel).

**Table 1. Baseline Clinical and Angiographic Characteristics**

	N=18
Age, years $\pm$ SD	62.1 $\pm$ 7.8
Male gender, n(%)	12 (67)
Current tobacco use, n(%)	2 (11)
Diabetes, n(%)	1 (6)
Hypertension, n(%)	11 (61)
Hypercholesterolemia, n(%)	13 (76)
Family history of coronary artery disease, n(%)	13 (72)
Stable angina	14 (78)
Unstable angina, n(%)	4 (22)
Prior MI, n(%)	2 (11)
Target vessel, n(%)	
RCA	4 (22)
LAD	8 (44)
LCX	6 (33)
Lesion length, mm $\pm$ SD	9.1 $\pm$ 3.6
ACC/AHA lesion classification, n(%)	
B1	9 (50)
B2	9 (50)

MI= myocardial infarction; RCA=right coronary artery; LAD=left anterior descending coronary artery; LCX= left circumflex coronary artery

**Table 2. MSCCT IVUS-Like Analysis Results**

	Scaffold (n=18)				Non-intervened (n=71)				Scaffold Vs. Non TV P value for changes
	18 months	5 years	Change	P value	18 months	5 years	Change	P value	
<b>Percent atheroma volume, %</b>									
Mean ±SD	49.3±10.5	48.1±8.7	-1.2±7.7	0.51	44.6±9.9	47.3±11.0	2.7±6.5	<0.01	0.03
<b>% change in total atheroma volume</b>									
Median (IQR)	0.6±22.0				11.9±25.6				0.09
<b>Normalized total atheroma volume, mm<sup>3</sup></b>									
Mean ±SD	94.2±34.6	92.6±32.2	-1.6±18.7	0.72	95.0±33.5	103.0±36.2	8.0±22.8	<0.01	0.10
<b>Normalized total lumen volume, mm<sup>3</sup></b>									
Mean ±SD	96.1±33.6	99.8±37.0	3.7±14.4	0.28	122.2±50.8	118.8±51.7	-3.4±19.83	0.16	0.16
<b>Normalized vessel volume, mm<sup>3</sup></b>									
Mean ±SD	190.3±54.9	192.4±57.5	2.1±16.4	0.59	217.2±69.7	221.8±67.6	4.6±29.0	0.18	0.72

**Table 3. Impact of therapy on atherosclerosis in recent natural progression/regression trials**

<b>Trial</b>	<b>Change in PAV,% Mean (95% CI)</b>	<b>% Change in TAV Mean (95% CI)</b>	<b>Follow-up</b>
SATURN(6)			26 months
Atorvastatin 80 mg	-0.99 (-1.19 to -0.63)	-	
Rosuvastatin 40mg	-1.22 (-1.52 to -0.90)	-	
PROSPECT (MSCT sub study)(10)	-0.07 (-1.43 to 1.57)	6.7 (1.0 to 12.43)	39 months
IBIS 4(17)			13 months
Rosuvastatin 40mg	-0.9 (-1.56 to -0.25)	-13.1 (-22.5 to -3.8)	
Present study			42 months
Scaffolded segments	-1.2 (-4.8 to 2.4)	0.65 (-9.54 to 10.84)	
Non-intervened segments segments	2.6 (1.16 to 4.2)	11.9 (5.99 to 17.91)	

PAV=percent atheroma volume; TAV=total atheroma volume

Figure 1.

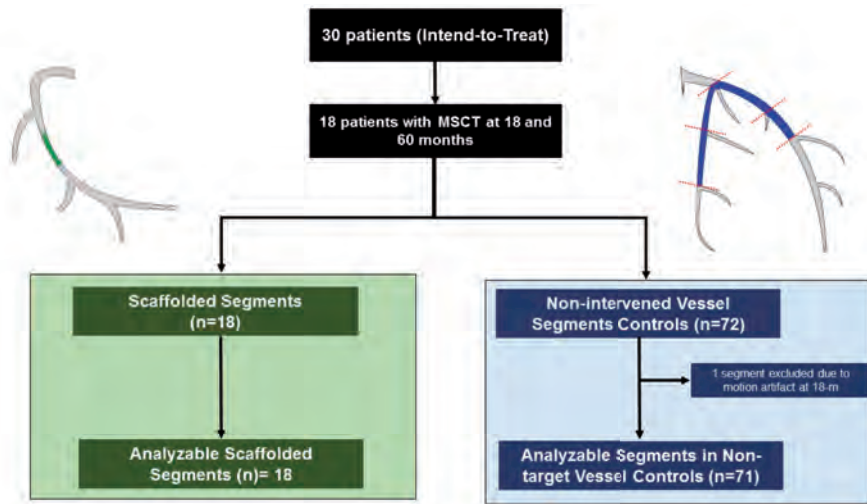


Figure 2.

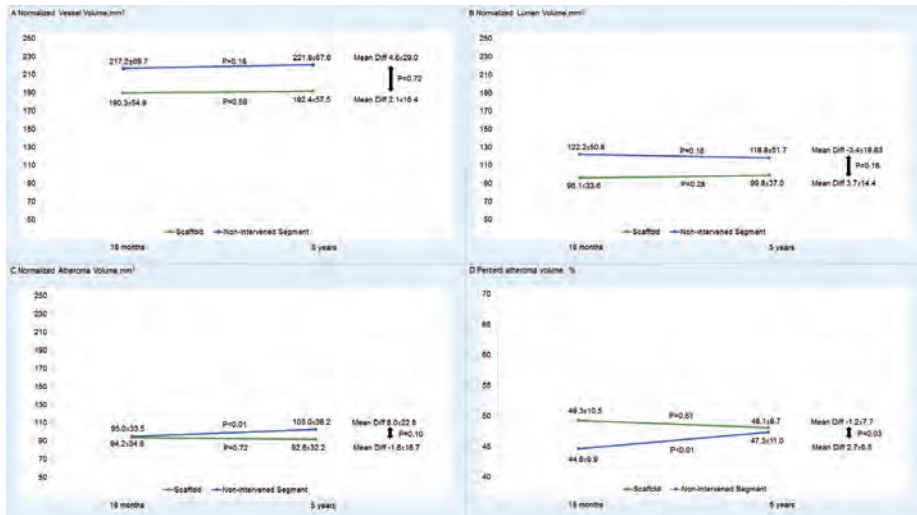


Figure 3.

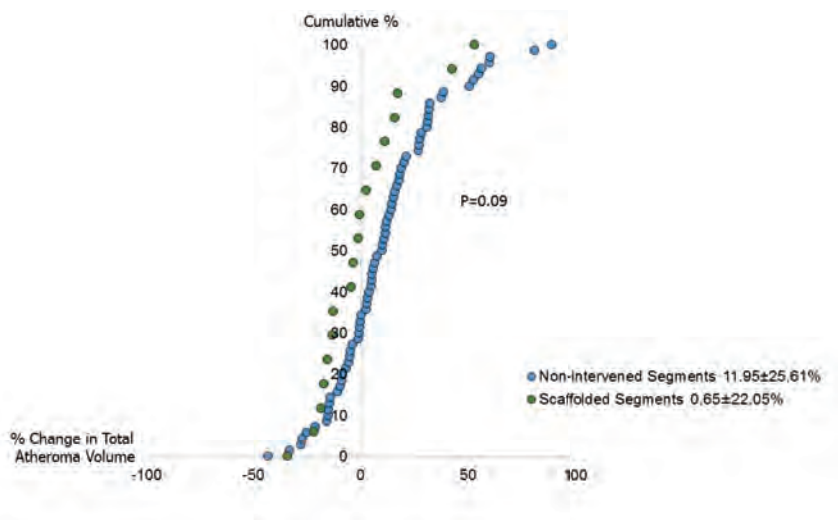
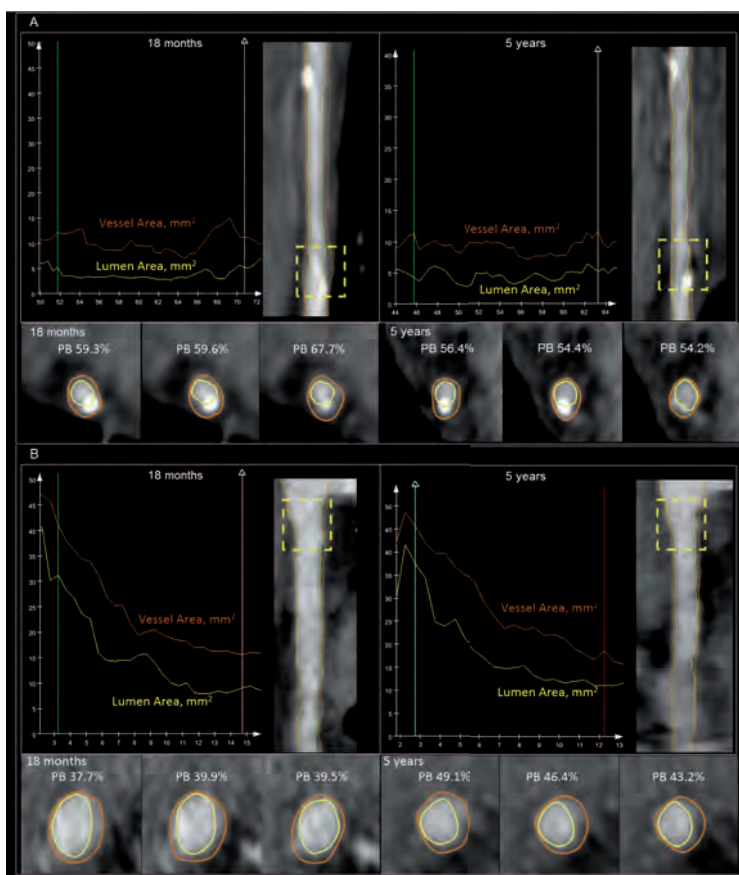


Figure 4.





## 2.7 Longitudinal follow-up of the Absorb BVS with multimodality imaging

Dynamics of vessel wall changes following the implantation of the Absorb everolimus-eluting bioresorbable vascular scaffold:  
A multi-imaging modality study at 6, 12, 24 and 36 months.

*Eurointervention.* 2014;9:1271-84.

[Original research paper, Impact Factor (2013): 3.758]

Serruys PW, Onuma Y, Garcia-Garcia HM, Muramatsu T, van Geuns RJ, de Bruyne B, Dudek D, Thuesen L, Smits PC, Chevalier B, McClean D, Koolen J, Windecker S, Whitbourn R, Meredith I, Dorange C, Veldhof S, Hebert KM, Rapoza R, Ormiston JA.





# Dynamics of vessel wall changes following the implantation of the Absorb everolimus-eluting bioresorbable vascular scaffold: a multi-imaging modality study at 6, 12, 24 and 36 months

Patrick W. Serruys<sup>1\*</sup>, MD, PhD; Yoshinobu Onuma<sup>1</sup>, MD; Hector M. Garcia-Garcia<sup>1,15</sup>, MD, PhD; Takashi Muramatsu<sup>1</sup>, MD, PhD; Robert-Jan van Geuns<sup>1</sup>, MD, PhD; Bernard de Bruyne<sup>2</sup>, MD, PhD; Dariusz Dudek<sup>3</sup>, MD; Leif Thuesen<sup>4</sup>, MD; Pieter C. Smits<sup>5</sup>, MD, PhD; Bernard Chevalier<sup>6</sup>, MD; Dougal McClean<sup>7</sup>, MD; Jacques Koolen<sup>8</sup>, MD, PhD; Stephan Windecker<sup>9</sup>, MD; Robert Whitbourn<sup>10</sup>, MD; Ian Meredith<sup>11</sup>, MD, PhD; Cecile Dorange<sup>12</sup>, MSc; Susan Veldhof<sup>12</sup>, RN; Karine Miquel Hebert<sup>12</sup>, PhD; Richard Rapoza<sup>13</sup>, PhD; John A. Ormiston<sup>14</sup>, MBChB, PhD

1. Thoraxcenter, Erasmus Medical Center, Rotterdam, The Netherlands; 2. Cardiovascular Center, Aalst, Belgium; 3. Jagiellonian University, Krakow, Poland; 4. Skejby Sygehus University Hospital, Aarhus, Denmark; 5. Maasstad Hospital, Rotterdam, The Netherlands; 6. Institut Jacques Cartier, Massy, France; 7. Christchurch Hospital, Christchurch, New Zealand; 8. Catharina Hospital, Eindhoven, The Netherlands; 9. Bern University Hospital, Bern, Switzerland; 10. St Vincent's Hospital, Fitzroy, Australia; 11. Monash Cardiovascular Research Centre, Melbourne, Australia; 12. Abbott Vascular, Diegem, Belgium; 13. Abbott Vascular, Santa Clara, CA, USA; 14. Auckland City Hospital, Auckland, New Zealand; 15. Cardialysis, Rotterdam, The Netherlands

P.W. Serruys and J.A. Ormiston are principal and co-principal investigators. P.W. Serruys and Y. Onuma had full access to the data, and co-wrote the manuscript.

GUEST EDITOR: William Wijns, MD, PhD, Onze-Lieve-Vrouweziekenhuis Aalst, OLV Hospital, Aalst, Belgium

This paper also includes accompanying supplementary data published online at: [http://www.pcronline.com/eurointervention/70th\\_issue/217](http://www.pcronline.com/eurointervention/70th_issue/217)

## KEYWORDS

- bioresorbable scaffold
- coronary artery disease
- coronary intervention

## Abstract

**Aims:** To assess observations with multimodality imaging of the Absorb bioresorbable everolimus-eluting vascular scaffold performed in two consecutive cohorts of patients who were serially investigated either at 6 and 24 months or at 12 and 36 months.

**Methods and results:** In the ABSORB multicentre single-arm trial, 45 patients (cohort B1) and 56 patients (cohort B2) underwent serial invasive imaging, specifically quantitative coronary angiography (QCA), intravascular ultrasound (IVUS), radiofrequency backscattering (IVUS-VH) and optical coherence tomography (OCT). Between one and three years, late luminal loss remained unchanged (6 months: 0.19 mm, 1 year: 0.27 mm, 2 years: 0.27 mm, 3 years: 0.29 mm) and the in-segment angiographic restenosis rate for the entire cohort B (n=101) at three years was 6%. On IVUS, mean lumen, scaffold, plaque and vessel area showed enlargement up to two years. Mean lumen and scaffold area remained stable between two and three years whereas significant reduction in plaque behind the struts occurred with a trend toward adaptive restrictive remodelling of EEM. Hyperechogenicity of the vessel wall, a surrogate of the bioresorption process, decreased from 23.1% to 10.4% with a reduction of radiofrequency backscattering for dense calcium and necrotic core. At three years, the count of strut cores detected on OCT increased significantly, probably reflecting the dismantling of the scaffold; 98% of struts were covered. In the entire cohort B (n=101), the three-year major adverse cardiac event rate was 10.0% without any scaffold thrombosis.

**Conclusions:** The current investigation demonstrated the dynamics of vessel wall changes after implantation of a bioresorbable scaffold, resulting at three years in stable luminal dimensions, a low restenosis rate and a low clinical major adverse cardiac events rate. Clinical Trial Registration Information: <http://www.clinicaltrials.gov/ct2/show/NCT00856856>

\*Corresponding author: Thoraxcenter, Ba-583, 's Gravendijkwal 230, 3015 CE Rotterdam, The Netherlands.  
E-mail: [p.w.j.c.serruys@erasmusmc.nl](mailto:p.w.j.c.serruys@erasmusmc.nl)

© Europa Digital & Publishing 2014. All rights reserved.

## Introduction

Bioresorbable scaffolds have to face multiple challenges which justify the careful evaluation of this novel technology. First of all, the polymeric scaffolds have to match the mechanical properties of metallic stents. It has been demonstrated that the acute recoil of a novel scaffold was not inferior to the one observed with an equivalent device in metal<sup>1,2</sup>. Secondly, it has been established in human testing that the mechanical integrity and the absence of recoil were maintained over a period of six months<sup>3</sup>. During that time lapse, the biological process of restenosis, consisting of neointimal formation and constrictive remodelling, is known to subside and therefore does not justify the implantation of a permanent metallic prosthesis<sup>4</sup>. In the following months, it has been shown that physiological and pharmacological vasomotion reappears, confirming the fact that the scaffold loses its mechanical stiffness as the amorphous tie chains between crystal lamellae of polylactide are hydrolysed (Figure 1)<sup>5</sup>. Afterwards, the polymer is progressively replaced by a malleable provisional matrix of proteoglycan<sup>6</sup>. Despite its malleable and deformable structure the scaffold does not undergo any reduction in area<sup>7</sup>. Following the coverage of struts and loss of mechanical support, it is assumed that the vessel can respond to pharmacological agents that reduce the plaque burden behind the struts without creating any malapposition, since the malleable and dismantling scaffold will follow the adaptive Glagovian remodelling of the vessel wall.

Optical coherence tomography (OCT) has provided the investigators with an extraordinary imaging tool capable of scrutinising micro-discontinuity of struts<sup>3</sup>, but this optical technique cannot differentiate the polylactide from proteoglycan which is one of the first structural changes to occur in vascular repair<sup>8</sup>. However, the technique can precisely quantify, in microns, the thickness of the tissue layers that isolate the superficial plaque from the lumen<sup>9</sup>. In contrast, ultrasonic interrogation of the polymeric strut can monitor the bioresorption process<sup>9,10</sup>. Palpography, using radiofrequency backscattering, has been able to analyse the subtle changes in vascular strain and can detect the return of the physiological cyclic strain<sup>11,12</sup>.

Rarely has a novel revascularisation technique been so intensively scrutinised during the early days of its development – the sequential assessment over three years provides new observations but potentially also raises new questions. The ultimate expectation of this novel technology is the occurrence of late lumen enlargement, associated with wall thinning and adaptive remodelling<sup>13</sup>.

The Absorb BVS device (Abbott Vascular, Santa Clara, CA, USA) was tested in 101 patients of the ABSORB Cohort B Trial which was subdivided into two groups of patients: the first group (B1) underwent invasive imaging with QCA, IVUS greyscale, IVUS-VH and OCT at six and 24 months, whereas the second group (B2) reported in detail in the current manuscript underwent invasive imaging at 12 months and at 36 months. The purpose of the present report is to describe the multimodality imaging performed post-procedure, at 6, 12, 24 and 36 months and to report the clinical follow-up at 36 months of the entire cohort of patients. (NCT00856856)

## STUDY POPULATION

The study population, study device, study procedure and definitions have been previously described<sup>3,7,9</sup>. Angiographic assessment, vasomotion test, IVUS greyscale analysis and IVUS-based radiofrequency backscattering were analysed in an independent core lab. The study was sponsored by Abbott Vascular (Santa Clara, CA, USA).

## STUDY DEVICE

The Absorb BVS consists of a polymer backbone of Poly (L-lactide) (PLLA) coated with a thin layer of a 1:1 mixture of Poly-D, L-lactide (PDLLA) polymer, and the antiproliferative drug everolimus to form an amorphous drug-eluting coating matrix containing 100 micrograms of everolimus/cm<sup>2</sup> of scaffold<sup>3,14</sup>. To enhance the mechanical strength of the struts and to reduce acute and late recoil, the strut design and the manufacturing process of the polymer were modified from the first version of the device. The new design has in-phase zigzag hoops linked by bridges that allow a more uniform strut distribution, reduce maximum circular unsupported surface area and provide more uniform vessel wall support and drug transfer. Additionally, a modified manufacturing process eliminated impurities such as monomer, oligomer and solvents, which resulted in a slower hydrolysis (*in vivo* degradation) rate of the polymer, thus preserving its mechanical integrity for a longer period of time. The actual duration of resorption of the second generation is *in vivo* approximately 18 months longer than the first generation, and the mass loss of the second-generation Absorb scaffold takes approximately 36 months.

## ANGIOGRAPHIC ASSESSMENT

In each patient, the scaffolded segment and the peri-scaffold segments (defined by a length of 5 mm, proximal and distal to the scaffold edge) were analysed by quantitative coronary angiography (QCA) post-procedure and at follow-up, using an interpolated method for the reference vessel diameter (RVD)<sup>3,7,9</sup>.

## VASOMOTION TEST

Changes in vasomotion (mean lumen diameter) prior to, and post-nitrate were assessed in paired matched angiographic view(s) in the scaffolded segment and in the 5 mm proximal and 5 mm distal adjacent segments<sup>3,7,9</sup>.

## IVUS GREYSCALE ANALYSIS

Treated vessels post-procedure and at follow-up were examined with phased array intravascular ultrasound catheters (EagleEye™; Volcano Corporation, Rancho Cordova, CA, USA) using a pullback speed of 0.5 mm per second. The region of interest, beginning 5 mm distal to, and extending 5 mm proximal to the treated segment, was examined<sup>15</sup>. There are three contours that can be delineated by IVUS: the endoluminal contour (lumen area), the leading edge of the struts (scaffold area), and the EEM area (vessel area). There are thus four compartments that can be quantified in IVUS: the luminal area, the neointimal area between the lumen and the scaffold contours (=scaffold area – lumen area), the plaque behind the area of the struts

(=vessel area–scaffold area) and the vessel area. Incomplete apposition was defined as one or more scaffold struts separated from the vessel wall, while acquired late incomplete apposition was defined as incomplete apposition at follow-up that was not present post-procedure<sup>15</sup>. For echogenicity assessment of polymeric struts at baseline and follow-up, a computer-aided greyscale value analysis programme for strut characterisation was used<sup>16,17</sup>.

### IVUS RADIOFREQUENCY ANALYSIS

Backscattering of radiofrequency signals provides information on vessel wall tissue composition (IVUS-VH)<sup>18,21</sup>. Four tissue components (necrotic core [NC] - red; dense calcium [DC] - white; fibrous [F] - green; and fibro-fatty [FF] - light green) were identified with autoregressive classification systems, and expressed as percentages (per cross-section, NC+DC+FF+F=100%)<sup>18,19</sup>. The change in quantitative analyses of these areas between implantation and follow-up was used as a surrogate assessment of the chemical and structural alteration of the polymeric struts<sup>3,7,9</sup>.

### OCT

As an optional investigation, intravascular OCT imaging using either a time-domain OCT (M3 system; LightLab Imaging [LLI], Westford, MA, USA) or a frequency-domain OCT (C7XR system; LLI) was performed at baseline and at follow-up<sup>14,22–26</sup>. None of the OCT acquisition was performed with an occlusion technique. The OCT measurements were performed either at 1 mm longitudinal intervals or at 200 micron intervals (strut core analysis) within the treated segment, using proprietary software for offline analysis (LLI). Details of the analysis method have been previously described<sup>3,27–29</sup>.

The thickness of the coverage was measured between the endoluminal side of the strut core and the boundary of the lumen, drawing the line of measurement from the mid part of the endoluminal edge of the black core of the struts toward the centre of gravity of the lumen in the analysed cross-section<sup>30</sup>. The threshold for the coverage is 30 microns, which corresponds to the average inter-observer measurement (300 struts analysed two times, 35±6 µm) of the endoluminal light backscattering frame of the strut. At three years, the appearance of the struts can be detected as a black core which sometimes displays irregular high-intensity areas, possibly indicative of the presence of *de novo* connective tissue (cellularisation) that progressively replaces the proteoglycan that is initially present after the resorption of the polymer.

### STATISTICAL ANALYSIS

For binary variables, percentages were calculated. Continuous variables are presented as mean and standard deviation. In cohort B2, overall comparison of serial measurement was assessed by applying the Friedman test, and pairwise comparisons between post-procedure and follow-up were performed by a Wilcoxon signed-rank test adjusted by the Bonferroni method.

For imaging assessment, serial analysis including pre-TLR assessment is presented in the tables, while truly serial analysis of each time point excluding pre-TLR values is presented in the supplement.

To assess the changes of imaging variables over time, the longitudinal repeated measurement analysis using a mixed effect model with five follow-up visits (at post-procedure, 6 months, 1 year, 2 years and 3 years) was performed in the SAS procedure PROC MIXED by pooling two cohorts (B1 and B2), as these two groups of patients were comparable in baseline characteristics. Compound symmetry covariance structure was used in the mixed model. In fact, there is no additional random effect beyond the residual error in this analysis. The PROC MIXED model is used for its capability to handle longitudinal data with certain missing patterns. The results are presented in the **Online data supplement**<sup>31</sup>.

As no formal hypothesis testing was planned for assessing the success of the study, no statistical adjustment was applied. P-values presented are exploratory analyses only and should therefore be interpreted cautiously.

## Results

### CLINICAL OUTCOME OF THE ENTIRE COHORT OF THE COHORT B (COHORTS B1 AND B2)

A total of 101 patients were enrolled in this study and the same investigational device (Absorb BVS first generation 1.1) was successfully implanted in all patients (**Table 1**). Additional metallic drug-eluting stents were implanted in three lesions. Clinical follow-up at three years was available in all but one patient who withdrew consent, although the vital status of the patient was available through the referring physician. During the three-year follow-up period, there were no possible, probable, or definite scaffold

**Table 1. Baseline characteristics.**

	Total (n=101)	Cohort B1 (n = 45)	Cohort B2 (n = 56)	p	
Age, years (mean±SD)	62±9	65±9	60±8	0.02	
Male gender, n (%)	73 (72)	33 (73)	40 (71)	0.83	
Current smokers, n (%)	17 (17)	5 (11)	12 (21)	0.18	
Diabetes, n (%)	17 (17)	6 (13)	11 (20)	0.4	
Hypertension requiring medication, n (%)	62 (62)	27 (60)	35 (64)	0.71	
Hyperlipidaemia requiring medication, n (%)	79 (78)	42 (93)	37 (66)	0.001	
Prior target vessel intervention, n (%)	6 (6)	4 (9)	2 (4)	0.4	
Prior myocardial infarction, n (%)	25 (25)	16 (36)	9 (16)	0.03	
Target vessel	Left anterior descending, n (%)	44 (43)	17 (38)	27 (47)	0.33
	Left circumflex, n (%)	24 (24)	12 (27)	12 (21)	–
	Right coronary artery, n (%)	34 (33)	16 (36)	18 (32)	0.67
AHA/ACC lesion classification	A, n (%)	1 (1)	1 (2)	0 (0)	0.44
	B1, n (%)	55 (55)	20 (45)	35 (63)	0.09
	B2, n (%)	40 (40)	22 (50)	18 (32)	0.07
	C, n (%)	4 (4)	1 (2)	3 (5)	0.63
Mean reference vessel diameter (mm)	2.61±0.37	2.65±0.46	2.58±0.29	0.37	
Minimum luminal diameter (mm)	1.06±0.28	1.06±0.32	1.06±0.23	0.91	
Diameter stenosis (%)	59±10	60±12	59±9	0.59	
Lesion length (mm)	9.9±3.6	10.2±3.9	9.7±3.4	0.44	

thromboses<sup>32</sup>. There were three non-Q-wave myocardial infarctions and seven ID-TLRs, which resulted in a three-year major adverse cardiac event rate of 10% (Table 2). Dual antiplatelet therapy was maintained in 98% (99/101), 81.2% (82/101), 24.0% (24/101) and 21.6% (21/97) at 6, 12, 24 and 36 months, respectively.

### CLINICAL OUTCOMES OF THE COHORT B2 WITH IMAGING FOLLOW-UP AT 12 AND 36 MONTHS

Clinical events up to 24 months have been previously reported<sup>3,7,9</sup>. Between one and three years, three ischaemia-driven (ID) target lesion revascularisations (TLR) and two non-ID TLR events occurred (Figure 2). The first patient received a 3.0×18 mm Absorb BVS in a large proximal LAD with a maximal diameter of 3.9 mm, resulting in 270 degrees of malapposition post-procedure. The one-year angiographic follow-up showed no restenosis in the scaffolded segment while OCT demonstrated extensive malapposition. The patient presented with Braunwald Class I unstable angina on day 564. Repeat angiography on day 567 revealed a significant in-scaffold restenosis, and the patient received a 3.0×18 mm XIENCE V® stent (Abbott Vascular). The three-year angiography revealed no restenosis in this metallic drug-eluting stent. The second patient had recurrent stable angina (CCS Class II) with reversible anterior ischaemia on myocardial scintigraphy. Follow-up coronary angiography at day 833 revealed a restenosis (% DS: 64%) of the scaffold in the mid LAD, which was treated with a 3.0×23 mm XIENCE V stent. The third patient, who had received a 3.0×18 mm Absorb

**Table 2. Non-hierarchical and hierarchical count of clinical events over 3 years in the entire cohort B (n=101).**

	30 days N=101	6 months N=101	12 months N=101	24 months N=100	36 months N=100
Cardiac death	0	0	0	0	0
Myocardial infarction, % (n)	2.0 (2)	3.0 (3)	3.0 (3)	3.0 (3)	3.0 (3)
Q-wave MI	0	0	0	0	0
Non-Q-wave MI, % (n)	2.0 (2)	3.0 (3)	3.0 (3)	3.0 (3)	3.0 (3)
Ischaemia-driven TLR, % (n)	0	2.0 (2)	4.0 (4)	6.0 (6)	7.0 (7)
CABG	0	0	0	0	0
PCI, % (n)	0	2.0 (2)	4.0 (4)	6.0 (6)	7.0 (7)
MACE, % (n)	2.0 (2)	5.0 (5)	6.9 (7)	9.0 (9)	10.0 (10)
TVF, % (n)	2.0 (2)	5.0 (5)	6.9 (7)	11.0 (11)	13.0 (13)

CABG: coronary artery bypass graft; MACE: major adverse cardiac events; MI: myocardial infarction; PCI: percutaneous coronary intervention; TLR: target lesion revascularisation; TVF: target vessel failure

BVS scaffold in the proximal RCA, underwent one-year planned angiography that revealed a progression of coronary stenoses in the distal RCA and the distal LM. The patient underwent CABG on day 439 but presented with unstable angina on day 590. Repeat angiography demonstrated a significant new lesion (% DS: 74%) in the mid RCA proximal and distal to the anastomosis of a coronary bypass, including the distal bifurcation. Despite the absence of

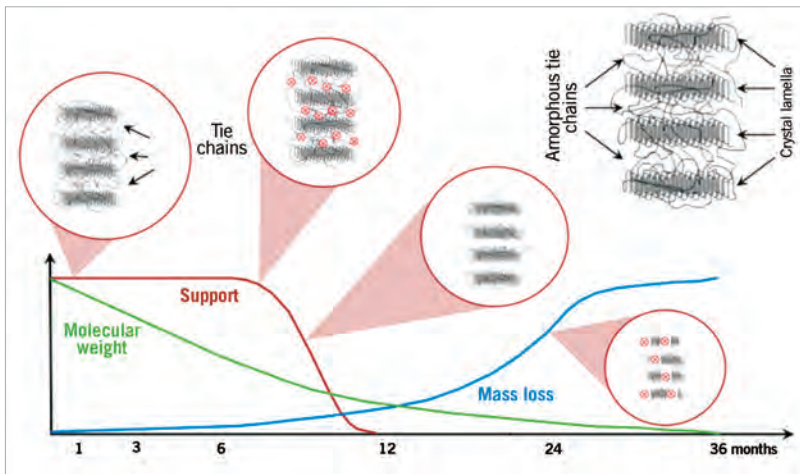


**Figure 1.** The Absorb bioresorbable vascular scaffold poly-L-lactide bioreabsorption process up to 36 months, when the polymeric device is expected to be fully resorbed. 1) Polymer hydration following implantation. Poly lactides are hydrophilic thus water can penetrate the implant. 2) Depolymerisation by hydrolysis, observed as a reduction in molecular weight (green line). 3) Polymer fragmentation into segments of low-weight polymer due to the scission of amorphous tie chains linking the crystalline regions, resulting in subsequent gradual loss of the radial strength (red line). 4) Assimilation or dissolution of monomers. The soluble monomer (e.g., L-lactate) is changed into pyruvate which eventually enters the Krebs cycle and is further converted into carbon dioxide and water, eliminated by the lung and kidney<sup>30</sup>.

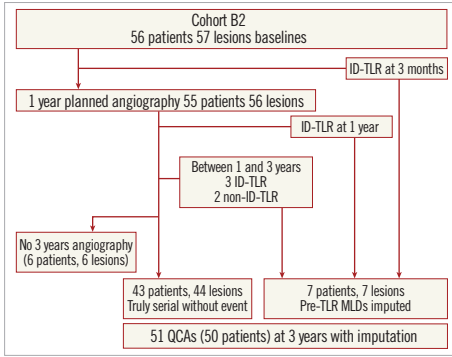


**Figure 2.** Patient flow chart of cohort B2. ID: ischaemia-driven; QCA: quantitative coronary angiography; TLR: target lesion revascularisation

restenosis in the Absorb BVS scaffold (in-segment late loss 0.02 mm, in-scaffold late loss 0.12 mm), a 4.0×38 mm Promus Element stent was placed across the new lesion in the mid RCA with a short overlap of the Absorb BVS scaffold. Because of the overlap, the event was adjudicated by the independent clinical events committee as ID-TLR, although the ARC definitions of TLR pertain specifically to repeat procedures due to restenosis of the device or its adjacent segments 5 mm proximal and distal to the device<sup>32</sup>.

One patient underwent a non-ID-TLR at two years due to persistent incomplete strut apposition observed on OCT without any evidence of ischaemia. The other patient (102913-012) had a non-ID-TLR in the proximal LAD at day 722 to treat a new stenosis in the left main trunk without binary restenosis in the Absorb BVS scaffold (in-scaffold LL: 0.55 mm, in-segment LL: 0.38 mm). During the process of stent implantation in the left main stem, the proximal part of the scaffold was dilated by a balloon and therefore the event was adjudicated as non-ID-TLR despite absence of binary restenosis in the scaffolded segment.

**QUANTITATIVE CORONARY ANGIOGRAPHY AT 6, 12, 24 AND 36 MONTHS**

The late loss at 6, 12, 24 and 36 months was 0.19, 0.27, 0.27 and 0.29 mm, respectively (Figure 3). In the group without TLR, the average late loss was similar at one year (0.22 mm) and three years (0.20 mm). For the entire cohort (n=101), there were six in-segment restenoses at three years with a binary restenosis rate of 6%.

In Table 3, the angiographic results of one and three-year follow-up, including pre-TLR values, are presented. Among the five cases with TLR between one year and three years, three were clinically driven while two were not. Among the three clinically driven TLR, two presented with a binary restenosis in the

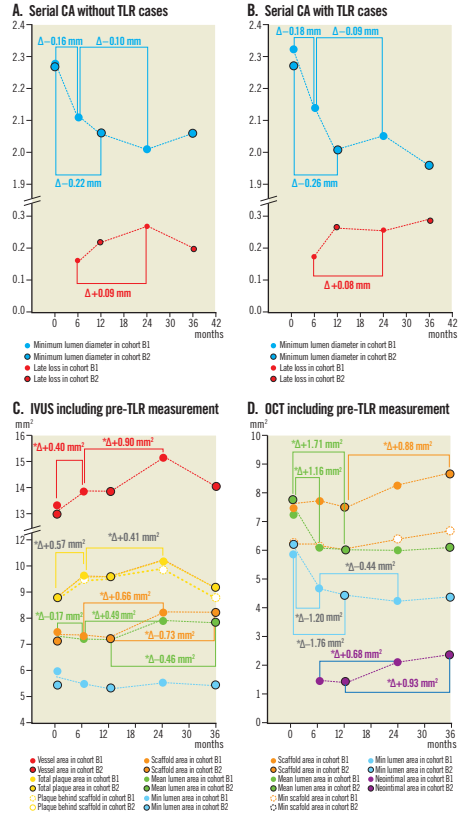


**Figure 3.** The four panels illustrate graphically the measurements in QCA without pre-TLR value (A), QCA with pre-TLR (B), IVUS (C) and OCT (D) performed post-procedure, at 6, 12, 24 and 36 months. The different parameters are colour-coded.

scaffolded segment (Figure 4). In carrying forward the last observation at the time of TLR, there were between one and three years, and no statistically significant differences in MLD, late loss, diameter stenosis and reference diameter in the patients with serial QCA data.

**VASOMOTION REACTION TO NITRATE (COHORT B2)**

In 47 patients the mean lumen diameter inside the scaffold measured prior to and following intracoronary injection of nitrate showed a significant increase in the scaffold from 2.45±0.37 mm to 2.50±0.39 mm (p=0.005). Figure 5 shows the relative changes of mean LD in the proximal, distal and scaffolded segments.

**Table 3. The results of quantitative angiographic analysis (QCA) in cohort B2 carrying forward the last QCA observation prior to the inter-current target lesion revascularisation.**

	Proximal	In-scaffold	Distal
<b>MLD (mm)</b>			
Post-procedure	2.44±0.37 (45)	2.27±0.23 (51)	2.17±0.36 (50)
At 1 year	2.34±0.38 (45)	2.01±0.34 (51)	2.10±0.32 (50)
At 3 years	2.31±0.42 (45)	1.96±0.45 (51)	2.05±0.37 (50)
P-value (post-1 year)	0.04	<0.001	0.10
P-value (post-3 years)	0.02	<0.001	0.06
P-value (1 year-3 years)	0.82	0.46	0.66
Late loss 1 year, mm	0.10±0.30 (43)	0.27±0.34 (50)	0.07±0.27 (49)
Late loss 3 years, mm	0.14±0.31 (44)	0.29±0.43 (51)	0.08±0.37 (49)
P-value (1 year-3 years)	0.26	1.00	0.76
<b>Diameter stenosis, %</b>			
Post-procedure	13.1±8.6 (45)	14.9±5.3 (51)	15.2±9.7 (50)
At 1 year	12.1±12.0 (45)	21.1±11.6 (51)	13.7±9.9 (50)
At 3 years	13.1±10.4 (45)	23.2±14.9 (51)	16.1±9.8 (50)
P-value (post-1 year)	0.46	0.002	0.10
P-value (post-3 years)	0.70	<0.001	0.95
P-value (1 year-3 years)	0.70	0.61	0.23
Binary restenosis 3 years	0% (0/45)	7.8% (4/51)	2.0% (1/50)
<b>RVD</b>			
Post-procedure	2.81±0.30 (45)	2.67±0.23 (51)	2.56±0.25 (50)
At 1 year	2.67±0.33 (45)	2.56±0.29 (51)	2.44±0.29 (50)
At 3 years	2.67±0.39 (45)	2.57±0.37 (51)	2.45±0.34 (50)
P-value (post-1 year)	<0.001	<0.001	<0.001
P-value (post-3 years)	0.002	0.003	0.006
P-value (1 year-3 years)	0.99	0.73	0.62

MLD: minimum lumen diameter; RVD: reference vessel diameter

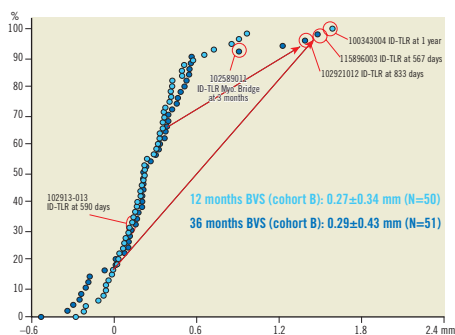


**Figure 4. Cumulative frequency distribution curves of angiographic late loss at one (light blue) and three years (dark blue) including QCA values at the time of target lesion revascularisation whenever it occurs (see text). The red arrows indicate the important changes in late loss between one and three years in patients who underwent ID-TLR (ischaemia-driven target lesion revascularisation).**

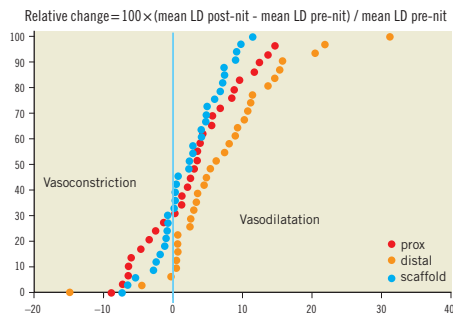


**Figure 5. Cumulative frequency distribution curves of relative changes (%) of mean lumen diameter after nitrate administration in the proximal (red), scaffold (blue) and distal (orange) segments. Relative change (in percentage) was calculated as changes in mean diameter prior to and after intracoronary nitrate administration divided by mean lumen diameter prior to nitrate. In the scaffold and proximal segments, one third of the lesions showed paradoxical vasoconstriction, while in the distal segment only 10% of the lesions showed such vasomotom.**

#### IVUS POST-PROCEDURE, AT 6, 12, 24 AND 36 MONTHS

IVUS analysis is available post-procedure and at 6, 12, 24 and 36 months (Figure 3). Results of the measurement at 6, 12 and 24 months have been previously published<sup>3-7,9</sup>. In the cohort B2, serial IVUS analysis is available post-procedure, at 12 and 36 months in 44 patients with 45 lesions, including three pre-TLR IVUS values (Table 4).

In the overall analysis (Figure 3 and Online data supplement), one of the most striking observations was the significant increase in mean scaffold, mean lumen, mean total plaque and mean vessel area between the first and the second year of observation. This enlargement of the scaffold accounted for the modest increase in neointimal area at two years (0.25 mm<sup>2</sup>) detected by ultrasound, so that the minimal lumen area remained unchanged at 12 and 24 months (Online data supplement).

Between two years and three years there was a substantial plaque reduction following the stepwise increase at six months, one year and two years. The result is a small non-significant increase between post-procedure and three years ( $\Delta+0.27$  mm<sup>2</sup>,  $p=0.08$ ). The expansive remodelling in vessel area documented at two years regressed considerably at three years in parallel with the reduction in plaque behind the struts.

In patients with serial IVUS at one and three years, incomplete apposition was observed at three years in three patients with an average malapposed area of 1.05±0.97 mm<sup>2</sup>. Two patients had malapposition at baseline, which resolved at one and three years. At one year, two patients presented with late acquired malappositions, which were resolved at three years. Three patients, who had no malapposition at baseline and one year, developed malapposition at three years.

**Table 4. Greyscale quantitative intravascular ultrasound carrying forward the last IVUS observation prior to the inter-current target lesion revascularisation if available.**

	BL	1 yr	3 yrs	Difference BL-1 yr	Difference 1 yr-3 yrs	Difference BL-3 yrs	p-values* BL-1 yr	p-values* 1 yr-3 yrs	p-values* BL-3 yrs	Friedman p-value
IVUS greyscale	(n=45)	(n=45)	(n=45)	45 pairs	45 pairs	45 pairs				
Mean vessel area, mm <sup>2</sup>	13.79±2.37	14.43±2.64	14.58±2.67	-0.64±1.62	-0.15±1.09	-0.79±1.54	0.03	0.41	0.002	0.18
Mean scaffold area, mm <sup>2</sup>	6.29±0.91	6.35±0.99	7.08±1.55	-0.06±0.59	-0.73±0.90	-0.80±1.26	n.s.	<0.001	<0.001	<0.001
Min scaffold area, mm <sup>2</sup>	5.08±0.90	5.09±0.90	5.33±1.21	-0.00±0.63	-0.25±0.73	-0.25±1.03	0.97	0.02	0.08	0.11
Neointimal hyperplasia area, mm <sup>2</sup>		0.08±0.13	0.28±0.41			-0.20±0.41		0.002		0.007
Minimum lumen area, mm <sup>2</sup>	5.08±0.90	4.99±0.94	5.08±1.35	0.09±0.72	-0.09±0.84	0.00±1.14	0.54	0.19	0.78	0.62
Mean lumen area, mm <sup>2</sup>	6.29±0.90	6.35±1.17	6.81±1.62	-0.06±0.88	-0.46±0.90	-0.52±1.32	n.s.	0.002	0.05	0.007
Plaque behind strut, mm <sup>2</sup>	7.50±1.82	8.08±2.03	7.49±1.76	-0.57±1.29	0.58±1.05	0.01±0.69	0.007	<0.001	n.s.	0.006
Total plaque area, mm <sup>2</sup>	7.50±1.82	8.08±1.94	7.77±1.73	-0.58±1.08	0.31±0.93	-0.27±0.84	<0.001	0.01	n.s.	0.004
Incomplete strut apposition, mm <sup>2</sup>	1.17±0.23 N=2	5.05±0.52 N=2	1.05±0.97 N=3							

BL: baseline; 1 yr: one year; 3 yrs: three years. \*A significant level for each paired comparison is 0.0167 after adjustment for multiplicity using the Bonferroni correction.

**IVUS ECHOGENICITY AND VH ANALYSIS POST-PROCEDURE, AT 6, 12, 24 AND 36 MONTHS**

The results at 6, 12 and 24 months have been published previously<sup>3,7,9</sup>. The results of echogenicity and VH analysis are presented in **Figure 6**. Percent hyperechogenicity on greyscale and radiofrequency backscattering from dense calcium and necrotic core decreased substantially between the first and third year, whereas fibrous and fibro-fatty tissue increased significantly between the first and third year.

**OPTICAL COHERENCE TOMOGRAPHY POST-PROCEDURE, AT 6, 12, 24 AND 36 MONTHS**

The results at 6, 12 and 24 months have been published previously<sup>3,7,9</sup>. The overall OCT analysis is graphically illustrated in **Figure 3**. After an initial decrease in minimal and mean lumen area, the stabilisation of these parameters was observed despite an increase in neointima between one and three years, which was compensated by the parallel increase in mean and minimum scaffold area.

At the time of the trial design the OCT investigation was optional. In cohort B2, 20 patients with 21 lesions underwent an OCT post-procedure. Out of these 21 lesions, 19 underwent serial OCT at one year and three years including two patients with OCT prior to TLR. In cohort B2, OCT measurements demonstrated a significant late scaffold area enlargement (**Table 5**, mean:  $\Delta 0.88 \pm 1.72$  mm<sup>2</sup>, p<0.001, minimum:  $\Delta 0.67 \pm 1.10$  mm<sup>2</sup>, p=0.03) between one and three years, and a significant increase in neointimal formation ( $\Delta 0.93 \pm 0.84$  mm<sup>2</sup>, p<0.001) with, as a result, the mean and minimal lumen area remaining stable between the two follow-up time points.

The number of struts counted in an all-frame analysis (200 micron interval) steadily increased from baseline (672.2±32.2) to one year (702.2±48.7) and to three years (726.4±70.1), probably

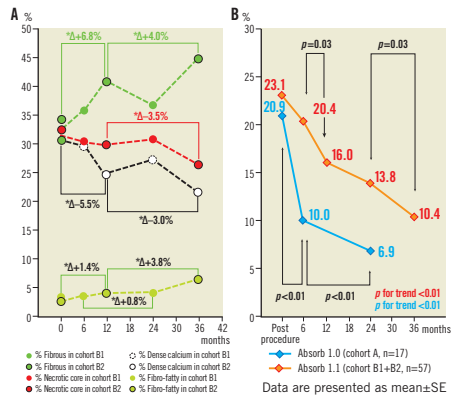


**Figure 6.** The two panels illustrate graphically the measurements in IVUS-VH (A) and echogenicity (B) performed post-procedure, at 6, 12, 24 and 36 months. Figure shows the changes in virtual histology over time – the polymeric struts are initially detected as pseudo dense calcium surrounded by necrotic core and interfere with the assessment of endogenous dense calcium and necrotic core. However, the sharp decrease in dense calcium and necrotic core between 24 and 36 months may also reflect the end of the inflammatory process with regression of the plaque behind the struts as illustrated in panel C of Figure 3. The steady increase of the fibrous and fibro-fatty component may correspond to the neointimal formation. Changes in % hyperechogenicity over time in the ABSORB cohort B (orange line) and cohort A (blue line). For echogenicity assessment of the polymeric struts at baseline and follow-up, a computer-aided greyscale value analysis programme for strut characterisation was used<sup>17,18</sup>.

**Table 5. Optical coherence tomography results carrying forward the last OCT observation prior to the inter-current target lesion revascularisation if available.**

	Post-procedure (n=19)	12 months (n=19)	36 months (n=19)	Difference BL-1 yr 19 pairs	Difference 1 yr-3 yrs 19 pairs	Difference BL-3 yrs 19 pairs	p-values# BL-1 yr	p-values# 1 yr-3 yrs	p-values# BL-3 yrs	Friedman p-value
Mean scaffold area, mm <sup>2</sup>	7.76±1.07	7.51±0.95	8.64±2.15	0.24±0.62	-0.88±1.72	-1.13±1.42	n.s.	0.002	n.s.	0.02
Min scaffold area, mm <sup>2</sup>	6.29±0.87	6.02±0.98	6.69±1.72	0.27±0.88	-0.67±1.10	-0.40±1.63	0.17	0.03	0.24	0.32
Mean black core area, mm <sup>2</sup>	0.19±0.03	0.16±0.02	0.20±0.03	0.03±0.04	-0.01±0.04	-0.04±0.03	0.010	<0.001	n.s.	0.002
Mean neointimal area, mm <sup>2</sup>		1.41±0.68	2.35±0.68		-0.93±0.84			<0.001		
Mean lumen area, mm <sup>2</sup>	7.72±1.17	6.01±1.29	6.09±1.67	1.70±1.31	-0.08±0.86	1.63±1.36	0.001	n.s.	0.001	<0.001
Min lumen area, mm <sup>2</sup>	6.18±0.96	4.43±1.08	4.34±1.48	1.76±1.19	0.09±0.93	1.84±1.47	<0.001	n.s.	<0.001	<0.001
Mean black core volume*, mm <sup>3</sup>	3.34	3.32	3.09	-0.02	-0.22	-0.25	0.92	0.04	0.12	
Uncovered struts, %		3.25±2.86	1.73±1.53		1.52±2.24			0.01		
Incomplete strut apposition, mm <sup>2</sup>	0.27±0.29 (n=16)	2.68±1.63 (n=3)	0.60±0.47 (n=3)							

BL: baseline; 1 yr: one year; 3 yrs: three years. \* This was measured with frame-by-frame analysis in 13 patients. # A significant level for each paired comparison is 0.0167 after adjustment for multiplicity using the Bonferroni correction.

reflecting the dismantling of the scaffold. The mean black core area was unchanged from baseline to three years. The contours of the black box were visually delineated by the analyst of the core lab (every mm frame analysis), resulting in unchanged quantitative assessment of the area. In an all-frame analysis available in 13 patients, the black core volume showed a modest but significant decrease from one to three years. Ninety-eight percent of struts were covered and three scaffolds showed malapposed struts with an average malapposition area of 0.60 mm<sup>2</sup>.

## Discussion

The main findings of the study are the following. 1) Echogenicity and VH analysis suggest advanced bioresorption of the polymeric device. 2) On IVUS, the mean and minimum scaffold areas significantly increase and compensate for the increase in neointimal hyperplasia - resulting in an increase of mean lumen area from one to three years with an unchanged minimal lumen area from one year to three years. The total plaque area shows a biphasic change with an increase between the first and second year and a plaque reduction between the second and third-year follow-up. 3) OCT confirms the IVUS findings regarding the increase in the scaffold area and neointimal area from one to three years. 4) Angiographic late luminal loss between one and three years remains unchanged with a binary in-segment restenosis of 6% for the entire cohort B. 5) The major adverse cardiac events rate at three years remains low.

### ADVANCED BIORESORPTION

**Figure 6** shows changes in % hyperechogenicity in serial pullbacks at six and 24 months and at one and three years. These two observations are combined since they have a similar rate of bioresorption that nevertheless has not yet reached its minimal value compared to the bioresorption of the cohort A device, using a first-generation scaffold with a faster resorption<sup>12</sup>. In the preclinical study, full resorption is complete at 36 months. The use of ultrasound to

monitor the degradation process of biopolymers has been proposed previously and tested in an *in vitro* set-up. Wu et al showed that the degradation rate of biodegradable polymers can be closely monitored by ultrasound techniques<sup>10</sup>.

At variance with this mode of investigation, OCT assessment of the black core volume showed a significant but modest decrease between one and three years. It is important to remember that this optical technique cannot differentiate the polylactide from the provisional matrix of proteoglycan. The preclinical studies have clearly demonstrated by gel permeation chromatography the absence of the polylactide at three years with its replacement by proteoglycan. The black core area was determined by visual contour delineation and does not take into account subtle change in greyiness of black cores or the appearance of light reflecting structures inside the black core (**Figure 7**). Obviously, assessment of light reflectivity should be applied to assess subtle modifications of light absorption and backscattering objectively<sup>33</sup>. Previous and current (unpublished data) preclinical assessments of histology and OCT have indicated that changes in strut appearance on OCT correspond to the cellularisation of the provisional matrix and the appearance of connective tissues surrounding the cell nuclei stained in black in a Movat histological preparation (**Figure 7**)<sup>6</sup>. Preclinical investigation of scaffolded porcine coronary artery models at two, three and four years combining OCT and histology indicated that the next phase will involve shrinkage of the connective tissue filling the strut footprints with, ultimately, the histological disappearance of strut footprints. This last integration process will result in late wall thinning. Wall thinning may impact on lumen enlargement and/or adaptive constrictive remodelling.

Noteworthy is that the persistence of black core on OCT at three years allows for the tracking of the outward displacement of individual struts and for documentation of the increase in scaffold area that clearly occurs between one and three years. At four years, this OCT information will no longer be available since the OCT signal will no longer be visible.

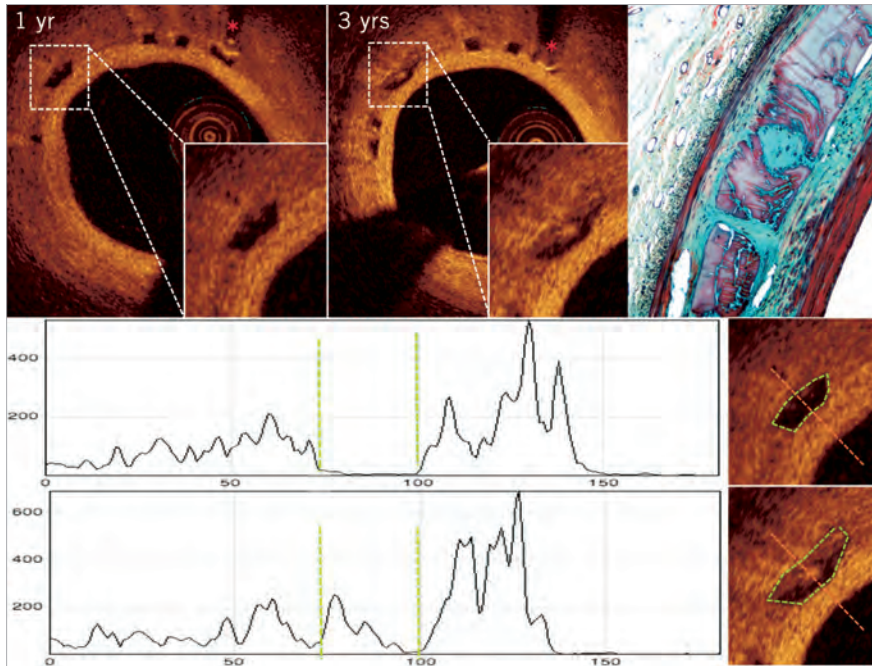


**Figure 7.** Matched OCT cross-sections according to the presence of distal metallic markers (red asterisks) at one and three years. One of the matched struts next to the marker (asterisk) was analysed by light reflectivity<sup>34</sup>. At three years, the strut core that was initially black became partially filled by a white nucleus exhibiting high light reflectivity. Tracings at the bottom showed graphically the light reflectivity along the scan line of incident light (red). The vertical green dotted lines correspond to the adluminal and abluminal boundaries of the black core either empty or partially occupied by white nucleus. Histological picture (Movat staining, 20×) of porcine coronary artery 36 months after implantation of Absorb scaffold showed provisional matrix (glycoconjugates) in purple, filling the void previously occupied by the polymeric strut. A cellularised (black dots) area with connective tissue (green staining) is located at the centre of the strut void and is connected by a peduncle to the subintima. Multi-layers of smooth muscle cells are overlying the strut voids. OCT images of the histological structures in a porcine model are very similar to those observed in human. The light intensity was analysed using an open source software (image J software).

#### SCAFFOLD ENLARGEMENT: A NEW CONVINCING OBSERVATION

Between one and three years, the OCT assessment documented an enlargement of the scaffold area (0.88 mm<sup>2</sup>) in parallel with an increase in neointima between and on top of the struts (0.93 mm<sup>2</sup>). The net result is on average an unchanged mean lumen area (58% showed an increase between one and three years while 42% showed a decrease). It seems that, at three years, a kind of equilibrium between the outward displacement of the scaffold and inward growth of neointimal tissue has been reached. The absence of late luminal loss between one and three years appears to be the net result of this equilibrium (**Figure 3**, **Figure 4**).

Preclinical studies demonstrated the full disappearance of the polylactide (gel permeation chromatography) at two years with the

first generation of the Absorb BVS (BVS 1.0) and at three years with the second generation (BVS 1.1). During that phase, giant cell granuloma can be observed in the vicinity of the struts and may explain the increase in plaque media in humans between the post-procedure, the six-month and the two-year follow-up. During that phase, the void previously occupied by the polymer is replaced by provisional matrix of proteoglycan that is ultimately going to be cellularised by connective tissues. At three years, granuloma and giant cells have completely disappeared in the histology of the porcine coronary artery implanted with the second-generation Absorb BVS (1.1) and may explain the (pseudo-) regression of the plaque behind the struts on IVUS in humans between two and three years. A similar process of pseudo-regression in cohort A has been previously described by our group<sup>34</sup>.

The IVUS confirms this outward displacement of the struts between one and two years, evolving in parallel with a plaque increase and outward expansive remodelling. During the third year, the plaque and EEM regress without further changes of the mean lumen and scaffold area. This observation exemplifies the dynamics of vessel wall changes following the implantation of a bioresorbable scaffold that has induced a transient inflammatory process.

#### DISCREPANCY BETWEEN CHANGES IN IVUS AREA AND OCT AREA BETWEEN 1 AND 3 YEARS

Between one and three years a significant increase in mean lumen area on IVUS with no changes in minimum lumen area was detected,

whereas on OCT an unchanged minimal and mean lumen area was seen. Lumen areas of native coronary arteries as measured by IVUS have been shown to be larger than the same areas measured by OCT, a difference that could be attributed to differences in resolution and the physics of backscattering of ultrasound and light from *in vivo* tissue<sup>35</sup>. When compared (n=19), the analysis of luminal areas over time is made more complex by the differences between the two techniques (Figure 8). This basic difference in detection of “luminal contour” is dynamically affected at follow-up as illustrated in Figure 8 and explains the absence of changes in mean lumen area (between one and three years) as assessed by OCT, in contrast to the increase in mean lumen area on IVUS.

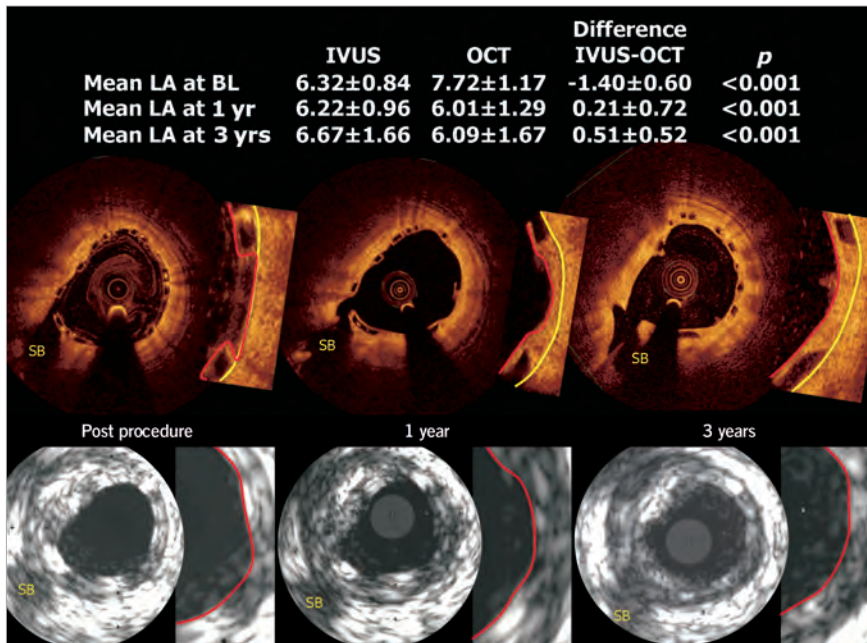


**Figure 8.** In 19 patients who had undergone both IVUS and OCT investigation, corresponding OCT and IVUS cross-sections (see side branch, SB) images are shown. The IVUS (20 MHz) primarily detected the highly reflective endoluminal surface of the polymeric struts, and is unable to detect with precision the endoluminal contour of the vessel wall between polymeric struts apposed but not embedded in the vessel wall. In other words, the delineation of the luminal contour on IVUS after scaffold implantation relies mainly on the bright interface created by the presence of polymeric struts. In contrast, the luminal dimension as measured by OCT truly reflects and delineates the endoluminal interface of the vessel wall behind the polymeric struts<sup>30</sup>: the polymeric struts do not create abluminal shadows allowing the detection of luminal contours behind and between the struts. At follow-up, neointimal tissue grows between polymeric struts and covers the top of the polymeric struts. This neointimal tissue (in between and on top of struts) is exquisitely detectable by OCT, showing the struts encapsulated by the neointima, whereas the lumen boundaries detected by IVUS were mainly determined by the blooming brightness of the polymeric struts that have not been resorbed. This basic difference in the detection of the “luminal contour” is dynamically affected at follow-up by tissue growth as illustrated in the figure and potentially explains the absence of changes in minimal lumen area (between one and three years) as assessed by OCT, vs. the increase in mean lumen area seen in IVUS. (See table included in the figure, p-value is for difference between IVUS and OCT, calculated by Wilcoxon signed-rank test).

## VASOMOTION AND STABLE LATE LOSS AT THREE YEARS

The QCA values described in **Table 2** were obtained post-intracoronary administration of nitrate with the exception of one patient who did not receive nitrate. The absolute and relative changes in mean lumen diameter of the scaffold are somewhat smaller than the changes observed in the proximal or distal segments (**Figure 5**). In this phase of the trial, the investigators were requested to record the blood pressure pre- and post-nitrate, and to wait for the normalisation of the blood pressure. Eventually, they had to reverse the decrease in blood pressure by volume expander if required. Notwithstanding, about 30% of the proximal segments and scaffold segments vasoconstricted, a phenomenon which may be attributed to the baroreceptor activation with a reflex increase in sympathetic tone and release of norepinephrine with secondary stimulation of alpha-1 receptors of the coronary vasculature<sup>36,37</sup>.

The restoration of the vasodilatory capacity seems to be an ongoing process over time. At six months, no significant vasomotion could be documented in a sequential test combining ergonovine and nitrates<sup>3</sup>. At one year, significant changes in vasoconstriction and vasodilatation were observed during the same test<sup>29</sup>. At two years, only intracoronary administration of nitrate was performed and a significant ( $p=0.035$ ) but modest ( $0.034\pm 0.09$  mm) vasodilatation was observed. At three years, the vasodilatation was accentuated ( $0.054\pm 0.12$  mm) and the overall effect was highly significant ( $p=0.005$ ).

In cases with (6 mo: 0.19, 1 yr: 0.27, 2 yrs: 0.27, 3 yrs: 0.29,  $p=0.138$ ) or without TLR (6 mo: 0.16, 1 yr: 0.22, 2 yrs: 0.27, 3 yrs: 0.20 mm,  $p=0.86$ ), there was no change in the late loss between one and three years. Cumulative frequency distribution curves of late loss at one and three years showed almost perfect superimposition of the two curves in their mid portion (**Figure 4**). Out of 10 patients showing a negative loss at one year, seven actually increased their negative late loss (or showed positive late gain) at three years. In all these cases, the positive late gain was not associated with malapposition of the struts on OCT.

## BINARY RESTENOSIS AND TLR

In the entire population ( $n=101$ ), the binary in-segment restenosis rate was 6%. ID-TLR was 7%: one patient received a metallic stent without binary in-segment restenosis, but rather for a new lesion located 10 mm distal to the scaffold. The re-PCI was adjudicated as ID-TLR, since the implanted metallic stent overlapped the previously implanted Absorb scaffold.

In cohort B1, there were two cases of in-segment restenosis which have been described previously<sup>39</sup>. In cohort B2, there were four in-segment restenoses (binary in-segment restenosis of 7.8%); one patient had a combination of in-scaffold and edge restenosis (**Table 2**). Of note, there were two very late (after one year, at 833 and 576 days) binary in-scaffold restenoses with ischaemic evidence and subsequent TLR treated with a metallic drug-eluting stent for which there is no aetiological explanation. In both cases, intravascular imaging confirmed the growth of neointimal tissue inside the scaffold, which was by no means crushed or encroached on by a growing plaque located outside the scaffold. These very late

restenoses are not a new entity specific to a bioresorbable scaffold: very late restenoses have also been documented after one year in metallic everolimus-eluting stents. In the SPIRIT II trial, 97 patients had serial angiographic QCA at six and 24 months; seven lesions exhibited an increase in LL of at least 0.8 mm between these two serial follow-up examinations (from  $-0.34, 0.37, -0.35, 0.37, -0.18, 0.08$  mm to  $1.15, 1.66, 0.66, 1.28, 0.63, 0.88$  mm, respectively). In the SPIRIT II trial, only two patients had ischaemia-driven TLR: one experienced very late stent thrombosis resulting in a non-Q-wave myocardial infarction between day 700 and day 721, and one underwent an ID-TLR at day 701.

In the ABSORB cohort B2, two patients with a myocardial bridge have been included. One with an ID-TLR at three months has been previously reported in great detail<sup>30</sup>. The second patient had aggravation of late loss from one year (0.96 mm) to three years (1.22 mm). However, this asymptomatic patient did not undergo a repeat procedure since the diameter stenosis, conventionally measured on the end-diastolic angiographic frame, was 48%. Of note, in this patient at one year the intracoronary administration of acetylcholine triggered a transient total occlusion which was immediately relieved by intracoronary nitrate. Currently, it is assumed that the systolic stress of a myocardial bridge on the scaffold ( $\pm 110,000$  cycles per day) is not compatible with an effective prevention of restenosis. It would be prudent to consider myocardial bridging as a contraindication for treatment with a bioresorbable scaffold.

## IVUS GREYSCALE INTERPRETATION OF THE ANGIOGRAPHIC STABLE LATE LUMINAL LOSS

The main long-term hypothesis is that late lumen enlargement will occur together with wall thinning and adaptive remodelling. Some signs heralding these changes were detectable on IVUS: at three-year follow-up, when compared to post-procedure, there is a significant increase in both mean scaffold area and mean lumen area with unchanged values of minimal scaffold area and minimal lumen area. In addition, there is a decrease in plaque behind the scaffold area between two and three years, which is accompanied by adaptive constrictive remodelling of the vessel area between two and three years (**Table 4, Figure 3**).

This would suggest that the expansive remodelling process observed in the first two years has been halted and followed by a plaque (pseudo-) regression between the second and third years with constriction of the EEM, suggesting an adaptive remodelling not seen in vessels caged with metallic stents<sup>38</sup>.

## CLINICAL OUTCOMES – PRELIMINARY COMPARISON WITH XIENCE V

The preliminary non-randomised comparison of clinical outcomes for the Absorb BVS scaffold and the XIENCE V metallic stent shows that these two devices have possibly similar event rates up to three years (**Figure 9**). For this comparison, 227 patients were selected from the SPIRIT I, II and III trials on the basis of a single implanted device with identical length and diameter ( $3.0\times 18$  mm).

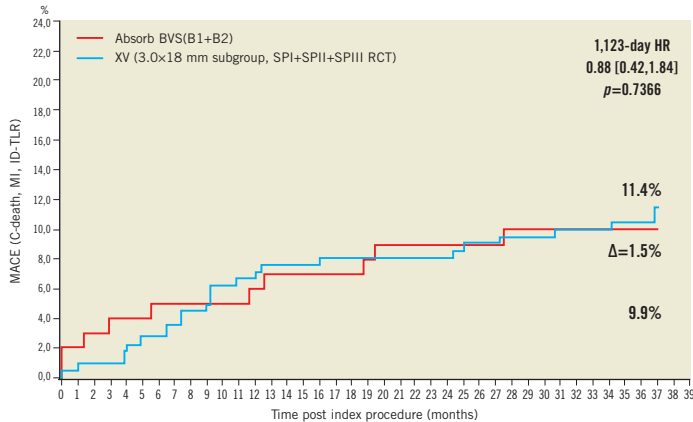


**Figure 9.** Kaplan-Meier estimates of cumulative major adverse cardiac events (cardiac mortality; any myocardial infarction or ischaemia-driven target lesion revascularisation) of the ABSORB cohort B (red,  $n=101$ ) and the 226 patients who received a single  $3.0 \times 18$  mm metallic everolimus-eluting stent in the SPIRIT I, II and III trials (blue).

This comparison should be viewed as a preamble to the ongoing randomised ABSORB II trial, enrolment to which has recently been completed<sup>39</sup>. More sophisticated adjusted comparisons using Cox regression analysis or propensity matching were precluded by the limited number of patients and events available, and this analysis should be viewed as hypothesis-generating.

### Limitations

The current analysis is limited by the fact that invasive imaging follow-up was sometimes not performed at one and three years. Six patients did not undergo angiography at three years: these patients had no events. In the angiographic analysis, however, pre-TLR minimal lumen diameter (therefore the worst MLD) was measured in all event cases, and those values are used as the MLD at three years. The MLD data derived from the current analysis are therefore still representative of the overall temporal changes in lumen dimensions. Conversely, in the patients who underwent TLR, pre-TLR IVUS or OCT are missing in three and two patients, respectively. The IVUS and OCT analysis might therefore under-represent the changes in lumen dimensions.

### Conclusion

The current investigation demonstrated the dynamics of vessel wall changes after implantation of an Absorb bioresorbable scaffold, resulting at three years in stable luminal dimensions, a low restenosis rate and a low clinical major adverse cardiac events rate.

### Guest Editor

This paper was Guest Edited by William Wijns, MD, PhD, Onze-Lieve-Vrouweziekenhuis Aalst, OLV Hospital, Aalst, Belgium.

### Conflict of interest statement

C. Dorange, S. Veldhof, K.M. Hebert and R. Rapoza are employees of Abbott Vascular. The other authors have no conflicts of interest to declare. The Guest Editor has received institutional research grants from several pharmaceutical and device companies, including Abbott Vascular and Biotronik and honoraria and fees on behalf of W. Wijns go to the Cardiovascular Research Center Aalst, Belgium.

### References

1. Tanimoto S, Serruys PW, Thuesen L, Dudek D, de Bruyne B, Chevalier B, Ormiston JA. Comparison of in vivo acute stent recoil between the bioabsorbable everolimus-eluting coronary stent and the everolimus-eluting cobalt chromium coronary stent: insights from the ABSORB and SPIRIT trials. *Catheter Cardiovasc Interv*. 2007;70:515-23.
2. Onuma Y, Serruys PW, Gomez J, de Bruyne B, Dudek D, Thuesen L, Smits P, Chevalier B, McClean D, Koolen J, Windecker S, Whitbourn R, Meredith I, Garcia-Garcia H, Ormiston JA. Comparison of in vivo acute stent recoil between the bioresorbable everolimus-eluting coronary scaffolds (revision 1.0 and 1.1) and the metallic everolimus-eluting stent. *Catheter Cardiovasc Interv*. 2011;78:3-12.
3. Serruys PW, Onuma Y, Ormiston JA, de Bruyne B, Regar E, Dudek D, Thuesen L, Smits PC, Chevalier B, McClean D, Koolen J, Windecker S, Whitbourn R, Meredith I, Dorange C, Veldhof S, Miquel-Hebert K, Rapoza R, Garcia-Garcia HM. Evaluation of the second generation of a bioresorbable everolimus drug-eluting vascular scaffold for treatment of de novo coronary artery stenosis: six-month clinical and imaging outcomes. *Circulation*. 2010;122:2301-12.
4. Waksman R. Biodegradable stents: they do their job and disappear. *J Invasive Cardiol*. 2006;18:70-4.

5. Oberhauser JP, Hossainy S, Rapoza RJ. Design principles and performance of bioresorbable polymeric vascular scaffolds. *EuroIntervention*. 2009;5:F15-22.
6. Onuma Y, Serruys PW, Ormiston JA, Regar E, Webster M, Thuesen L, Dudek D, Veldhof S, Rapoza R. Three-year results of clinical follow-up after a bioresorbable everolimus-eluting scaffold in patients with de novo coronary artery disease: the ABSORB trial. *EuroIntervention*. 2010;6:447-53.
7. Serruys PW, Onuma Y, Dudek D, Smits PC, Koolen J, Chevalier B, de Bruyne B, Thuesen L, McClean D, van Geuns RJ, Windecker S, Whitbourn R, Meredith I, Dorange C, Veldhof S, Hebert KM, Sudhir K, Garcia-Garcia HM, Ormiston JA. Evaluation of the second generation of a bioresorbable everolimus-eluting vascular scaffold for the treatment of de novo coronary artery stenosis: 12-month clinical and imaging outcomes. *J Am Coll Cardiol*. 2011;58:1578-88.
8. Brugaletta S, Radu MD, Garcia-Garcia HM, Heo JH, Farooq V, Girasis C, van Geuns RJ, Thuesen L, McClean D, Chevalier B, Windecker S, Koolen J, Rapoza R, Miquel-Hebert K, Ormiston J, Serruys PW. Circumferential evaluation of the neointima by optical coherence tomography after ABSORB bioresorbable vascular scaffold implantation: can the scaffold cap the plaque? *Atherosclerosis*. 2012;221:106-12.
9. Ormiston JA, Serruys PW, Onuma Y, van Geuns RJ, de Bruyne B, Dudek D, Thuesen L, Smits PC, Chevalier B, McClean D, Koolen J, Windecker S, Whitbourn R, Meredith I, Dorange C, Veldhof S, Hebert KM, Rapoza R, Garcia-Garcia HM. First serial assessment at 6 months and 2 years of the second generation of absorb everolimus-eluting bioresorbable vascular scaffold: a multi-imaging modality study. *Circ Cardiovasc Interv*. 2012;5:620-32.
10. Wu HC, Shen FW, Hong X, Chang WV, Winet H. Monitoring the degradation process of biopolymers by ultrasonic longitudinal wave pulse-echo technique. *Biomaterials*. 2003;24:3871-6.
11. Brugaletta S, Gogas BD, Garcia-Garcia HM, Farooq V, Girasis C, Heo JH, van Geuns RJ, de Bruyne B, Dudek D, Koolen J, Smits P, Veldhof S, Rapoza R, Onuma Y, Ormiston J, Serruys PW. Vascular compliance changes of the coronary vessel wall after bioresorbable vascular scaffold implantation in the treated and adjacent segments. *Circ J*. 2012;76:1616-23.
12. Serruys PW, Ormiston JA, Onuma Y, Regar E, Gonzalo N, Garcia-Garcia HM, Nieman K, Bruining N, Dorange C, Miquel-Hebert K, Veldhof S, Webster M, Thuesen L, Dudek D. A bioabsorbable everolimus-eluting coronary stent system (ABSORB): 2-year outcomes and results from multiple imaging methods. *Lancet*. 2009;373:897-910.
13. Serruys PW, Garcia-Garcia HM, Onuma Y. From metallic cages to transient bioresorbable scaffolds: change in paradigm of coronary revascularization in the upcoming decade? *Eur Heart J*. 2012;33:16-25.
14. Okamura T, Garg S, Gutiérrez-Chico J, Shin E, Onuma Y, Garcia-Garcia H, Rapoza R, Sudhir K, Regar E, Serruys P. In vivo evaluation of stent strut distribution patterns in the bioabsorbable everolimus-eluting device: an OCT ad hoc analysis of the revision 1.0 and revision 1.1 stent design in the ABSORB clinical trial. *EuroIntervention*. 2010;5:932-8.
15. Mintz GS, Nissen SE, Anderson WD, Bailey SR, Erbel R, Fitzgerald PJ, Pinto FJ, Rosenfield K, Siegel RJ, Tuzcu EM, Yock PG. American College of Cardiology Clinical Expert Consensus Document on Standards for Acquisition, Measurement and Reporting of Intravascular Ultrasound Studies (IVUS). A report of the American College of Cardiology Task Force on Clinical Expert Consensus Documents. *J Am Coll Cardiol*. 2001;37:1478-92.
16. Tanimoto S, Bruining N, van Domburg RT, Rotger D, Radeva P, Ligthart JM, Serruys PW. Late stent recoil of the bioabsorbable everolimus-eluting coronary stent and its relationship with plaque morphology. *J Am Coll Cardiol*. 2008;52:1616-20.
17. Bruining N, de Winter S, Roelandt JR, Regar E, Heller I, van Domburg RT, Hamers R, Onuma Y, Dudek D, Webster MW, Thuesen L, Ormiston JA, Cheong WF, Miquel-Hebert K, Veldhof S, Serruys PW. Monitoring in vivo absorption of a drug-eluting bioabsorbable stent with intravascular ultrasound-derived parameters a feasibility study. *JACC Cardiovasc Interv*. 2010;3:449-56.
18. Nair A, Kuban BD, Tuzcu EM, Schoenhagen P, Nissen SE, Vince DG. Coronary plaque classification with intravascular ultrasound radiofrequency data analysis. *Circulation*. 2002;106:2200-6.
19. Nair A, Margolis MP, Kuban BD, Vince DG. Automated coronary plaque characterisation with intravascular ultrasound backscatter: ex vivo validation. *EuroIntervention*. 2007;3:113-20.
20. Shin ES, Garcia-Garcia HM, Garg S, Ligthart J, Thuesen L, Dudek D, Ormiston JA, Serruys PW. Assessment of the serial changes of vessel wall contents in atherosclerotic coronary lesion with bioresorbable everolimus-eluting vascular scaffolds using Shin's method: an IVUS study. *Int J Cardiovasc Imaging*. 2011;27:931-7.
21. Shin ES, Garcia-Garcia HM, Sarno G, Thuesen L, Dudek D, Ormiston JA, Serruys PW. Reproducibility of Shin's method for necrotic core and calcium content in atherosclerotic coronary lesions treated with bioresorbable everolimus-eluting vascular scaffolds using volumetric intravascular ultrasound radiofrequency-based analysis. *Int J Cardiovasc Imaging*. 2012;28:43-9.
22. Sihan K, Botha C, Post F, de Winter S, Gonzalo N, Regar E, Serruys PJ, Hamers R, Bruining N. Fully automatic three-dimensional quantitative analysis of intracoronary optical coherence tomography: method and Validation. *Catheter Cardiovasc Interv*. 2009;74:1058-65.
23. Prati F, Regar E, Mintz GS, Arbustini E, Di Mario C, Jang IK, Akasaka T, Costa M, Guagliumi G, Grube E, Ozaki Y, Pinto F, Serruys PW. Expert review document on methodology, terminology, and clinical applications of optical coherence tomography: physical principles, methodology of image acquisition, and clinical application for assessment of coronary arteries and atherosclerosis. *Eur Heart J*. 2010;31:401-15.
24. Gonzalo N, Serruys PW, Okamura T, Shen ZJ, Onuma Y, Garcia-Garcia HM, Sarno G, Schultz C, van Geuns RJ, Ligthart J, Regar E. Optical coherence tomography assessment of the acute effects of stent implantation on the vessel wall: a systematic quantitative approach. *Heart*. 2009;95:1913-9.

25. Regar E, Leeuwen AMGJv, Serruys PW. Optical Coherence Tomography in Cardiovascular Research. London, UK: Informa Healthcare; 2007.
26. Gonzalo N, Serruys PW, Garcia-Garcia HM, van Soest G, Okamura T, Ligthart J, Knaapen M, Verheye S, Bruining N, Regar E. Quantitative ex vivo and in vivo comparison of lumen dimensions measured by optical coherence tomography and intravascular ultrasound in human coronary arteries. *Rev Esp Cardiol*. 2009;62:615-24.
27. Gomez-Lara J, Brugaletta S, Diletti R, Garg S, Onuma Y, Gogas BD, van Geuns RJ, Dorange C, Veldhof S, Rapoza R, Whitbourn R, Windecker S, Garcia-Garcia HM, Regar E, Serruys PW. A comparative assessment by optical coherence tomography of the performance of the first and second generation of the everolimus-eluting bioresorbable vascular scaffolds. *Eur Heart J*. 2011;32:294-304.
28. Gomez-Lara J, Radu M, Brugaletta S, Farooq V, Diletti R, Onuma Y, Windecker S, Thuesen L, McClean D, Koolen J, Whitbourn R, Dudek D, Smits PC, Regar E, Veldhof S, Rapoza R, Ormiston JA, Garcia-Garcia HM, Serruys PW. Serial analysis of the malapposed and uncovered struts of the new generation of everolimus-eluting bioresorbable scaffold with optical coherence tomography. *JACC Cardiovasc Interv*. 2011;4:992-1001.
29. Onuma Y, Serruys PW. Bioresorbable scaffold: the advent of a new era in percutaneous coronary and peripheral revascularization? *Circulation*. 2011;123:779-97.
30. Tsuchida K, Serruys PW, Bruining N, Dudek D, Drzewiecki J, Banning AP, Zmudka K, Schiele F, Zhou Z, Rademaker TA, van Es GA, Koglin J, Russell ME, Colombo A. Two-year serial coronary angiographic and intravascular ultrasound analysis of in-stent angiographic late lumen loss and ultrasonic neointimal volume from the TAXUS II trial. *Am J Cardiol*. 2007;99:607-15.
31. Littell RC, Milliken GA, Stroup WW, Wolfinger RD, Schabenberger O. SAS for Mixed Models. 2nd edition ed: SAS Institute; 2006.
32. Cutlip DE, Windecker S, Mehran R, Boam A, Cohen DJ, van Es GA, Steg PG, Morel MA, Mauri L, Vranckx P, McFadden E, Lansky A, Hamon M, Krucoff MW, Serruys PW. Clinical end points in coronary stent trials: a case for standardized definitions. *Circulation*. 2007;115:2344-51.
33. Sheehy A, Gutierrez-Chico JL, Diletti R, Oberhauser JP, Glauser T, Harrington J, Kossuth MB, Rapoza RJ, Onuma Y, Serruys PW. In vivo characterisation of bioresorbable vascular scaffold strut interfaces using optical coherence tomography with Gaussian line spread function analysis. *EuroIntervention*. 2012;7:1227-35.
34. Sarno G, Onuma Y, Garcia Garcia HM, Garg S, Regar E, Thuesen L, Dudek D, Veldhof S, Dorange C, Ormiston JA, Serruys PW. IVUS radiofrequency analysis in the evaluation of the polymeric struts of the bioabsorbable everolimus-eluting device during the bioabsorption process. *Catheter Cardiovasc Interv*. 2010;75:914-8.
35. Okamura T, Onuma Y, Garcia-Garcia HM, van Geuns RJ, Wykrzykowska JJ, Schultz C, van der Giessen WJ, Ligthart J, Regar E, Serruys PW. First-in-man evaluation of intravascular optical frequency domain imaging (OFDI) of Terumo: a comparison with intravascular ultrasound and quantitative coronary angiography. *EuroIntervention*. 2011;6:1037-45.
36. Ertl G, Hu K. Anti-ischemic potential of drugs related to the renin-angiotensin system. *J Cardiovasc Pharmacol*. 2001;37:S11-20.
37. Camm AJ, Lüscher TF, Serruys PW. The ESC textbook of cardiovascular medicine. 2nd revised edition ed. Oxford: Oxford University Press; 2009.
38. Claessen BE, Beijk MA, Legrand V, Ruzyllo W, Manari A, Varenne O, Suttorp MJ, Tijssen JG, Miquel-Hebert K, Veldhof S, Henriques JP, Serruys PW, Piek JJ. Two-year clinical, angiographic, and intravascular ultrasound follow-up of the XIENCE V everolimus-eluting stent in the treatment of patients with de novo native coronary artery lesions: the SPIRIT II trial. *Circ Cardiovasc Interv*. 2009;2:339-47.
39. Diletti R, Serruys PW, Farooq V, Sudhir K, Dorange C, Miquel-Hebert K, Veldhof S, Rapoza R, Onuma Y, Garcia-Garcia HM, Chevalier B. ABSORB II randomized controlled trial: a clinical evaluation to compare the safety, efficacy, and performance of the Absorb everolimus-eluting bioresorbable vascular scaffold system against the XIENCE everolimus-eluting coronary stent system in the treatment of subjects with ischemic heart disease caused by de novo native coronary artery lesions: rationale and study design. *Am Heart J*. 2012;164:654-63.

### Online data supplement

**Online Figure 1.** Flow chart of IVUS imaging follow-up.

**Online Figure 2.** Flow chart of OCT follow-up.

**Online Table 1.** The results of longitudinal repeated measurement analysis using a mixed effect model with five follow-up visits (at post-procedure, 6 months, 1 year, 2 years and 3 years).

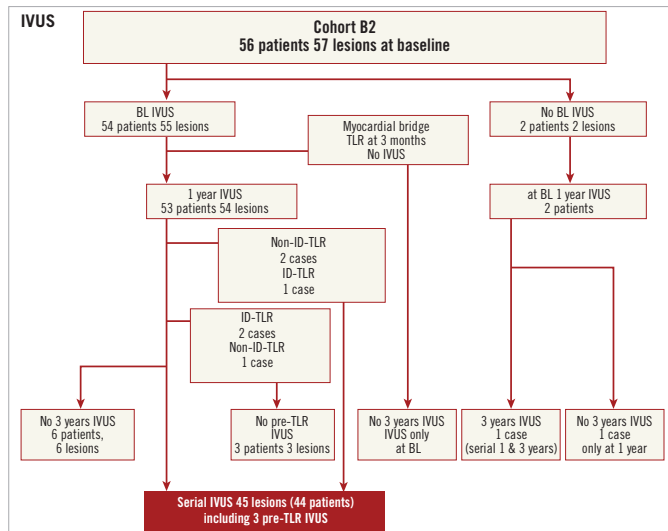
**Online Table 2.** The results of quantitative angiographic analysis in a truly serial population.

**Online Table 3.** Greyscale quantitative intravascular ultrasound without imputation.

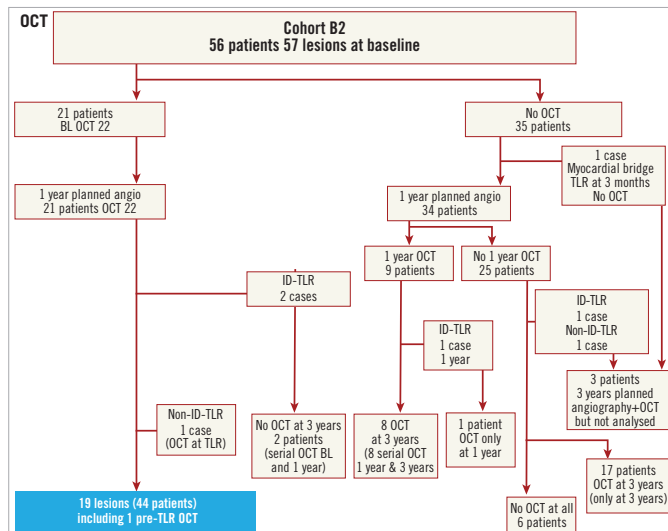
**Online Table 4.** Intravascular ultrasound radiofrequency virtual histology backscattering (virtual histology) in a truly serial population.

**Online Table 5.** Optical coherence tomography results in a truly serial population.

# Online data supplement



Online Figure 1. Flow chart of IVUS imaging follow-up.



Online Figure 2. Flow chart of OCT follow-up.

Online Table 1. The results of longitudinal repeated measurement analysis using a mixed effect model with five follow-up visits (at post-procedure, 6 months, 1 year, 2 years and 3 years).

Quantitative coronary angiography analysis	Post-procedure (cohorts B1+B2)	6 months (cohort B1)	1 year (cohort B2)	2 years (cohort B1)	3 years (cohort B2)	p-value					Overall			
	(N= 101)	(N= 45)	(N= 56)	(N= 45)	(N= 56)	Post-proc vs. 6 mo	Post-proc vs. 1 yr	Post-proc vs. 2 yrs	Post-proc vs. 3 yrs	6 mo vs. 1 yr	1 yr vs. 2 yrs	2 yrs vs. 3 yrs		
Reference vessel diameter (mm, mean±SD)	In-scaffold	2.71±0.30 (102)	2.66±0.36 (42)	2.56±0.30 (57)	2.57±0.34 (38)	2.57±0.37 (51)	0.0077	<0.0001	0.0001	0.0001	0.3373	0.9302	0.7265	<0.0001
	Proximal segment	2.82±0.35 (95)	2.72±0.36 (42)	2.65±0.32 (50)	2.67±0.36 (38)	2.67±0.39 (45)	0.0001	<0.0001	<0.0001	<0.0001	0.7137	0.9077	0.9286	<0.0001
	Distal segment	2.59±0.31 (100)	2.55±0.37 (41)	2.44±0.31 (56)	2.45±0.32 (37)	2.45±0.34 (50)	0.011	<0.0001	<0.0001	0.0003	0.1476	0.8537	0.3388	<0.0001
	In-scaffold	2.29±0.25 (102)	2.14±0.29 (42)	2.01±0.30 (57)	2.03±0.28 (38)	1.96±0.45 (51)	0.0002	<0.0001	<0.0001	<0.0001	0.059	0.8956	0.3609	<0.0001
Minimal luminal diameter (mm, mean±SD)	In-scaffold	2.44±0.44 (95)	2.39±0.49 (42)	2.31±0.37 (50)	2.25±0.54 (38)	2.31±0.42 (45)	0.0852	0.0034	0.002	0.002	0.4281	0.7303	0.8918	0.0005
	Proximal segment	2.20±0.39 (100)	2.16±0.36 (41)	2.10±0.33 (56)	2.11±0.35 (37)	2.05±0.37 (50)	0.118	0.014	0.1883	0.0019	0.6383	0.5456	0.2557	0.0112
	Distal segment	1.53±0.50 (99)	1.92±0.71 (42)	2.11±1.12 (57)	2.01±0.71 (38)	2.16±1.45 (51)	0.0166	<0.0001	0.0007	<0.0001	0.293	0.9494	0.2758	<0.0001
	In-scaffold	1.53±0.48 (100)	1.48±0.50 (41)	1.35±0.49 (56)	1.38±0.52 (37)	1.61±0.49 (45)	0.4443	0.5742	0.3923	0.9111	0.8539	0.2817	0.5617	0.6158
Diameter stenosis (%; mean±SD)	Proximal segment	14.86±9.50 (41)	13.58±9.89 (56)	13.85±7.18 (37)	16.14±9.77 (50)	0.7714	0.2607	0.1871	0.5332	0.5546	0.762	0.1237	0.37	
	Distal segment	0.07±0.28 (42)	0.12±0.29 (48)	0.12±0.36 (38)	0.14±0.31 (44)					0.4729	0.9266	0.7414	0.485	
	In-scaffold	0.19±0.18 (42)	0.27±0.32 (56)	0.27±0.19 (38)	0.29±0.43 (51)					0.1627	0.9168	0.7595	0.138	
Late loss (mm, mean±SD)	Proximal segment	0.06±0.29 (41)	0.07±0.27 (55)	0.04±0.25 (37)	0.08±0.37 (49)					0.6373	0.5265	0.5377	0.9291	
	Distal segment													
	In-scaffold													
IVUS grey-scale analysis	Post-procedure (cohorts B1+B2)	(N= 101)	(N= 45)	(N= 56)	(N= 45)	(N= 56)	p-value	p-value	p-value	p-value	p-value	p-value	p-value	Overall
		(N= 102)	(N= 45)	(N= 57)	(N= 45)	(N= 57)	Post-proc vs. 6 mo	Post-proc vs. 1 yr	Post-proc vs. 2 yrs	Post-proc vs. 3 yrs	6 mo vs. 1 yr	1 yr vs. 2 yrs	2 yrs vs. 3 yrs	p-value
	Mean vessel area (mm <sup>2</sup> )	14.13±3.37 (95)	14.52±3.94 (40)	14.57±3.02 (56)	15.31±3.90 (38)	14.54±2.65 (46)	0.2224	0.0014	<0.0001	<0.0001	0.2375	0.0165	0.0951	<0.0001
	Mean scaffold area (mm <sup>2</sup> )	6.41±1.02 (95)	6.45±1.07 (40)	6.32±0.97 (56)	7.11±1.71 (38)	7.06±1.54 (46)	0.3842	0.3794	<0.0001	<0.0001	0.4805	0.0009	0.1374	<0.0001
	Minimum scaffold area (mm <sup>2</sup> )	5.29±0.99 (95)	5.29±0.92 (40)	5.04±0.93 (56)	5.37±1.28 (38)	5.29±1.23 (46)	0.0746	0.3396	0.6791	0.0395	0.4438	0.7609	0.1374	0.00429
	Mean lumen area (mm <sup>2</sup> )	6.43±1.06 (95)	6.59±1.08 (40)	6.31±1.17 (56)	6.89±1.74 (38)	6.79±1.61 (46)	0.1911	0.8395	0.0171	0.0009	0.368	0.0404	0.8247	<0.0001
	Minimum lumen area (mm <sup>2</sup> )	5.28±0.99 (95)	5.21±0.95 (40)	4.96±0.98 (56)	5.17±1.26 (38)	5.04±1.35 (46)	0.0628	0.0858	0.1013	0.5655	0.7111	0.8697	0.833	0.1427
Mean plaque area (mm <sup>2</sup> )	7.70±2.64 (95)	8.13±2.70 (40)	8.26±2.31 (56)	8.42±2.74 (38)	7.75±1.72 (46)	0.0005	<0.0001	<0.0001	0.0381	0.7097	0.067	0.001	<0.0001	
Plaque behind scaffold area (mm <sup>2</sup> )	7.72±2.68 (95)	8.07±2.71 (40)	8.26±2.40 (56)	8.20±2.72 (38)	7.88±1.74 (46)	0.0056	<0.0001	<0.0001	0.9179	0.51	0.4777	0.0007	<0.0001	

Online Table 1. The results of longitudinal repeated measurement analysis using a mixed effect model with five follow-up visits (at post-procedure, 6 months, 1 year, 2 years and 3 years). (continued)

IVUS-VH	Post-procedure (cohorts B1+B2)	6 months (cohort B1)	1 year (cohort B2)	2 years (cohort B1)	3 years (cohort B2)	p-value proc vs. 6 mo	Post- proc vs. 1 yr	Post- proc vs. 2 yrs	Post- proc vs. 3 yrs	p-value 6 mo vs. 1 yr	p-value 1 yr vs. 2 yrs	p-value 2 yrs vs. 3 yrs	Overall p-value
	(N= 101)	(N= 45)	(N= 56)	(N= 45)	(N= 56)								
% Dense calcium of VH plaque	29.84±1.05 (90)	28.16±1.044 (37)	24.25±7.86 (52)	27.74±7.45 (32)	21.52±7.94 (44)	0.1696	<0.0001	0.0139	<0.0001	0.0231	0.2166	0.0047	<0.0001
% Necrotic core of VH plaque	31.51±7.07 (90)	30.11±7.35 (37)	30.00±6.83 (52)	31.67±4.64 (32)	26.49±6.21 (44)	0.3616	0.116	0.8761	<0.0001	0.686	0.2046	0.0006	0.0004
% Fibro-fatty VH plaque	3.22±3.38 (90)	3.92±4.05 (37)	4.61±2.53 (52)	4.10±2.84 (32)	6.77±3.59 (44)	0.234	0.001	0.0595	<0.0001	0.1653	0.4485	0.0001	<0.0001
% Fibrous VH plaque	35.43±1.91 (90)	37.80±11.61 (37)	41.13±6.53 (52)	36.49±7.03 (32)	45.22±9.14 (44)	0.2194	0.0001	0.2779	<0.0001	0.0667	0.0674	0.0004	<0.0001
Dense calcium area (mm <sup>2</sup> )	1.23±0.79 (90)	1.33±0.87 (37)	1.13±0.50 (52)	1.37±0.69 (32)	0.94±0.43 (44)	0.0351	0.0384	0.199	<0.0001	0.0024	0.0177	0.0001	0.0001
Necrotic core area (mm <sup>2</sup> )	1.40±0.93 (90)	1.51±4.03 (37)	1.52±0.89 (52)	1.61±0.77 (32)	1.22±0.56 (44)	0.0086	0.683	0.0029	0.0394	0.069	0.0311	0.0002	0.0015
Fibro-fatty area (mm <sup>2</sup> )	0.15±0.23 (90)	0.24±0.37 (37)	0.25±0.23 (52)	0.25±0.31 (32)	0.31±0.22 (44)	0.0271	0.0003	0.0019	<0.0001	0.4455	0.9075	0.1318	<0.0001
Fibrous area (mm <sup>2</sup> )	1.56±1.17 (90)	1.96±1.36 (37)	2.10±1.20 (52)	1.91±1.21 (32)	2.08±0.90 (44)	0.0003	<0.0001	<0.0001	<0.0001	0.8348	0.4429	0.8039	<0.0001
OCT	Post-procedure (cohorts B1+B2)	6 months (cohort B1)	1 year (cohort B2)	2 years (cohort B1)	3 years (cohort B2)	p-value proc vs. 6 mo	Post- proc vs. 1 yr	Post- proc vs. 2 yrs	Post- proc vs. 3 yrs	p-value 6 mo vs. 1 yr	p-value 1 yr vs. 2 yrs	p-value 2 yrs vs. 3 yrs	Overall p-value
	(N= 101)	(N= 45)	(N= 56)	(N= 45)	(N= 56)								
Mean luminal area (mm <sup>2</sup> )	7.50±1.24 (51)	6.35±1.50 (28)	5.91±1.69 (31)	5.93±1.75 (27)	6.06±1.70 (45)	<0.0001	<0.0001	<0.0001	<0.0001	0.3131	0.7483	0.8225	<0.0001
Minimum luminal area (mm <sup>2</sup> )	6.05±1.10 (51)	4.89±1.43 (28)	4.29±1.39 (31)	4.22±1.45 (27)	4.45±1.55 (45)	<0.0001	<0.0001	<0.0001	<0.0001	0.1632	0.7278	0.6911	<0.0001
Mean scaffold area (mm <sup>2</sup> )	7.60±1.10 (51)	7.91±1.40 (28)	7.42±1.22 (31)	8.12±1.92 (27)	8.50±1.93 (45)	0.3849	0.9152	0.0125	0.0001	0.4613	0.0483	0.8829	<0.0001
Minimum scaffold area (mm <sup>2</sup> )	6.28±1.07 (51)	6.38±1.44 (28)	5.96±1.14 (31)	6.30±1.47 (27)	6.66±1.67 (45)	0.8726	0.4224	0.7015	0.0398	0.6172	0.3662	0.1943	0.0527

Values are presented as mean±standard deviation (number of observations). A significant level for each paired comparison is 0.01 after adjustment for multiplicity using the Bonferroni correction. L: lesions; Post-proc: post-procedure; 6 mo: 6 months; 1 yr: 1 year; 2 yrs: 2 years; 3 yrs: 3 years

**Online Table 2. The results of quantitative angiographic analysis in a truly serial population.**

		Proximal	In-scaffold	Distal
MLD (mm)	Post-procedure	2.47±0.37 (39)	2.27±0.23 (44)	2.18±0.38 (43)
	At 1 year	2.39±0.37 (39)	2.06±0.26 (44)	2.10±0.34 (43)
	At 3 years	2.36±0.43 (39)	2.06±0.32 (44)	2.08±0.34 (43)
	P-value (post-1 yr)	0.1494	<0.0001	0.1105
	P-value (post-3 yrs)	0.0571	<0.0001	0.1208
	P-value (1 yr-3 yrs)	0.7372	0.5812	0.9510
	Late loss 1 yr, mm	0.09±0.28 (37)	0.22±0.27 (43)	0.08±0.28 (42)
	Late loss 3 yrs, mm	0.13±0.29 (38)	0.20±0.31 (44)	0.06±0.35 (42)
P-value (1 yr-3 yrs)	0.2700	0.8587	0.9392	
Diameter stenosis, %	Post-procedure	13.05±8.70 (39)	15.53±5.15 (44)	15.08±10.05 (43)
	At 1 year	11.12±11.61 (39)	18.93±8.31 (44)	13.43±9.37 (43)
	At 3 years	11.94±9.53 (39)	19.23±8.50 (44)	14.72±6.84 (43)
	P-value (post-1 yr)	0.2728	0.0408	0.0910
	P-value (post-3 yrs)	0.3252	0.0166	0.5971
	P-value (1 yr-3 yrs)	0.8766	0.9953	0.3740
	In-scaffold binary restenosis 3 yrs	0.0% (0/39)	0.0% (0/44)	0.0% (0/43)
RVD	Post-procedure	2.84±0.30 (39)	2.69±0.23 (44)	2.56±0.25 (43)
	At 1 year	2.69±0.30 (39)	2.56±0.28 (44)	2.43±0.28 (43)
	At 3 years	2.67±0.38 (39)	2.56±0.37 (44)	2.44±0.35 (43)
	P-value (post-1 yr)	0.0006	0.0001	<0.0001
	P-value (post-3 yrs)	0.0001	0.0005	0.0067
	P-value (1 yr-3 yrs)	0.6861	0.6173	0.6141

**Online Table 3. Greyscale quantitative intravascular ultrasound without imputation.**

IVUS greyscale	BL (n=42)	1 yr (n=42)	3 yrs (n=42)	Difference 1 yr-BL* 42 pairs	Difference 3 yrs-1 yr* 42 pairs	Difference 3 yrs-BL* 42 pairs	p-values BL-1 yr	p-values 1 yr-3 yrs	p-values BL-3 yrs
Mean vessel area, mm <sup>2</sup>	13.91±2.37	14.38±2.47	14.54±2.61	0.47±1.37	0.17±1.10	0.64±1.41	0.0765	0.3513	0.0072
Mean scaffold area, mm <sup>2</sup>	6.30±0.93	6.34±0.99	7.03±1.47	0.04±0.58	0.69±0.82	0.73±1.15	0.6986	<0.0001	<0.0001
Min scaffold area, mm <sup>2</sup>	5.08±0.93	5.08±0.92	5.32±1.22	-0.01±0.65	0.24±0.74	0.23±1.05	0.916	0.0191	0.1118
Neointimal hyperplasia area, mm <sup>2</sup>		0.07±0.12	0.21±0.27		0.14±0.26			<0.0001	
Minimum lumen area, mm <sup>2</sup>	5.08±0.93	4.99±0.97	5.12±1.27	-0.10±0.74	0.13±0.73	0.04±1.09	0.6018	0.1545	0.667
Mean lumen area, mm <sup>2</sup>	6.30±0.93	6.33±1.16	6.82±1.53	0.03±0.86	0.48±0.85	0.51±1.22	0.3261	0.0002	0.0098
Plaque behind strut, mm <sup>2</sup>	7.61±1.80	8.04±1.88	7.52±1.75	0.43±1.07	-0.52±0.85	-0.09±0.61	0.0088	<0.0001	0.3079
Total plaque area, mm <sup>2</sup>	7.60±1.80	8.04±1.82	7.72±1.76	0.44±0.86	-0.32±0.74	0.12±0.65	0.0011	0.002	0.2736
Incomplete strut apposition, mm <sup>2</sup>	1.17±0.23 N=2	5.41±NA N=1	1.05±0.97 N=3						

BL: baseline, 1 yr: one year, 3 yrs: three years

**Online Table 4. Intravascular ultrasound radiofrequency virtual histology backscattering (virtual histology) in a truly serial population.**

	BL n=36	12 months n=36	36 months n=36	Difference 3 yrs-1 yr	Difference 3 yrs-BL	p-values 1 yr-3 yrs	p-values BL-3 yrs
Dense calcium area, %	30.74±10.11	24.95±8.28	21.84±8.41	-3.11±5.21	-8.90±9.68	0.0015	<0.0001
Necrotic core area, %	32.10±6.62	30.01±6.29	26.11±5.99	-3.90±8.32	-5.99±9.00	0.0058	<0.0001
Fibro-fatty, %	2.94±2.43	4.23±2.29	6.87±3.66	2.63±3.30	3.92±4.19	<0.0001	<0.0001
Fibrous, %	34.22±10.05	40.80±9.60	45.18±9.38	4.38±9.59	10.96±12.51	0.0076	<0.0001

BL: baseline; 1 yr: one year; 3 yrs: three years

**Online Table 5. Optical coherence tomography results in a truly serial population.**

OCT	Post-procedure (n=18)	12 months (n=18)	36 months (n=18)	Difference 1 yr-BL* 18 pairs	Difference 3 yrs-1 yr* 18 pairs	Difference 3 yrs-BL* 18 pairs	p-values BL-1 yr	p-values 1 yr-3 yrs	p-values BL-3 yrs
Mean scaffold area, mm <sup>2</sup>	7.73±1.09	7.44±0.92	8.32±1.67	-0.29±0.60	0.88±0.96	0.59±1.21	0.0599	0.0016	0.0814
Min scaffold area, mm <sup>2</sup>	6.23±0.85	6.00±1.00	6.59±1.71	-0.23±0.89	0.60±1.08	0.37±1.67	0.2691	0.0483	0.2986
Mean black core area, mm <sup>2</sup>	0.19±0.03	0.16±0.02	0.20±0.03	-0.02±0.03	0.04±0.03	0.01±0.04	0.0066	<0.0001	0.2121
Mean neointimal area, mm <sup>2</sup>		1.49±0.60	2.26±0.56		0.77±0.41			<0.0001	
Mean lumen area, mm <sup>2</sup>	7.69±1.19	5.79±0.85	5.86±1.37	-1.91±1.00	0.07±0.88	-1.83±1.06	<0.0001	0.7019	<0.0001
Minimal lumen area, mm <sup>2</sup>	6.13±0.96	4.31±0.96	4.25±1.46	-1.82±1.19	-0.06±0.95	-1.88±1.51	<0.0001	0.7742	<0.0001
Uncovered struts, %		3.19±2.93	1.65±1.53		-1.55±2.30			0.0150	
Incomplete strut apposition, mm <sup>2</sup>	0.23±0.24 (n=15)	3.05±2.11 (n=2)	0.66±0.65 (n=2)						

BL: baseline; 1 yr: one year; 3 yrs: three years



# Chapter 3

## Anatomical and Functional Lesion Assessment with Three Dimensional Imaging Techniques

### 3.1 Validation of 3D-QCA in bifurcation phantom model

Advanced three-dimensional quantitative coronary angiographic assessment of bifurcation lesions: methodology and phantom validation.

*Eurointervention.* 2013;8:1451-60.

[Original research paper, Impact Factor (2013): 3.758]

Girasis C, Schuurbiers JCH, Muramatsu T, Aben JP, Onuma Y, Soekhradj S, Morel MA, van Geuns RJ, Wentzel JJ, Serruys PW.





# Advanced three-dimensional quantitative coronary angiographic assessment of bifurcation lesions: methodology and phantom validation

Chrysafios Girasis<sup>1</sup>, MD; Johan C.H. Schuurbiens<sup>2</sup>, BSc; Takashi Muramatsu<sup>1</sup>, MD; Jean-Paul Aben<sup>3</sup>, BSc; Yoshinobu Onuma<sup>1</sup>, MD; Satishkumar Soekhradj<sup>3</sup>, MSc; Marie-angèle Morel<sup>4</sup>, BSc; Robert-Jan van Geuns<sup>1</sup>, MD, PhD; Jolanda J. Wentzel<sup>2</sup>, PhD; Patrick W. Serruys<sup>\*1</sup>, MD, PhD

1. Thoraxcenter, Erasmus MC, Rotterdam, The Netherlands; 2. Biomedical Engineering, Erasmus MC, Rotterdam, The Netherlands; 3. Pie Medical Imaging, Maastricht, The Netherlands; 4. Cardialysis B.V., Rotterdam, The Netherlands

This paper also includes accompanying supplementary data published at the following website: [www.eurointervention.org](http://www.eurointervention.org)

## KEYWORDS

- angiography
- coronary bifurcation
- quantitative coronary angiography
- three-dimensional

## Abstract

**Aims:** Validation of new three-dimensional (3-D) bifurcation quantitative coronary angiography (QCA) software.

**Methods and results:** Cardiovascular Angiography Analysis System (CAAS 5v10) allows 3-D angiographic reconstructions based on two or more 2-D projection images. Measurements for minimal lumen diameter (MLD), reference vessel diameter (RVD), percent diameter stenosis (DS) and bifurcation angle (BA) were validated against precision manufactured phantom bifurcations. Length measurements were validated against angiographic measurement catheters inserted into a plexiglas bifurcation phantom. In 3-D reconstructions based on two 2-D images, acquired at variable rotation and angulation, accuracy and precision (mean difference  $\pm$  SD) of the 11-segment model for MLD, RVD and DS were  $0.013\pm 0.131$  mm,  $-0.052\pm 0.039$  mm and  $-1.08\pm 5.13\%$ , respectively; inter-observer variability was 0.141 mm, 0.058 mm and 5.42%, respectively. Adding the antero-posterior (optimal) projection to these basic reconstructions resulted in reduced variability (0.101 mm, 0.041 mm and 3.93% for MLD, RVD and DS,  $p<0.01$  for all) and showed a trend towards improved precision (0.109 mm, 0.031 mm and 4.26%, respectively,  $p>0.05$  for all). In basic reconstructions, accuracy and precision for BA was  $-1.3\pm 5.0^\circ$ , whereas inter-observer variability was  $7.5^\circ$ ; respective measures for length were  $0.15\pm 0.26$  mm and 0.54 mm. Adding the antero-posterior projection resulted in decreased precision (0.47 mm,  $p<0.01$ ) and increased variability (1.03 mm,  $p<0.01$ ) for length measurements; precision ( $5.4^\circ$ ) and variability ( $7.9^\circ$ ) for BA did not change significantly ( $p>0.30$ ).

**Conclusions:** Advances in the methodology of 3-D reconstruction and quantitative analysis for bifurcation lesions translated into highly accurate, precise and reproducible measures of diameter, length and BA.

\*Corresponding author: Thoraxcenter, Ba-583, 's Gravendijkwal 230, 3015 CE Rotterdam, The Netherlands.  
E-mail: [p.w.j.c.serruys@erasmusmc.nl](mailto:p.w.j.c.serruys@erasmusmc.nl)

© Europa Digital & Publishing 2013. All rights reserved.

## Introduction

Percutaneous coronary interventions (PCIs) for the treatment of coronary bifurcation lesions require optimal angiographic analysis<sup>1</sup>; whereas visual assessment of lesion severity is still highly variable even among experts in this field<sup>2</sup>, quantitative coronary angiography (QCA) analysis has seen improvements in performance. Dedicated two-dimensional (2-D) bifurcation QCA software acknowledges the “step-down” in vessel calibre from the proximal main vessel into the distal main vessel and the side branch<sup>3</sup> by determining reference vessel diameter (RVD) based on each of the three branches separately<sup>4,5</sup>. Thereby, higher precision in RVD and percent diameter stenosis (DS) values are attained, facilitating accurate balloon and stent sizing. In addition, reporting results over an increased number of bifurcation vessel segments facilitates accurate disease localisation and consistency in serial angiographic studies<sup>1</sup>.

Nevertheless, the validity of 2-D QCA is dependent on the angiographic view analysed and can be affected by foreshortening and variable magnification; tortuous and/or overlapping coronary structures could impose further limitations<sup>6</sup>. By eliminating these potential sources of error, 3-D QCA algorithms have been shown to provide accurate, precise and reproducible diameter, area and length measurements<sup>7-10</sup> for single-vessel lesions in real time. Experience with 3-D bifurcation reconstructions has been reported comparing results with 2-D analysis<sup>11,12</sup>; however, accuracy and precision of 3-D bifurcation QCA measurements has not been established compared to a gold standard.

Dedicated 3-D bifurcation QCA software incorporated in the latest version of Cardiovascular Angiography Analysis System (CAAS 5v10; Pie Medical Imaging, Maastricht, The Netherlands) adopts algorithms already validated in the 2-D software<sup>4,13</sup> and applies them to the 3-D reconstructions. Furthermore, the methodology has been revised compared to the previous version<sup>14</sup>, in order to allow reconstructions of more than two 2-D projections. In this report we present the theoretical provisions of this software and the results of *in vitro* validation for measures of diameter, length and bifurcation angle (BA).

## Materials and methods

### THEORETICAL PROVISIONS

A 3-D reconstruction requires at least two angiographic images separated by a viewing angle  $\geq 30^\circ$ ; up to four images acquired by a biplane, monoplane or a rotational angiographic system can be combined. Analysis is initiated by demarcating the bifurcation to be analysed on the first selected angiographic image. Subsequently, automatic contour detection is performed via a validated algorithm featuring improved analysis for small vessel lumens<sup>13</sup>. The region of interest is automatically indicated in the other selected image(s), thereby assisting the analyst in correctly placing the delimiter points around the bifurcation, which is then contoured with the same algorithm.

### 3-D RECONSTRUCTION

The acquisition geometry of the projection images provided through the DICOM (Digital Imaging and Communications in Medicine) headers of the angiographic system is not sufficient to obtain an accurate

3-D reconstruction due to the isocentre offset of the gantry. The isocentre offset is the spatial difference between the centres of rotation (isocentres) of the frontal and lateral C-arms in a biplane gantry, attributable mainly to the imperfect alignment of both C-arms but also to gravity; even in a monoplane system active gantry rotation could result in a significant shift of its isocentre. In order to correct for this system distortion, a common image point (CIP) is determined by correlating the videodensitometric information obtained from the 2-D images. Subsequently, the 3-D centrelines for the bifurcation branches are reconstructed by means of an adaptive 3-D epipolar geometry algorithm<sup>14</sup>. Respective 3-D cross-sections are constructed assuming an elliptical model, by using the luminal diameters of the corresponding 2-D cross-sections and their spatial orientations to define the ellipse axes. In cases where  $>2$  projections are used, already existing cross-sections are modified by integrating contour information from each additional 2-D image, while retaining an elliptical shape. In this fitting process, axes between adjacent cross-sections are kept aligned, in order to prevent the 3-D model from twisting along its centreline. For true 3-D quantitative analysis the elliptical model is then converted into a 3-D triangular surface mesh by means of a marching cubes algorithm<sup>15</sup>.

### 3-D QUANTITATIVE ANALYSIS

Analogous to previous publications on bifurcation QCA analysis<sup>14-16</sup>, the polygon of confluence (POC) is defined as the central bifurcation region which behaves differently from a single-vessel segment. Outside the POC, the cross-sectional area is defined perpendicular to the centre of the lumen; within the POC, the cross-sectional area is defined by using the “minimum energy” cross-section, i.e., the smoothest possible surface that spans the lumen at each centre line position. This “minimisation” is performed by using a level set algorithm<sup>17</sup> and will result in curved cross-sections within the central bifurcation region (**Figure 1**).

Automatic calculation of reference cross-sectional area adopts the methodology described for 2-D bifurcation QCA and applies it to the 3-D reconstructed model. Outside the POC, a 3-D equivalent of the algorithm used in single-vessel segments is employed<sup>13,18</sup>. Within the POC, the reference area is derived by applying an interpolation technique between the “healthy” reconstructed 3-D branches. Based on the respective cross-sectional areas, lumen diameter and RVD are defined as the equivalent diameters based on the assumption of circularity. Finally, proximal and distal BA values are derived according to the methodology already described<sup>14</sup>.

The CAAS 5v10 analysis software has no restriction regarding the number of bifurcations the 3-D model consists of: it is possible to reconstruct and analyse a vascular tree which consists of multiple bifurcations. We chose to focus on 3-D reconstructions of one bifurcation at a time, in order to mimic routine angiographic practice. Analysis regarding full-tree reconstructions of bifurcation phantoms is presented in an **Online appendix**.

### VALIDATION

#### DIAMETER AND BA

Six precision-manufactured plexiglas phantoms, each mimicking a vessel with three successive bifurcations lesions, were used for

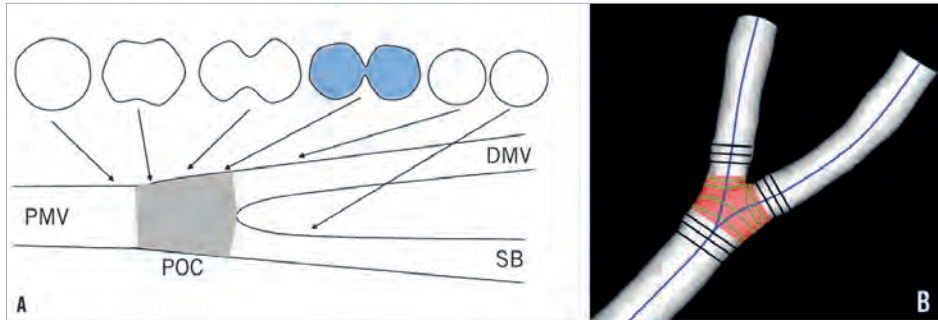


**Figure 1.** Definition of polygon of confluence (POC). A) Within POC (grey) the vessel is slowly widening, but at the same time the top and bottom are slowly collapsing towards a single point (figure-of-eight shape, in blue) after which we have two “normal”-shaped vessels. B) The start of the POC (in red) is defined as the position where plane cross-sections give way to curved ones; exactly the opposite marks the end of the POC. DMV: distal main vessel; PMV: proximal main vessel; SB: side branch

the validation of minimal lumen diameter (MLD), RVD, DS and BA measurements. Their design has already been described in detail<sup>19</sup>. In total, 54 phantom vessel segments of reference diameter 1.40-4.00 mm were evaluated; 33 of them had a stenosis within 3-5 mm of the bifurcation (DS 40.6-80.5%; MLD 0.53-1.96 mm), whereas the rest were free of stenoses (MLD 1.40-4.00 mm). Proximal and distal BA range was 90.4-159° and 39.5-102.9°, respectively. Digital angiograms were acquired on a biplane angiographic

system (Axiom Artis™; Siemens, Forchheim, Germany); all phantoms were filled with 100% Iodixanol 320 (Visipaque™; GE Healthcare, Cork, Ireland) and imaged at 30 frames per second in a 20 cm field of view. Multiple projections were acquired for variable degrees of gantry rotation and angulation. For validation purposes, five 2-D projections including the anteroposterior (AP) projection were employed in multiple combinations. Our reconstruction protocol is shown in **Figure 2**.

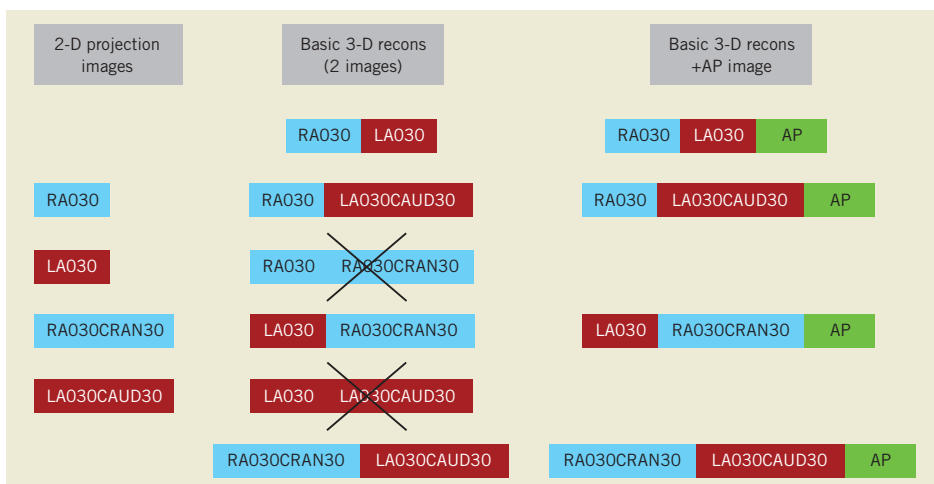


**Figure 2.** 3-D reconstruction protocol. For every phantom bifurcation, four 2-D projection images were combined into four separate 3-D reconstructions using two 2-D images at a time. Two potential combinations were a priori excluded, on the basis of providing limited information. The anteroposterior image (AP) was added to every one of these basic reconstructions, creating a second set of replicate 3-D QCA measurements. RAO/LAO: right/left anterior oblique (rotation); CRAN/CAUD: cranial/caudal angulation

A standard operator procedure for angiographic analysis was followed, wherein: 1) analysis was performed on the middle frame of every angiographic image acquisition; 2) delimiter points were placed at the furthest possible distance from the bifurcation to be analysed, but not touching the adjacent bifurcation lesions or the phantom borders; 3) manual contour correction was not allowed; however, contour detection could be adjusted by using the “restriction” option, thereby excluding gross image artefacts without manually redefining the detected contours<sup>18</sup>; 4) if the location of the automatically defined CIP differed between images, the user could manually reposition it to an easily identifiable landmark, preferably the centre of the bifurcation.

Reconstruction resulted in a 3-D representation of the analysed bifurcation, displayed in the optimal projection, which was defined as the projection where mean foreshortening of the bifurcated vessels was minimised; quantitative analysis was reported according to the validated 11- and 6-segment models (Figure 3)<sup>4,13</sup>. Segments 2, 3 and 5 of either model reflect the segments, where in clinical practice the stent would be placed in the proximal main vessel, distal main vessel and side branch, respectively. MLD, RVD and DS values for these segments were pooled together and compared to the phantom values. Angle calculations are independent of the bifurcation segment model used. Proximal and distal BA values were pooled together and compared to the phantom angles.

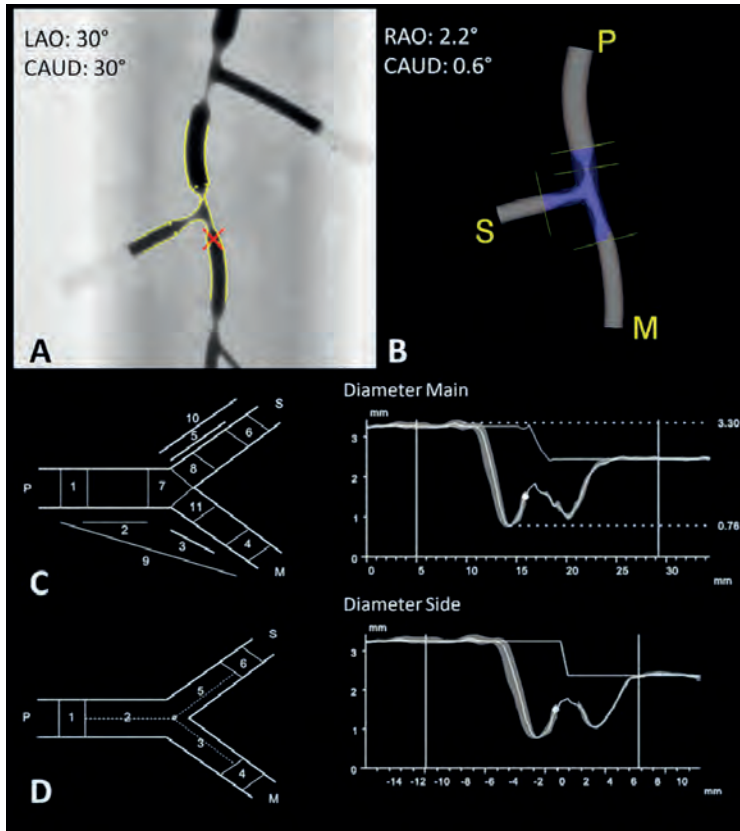


**Figure 3.** 3-D reconstruction and quantitative analysis (compilation). Phantom 2, bifurcation 2 was analysed in two projection images, one acquired at LAO30CAUD30 (A) and one at RAO30CRAN30 (not shown); the red cross indicates the common image point (CIP). B) 3-D reconstruction is shown in the optimal projection; P, M and S stand for PMV, DMV and SB. C) 11-segment model. Left: schematic; right: diameter graph with RVD curve for PMV into DMV. D) 6-segment model. Left: schematic; right: diameter graph with RVD curve for PMV into SB. RVD function is independent of segment model used. In both graphs, automatic reference analysis was applied. RAO/LAO: right/left anterior oblique (rotation); CRAN/CAUD: cranial/caudal angulation

## LENGTH

Due to the lack of reproducibly identifiable markers on the aforementioned bifurcation phantoms, we used a different experimental set-up for the validation of length measurements (Figure 4). Two 5 Fr Cook measurement catheters (Cook Medical, Bloomington, IN, USA) with a marker distance of 10 mm were inserted into a hollow plexiglas bifurcation phantom with an inner diameter of 4.3 mm. Measurement catheters were aligned in the proximal main vessel, one extending into the distal main vessel, the second one extending into the side branch. In order to distinguish between the two branches, a copper marker was mounted on the distal main vessel. The phantom was imaged on the same angiographic system at 30 frames per second in a 25 cm field of view, and the same reconstructions protocol was followed. Within each 3-D reconstruction, 18 inter-marker segments of variable length (ranging from 20 mm up to 80 mm) were measured from leading edge to leading edge, all of these segments covering the central bifurcation region.

All QCA analyses were performed off-line by two experienced analysts (CG, TM), independently from each other.

## STATISTICS

Statistical analysis was performed using SPSS 17.0 for Windows (SPSS Inc., Chicago, IL, USA). Continuous variables are presented as mean  $\pm$  1 standard deviation and compared with the paired-samples

t-test; categorical variables are presented as counts. Replicate measurements reflecting multiple 3-D reconstructions of the same bifurcation were averaged separately for each analyst. The within-segment deviation of these replicate measurements was reported as the measurement error<sup>20</sup> and was integrated in the calculation of the final precision/variability estimates following Bland-Altman methodology<sup>21</sup>.

The first analyst carried out two full rounds of measurements with a time interval of two weeks, in order to determine intra-observer variability. The first round of measurements was compared both with the measurements of the second analyst to determine inter-observer variability and with the corresponding true values for the purpose of validating the software against the ground truth. Bland-Altman analysis was performed for all comparisons<sup>22</sup>.

Regarding intra- and inter-observer comparisons, the mean difference (bias) and its standard deviation were calculated; the repeatability coefficient ( $1.96 \times$  standard deviation) was determined as the measure of variability. For validation purposes, the signed differences between QCA measurements and the true values were averaged: the mean of these signed differences is a measure of accuracy, and the standard deviation is a measure of precision. Measures of accuracy were compared with the paired t-test; measures of precision/variability were compared with the F-test. As the true values were known, we chose to plot these on the X-axis of the Bland-Altman plot against the signed differences and computed the corresponding 95% limits of agreement<sup>22</sup>.

All statistical tests were two-sided and a p-value  $<0.05$  was considered statistically significant.

## Results

### MLD-RVD-DS

Accuracy and precision for 3-D reconstructions of individual phantom bifurcations are shown in Table 1. MLD values for 3-D reconstructions of two projections (basic reconstructions) had an accuracy and precision of  $0.013 \pm 0.131$  mm and  $-0.024 \pm 0.150$  mm for the 11- and 6-segment models, respectively, not being significantly different from phantom values (p-value 0.44 and 0.24). The reference size of phantom vessels was underestimated by an average 0.05 mm in both models, whereas DS estimates did not differ significantly from true values, precision being in the order of 5%. Adding the AP projection to the basic reconstructions resulted in improved precision for MLD, RVD and DS values for the 11-segment model (0.109 mm, 0.031 mm and 4.26%, respectively) (Figure 5); however, improvement did not reach statistical significance for any parameter ( $p > 0.05$ ).

### VARIABILITY

Bias, standard deviation and repeatability coefficient for the basic reconstructions are reported in Table 2. Adding the AP projection to the basic reconstructions resulted in increased inter-observer reproducibility for the 11-segment model, the repeatability coefficient being 0.101 mm for MLD, 0.041 mm for RVD and 3.93% for DS ( $p \leq 0.01$  for every parameter). On the contrary, variability did not change significantly for the 6-segment model ( $p > 0.05$  for every parameter).

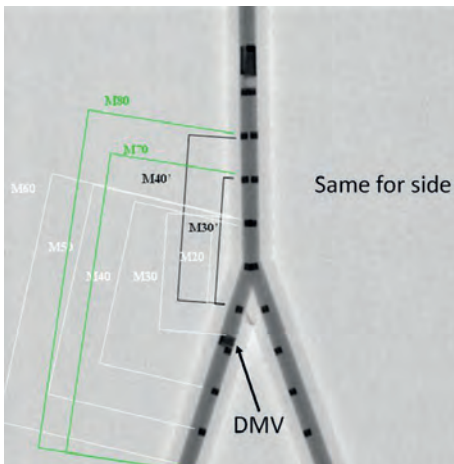


**Figure 4.** Experimental set-up for validation of length measurements. Measurement catheters aligned in a plexiglas bifurcation phantom, one extending into the DMV, the second one extending into the side branch; DMV is identified by a copper marker on the catheter (arrow). Inter-marker segments of variable length are indicated on the DMV side, all of them covering the central bifurcation region. The same segments were defined and measured on the second catheter as well. DMV: distal main vessel

**Table 1. Validation of segment models vs. phantom dimensions (3-D reconstructions of individual bifurcations).**

		2 images (basic)			3 images			p-value		
		Accuracy	Measurement error	Precision	Accuracy	Measurement error	Precision	Basic vs. phantom	3 images vs. phantom	Basic vs. 3 images*
BSM11	MLD, mm	0.013	0.044	0.131	0.003	0.039	0.109	0.44	0.84	0.07 (0.09)
	RVD, mm	-0.052	0.023	0.039	-0.055	0.016	0.031	<0.001	<0.001	0.07 (0.06)
	DS, %	-1.08	1.68	5.13	-0.79	1.46	4.26	0.11	0.16	0.18 (0.09)
BSM6	BA, °	-1.3	3.0	5.0	-1.9	3.1	5.4	0.09	0.02	0.15 (0.33)
	MLD, mm	-0.024	0.041	0.150	-0.031	0.041	0.159	0.24	0.15	0.09 (0.34)
	RVD, mm	-0.051	0.024	0.039	-0.054	0.016	0.032	<0.001	<0.001	0.06 (0.08)
	DS, %	0.22	1.52	4.85	0.37	1.62	5.04	0.73	0.58	0.41 (0.39)
	BA, °	-1.3	3.0	5.0	-1.9	3.1	5.4	0.09	0.02	0.15 (0.33)

BA: bifurcation angle; BSM: bifurcation segment model; DS: percent diameter stenosis; MLD: minimal lumen diameter; RVD: reference vessel diameter. \* values relate to the comparison between accuracy measures, values in parentheses relate to the comparison between precision measures.

**Table 2. Intra- and inter-observer variability in basic 3-D reconstructions of individual bifurcations.**

	Intra-BSM11			Intra-BSM6			Inter-BSM11			Inter-BSM6		
	bias	SD	repeat	bias	SD	repeat	bias	SD	repeat	bias	SD	repeat
MLD, mm	0.002	0.062	0.121	0	0.053	0.104	0.006	0.072	0.141	-0.002	0.058	0.114
RVD, mm	0	0.029	0.056	0	0.029	0.057	0.004	0.030	0.058	0.004	0.028	0.054
DS, %	-0.08	2.36	4.64	-0.01	1.96	3.84	-0.18	2.76	5.42	0.10	2.08	4.07
BA, °	0.0	4.0	7.8	0.0	4.0	7.8	0.1	3.8	7.5	0.1	3.8	7.5

BA: bifurcation angle; BSM: bifurcation segment model; DS: percent diameter stenosis; MLD: minimal lumen diameter; repeat: repeatability coefficient; RVD: reference vessel diameter; SD: standard deviation

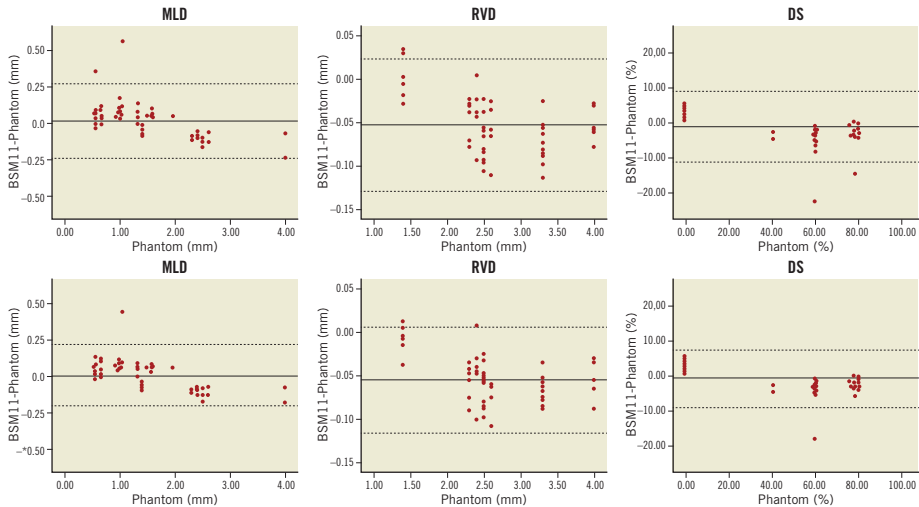


**Figure 5. Bland-Altman plots comparing 11-segment model results to the phantom values. 3-D reconstructions combining two (upper panel) or three 2-D images (lower panel) were validated for measures of minimal lumen diameter (MLD), reference vessel diameter (RVD) and percent diameter stenosis (DS). Automatic reference obstruction analysis was always used. Solid lines represent the mean difference; dotted lines represent the 95% limits of agreement ( $\pm 1.96$  SD). BSM11: 11-segment model**

## INTER-MODEL AGREEMENT

In basic reconstructions, the 11-segment model provided significantly larger ( $p=0.02$ ) and slightly more precise ( $p=0.16$ ) MLD values compared to the 6-segment model; as expected, DS estimates were significantly smaller ( $p=0.02$ ) and also more precise ( $p=0.34$ ). However, the 6-segment model had a higher inter-observer reproducibility for DS and MLD ( $p$ -value 0.02 and 0.11, respectively). Adding the AP projection augmented the difference in precision in favour of the 11-segment model for MLD ( $p<0.01$ ) and DS ( $p=0.11$ ) values; there was also a trend towards higher reproducibility compared to the 6-segment model ( $p>0.05$  for both MLD and DS).

## BA

Basic 3-D reconstructions underestimated BA by  $1.3^\circ$  ( $p=0.09$ ) having a precision of  $5.0^\circ$  (Table 2). Intra- and inter-observer bias was close to zero, whereas the repeatability coefficient was  $7.8^\circ$  and  $7.5^\circ$ , respectively. Adding the AP projection resulted in a larger underestimation ( $-1.9^\circ$ ,  $p=0.02$ ) and slightly reduced precision ( $5.4^\circ$ ,  $p=0.33$ ) (Figure 6), whereas inter-observer variability was  $7.9^\circ$  ( $p=0.38$ ).

During the analysis the rates of applying restriction were uniformly low, namely 3.9% for reconstructions using either two or three images. The rates of CIP relocation were low for basic 3-D reconstructions (11.1%), whereas they were higher for reconstructions of

three projections (31.0%). The CIP had to be relocated most frequently in reconstructions using angulated views.

## LENGTH MEASUREMENTS

Compared to true inter-marker distances ( $46.67\pm 19.40$  mm), basic reconstructions showed an accuracy and precision of  $0.15\pm 0.26$  mm and a measurement error of 0.23 mm; inter-observer bias was 0.07 mm, whereas variability was 0.54 mm. Adding the AP projection resulted in an accuracy and precision of  $0.04\pm 0.47$  mm ( $p<0.01$  for precision) and a measurement error of 0.50 mm; inter-observer variability was increased (1.03 mm,  $p<0.01$ ). Relatively large variability between replicate measurements compared to the overall precision estimates resulted in apparently wide limits of agreement around the averaged length values (Figure 6). Nevertheless, both precision and measurement error were negligible when compared with true inter-marker distances.

## Discussion

The main findings of this study are: 1) the new 3-D bifurcation QCA algorithm is highly accurate, precise and reproducible in terms of RVD; 2) in terms of MLD and DS, 3-D reconstructions using two 2-D projections are highly accurate and quite precise and reproducible; when adding a third projection, a higher level of precision and reproducibility is achieved; 3) BA measurements slightly

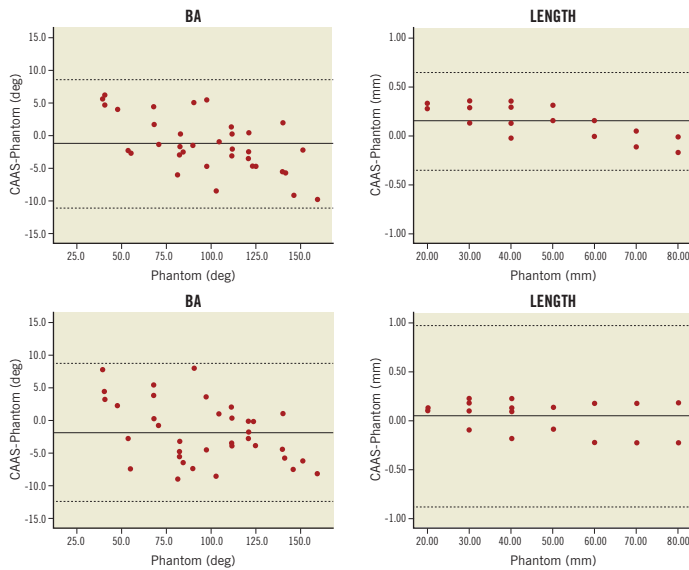


**Figure 6.** Bland-Altman plots for BA values and length measurements. 3-D reconstructions combining two (upper panel) or three 2-D images (lower panel) were employed. Solid lines represent the mean difference; dotted lines represent the 95% limits of agreement ( $\pm 1.96$  SD). Apparently wide limits of agreement for length measurements resulted from the relatively large variability between replicate measurements compared to the overall precision.

underestimate the true values, though precision and reproducibility are quite high and relatively unaffected by adding a third projection; 4) length measurements have excellent accuracy and precision and high reproducibility.

A number of major randomised trials are under way in the field of bifurcation PCI. The EXCEL trial will evaluate the effectiveness of left main coronary artery revascularisation comparing PCI using second-generation drug-eluting stents to coronary artery bypass grafting. Bifurcation lesions are expected to represent the largest category of lesions treated<sup>23</sup>. On the other hand, TRYTON will evaluate the safety and effectiveness of a dedicated bifurcation stent in the treatment of *de novo* bifurcation lesions. Whereas workhorse angiographic analysis is going to be based on 2-D QCA, 3-D QCA is involved in the evaluation of a sizeable number of patients. Hence, validation of the software's performance is imperative.

### DIAMETER-DERIVED PARAMETERS

Earlier versions of 3-D reconstruction software were validated for measures of vessel diameter in the late 1990s; full coronary tree reconstruction, however, came at the cost of fair accuracy (3%-7% relative error in calculation) and increased time requirements (several hours down to 10 minutes)<sup>24,25</sup>. Next-generation algorithms focused on the reconstruction of single-vessel segments rather than entire coronary arteries, thereby enabling reliable results to be available in real time<sup>7-10,26</sup>.

Achieving similar results in the 3-D reconstruction of coronary bifurcations is not a trivial task. For any given bifurcation there is usually one single optimal projection<sup>1</sup>. It follows that in any other projection certain parts of the anatomy, usually the ostia of the daughter branches, are obscured due to overlap. The new algorithm can retrieve missing information even from a combination of sub-optimal views<sup>14</sup>; however, a reconstruction including the optimal 2-D projection would be expected to be even more robust.

In our study, the basic 3-D reconstructions did not include the AP view, which was the optimal 2-D view due to the phantoms' orientation. Nevertheless, compared to analysis performed on the same phantom bifurcations using 2-D CAAS, 3-D software showed similar accuracy and precision: in images acquired at 30° rotation respective 2-D measures were 0.035±0.10 mm for MLD, -0.004±0.041 mm for RVD and -0.74±4.52% for DS<sup>13</sup>. Moreover, since the same contour detection algorithm was used, the extent of overestimation for small true MLD values (≤0.70 mm) was uniformly limited in both 2-D and 3-D analysis. However, whereas full automatic calibration was readily available in 3-D QCA, for the purpose of 2-D validation the pixel size had to be derived off-line based on geometric calibration. Contrary to our phantoms, the course of coronary vessels does not usually lie on a single plane inside the human thorax. Hence, vessel segments analysed on a 2-D angiographic image are subject to errors from variable magnification, since an automatically derived pixel size can be valid on only one plane<sup>10</sup>. Naturally the same phenomenon applies to catheter calibration as well.

Adding the AP view to the basic 3-D reconstructions resulted in improved precision and reproducibility for all diameter-derived

parameters in our study. One may argue that combining more than two 2-D images is rarely feasible at any stage during a procedure, at least not retrospectively, as there are simply not enough images available which are also suitable for a 3-D reconstruction<sup>27</sup>. However, when used on-line, this innovation can be clinically relevant. Even if the optimal view is not among the images initially acquired, it can be suggested by a 3-D reconstruction based on two suboptimal views; time requirements (<10 sec for reconstruction of two images, <60 sec for three images) should not be an issue. However, limitations imposed by patient anatomy (vessel overlap) or proximity between the gantry and the patient/table may make it difficult to acquire the optimal view exactly as suggested<sup>10</sup>.

### RVD-DS

Highly accurate, precise and reproducible RVD measurements were achieved by combining a validated algorithm for automatic RVD derivation in bifurcation lesions with genuine 3-D calculations. Thereby, instead of performing a tedious and arbitrary single-vessel analysis for all three branches separately, RVD and DS values can be derived in the time of a single analysis, having at the same time all the advantages of the 3-D reconstruction. When applied on-line, 3-D QCA-derived information may potentially complement or even substitute invasive imaging modalities in stent sizing and deployment, thereby minimising adverse event rates.

Furthermore, 3-D QCA-derived MLD and DS values for bifurcation lesions should be expected to have a better correlation with respective fractional flow reserve (FFR) values, when compared to 2-D measures<sup>28,29</sup>. It is not implied that a single angiographic measure can fully reflect all anatomic and haemodynamic parameters that determine the functional significance of a lesion<sup>30</sup>; however, we believe that spatially accurate measurements will help improve periprocedural strategy in bifurcation PCI.

### SEGMENT MODELS

Agreement between models in the new software looks diminished compared to 2-D validation; however, the difference in results for MLD and DS was largely driven by a small number of outliers in MLD detection, resulting from different segment definitions between models<sup>13</sup>. Cases where the MLD was located in the POC rather than segments 2, 3 or 5 resulted in overestimates for the 11-segment model. On the contrary, cases where a stenosis-free proximal main vessel impinged on a distal stenosis resulted in underestimates for the 6-segment model. Similar differences were already observed in 2-D analysis, only to be inflated in the process of 3-D reconstruction. The fact remains that the 6-segment model offers a quick overview of results during a procedure, whereas the 11-segment model is more of a research tool providing more detailed information. Nevertheless, it appears that the algorithms are not mutually interchangeable when it comes to long-term angiographic analysis: whichever algorithm is adopted for reporting results pre- and post-procedure would have to be used at follow-up as well.

### BA

Angle calculations have recently gained attention due to growing evidence that wider distal BA values might lead to a worse outcome, especially with two-stent techniques<sup>27,31,32</sup>. To our knowledge, there

is a single validation study on 3-D derived BA reporting an underestimation of the phantom values by 2.6° and a standard error of the estimate equal to 0.77<sup>25</sup>. In our study, BA accuracy and precision were improved compared to the 2-D QCA software validation (-3.1±6.2° in rotated views), which was not unexpected. This difference might have been more pronounced if our phantom bifurcations had lain in more than one plane. This could also explain the lack of improvement seen following the addition of the optimal view. Currently, there is a binary approach regarding BA size: several cut-off values (50°, 70°) have been proposed; however, definitions and measurement methods are still at variance. Pending more detailed data from 3-D QCA-based computations regarding the effect of BA on outcome, precision of 5.0° is considered high.

#### LENGTH

One of the most acknowledged advantages of 3-D QCA is its accuracy in length derivation. Foreshortening in 2-D analysis may result in erroneous sizing and deployment of stents. This could translate either into incomplete lesion coverage and the need for additional stents or into excessive stent length, jailing of a side branch and increased restenosis rates<sup>33</sup>. This is why length measurements have the most comprehensive validation. Demarcated wires<sup>8</sup>, wire phantoms<sup>10</sup>, stent balloons<sup>9</sup> or stented coronary segments, identified by radio-opaque markers<sup>34</sup>, and 3-D reconstructions based on fusion of angiography and intravascular ultrasound<sup>26</sup> have all been used as a gold standard. In our study, length measurements were performed on demarcated catheter segments spanning the phantom bifurcation, thereby proving that they are consistent and impervious to bifurcation region definitions. Variability, albeit negligible, is assumed to correlate with the marker placement procedure, which was not automated but relied on the analysts' visual perception.

#### LIMITATIONS

*In vitro* validation has the obvious limitation of being based on static objects, acquired under ideal angiographic conditions. In our phantom bifurcations, lesions were circular-shaped in cross-sectional view for design simplicity and due to manufacturing constraints<sup>19</sup>. On the contrary, more than 50% of coronary lesions are asymmetric, where 2-D analysis is known to be inaccurate<sup>35</sup>. Furthermore, as opposed to straight phantom vessel segments, coronary vessels usually have curved trajectories, which augment the effect of foreshortening in 2-D projection images<sup>10,11</sup>. Taking the calibration issues already mentioned into account, we have to assume that the incremental value of 3-D bifurcation QCA as compared to 2-D analysis may have been underestimated.

Recently, minimal lumen area and percent area stenosis were shown to have a higher power for predicting reduced FFR values, when compared to the respective diameter-derived parameters<sup>29</sup>. In our study only diameter-derived measures were reported. However, due to the symmetric design of the phantom bifurcation lesions and because of the circularity assumption in diameters' derivation from respective cross-sectional areas, our findings are transferable to area-derived parameters as well.

#### Conclusions

The new dedicated 3-D bifurcation QCA software allows angiographic reconstructions of more than two 2-D projection images, and features novel 3-D quantitative analysis of bifurcation lesions. These advances translate into accurate, precise and reproducible measures of diameter, length and bifurcation angle. There is still work to be done regarding the *in vivo* validation of this software, in order to determine the clinical relevance of these data.

#### Conflict of interest statement

JP. Aben and S. Soekhradjare are employees of Pic Medical Imaging. MA. Morel is an employee of Cardialyis BV. The other authors have no conflicts of interest to declare.

#### References

1. Lansky A, Tuinburg J, Costa M, Maeng M, Koning G, Popma J, Cristea E, Gavit L, Costa R, Rares A, Van Es GA, Lefevre T, Reiber H, Louvard Y, Morice MC; European Bifurcation Angiographic Subcommittee. Quantitative angiographic methods for bifurcation lesions: a consensus statement from the European Bifurcation Group. *Catheter Cardiovasc Interv.* 2009;73:258-66.
2. Girasis C, Onuma Y, Schuurbiens JC, Morel MA, van Es GA, van Geuns RJ, Wentzel JJ, Serruys PW. 5<sup>th</sup> meeting of the European Bifurcation Club. Validity and variability in visual assessment of stenosis severity in phantom bifurcation lesions: a survey in experts during the fifth meeting of the European Bifurcation Club. *Catheter Cardiovasc Interv.* 2012;79:361-8.
3. Finet G, Gilard M, Perrenot B, Rioufol G, Motreff P, Gavit L, Prost R. Fractal geometry of arterial coronary bifurcations: a quantitative coronary angiography and intravascular ultrasound analysis. *EuroIntervention.* 2008;3:490-8.
4. Girasis C, Schuurbiens JC, Onuma Y, Aben JP, Weijers B, Boersma E, Wentzel JJ, Serruys PW. Two-dimensional quantitative coronary angiographic models for bifurcation segmental analysis: in vitro validation of CAAS against precision manufactured plexiglas phantoms. *Catheter Cardiovasc Interv.* 2011;77:830-9.
5. Tuinburg JC, Koning G, Rares A, Janssen JP, Lansky AJ, Reiber JH. Dedicated bifurcation analysis: basic principles. *Int J Cardiovasc Imaging.* 2011;27:167-74.
6. Green NE, Chen SY, Hansgen AR, Messenger JC, Groves BM, Carroll JD. Angiographic views used for percutaneous coronary interventions: a three-dimensional analysis of physician-determined vs. computer-generated views. *Catheter Cardiovasc Interv.* 2005;64:451-9.
7. Ramcharitar S, Daeman J, Patterson M, van Geuns RJ, Boersma E, Serruys PW, van der Giessen WJ. First direct in vivo comparison of two commercially available three-dimensional quantitative coronary angiography systems. *Catheter Cardiovasc Interv.* 2008;71:44-50.
8. Agostoni P, Biondi-Zoccai G, Van Langenhove G, Cornelis K, Vermeersch P, Convens C, Vassanelli C, Van Den Heuvel P, Van Den Branden F, Verhey S. Comparison of assessment of native coronary arteries by standard versus three-dimensional coronary angiography. *Am J Cardiol.* 2008;102:272-9.

9. Rittger H, Schertel B, Schmidt M, Justiz J, Brachmann J, Sinha AM. Three-dimensional reconstruction allows accurate quantification and length measurements of coronary artery stenoses. *EuroIntervention*. 2009;5:127-32.
10. Tu S, Koning G, Jukema W, Reiber JH. Assessment of obstruction length and optimal viewing angle from biplane X-ray angiograms. *Int J Cardiovasc Imaging*. 2010;26:5-17.
11. Dvir D, Assali A, Lev El, Ben-Dor I, Battler A, Kornowski R. Percutaneous interventions in unprotected left main lesions: novel three-dimensional imaging and quantitative analysis before and after intervention. *Cardiovasc Revasc Med*. 2010;11:236-40.
12. Galassi AR, Tomasello SD, Capodanno D, Seminara D, Canonico L, Occhipinti M, Tamburino C. A novel 3D reconstruction system for the assessment of bifurcation lesions treated by the mini-crush technique. *J Interv Cardiol*. 2010;23:46-53.
13. Girasis C, Schuurbijs JC, Onuma Y, Aben JP, Weijers B, Morel MA, Wentzel JJ, Serruys PW. Advances in two-dimensional quantitative coronary angiographic assessment of bifurcation lesions: improved small lumen diameter detection and automatic reference vessel diameter derivation. *EuroIntervention*. 2012;7:1326-35.
14. Onuma Y, Girasis C, Aben JP, Sarno G, Piazza N, Lokkerbol C, Morel MA, Serruys PW. A novel dedicated 3-dimensional quantitative coronary analysis methodology for bifurcation lesions. *EuroIntervention*. 2011;7:629-35.
15. Lorensen W, Cline H. Marching cubes: a high resolution 3D surface construction algorithm. *Computer Graphics*. 1987;21:163-9.
16. Ramcharitar S, Onuma Y, Aben JP, Consten C, Weijers B, Morel MA, Serruys PW. A novel dedicated quantitative coronary analysis methodology for bifurcation lesions. *EuroIntervention*. 2008;3:553-7.
17. Sethian J. Level Set Methods and Fast Marching Methods: Evolving Interfaces in Computational Geometry, Fluid Mechanics, Computer Vision, and Materials Science. Cambridge: Cambridge University Press; 1999.
18. Gronenschild E, Janssen J, Tijdens F. CAAS. II: A second generation system for off-line and on-line quantitative coronary angiography. *Cathet Cardiovasc Diagn*. 1994;33:61-75.
19. Girasis C, Schuurbijs JC, Onuma Y, Serruys PW, Wentzel JJ. Novel bifurcation phantoms for validation of quantitative coronary angiography algorithms. *Catheter Cardiovasc Interv*. 2011;77:790-7.
20. Bland JM, Altman DG. Measurement error. *BMJ*. 1996;313:744.
21. Bland JM, Altman DG. Measuring agreement in method comparison studies. *Stat Methods Med Res*. 1999;8:135-60.
22. Bland JM, Altman DG. Statistical methods for assessing agreement between two methods of clinical measurement. *Lancet*. 1986;1:307-10.
23. Stone GW. Motivation, objective and implication of EXCEL study. Presented at: Transcatheter Therapeutics Asia Pacific; April 28, 2010; Seoul, South Korea.
24. Wellhofer E, Wahle A, Mugaragu I, Gross J, Oswald H, Fleck E. Validation of an accurate method for three-dimensional reconstruction and quantitative assessment of volumes, lengths and diameters of coronary vascular branches and segments from biplane angiographic projections. *Int J Card Imaging*. 1999;15:339-53; discussion 355-6.
25. Messenger JC, Chen SY, Carroll JD, Burchenal JE, Kioussopoulos K, Groves BM. 3D coronary reconstruction from routine single-plane coronary angiograms: clinical validation and quantitative analysis of the right coronary artery in 100 patients. *Int J Card Imaging*. 2000;16:413-27.
26. Schuurbijs JC, Lopez NG, Ligthart J, Gijzen FJ, Dijkstra J, Serruys PW, Van der Steen AF, Wentzel JJ. In vivo validation of CAAS QCA-3D coronary reconstruction using fusion of angiography and intravascular ultrasound (ANGUS). *Catheter Cardiovasc Interv*. 2009;73:620-6.
27. Girasis C, Serruys PW, Onuma Y, Colombo A, Holmes DR Jr, Feldman TE, Bass EJ, Leadley K, Dawkins KD, Morice MC. 3-Dimensional bifurcation angle analysis in patients with left main disease: a substudy of the SYNTAX trial (SYNERgy Between Percutaneous Coronary Intervention with TAXus and Cardiac Surgery). *JACC Cardiovasc Interv*. 2010;3:41-8.
28. Sarno G, Garg S, Onuma Y, Girasis C, Tonino P, Morel MA, van Es GA, Pijls N, Serruys PW. Bifurcation lesions: Functional assessment by fractional flow reserve vs. anatomical assessment using conventional and dedicated bifurcation quantitative coronary angiogram. *Catheter Cardiovasc Interv*. 2010;76:817-23.
29. Yong AS, Ng AC, Brieger D, Lowe HC, Ng MK, Kritharides L. Three-dimensional and two-dimensional quantitative coronary angiography, and their prediction of reduced fractional flow reserve. *Eur Heart J*. 2011;32:345-53.
30. Seiler C. Aiming at a disorder's concept by 3D QCA vs. FFR: a case of advanced ballistics. *Eur Heart J*. 2011;32:261-3.
31. Dzavik V, Kharbada R, Ivanov J, Ing DJ, Bui S, Mackie K, Ramsamujh R, Barolet A, Schwartz L, Seidelin PH. Predictors of long-term outcome after crush stenting of coronary bifurcation lesions: importance of the bifurcation angle. *Am Heart J*. 2006;152:762-9.
32. Adriaenssens T, Byrne RA, Dibra A, Iijima R, Mehilli J, Bruskina O, Schomig A, Kastrati A. Culotte stenting technique in coronary bifurcation disease: angiographic follow-up using dedicated quantitative coronary angiographic analysis and 12-month clinical outcomes. *Eur Heart J*. 2008;29:2868-76.
33. Gollapudi RR, Valencia R, Lee SS, Wong GB, Teirstein PS, Price MJ. Utility of three-dimensional reconstruction of coronary angiography to guide percutaneous coronary intervention. *Catheter Cardiovasc Interv*. 2007;69:479-82.
34. Bruining N, Tanimoto S, Otsuka M, Weustink A, Ligthart J, de Winter S, van Mieghem C, Nieman K, de Feyter PJ, van Domburg RT, Serruys PW. Quantitative multi-modality imaging analysis of a bio-absorbable poly-L-lactic acid stent design in the acute phase: a comparison between 2- and 3D-QCA, QCU and QMSCT-CA. *EuroIntervention*. 2008;4:285-91.
35. Serruys PW, Reiber JH, Wijns W, van den Brand M, Kooijman CJ, ten Katen HJ, Hugenholz PG. Assessment of percutaneous transluminal coronary angioplasty by quantitative coronary angiography: diameter versus densitometric area measurements. *Am J Cardiol*. 1984;54:482-8.

## Online data supplement

### APPENDIX

Software validation for full-tree 3-D reconstructions of bifurcation phantoms.

# Online data supplement

## ONLINE APPENDIX

Software validation for full-tree 3-D reconstructions of bifurcation phantoms

This appendix complements the main manuscript “Advanced three-dimensional quantitative coronary angiographic assessment of bifurcation lesions: methodology and phantom validation” and provides the results from additional analyses.

The new three-dimensional (3-D) bifurcation quantitative coronary angiography (QCA) algorithm has no restriction regarding the number of bifurcations the 3-D model consists of; it is possible to reconstruct and analyse a vascular tree which consists of multiple bifurcations.

## Methods

In order to investigate the accuracy, precision and reproducibility of this methodology, we performed full-tree 3-D reconstructions for the entire series of bifurcation phantoms<sup>1</sup>: images acquired at 30° rotation, in right and left anterior oblique (RAO-LAO) projection were combined. The operator procedure for angiographic analysis was amended accordingly, wherein: 1) for every given phantom, delimiter points were placed in the proximal main vessel of the proximal bifurcation, in the distal main vessel of the distal bifurcation and in a side branch of any of the three bifurcations; by default we chose to begin with the side branch of the proximal bifurcation; 2) the remaining side branches were added to the phantom tree (one at a time), by indicating the junction point with the contoured main vessel and a distal delimiter; the first two steps were then repeated in the next image; 3) reconstruction was performed for the entire phantom, and the common image point (CIP) was relocated as appropriate; 4) in the 3-D reconstructed phantoms one bifurcation was selected and analysed at a time (region of interest could be edited in order that analysis was not influenced by adjacent bifurcation lesions); 5) quantitative analysis was performed and reported for minimal lumen diameter (MLD), reference vessel diameter (RVD), percent diameter stenosis (DS) and bifurcation angles (BAs) as described in the main manuscript. Results were compared with the true phantom values and with separate 3-D reconstructions of individual bifurcations using the same combinations of images (30° RAO-LAO).

## Results

### MLD-RVD-DS

Accuracy and precision for full-tree and individual 3-D reconstructions are shown in **Table 1**. MLD values for full-tree reconstructions had an accuracy and precision of 0.012±0.135 mm and -0.021±0.155 mm for the 11- and 6-segment models, respectively, not being significantly different from phantom values (p-value 0.51 and 0.33). The reference size of phantom vessels was underestimated by an average 0.06 mm in both models, whereas DS estimates did not significantly differ from true values, precision being in the order of 5%. Accuracy and precision did not differ significantly between full-tree and individual reconstructions.

Inter-observer variability for 11- and 6-segment models was 0.146/0.155 mm for MLD, 0.038/0.039 mm for RVD and 5.59/5.41% for DS values.

The 11-segment model was more accurate (p=0.05) and precise (p=0.16) for MLD, while the 6-segment model was more accurate (p=0.04) for DS values; difference in DS precision was not significant (p=0.47).

### BA

Full-tree 3-D reconstructions underestimated BA by 2.1° (p=0.01) having a precision of 4.7°; individual reconstructions had slightly increased accuracy (-0.9°, p=0.16) but equal precision. Inter-observer bias was 0.7°, whereas the repeatability coefficient was 8.8°.

## SUMMARY

The performance of the new 3-D bifurcation QCA software in full-tree reconstructions of the bifurcation phantoms was comparable, but slightly inferior to the results attained from reconstructions performed separately for each individual phantom bifurcation.

## Reference

1. Girasis C, Schuurbiens JC, Onuma Y, Serruys PW, Wentzel JJ. Novel bifurcation phantoms for validation of quantitative coronary angiography algorithms. *Catheter Cardiovasc Interv*. 2011;77:790-7.

**Table 1. Validation of segment models vs. phantom dimensions (full-tree 3-D reconstructions of bifurcation phantoms).**

		Full-tree		Individual		p-value		
		Accuracy	Precision	Accuracy	Precision	Full-tree vs. phantom	Individual vs. phantom	Full-tree vs. individual*
BSM11	MLD, mm	0.012	0.135	0.001	0.118	0.51	0.97	0.30 (0.17)
	RVD, mm	-0.059	0.037	-0.056	0.040	<0.001	<0.001	0.29 (0.29)
	DS, %	-1.18	5.25	-0.71	4.75	0.10	0.28	0.25 (0.23)
BSM6	MLD, mm	-0.021	0.155	-0.038	0.146	0.33	0.06	0.07 (0.33)
	RVD, mm	-0.058	0.037	-0.056	0.041	<0.001	<0.001	0.27 (0.23)
	DS, %	0.04	5.20	0.67	4.80	0.96	0.31	0.12 (0.28)

BSM: bifurcation segment model; DS: percent diameter stenosis; MLD: minimal lumen diameter; RVD: reference vessel diameter. \*values relate to the comparison between accuracy measures, values in parentheses relate to the comparison between precision measures.



### 3.2 Virtual functional assessment of coronary artery narrowings using 3D-QCA

Fast virtual functional assessment of intermediate coronary lesions using routine angiographic data and blood flow simulation in humans: comparison with pressure wire-fractional flow reserve.

*Eurointervention.* 2014;10:574-83.

[Original research paper, Impact Factor (2013): 3.758]

Papafaklis MI, Muramatsu T\*, Ishibashi Y, Lakkas LS, Nakatani S, Bourantas CV, Ligthart JM, Onuma Y, Echavarría-Pinto M, Tsirka G, Kotsia A, Nikas DN, Mogabgab O, van Geuns RJ, Naka KK, Fotiadis DI, Brilakis ES, Garcia-Garcia HM, Escaned J, Zijlstra F, Michalis LK, Serruys PW.

\* Equally contributed to the first author





# Fast virtual functional assessment of intermediate coronary lesions using routine angiographic data and blood flow simulation in humans: comparison with pressure wire – fractional flow reserve

Michail I. Papafaklis<sup>1,2</sup>, MD, PhD, FESC; Takashi Muramatsu<sup>3</sup>, MD; Yuki Ishibashi<sup>3</sup>, MD; Lampros S. Lakkas<sup>1</sup>, MD; Shimpei Nakatani<sup>3</sup>, MD; Christos V. Bourantas<sup>3</sup>, MD, PhD; Jurgen Ligthart<sup>3</sup>, BSc; Yoshinobu Onuma<sup>3</sup>, MD, PhD; Mauro Echavarría-Pinto<sup>4</sup>, MD; Georgia Tsirka<sup>1</sup>, MD; Anna Kotsia<sup>5</sup>, MD; Dimitrios N. Nikas<sup>1</sup>, MD, PhD, FESC; Owen Mogabgab<sup>5</sup>, MD; Robert-Jan van Geuns<sup>3</sup>, MD, PhD; Katerina K. Naka<sup>1</sup>, MD, PhD, FESC; Dimitrios I. Fotiadis<sup>6</sup>, PhD; Emmanouil S. Brilakis<sup>5</sup>, MD, PhD; Héctor M. García-García<sup>3</sup>, MD, PhD; Javier Escaned<sup>4</sup>, MD, PhD, FESC; Felix Zijlstra<sup>3</sup>, MD, PhD; Lampros K. Michalis<sup>1</sup>, MD, MRCP, FESC; Patrick W. Serruys<sup>3,7\*</sup>, MD, PhD, FESC

1. Department of Cardiology, Medical School, University of Ioannina, Ioannina, Greece; 2. Harvard-MIT Division of Health Sciences and Technology, Massachusetts Institute of Technology, Cambridge, MA, USA; 3. Thoraxcenter, Erasmus Medical Centre, Rotterdam, The Netherlands; 4. San Carlos University Hospital, Madrid, Spain; 5. Veterans Administration North Texas Healthcare System and University of Texas Southwestern Medical School, Dallas, TX, USA; 6. Department of Materials Science and Engineering, University of Ioannina, Ioannina, Greece; 7. International Centre for Circulatory Health, National Heart and Lung Institute, Imperial College London, London, United Kingdom

M.I. Papafaklis and T.Muramatsu contributed equally to this work.

GUEST EDITOR: Nicolas Foin, MSc, PhD; National Heart Centre, Singapore

This paper also includes accompanying supplementary data published online at: [http://www.pronline.com/eurointervention/76th\\_issue/100](http://www.pronline.com/eurointervention/76th_issue/100)

## KEYWORDS

- computational fluid dynamics
- fractional flow reserve
- functional assessment
- quantitative coronary angiography

## Abstract

**Aims:** To develop a simplified approach of virtual functional assessment of coronary stenosis from routine angiographic data and test it against fractional flow reserve using a pressure wire (wire-FFR).

**Methods and results:** Three-dimensional quantitative coronary angiography (3D-QCA) was performed in 139 vessels (120 patients) with intermediate lesions assessed by wire-FFR (reference standard:  $\leq 0.80$ ). The 3D-QCA models were processed with computational fluid dynamics (CFD) to calculate the lesion-specific pressure gradient ( $\Delta P$ ) and construct the  $\Delta P$ –flow curve, from which the virtual functional assessment index (vFAI) was derived. The discriminatory power of vFAI for ischaemia-producing lesions was high (area under the receiver operator characteristic curve [AUC]: 92% [95% CI: 86–96%]). Diagnostic accuracy, sensitivity and specificity for the optimal vFAI cut-point ( $\leq 0.82$ ) were 88%, 90% and 86%, respectively. Virtual-FAI demonstrated superior discrimination against 3D-QCA–derived % area stenosis (AUC: 78% [95% CI: 70–84%];  $p < 0.0001$  compared to vFAI). There was a close correlation ( $r = 0.78$ ,  $p < 0.0001$ ) and agreement of vFAI compared to wire-FFR (mean difference:  $-0.0039 \pm 0.085$ ,  $p = 0.59$ ).

**Conclusions:** We developed a fast and simple CFD-powered virtual haemodynamic assessment model using only routine angiography and without requiring any invasive physiology measurements/hyperaemia induction. Virtual-FAI showed a high diagnostic performance and incremental value to QCA for predicting wire-FFR; this “less invasive” approach could have important implications for patient management and cost.

\*Corresponding author: International Centre for Circulatory Health, National Heart and Lung Institute, Imperial College London, London, United Kingdom. E-mail: [patrick.w.j.c.serruys@gmail.com](mailto:patrick.w.j.c.serruys@gmail.com)

© Europa Digital & Publishing 2014. All rights reserved.

SUBMITTED ON 26/05/2014 - REVISION RECEIVED ON N/A - EHI Transfer - ACCEPTED ON 17/06/2014

## Introduction

Measurement of the fractional flow reserve (FFR) in the catheterisation laboratory has become the gold standard for assessing the haemodynamic significance of intermediate stenoses<sup>1,2</sup>. FFR reliably identifies ischaemia-producing lesions and improves clinical decision making as well as patient outcomes when used for PCI guidance<sup>3-5</sup>. However, FFR assessment requires insertion of a costly pressure-sensor guidewire in the coronary artery and administration of a vasodilator for inducing hyperaemia, which, among other factors, may contribute to the low adoption rate of FFR in clinical practice (<10% of intermediate stenoses evaluated by FFR in the recent US CathPCI Registry)<sup>6</sup>.

While obstructive coronary anatomy is directly linked to haemodynamic sequelae and, consequently, the production of ischaemia/anginal symptoms in patients, the accuracy of stand-alone anatomic measures (e.g., %diameter stenosis [%DS]) derived from invasive angiography or coronary computed tomographic angiography [CCTA]) is limited when assessing the functional significance of stenoses<sup>7,8</sup>. This is not surprising given the multitude of geometric features along with the specific flow rate that contribute to the calculation of the translational pressure gradient as initially observed by Gould<sup>9</sup> and Young<sup>10</sup>. Physiology models for the coronary circulation using basic principles of physics have been proposed previously; early efforts attempted to use simplified coronary artery dimensions assessed by quantitative arteriography for computing pressure gradients at pre-specified flow rates, thereby evaluating the haemodynamics of a stenosis from anatomy<sup>11,12</sup>, while dedicated indices like stenosis flow reserve were also presented<sup>13,14</sup>. Recently, advanced computational fluid dynamics (CFD) techniques have been applied to human CCTA imaging datasets providing a more comprehensive approach; these were shown to enhance the diagnostic performance of CCTA for predicting FFR<sup>15-17</sup>.

In the current report, we extend the previous work and present an approach for fast and simplified virtual functional assessment of coronary stenoses using three-dimensional quantitative coronary angiography (3D-QCA) and blood flow simulation. We test the diagnostic performance of the derived virtual index in a real-world patient population with intermediate lesions that were haemodynamically assessed by a pressure-sensor guidewire (wire-FFR).

## Methods

A detailed description of the methods is included in the [Online Appendix](#).

### PATIENT POPULATION

Patients from four tertiary University Hospitals who underwent coronary angiography and FFR measurements for assessing intermediate lesions were retrospectively included in this study (data spanning from June 2005 to July 2013). Patients presenting with stable or unstable angina or non-ST-elevation myocardial infarction and stenoses in a major epicardial artery (left anterior descending artery [LAD], left circumflex [LCx]/oblique marginal [OM] and right coronary artery [RCA]) were eligible for inclusion in the

study. Exclusion criteria were: significant left main stem disease; vessels with bifurcational lesions; infarct-related vessels; vessels distally protected by bypass grafts; vessels with ostial stenoses; and presence of chronic total occlusions. All lesions included in the study had documented adenosine administration and wire-FFR/pressure recordings, as well as suitable angiographic projections for 3D-QCA (as described in the Methods and the [Online Appendix](#)). The study protocol was approved by the local ethics committees and written informed consent was provided by each patient for using the data for research purposes.

### CARDIAC CATHETERISATION AND WIRE-FFR DATA ACQUISITION

Wire-FFR assessment was performed in vessels with intermediate lesions (30-70 %DS by visual estimation) as clinically indicated at the discretion of the operator. The recording of the position of the pressure wire distally in the coronary artery at the time of wire-FFR assessment was available, and enabled the comparison of the virtual functional assessment against the measured wire-FFR at the same location. Wire-FFR values  $\leq 0.80$  were considered diagnostic of ischaemia<sup>4</sup>.

### QUANTITATIVE CORONARY ANGIOGRAPHY AND BLOOD FLOW SIMULATION

Three-dimensional QCA was performed off-line with the validated CAAS QCA-3D system (Pie Medical Imaging, Maastricht, The Netherlands)<sup>18</sup>. The end-diastolic frames of the best two full-contrast angiographic views (angle difference  $>30^\circ$ ) of the studied artery before insertion of guidewires were used for 3D-QCA reconstruction. Percentage area stenosis (%AS), %DS, minimum luminal area (MLA) and minimum luminal diameter (MLD) were derived from the 3D-QCA model. Additionally, conventional two-dimensional-QCA (2D-QCA) analysis of both projections used in 3D-QCA was performed for calculating max %DS, which may reflect daily practice in the catheterisation laboratory better.

The obtained 3D lumen geometries were further processed with computational fluid dynamics (CFD) techniques for solving the 3D transport equations governing the conservation of mass and momentum. A reference pressure of 100 mmHg (corresponding to the average aortic pressure in humans) was imposed at the inlet. Blood flow was assumed to be laminar and incompressible, and steady flow (fully developed) was specified as boundary condition at the outlet; two separate simulations with a steady flow of 1 and 3 ml/s (approximately corresponding to the average flow at rest and the hyperaemic flow increase in human coronary arteries, respectively)<sup>19,20</sup> were performed. The pressure gradient at these two flow rates was calculated from the difference of the average pressure at the inlet (Pa) and outlet (Pd) of the CFD simulations.

### DATA ANALYSIS AND CALCULATION OF THE VIRTUAL FUNCTIONAL ASSESSMENT INDEX

The simulation results were further processed in order to construct the artery-specific pressure gradient ( $\Delta P$ )–flow relationship which

is characteristic for every coronary obstruction<sup>21</sup>. The computed  $\Delta P$  values at 1 and 3 ml/s were used to define a quadratic equation:  $\Delta P=0+f_v Q+f_s Q^2$  (i.e., zero intercept), where  $\Delta P$  is the pressure gradient (mmHg),  $Q$  is the flow rate (ml/s),  $f_v$  (mmHg s/ml) is the coefficient of pressure loss due to viscous friction and  $f_s$  (mmHg s<sup>2</sup>/ml<sup>2</sup>) is the coefficient of pressure loss due to flow separation<sup>9,11</sup>. From the  $\Delta P-Q$  curve, the relationship of the Pd/Pa ratio vs. flow was calculated. Finally, we calculated the virtual Functional Assessment Index (vFAI) as the ratio of the area, defined by the constant Pd/Pa vs. flow relationship in a normal artery up to 4 ml/s (chosen as a universal and fixed upper limit corresponding approximately to the mean+2SD hyperaemic flow rate increase in normal human coronary arteries starting from an average flow rate of 1 ml/s at rest<sup>20</sup>, although it is an unrealistic hyperaemic flow rate in some subjects as presented in the Supplemental results in the **Online Appendix** and discussed in the limitations section), which is covered by the area of the artery-specific Pd/Pa vs. flow relationship. Note that the numeric value for vFAI as computed here is not mathematically equal to the value for wire-FFR (**Online Appendix** and **Online Figure 1**).

### STATISTICS

The correlation between derived variables (vFAI and anatomic measures) and wire-FFR was investigated using the Pearson ( $r$ ) and Spearman ( $r_s$ ) correlation coefficients. Bland-Altman analysis was performed with wire-FFR as the standard of reference, and the paired t-test was used to test any significant difference between the vFAI and wire-FFR. Receiver operator characteristic (ROC) curve analysis was performed to evaluate the discrimination of vFAI and QCA-derived anatomic measures (e.g., %AS) for predicting wire-FFR  $\leq 0.80$  (reference standard). Diagnostic measures including sensitivity, specificity, positive/negative predictive value and accuracy were calculated, and the optimal cut-off for vFAI and anatomic measures was determined. Except for the patient characteristics, analyses were performed on a per-vessel basis. A two-sided p-value  $< 0.05$  was considered significant.

### Results

CFD processing was successfully completed in all of the selected vessels (mean length of 3D-QCA models: 59.43 $\pm$ 21.01 mm). The average total time required for the procedure, including the extraction of the 3D-QCA anatomy ( $\approx$ 5 minutes), the CFD mesh construction ( $\approx$ 3 minutes) and the CFD computational time ( $\approx$ 7 minutes), was approximately 15 minutes per vessel using an off-the-shelf workstation with a quad-core 2.4 GHz (Intel core i7-3630QM) processor unit (8 GB of RAM). The average time required for the 2D-QCA analysis of the two projections was approximately five minutes/vessel.

### CLINICAL AND LESION CHARACTERISTICS

A total of 139 vessels in 120 patients were studied (**Table 1**). The majority of patients presented with stable disease (65.8%). More than a third of the patients had a prior revascularisation procedure and 31% had a history of prior myocardial infarction.

**Table 1. Characteristics of patients and vessels studied.**

Clinical characteristic	All patients (n=120)
Male gender	87 (72.5%)
Age, years	64.0 $\pm$ 9.6
Dyslipidaemia	78 (65%)
Hypertension	70 (58.3%)
Diabetes mellitus	34 (28.3%)
Current smoker (last 1 year)	33 (27.5%)
History of prior myocardial infarction	37 (30.8%)
History of prior PCI	48 (40%)
History of prior CABG	3 (4.1%)
Peripheral arterial disease	3 (2.5%)
Chronic kidney disease	4 (3.3%)
Clinical presentation	
Stable angina	79 (65.8%)
Unstable angina	33 (27.5%)
Non-ST-elevation myocardial infarction	8 (6.7%)
Vessel disease	
Single-vessel	37 (30.8%)
Two-vessel	39 (32.5%)
Three-vessel	29 (24.2%)
Vessel characteristic	All vessels (n=139)
Vessel studied	
Left anterior descending artery	90 (64.7%)
Left circumflex/obtuse marginal	19 (13.7%)
Right coronary artery	30 (21.6%)
Lesions	
Focal	75 (54%)
Diffuse disease/tandem lesions*	58 (41.7%)
In-stent restenotic	6 (4.3%)

CABG: coronary artery bypass grafting; PCI: percutaneous coronary intervention. \*Diffuse disease was defined as a lumen stenosis with either a length of more than 20 mm or a vessel diameter of  $< 2$  mm at least 75% of the length of the stenosis. Tandem lesions were defined as serial lumen stenoses that were more than 3 vessel reference diameters apart.

The majority of vessels had focal lesions (54%). Mean max %DS by 2D-QCA was 43.4 $\pm$ 11.6%, whereas mean %AS and %DS by 3D-QCA were 61.4 $\pm$ 13.1 and 38.8 $\pm$ 10.9%, respectively. The majority of vessels had 25-50 max %DS by 2D-QCA (n=95; 68%), while there were 37 (27%) with 50-75 max %DS. Wire-FFR assessment showed that there were functionally significant lesions (wire-FFR  $\leq 0.80$ ) in 52 vessels (37%). The majority of cases had a wire-FFR value between 0.70 and 0.90 (n=84; 60%) reflecting the intermediate severity of the lesions studied (median FFR: 0.84 [0.75-0.90]). Computed haemodynamic indices including vFAI as well as QCA-based anatomic measures were significantly different between the two wire-FFR groups ( $\leq 0.80$  vs.  $> 0.80$ ; **Online Table 1**).

### DIAGNOSTIC ACCURACY OF vFAI FOR IDENTIFYING HAEMODYNAMICALLY SIGNIFICANT DISEASE

Discriminatory power of vFAI against wire-FFR was very good (AUC: 91.9% [95% CI: 86.3-96%]), and the optimal cut-point for vFAI was 0.82 (Figure 1). Diagnostic performance based on the optimal vFAI cut-point is listed in Table 2. There were 47 true positives (33.8%), 75 true negatives (54%), 12 false positives (8.6%) and five false negatives (3.6%). Sensitivity, specificity and overall diagnostic accuracy were 90.4%, 86.2% and 87.8%, respectively. A vFAI value above 0.90 had a 100% negative predictive value indicating perfect accuracy for detecting functionally non-significant disease. Representative examples of vessels with and

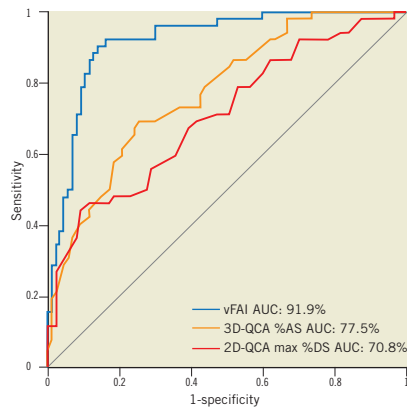


**Figure 1.** Receiver operator characteristic (ROC) curve analysis for the virtual functional assessment index (vFAI) against the fractional flow reserve cut-point ( $\leq 0.80$ ; reference standard). The area under the ROC curve (AUC) was 91.9% (95% CI: 86-96%). The respective AUC for 3D-QCA %area stenosis (%AS; AUC: 77.5% [95% CI: 69.9-84.3%]; values on the ROC curve represent 1-AS) and 2D-QCA max %diameter stenosis (%DS; AUC: 70.8% [95% CI: 62.2-77.9%]; values on the ROC curve represent 1-DS) showed that vFAI had significantly higher discriminatory power ( $p < 0.001$  for both).

**Table 2.** Diagnostic performance of the virtual functional assessment index (vFAI) and the anatomic measures from 3D- and 2D-quantitative coronary angiography (QCA) using the optimal cut-points (receiver operator characteristic curve analysis). Fractional flow reserve ( $\leq 0.80$ ) measured using the pressure wire was used as the reference standard.

Diagnostic measure	vFAI $\leq 0.82$	3D-QCA %AS $> 64\%$	3D-QCA MLA $\leq 1.66 \text{ mm}^2$	3D-QCA %DS $> 41\%$	2D-QCA max %DS $> 51\%$
Diagnostic accuracy	87.8% (81.1-92.7%)	72.7% (64.5-79.9%)	79.1% (71.4-85.6%)	74.1% (66-81.2%)	73.4% (65.2-80.5%)
Sensitivity	90.4% (79-96.8%)	69.2% (54.9-81.3%)	80.8% (67.5-90.4%)	65.4% (50.9-78%)	44.2% (30.5-58.7%)
Specificity	86.2% (77.2-92.7%)	74.7% (64.3-83.4%)	78.2% (68-86.3%)	79.3% (69.3-87.3%)	90.8% (82.7-96%)
Positive predictive value	79.7% (67.2-89%)	62.1% (48.4-74.5%)	68.9% (55.7-80.1%)	65.4% (50.9-78%)	25.8% (11.9-44.6%)
Negative predictive value	93.8% (86.01-97.9%)	80.3% (69.9-88.3%)	87.2% (77.7-93.7%)	79.3% (69.3-87.3%)	73.2% (63.8-81.2%)

Values are presented as estimates (95% CI); %AS: percent area stenosis; %DS: percent diameter stenosis; MLA: minimum lumen area

without ischaemia-producing lesions are illustrated in Figure 2 and Figure 3, respectively (additional data in Online Figure 2).

Although vFAI values are not intended to be mathematically equivalent to wire-FFR values, enforcing the same cut-point ( $\leq 0.80$ ) for vFAI as for wire-FFR yielded only a small decrease in vFAI diagnostic performance: 85.6% accuracy (95% CI: 78.7-91%); 78.8% sensitivity (95% CI: 65.3-88.9%), 89.7% specificity (95% CI: 81.3-95.2%), positive predictive value of 82% (95% CI: 68.6-91.4%) and negative predictive value of 87.6% (95% CI: 79-93.7%).

### DIAGNOSTIC PERFORMANCE OF VIRTUAL FUNCTIONAL ASSESSMENT AGAINST QCA

In our exploratory analyses of diagnostic performance using wire-FFR as the reference standard, vFAI (AUC: 91.9%) demonstrated superior discrimination to QCA anatomic measures: (i) 3D-QCA %AS (AUC: 77.5%;  $p < 0.001$ ; Figure 1), (ii) 3D-QCA MLA (AUC: 83.9%;  $p < 0.001$ ) and (iii) 2D-QCA max %DS (AUC: 70.8%;  $p < 0.001$ ; Figure 1). Of note, 3D-QCA %AS had a borderline trend for superiority against 2D-QCA max %DS ( $p = 0.053$ ).

The optimal vFAI cut-point (0.82) had a higher performance for all diagnostic measures compared to the respective values of the optimal cut-points for %AS ( $> 64\%$ ) and MLA ( $\leq 1.66 \text{ mm}^2$ ) by 3D-QCA, and max %DS ( $> 51\%$ ) by 2D-QCA as presented in Table 2.

### CORRELATION AND AGREEMENT BETWEEN VIRTUAL FUNCTIONAL ASSESSMENT AND WIRE-FFR

There was a close correlation between vFAI and wire-FFR values ( $r = 0.78$ ,  $p < 0.0001$ ;  $r_s = 0.73$ ,  $p < 0.0001$ ; Figure 4A), and the agreement was good (mean difference:  $-0.0039 \pm 0.085$ ,  $p = 0.59$ ; Figure 4B).

### CORRELATION BETWEEN QCA ANATOMIC MEASURES AND WIRE-FFR

There was a weaker correlation between wire-FFR and (i) %AS ( $r = -0.42$ ,  $p < 0.0001$ ;  $r_s = -0.49$ ,  $p < 0.0001$ ), MLA ( $r = 0.53$ ,  $p < 0.0001$ ;  $r_s = 0.61$ ,  $p < 0.0001$ ), %DS ( $r = -0.42$ ,  $p < 0.0001$ ;  $r_s = -0.47$ ,  $p < 0.0001$ ) by 3D-QCA, (ii) max %DS by 2D-QCA ( $r = -0.39$ ,  $p < 0.0001$ ;  $r_s = -0.36$ ,  $p < 0.0001$ ) compared to the correlation of vFAI with wire-FFR (Online Figure 3).

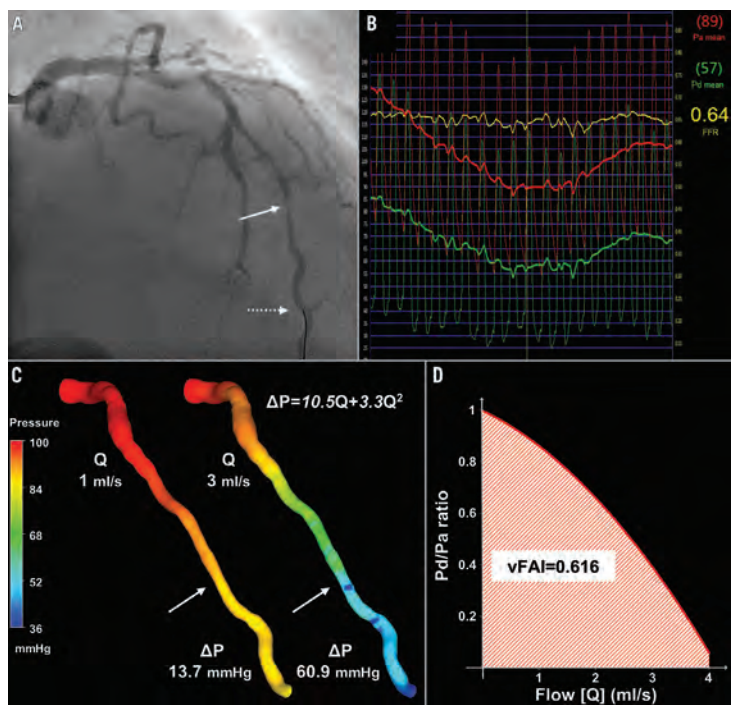


**Figure 2.** Intermediate lesion with haemodynamic significance. (A) Representative example of a left anterior descending artery (LAD) with a moderate lesion (arrow: maximal stenosis) in angiography (3D-QCA %diameter stenosis: 35%) that had (B) a low fractional flow reserve (FFR=0.64) measured at a distal location (dotted arrow) using the pressure wire. (C) 3D-QCA coronary lumen reconstruction with the pressure distribution in a colour-coded map for two different flow rates ( $Q$ ), which resulted in a pressure gradient ( $\Delta P$ ) of 13.7 and 60.9 mmHg. The computed artery-specific  $\Delta P$ - $Q$  relationship is provided. The arrows denote the location of maximal stenosis. (D) Relationship between the ratio of distal to aortic pressure ( $Pd/Pa$ ) and flow for the studied artery, and calculation of the artery-specific virtual functional assessment index (vFAI: 0.62) shows the good agreement with wire-FFR.

#### COMPARISON OF vFAI PRE- AND POST-INTERVENTION

Separate pairwise analysis was performed for post-PCI vFAI assessment in 27 cases with  $FFR \leq 0.80$  (52%) and available suitable post-PCI angiographic projections for 3D-QCA. Post-PCI vFAI was significantly increased compared to the corresponding pre-PCI value ( $0.70 \pm 0.14$  vs.  $0.89 \pm 0.05$ ,  $p < 0.001$ ).

#### Discussion

We have developed a simplified approach for fast virtual functional assessment of diseased coronary arteries using 3D-QCA and CFD modelling based only on routine coronary angiographic data; our workflow does not require any additional patient-specific information and pressure measurements at any stage of the process, enabling both prospective and retrospective physiology assessment. The diagnostic testing of vFAI that we performed in real-world patients with intermediate coronary lesions demonstrated

that this approach has a high diagnostic accuracy, correlates well with wire-FFR showing no bias, yet with wide standard deviation, and presents superior discriminatory power/diagnostic performance against stand-alone 2D/3D-QCA-derived anatomic measures of lesion severity. Our approach can be potentially implemented in any catheterisation laboratory using commercially available 3D-QCA and CFD software without requiring any additional costly systems. Currently, this is the first study testing the application of CFD in conventional angiography for “less invasive” assessment of the haemodynamic significance of coronary stenoses without requiring either the pressure wire or any vasodilator administration.

#### COMPARISON OF vFAI TO PREVIOUS VIRTUAL PHYSIOLOGY MODELS

Early simple and latest advanced physiology models for the coronary circulation have been proposed exploiting the information

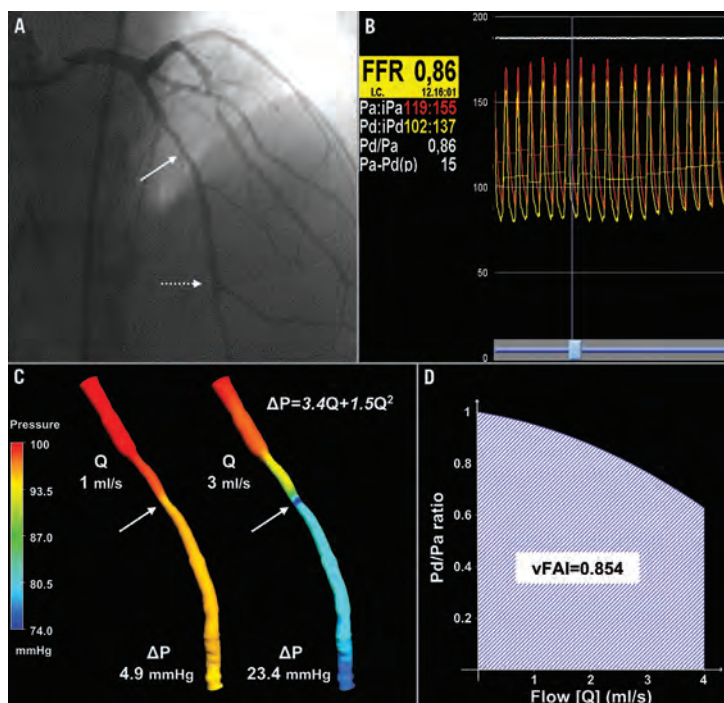


**Figure 3.** Intermediate lesion without haemodynamic significance. (A) Representative example of a LAD with a moderate lesion (arrow: maximal stenosis) in angiography (3D-QCA %diameter stenosis: 51%) that had (B) a high FFR (0.86) measured at a distal location (dotted arrow) using the pressure wire. (C) 3D-QCA coronary lumen reconstruction with the pressure distribution in a colour-coded map for the different flow rates. The arrows denote the location of maximal stenosis. (D) Artery-specific vFAI (0.85) shows good agreement with FFR.

within the images from cardiovascular patients<sup>14-17,22,23</sup>. The current method only requires routine coronary angiographic data for 3D-QCA, proposing a “less invasive” functional assessment without the need for the pressure wire and drug-induced vasodilation as compared to wire-FFR assessment. This is similar to the workflow applied by Morris et al<sup>22</sup> to a very limited sample (Table 3); however, they used rotational coronary angiography for acquiring coronary geometry data, which is both less readily available and more demanding to perform. Additionally, they employed a lumped approach (Windkessel) to model the downstream boundary conditions of resistance, which is based on empirically derived pressure values over the heart cycle (i.e., pulsatile pressure profile), thereby requiring invasive measurements similar to the ones performed during the wire-FFR procedure for optimisation purposes. Furthermore, owing to pulsatile flow CFD simulations, which are much more time-consuming ( $\approx 24$  hrs), their workflow would be hard to implement in the future in an on-line fashion in the catheterisation laboratory. In contrast, we present

a simplified approach taking advantage of fundamental haemodynamic relationships and CFD applications in patient-specific coronary geometries, thus providing fast virtual functional assessment without requiring any additional personalised data, such as pressure measurements, at any stage of the process. Our approach also enables vFAI calculation between any two locations selected along the single artery studied (e.g., as would be required for separate assessment of tandem lesions).

Recently, CCTA-FFR was developed to provide non-invasive functional/anatomical assessment of the coronary tree. CCTA-FFR uses CFD coupled with an elaborate combination of lumped models for both the systemic circulation and the coronary microcirculation requiring approximately five hours of processing time per patient<sup>24,25</sup>. The CCTA-FFR studies showed that the non-invasive virtual index correlated well with wire-FFR ( $r \approx 0.6-0.8$ ; Table 3) and had significantly increased discriminatory power against stand-alone CCTA considering wire-FFR as the reference standard<sup>15-17</sup>. The latest data from the NXT trial reflecting close adherence to

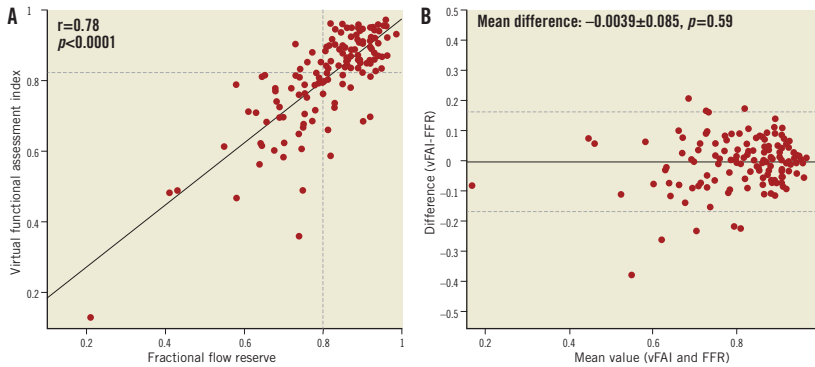


**Figure 4.** (A) There was a close correlation between the virtual functional assessment index (vFAI) and fractional flow reserve (FFR;  $r=0.78$ ). The horizontal dashed line indicates the optimal cut-point (0.82) derived from the receiver operator characteristic curve analysis. (B) The Bland-Altman plot (provided for comparison purposes only since vFAI and FFR are not intended to be mathematically equivalent) for the agreement between vFAI and FFR showed a mean difference of  $-0.0039$  (solid line); the dashed lines represent the values at  $\text{mean}\pm 2\text{SD}$ .

CTA image acquisition protocols and technological improvements demonstrated a per-vessel diagnostic accuracy of 86%<sup>17</sup>.

The correlation between vFAI and wire-FFR was in the same range as in previous studies presenting physiology models (Table 3), while agreement and diagnostic performance (accuracy: 88%) were very good; vFAI also provided superior discrimination/diagnostic performance against the QCA anatomic measures, thereby justifying its potential use as an adjunctive modality in the patient-management workflow. However, it becomes evident from previous work as well as from our own that all virtual indices perform similarly with reasonable behaviour for the group (i.e., small mean difference) but demonstrate a significant scatter (i.e., substantial standard deviation) in comparison with wire-FFR, which may remain insufficient for individual patient decisions.

#### CHALLENGES AND CLINICAL IMPLICATIONS OF VIRTUAL FUNCTIONAL ASSESSMENT USING ROUTINE ANGIOGRAPHY

Blood flow simulation can provide a comprehensive approach by taking full advantage of the 3D anatomical data and by directly adding the missing functional element. Nonetheless, realistic artery-specific anatomy is the foundation for any CFD process and, thus, both the resolution of raw images and the accuracy of the 3D reconstruction by existing algorithms and their approximations are critical for the simulation results.

Physiological parameters of coronary microcirculation and resistance of the underlying myocardium as well as their influence in coronary flow during hyperaemia are difficult to model, even with sophisticated algorithms. Reduced vasodilation of arterioles with increased resistance after hyperaemia induction, such as in

**Table 3.** Comparison of the performance of vFAI to previously reported physiology models using pressure-wire fractional flow reserve (FFR) as the reference standard.

Model/study	Sample size	Imaging modality	Correlation vs. FFR <sup>a</sup>	AUC	Bias $\pm$ SD
vFAI	139	Conventional angiography	0.78	0.92	0.00 $\pm$ 0.085
CCTA-FFR		Coronary			
DISCOVER-FLOW <sup>15</sup>	159	Computed	0.68	0.90	0.02 $\pm$ 0.116
DeFACTO <sup>16</sup>	407	Tomographic	0.63	0.81 <sup>b</sup>	0.06 <sup>c</sup>
HeartFlowNXT <sup>17</sup>	484	Angiography	0.82	0.93	0.02 $\pm$ 0.074
Virtual FFR-VIRTU-1 <sup>22</sup>	35 <sup>d</sup>	Rotational angiography	0.84 <sup>e</sup>	–	0.02 $\pm$ 0.08
Vascular resistance ratio (VRR) <sup>23</sup>	21	OCT	0.81	–	0.05 $\pm$ 0.082
Stenosis flow reserve (SFR) <sup>14</sup>	110	Conventional angiography	0.61	–	–

Reported values correspond to the pre-intervention per-vessel analysis (sample size=number of vessels studied). <sup>a</sup>Pearson correlation coefficient; <sup>b</sup>Corresponds to the per-patient analysis because the value for the per-vessel one was not reported; <sup>c</sup>SD was not reported; <sup>d</sup>Includes both pre- and post-intervention in the analysis as reported; <sup>e</sup>Pearson correlation coefficient for the best fit line passing through the origin. OCT: optical coherence tomography

cases of dysfunction (e.g., diabetes) or damage (i.e., myocardial infarct), certainly pose a challenge for modelling purposes. In such cases, virtual functional assessment would overestimate the haemodynamic lesion severity compared to wire-FFR, which, conversely, is known to yield higher FFR values than expected<sup>21</sup>.

Despite the challenges of modelling physiology, virtual functional assessment is a promising approach providing an incremental value to stand-alone coronary imaging. Coupled with the superior resolution of invasive angiography, which remains the cornerstone for coronary disease diagnosis, playing an essential role in the path towards intervention, virtual functional assessment – as presented in the current study – could prove to be a valuable tool, overcoming the limitations of angiography as shown by the superiority of vFAI vs. 2D/3D-QCA metrics. However, we acknowledge that the point-by-point comparison of vFAI vs. wire-FFR presents quite a large variation, as was also the case in previous studies exploring similar virtual indices (Table 3), thereby making this approach too imprecise for substituting the well-established wire-FFR in clinical practice. Still, rather than considering the proposed approach as competitive with wire-FFR assessment, we would emphasise the complementary role that our proposed approach could acquire for clinical use. Given the high diagnostic accuracy and, particularly, the high negative predictive performance of vFAI (a vFAI value above 0.90 had a 100% negative predictive value in our patient population), vFAI could potentially guide clinical decisions by defining a group of patients that would not need further evaluation with wire-FFR, thereby reducing the additional use of the pressure wire/vasodilators. Of note, following such a strategy would translate into 27% of the cases (i.e., those with vFAI >0.90) being deferred from wire-FFR assessment according to the results in our population with intermediate lesions. Consequently, this less expensive and less invasive strategy could broaden the application of haemodynamic assessment in catheterisation laboratories, thereby increasing the number of well-informed clinical decisions and overall, could be proven to be time- and cost-effective.

#### LIMITATIONS

This is a medium-sized population study and thus further prospective studies with much larger patient populations are warranted for validating our approach. Additionally, our CFD models did not include the effect of any side branches and therefore made the assumption that coronary flow remains the same along the length of each single artery across proximal or more distal lesions. Incorporation of at least one major side branch in the 3D model, which is feasible with existing 3D-QCA software, could be added in future work and would address this issue to a large extent, at least when evaluating stenoses in proximal and middle coronary segments where clinical interest is primarily focused. Nonetheless, we acknowledge that modelling of a large branched network would be highly demanding, increasing the complexity of the 3D-CFD process. Also, due to the use of pre-specified uniform flow values, the mass and functional capacity of the distal myocardial bed, which affect coronary flow, are not incorporated into the proposed model. Our simulations show

that a universal hyperaemic flow limit of 4 ml/sec produces implausible pressure gradients in some cases. Therefore, our assumption of a fixed value oversimplifies a complex boundary condition; further work on vFAI will explore methods to adjust the maximum flow rate. Finally, 3D-QCA is not widely available in catheterisation laboratories and may pose an additional cost.

#### Conclusions

This study investigated the diagnostic performance of a virtual functional assessment approach from routine angiographic data empowered with CFD analysis. The proposed approach does not require any pressure measurements/hyperaemia induction and provides virtual functional assessment in a simplified and fast manner, enabling on-line prospective or *post hoc*/retrospective (off-line) evaluations. Our analysis in a real-world patient population, with lesions of intermediate angiographic severity, namely those of great clinical interest, showed that our derived virtual index has superior diagnostic performance to stand-alone angiographic measures for predicting wire-FFR. Therefore, the proposed approach is promising and worthy of further investigation that would also test the potential benefit in patient management and cost.

#### Impact on daily practice

Fractional flow reserve measured invasively using the pressure wire after hyperaemia induction has been established as a valuable method for assessing the haemodynamic significance of coronary stenoses and guiding percutaneous coronary intervention, but it is not widely adopted in clinical practice. Conventional angiography has a pivotal role in coronary artery disease diagnosis and, as shown in this study, can also be used for virtual functional assessment of coronary lesions employing three-dimensional quantitative coronary angiography and blood flow simulation techniques. This less invasive strategy, based on routine angiographic data without requiring the pressure wire and vasodilator-induced hyperaemia, could be applied in daily practice for easier, wider, and potentially less expensive application of haemodynamic assessment of coronary lesions in the catheterisation laboratory.

#### Guest Editor

This paper was guest edited by Nicolas Foin, MSc, PhD; National Heart Centre, Singapore.

#### Acknowledgements

We acknowledge the support of the George D. Behrakis Fellowship. We thank Antonis Sakellarios, BSc, for technical support with the CFD simulations.

#### Funding

This work is partly funded by the European Union (European Regional Development Fund - ERDF) and the Greek national funds through the Operational Program “THESSALY - MAINLAND

GREECE AND EPIRUS - 2007-2013" of the National Strategic Reference Framework (NSRF 2007-2013; MIS 348133).

### Conflict of interest statement

The authors have no conflicts of interest to declare. The Guest Editor has no conflicts of interest to declare.

### References

1. Levine GN, Bates ER, Blankenship JC, Bailey SR, Bittl JA, Cercek B, Chambers CE, Ellis SG, Guyton RA, Hollenberg SM, Khot UN, Lange RA, Mauri L, Mehran R, Moussa ID, Mukherjee D, Nallamothu BK, Ting HH; American College of Cardiology Foundation; American Heart Association Task Force on Practice Guidelines; Society for Cardiovascular Angiography and Interventions. 2011 ACCF/AHA/SCAI Guideline for Percutaneous Coronary Intervention. A report of the American College of Cardiology Foundation/American Heart Association Task Force on Practice Guidelines and the Society for Cardiovascular Angiography and Interventions. *J Am Coll Cardiol.* 2011;58:e44-122.
2. Task Force on Myocardial Revascularization of the European Society of Cardiology (ESC) and the European Association for Cardio-Thoracic Surgery (EACTS); European Association for Percutaneous Cardiovascular Interventions (EAPCI), Wijns W, Kolh P, Danchin N, Di Mario C, Falk V, Folliguet T, Garg S, Huber K, James S, Knuuti J, Lopez-Sendon J, Marco J, Menicanti L, Ostojic M, Piepoli MF, Pirtel C, Pomar JL, Reifart N, Ribichini FL, Schali J, Sergeant P, Serruys PW, Silber S, Sousa Uva M, Taggart D. Guidelines on myocardial revascularization. *Eur Heart J.* 2010;31:2501-55.
3. Pijls NH, van Schaardenburgh P, Manoharan G, Boersma E, Bech JW, van't Veer M, Bar F, Hoortje J, Koolen J, Wijns W, de Bruyne B. Percutaneous coronary intervention of functionally non-significant stenosis: 5-year follow-up of the DEFER Study. *J Am Coll Cardiol.* 2007;49:2105-11.
4. Tonino PA, De Bruyne B, Pijls NH, Siebert U, Ikeno F, van't Veer M, Klauss V, Manoharan G, Engstrom T, Oldroyd KG, Ver Lee PN, MacCarthy PA, Fearon WF. Fractional flow reserve versus angiography for guiding percutaneous coronary intervention. *N Engl J Med.* 2009;360:213-24.
5. De Bruyne B, Pijls NH, Kalesan B, Barbato E, Tonino PA, Piroth Z, Jagic N, Mobius-Winkler S, Rioufol G, Witt N, Kala P, MacCarthy P, Engstrom T, Oldroyd KG, Mavromatis K, Manoharan G, Verlee P, Frobert O, Curzen N, Johnson JB, Juni P, Fearon WF. Fractional flow reserve-guided PCI versus medical therapy in stable coronary disease. *N Engl J Med.* 2012;367:991-1001.
6. Dehmer GJ, Weaver D, Roe MT, Milford-Beland S, Fitzgerald S, Hermann A, Messenger J, Moussa I, Garratt K, Rumsfeld J, Brindis RG. A contemporary view of diagnostic cardiac catheterization and percutaneous coronary intervention in the United States: a report from the CathPCI Registry of the National Cardiovascular Data Registry, 2010 through June 2011. *J Am Coll Cardiol.* 2012;60:2017-31.
7. Meijboom WB, Van Mieghem CA, van Pelt N, Weustink A, Pugliese F, Mollet NR, Boersma E, Regar E, van Geuns RJ, de

- Jaegere PJ, Serruys PW, Krestin GP, de Feyter PJ. Comprehensive assessment of coronary artery stenoses: computed tomography coronary angiography versus conventional coronary angiography and correlation with fractional flow reserve in patients with stable angina. *J Am Coll Cardiol.* 2008;52:636-43.
8. Yong AS, Ng AC, Brieger D, Lowe HC, Ng MK, Kritharides L. Three-dimensional and two-dimensional quantitative coronary angiography, and their prediction of reduced fractional flow reserve. *Eur Heart J.* 2011;32:345-53.
9. Gould KL. Pressure-flow characteristics of coronary stenoses in unsedated dogs at rest and during coronary vasodilation. *Circ Res.* 1978;43:242-53.
10. Young DF. Fluid Mechanics of Arterial Stenoses. *J Biomech Eng.* 1979;101:157-75.
11. Brown BG, Bolson E, Frimer M, Dodge HT. Quantitative coronary arteriography: estimation of dimensions, hemodynamic resistance, and atheroma mass of coronary artery lesions using the arteriogram and digital computation. *Circulation.* 1977;55:329-37.
12. Zijlstra F, van Ommeren J, Reiber JH, Serruys PW. Does the quantitative assessment of coronary artery dimensions predict the physiologic significance of a coronary stenosis? *Circulation.* 1987;75:1154-61.
13. Gould KL, Kirkeide RL, Buchi M. Coronary flow reserve as a physiologic measure of stenosis severity. *J Am Coll Cardiol.* 1990;15:459-74.
14. Bartunek J, Sys SU, Heyndrickx GR, Pijls NH, De Bruyne B. Quantitative coronary angiography in predicting functional significance of stenoses in an unselected patient cohort. *J Am Coll Cardiol.* 1995;26:328-34.
15. Koo BK, Erglis A, Doh JH, Daniels DV, Jegere S, Kim HS, Dunning A, DeFrance T, Lansky A, Leipsic J, Min JK. Diagnosis of ischemia-causing coronary stenoses by noninvasive fractional flow reserve computed from coronary computed tomographic angiograms. Results from the prospective multicenter DISCOVER-FLOW (Diagnosis of Ischemia-Causing Stenoses Obtained Via Noninvasive Fractional Flow Reserve) study. *J Am Coll Cardiol.* 2011;58:1989-97.
16. Min JK, Leipsic J, Pencina MJ, Berman DS, Koo BK, van Mieghem C, Erglis A, Lin FY, Dunning AM, Apruzzese P, Budoff MJ, Cole JH, Jaffer FA, Leon MB, Malpeso J, Mancini GB, Park SJ, Schwartz RS, Shaw LJ, Mauri L. Diagnostic accuracy of fractional flow reserve from anatomic CT angiography. *JAMA.* 2012;308:1237-45.
17. Norgaard BL, Leipsic J, Gaur S, Seneviratne S, Ko BS, Ito H, Jensen JM, Mauri L, De Bruyne B, Bezerra H, Osawa K, Marwan M, Naber C, Erglis A, Park SJ, Christiansen EH, Kalltoft A, Lassen JF, Botker HE, Achenbach S. Diagnostic performance of noninvasive fractional flow reserve derived from coronary computed tomography angiography in suspected coronary artery disease: the NXT trial (Analysis of Coronary Blood Flow Using CT Angiography: Next Steps). *J Am Coll Cardiol.* 2014;63:1145-55.
18. Schuurbers JC, Lopez NG, Ligthart J, Gijzen FJ, Dijkstra J, Serruys PW, Van der Steen AF, Wentzel JJ. In vivo validation of

CAAS QCA-3D coronary reconstruction using fusion of angiography and intravascular ultrasound (ANGUS). *Catheter Cardiovasc Interv.* 2009;73:620-6.

19. Nichols WW, O'Rourke MF. McDonald's Blood Flow in Arteries: Theoretical, Experimental and Clinical Principles. London: Arnold, 1998.

20. Kern MJ, Bach RG, Mechem CJ, Caracciolo EA, Aguirre FV, Miller LW, Donohue TJ. Variations in normal coronary vasodilatory reserve stratified by artery, gender, heart transplantation and coronary artery disease. *J Am Coll Cardiol.* 1996;28:1154-60.

21. Kern MJ, Lerman A, Bech JW, De Bruyne B, Eeckhout E, Fearon WF, Higano ST, Lim MJ, Meuwissen M, Piek JJ, Pijls NH, Siebes M, Spaan JA. Physiological assessment of coronary artery disease in the cardiac catheterization laboratory: a scientific statement from the American Heart Association Committee on Diagnostic and Interventional Cardiac Catheterization, Council on Clinical Cardiology. *Circulation.* 2006;114:1321-41.

22. Morris PD, Ryan D, Morton AC, Lycett R, Lawford PV, Hose DR, Gunn JP. Virtual fractional flow reserve from coronary angiography: modeling the significance of coronary lesions: results from the VIRTU-1 (VIRTUal Fractional Flow Reserve From Coronary Angiography) study. *JACC Cardiovasc Interv.* 2013;6:149-57.

23. Guagliumi G, Sirbu V, Petroff C, Capodanno D, Musumeci G, Yamamoto H, Elbasiony A, Brushett C, Matiashvili A,

Lortkipanidze N, Valsecchi O, Bezerra HG, Schmitt JM. Volumetric assessment of lesion severity with optical coherence tomography: relationship with fractional flow. *EuroIntervention.* 2013;8:1172-81.

24. Kim HJ, Vignon-Clementel IE, Coogan JS, Figueroa CA, Jansen KE, Taylor CA. Patient-specific modeling of blood flow and pressure in human coronary arteries. *Ann Biomed Eng.* 2010;38:3195-209.

25. Taylor CA, Fonte TA, Min JK. Computational fluid dynamics applied to cardiac computed tomography for noninvasive quantification of fractional flow reserve: scientific basis. *J Am Coll Cardiol.* 2013;61:2233-41.

### Online data supplement

**Online Appendix.** Supplemental methods and results.

**Online Table 1.** QCA anatomic measures (three- and two-dimensional) and virtual haemodynamic indices according to functional significance assessed by wire-FFR.

**Online Figure 1.** Calculation of the virtual functional assessment index (vFAI).

**Online Figure 2.** Pairs of projections used for three-dimensional quantitative coronary angiography (3D-QCA) reconstruction of the example cases.

**Online Figure 3.** Correlation between 2D/3D-QCA-derived anatomic measures and fractional flow reserve using the pressure wire.

# Online data supplement

## Appendix. Supplemental methods

### CARDIAC CATHETERISATION AND WIRE-FFR DATA ACQUISITION

Routine cardiac catheterisation and coronary angiography were performed according to standard clinical practice, and angiographic images were acquired using monoplane or biplane systems with or without flat panel detectors (AXIOM-Artis; Siemens Healthcare, Munich, Germany; Integris Allura, Allura Xper, Integris H; Philips Medical Systems, Amsterdam, The Netherlands). At least two full-contrast projections optimised for angle according to cardiac position were available in all studied arteries. Wire-FFR assessment was performed in vessels with intermediate lesions (30-70 %DS by visual estimation) as clinically indicated at the discretion of the operator. After administration of nitroglycerine, a pressure-sensor guidewire (PressureWire/RadiAnalyzer; St. Jude Medical Systems, Uppsala, Sweden; PrimeWire Prestige or ComboWire; Volcano Corporation, San Diego, CA, USA) was advanced distally in the coronary artery past a region with luminal stenosis(es). The recording of the position of the pressure wire distally in the coronary artery at the time of wire-FFR assessment was available and enabled the comparison of the virtual functional assessment against the measured wire-FFR at the same location. In a minority of cases where a projection with the pressure wire was not available, the location for wire-FFR assessment was selected based on an anatomical landmark (side branch) distal to the lesion. Maximal hyperaemia was induced by administration of either intravenous (140 µg/kg per minute) or intracoronary (60 and 50 µg in the left and right coronary artery, respectively) adenosine. Wire-FFR was measured as the ratio of mean distal coronary pressure (Pd) to mean aortic coronary pressure (Pa) during hyperaemia. Wire-FFR values  $\leq 0.80$  were considered diagnostic of ischaemia<sup>4</sup>.

### QUANTITATIVE CORONARY ANGIOGRAPHY AND BLOOD FLOW SIMULATION

Three-dimensional QCA was performed off-line with the validated CAAS QCA-3D system (Pie Medical Imaging, Maastricht, The Netherlands)<sup>8</sup>. The end-diastolic frames of the best two full-contrast angiographic views (angle difference  $>30^\circ$ ) of the studied artery before insertion of guidewires were used for 3D-QCA reconstruction. All cases included in the study had angiographic data with documented values for the angulation and source-to-image intensifier distance in the DICOM files as needed for the 3D-QCA procedure. Proximal and distal landmarks for 3D-QCA were defined manually as (i) the ostium of the epicardial artery studied (i.e., ostium of LAD, LCx or RCA; the left main artery was not included in the model of the left arteries), and (ii) the location corresponding to the position of the pressure-sensor guidewire distally where the wire-FFR measurement was performed or a side branch distal to the lesion(s) assessed. Percentage area stenosis (%AS), %DS, minimum luminal area (MLA) and minimum luminal diameter (MLD) were derived from

the 3D-QCA model. Additionally, conventional 2D-QCA analysis of the two projections used in 3D-QCA was performed for all cases for calculating max %DS by 2D-QCA, which may reflect daily practice in the catheterisation laboratory better.

The obtained 3D lumen geometries were further processed with computational fluid dynamics (CFD) techniques that can provide the detailed characteristics of intravascular blood flow and the pressure field, thus enabling the computation of the pressure gradient between the inlet and outlet of the studied coronary segment. A finite volume mesh of approximately 1.4 million tetrahedrons on average was generated in order to perform blood flow simulation by solving the 3D transport equations governing the conservation of mass and momentum (ICEM CFD and CFX 11; Ansys, Canonsburg, PA, USA). Blood was treated as a homogeneous and Newtonian fluid with a dynamic viscosity of 0.0035 Pa·s and a density of 1,050 kg/m<sup>3</sup>. The arterial wall was considered to be rigid and no-slip conditions were applied at the vessel wall, while a reference pressure of 100 mmHg (corresponding to the average aortic pressure in humans) was imposed at the inlet. Blood flow was assumed to be laminar and incompressible and steady flow (fully developed) was specified as boundary condition at the outlet. Two separate simulations with a steady flow of 1 and 3 ml/s (approximately corresponding to the average flow at rest and the hyperaemic flow increase in human coronary arteries, respectively)<sup>19,20</sup> were performed. The pressure gradient at these two flow rates was calculated from the difference of the average pressure at the inlet (Pa) and outlet (Pd) of the CFD simulations.

### RATIONALE AND CALCULATION OF THE VIRTUAL FUNCTIONAL ASSESSMENT INDEX

The difficulty in virtually assessing FFR primarily arises from the fact that a boundary condition of coronary flow (e.g., at the outlet of the coronary artery studied) is required to perform the CFD simulation. However, hyperaemic flow, as required for FFR assessment, is variable, not known, and difficult to quantify for each specific artery without inserting a catheter<sup>26</sup>, since flow intrinsically depends on the vasodilation of the underlying myocardium (i.e., resistance of coronary microcirculation) and the haemodynamic status of the patient<sup>27</sup>.

The foundation of our approach for calculating the virtual functional assessment index (vFAI) is the artery-specific quadratic pressure gradient ( $\Delta P$ )–flow relationship:  $\Delta P = 0 + f_v Q + f_s Q^2$  (i.e., zero intercept; Equation 1), where  $\Delta P$  is the pressure gradient (mm Hg),  $Q$  is the flow rate (ml/s),  $f_v$  (mmHg s/ml) is the coefficient of pressure loss due to viscous friction and  $f_s$  (mmHg s<sup>2</sup>/ml<sup>2</sup>) is the coefficient of pressure loss due to flow separation<sup>9,11</sup>. In each case studied, the two computed  $\Delta P$  values at 1 and 3 ml/s from the CFD simulations were used in order to solve the fully determined system of this quadratic equation with two unknown parameters (i.e., the two coefficients  $f_v$  and  $f_s$ ).

From the  $\Delta P$ - $Q$  equation, the equation describing the relationship of the Pd/Pa ratio vs. flow was calculated as  $Pd/Pa = 1 - f_v \cdot Q/Pa - f_s \cdot Q^2/Pa$  by substituting  $\Delta P$  with  $(Pa - Pd)$  in Equation 1 and then transforming Equation 1 (i.e., by dividing both sides of the equation with Pa) so that in the end Pd/Pa is calculated. A reference value of 100 mmHg (mean aortic pressure in humans) was used for Pa and since the two coefficients were calculated in the previous step, all parameters on the right side of the Pd/Pa vs. flow equation are known. To account for the “overall behaviour” of the artery/stenosis-specific Pd/Pa vs. flow relationship in each case, the area under the Pd/Pa vs. flow curve was calculated (i.e., calculation of the integral of the equation); the area was calculated for a flow range of 0 to 4 ml/sec (corresponding approximately to the mean+2SD hyperaemic flow rate increase in normal human coronary arteries starting from an average flow rate of 1 ml/s at rest)<sup>20</sup>. In the large epicardial coronary arteries without atherosclerotic disease/stenoses, resistance is trivial and thus there is virtually no pressure drop and the Pd/Pa ratio is equal to 1; consequently, in normal arteries the Pd/Pa vs. flow relationship can be considered to be approximately constant, and the area under the horizontal line for a flow range from 0 to 4 ml/sec is also known (reference area for normal artery without a stenosis). Finally, vFAI was calculated as the ratio of the area under the artery-specific Pd/Pa vs. flow curve to the reference area (**Online Figure 1**).

Note that vFAI is not mathematically equivalent to wire-FFR since

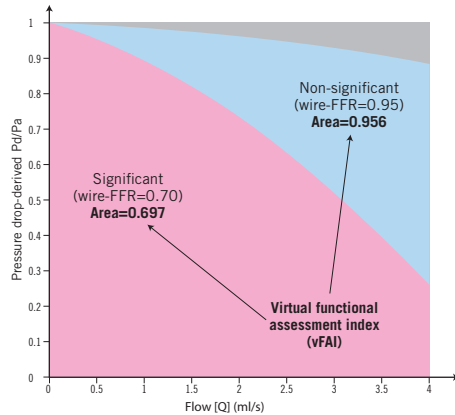
$$vFAI - wireFFR = \frac{1 \cdot f_v \cdot 4}{2 \cdot Pa} + \frac{2 \cdot f_s \cdot 4 \cdot 4}{3 \cdot Pa}$$

using a flow range of 0 to 4 ml/sec. While FFR has an accepted physiologic interpretation, namely the ratio of maximum flow with the stenosis to maximum flow without the stenosis, vFAI has only a geometric interpretation. Namely, vFAI equals the ratio of the area (up to a universal and fixed flow limit) under the pressure drop versus flow curve with the stenosis to the ideal area without a stenosis. Although FFR values generally do not fall below about 0.2 due to a complex interplay among collateral flow, zero-flow pressure, and/or venous pressure, this area contributes to vFAI for every stenosis regardless of severity.

## STATISTICS

Categorical variables are presented as counts and percentages, and continuous variables as mean±SD and median [interquartile range] as appropriate. The unpaired t-test was used to compare normally distributed continuous variables between two groups, whereas the Mann-Whitney U test was used for non-normally distributed variables. The correlation between derived variables (vFAI and anatomic measures) and wire-FFR was investigated using the Pearson ( $r$ ) and Spearman ( $r_s$ ) correlation coefficients. Bland-Altman analysis was performed with wire-FFR as the standard of reference, and the paired t-test was used to test any significant difference between the vFAI and wire-FFR. Receiver operator characteristic (ROC) curve analysis was performed to evaluate the discrimination of vFAI and QCA-derived anatomic measures (e.g., %AS) for predicting wire-FFR  $\leq 0.80$  (gold standard); the

areas under the ROC curve (AUCs) were calculated with binomial exact confidence intervals and were compared using the DeLong method. Diagnostic measures including sensitivity, specificity, positive/negative predictive value and accuracy were calculated, and the optimal cut-off for vFAI and anatomic measures was determined (ROC criterion:  $\max[\text{sensitivity} + \text{specificity}]$ ). Except for the patient characteristics, analyses were performed on a per-vessel basis (assuming independence of lesion-specific ischaemia in vessels) using SPSS 17.0 (SPSS Inc., Chicago, IL, USA) and Stata 10.0 (StataCorp LP, College Station, TX, USA). A two-sided p-value  $< 0.05$  was considered significant.



**Online Figure 1.** Calculation of the virtual functional assessment index (vFAI). The relationship of the Pd/Pa ratio vs. flow was calculated as  $Pd/Pa = 1 - f_v \cdot Q/Pa - f_s \cdot Q^2/Pa$ , where Pa is the aortic pressure, Pd the coronary pressure distal to the stenosis, Q is the flow rate (ml/s), and  $f_v$  (mmHg s/ml) and  $f_s$  (mmHg s<sup>2</sup>/ml<sup>2</sup>) are the coefficients of pressure loss due to viscous friction and flow separation, respectively. A reference value of 100 mmHg (mean aortic pressure in humans) was used for Pa. To calculate vFAI, (1) we consider that there is no pressure loss through normal arteries (i.e., Pa is transmitted completely along a normal artery), and thus Pd/Pa is constant and equal to 1; (2) the area under the curve of a normal artery up to  $Q = 4$  ml/s (i.e., approximately the mean+2SD of hyperaemic flow in human coronary arteries) is used as a normal reference value; and (3) the area-under-the curve of the studied coronary segment is calculated based on the specific Pd/Pa vs. flow curve and is expressed as a ratio compared to the reference area. The figure demonstrates two representative examples of an artery with haemodynamically significant stenosis (wire-FFR=0.70) and vFAI=0.697 (red area) and an artery with non-significant stenosis (wire-FFR=0.95; vFAI=0.956). The grey area represents the difference between the reference area (i.e., normal artery) and the area of the artery with non-significant stenosis, while the blue area represents the difference in areas between the two arteries.

## Supplemental results

### PRESSURE GRADIENT USING A UNIVERSAL UPPER LIMIT FOR FLOW RATE

We tested our fixed hyperaemic flow limit by performing additional simulations for all cases using a boundary condition of 4 ml/sec for coronary flow. Given the range of derived pressure gradients at this high flow rate (mean: 48.96±54.36 mmHg; interquartile range: 22.78-59.1 mmHg; 5-95% percentile: 11.81-104.83 mmHg; max: 573.1 mmHg; min: 9.7 mmHg), the selection of a pre-specified aortic pressure value and hyperaemic flow limit poses a problem since there were even some cases with a pressure gradient of >200 mmHg, which is above any values (even in hypertensive cases) present in human conditions. However, we also note that in most cases (as presented by the 95% percentile: 104.83 mmHg) the above-mentioned selection yields a rather realistic value of pressure gradient for human coronaries, reflecting our original assumption corresponding to the mean +2SD hyperaemic flow rate increase in normal human coronary arteries starting from an average flow rate of 1 ml/s at rest<sup>4</sup>.

### Online references

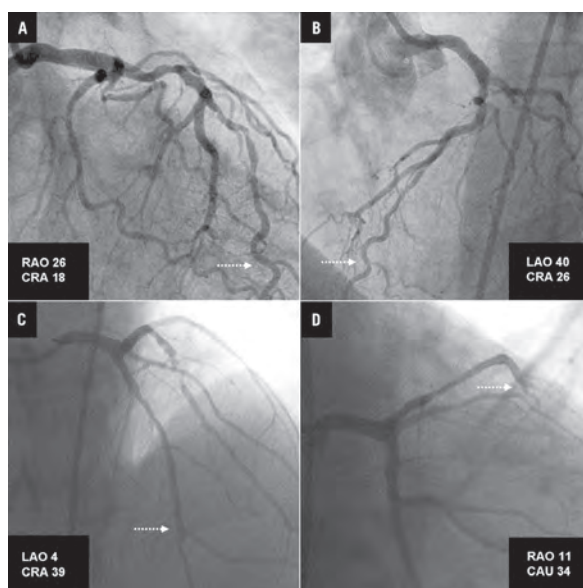
26. Wong JT, Le H, Suh WM, Chalyan DA, Mehraien T, Kern MJ, Kassab GS, Molloy S. Quantification of fractional flow reserve based on angiographic image data. *Int J Cardiovasc Imaging*. 2012;28:13-22.

27. de Bruyne B, Bartunek J, Sys SU, Pijls NH, Heyndrickx GR, Wijns W. Simultaneous coronary pressure and flow velocity measurements in humans. Feasibility, reproducibility, and hemodynamic dependence of coronary flow velocity reserve, hyperemic flow versus pressure slope index, and fractional flow reserve. *Circulation*. 1996;94:1842-9.

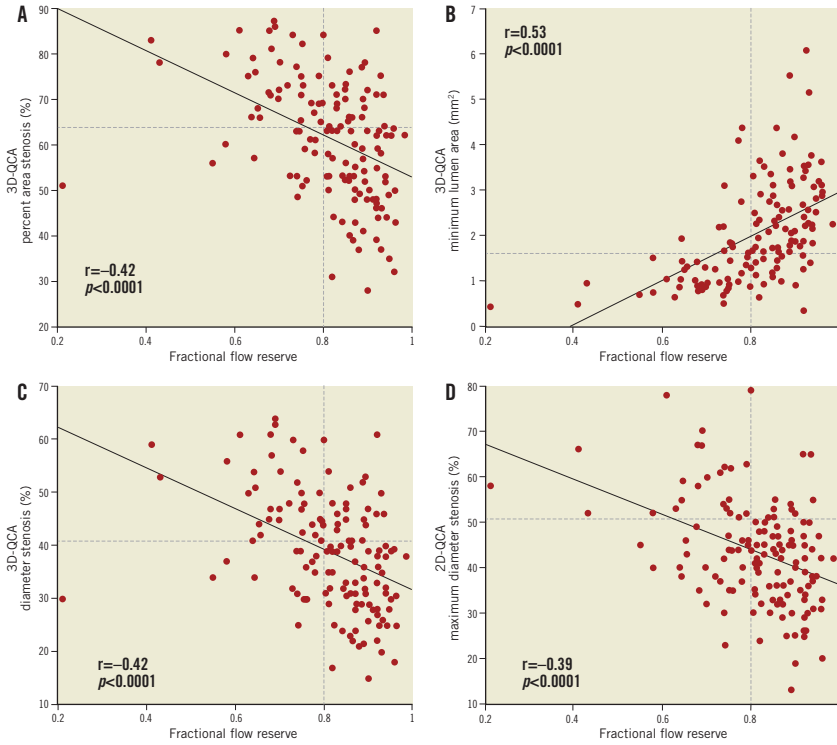
**Online Table 1. QCA anatomic measures (three- and two-dimensional) and virtual haemodynamic indices according to functional significance assessed by wire-FFR.**

Parameter	Wire-FFR ≤0.80 (n=52)	Wire-FFR >0.80 (n=87)	p-value
2D-QCA maxDS (%)	49.1±12.3	39.9±9.8	<0.001
3D-QCA AS (%)	69.3±10.7	56.6±12.2	<0.001
3D-QCA DS (%)	45.4±10.0	34.9±9.4	<0.001
3D-QCA MLA (mm <sup>2</sup> )	1.10 [0.87-1.59]	2.32 [1.73-3.09]	<0.001
3D-QCA MLD (mm)	1.26±0.34	1.72±0.37	<0.001
Coefficient $f_v$ (mmHg s/ml)	5.87 [4.39-8.75]	2.45 [1.32-3.48]	<0.001
Coefficient $f_s$ (mmHg s <sup>2</sup> /ml <sup>2</sup> )	2.61 [2.11-3.42]	1.14 [0.76-1.64]	<0.001
Virtual Functional Assessment Index	0.73 [0.62-0.80]	0.89 [0.84-0.93]	<0.001

Values are presented as mean±SD or median [interquartile range]. FFR: fractional flow reserve; MLD: minimum lumen diameter; QCA: quantitative coronary angiography;  $f_v$ : coefficient for viscous losses;  $f_s$ : coefficient for flow separation losses



**Online Figure 2.** Pairs of projections used for 3D-QCA reconstruction of the coronary segments presented in the examples of Figure 2 (corresponding to A and B in this figure) and Figure 3 (corresponding to C and D in this figure) of the main manuscript. The dotted arrows mark the location of the distal landmark of the reconstruction where the pressure wire was positioned for fractional flow reserve assessment.



**Online Figure 3.** There was a moderate correlation between 2D/3D-QCA-derived anatomic measures (A: % area stenosis; B: minimum lumen area; C: % diameter stenosis; D: maximum % diameter stenosis) and fractional flow reserve by the pressure wire. Horizontal dashed lines indicate the optimal cut-points (64%, 1.66 mm<sup>2</sup>, 41%, and 51%, respectively) derived from the receiver operator characteristic curve analysis. QCA: quantitative coronary angiography.

### 3.3 Comparison between 2D- and 3D-QCA in bifurcation lesions

Comparison between two-dimensional and three-dimensional quantitative coronary angiography bifurcation analyses for the assessment of bifurcation lesions: A sub-analysis of the TRYTON pivotal IDE coronary bifurcation trial.

(Submitted)

[Original research paper]

Muramatsu T, Grundeken MJ, Ishibashi Y, Nakatani S, Campos CA, Morel MA, Jonker H, Girasis C, de Winter RJ, Wykrzykowska JJ, García-García HM, Leon MB, Serruys PW, Onuma Y.





# **Comparison Between Two-dimensional and Three-dimensional**

## **Quantitative Coronary Angiography Bifurcation Analyses**

### **For the Assessment of Bifurcation Lesions:**

#### **A Sub-analysis of the TRYTON pivotal IDE Coronary Bifurcation Trial**

Takashi Muramatsu, MD, PhD,\* † Maik J. Grundeken, MD,‡ Yuki Ishibashi, MD, PhD, \*

Shimpei Nakatani, MD,\* Carlos A. Campos, MD,\* Marie-Angèle Morel, BSc,§ Hans Jonker,

BSc,§ Chrysafios Girasis, MD,\* Robbert J. de Winter, MD, PhD, ‡ Joanna J. Wykrzykowska,

MD, PhD,‡ Hector M. García-García, MD, PhD,\* § Martin B. Leon, MD, || Patrick W. Serruys,

MD, PhD, ¶ Yoshinobu Onuma, MD, PhD\*

On behalf of the TRYTON pivotal IDE coronary bifurcation trial investigators

\* Thoraxcenter, Erasmus Medical Center, Rotterdam, The Netherlands.

† Department of Cardiology, Fujita Health University Hospital, Toyoake, Japan.

‡ Academic Medical Center, Amsterdam, The Netherlands

§ Cardialysis, B.V., Rotterdam, the Netherlands.

|| Cardiovascular Research Foundation (CRF)/ Columbia University Medical Center-New

York Presbyterian Hospital, New York, NY.

¶ International Centre for Circulatory Health, NHLI, Imperial College London, London,  
The United Kingdom.

**Word counts:** 4,290words

**Number of Tables:** 3

**Number of Figures:** 6

**Brief title:** 2-D vs. 3-D QCA in bifurcation

**Clinical trial registration information:** ClinicalTrials.gov NCT01258972.

**Conflict of interest:**

The TRYTON IDE trial have been sponsored and funded by Tryton Medical, Inc. All other authors have reported that they have no relationships relevant to the contents of this paper to disclose.

**Address for correspondence:**

Professor Patrick W. Serruys, MD, PhD.

International Centre for Circulatory Health, NHLI, Imperial College London, London,

The United Kingdom

P.O. Box 2125, 3000 CC Rotterdam, The Netherlands

Email: [patrick.w.j.c.serruys@gmail.com](mailto:patrick.w.j.c.serruys@gmail.com)

Telephone: +31-102062828

Fax: +31-102062884

### **Abbreviations and acronyms**

BA = bifurcation angle

BSM = bifurcation segment model

DES = drug-eluting stent(s)

DS = diameter stenosis

MLD = minimal luminal diameter

PCI = percutaneous coronary intervention

MB = main branch

QCA = quantitative coronary angiography

RVD = reference vessel diameter

SB = side branch

SBBA = side branch balloon angioplasty

### **Abstract (261 words)**

**Background:** Three-dimensional (3D) quantitative coronary angiography (QCA) provides more accurate measurements by minimizing inherent limitations of two-dimensional (2D) QCA. The aim of this study was to compare the measurements between 2D and 3D QCA analyses in bifurcation lesions using validated bifurcation QCA algorithm.

**Methods and Results:** A total of 114 cases with non-left main bifurcation lesions in the TRYTON pivotal IDE Coronary Bifurcation Trial (ClinicalTrials.gov: NCT01258972) were analyzed with a dedicated bifurcation QCA software (CAAS 5.10, Pie Medical Imaging, Maastricht, the Netherlands). All cases were analyzed by applying matched projections between pre- and post-procedure. The 2D analyses were performed using one of two angiographic images used for 3D reconstruction with the largest distal bifurcation angle. In the treated segments (stent and balloon), there were no differences in minimal luminal diameter (MLD) between 2D and 3D, while diameter stenosis (DS) was significantly larger in 2D compared to 3D both pre-procedure and post-procedure (53.9% for 2D vs. 52.1% for 3D pre-procedure,  $p<0.01$ ; 23.2% for 2D vs. 20.9% for 3D post-procedure,  $p=0.01$ ). In the sub-segment level analysis, lengths of proximal main branch, distal main branch, and side branch were consistently shorter in 2D compared to 3D both pre-procedure and post-procedure. The site of smallest MLD and largest %DS were also different between 2D and 3D in a considerable proportion of the patients (kappa values: 0.50 for MLD, 0.55 for %DS).

**Conclusions:** There are differences between in-vivo 2D and 3D QCA analysis of coronary bifurcation lesions. Our results are crucial in determining the methodology of QCA analysis for bifurcation lesions when designing future clinical studies.

**Key words:** coronary bifurcation, three-dimensional, quantitative coronary angiography.

## **Introduction**

Quantitative coronary angiography (QCA) has been introduced in the mid-eighties to overcome the shortcomings of visual assessment of stenosis severity, such as a marked inter- and intra-observer variability (1-4). Conventional two-dimensional (2D) QCA has been accepted as an objective and reproducible method to quantify coronary lesion severity, and QCA parameters have been accepted as surrogate endpoints in numerous randomized clinical trials evaluating the efficacy of new technologies in percutaneous coronary interventions (PCI) and the effect of new pharmaceutical agents on coronary artery disease progression/regression (5-7).

Even in the era of drug-eluting stents (DES), bifurcation lesions have still been recognized as one of the most challenging lesion subsets (8;9). As a consequence of the fractal geometry of the coronary tree, there is a natural tapering of bifurcations, with differences in the reference vessel diameters proximal and distal to the bifurcation (10;11). The interpolation method of the single-vessel QCA algorithms to estimate the reference vessel diameter (RVD) is therefore inaccurate, structurally underestimating the RVD and percentage diameter stenosis (%DS) in the proximal main branch (MB), and overestimating the RVD and DS of the distal MB and side branch (SB) (11). Dedicated bifurcation 2D QCA algorithms have therefore been developed to improve

the accuracy of QCA in bifurcation lesions (12;13).

However, 2D bifurcation techniques also include several inherent limitations, such as vessel overlap and foreshortening that can lead to inaccurate angiographic assessment. Three-dimensional (3D) QCA techniques have been developed to overcome these limitations, improving the accuracy of QCA, as shown in a phantom bifurcation model (14). To date, however, comparisons between 2D and 3D bifurcation QCA have not yet been performed in real life. The aim of this study was therefore to compare the angiographic measurements between 2D and 3D QCA analyses in human coronary bifurcation lesions using validated bifurcation QCA analysis software.

## **Methods**

### ***Study overview***

The TRYTON pivotal IDE (Investigational Device Exemption) Coronary Bifurcation Trial is a prospective, multicenter, single-blind, randomized controlled study to evaluate the safety and efficacy of the Tryton side branch stent (Tryton Medical, Inc., Durham, NC) in the treatment of *de novo* coronary bifurcation lesions. Per protocol, symptomatic patients aged  $\geq 18$  years with a single *de novo* lesion in a non-left main bifurcation were considered eligible for enrollment. Main angiographic inclusion

criteria were a %DS between 50% and 100% in both MB and SB, with an RVD of the MB of  $\geq 2.5$  and  $\leq 4.0$  mm, and with an RVD of the SB of  $\geq 2.5$  and  $\leq 3.0$  mm, both on visual estimation. Eligible patients were randomized in a 1:1 fashion to either the Tryton stent or side branch balloon angioplasty (SBBA), both in conjunction with a DES in the MB. The study protocol was approved by the institutional review boards or medical ethics committees at each participating center. This study was registered at ClinicalTrials.gov (identifier: NCT01258972). Written informed consent was obtained for all enrolled patients. In the present analysis, angiographic data were pooled and analyzed regardless of randomization.

### ***Study device and treatment procedure***

The details of the Tryton side branch stent were described elsewhere.(15;16). In brief, the Tryton stent is a balloon-expandable bare-metal stent made of L-605 cobalt chromium (CoCr) with strut thickness of 84  $\mu\text{m}$ . The Tryton stent is comprised of three zones: a distal side branch zone that is deployed within the SB, a transition zone that resides at the SB ostium, and a proximal MB zone that is placed within the proximal MB. Before Tryton implantation, both distal MB and SB are wired. After successful implantation of the Tryton stent, the SB guide wire was then re-wired into the distal MB.

After MB pre-dilation, an approved conventional DES was then implanted in the MB, overlapping the proximal MB zone. Per-protocol, it was mandated to finalize the procedure with final kissing balloon inflation.

### *Quantitative coronary angiography assessment*

Off-line QCA analyses were performed using the Cardiovascular Angiography Analysis System software (CAAS 5.10, Pie Medical Imaging, Maastricht, The Netherlands) in an independent angiographic core laboratory (Cardialysis B.V., Rotterdam, The Netherlands). The MB was defined as the branch in which the DES was implanted, whereas the SB was defined as the branch in which the Tryton stent was implanted or SBBA performed. The treated segments were defined by three borders: the proximal MB border was defined by the proximal MB DES stent edge, the distal MB border was defined by the distal MB DES stent edge, and the SB border was defined by either the distal Tryton stent edge or the distal marker of the most distal balloon used in the case of SBBA (**Figure 1**). The in-segment analyses included the treated segment plus 5-mm proximally to the proximal border of MB, and 5-mm distally to the distal borders of MB and SB.

Per imaging analysis protocol, only matched pre- and post-procedural projections were used for QCA analyses. Calibration was performed automatically in both 2D and 3D analysis with the geometric data of acquisitions provided through the DICOM headers. In the present study, 3D QCA analyses were performed first, using two angiographic images separated by a viewing angle of  $\geq 30^\circ$ . Subsequently 2D analyses were performed by using one of the two angiographic images in which the largest BA between the distal MB and SB was visible on visual estimation (**Figure 2**). The same cine-film, end-diastolic frame, and segmentations used for the 3D analysis were used for the 2D analysis.

MLD, %DS, and RVD were quantified pre- and post-procedurally. Diameter values from the 3D QCA analysis were derived from the so-called “equivalent diameters”, as previously published (17). In short, this means that in the case the 3D QCA-derived cross-sectional lumen area has an elliptical shape, the “equivalent” lumen diameter of that cross section was defined as the diameter of a virtual circle with the same area as the elliptical lumen (*Supplementary material, Figure S1*). Accordingly, MLD in 3D QCA corresponds to the “equivalent diameter” of the absolute minimal lumen area. Respective values for corresponding sub-segments were obtained from the bifurcation 6-segment model (BSM6)(13). In addition, quantitative parameters for the

3-mm ostial SB segment, derived from the bifurcation 11-segment model (BSM11), were also assessed (**Figure 3**) (13). Bifurcation angle (BA) values were calculated according to the methodology described previously (12;17). Binary stenosis was defined as the presence of stenosis with a DS of  $\geq 50\%$ .

In sub-segment level analyses, measurements in sub-segments based on BSM6 and ostial SB were presented. In treated segment level analyses, the smallest MLD and the largest DS among the sub-segments based on BSM6 were used for the analyses

### *Statistical analysis*

Continuous variables were expressed as mean  $\pm$  SD and categorical variables as counts and percentages. Comparisons were performed by paired t-test for continuous variables and chi-square test for categorical variables. Agreements between 2D and 3D analyses in detecting the sub-segment with the smallest MLD or the largest %DS were evaluated using kappa statistics. Statistical analyses were performed using SPSS Statistics version 21 (IBM, Inc., Armonk, NY).

## **Results**

### *Study population and baseline characteristics*

A total of 114 patients (114 bifurcation lesions) were used for the current analyses. These cases provided the paired QCA datasets with 2D and 3D by using matched angiographic projections between pre- and post-procedure (*Supplementary material, Figure S2*).

### *Sub-segment level analysis*

Sub-segment analyses based on the BSM6 model are shown in **Table 1**.

Pre-procedurally, 2D-MLD was smaller than 3D-MLD in the proximal MB, while the 2D-MLD was larger than 3D-MLD in the SB. Post-procedurally, 2D-MLD was smaller than 3D-MLD in the distal MB. Specifically at the ostial SB, there were no differences in MLD between 2D and 3D QCA (both pre- and post-procedure). Pre-procedural RVD was consistently larger in 2D QCA than in 3D QCA in the proximal MB, distal MB, and SB. Post-procedural RVD was larger with 2D QCA only in the proximal MB, while in the other segments the RVD was similar between 2D QCA and 3D QCA. These differences in MLD and RVD resulted in differences in pre- and post-procedural %DS in the proximal MB and ostial SB (**Figure 4A**). Segment lengths were consistently shorter with 2D QCA than with 3D QCA in all sub-segments, both pre- and post-procedure.

### ***Treated segment level analysis***

There were no differences in either in-segment MLD or treated segment MLD between 2D and 3D QCA both pre- and post-procedure (**Table 2**). Conversely, 2D QCA showed a trend toward a larger in-segment %DS compared to 3D QCA, while in the treated segment %DS appeared to be significantly larger in 2D QCA than in 3D QCA both pre-procedure ( $53.9\% \pm 12.4\%$  vs.  $52.1\% \pm 11.3\%$ ,  $p < 0.01$ ) and post-procedure ( $23.2\% \pm 10.9$  vs.  $20.9\% \pm 11.9\%$ ,  $p = 0.01$ ) (**Figure 4B**).

### ***Bifurcation angle analysis***

Bifurcation angle analyses are shown in **Table 3**. Proximal bifurcation angles ( $BA_{PMB-SB}$ ) were significantly greater in 2D QCA than in 3D QCA both pre-procedure and post-procedure, while there were no differences in pre- and post-procedural distal bifurcation angles ( $BA_{DMB-SB}$ ) between 2D and 3D QCA. Post-procedurally  $BA_{PMB-SB}$  became significantly greater and  $BA_{DMB-SB}$  became significantly smaller in both 2D and 3D QCA.

### ***Comparisons of locations with the smallest MLD or the largest %DS between 2D and 3D QCA***

Pre-procedural locations with the smallest MLD and the largest %DS among

sub-segments based on the BSM6 model are shown in **Figure 5**. There were apparent inconsistencies in location (i.e., sub-segments) having in-segment smallest MLD and largest %DS between 2D and 3D analyses. In the BSM6 model, 2D QCA indicated 49 cases and 3D QCA indicated 63 cases having the smallest pre-procedural MLD within the SB (segment 5 in the BSM6 model). Similarly, 2D and 3D QCA indicated the SB as the location of largest pre-procedural %DS in 27 and 40 cases, respectively. For the agreement between 2D and 3D QCA in determining the location of the sub-segment with the smallest pre-procedural MLD, the kappa value was 0.50. For the agreement to determine the location of the largest pre-procedural %DS, the kappa value was 0.55.

## **Discussion**

The main findings of this study can be summarized as follows: 1) %DS were estimated to be more severe when 2D QCA was used as compared when 3D QCA was used, specifically within the SB ostium; 2) in most sub-segments, this difference was based on larger RVD as measured with 2D QCA, while MLDs were similar between 2D and 3D, except for the proximal MB (pre-procedure), distal MB, and ostial SB (both post-procedure), in which the difference in MLD was explained by a smaller MLD measured by 2D QCA; 3) segment lengths appeared to be shorter in 2D than in 3D

QCA; 4) bifurcation angles were influenced by 2D and 3D analyses; and 5) the agreement between 2D and 3D QCA to define the locations with the smallest MLD and the largest %DS was poor in non-left main bifurcation lesions.

There have been two studies that compared 2D and 3D QCA in bifurcation lesions (18;19). A limitation of these studies was that different software with different analysis algorithms were used for the 2D and 3D QCA analyses. In a previous study it has been shown that the CardiOp-B system (Paeion Medical, Rosh Ha'ayin, Israel) which was used for the 3D QCA analyses in both studies, was less accurate with respect to the measurements of luminal diameter and area when compared to the CAAS system (20). We applied the CAAS bifurcation analysis algorithms systematically to 2D and 3D QCA that has been validated in the plexiglas bifurcation phantom models with excellent inter- and intra-observer reproducibility (13;14;21). In the present study, sub-segment level analysis based on the BSM6 model showed a trend toward larger %DS in 2D QCA than in 3D QCA. The differences in %DS between the two QCA approaches could partially be explained by a larger RVD found with 2D QCA. The RVD at the MLD site is an interpolated reference diameter based on the non-stenotic lumens of the analyzed region of interest. In some sub-segments, a larger RVD determined with 2D analysis might imply an overestimation of the non-stenotic regions, resulting in a larger

interpolated RVD at the MLD site as compared to 3D analysis. Another possible explanation could be that the luminal shape at the MLD site is often not circular (concentric plaque), but elliptical (eccentric plaque). 3D QCA derived MLD is calculated as an “equivalent diameter” based on the circular assumption of the cross-section (*Supplementary material, Figure S1*). For the current study, 2D analysis was based on a single projection, which could result in a smaller MLD if the projection was perpendicular on the smallest diameter of the elliptical lumen. Furthermore, we found a low agreement between 2D and 3D QCA to define the location of the smallest in-segment MLD. As a result, there might also be a difference in %DS because the MLD was located in a somewhat different site, even in the same sub-segment, because the two modalities uses different methodology to calculate the MLD (smallest area in 3D vs. smallest diameter in 2D) as mentioned above. Consequently, the interpolated RVD might be larger at that site leading to larger %DS.

Accuracy in length derivation is one of advantages of 3D QCA by minimizing possible vessel foreshortening commonly seen in 2D QCA (14;17;22). In the present study, the length of each sub-segment (proximal MB, distal MB, and SB) appeared to be significantly shorter in 2D than in 3D QCA. This finding is in line with previous studies that showed the superiority of 3D to 2D QCA in determining the segment length

(20;22-25). This advantage of 3D QCA may help interventional cardiologists in their decision making of appropriate device length when treating bifurcation lesions.

Recently more attention has been drawn to the BA assessment since the relative changes between systolic and diastolic BA was related to clinical outcomes after distal left main PCI, with patients having the smallest difference in systolic and diastolic BA are at higher risk for major adverse cardiac events such as death, myocardial infarction, repeat revascularization and stent thrombosis than patients with a relative larger difference (26;27). Theoretically 3D QCA provides more accurate BA compared to 2D QCA by calculating the vectors of proximal MB, distal MB, and SB separately in a three-dimensional approach that can minimize the influence of vessel overlap (17). In the present study, however, significant differences were observed only in  $BA_{PMB-SB}$ , not in  $BA_{DMB-SB}$ . This finding might be attributed to the fact that we applied one projection showing greater  $BA_{DMB-SB}$  to 2D QCA analysis (**Figure 3**). Such a 2D image could be considered as a better view for the BA assessment because of less overlap of distal MB and SB, resulting in minimal difference in  $BA_{DMB-SB}$  between 2D and 3D QCA. It should be emphasized, however, that 2D BA assessment is highly depending on the selected view (*Supplementary material, Figure S3*), thus 3D QCA approach should be recommended for BA assessment. However, if 3D QCA is not available, we

recommend to assess the  $BA_{\text{DMB-SB}}$  only in the view with the largest distal  $BA_{\text{DMB-SB}}$ .

The present study also highlights the fact that 2D and 3D QCA detected different locations of the smallest pre-procedural MLD or the largest pre-procedural %DS in bifurcation lesions. Indeed the kappa values suggested insufficient agreement between the two analysis approaches (kappa: 0.50 for the smallest MLD sites and 0.55 for the largest %DS sites). From the clinical perspective, it has been reported that %DS measured by dedicated 2D bifurcation QCA algorithm showed a better correlation with invasive fractional flow reserve (FFR) compared to that by a conventional single-vessel 2D QCA technique, and this advantage was more pronounced in SB (28). It is also noteworthy that Yong et al. demonstrated that 3D QCA derived measurements showed better predictive ability in detecting functionally significant stenosis determined by invasive FFR as compared to 2D QCA derived measurements in simple lesions. Therefore, the dedicated bifurcation 3D QCA algorithm may provide more accurate information not only on anatomical severity but also on location of stenosis to be treated in the clinical settings, although we cannot use the current data to support this statement.

### *Study limitations*

First, we presented neither inter- nor intra-observer reproducibility of QCA analyses in the present study. Our group has already reported the excellent inter- and intra-observer reproducibility in both 2D and 3D QCA analyses in the previous literature (13;14;21). The results may be different when using other software with different algorithms for bifurcation analysis. Second, we consistently applied one of two angiographic images with greater  $BA_{DMB-SB}$  to the 2D analysis since such a view is usually considered as a better 2D view specifically for the anatomical evaluation of ostial SB that is the most susceptible part of bifurcation to vessel overlap (**Figure 3**). Nevertheless, image selection may have an impact on the comparison between 2D and 3D QCA derived parameters.

## **Conclusions**

There are differences between in-vivo 2D and 3D QCA analyses of coronary bifurcation lesions. Whereas %DS was in general larger with 2D QCA, lesion length was in general shorter with 2D QCA than with 3D QCA. Surprisingly, no differences could be detected in distal bifurcation angles ( $BA_{DMB-SB}$ ), although a difference in the proximal bifurcation angles ( $BA_{PMB-SB}$ ) was evident between the two algorithms. The MLD sites or the largest %DS sites were not always the same in 2D assessment as in 3D

in a considerable proportion of the patients. Our results are crucial in determining the methodology of QCA analysis for bifurcation lesions when designing future clinical studies. More studies are needed to investigate the potential clinical benefit in using 3D approach over 2D QCA for the assessment of bifurcation lesions.

### **Acknowledgements**

The authors wish to express their sincere appreciation to Mr. Folkert Tijdens (Pie Medical Imaging, Maastricht, The Netherlands) for technical assistance. The TRYTON pivotal IDE Coronary Bifurcation Trial was sponsored and funded by the Tryton Medical, Inc., Durham, NC.

## **References**

- (1) Serruys PW, Reiber JH, Wijns W, van den Brand M, Kooijman CJ, ten Katen HJ et al. Assessment of percutaneous transluminal coronary angioplasty by quantitative coronary angiography: diameter versus densitometric area measurements. *Am J Cardiol* 1984;54(6):482-488.
- (2) Reiber JH, Serruys PW, Kooijman CJ, Wijns W, Slager CJ, Gerbrands JJ et al. Assessment of short-, medium-, and long-term variations in arterial dimensions from computer-assisted quantitation of coronary cineangiograms. *Circulation* 1985;71(2):280-288.
- (3) Zir LM, Miller SW, Dinsmore RE, Gilbert JP, Harthorne JW. Interobserver variability in coronary angiography. *Circulation* 1976;53(4):627-632.
- (4) Galbraith JE, Murphy ML, de SN. Coronary angiogram interpretation. Interobserver variability. *JAMA* 1978;240(19):2053-2056.
- (5) Garg S, Serruys PW. Coronary stents: current status. *J Am Coll Cardiol* 2010;56(10 Suppl):S1-42.
- (6) Lichtlen PR, Hugenholtz PG, Rafflenbeul W, Hecker H, Jost S, Deckers JW. Retardation of angiographic progression of coronary artery disease by nifedipine. Results of the International Nifedipine Trial on Antiatherosclerotic Therapy (INTACT). INTACT Group Investigators. *Lancet* 1990;335(8698):1109-1113.
- (7) de Feyter PJ, Vos J, Deckers JW. Progression and regression of the atherosclerotic plaque. *Eur Heart J* 1995;16 Suppl I:26-30.
- (8) Rathore S, Terashima M, Katoh O, Matsuo H, Tanaka N, Kinoshita Y et al. Predictors of angiographic restenosis after drug eluting stents in the coronary arteries: contemporary practice in real world patients. *EuroIntervention* 2009;5(3):349-354.
- (9) van Werkum JW, Heestermans AA, Zomer AC, Kelder JC, Suttorp MJ, Rensing BJ et al. Predictors of coronary stent thrombosis: the Dutch Stent Thrombosis Registry. *J Am Coll Cardiol* 2009;53(16):1399-1409.
- (10) Finet G, Gilard M, Perrenot B, Rioufol G, Motreff P, Gavit L et al. Fractal geometry of arterial coronary bifurcations: a quantitative coronary angiography and intravascular ultrasound analysis. *EuroIntervention* 2008;3(4):490-498.
- (11) Lansky A, Tuinenburg J, Costa M, Maeng M, Koning G, Popma J et al. Quantitative angiographic methods for bifurcation lesions: a consensus statement from the European Bifurcation Group. *Catheter Cardiovasc Interv* 2009;73(2):258-266.
- (12) Ramcharitar S, Onuma Y, Aben JP, Consten C, Weijers B, Morel MA et al. A novel dedicated quantitative coronary analysis methodology for bifurcation

lesions. *EuroIntervention* 2008;3(5):553-557.

- (13) Girasis C, Schuurbiers JC, Onuma Y, Aben JP, Weijers B, Boersma E et al. Two-dimensional quantitative coronary angiographic models for bifurcation segmental analysis: in vitro validation of CAAS against precision manufactured plexiglas phantoms. *Catheter Cardiovasc Interv* 2011;77(6):830-839.
- (14) Girasis C, Schuurbiers JC, Muramatsu T, Aben JP, Onuma Y, Soekhradj S et al. Advanced three-dimensional quantitative coronary angiographic assessment of bifurcation lesions: methodology and phantom validation. *EuroIntervention* 2013;8(12):1451-1460.
- (15) Grundeken MJ, Asgedom S, Damman P, Lesiak M, Norell MS, Garcia E et al. Six-month and one-year clinical outcomes after placement of a dedicated coronary bifurcation stent: a patient-level pooled analysis of eight registry studies. *EuroIntervention* 2013;9(2):195-203.
- (16) Grundeken MJ, Stella PR, Wykrzykowska JJ. The Tryton Side Branch Stent for the treatment of coronary bifurcation lesions. *Expert Rev Med Devices* 2013;10(6):707-716.
- (17) Onuma Y, Girasis C, Aben JP, Sarno G, Piazza N, Lokkerbol C et al. A novel dedicated 3-dimensional quantitative coronary analysis methodology for bifurcation lesions. *EuroIntervention* 2011;7(5):629-635.
- (18) Galassi AR, Tomasello SD, Capodanno D, Seminara D, Canonico L, Occhipinti M et al. A novel 3-d reconstruction system for the assessment of bifurcation lesions treated by the mini-crush technique. *J Interv Cardiol* 2010;23(1):46-53.
- (19) Dvir D, Assali A, Lev EI, Ben-Dor I, Battler A, Kornowski R. Percutaneous interventions in unprotected left main lesions: novel three-dimensional imaging and quantitative analysis before and after intervention. *Cardiovasc Revasc Med* 2010;11(4):236-240.
- (20) Ramcharitar S, Daeman J, Patterson M, van Guens RJ, Boersma E, Serruys PW et al. First direct in vivo comparison of two commercially available three-dimensional quantitative coronary angiography systems. *Catheter Cardiovasc Interv* 2008;71(1):44-50.
- (21) Girasis C, Schuurbiers JC, Onuma Y, Aben JP, Weijers B, Morel MA et al. Advances in two-dimensional quantitative coronary angiographic assessment of bifurcation lesions: improved small lumen diameter detection and automatic reference vessel diameter derivation. *EuroIntervention* 2012;7(11):1326-1335.
- (22) Meerkin D, Marom H, Cohen-Biton O, Einav S. Three-dimensional vessel analyses provide more accurate length estimations than the gold standard QCA. *J Interv Cardiol* 2010;23(2):152-159.
- (23) Tsuchida K, van der Giessen WJ, Patterson M, Tanimoto S, Garcia-Garcia HM,

Regar E et al. In vivo validation of a novel three-dimensional quantitative coronary angiography system (CardiOp-B): comparison with a conventional two-dimensional system (CAAS II) and with special reference to optical coherence tomography. *EuroIntervention* 2007;3(1):100-108.

- (24) Bruining N, Tanimoto S, Otsuka M, Weustink A, Ligthart J, de WS et al. Quantitative multi-modality imaging analysis of a bioabsorbable poly-L-lactic acid stent design in the acute phase: a comparison between 2- and 3D-QCA, QCU and QMSCT-CA. *EuroIntervention* 2008;4(2):285-291.
- (25) Yong AS, Ng AC, Brieger D, Lowe HC, Ng MK, Kritharides L. Three-dimensional and two-dimensional quantitative coronary angiography, and their prediction of reduced fractional flow reserve. *Eur Heart J* 2011;32(3):345-353.
- (26) Girasis C, Serruys PW, Onuma Y, Colombo A, Holmes DR, Jr., Feldman TE et al. 3-Dimensional bifurcation angle analysis in patients with left main disease: a substudy of the SYNTAX trial (SYnergy Between Percutaneous Coronary Intervention with TAXus and Cardiac Surgery). *JACC Cardiovasc Interv* 2010;3(1):41-48.
- (27) Girasis C, Farooq V, Diletti R, Muramatsu T, Bourantas CV, Onuma Y et al. Impact of 3-dimensional bifurcation angle on 5-year outcome of patients after percutaneous coronary intervention for left main coronary artery disease: a substudy of the SYNTAX trial (synergy between percutaneous coronary intervention with taxus and cardiac surgery). *JACC Cardiovasc Interv* 2013;6(12):1250-1260.
- (28) Sarno G, Garg S, Onuma Y, Girasis C, Tonino P, Morel MA et al. Bifurcation lesions: Functional assessment by fractional flow reserve vs. anatomical assessment using conventional and dedicated bifurcation quantitative coronary angiogram. *Catheter Cardiovasc Interv* 2010;76(6):817-823.

**Table 1. Sub-segment level analysis (paired samples N=114)**

Variables	Paired samples (N=114)		p value
	2-D QCA	3-D QCA	
<b>Pre-procedure</b>			
Proximal Main Branch (segment 2 in BSM6)			
MLD, mm	1.75 ± 0.65	1.84 ± 0.61	<0.01
RVD, mm	3.00 ± 0.57	2.71 ± 0.51	<0.01
DS, %	41.4 ± 19.5	31.7 ± 19.4	<0.01
Length, mm	8.34 ± 4.23	9.25 ± 4.72	<0.01
Binary stenosis rate, n(%)	40 (35.1)	25 (21.9)	0.03
Distal Main Branch (segment 3 in BSM6)			
MLD, mm	1.32 ± 0.36	1.33 ± 0.37	0.68
RVD, mm	2.24 ± 0.40	2.21 ± 0.40	0.08
DS, %	40.2 ± 15.6	38.9 ± 15.3	0.28
Length, mm	9.87 ± 5.27	11.63 ± 6.56	<0.01
Binary stenosis rate, n(%)	36 (31.6)	27 (23.7)	0.18
Side Branch (segment 5 in BSM6)			
MLD, mm	1.29 ± 0.38	1.22 ± 0.41	0.02
RVD, mm	2.08 ± 0.36	1.99 ± 0.33	<0.01
DS, %	37.8 ± 15.8	38.9 ± 16.7	0.46
Length, mm	6.23 ± 1.86	6.79 ± 2.23	<0.01
Binary stenosis rate, n(%)	30 (26.3)	29 (25.4)	0.88
Ostial Side Branch (segment 8 in BSM11)			
MLD, mm	1.42 ± 0.41	1.44 ± 0.45	0.63
RVD, mm	2.08 ± 0.35	1.99 ± 0.33	<0.01
DS, %	31.6 ± 16.3	28.1 ± 16.9	0.02
Length, mm	2.95 ± 0.39	2.94 ± 0.41	0.57
Binary stenosis rate, n(%)	18 (15.8)	9 (7.9)	0.07
<b>Post-procedure</b>			
Proximal Main Branch (segment 2 in BSM6)			
MLD, mm	2.89 ± 0.39	2.89 ± 0.38	0.91
RVD, mm	3.28 ± 0.44	3.11 ± 0.42	<0.01

DS, %	11.52 ± 7.25	6.86 ± 6.64	<0.01
Length, mm	8.01 ± 4.02	8.70 ± 4.35	<0.01
Binary stenosis rate, n(%)	0 (0.0)	0 (0.0)	1.00
Distal Main Branch (segment 3 in BSM6)			
MLD, mm	2.38 ± 0.32	2.42 ± 0.34	0.04
RVD, mm	2.66 ± 0.32	2.66 ± 0.31	0.84
DS, %	10.35 ± 8.37	9.28 ± 6.11	0.14
Length, mm	10.05 ± 5.04	11.40 ± 6.03	<0.01
Binary stenosis rate, n(%)	0 (0.0)	0 (0.0)	1.00
Side Branch (segment 5 in BSM6)			
MLD, mm	1.78 ± 0.39	1.75 ± 0.40	0.23
RVD, mm	2.18 ± 0.31	2.15 ± 0.42	0.37
DS, %	18.28 ± 14.13	18.61 ± 13.17	0.77
Length, mm	6.41 ± 2.03	6.66 ± 2.23	0.09
Binary stenosis rate, n(%)	4 (3.5)	2 (1.8)	0.41
Ostial Side Branch (segment 8 in BSM11)			
MLD, mm	1.81 ± 0.40	1.85 ± 0.39	0.08
RVD, mm	2.19 ± 0.31	2.16 ± 0.42	0.3
DS, %	17.58 ± 13.66	14.14 ± 11.62	<0.01
Length, mm	2.97 ± 0.44	2.96 ± 0.43	0.61
Binary stenosis rate, n(%)	4 (3.5)	1 (0.9)	0.18

MLD = minimal luminal diameter, RVD = reference vessel diameter, DS = diameter stenosis, BSM = bifurcation segment model.

**Table 2. Treated segment level analysis**

Variables	Paired samples (N=114)		
	2D QCA	3D QCA	p value
<b>In-segment (whole segment in BSM6)</b>			
Smallest MLD, mm			
Pre-procedure	1.07 ± 0.27	1.05 ± 0.29	0.43
Post-procedure	1.56 ± 0.34	1.0 ± 0.34	0.08
Largest DS, %			
Pre-procedure	53.96 ± 12.25	52.09 ± 11.31	0.06
Post-procedure	32.39 ± 10.93	28.66 ± 10.40	0.08
<b>Treated segment (segment 2, 3, 5 in BSM6)</b>			
Smallest MLD, mm			
Pre-procedure	1.07 ± 0.28	1.05 ± 0.30	0.47
Post-procedure	1.76 ± 0.37	1.74 ± 0.39	0.36
Largest DS, %			
Pre-procedure	53.87 ± 12.40	52.09 ± 11.31	<0.01
Post-procedure	23.21 ± 10.88	20.89 ± 11.89	0.01

BSM = bifurcation segment model, MLD = minimal luminal diameter, DS = diameter stenosis.

**Table 3. Bifurcation Angle Analysis (paired sample N=114)**

Bifurcation Angle, degree	Paired samples (N=114)		p value
	2-D QCA	3-D QCA	
Pre-procedure			
Proximal MB-SB	141.3 ± 22.8	137.4 ± 17.5	0.04
Distal MB-SB	61.9 ± 21.9	59.0 ± 16.2	0.08
Post-procedure			
Proximal MB -SB	153.0 ± 18.2	144.3 ± 14.3	<0.01
Distal MB-SB	51.7 ± 18.9	51.4 ± 13.8	0.85

Bifurcation Angle, degree	Paired samples (N=114)		p value
	Pre-procedure	Post-procedure	
2-D QCA			
Proximal MB -SB	141.3 ± 22.8	153.0 ± 18.2	<0.01
Distal MB -SB	61.9 ± 21.9	51.7 ± 18.9	<0.01
3-D QCA			
Proximal MB -SB	137.4 ± 17.5	144.3 ± 14.4	<0.01
Distal MB -SB	59.0 ± 16.2	51.4 ± 13.8	<0.01

MB = main branch, SB = side branch.

**Figure 1.**

**Title:** Treatment procedure using the Tryton stent and the definition of the treated segment.

**Caption:** A bifurcation lesion was observed in the mid segment of left anterior descending artery and a diagonal branch (left in panel A). After pre-dilatation, a tryton stent was implanted toward the side branch (center left), then a drug-eluting stent was implanted through the Tryton stent in the main vessel (center right). The final angiogram showed fine results (right). The treated segments were delineated using 3 white lines (see white arrows) at the proximal main branch (PMB), distal main branch (DMB), and side branch (SB) in the matched projections (white arrows, pre-procedure in panel B and post-procedure in panel C). Specifically, the proximal and distal borders of the main vessel were set at the proximal and distal edge of the DES implanted, respectively. In this case, the distal border of side branch was defined as the distal edge of the Tryton stent.

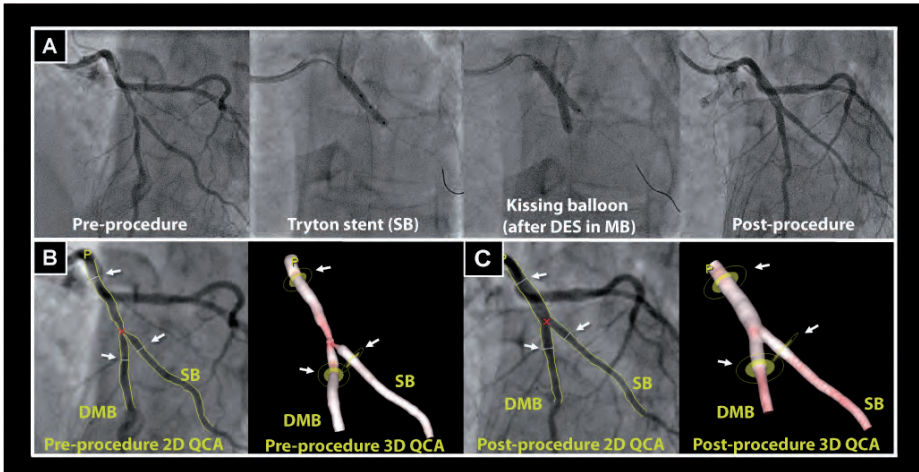


**Figure 2.**

**Title:** Two-dimensional (2D) and three-dimensional (3D) QCA assessments.

**Caption:** Severe stenosis was evident at the ostium of side branch (yellow arrows) in the LAO cranial view (panel A), while this part was overlapped and ‘hidden’ by the overlapping main vessel in the RAO cranial view (panel B). An angiogram with the largest bifurcation angle between distal main branch and side branch was used for 2D quantitative coronary angiography assessment in the current analysis (e.g., the panel A in this case).

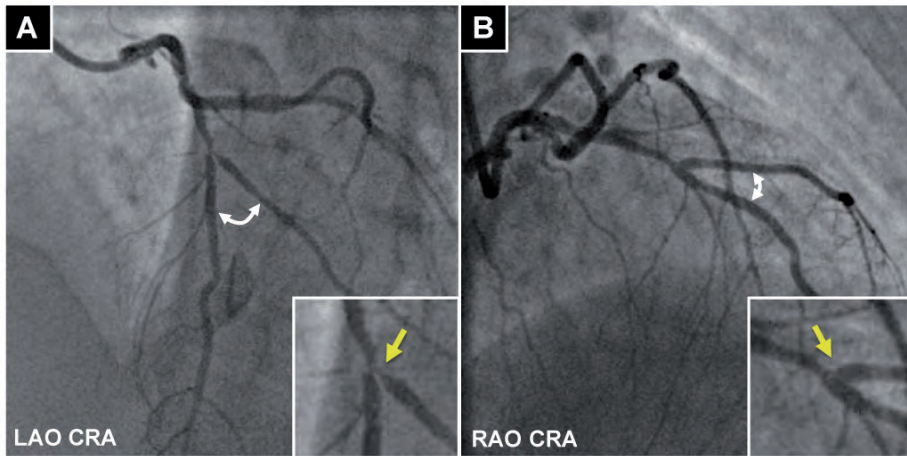


**Figure 3.**

**Title:** Bifurcation segment models in the Cardiovascular Angiography Analysis System (CAAS).

**Caption:** Segments 2, 3 and 5 in bifurcation 6-segment model (BSM6) correspond to the treated segment, where the stents were implanted or balloons were dilated, including the proximal main branch (PMB), distal main branch (DMB) and side branch (SB) respectively. These three sub-segments are divided by the point of bifurcation (POB) defined as the point where all the centerlines meet and the midpoint of the largest circle/sphere that can reach all three contours in bifurcation.<sup>9</sup> Segments 1, 4 and 6 correspond to 5-mm segments beyond the treated segment (left panel). Segments 8 in BSM11 reflect 3-mm ostial segments of SB (right panel). In this study, the aforementioned treated segment corresponded to segments 2, 3, and 5 of BSM6, and in-segment corresponded to entire segments in BSM6.

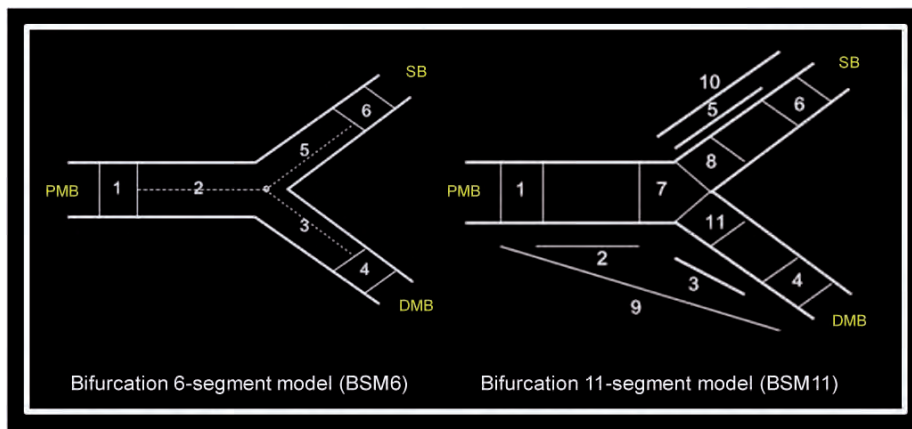


### Figure 4A.

**Title:** Bland-Altman plots and cumulative frequency distribution (CFD) curves of MLD and %DS in the ostial side branch.

**Caption:** In the Bland-Altman plots (upper panels), solid lines indicate the mean difference between 2D and 3D analyses and dotted lines indicate the upper and lower limit of agreement (LOA). In the CFD curves (lower panels), blue circles indicate 2D QCA and red squares indicate 3D QCA (lower panels). MLD = minimal luminal diameter, %DS = percentage diameter stenosis.

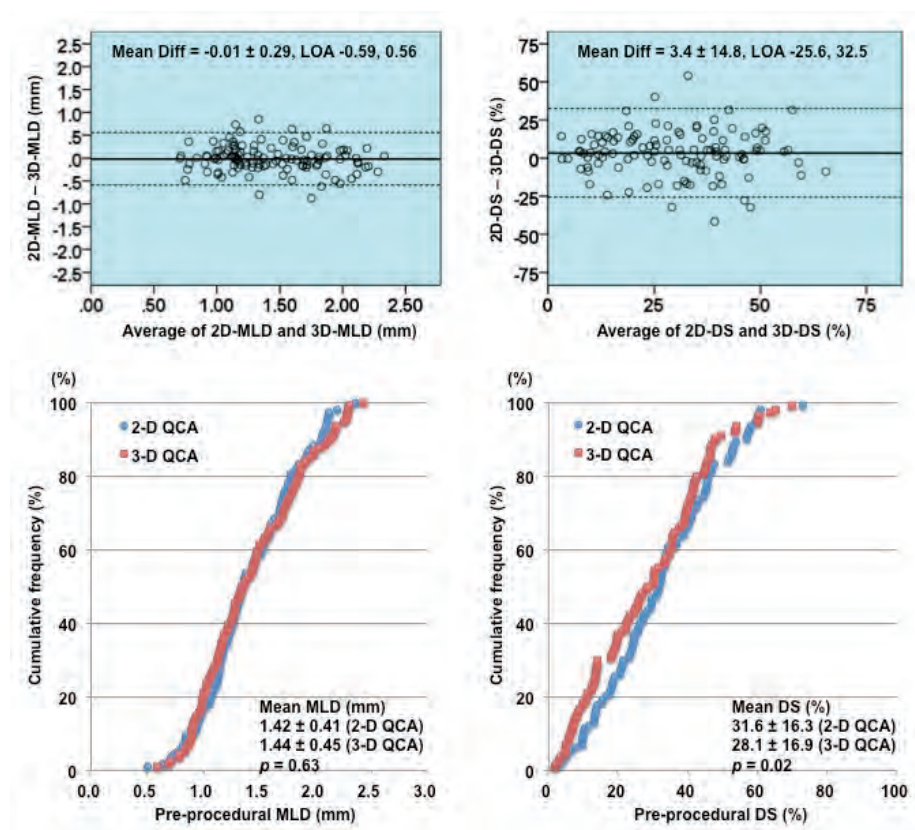
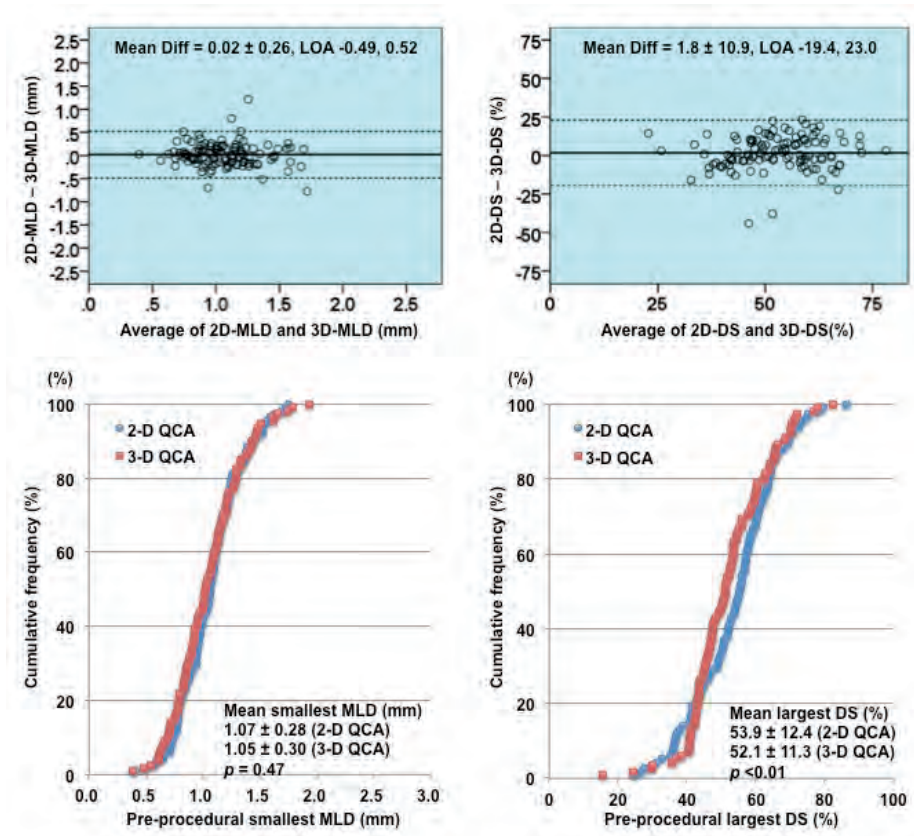


**Figure 4B.**

**Title:** Bland-Altman plots and cumulative frequency distribution (CFD) curves of the smallest MLD and the largest %DS in the treated segment.

**Caption:** In the Bland-Altman plots (upper panels), solid lines indicate the mean difference between 2D and 3D analyses and dotted lines indicate the upper and lower limit of agreement (LOA). In the CFD curves (lower panels), blue circles indicate 2D QCA and red squares indicate 3D QCA (lower panels). MLD = minimal luminal diameter, %DS = percentage diameter stenosis.





*Supplementary materials*

**Figure S1.**

**Title:** Schematic representation of diameter measurements in the 3D QCA analysis.

**Caption:** The measured area in an elliptical cross-section is converted to a circle with the same area. The diameter of such a circle is called as an equivalent diameter.

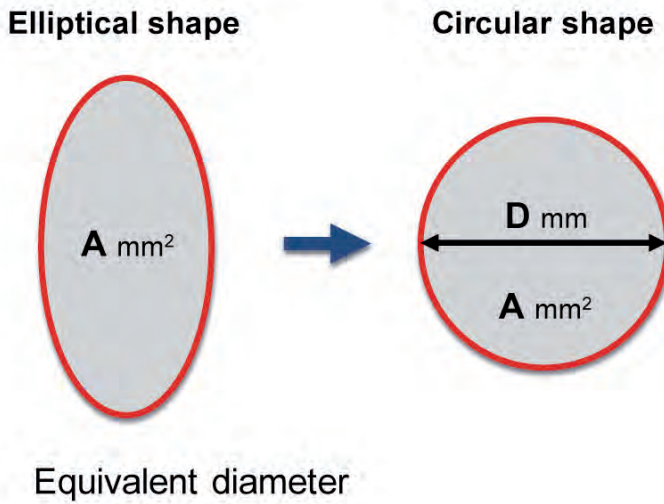


**Figure S2. Title:** Flow diagram of this study.

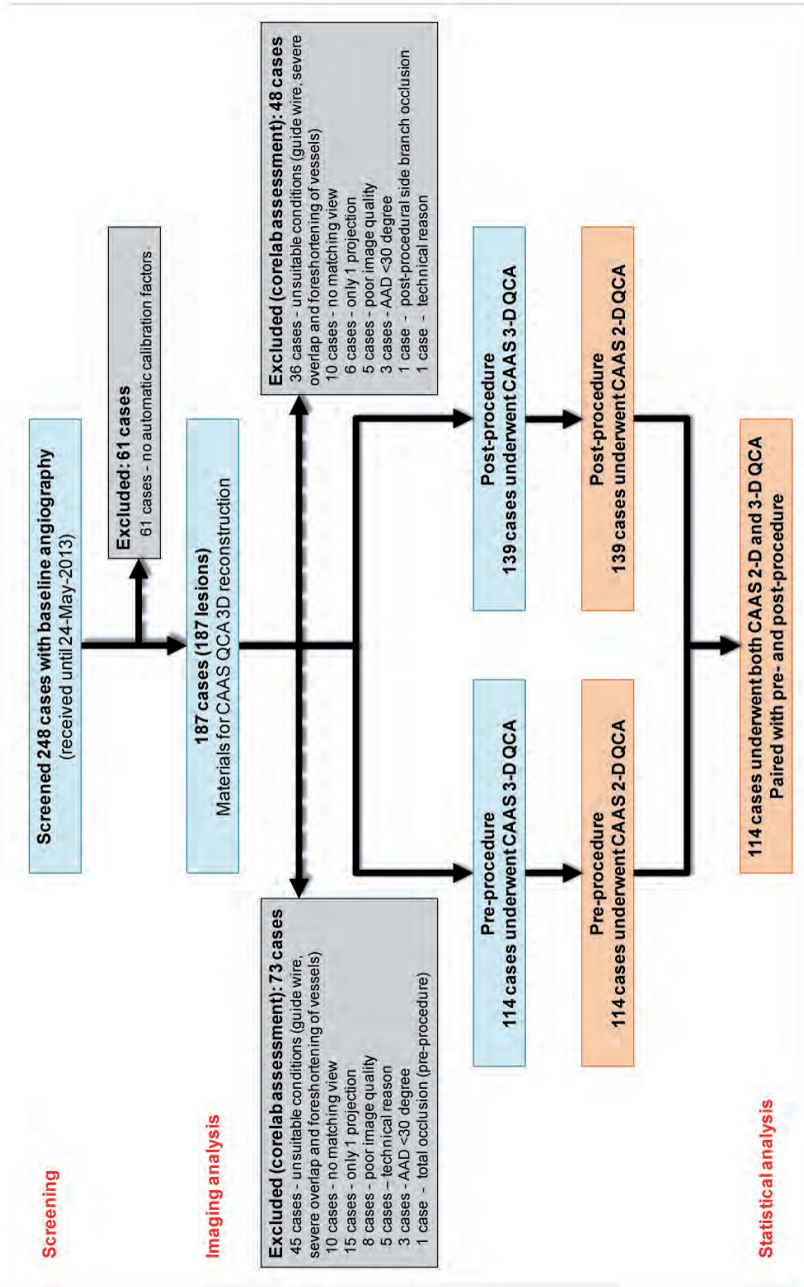
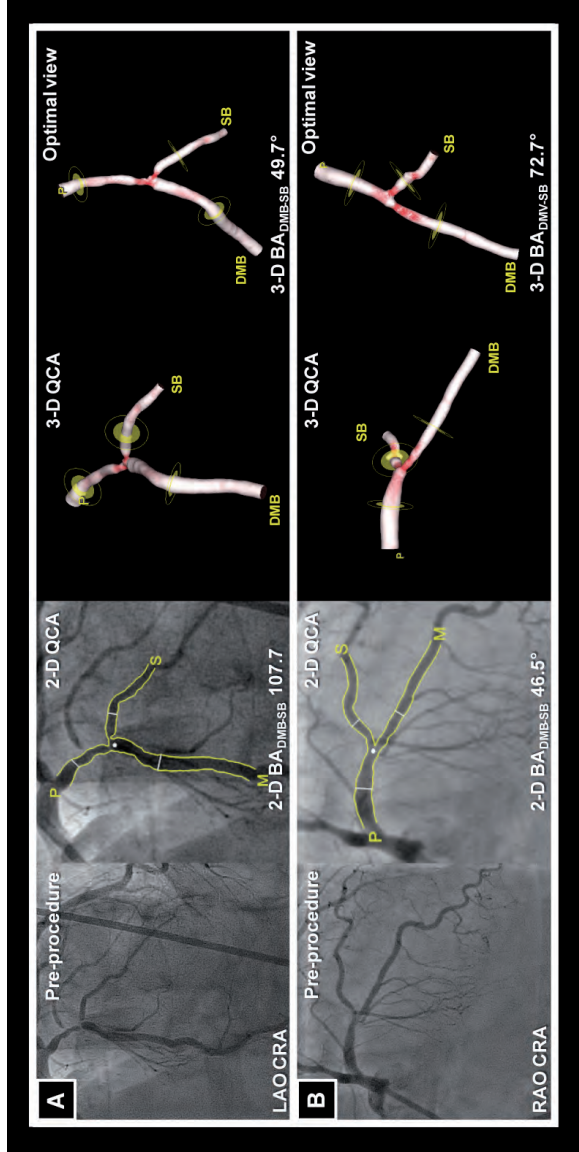


**Figure S3.**

**Title:** Examples of distal bifurcation angle assessment in 2D and 3D QCA.

**Caption:** Pre-procedural angiograms revealed bifurcation lesions located in the left anterior descending artery and a diagonal branch. In both cases, distal main branch (MB) and side branch (SB) were well separated in the first images selected for 2D analysis. In panel A, 2D QCA showed a distal bifurcation angle ( $BA_{DMB-SB}$ ) of 107.7 degree, while 3D QCA showed a distal bifurcation angle of 49.7 degree, suggesting overestimation of 2D analysis compared to 3D analysis. Conversely, panel B, 2D QCA showed a  $BA_{DMV-SB}$  of 46.5 degree, while in 3D QCA this was shown to be 72.7 degree, suggesting underestimation of 2D analysis compared to 3-D analysis.



### 3.4 Three-dimensional OCT assessment of bioresorbable magnesium alloy in bifurcation

Serial 2-Dimensional and 3-Dimensional optical coherence tomography assessment of overhanging struts of drug-eluting absorbable metal scaffold. “DREAMS” for jailed side branch?

*JACC Cardiovasc Interv.* 2014;7:575-6.  
[Case report, Impact Factor (2013): 7.440]

Muramatsu T, García-García HM, Serruys PW, Waksman R, Verheye S.





## Serial 2-Dimensional and 3-Dimensional Optical Coherence Tomography Assessment of Overhanging Struts of Drug-Eluting Absorbable Metal Scaffold

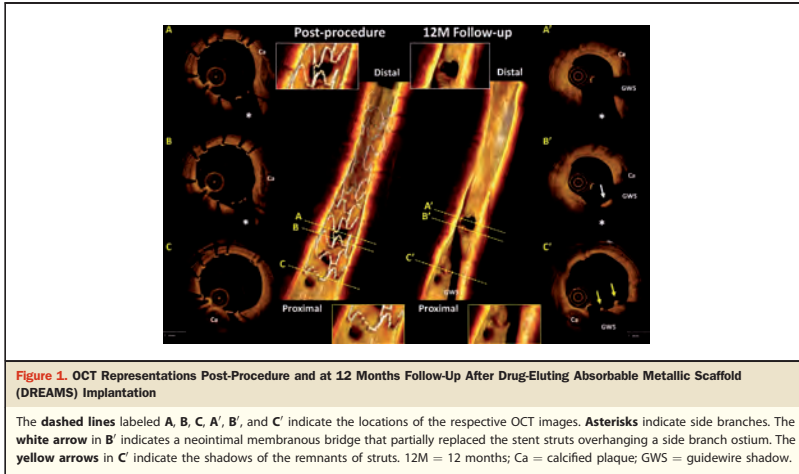
### “DREAMS” for Jailed Side Branch?

Takashi Muramatsu, MD, PhD,\*† Hector M. García-García, MD, PhD,\*‡  
Patrick W. Serruys, MD, PhD,\* Ron Waksman, MD,§ Stefan Verheye, MD,||  
on behalf of the BIOSOLVE-I Investigators

Rotterdam, the Netherlands; Toyoko, Japan; Washington, DC; and Antwerpen, Belgium

A 75-year-old woman with stable angina pectoris underwent percutaneous coronary intervention of the left anterior descending coronary artery,

whereby a 3.25/16-mm paclitaxel-eluting absorbable metal scaffold (DREAMS, Biotronik, Bülach, Switzerland) was successfully implanted.



From the \*Thoraxcenter, Erasmus Medical Center, Rotterdam, the Netherlands; †Department of Cardiology, Fujita Health University Hospital, Toyoko, Japan; ‡Cardialysis B.V., Rotterdam, the Netherlands; §MedStar Washington Hospital Center, Washington, DC; and the ||ZNA Middelheim, Antwerpen, Belgium. Dr. Waksman has received research grant support and consulting fees from Biotronik. All other authors have reported that they have no relationships relevant to the contents of this paper to disclose.

Manuscript received June 20, 2013; accepted July 18, 2013.

Post-procedural angiography showed excellent results without pinching of the side branch ostium. The patient experienced no procedure-related complications, and was discharged 48 h after the procedure on dual antiplatelet therapy. Optical coherence tomography (OCT) (LightLab Imaging, Westford, Massachusetts) was performed post-procedure and at 12 months follow-up. Post-procedurally, the

scaffold was well expanded with good apposition of struts to the vessel wall, and a side branch was jailed by the struts of DREAMS (Figs. 1A and 1B). At 12 months follow-up, OCT showed a smooth luminal surface with moderate neointimal hyperplasia in the scaffolded segment. Some remnants of struts were still visible with shadows (Fig. 1C', yellow arrows). Interestingly, the struts overhanging a side branch ostium were partially replaced by a neointimal membranous bridge (Fig. 1B', white arrow), whereas 3-dimensional OCT revealed the unobstructed and widely opened ostium of the side branch.

This is the first report to our knowledge of a serial OCT assessment in a case of overhanging struts at the ostium of a side branch after DREAMS implantation. Fully bioresorbable scaffolds are a novel therapeutic approach because they provide transient vessel support, in contrast to the permanent metallic stents. The DREAMS absorbable metal scaffold is made of a magnesium alloy, and is programmed to be absorbed and ultimately converted to hydroxyapatite 9 to 12 months following implantation (1). Previously, a similar case had been reported with the everolimus-eluting polymeric bioresorbable scaffold (Absorb BVS, Abbott Vascular, Santa Clara, California), but with a longer period (24 months) of bioresorption than in this case

(2). This case highlights the resorption of the magnesium struts overhanging a side branch ostium, as illustrated in 3-dimensional OCT (3).

---

**Reprint requests and correspondence:** Dr. Hector M. García-García, Thoraxcenter, Erasmus Medical Center, z120, Dr Molewaterplein 40, 3015 GD, Rotterdam, the Netherlands. E-mail: h.garciagarcia@erasmusmc.nl

---

#### REFERENCES

1. Haude M, Erbel R, Erne P, et al. Safety and performance of the drug-eluting absorbable metal scaffold (DREAMS) in patients with de-novo coronary lesions: 12 month results of the prospective, multicentre, first-in-man BIOSOLVE-I trial. *Lancet* 2013;381:836–44.
2. Okamura T, Serruys PW, Regar E. Cardiovascular flashlight. The fate of bioresorbable struts located at a side branch ostium: serial three-dimensional optical coherence tomography assessment. *Eur Heart J* 2010; 31:2179.
3. Farooq V, Gogas BD, Okamura T, et al. Three-dimensional optical frequency domain imaging in conventional percutaneous coronary intervention: the potential for clinical application. *Eur Heart J* 2013;34: 875–85.

---

**Key Words:** bioresorbable scaffold ■ optical coherence tomography ■ side branch.

# Chapter 4

## Light-based Imaging Assessment for Acute Myocardial Infarction and Clinical Implications of Bioresorbable Scaffolds

### 4.1 Methodology to quantify in-stent structures

Quantitative optical frequency domain imaging assessment of in-stent structures in patients with ST-segment elevation myocardial infarction: impact of imaging sampling rate.

*Circ J.* 2012;76:2822-31.

[Original research paper, Impact Factor (2012): 3.578]

Muramatsu T, Garcia-Garcia HM, Lee IS, Bruining N, Onuma Y, Serruys PW.





# Quantitative Optical Frequency Domain Imaging Assessment of In-Stent Structures in Patients With ST-Segment Elevation Myocardial Infarction

## – Impact of Imaging Sampling Rate –

Takashi Muramatsu, MD, PhD; Hector M. García-García, MD, PhD; Il Soo Lee, MD, PhD;  
Nico Bruining, PhD; Yoshinobu Onuma, MD; Patrick W. Serruys, MD, PhD

**Background:** The impact of the sampling rate (SR) of optical frequency domain imaging (OFDI) on quantitative assessment of in-stent structures (ISS) such as plaque prolapse and thrombus remains unexplored.

**Methods and Results:** OFDI after stenting was performed in ST-segment elevation myocardial infarction (STEMI) patients using a TERUMO OFDI system (Terumo Europe, Leuven, Belgium) with 160 frames/s and pullback speed of 20 mm/s. A total of 126 stented segments were analyzed. ISS were classified as either attached or non-attached to stent area boundaries. The volume, mean area and largest area of ISS were assessed according to 4 frequencies of SR, corresponding to distances between the analyzed frames of 0.125, 0.25, 0.50 and 1.0 mm. ISS volume was calculated by integrating cross-sectional ISS areas multiplied by each sampling distance using the disk summation method. The volume and mean area of ISS became significantly larger, while the largest area became significantly smaller as sampling distance became larger (1.11 mm<sup>2</sup> for 0.125 mm vs. 1.00 mm<sup>2</sup> for 1.0 mm, P for trend=0.036). In addition, variance of difference was positively associated with increasing width of sampling distance.

**Conclusions:** Quantification of ISS is significantly influenced by the applied frequency of SR. This should be taken into account when designing future OFDI studies in which quantitative assessment of ISS is critical for the evaluation of STEMI patients. (*Circ J* 2012; **76**: 2822–2831)

**Key Words:** Acute myocardial infarction; Coronary artery disease; Coronary thrombosis; Optical coherence tomography; Prolapse

Intravascular optical coherence tomography (OCT) is a light-based imaging modality that provides high-resolution images of the coronary arteries.<sup>1–3</sup> The recently developed optical frequency domain imaging (OFDI) technique, or Fourier-domain OCT, provides higher image acquisition speed, greater penetration depth, and higher-quality image resolution compared to the conventional time-domain OCT.<sup>4–7</sup> Furthermore, its higher frame rate and higher pullback speed reduce the impact of possible motion artifacts and improve longitudinal resolution, facilitating a more detailed depiction and more accurate quantitative analysis of coronary arteries compared to the time-domain OCT.<sup>8,9</sup>

Recent OCT/OFDI studies applied various sampling rates (SRs) for qualitative and quantitative cross-sectional image analysis. The SR, which can be translated into the distance be-

tween 2 sampled frames along the longitudinal axis (ie, sampling distance), varied from 0.33 to 1.0 mm.<sup>10–14</sup> Interestingly, a previous study demonstrated that lumen and stent areas showed low variability (<10%) within the various sampling distances ranging from 0.3 to 2.4 mm.<sup>15</sup> The variability in detecting uncovered stent struts, however, increased across the sampling distances, and the relative difference reached more than 50% at 0.90-mm analysis compared to 0.06-mm analysis as a reference. This suggests that quantification of lumen and stent areas is stable over a wide range of SR but that heterogeneously distributed structures such as uncovered struts are influenced by SR.

This then prompts the question of how different SRs might possibly affect quantification of intraluminal masses (ie, plaque prolapse and thrombus), which are also heterogeneously dis-

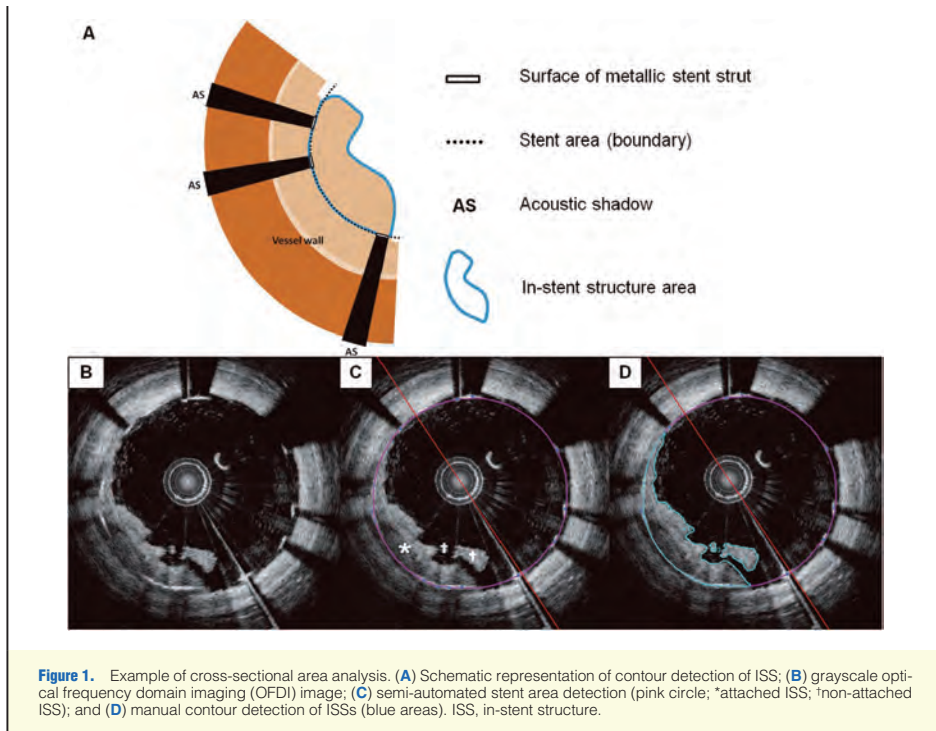
Received April 24, 2012; revised manuscript received July 9, 2012; accepted July 27, 2012; released online August 29, 2012 Time for primary review: 15 days

Thoraxcenter, Erasmus Medical Center, Rotterdam (T.M., H.M.G.-G., I.S.L., N.B., Y.O., P.W.S.); Cardialysis BV, Rotterdam (H.M.G.-G.), The Netherlands

Mailing address: Yoshinobu Onuma, MD, Department of Interventional Cardiology, Thoraxcenter, Erasmus Medical Center, 's-Gravendijkwal 230, 3015 CE, Rotterdam, The Netherlands. E-mail: yoshinobuonuma@gmail.com

ISSN-1346-9843 doi:10.1253/circj.CJ-12-0536

All rights are reserved to the Japanese Circulation Society. For permissions, please e-mail: cj@j-circ.or.jp



tributed in coronary arteries. This issue is crucial in the design of longitudinal studies for the evaluation of intraluminal masses. Therefore, the aim of this study was to examine the impact of different SRs on quantitative OFDI assessment of intraluminal masses after stent implantation in patients with ST-segment elevation myocardial infarction (STEMI).

## Methods

### Subjects

This is a sub-study of the TROFI trial, which was a prospective, randomized controlled, single-blinded, multicenter clinical study enrolling 141 STEMI patients at 5 European centers (ClinicalTrials.gov identifier: NCT01271361). Briefly, STEMI patients having an angiographically visible stenosis (>30%) or pre-procedural TIMI flow grade  $\leq 2$  in a single de novo, native, unstented vessel were considered for enrollment. Patients were randomized in a 1:1 fashion to receive either primary percutaneous coronary intervention (PCI) with thrombectomy (n=71) or without thrombectomy (n=70) prior to biolimus-A9 eluting metallic stent (Nobori®; Terumo Europe, Leuven, Belgium) implantation. The primary endpoint was defined as post-procedural minimal flow area quantified on OFDI. In this sub-study, the OFDI data were pooled regardless of the treatment arm. This study protocol was approved by the local ethics committee at each participating center, and written informed con-

sent was obtained from all enrolled patients.

### Image Acquisition

The primary PCI procedure was performed using a 6-Fr guiding catheter. As long as the patient's hemodynamics were stable, 0.2 mg i.c. nitroglycerin was given before the OFDI procedure. This imaging procedure was performed with a TERUMO OFDI system (Terumo Europe, Leuven, Belgium) using a non-occlusive technique at an image acquisition rate of 160 frames/s during an automated pullback at a speed of 20 mm/s. The pullback was performed during continuous i.c. injection of contrast medium through the guiding catheter using an injection pump at a flow rate of 3–4 ml/s for a maximum of 4 s. The imaging data once saved in the console were converted into AVI files and then transferred for off-line quantitative analysis.

### Definition of In-Stent Structure and Contour Detection

The region of interest (ROI) was selected as the stented segment, which was defined as the region between the first and the last frame where metallic stent struts were visible around the whole vessel circumference.<sup>7</sup> Quantitative analysis software (QCU-CMS version 4.50; LKEB, Leiden University, Leiden, The Netherlands) was used for off-line OFDI analysis.

In each cross-section, we analyzed all individual masses within the stent area, which was defined as in-stent structure (ISS). In cases of incomplete stent apposition, masses located

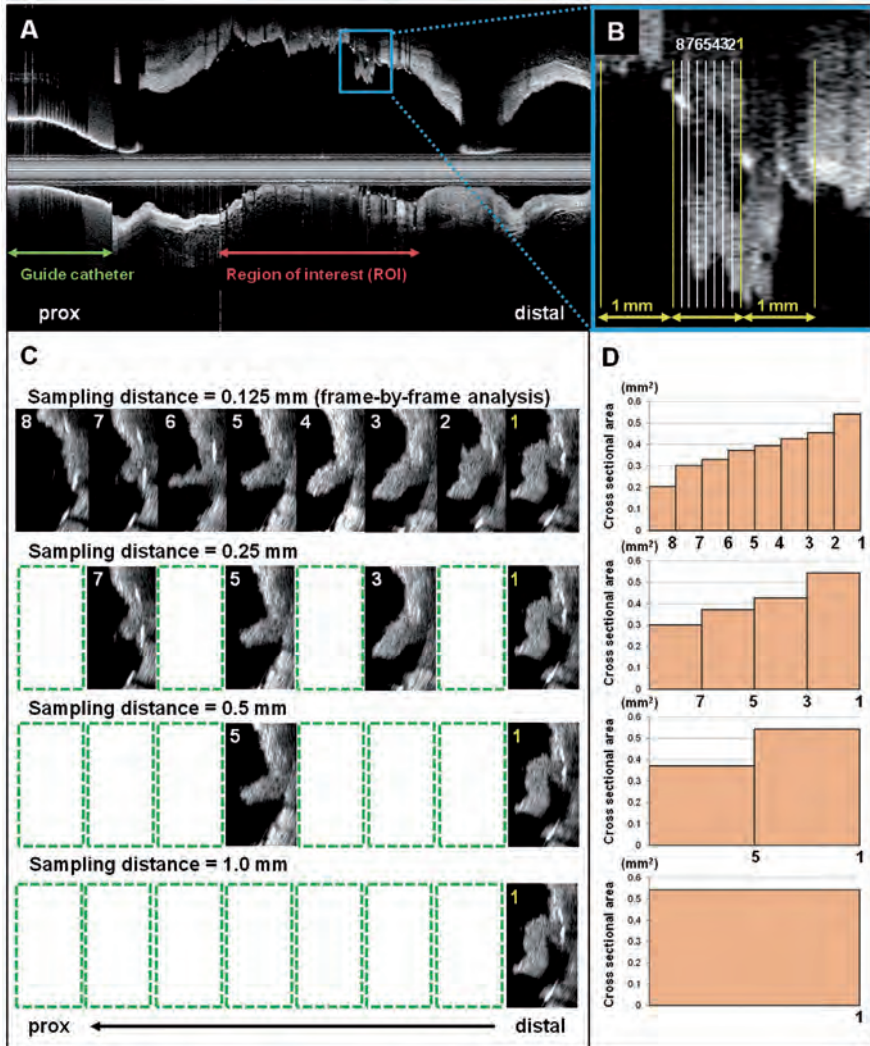


**Figure 2.** Example of sampling frames and volumetric assessment. **(A)** Focally protruding mass is shown on longitudinal view (blue box). **(B)** In the magnified image, each cross-section is numbered and indicated by yellow and white lines. **(C)** Cross-sectional area analysis was performed in all frames (sampling distance of 0.125mm), every 3<sup>rd</sup> frame (0.25mm), every 5<sup>th</sup> frame (0.50mm), and every 9<sup>th</sup> frame (1.0mm). **(D)** Schematic representation of volumetric estimation of in-stent structure (ISS) for corresponding sampling distance. ISS volume can be calculated by numerical integration of cross-sectional area multiplied by corresponding sampling distance (disk summation method). The estimated ISS volume can be expressed as the total bar (disk) area.

Table 1. Frames With ISS vs. Sampling Rate					
	0.125 mm	0.25 mm	0.5 mm	1.0 mm	P for trend <sup>†</sup>
<b>No. analyzed frames</b>	21,703	10,887	5,475	2,770	
<b>No. frames with ISS</b>					
Attached	14,269 (65.7)	7,247 (66.6)	3,722 (68.0)	1,986 (71.7)	
Non-attached	1,657 (7.6)	835 (7.7)	430 (7.9)	242 (8.7)	
Any	14,513 (66.9)	7,383 (67.8)	3,808 (69.6)	2,044 (73.8)	
<b>No. sub-segments with ISS</b>					
Attached	923	654	430	293	
Non-attached	308	139	61	39	
Any	878	633	413	284	
<b>No. frames with ISS per ROI</b>					
Attached	113.3±53.1	57.5±26.7	29.5±13.4	15.8±7.1	<0.001
Non-attached	13.2±16.4	6.6±8.2	3.4±4.2	1.9±2.4	<0.001
Any	115.2±53.2	58.6±26.7	30.2±13.5	16.2±7.2	<0.001
<b>No. sub-segments with ISS per ROI</b>					
Attached	7.3±4.1	5.2±2.9	3.4±1.9	2.3±1.3	<0.001
Non-attached	2.4±3.1	1.1±1.6	0.5±0.8	0.3±0.6	<0.001
Any	7.0±4.1	5.0±3.0	3.3±1.9	2.3±1.3	<0.001

Data given as mean±SD or n (%).

<sup>†</sup>ANOVA after logarithmic transformation. Sub-segment was defined as the presence of ISS in at least 2 sequential frames.

ISS, in-stent structure; ROI, region of interest.

outside the stent area were not taken into account for this analysis. ISS was categorized into 2 variables: attached ISS and non-attached ISS. Attached ISS was defined as a plaque prolapse or an intraluminal mass that was attached to the vessel wall or stent struts within the ROI. Non-attached ISS referred to an intraluminal mass separated from the vessel wall and stent struts. These definitions were based on the following concepts.<sup>16</sup> Plaque prolapse has been defined as a convex-shaped protrusion of tissue between adjacent stent struts towards the lumen without disruption of the continuity of the luminal vessel surface. At variance with this definition, plaque prolapse as seen in acute myocardial infarction may have a disrupted and irregular surface, and adjacent struts may be embedded or even buried in the prolapsing masses. Consequently, plaque prolapse is frequently indistinguishable from an intraluminal mass attached to the vessel wall, which is presumably thrombus. Therefore, in this study, plaque prolapse and thrombus attached to the vessel wall were categorized as a single variable, attached ISS.

An example of a cross-sectional area analysis is shown in **Figure 1**. As for the contour detection of attached ISS, the boundary that connected the surfaces of adjacent stent struts was determined on semi-automated stent area detection, and then contour was manually traced. Cross-sectional ISS area analysis was performed by 2 skilled observers for every frame along the whole ROI.

### Measurement of Interest

When more than 1 attached or non-attached ISS was detected in an analyzed cross-section, the ISS area was calculated by summing all individual ISS areas. If there was no ISS in an analyzed cross-section, ISS area was regarded as zero.

ISS volume was calculated using numerical integration based on the disk summation method,<sup>17–19</sup> the formula for which is as follows:

$$\text{ISS volume (mm}^3\text{)} = \sum_{i=1}^n \{\text{ISSarea}(i)\} \times h,$$

where n is the number of analyzed frames in an ROI and h is the width of the sampling distance.

Mean ISS area was calculated as follows:

$$\text{Mean ISS area (mm}^2\text{)} = \frac{\sum_{i=1}^n \{\text{ISSarea}(i)\}}{n},$$

where n is the number of analyzed frames in an ROI.

Given the frame rate of 160 frames/s and the pullback speed of 20 mm/s, the minimum sampling distance was determined as 0.125 mm. Therefore, we calculated the ISS volume and mean ISS area according to 4 different sampling distances. Specifically, the sampling distances of 0.125, 0.25, 0.50 and 1.0 mm corresponded to all, every 3<sup>rd</sup>, every 5<sup>th</sup> and every 9<sup>th</sup> frame starting from the most distal frame in an ROI, respectively (**Figure 2**). In addition, we counted the number of sub-segments with ISS, which was defined as the presence of ISS in at least 2 sequential frames in an ROI.

### Statistical Analysis

Descriptive data are presented as mean±SD for continuous variables or percentages. Interobserver reproducibility of measurement was assessed using Lin's concordance correlation coefficient.<sup>20</sup> Comparisons of measurements between the different SRs were done using non-parametric Wilcoxon signed-rank test, and linear trends across the 4 frequencies of SR were tested using 1-way analysis of variance (ANOVA) after logarithmic transformation. We consistently used the 0.125-mm analysis with the most frequent SR as a reference when comparing the measurements between the different SRs. Correlations were tested with Spearman's rank correlation coefficient ( $\rho$ ). Agreement of measurement was assessed by determining the range of difference (mean±2SD) according to the Bland-Altman method.<sup>21</sup> We also compared the variance (ie, square of SD) of difference between the different pairs of SRs using the Pitman-Morgan test.<sup>22,23</sup> All statistical analysis was done using SPSS 18.0 (SPSS, Chicago, IL, USA). P<0.05 was considered statistically significant.

Table 2. Area and Volumetric Analysis vs. Sampling Rate					
	0.125 mm	0.25 mm	0.50 mm	1.0 mm	P for trend
<b>Attached ISS</b>					
Volume (mm <sup>3</sup> )	5.26±4.87	5.41±4.91*	5.76±5.07*†	6.48±5.52*†‡	0.006
Absolute difference (mm <sup>3</sup> )	0 (Reference)	0.15	0.51	1.22	
Relative difference (%)	0 (Reference)	2.9	9.7	23.2	
Mean area (mm <sup>2</sup> )	0.25±0.19	0.25±0.19*	0.26±0.19*†	0.29±0.20*†‡	0.008
Absolute difference (mm <sup>2</sup> )	0 (Reference)	0.01	0.02	0.05	
Relative difference (%)	0 (Reference)	2.3	7.9	19.2	
Largest area (mm <sup>2</sup> )	1.10±0.56	1.08±0.56*	1.04±0.56*†	0.98±0.55*†‡	0.029
Absolute difference (mm <sup>2</sup> )	0 (Reference)	-0.02	-0.07	-0.12	
Relative difference (%)	0 (Reference)	-1.9	-6.1	-10.8	
<b>Non-attached ISS</b>					
Volume (mm <sup>3</sup> )	0.16±0.36	0.17±0.39	0.19±0.47	0.25±0.71*†‡	<0.001
Absolute difference (mm <sup>3</sup> )	0 (Reference)	0.01	0.03	0.09	
Relative difference (%)	0 (Reference)	6.2	17.3	56.7	
Mean area (mm <sup>2</sup> )	0.008±0.020	0.008±0.021	0.009±0.024	0.012±0.032*†‡	<0.001
Absolute difference (mm <sup>2</sup> )	0 (Reference)	0.001	0.001	0.003	
Relative difference (%)	0 (Reference)	3.8	11.3	42.8	
Largest area (mm <sup>2</sup> )	0.17±0.25	0.15±0.24*	0.12±0.24*†	0.11±0.24*†‡	0.082
Absolute difference (mm <sup>2</sup> )	0 (Reference)	-0.02	-0.05	-0.06	
Relative difference (%)	0 (Reference)	-12.4	-28.2	-35.2	
<b>Total</b>					
Volume (mm <sup>3</sup> )	5.41±4.99	5.58±5.03*	5.95±5.22*†	6.73±5.75*†‡	0.005
Absolute difference (mm <sup>3</sup> )	0 (Reference)	0.16	0.53	1.31	
Relative difference (%)	0 (Reference)	3.0	9.9	24.2	
Mean area (mm <sup>2</sup> )	0.25±0.20	0.26±0.20*	0.27±0.20*†	0.30±0.21*†‡	0.006
Absolute difference (mm <sup>2</sup> )	0 (Reference)	0.01	0.02	0.05	
Relative difference (%)	0 (Reference)	2.4	8.0	20.0	
Largest area (mm <sup>2</sup> )	1.11±0.56	1.09±0.56*	1.05±0.57*†	1.00±0.55*†‡	0.036
Absolute difference (mm <sup>2</sup> )	0 (Reference)	-0.02	-0.07	-0.12	
Relative difference (%)	0 (Reference)	-2.1	-6.0	-10.5	

Data given as mean ± SD or n (%).

\*ANOVA after logarithmic transformation. \*P<0.05 vs. 0.125 mm, †P<0.05 vs. 0.25 mm, ‡P<0.05 vs. 0.50 mm (Wilcoxon signed-rank test).

ISS, in-stent structure.

## Results

### Segment Characteristics

Among 142 ROI in 141 patients, 16 ROI in 16 patients had to be excluded due to poor image quality. Consequently, 126 ROI in 125 patients containing 21,703 frames were analyzed. The analyzed segments were located in the left anterior descending (50 ROI, 8,544 frames), left circumflex (13 ROI, 2,019 frames), right coronary arteries (54 ROI, 9,687 frames), diagonal branch (7 ROI, 1,124 frames) and obtuse marginal branch (2 ROI, 329 frames). The mean stent length and mean number of frames per ROI were 21.4 mm and 172 frames, respectively. The mean number of subsegments with ISS per ROI became smaller as sampling distance became larger (7.3 for 0.125 mm and 2.3 for 1.0 mm, P for trend <0.001; **Table 1**). Attached ISS were detected in all ROI, although non-attached ISS could not be detected in 10 ROI.

### Inter-Observer Reproducibility

Concordance correlation coefficients in 15 randomly selected ROI showed excellent reproducibility between the 2 observers (0.90, 0.94 and 0.89 in volume, mean area and largest area of

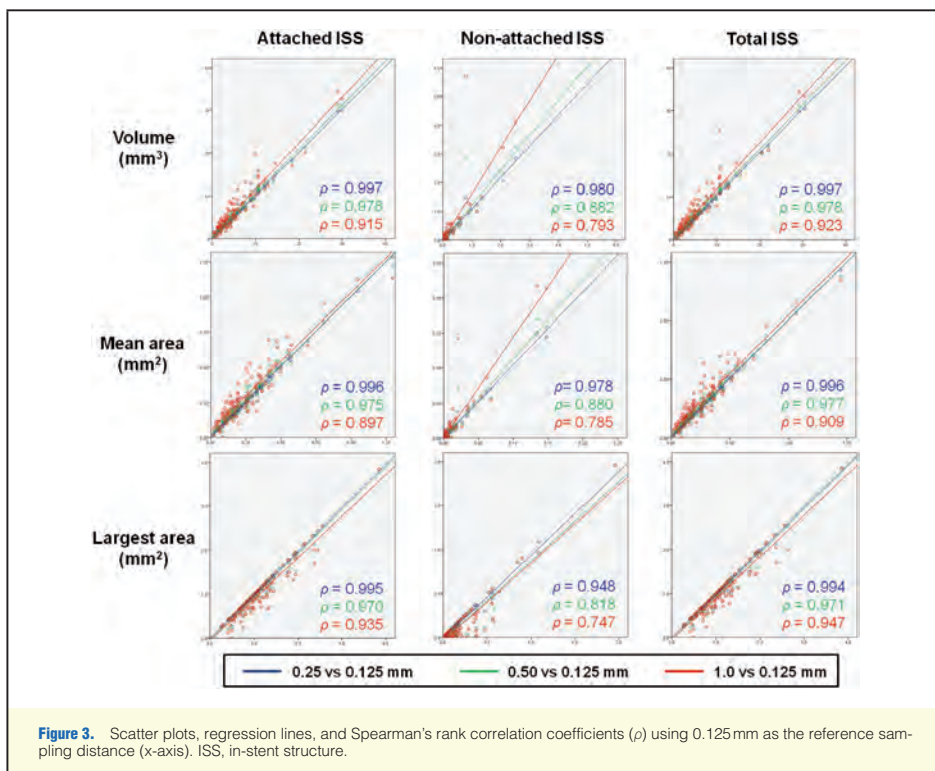
total ISS, respectively).

### Area and Volumetric Analyses

The calculated volume and areas of non-attached ISS were much smaller than those of attached ISS (**Table 2**). The volume and mean area significantly became larger as sampling distance became larger in both attached and non-attached ISS. In contrast, the largest area of attached ISS significantly became smaller as sampling distance became larger. The largest area of non-attached ISS showed a similar trend but did not reach statistical significance (P for trend=0.082). With respect to total ISS, all measurements were significantly different between the 4 frequencies of SR.

### Correlations With SR

Although correlation coefficients of non-attached ISS were generally smaller than those of attached and total ISS, all measurements showed good correlations with the reference sampling distance of 0.125 mm (**Figure 3**). In contrast, the coefficient was consistently higher as paired sampling distance became smaller than the reference distance of 0.125 mm. The volume and mean area of non-attached ISS had the greatest divergence of



regression lines than the other measurements, suggesting greater difference between SRs.

#### Agreement and Variability in Different SRs

The ranges of agreement consistently became wider as sampling distance became larger in both ISS volume (Figure 4A) and mean ISS area (Figure 4B). The variance of difference (VOD) between the different pairs of SRs is shown in Figure 5. An increase of VOD was significantly associated with increased sampling distance.

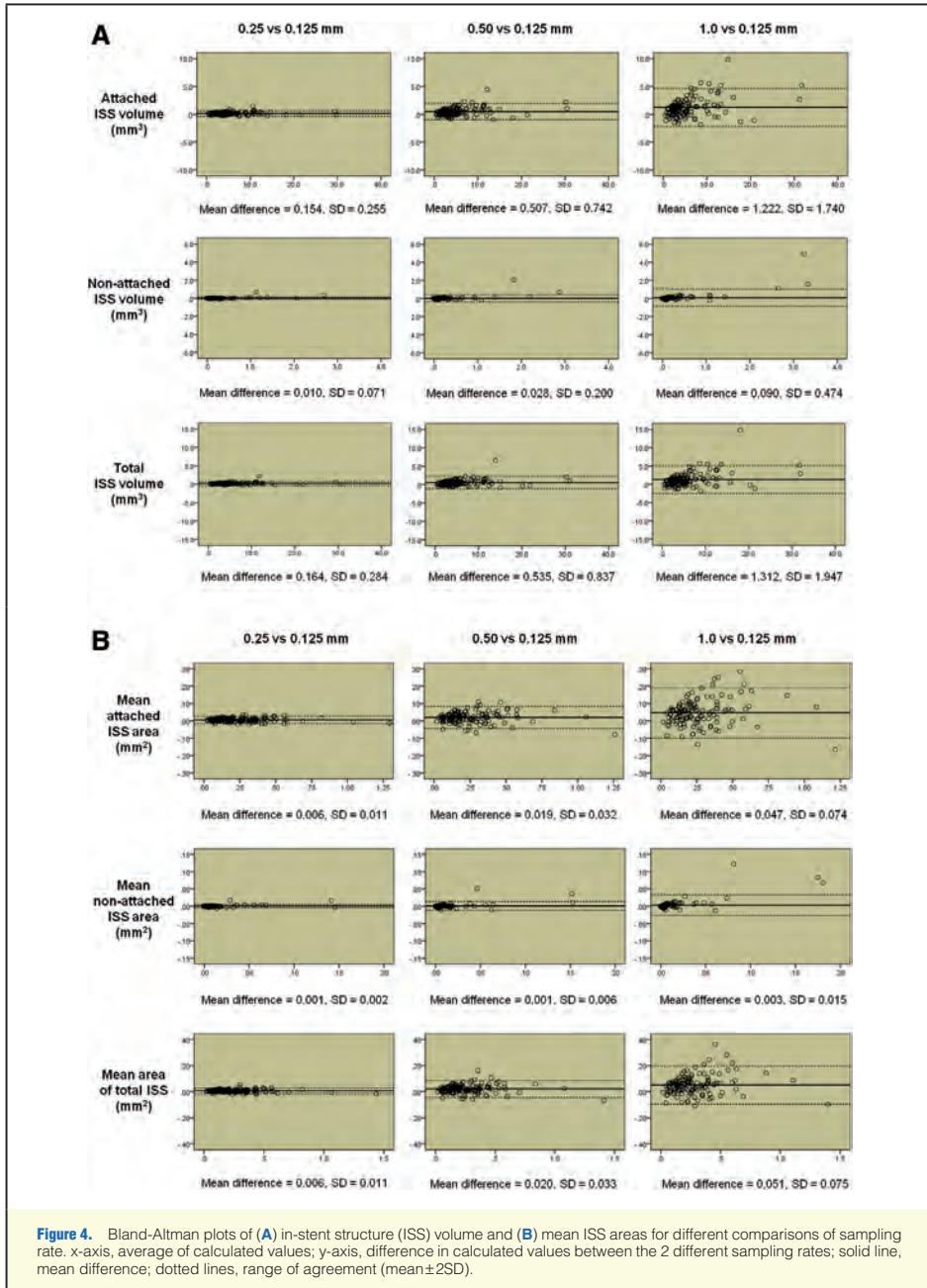
#### Discussion

To our knowledge, the present study is the first to evaluate the impact of SR in OCT/OFDI analysis on the quantitative assessment of intraluminal mass. The main findings of this study are: (1) ISS volume and mean ISS area were more likely to be overestimated, and the largest ISS area was more likely to be underestimated in larger sampling distance compared to the reference of 0.125 mm; and (2) larger variability of calculation was associated with increased sampling distance.

Recent developments in OCT/OFDI technology have resulted in an intracoronary imaging system with much higher resolution than the other imaging modalities. In STEMI patients,

OFDI has an advantage in detecting small intraluminal masses with irregular shapes and heterogeneous distribution not only in cross-sectional (ie, 2-dimensional [D]) images but also in reconstructed 3-D images.<sup>24</sup> Recent studies have demonstrated that plaque prolapse and thrombus were more clearly visible and detectable on OCT/OFDI compared to intravascular ultrasound (IVUS).<sup>12,25</sup> The prevalence of post-procedural plaque prolapse or thrombus as assessed on IVUS varied from 34% to 69% in patients with acute myocardial infarction,<sup>26,27</sup> whereas Gonzalo et al reported that post-procedural plaque prolapse could be detected on OCT in all patients with unstable angina.<sup>16</sup> The present results confirmed these findings of previous OCT/OFDI studies.

The present study demonstrates that the measurement of ISS was influenced by SR and that plaque prolapse and thrombus could be observed heterogeneously and randomly even within a short segment of <1.0 mm in the stented segment. In contrast, in 10 randomly selected ROI for which we performed frame-by-frame analysis of stent/lumen areas (total 1,118 frames), the mean stent area and the mean lumen area were similar between the 0.125-mm and 1.0-mm analyses (0.125-mm vs. 1.0-mm:  $8.55 \pm 1.59 \text{ mm}^2$  vs.  $8.56 \pm 1.54 \text{ mm}^2$  in mean stent area,  $P=0.65$ ;  $8.45 \pm 1.65 \text{ mm}^2$  vs.  $8.47 \pm 1.60 \text{ mm}^2$  in mean lumen area,  $P=0.50$ ; respectively). The metallic structure seems to be more even



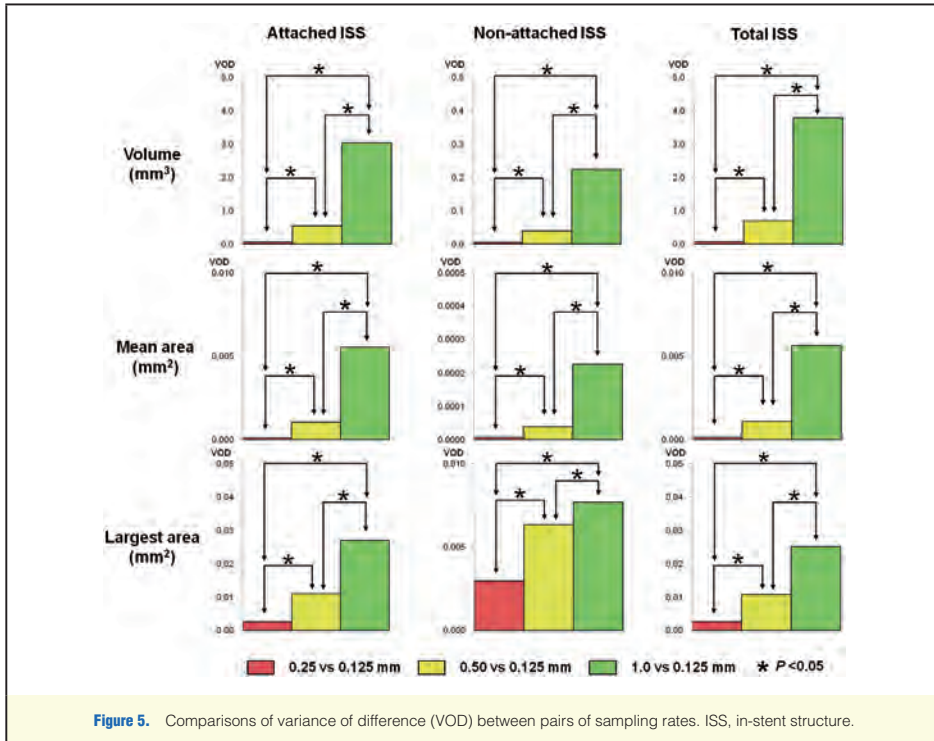


Figure 5. Comparisons of variance of difference (VOD) between pairs of sampling rates. ISS, in-stent structure.

throughout the stented segment, so that the stent area would be less influenced by SR.

In the current analysis, the mean number of ISS per ROI became smaller as sampling distance became larger, while ISS volume showed an inverse association (Table 1). According to our definition and methodology, when intraluminal masses are detected in 2 or more sequential sampled frames, it should be recognized as 1 continuous structure. Therefore multiple ISS, which existed separately on the longitudinal axis, could be misclassified as a sole structure when the intervals between separate ISS were interpolated in the non-sampled frames. Such misclassification presumably resulted in underestimation with respect to the number of ISS. Similarly, larger sampling distance was more likely to skip the frames without ISS in the non-sampled frames, resulting in overestimation of ISS volume (Figure 2). These variances of measurements can largely be influenced by the distribution of ISS. Therefore the present study suggests that in the setting of STEMI, 1.0mm-analysis is not sufficient for the quantitative OCT/OFDI assessment compared to the frame-by-frame analysis.

We calculated the ISS volume using the disk summation method given by

$$\int_a^b f(x) dx \approx \sum_{i=a}^b f(x_i) \times h,$$

where  $h$  is the sampling distance. This method applies the simple principle among the mathematical methods such as, for

example, the Simpson's rule given by

$$\int_a^b f(x) dx \approx \frac{b-a}{6} [f(a) + 4f\left(\frac{a+b}{2}\right) + f(b)]$$

in terms of numerical integration.<sup>28</sup> Indeed, the disk summation method has been used in commercially available software applying 3-D IVUS reconstruction.<sup>29,30</sup> We should, however, mention a limitation of our methodology with respect to ROI length. In the present study, frame-level analysis consistently started from the same most distal frame in the stented segment regardless of SR, where the metallic stent struts were first visible around the whole vessel circumference during the pullback. Consequently, the most proximal frame was determined in the sampled frames according to SR, therefore in 106 out of 126 stented segments the most proximal frames were different among SRs, resulting in different ROI lengths. Including the same most proximal frames to adjust ROI length among SRs, the respective total ISS volume in 0.125-mm, 0.25-mm, 0.5-mm, and 1.0-mm-analyses was 5.41, 5.61 ( $\Delta$  with original data, 0.03), 6.03 ( $\Delta$  with original data, 0.08), and 6.91 ( $\Delta$  with original data, 0.18) mm<sup>3</sup> ( $P < 0.05$  between any pairs of SRs and  $P$  for trend=0.005). Therefore the present results were consistent even when including the most proximal frame in ROI, and the results would not be significantly influenced unless a large amount of ISS was located at the most proximal frame.

Plaque prolapse or thrombus after stenting is frequently observed on IVUS.<sup>31-33</sup> A previous IVUS study demonstrated that

plaque prolapse after stent implantation was commonly accompanied by thrombus and associated with greater levels of CK-MB<sup>34</sup> and early stent thrombosis<sup>27,35</sup> in patients with acute myocardial infarction. In addition, another issue was raised in a recent study that demonstrated that plaque/thrombus protrusion was an independent predictor of late acquired malapposition in patients with acute myocardial infarction.<sup>36</sup> In contrast, several studies showed that prolapse after stenting was not associated with long-term clinical outcomes in patients with acute myocardial infarction<sup>26,27</sup> or stable coronary artery disease.<sup>33</sup> The discrepancy between short- and long-term outcomes might partially be attributed to the fact that prolapse once detected on IVUS at baseline procedure disappeared at 13-month follow-up.<sup>26</sup> The impact of OCT/OFDI assessment of plaque prolapse or thrombus on clinical outcome, however, has not been explored.

Despite the superiority of OCT/OFDI over IVUS in detecting plaque prolapse and thrombus,<sup>12,26</sup> the methodology and appropriate SR for quantitative OCT/OFDI ISS assessment has not been fully investigated. In the present OFDI data, absolute differences in volume and in the largest area of total ISS between the 0.125-mm analysis and 1.0-mm analysis were 1.31 mm<sup>3</sup> and 0.12 mm<sup>2</sup>, respectively. Although these differences were relatively small, differences in SR should be considered when designing future longitudinal studies, particularly addressing plaque prolapse or thrombus by OFDI.

Higher SR is theoretically ideal to obtain a more accurate quantification. This comes at the cost, however, of longer analysis time and greater effort compared to the current de facto analysis approaches using a sampling distance of 1.0 mm. Indeed, area and volumetric estimation of ISS showed good correlation between the different SRs even in 0.125-mm vs. 1.0-mm analyses. Nevertheless, we also noted the statistically significant differences in calculated values and variability among SRs, suggesting that higher SR facilitates more accurate and less variable assessment of ISS. Taken together, the choice of SR must be considered in the light of the subject group, measurement type and analysis method.

### Study Limitations

First, the intraluminal masses outside the stent area were not taken into account in this study. In STEMI patients, the stent struts might be buried in thrombotic masses and potentially some amount of thrombus could exist in the space between the struts and vessel wall. It was also challenging to identify the precise boundary between the vessel wall and thrombus behind the stent struts because of acoustic shadow and light-intensity attenuation by red thrombus.<sup>37</sup> In this methodological study, we thus focused on the intraluminal masses inside the stent area, named ISS, with the aim of highly reproducible contour detection. Second, we classified SR into 4 sampling distances of 1.0 mm, 0.5 mm, 0.25 mm and 0.125 mm. Such classification was based on the image acquisition setting of the TERUMO OFDI system and imaging protocol of the TROFI trial. Further evaluation, however, will be required if OFDI systems become available with even higher frame acquisition rates than the currently available systems.

### Conclusion

Quantification of ISS is significantly influenced by the analyzed SR. This should be taken into account when designing future OFDI studies in which quantitative assessment of ISS is critical for evaluation of STEMI patients.

### Disclosures

Conflict of interest: There is no conflict of interest to declare.

### References

- Jang IK, Tearney G, Bouma B. Visualization of tissue prolapse between coronary stent struts by optical coherence tomography: Comparison with intravascular ultrasound. *Circulation* 2001; **104**: 2754.
- Jang IK, Bouma BE, Kang DH, Park SJ, Park SW, Seung KB, et al. Visualization of coronary atherosclerotic plaques in patients using optical coherence tomography: Comparison with intravascular ultrasound. *J Am Coll Cardiol* 2002; **39**: 604–609.
- Yabushita H, Bouma BE, Houser SL, Aretz HT, Jang IK, Schliendorf KH, et al. Characterization of human atherosclerosis by optical coherence tomography. *Circulation* 2002; **106**: 1640–1645.
- Yun S, Tearney G, de Boer J, Ifimia N, Bouma B. High-speed optical frequency-domain imaging. *Opt Express* 2003; **11**: 2953–2963.
- Gonzalo N, Tearney GJ, Serruys PW, van Soest G, Okamura T, Garcia-Garcia HM, et al. Second-generation optical coherence tomography in clinical practice: High-speed data acquisition is highly reproducible in patients undergoing percutaneous coronary intervention. *Rev Esp Cardiol* 2010; **63**: 893–903.
- Takarada S, Imanishi T, Liu Y, Ikejima H, Tsuchioka H, Kuroi A, et al. Advantage of next-generation frequency-domain optical coherence tomography compared with conventional time-domain system in the assessment of coronary lesion. *Catheter Cardiovasc Interv* 2010; **75**: 202–206.
- Okamura T, Gonzalo N, Gutierrez-Chico JL, Serruys PW, Bruining N, de Winter S, et al. Reproducibility of coronary Fourier domain optical coherence tomography: Quantitative analysis of in vivo stented coronary arteries using three different software packages. *EuroIntervention* 2010; **6**: 371–379.
- Yun SH, Tearney G, de Boer J, Bouma B. Motion artifacts in optical coherence tomography with frequency-domain ranging. *Opt Express* 2004; **12**: 2977–2998.
- Ha J, Yoo H, Tearney GJ, Bouma BE. Compensation of motion artifacts in intracoronary optical frequency domain imaging and optical coherence tomography. *Int J Cardiovasc Imaging* 2011 Oct 14 [Epub ahead of print].
- Barlis P, Regar E, Serruys PW, Dimopoulos K, van der Giessen WJ, van Geuns RJ, et al. An optical coherence tomography study of a biodegradable vs. durable polymer-coated limus-eluting stent: A LEADERS trial sub-study. *Eur Heart J* 2010; **31**: 165–176.
- Gutierrez-Chico JL, van Geuns RJ, Regar E, van der Giessen WJ, Kelbaek H, Saunamaki K, et al. Tissue coverage of a hydrophilic polymer-coated zotarolimus-eluting stent vs. a fluoropolymer-coated everolimus-eluting stent at 13-month follow-up: An optical coherence tomography substudy from the RESOLUTE All Comers trial. *Eur Heart J* 2011; **32**: 2454–2463.
- Okamura T, Onuma Y, Garcia-Garcia HM, van Geuns RJ, Wykrzykowska JJ, Schultz C, et al. First-in-man evaluation of intravascular optical frequency domain imaging (OFDI) of Terumo: A comparison with intravascular ultrasound and quantitative coronary angiography. *EuroIntervention* 2011; **6**: 1037–1045.
- Gomez-Lara J, Radu M, Brugaletta S, Farooq V, Diletti R, Onuma Y, et al. Serial analysis of the malapposed and uncovered struts of the new generation of everolimus-eluting bioresorbable scaffold with optical coherence tomography. *JACC Cardiovasc Interv* 2011; **4**: 992–1001.
- Guagliumi G, Costa MA, Sirbu V, Musumeci G, Bezerra HG, Suzuki N, et al. Strut coverage and late malapposition with paclitaxel-eluting stents compared with bare metal stents in acute myocardial infarction: Optical coherence tomography substudy of the Harmonizing Outcomes with Revascularization and Stents in Acute Myocardial Infarction (HORIZONS-AMI) Trial. *Circulation* 2011; **123**: 274–281.
- Tahara S, Chamie D, Baibars M, Alraies C, Costa M. Optical coherence tomography endpoints in stent clinical investigations: Strut coverage. *Int J Cardiovasc Imaging* 2011; **27**: 271–287.
- Gonzalo N, Serruys PW, Okamura T, Shen ZJ, Onuma Y, Garcia-Garcia HM, et al. Optical coherence tomography assessment of the acute effects of stent implantation on the vessel wall: A systematic quantitative approach. *Heart* 2009; **95**: 1913–1919.
- Degerekin M, Regar E, Tanabe K, Lemos P, Lee CH, Smits P, et al. Evaluation of coronary remodeling after sirolimus-eluting stent implantation by serial three-dimensional intravascular ultrasound. *Am J Cardiol* 2003; **91**: 1046–1050.
- Onuma Y, Serruys PW, den Heijer P, Joeseef KS, Duckers H, Regar E, et al. MAHOROBA, first-in-man study: 6-month results of a bio-

- degradable polymer sustained release tacrolimus-eluting stent in de novo coronary stenoses. *Eur Heart J* 2009; **30**: 1477–1485.
19. Prati F, Regar E, Mintz GS, Arbustini E, Di Mario C, Jang IK, et al. Expert review document on methodology, terminology, and clinical applications of optical coherence tomography: Physical principles, methodology of image acquisition, and clinical application for assessment of coronary arteries and atherosclerosis. *Eur Heart J* 2010; **31**: 401–415.
  20. Lin LI. A concordance correlation coefficient to evaluate reproducibility. *Biometrics* 1989; **45**: 255–268.
  21. Bland JM, Altman DG. Statistical methods for assessing agreement between two methods of clinical measurement. *Lancet* 1986; **1**: 307–310.
  22. Pitman EJJ. A note on normal correlation. *Biometrika* 1939; **31**: 9–12.
  23. Morgan WA. A test for the significance of the difference between the two variances in a sample from a normal bivariate population. *Biometrika* 1939; **31**: 13–19.
  24. Muramatsu T, Serruys PW, Onuma Y. Thrombotic arch in ST-segment elevation myocardial infarction: Comparison between two-dimensional and three-dimensional optical frequency domain imaging. *Eur Heart J* 2012; **33**: 1510.
  25. Kubo T, Imanishi T, Takarada S, Kuroi A, Ueno S, Yamano T, et al. Assessment of culprit lesion morphology in acute myocardial infarction: Ability of optical coherence tomography compared with intravascular ultrasound and coronary angiography. *J Am Coll Cardiol* 2007; **50**: 933–939.
  26. Maehara A, Mintz GS, Lansky AJ, Witzentichler B, Guagliumi G, Brodie B, et al. Volumetric intravascular ultrasound analysis of Paclitaxel-eluting and bare metal stents in acute myocardial infarction: The harmonizing outcomes with revascularization and stents in acute myocardial infarction intravascular ultrasound substudy. *Circulation* 2009; **120**: 1875–1882.
  27. Hong YJ, Jeong MH, Choi YH, Song JA, Kim DH, Lee KH, et al. Impact of tissue prolapse after stent implantation on short- and long-term clinical outcomes in patients with acute myocardial infarction: An intravascular ultrasound analysis. *Int J Cardiol* 2011 December 14 [E-pub ahead of print].
  28. Sili E, Mayers D. An introduction to numerical analysis. Cambridge: Cambridge University Press, 2003.
  29. Hamers R, Bruining N, Knook M, Sabate M, Roelandt JRJC. A novel approach to quantitative analysis of intra vascular ultrasound images. *Computers Cardiol* 2001; **28**: 589–592.
  30. Tani S, Watanabe I, Anazawa T, Kawamata H, Tachibana E, Furukawa K, et al. Effect of pravastatin on malondialdehyde-modified low-density lipoprotein levels and coronary plaque regression as determined by three-dimensional intravascular ultrasound. *Am J Cardiol* 2005; **96**: 1089–1094.
  31. Bocksch W, Scharl M, Beckmann S, Dreyse S, Fleck E. Intravascular ultrasound imaging in patients with acute myocardial infarction. *Eur Heart J* 1995; **16**(Suppl J): 46–52.
  32. Hong MK, Park SW, Lee CW, Kang DH, Song JK, Kim JJ, et al. Long-term outcomes of minor plaque prolapsed within stents documented with intravascular ultrasound. *Catheter Cardiovasc Interv* 2000; **51**: 22–26.
  33. Futamatsu H, Sabate M, Angiolillo DJ, Jimenez-Quevedo P, Corros C, Morikawa-Futamatsu K, et al. Characterization of plaque prolapse after drug-eluting stent implantation in diabetic patients: A three-dimensional volumetric intravascular ultrasound outcome study. *J Am Coll Cardiol* 2006; **48**: 1139–1145.
  34. Hong YJ, Jeong MH, Ahn Y, Sim DS, Chung JW, Cho JS, et al. Plaque prolapse after stent implantation in patients with acute myocardial infarction: An intravascular ultrasound analysis. *JACC Cardiovasc Imaging* 2008; **1**: 489–497.
  35. Choi SY, Witzentichler B, Maehara A, Lansky AJ, Guagliumi G, Brodie B, et al. Intravascular ultrasound findings of early stent thrombosis after primary percutaneous intervention in acute myocardial infarction: A Harmonizing Outcomes with Revascularization and Stents in Acute Myocardial Infarction (HORIZONS-AMI) substudy. *Circ Cardiovasc Interv* 2011; **4**: 239–247.
  36. Guo N, Maehara A, Mintz GS, He Y, Xu K, Wu X, et al. Incidence, mechanisms, predictors, and clinical impact of acute and late stent malapposition after primary intervention in patients with acute myocardial infarction: An intravascular ultrasound substudy of the Harmonizing Outcomes with Revascularization and Stents in Acute Myocardial Infarction (HORIZONS-AMI) trial. *Circulation* 2010; **122**: 1077–1084.
  37. Kume T, Akasaka T, Kawamoto T, Ogasawara Y, Watanabe N, Toyota E, et al. Assessment of coronary arterial thrombus by optical coherence tomography. *Am J Cardiol* 2006; **97**: 1713–1717.

#### 4.2 Morphologic assessment of thrombus with three-dimensional approach

Thrombotic arch in ST-segment elevation myocardial infarction: comparison between 2-dimensional and 3-dimensional optical frequency domain imaging.

*Eur Heart J.* 2012;33:1510.

[Case report, Impact Factor (2012): 14.097]

Muramatsu T, Serruys PW, Onuma Y.





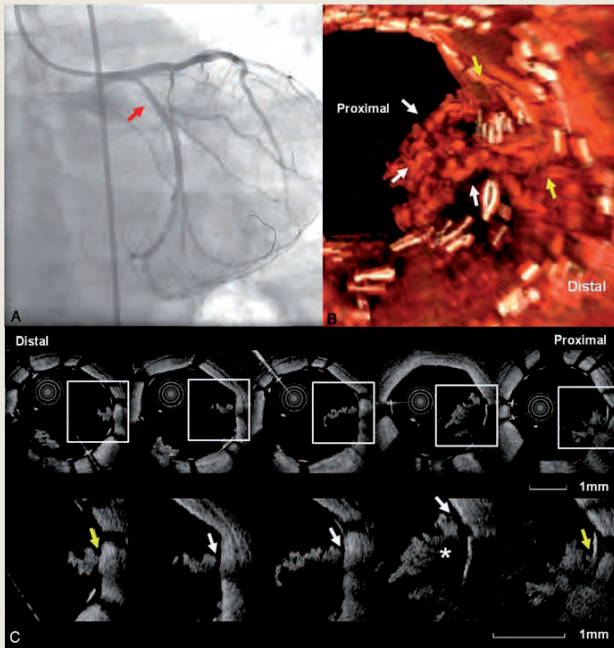
## Thrombotic arch in ST-segment elevation myocardial infarction: comparison between two-dimensional and three-dimensional optical frequency domain imaging

Takashi Muramatsu, Patrick W. Serruys, and Yoshinobu Onuma\*

Department of Interventional Cardiology, Thoraxcenter, Erasmus MC, 's-Gravendijkwal 230, 3015 CE Rotterdam, The Netherlands

\* Corresponding author. Tel: +31 10 463 5260, Fax: +31 10 463 5258, Email: yoshinobuonuma@gmail.com

A 54-year-old female presented with inferoposterior ST-segment elevation myocardial infarction. Coronary angiogram revealed total occlusion of the proximal left circumflex artery. Following a thrombus aspiration, without administration of glycoprotein IIb/IIIa inhibitor, direct stenting with a drug-eluting metallic stent was performed. After stent implantation, angiogram showed thrombolysis in myocardial infarction (TIMI) grade III flow, without any evidence of intraluminal defect within the culprit lesion (Panel A, red arrow). Subsequently, we performed the optical frequency domain imaging (OFDI; Terumo Europe N.V., Leuven, Belgium) with a pullback speed of 20 mm/s. During image acquisition, contrast medium was continuously injected to exclude blood in the lumen. In contrast to the angiogram, a reconstructed three-dimensional OFDI image showed a lot of thrombi protruding into the lumen within the metallic stent (see Supplementary material online, Video S1), and a focal structure with arch-like formation could be clearly imaged in the proximal segment (Panel B, yellow and white arrows). Interestingly, corre-



sponding two-dimensional images showed that both ends of this thrombus were attached to the vessel wall (Panel C, yellow arrows), while its body was free from the vessel wall and looked like floating inside the lumen (Panel C, white arrows). Strut-level analysis in the segment with the thrombus showed 160 apposed struts (96.4%) and 6 malapposed struts (3.6%) located at the opposite side of the thrombus. Considering the absence of malapposed strut behind the thrombus, heterogeneous signal intensity, and inconsistent intensity attenuation (Panel C, asterisk), this structure is considered as a mixed type of thrombus which could not be removed by thrombectomy. This case highlights the efficacy of OFDI in detecting intracoronary thrombus not visible on angiography and facilitates our understanding of intracoronary thrombus morphology.

Supplementary material is available at *European Heart Journal* online.

Published on behalf of the European Society of Cardiology. All rights reserved. © The Author 2012. For permissions please email: journals.permissions@oup.com



### 4.3 Impact of thrombus aspiration on OFDI measurements and clinical outcomes in STEMI patients

Short- and mid-term results of the randomized TROFI trial.

Onuma Y, et al. *Eur Heart J*. 2013;34:1050-60.

Garcia-Garcia HM, et al. *Eur Heart J Cardiovasc Imaging*. 2014;15:987-95.

[This chapter merged two papers.]

Muramatsu T, Onuma Y, Garcia-Garcia HM, Serruys PW.





## Short- and mid-term results of the randomized TROFI trial

Takashi Muramatsu\*, Yoshinobu Onuma\*, Hector M. Garcia-Garcia\*, Patrick W. Serruys\*;  
On behalf of the TROFI Investigators.

\* Thoraxcenter, Erasmus Medical Center, Rotterdam, the Netherlands.

This chapter merged following two papers:

Onuma Y, et al. *Eur Heart J*. 2013;34:1050-60.

Garcia-Garcia HM, et al. *Eur Heart J Cardiovasc Imaging*. 2014;15:987-95.

### Introduction

Primary percutaneous coronary intervention (PPCI) has been well established as the treatment of choice for the majority of patients presenting with acute ST-elevation myocardial infarction (STEMI), and previous trials have demonstrated its superiority to conventional thrombolytic treatment.[1] PPCI achieves more frequently a thrombolysis in myocardial infarction (TIMI) 3 coronary flow grade and a greater ventricular preservation when compared with pharmacological thrombolysis.[2,3] Despite successful PPCI with patent infarct-related artery, up to 30% of patients do not achieve adequate myocardial reperfusion.[4-6] The so-called no-reflow phenomenon has been ascribed to distal embolization of thrombus or plaque debris, vasoconstriction, and reperfusion injury.[7] Micro-embolization can lead to the occlusion of arterioles in the microcirculation and impair the capillary bed circulation, while embolization of larger atherosclerotic particles can lead to the occlusion of pre-arterioles and side branches.[8,9] The use of thrombectomy (TB) devices during PPCI has been recently shown to result in less macro-/microembolization and to improve epicardial, angiographical TIMI flow, blush score, and myocardial perfusion.[4-6] Moreover, thrombus aspiration or rheolysis has been shown to decrease cardiac death and repeat myocardial infarction, although the study was not powered to detect any difference in mortality.[10]

Furthermore, it is deemed that late stent malapposition is common after PPCI, and may predispose to stent thrombosis. Late malapposition may be related to under-deployment of stents at the time of PPCI, and this may be due in part (i) to thrombus behind struts, which subsequently resolves and leads to stent malapposition; (ii) to late vasorelaxation of the vasoconstricted vessel in the acute phase of STEMI. Removal of thrombus before stenting potentially could lead to better stent expansion and less late malapposition.

However, in the setting of STEMI, the impact of thrombus removal on acute and chronic luminal dimension is still unclear. After stenting, such thrombus either protrudes into the lumen through the mesh of metallic stent struts or is squeezed between the vessel wall and stent; protruding thrombus can partially fill in the luminal metallic conduit immediately after stenting, a specific feature that has not been investigated, due to the limited ability of the conventional angiography and intravascular

ultrasound (IVUS) in detecting thrombus. Optical frequency domain imaging (OFDI) - a high-resolution imaging technique - provides valuable information in the setting of acute myocardial infarction.[11] This imaging modality has been shown to be even more sensitive in detecting intraluminal mass (i.e. thrombus) and offers unique possibilities in the analysis of coronary intervention in acute myocardial infarction.[12,13]

We hypothesize that in patients with STEMI, PPCI with TB using an Eliminate aspiration catheter will reduce intraluminal thrombus and create a larger flow area on OFDI compared with PPCI without TB. The current study tests this hypothesis and the study reports the primary results of 141 patients enrolled in a prospective randomized controlled, multi-centre study (NCT01271361). In addition, we sought to investigate the incidence of incomplete stent apposition (ISA) and to explore the impact of the presence of thrombus and protruding plaque after stent implantation on neointima formation at mid-term follow-up in STEMI patients with serial OFDI investigations.

### Methods

#### Patient selection

TROFI was a prospective, randomized, controlled, single-blind, multicenter clinical study enrolling 141 patients with STEMI, 12 h from the onset of the chest pain. Patients were randomized in a 1:1 ratio to receive PPCI using drug-eluting stent (DES, Nobori, Terumo Europe, Leuven, Belgium) with TB or without TB prior to stenting. Patients aged  $\geq 18$  years with STEMI documented with  $\geq 2$  mm ST-segment elevation in at least two contiguous leads prior to PPCI, presenting in the cath lab, 12 h after the onset of symptoms lasting  $\geq 20$  min and having an angiographically visible stenosis ( $>30\%$ ) or TIMI  $\leq II$  in a single de novo, native, previously unstented vessel were considered for enrolment. Per protocol, a total of 49 patients underwent angiography and OFDI follow-up at 6 months in 3 predefined enrolling centers.

#### Procedure

Following confirmation of clinical and angiographic eligibility and having obtained informed consent, subjects were randomly assigned to one of the treatment arms (PPCI with or without TB), according to computer-generated blocks stratified by center. If multiple lesions were to be treated, all lesions had

to receive the treatment that has been assigned per randomization.

When the patient was allocated to TB arm, multiple pullbacks with the TB catheter (Eliminate, Terumo Clinical Supply, Gifu, Japan) were performed until no further decrease of the intraluminal mass on angiography could be obtained. At least two thrombus aspirations had to be done and the TB procedure could be stopped only when there was no more thrombotic material in the aspirate for at least two consecutive aspirations. In case of angiographic luminal defect after stenting, an additional aspiration could be performed. The operator was blinded to the OFDI results.

The Nobori DES was used for stenting procedure. Direct stenting or/and pre-dilatation were allowed at the discretion of the investigator. If pre-dilatation was performed, the use of a commercially available balloon with a length not exceeding the length of the stent to be implanted was recommended. Full lesion coverage had to be ensured by implantation of one or multiple stents. Post-dilatation after stenting could be performed at the discretion of the investigator in either treatment arm.

### OFDI investigation

After the post-procedure angiography, OFDI was obtained with TERUMO OFDI system (Terumo Corporation, Tokyo, Japan) with imaging element rotating at 9600 rpm allowing imaging at 160 frames/s. Under fluoroscopic guidance, the OFDI catheter was advanced into the vessel, placing the optical lens  $\geq 5$  mm distal to the stent. Imaging calibration was performed as previously described.[14] OFDI pullbacks with a speed of 20 mm/s were performed during the continuous injection of a maximum of 16 mL of 100% contrast medium (Iodixanol 320, Visipaque™, GE Health Care, Cork Ireland) through the guiding catheter using an injection pump (Mark-V ProVis, Medrad, Inc., Indianola, PA, USA) or manually. The contrast was injected at a pressure of 300 p.s.i with a flow rate of 3-4 mL/s for a maximum of 4 sec. The images were electronically exported for offline analysis.

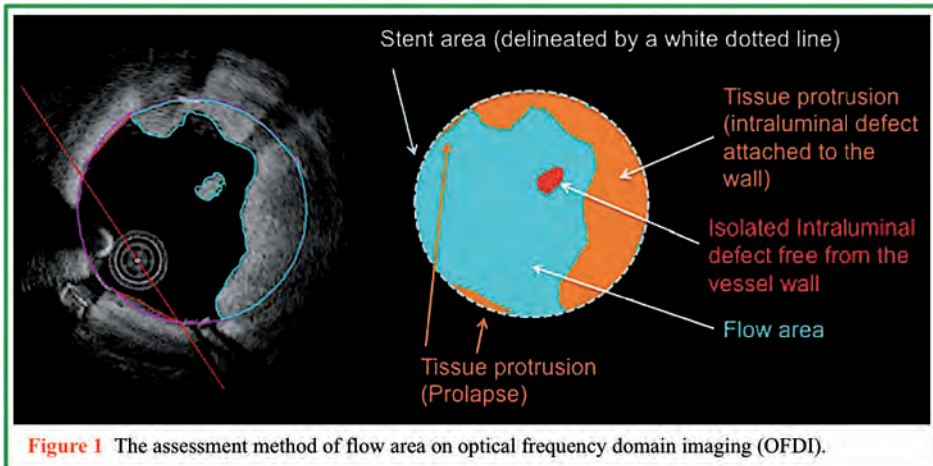
The operator was blinded to the OFDI results. All decisions about the adequacy of stent placement, expansion, and additional post-dilatation had to be made by angiographic evaluation only. The procedure was considered complete after final angiographic and OFDI recordings of the treatment area whenever the guiding catheter has been removed from the patient.

### Data monitoring

The monitoring for this study was conducted by whether sponsor or sponsor designee in all centers. One hundred per cent source data verification was performed including device malfunctions and serious events. The independent Clinical Events Committee (CEC), which is composed of interventional and/or non-interventional cardiologists, adjudicated all clinical events and clinical endpoints based on protocol. The CEC members were not participants in the study and were blind to any imaging results of the study. The Data Safety Monitoring Board was also organized as an independent committee that potentially provide confidential recommendations, when necessary, of study termination based on the safety stopping rules or the occurrence of clinically significant results in safety analyses of the data.

### QCA, ECG, and OFDI analysis

An independent core laboratory (Cardialysis BV, Rotterdam, The Netherlands) reviewed all coronary angiograms and OFDI images and performed qualitative and quantitative analysis. On pre-procedural angiography, in case of total occlusion, quantitative coronary angiography (QCA) analysis was performed preferably as far as possible from the point of occlusion but distal to the most proximal take off of the side branch. In QCA, three different regions were identified: stented segment and the segments 5 mm proximal and distal to the stent. Intracoronary thrombus was angiographically identified and scored in five grades as previously described.[15] Thrombus grade was assessed before procedure and after flow achievement



with guide-wire crossing. Thrombosis in myocardial infarction flow and myocardial blush were assessed as previously reported.[16] The QCA measurements included percentage diameter stenosis, lesion length, minimal lumen diameter, maximal lumen diameter, and reference vessel diameter (RVD; CAAS II, Pie-Medical, Maastricht, The Netherlands). ST-segment resolution was calculated as described previously.[17]

For the OFDI analyses, one frame per millimeter was selected and analyzed by analysts unaware of QCA results and blinded to the treatment arm. Whenever intraluminal mass or tissue protrusion was detected, then an all-frame analysis (0.125 mm/slice) was performed to compute the volumes. The OFDI analysis was performed using a customized off-line software (QCU-CMS, LKEB, Leiden University, The Netherlands).

Region of interest (ROI) was selected as the stented segment, which was defined as the segment between the most distal and proximal frame where metallic stent struts were visible around the whole vessel circumference.[18] The stent and lumen areas were semi-automatically traced at every 1 mm. Neointima area was defined as the difference between stent and lumen areas (in absence of ISA). Definitions of ISA and coverage have been consistently described and reported in the literature.[19] In addition, we analyzed all individual masses within the stent area which were defined as ISS. ISS was categorized into ISS

attached to vessel wall (i.e. thrombus or prolapse) and non-attached ISS.[20] In order to achieve a more accurate estimation for ISS volume, the cross-sectional ISS analysis was performed in every frame along the whole stented region. When more than two attached or non-attached ISS were detected in an analyzed cross-section, the ISS area was calculated by cumulating all individual ISS areas. If there is no ISS in an analyzed cross-section, ISS area was regarded as zero. ISS volume was calculated by numerical integration based on the disk summation method, which formula is shown as follows:

$$ISS \text{ volume (mm}^3\text{)} = \sum_{i=1}^n \{ ISS \text{ area (} i \text{)} \}$$

where n indicates the number of analyzed frames in ROI and h indicates the width of sampling distance (0.125 mm).

The OCT healing score is a weighted index that combines the following parameters:

- (i) presence of ISS is assigned weight of '4';
- (ii) presence of both malapposed and uncovered struts (%MU) is assigned a weight of '3';
- (iii) presence of uncovered struts alone (%U) is assigned a weight of '2';
- and finally,
- (iv) presence of malapposition alone (%M) is assigned a weight

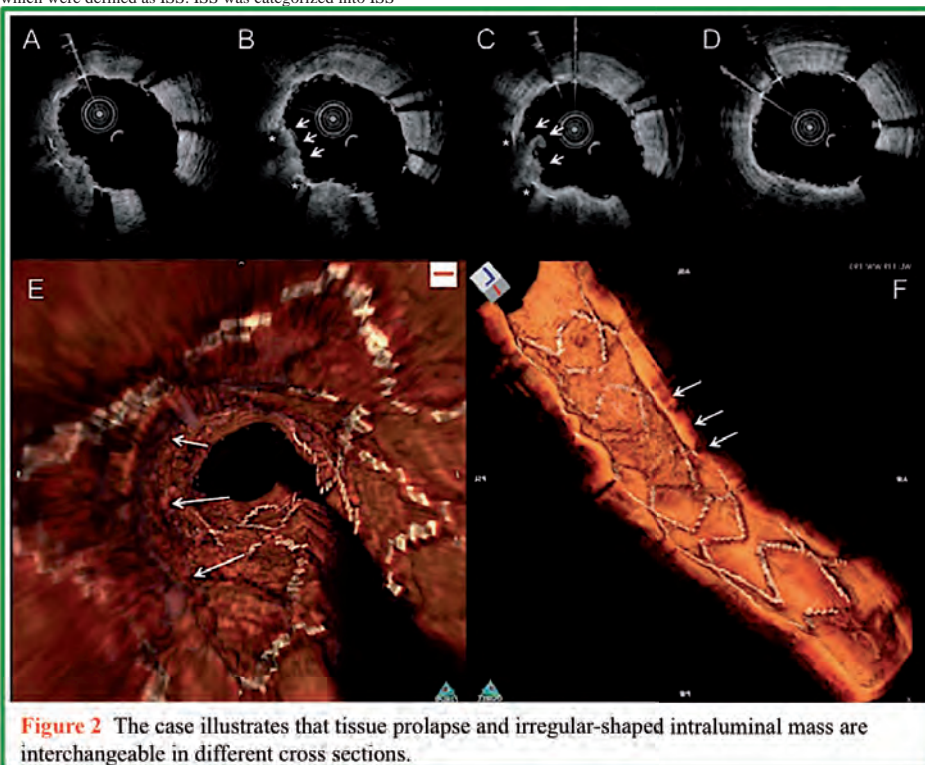


**Figure 2** The case illustrates that tissue prolapse and irregular-shaped intraluminal mass are interchangeable in different cross sections.

of '1'.

Neointimal healing score = (%ISS × '4') + (%MU × '3') + (%U × '2') + (%M × '1')

Three-dimensional OFDI was reconstructed according to the previously published method to illustrate three-dimensional distribution of protrusion.[21]

### Study endpoints and definitions

The primary endpoint is minimum flow area (MinFA) immediately after PPCI assessed by OFDI. Flow area is defined as: [stent area + incomplete stent apposition (ISA) area] - (tissue protrusion + isolated intraluminal defect area) (Figure 1).

In the assessment of flow area, there are three parameters involved: protrusion, intraluminal defect, and ISA. The term protrusion is purely descriptive and refers to biological material protruding toward the lumen beyond the boundaries of the struts. Tissue prolapse in stable and unstable patients has been previously defined as a convex-shaped, protrusion of tissue between adjacent stent struts towards the lumen, without disruption of the continuity of the luminal vessel surface.[22] At variance with this definition, tissue protrusion in acute myocardial infarction may have a disrupted and irregular surface and adjacent struts may be embedded or even buried in the prolapsing mass. The biological material involved in the protrusion can be either intimal/connective tissue of the vessel wall, necrotic core abutting the lumen vessel, or thrombus covering plaque ruptures (Figure 2).

Isolated intraluminal defect refers to a fix structure separated from the vessel wall seen in the analyzed cross section and likely attached to the vessel wall at a proximal or distal site in a

different cross section. Intra-stent structure area was defined as a sum of tissue protrusion area and isolated intraluminal defect area. Malapposition has been consistently described and reported in the literature.[23,24]

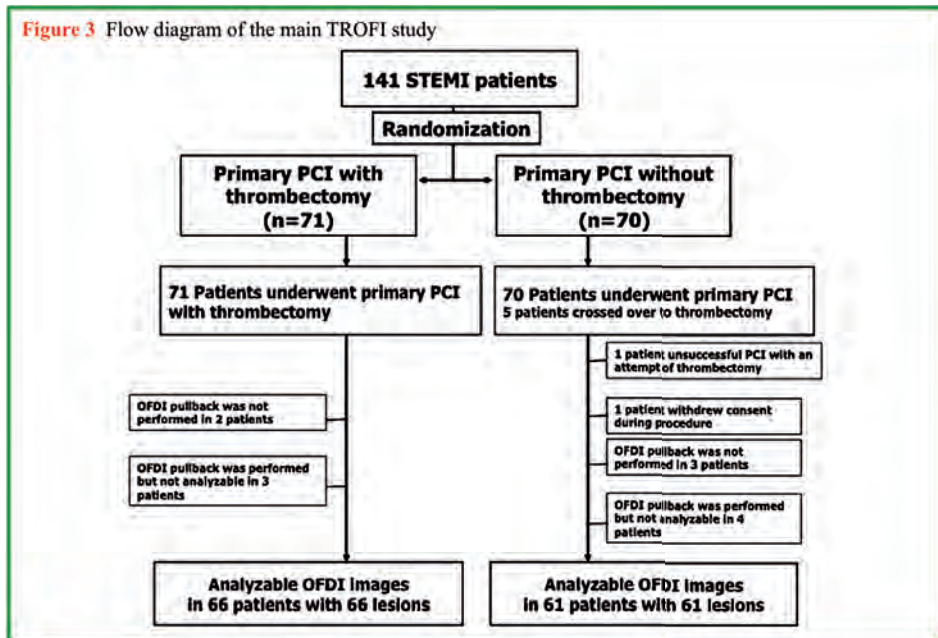
### Clinical events

Major adverse cardiac event was defined as a composite of cardiac death, reinfarction in the territory of infarction-related vessel (Q-wave and non-Q-wave), or clinically driven target vessel revascularization, exactly the same as target vessel failure (TVF). Stent thrombosis was adjudicated according to academic research consortium definition.[25]

### Sample size calculations and statistical analysis

The sample size calculations for the TROFI study were based on pooled data of Cardialysis database from multiple trials in acute coronary syndrome where the MinFA was  $4.95 + 1.39 \text{ mm}^2$ . Based on these numbers, the sample size of 60 patients in each group would achieve 80% power to detect a difference of  $0.72 \text{ mm}^2$  between the null hypothesis that both group means are  $4.95 \text{ mm}^2$  and the alternative hypothesis that the mean of the actively treated group is  $5.67 \text{ mm}^2$  with estimated standard deviations of  $1.39 \text{ mm}^2$  in both group and with a significance level (alpha) of 0.05 using a two-sided two-sample t-test. Categorical variables were expressed as percentages and were compared by Fisher's exact test. Continuous variables are presented as mean with standard deviation. Normally distributed variables were compared by t-test, whereas non-parametric Wilcoxon rank-sum test was used for variables without normal

Figure 3 Flow diagram of the main TROFI study



distribution. The prespecified primary analyses were to be performed on the basis of the intention to treat. But two additional analytical plans were considered: a per-protocol analysis (successful TB implying lesion crossing and thrombus aspiration; successful stent implantation; analysable OFDI pullback; no protocol exclusion/violation) and one analysis according to the actually received treatment. All statistical tests were two tailed, and P-value of <0.05 was considered as statistically significant. All statistical analyses were performed using SAS version 9.1 (SAS Institute, Inc., Cary, NC).

## Results

### Primary results

Between 24 November 2010 and 11 October 2011, 141 patients were enrolled at five European sites and randomized to receive PPCI with initial TB (n=71) or conventional PPCI without TB (n=70) (Figure 3). Of 70 patients allocated to conventional percutaneous coronary intervention (PCI), one patient did not undergo PCI, because the operator failed to cross the lesion with a wire. Another patient withdrew informed consent during procedure and five patients received TB by operator's clinical decision despite the initial assignment to conventional PCI arm. Of five patients, TB was performed before stenting without pre-dilatation in three cases, whose angiographic thrombus grade were 4 in two cases and 5 in one case. In two cases, TB was performed after stenting, due to the remaining thrombus in the stent or due to embolization of thrombus in the distal segment.

Baseline characteristics of the patients were well matched between the two groups (Table 1). There were no differences in complication before PPCI (Table 2). Although glycoprotein IIb/IIIa inhibitors were given numerically more frequently in non-TB arm than in TB arm, the difference was not statistically significant (P=0.09). Femoral approach was more frequently used in the TB than in the non-TB but the difference did not reach statistical significance (P=0.06). The TB device reached and crossed the lesion in all cases, and thrombotic material was successfully removed in all but one patient. The number of aspiration was 1.70±0.54. Five patients from the non-TB group 'crossed over' to the TB group, four of the five lesions could be reached, crossed, and thrombus could be aspirated. As far as the procedure is concerned, number of stent per lesion, total stent length, and diameter are comparable between two groups.

In the pre-procedural angiographic assessment, grades of TIMI flow were comparable in both groups (Table 3). Pre-procedural QCA did not differ statistically from each other. However, post-procedure, minimal lumen diameter as well as RVD was significantly larger in the TB group than in the non-TB group. Thrombolysis in myocardial infarction flow grade post-procedure remained comparable. Post-procedure, the presence of thrombus is diagnosed angiographically in four and seven patients in the TB and non-TB arms, respectively.

Implanted stent had comparable length in both groups, but the maximal and minimal stent area in the TB group was non-significantly larger than in the non-TB group. The amount of protrusion and intraluminal defect as well as ISA was very similar as shown in Table 4. Accordingly, the minimum flow

**Table 1** Baseline characteristics

Demographics	TB 71 patients	Non-TB 70 patients
Age, years	61.1 ± 11.8	60.9 ± 12.7
Male, %	75.7	69.1
Heart Rate, b.p.m.	73.8 ± 18.8	73.6 ± 14.1
<b>Risk factors</b>		
Diabetes mellitus, n/N (%)	6/71 (8.4)	9/68 (13.2)
Insulin dependent, n/N (%)	1/6 (16.7)	1/7 (14.3)
Current smoking, %	45.1	46.3
Hypercholesterolaemia, %	29.6	28.6
Hypertension, %	38.0	35.7
Family history of coronary artery disease, %	33.8	47.1
<b>Any other complication that requires treatment</b>		
Sustained ventricular tachycardia, %	1.4	0
Ventricular fibrillation, %	0	2.9
<b>STEMI treatment before PCI</b>		
Haemodynamic support, %	1.4	1.4
Heparin (in ambulance), %	42.2	42.8
<b>Killip classification before PCI, %</b>		
Class I	73.2	70.0
Class II	2.8	1.4
Class III	0.0	0.0
Class IV	1.4	1.4

**Table 2** Peri-procedural medication and procedural data

	TB 71 patients	Non-TB 70 patients
Aspirin, %	100	100
Clopidogrel, %	84.0	90.6
Prasugrel, %	14.7	9.4
Ticlopidine, %	1.3	0
Glycoprotein IIb/IIIa inhibitors, %	47.8	62.8
Inotropic agents, %	2.7	0.0
<b>Vascular access</b>		
Femoral, %	85.9	71.4
Radial, %	14.1	27.1
<b>Procedural details</b>		
<b>Treated vessels</b>		
RCA, %	37.0	44.3
LAD, %	44.7	42.9
LCx, %	18.3	10.0
Stents implanted per lesion	1.2 ± 0.5	1.3 ± 0.7
Mean total stent length/lesion (mm, nominal)	21.7 ± 9.4	23.4 ± 11.1
Mean stent diameter (mm, nominal)	3.2 ± 0.4	3.1 ± 0.4
Number of aspiration catheter insertion	1.76 ± 0.54	2.0 ± 0.0 <sup>a</sup>
Number of passage of aspiration catheter to the lesion	2.00 ± 0.86	1.67 ± 0.58 <sup>a</sup>
Aspiration device successfully reached, %	100	80 <sup>a</sup>
Aspiration device successfully crossed, %	100	80 <sup>a</sup>
Thrombus successfully removed, % <sup>a</sup>	98.5	100 <sup>a</sup>

**Table 3 Peri- and post-procedural QCA analysis**

	TB group 71 patients 72 lesions	Non-TB group 70 patients 70 lesions	P value
<b>Pre-procedure</b>			
TIMI flow			
0	42.5%	40.8%	0.71
1	5.5%	5.6%	
2	26.0%	19.7%	
3	26.0%	33.8%	
Thrombus burden before wiring			
0	1.4%	1.4%	0.85
1	8.5%	8.7%	
2	4.2%	7.2%	
3	32.4%	30.4%	
4	11.3%	17.4%	
5	42.3%	34.8%	
Thrombus burden after wiring			
0	1.8%	2.2%	0.95
1	5.3%	6.7%	
2	12.3%	8.9%	
3	40.4%	44.4%	
4	31.6%	33.3%	
5	8.8%	4.4%	
Lesion length, mm	13.35 ± 6.35	13.68 ± 6.66	0.82
RVD non-total occlusion, mm	2.86 ± 0.43	2.70 ± 0.49	0.14
RVD total occlusion, mm	2.98 ± 0.55	2.82 ± 0.68	0.28
MLD, mm	0.46 ± 0.49	0.48 ± 0.54	0.82
% Diameter stenosis	84.1 ± 15.7	82.4 ± 19.1	0.57
<b>Post-procedure</b>			
TIMI flow			
0	0.0%	0.0%	0.63
1	3.1%	6.0%	
2	4.6%	7.5%	
3	92.3%	86.6%	
Stent length			
	19.25 ± 9.63	20.59 ± 8.97	0.21
RVD post-procedure	3.01 ± 0.46	2.79 ± 0.46	0.007
MLD, mm	2.89 ± 0.47	2.49 ± 0.46	0.01
% Diameter stenosis	10.50 ± 7.30	10.56 ± 6.53	0.56
<b>Angiographic complication</b>			
Dissection	2.9%	1.5%	1.00
Thrombus	5.8%	10.3%	0.33
Coronary spasm	1.4%	4.5%	0.36
Distal embolism	4.3%	2.8%	0.49
No-reflow	1.5%	0.0%	1.00
<b>ECG</b>			
ST segment resolution			
<30%	13.1%	15.5%	0.93
30 - 70%	27.9%	27.6%	
>70%	59.0%	56.9%	
<b>Myocardial blush grade</b>			
0 or 1	15.5%	11.6%	0.64
2	49.3%	47.8%	
3	35.2%	40.6%	

area tended to be larger in the TB group than in the non-TB group, but the difference ( $\Delta 0.57 \text{ mm}^2$ ,  $P=0.12$ ) was lower than the expected difference of  $0.72 \text{ mm}^2$ , and therefore, the primary endpoint was not reached. The total volume of intra-stent structure (protrusion and intraluminal defect) is presented in Figure 4 and was not different between two groups (non-TB:  $5.27 \pm 4.20 \text{ mm}^3$ , TB:  $5.55 \pm 5.65 \text{ mm}^3$ ,  $P=0.75$ ).

### Six-month follow-up results

In three predefined centers, the enrolled patients were followed up angiographically and with OFDI at 6 months (26 patients in the TB arm and 25 patients in the non-TB arm). Paired (post-procedure and follow-up) OFDI recordings were available in 25 and 24 patients in the TB and the non-TB arms, respectively.

At 6 months follow-up, there were also no differences in lumen, ISA or neointima areas between the two groups. Per strut-level analysis, percentage of ISA struts was  $0.42 \pm 0.94$  vs.  $0.38 \pm 0.77$  ( $P=0.76$ ), and percentage of covered struts was  $92.7 \pm 7.2$  vs.  $94.4 \pm 9.2$  ( $P=0.47$ ) in the TB and non-TB groups, respectively. The OCT healing score considerably decreased from baseline in both groups, but was not significantly different between the two groups ( $17 \pm 16$  in the TB and  $13 \pm 20$  in non-TB group,  $P=0.49$ ) (Table 5).

The three components that determine the flow area (where the blood flows) are: (i) ISS area (attached and non-attached) and (ii) ISA; therefore, their isolated or combined presence was analyzed in 2400 (1189 at baseline and 1211 at follow-up) frames within ROI. In the Venn diagrams at post-procedure (Figure 5), it appears that the most common isolated observation was prolapse of the material into the lumen (54.3%). The non-attached ISS consistently co-existed with prolapse (5.97%), with malapposition (0.17%) or with both (1.51%), but not isolated. In the same cross-section, prolapse and malapposition (11.9%) could co-exist. Malapposition alone was a quite rare phenomenon (2.27%). At 6 months follow-up, most of frames showed only neointima (81.1%), or in combination with either non-attached ISS (1.24%) or with ISA (1.16%). Only 0.83% of the frames showed neointima, non-attached ISS, and ISA. More importantly, there were 15.7% of the frames without any neointima that showed the clustering of the uncovered struts.

There was a moderate, positive correlation between ISS volume at post-procedure and the neointima volume at 6 months follow-up (Pearson's  $r=0.409$ ,  $P=0.04$ ) (Figure 6).

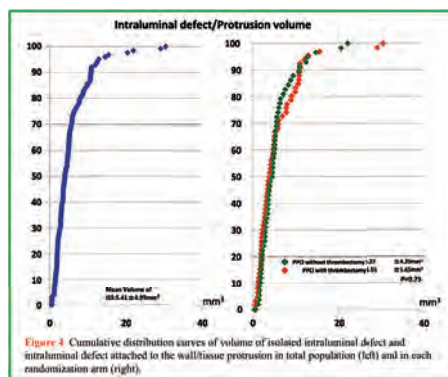
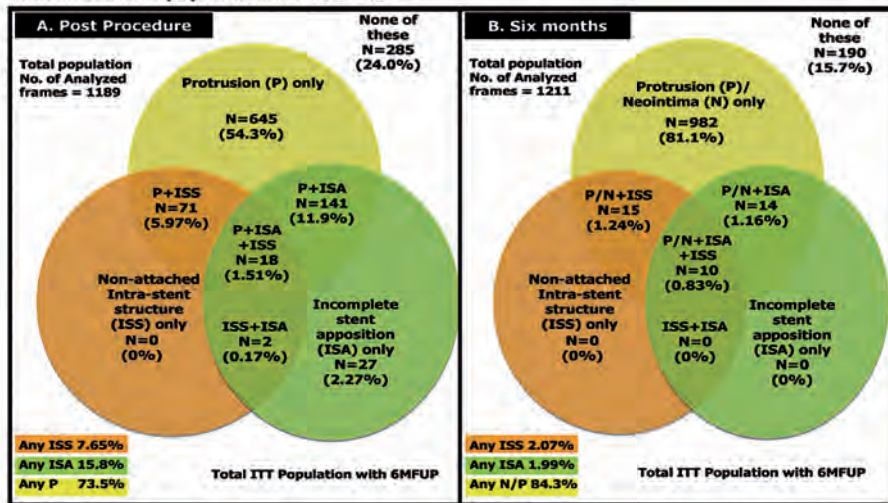


Figure 4 Cumulative distribution curves of volume of isolated intraluminal defect and intraluminal defect attached to the wall/tissue protrusion in total population (left) and in each randomization arm (right).

**Table 4** Quantitative OFDI analysis

	TB 66 patients, 66 lesions	Non-TB 61 patients, 61 lesions	Difference in means	P
Stent length, mm	22.0 ± 9.86	21.07 ± 7.69	0.93	0.56
Mean stent area, mm <sup>2</sup>	8.99 ± 2.35	8.29 ± 2.09	0.7	0.08
Mean intra-stent structure area (protrusion + isolated intraluminal mass), mm <sup>2</sup>	0.36 ± 0.22	0.34 ± 0.21	0.03	0.46
Incomplete strut apposition area, mm <sup>2</sup>	0.14 ± 0.27	0.14 ± 0.26	0.01	0.91
Mean flow area, mm <sup>2</sup>	8.71 ± 2.28	8.04 ± 2.13	0.67	0.09
Minimum flow area, mm <sup>2</sup>	7.08 ± 2.14	6.51 ± 1.99	0.57	0.12
Minimum stent area, mm <sup>2</sup>	7.62 ± 2.26	7.07 ± 2.09	0.55	0.16
Minimum lumen area, mm <sup>2</sup>	7.10 ± 2.13	6.52 ± 1.99	0.58	0.11
Minimum lumen diameter, mm	2.54 ± 0.48	2.50 ± 0.45	0.05	0.56

**Patient N=49 ITT population with 6M FUP**



**Figure 5** The Venn diagram showing the relationship among three components of flow area.

### Subgroup analysis

Post hoc subgroup analysis was performed to investigate the impact of pre-procedural thrombus burden on MinFA. In 66 patients with a thrombus grade of 4 or 5, the MinFA were  $6.52 \pm 1.97 \text{ mm}^2$  in non-TB vs.  $7.54 \pm 2.30 \text{ mm}^2$  in TB ( $P=0.043$ ), while in the patients with a less thrombus burden, the MinFA was  $6.54 \pm 2.02 \text{ mm}^2$  vs.  $6.53 \pm 1.81 \text{ mm}^2$  ( $P=0.81$ ,  $P$  for interaction = 0.09).

### Clinical outcomes

The clinical outcome of these patients before discharge is presented in **Table 6**. There were no differences between the two groups. In the non-TB arm, one patient experienced a stroke, while two patients experienced non-target vessel revascularization. In the TB arm, one patient had an acute stent thrombosis and target lesion revascularization. Due to lasting symptom caused by a side branch occlusion, the other patient

underwent a target lesion revascularization to re-open the small right ventricular branch. Two patients experienced non-target vessel revascularization.

At up to 12 months, there have been two patients having TVF in the TB group (**Table 6**). One of them has had stent thrombosis within hospitalization and there has been one patient with MI. In the non-TB group, there have been four patients with TVF. One of them had died between 1 and 6 months follow-up.

### Discussion

The TROFI study demonstrated that aspiration TB during PPCI was not associated with a significantly larger flow area compared with patients with non-TB. The amount of intraluminal mass attached to or free from the vessel wall was similar between the two groups. A per-treatment and per-protocol analyses did not affect the statistical outcomes.

**Table 5** Serial OFDI follow-up results

Post-procedure	Thrombectomy (N = 25)	Non-Thrombectomy (N = 24)	P-value
Stent length (mm)	24.8 ± 12.1	21.8 ± 7.9	0.44
Mean stent area (mm <sup>2</sup> )	8.4 ± 2.5	8.2 ± 2.2	0.75
Minimum stent area (mm <sup>2</sup> )	7.1 ± 2.2	6.9 ± 2.2	0.82
Mean flow area (mm <sup>2</sup> )	8.0 ± 2.2	7.9 ± 2.1	0.84
Minimum flow area (mm <sup>2</sup> )	6.5 ± 2.0	6.4 ± 2.1	0.82
Mean attached intra-stent structure (prolapse) (mm <sup>2</sup> )	0.42 ± 0.29	0.31 ± 0.14	0.10
Mean Non-attached intra-stent structure (mm <sup>2</sup> )	0.01 ± 0.01	0.01 ± 0.02	0.31
Mean lumen area (mm <sup>2</sup> )	8.0 ± 2.2	7.9 ± 2.1	0.84
Minimum lumen area (mm <sup>2</sup> )	6.5 ± 2.0	6.4 ± 2.1	0.82
Minimum lumen diameter (mm)	2.5 ± 0.46	2.5 ± 0.45	0.97
Mean incomplete strut apposition area (mm <sup>2</sup> )	0.12 ± 0.20	0.07 ± 0.11	0.75
ISA struts (%)	5.9 ± 9.1	3.1 ± 3.5	0.47
Healing score	202 ± 45	196 ± 17	0.49
<b>Follow-up</b>			
Mean stent area (mm <sup>2</sup> )	8.2 ± 2.6	7.8 ± 2.1	0.52
Minimum stent area (mm <sup>2</sup> )	6.9 ± 2.2	6.7 ± 2.2	0.70
Mean flow area (mm <sup>2</sup> )	7.6 ± 2.5	7.1 ± 2.0	0.43
Minimum flow area (mm <sup>2</sup> )	6.1 ± 2.2	5.6 ± 2.1	0.48
Mean lumen area (mm <sup>2</sup> )	7.6 ± 2.5	7.1 ± 2.0	0.43
Minimum lumen area, mm <sup>2</sup>	6.1 ± 2.2	5.6 ± 2.1	0.48
Minimum lumen diameter (mm)	2.5 ± 0.48	2.4 ± 0.48	0.41
Mean ISA area (mm <sup>2</sup> )	0.03 ± 0.06	0.02 ± 0.05	0.72
Maxi ISA area (mm <sup>2</sup> )	0.24 ± 0.48	0.37 ± 0.80	0.48
Mean number of struts	249 ± 139	225 ± 74	0.79
ISA struts (%)	0.42 ± 0.94	0.38 ± 0.77	0.76
Covered struts (%)	92.7 ± 7.2	94.4 ± 9.2	0.47
Healing score	17 ± 16	13 ± 20	0.49
Neointima area (mm <sup>2</sup> )	0.69 ± 0.45	0.78 ± 0.46	0.37
Neointima volume (mm <sup>3</sup> )	15.8 ± 16.9	13.7 ± 9.2	0.80

The pre-determined statistical assumption of 0.72 mm<sup>2</sup> difference used for sample size calculation was relying on a limited database from all-comer registries, collected at the central research organization of Cardialysis in Rotterdam, since trial design or endpoint based on optical coherence tomography have so far not been described and used in the literature. In that respect, the difference in minimum flow area of the historical cohort (4.95±1.39 mm<sup>2</sup>) and the present series (6.51±1.99 mm<sup>2</sup>) is striking, suggesting selection bias (e.g. unselected patients from practice vs. selected patients, lesion, and anatomy in the randomized trial).

The pre-procedural thrombus burden might influence the efficacy of TB device. The subgroup analysis on thrombus grade suggests that TB with aspiration catheter is more effective

in patients with a large thrombus burden than those with a small thrombus, where the macroscopic extraction of thrombotic material overrules the distal micro-embolization caused by the device passage. With manual aspiration catheters, the zone of effect is limited to that area directly adjacent to the inlet port so that the small thrombus/protrusion attached to the vessel wall, located on the other side of the inlet port, might not be aspirated by the catheter. Especially in the patients with a low thrombus burden, a strategy of sole stenting might be enough for restoration of flow area.

Previous all-comer studies using DESs showed that indication of acute coronary syndrome (ACS) and STEMI was one of independent predictors for acute/subacute or late stent thrombosis.[26-28] The potential explanation was that patients

**Table 6** Clinical outcomes up to 12 months follow-up

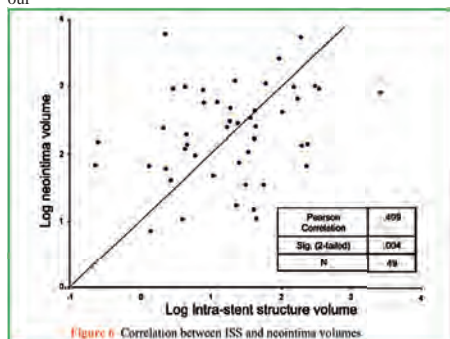
N (%)	TB (N = 71)				Non-TB (N = 70)			
	Discharge	<1 month	<6 months	Total 12 months	Disch	<1 month	<6 months	Total 12 months
TVF	1 (1.4)	1 (1.4)	1 (1.4)	2 (2.8)	1 (1.4)	1 (1.4)	3 (4.3)	4 (5.7)
All-cause mortality	0	0	0	0	0	0	1 (1.4)	1 (1.4)
Cardiac death	0	0	0	0	0	0	1 (1.4)	1 (1.4)
Non-cardiovascular death	0	0	0	0	0	0	0	0
Vascular death	0	0	0	0	0	0	0	0
Any myocardial (re) infarction	0	0	0	1 (1.4)	0	0	0	0
Target vessel revascularization	1 (1.4)	1 (1.4)	1 (1.4)	2 (2.8)	1 (1.4)	1 (1.4)	2 (2.8)	3 (4.3)
Stent thrombosis	1 (1.4)	1 (1.4)	1 (1.4)	1 (1.4)	0	0	0	0

with ACS might have a high thrombus burden at the time of stent implantation, which upon dissolution might result in late acquired stent malapposition and altered flow dynamics around stent struts. In the current study, the tissue protrusion/thrombus occupied only a small percentage of stent volume irrespective of treatment arm (TB:  $4.02 \pm 1.95\%$  vs. non-TB:  $4.18 \pm 2.27\%$ ,  $P=0.66$ ). In addition, there was only one case of acute/subacute thrombosis, which seemed to be associated with the distal edge dissection (Figure 6). This suggests that even in STEMI population, the in-stent protrusion/thrombus is small and might not to be associated with stent thrombosis.

Larger stent area and flow area in the TB arm are in itself a puzzling observation. Although the angiographic pre-procedural vessel reference did not statistically differ between the two groups (TB:  $2.91 \pm 0.49$  mm, non-TB:  $2.75 \pm 0.56$  mm;  $\Delta 0.16$  mm,  $P=0.09$ ), this non-significant difference of 0.16 mm could be partially contributed to the selection of larger stent size and the larger stent area post-procedure on OFDI when the area is calculated by the second power of diameter.

These differences in vessel size, MinFA, and stent area could be the result of non-documented treatment effects of TB. Thrombectomy not only aspirates particulated debris but also soluble vasoconstrictors, thrombogenic, and inflammatory mediators released during plaque rupture and contributing to microcirculatory impairment. Among them, endothelin, serotonin, thromboxane, and tumour necrosis factor alpha (TNF- $\alpha$ ) have been identified.[29-31] It has been demonstrated using coronary aspirate that serotonin is the main coronary vasoconstrictor after stenting and thromboxane, and TNF- $\alpha$  potentiates the serotonin response. Unfortunately, in our study, none of these assessments was performed and vasomotor tone of the coronary vasculature immediately post-TB was not assessed even by quantitative coronary angiography. Ideally, in future studies, quantitative assessment of OFDI prior to TB and immediately post-TB as well as post-stenting should be performed to quantify changes in vasomotor tone.

The post-procedural incidence of malapposition is a rather frequent observation (85.8% in a patient-level analysis without differences between groups) and seems higher than the incidence observed in the paclitaxel arm of the HORIZONS-AMI trial with IVUS (34.3%).[32] presumably due to higher resolution of OFDI than IVUS.[14] On the contrary to our



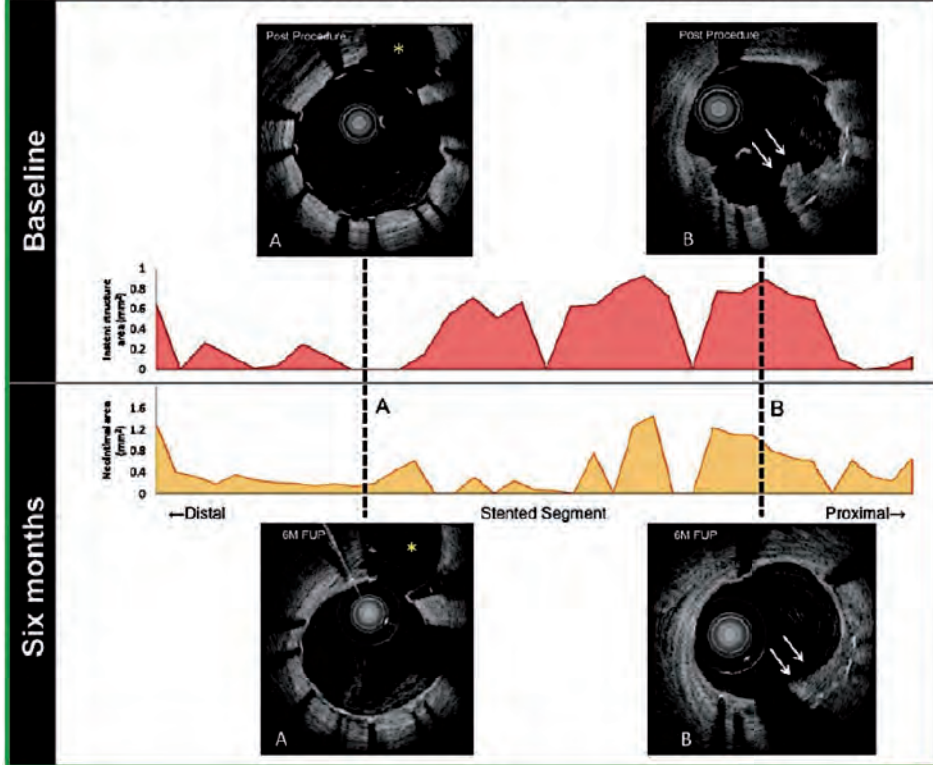
assumption of the dissolution of thrombus existing between stent struts and vessel wall together with the profound neointima inhibition due to high concentration of the antiproliferative drug, the incidence of late ISA in STEMI patients was very low at 6 months follow-up in the present study. Specifically in the serial population, an incidence of ISA was 15.8% post-procedure and 2.0% at 6 months follow-up. Furthermore, the healing score was dramatically decreased from 200 to 15. It thus seems unreasonable to recommend a targeted post-dilatation of the malapposed/ISA struts, and from that point of view, the use of self-expanding device might be more relevant for the treatment of prolapse than for malapposition.[33]

The results of current trial showed no difference in plaque protrusion or intraluminal defects after stent implantation between TB and non-TB as well as TIMI flow. In the previous literatures, however, plaque prolapse after stent implantation, as assessed by IVUS, was shown to be associated with greater levels of creatine kinase isoenzyme MB[34] and early stent thrombosis[28,35] in patients with acute myocardial infarction. Conflicting results however exist on the fact that prolapse after stenting was not associated with long-term clinical outcomes in patients with acute myocardial infarction.[27,28] or stable coronary artery disease.[36] Interestingly, we found a moderate positive relationship between the post-procedural ISS volume and neointima formation at 6 months follow-up. An example case demonstrated that the location of ISS at post-procedure well matched that of neointima at follow-up (Figure 7). It has been described that the thrombus can nest and promote the growth of smooth muscle cells. This may be due to the presence of chemoattractants and growth factors in the thrombotic milieu.[37] Considering that the number of patients included is too small to correlate OFDI findings with clinical events, the clinical significance of intraluminal protrusion on OFDI remained unclear.

### Limitation

The fate of intraluminal thrombi can be two-fold: Either they can be removed backward (by aspiration device) or pushed forward by the TB catheter itself. To date, this 'double-edged sword' impact of advancing and pulling back a TB catheter through thrombotic area has not been fully documented and elucidated. In that respect, our study was focalized on the intra-stent area post-treatment and must be viewed as a pure mechanistic analysis without any specific consideration for all the other relevant physiological implications, such as peripheral embolization, microcirculatory, and myocardial injury with their eventual clinical sequelae. In sample size calculations, the potential crossovers from non-TB to TB were not taken into account. The study population represents a relatively non-complicated population compared with all-comer population in daily practice because cardiogenic shock is one of exclusion criteria. Due to the strict requirement of the informed consent at emergent situation, severely ill patients with potentially large thrombus burden could be excluded from the study. In a recent meta-analysis of the HORIZONS-AMI and CADILLAC populations,[38] 68% of these studies population had an initial TIMI 0-1 flow, while in the current TROFI trial, 46% of patients presented TIMI 0-1.

**Figure 7** A representative case showing the relationship between ISS and neointima.



## Conclusions

The current randomized controlled trial using a high-resolution OFDI device showed no significant difference in OFDI parameters including minimal flow area between PPCI with TB and PPCI without TB at both post-procedure and 6 months follow-up. However, ISS volume at post-procedure was positively associated with neointimal volume at 6 months follow-up. DES with biodegradable polymer showed to be safe with very low adverse events rate up to 1 year. The potential impact of OFDI guidance needs to be further elucidated in future studies.

## Disclosure

The TROFI study was sponsored by TERUMO Europe NV (Leuven, Belgium). The authors have no conflict of interest related to the context of this chapter.

## References

1. Van de Werf F, Bax J, Betriu A, et al. Management of acute myocardial infarction in patients presenting with persistent ST-segment elevation: the Task Force on the Management of ST-Segment Elevation Acute Myocardial Infarction of the European Society of Cardiology. *Eur Heart J* 2008;29:2909–2945.
2. Zijlstra F, Hoorntje JC, de Boer MJ, et al. Long-term benefit of primary angioplasty as compared with thrombolytic therapy for acute myocardial infarction. *N Engl J Med* 1999;341:1413–1419.
3. Grines CL, Cox DA, Stone GW, et al. Coronary angioplasty with or without stent implantation for acute myocardial infarction. Stent Primary Angioplasty in Myocardial Infarction Study Group. *N Engl J Med* 1999;341:1949–1956.
4. Silva-Orrego P, Colombo P, Bigi R, et al. Thrombus aspiration before primary angioplasty improves myocardial reperfusion in acute myocardial infarction: the DEAR-MI (Dethrombosis to Enhance Acute Reperfusion in Myocardial Infarction) study. *J Am Coll Cardiol* 2006;48:1552–1559.

5. Sardella G, Mancone M, Bucciarelli-Ducci C, et al. Thrombus aspiration during primary percutaneous coronary intervention improves myocardial reperfusion and reduces infarct size: the EXPIRA (thrombectomy with export catheter in infarct-related artery during primary percutaneous coronary intervention) prospective, randomized trial. *J Am Coll Cardiol* 2009;53:309–315.
6. Burzotta F, Trani C, Romagnoli E, et al. Manual thrombus-aspiration improves myocardial reperfusion: the randomized evaluation of the effect of mechanical reduction of distal embolization by thrombus-aspiration in primary and rescue angioplasty (REMEDIA) trial. *J Am Coll Cardiol* 2005;46:371–376.
7. Reffelmann T, Hale SL, Dow JS, et al. No-reflow phenomenon persists long term after ischemia/reperfusion in the rat and predicts infarct expansion. *Circulation* 2003;108:2911–2917.
8. Skyschally A, Leineweber K, Gres P, et al. Coronary microembolization. *Basic Res Cardiol* 2006;101:373–382.
9. Iwakura K, Ito H, Kawano S, et al. Assessing myocardial perfusion with the transthoracic Doppler technique in patients with reperfused anterior myocardial infarction: comparison with angiographic, enzymatic and electrocardiographic indices. *Eur Heart J* 2004;25:1526–1533.
10. Vlaar PJ, Svilaas T, van der Horst IC, et al. Cardiac death and reinfarction after 1 year in the Thrombus Aspiration during Percutaneous coronary intervention in Acute myocardial infarction Study (TAPAS): a 1-year follow-up study. *Lancet* 2008;371:1915–1920.
11. Muramatsu T, Serruys PW, Onuma Y. Thrombotic arch in ST-segment elevation myocardial infarction: comparison between two-dimensional and three dimensional optical frequency domain imaging. *Eur Heart J* 2012;27:141–154.
12. Kubo T, Imanishi T, Takarada S, et al. Assessment of culprit lesion morphology in acute myocardial infarction: ability of optical coherence tomography compared with intravascular ultrasound and coronary angiography. *J Am Coll Cardiol* 2007;50:933–939.
13. Gonzalo N, Barlis P, Serruys PW, et al. Incomplete stent apposition and delayed tissue coverage are more frequent in drug-eluting stents implanted during primary percutaneous coronary intervention for ST-segment elevation myocardial infarction than in drug-eluting stents implanted for stable/unstable angina: insights from optical coherence tomography. *JACC Cardiovasc Interv* 2009;2:445–452.
14. Okamura T, Onuma Y, Garcia-Garcia HM, et al. First-in-man evaluation of intravascular optical frequency domain imaging (OFDI) of Terumo: a comparison with intravascular ultrasound and quantitative coronary angiography. *EuroIntervention* 2011;6:1037–1045.
15. Sianos G, Papafaklis MI, Daemen J, et al. Angiographic stent thrombosis after routine use of drug-eluting stents in ST-segment elevation myocardial infarction: the importance of thrombus burden. *J Am Coll Cardiol* 2007;50:573–583.
16. van 't Hof AW, Liem A, Suryapranata H, et al. Angiographic assessment of myocardial reperfusion in patients treated with primary angioplasty for acute myocardial infarction: myocardial blush grade. *Zwolle Myocardial Infarction Study Group. Circulation* 1998;97:2302–2306.
17. Schroder R. Prognostic impact of early ST-segment resolution in acute ST-elevation myocardial infarction. *Circulation* 2004;110:e506–e510.
18. Okamura T, Gonzalo N, Gutierrez-Chico JL, et al. Reproducibility of coronary Fourier domain optical coherence tomography: quantitative analysis of in vivo stented coronary arteries using three different software packages. *EuroIntervention* 2010;6:371–9.
19. Gonzalo N, Garcia-Garcia HM, Serruys PW, et al. Reproducibility of quantitative optical coherence tomography for stent analysis. *EuroIntervention* 2009;5:224–32.
20. Muramatsu T, Garcia-Garcia HM, Lee IS, et al. Quantitative optical frequency domain imaging assessment of in-stent structures in patients with ST-segment elevation myocardial infarction. *Circ J* 2012;76:2822–31.
21. Okamura T, Onuma Y, Garcia-Garcia HM, et al. 3-Dimensional optical coherence tomography assessment of jailed side branches by bioresorbable vascular scaffolds: a proposal for classification. *JACC Cardiovasc Interv* 2010;3:836–844.
22. Gonzalo N, Serruys PW, Okamura T, et al. Optical coherence tomography assessment of the acute effects of stent implantation on the vessel wall: a systematic quantitative approach. *Heart* 2009;95:1913–1919.
23. Prati F, Regar E, Mintz GS, et al. Expert review document on methodology, terminology, and clinical applications of optical coherence tomography: physical principles, methodology of image acquisition, and clinical application for assessment of coronary arteries and atherosclerosis. *Eur Heart J* 2010;31:401–415.
24. Tanigawa J, Barlis P, Di Mario C. Intravascular optical coherence tomography: optimization of image acquisition and quantitative assessment of stent strut apposition. *EuroIntervention* 2007;3:128–136.
25. Cutlip DE, Windecker S, Mehran R, et al. Clinical end points in coronary stent trials: a case for standardized definitions. *Circulation* 2007;115:2344–2351.
26. Daemen J, Wenaweser P, Tsuchida K, et al. Early and late coronary stent thrombosis of sirolimus-eluting and paclitaxel-eluting stents in routine clinical practice: data from a large two-institutional cohort study. *Lancet* 2007;369:667–678.
27. Park DW, Park SW, Park KH, et al. Frequency of and risk factors for stent thrombosis after drug-eluting stent implantation during long-term follow-up. *Am J Cardiol* 2006;98:352–356.
28. Wenaweser P, Daemen J, Zwahlen M, et al. Incidence and correlates of drug-eluting stent thrombosis in routine clinical practice. 4-year results from a large 2-institutional cohort study. *J Am Coll Cardiol* 2008;52:1134–1140.
29. Adlbrecht C, Bonderman D, Plass C, et al. Active endothelin is an important vasoconstrictor in acute coronary thrombi. *Thromb Haemost* 2007;97:642–649.
30. Bonderman D, Teml A, Jakowitsch J, et al. Coronary no-reflow is caused by shedding of active tissue factor from dissected atherosclerotic plaque. *Blood* 2002;99:2794–2800.
31. Brambilla M, Camera M, Colnago D, et al. Tissue factor in patients with acute coronary syndromes: expression in platelets,

- leukocytes, and platelet-leukocyte aggregates. *Arterioscler Thromb Vasc Biol* 2008;28:947–953.
32. Guo N, Maehara A, Mintz GS, et al. Incidence, mechanisms, predictors, and clinical impact of acute and late stent malapposition after primary intervention in patients with acute myocardial infarction: an intravascular ultrasound substudy of the Harmonizing Outcomes with Revascularization and Stents in Acute Myocardial Infarction (HORIZONS-AMI) trial. *Circulation* 2010;122:1077–1084.
33. Amoroso G, van Geuns RJ, Spaulding C, et al. Assessment of the safety and performance of the STENTYS self-expanding coronary stent in acute myocardial infarction: results from the APPOSITION I study. *EuroIntervention* 2011;7:428–436.
34. Hong YJ, Jeong MH, Ahn Y, et al. Plaque prolapse after stent implantation in patients with acute myocardial infarction: An intravascular ultrasound analysis. *JACC Cardiovasc Imaging* 2008;1:489–497.
35. Choi SY, Witzenbichler B, Maehara A, et al. Intravascular ultrasound findings of early stent thrombosis after primary percutaneous intervention in acute myocardial infarction: A Harmonizing Outcomes with Revascularization and Stents in Acute Myocardial Infarction (HORIZONS-AMI) substudy. *Circ Cardiovasc Interv* 2011;4:239–247.
36. Futamatsu H, Sabate M, Angiolillo DJ, et al. Characterization of plaque prolapse after drug-eluting stent implantation in diabetic patients: A three-dimensional volumetric intravascular ultrasound outcome study. *J Am Coll Cardiol* 2006;48:1139–1145.
37. MacLeod DC, Strauss BH, de Jong M, et al. Proliferation and extracellular matrix synthesis of smooth muscle cells cultured from human coronary atherosclerotic and restenotic lesions. *J Am Coll Cardiol* 1994;23:59–65.
38. Brener SJ, Mehran R, Brodie BR, et al. Predictors and implications of coronary infarct artery patency at initial angiography in patients with acute myocardial infarction (from the CADILLAC and HORIZONS-AMI Trials). *Am J Cardiol* 2011;108:918–923.

#### 4.4 Early clinical experience of polylactide bioresorbable scaffold for STEMI and NSTEMI in the Thoraxcenter

Early and late optical coherence tomography findings following everolimus-eluting bioresorbable vascular scaffold implantation in myocardial infarction: a preliminary report.

*Hellenic J Cardiol* 2015;56:125-35.

[Original research paper, Impact Factor (2013): 0.785]

Karanasos A, Muramatsu T, Diletti R, Nauta S, Onuma Y, Lenzen M, Nakatani S, van Mieghem NM, Schultz C, de Jaegere PP, Serruys PW, Zijlstra F, Regar E, van Geuns RJ.





# Early and Late Optical Coherence Tomography Findings Following Everolimus-Eluting Bioresorbable Vascular Scaffold Implantation in Myocardial Infarction: A Preliminary Report

ANTONIOS KARANASOS, TAKASHI MURAMATSU, ROBERTO DILETTI, SJOERD NAUTA, YOSHINOBU ONUMA, MATTIE LENZEN, SHIMPEI NAKATANI, NICOLAS M. VAN MIEGHEM, CARL SCHULTZ, PETER P. DE JAEGERE, PATRICK W. SERRUYS, FELIX ZIJLSTRA, EVELYN REGAR, ROBERT-JAN VAN GEUNS

*Thoraxcenter, Erasmus Medical Center, Rotterdam, the Netherlands*

**Key words:**  
**Bioresorbable vascular scaffold, optical coherence tomography, ST-elevation myocardial infarction, non-ST-elevation myocardial infarction.**

*Manuscript received:*  
May 30, 2014;  
*Accepted:*  
September 8, 2014.

*Address:*  
Robert-Jan van Geuns

*Department of  
Cardiology, Thoraxcenter  
Room Ba585, Erasmus  
Medical Center  
Molewaterplein 40  
3015 RD, Rotterdam  
The Netherlands  
[r.vangeuns@erasmusmc.nl](mailto:r.vangeuns@erasmusmc.nl)*

**Introduction:** Although bioresorbable vascular scaffolds (BVS) have been used with promising results in patients with stable and unstable angina, little is known about the acute vascular response following BVS implantation in myocardial infarction. We present angiographic and OCT findings from the first patients undergoing bioresorbable vascular scaffold (BVS) implantation for non-ST-elevation myocardial infarction (NSTEMI) or ST-elevation myocardial infarction (STEMI) in our institution.

**Methods:** The first 5 patients with NSTEMI and the first 5 patients with STEMI who underwent BVS implantation in our institution, followed by optical coherence tomography (OCT) imaging of the treated culprit vessel, were included in this series. All patients underwent angiographic analysis pre- and post- BVS implantation, as well as OCT analysis, including qualitative and quantitative assessment.

**Results:** Implantation was successful in all cases, as assessed by angiography and OCT. There were no cases with coronary spasm, distal embolization or no-reflow. No adverse clinical events were recorded in any patient at the 6-month follow up. Specific illustrative cases demonstrating the challenges of BVS implantation in myocardial infarction are presented.

**Conclusions:** BVS implantation can potentially be used in the setting of thrombotic lesions encountered in myocardial infarction; however, the role of this treatment approach warrants systematic evaluation in prospective studies.

**I**mplantation of metallic platform drug-eluting stents constitutes the mainstay of revascularization in acute myocardial infarction.<sup>1</sup> However, their use has been associated with an impaired vascular healing response, while concerns have been raised over their long-term performance. Bioresorbable vascular scaffolds (BVS) could help overcome such long-term pitfalls of metallic platforms.<sup>2</sup> Although bioresorbable scaffolds have shown promising results in stable

and unstable angina,<sup>3,4</sup> the acute vascular response following BVS implantation in myocardial infarction has not been extensively studied.<sup>5-7</sup>

As of September 1st, 2012, the ABSORB™ BVS (Abbott Vascular, Santa Clara, CA, USA) has been commercially available in the Netherlands. Based on available evidence,<sup>3,4</sup> our department selected these devices as the first option for younger patients presenting for percutaneous coronary intervention (PCI) in every-

day clinical practice. As lesions in these patients might be more complex compared to those of trial investigational patients, the BVS-EXPAND registry was initiated. In this registry, follow-up data are collected as part of the hospital routine for monitoring outcomes after PCI and the introduction of a different generation of stent or scaffold. The BVS-EXPAND includes patients with stable disease, but also patients with unstable angina or non-ST-elevation myocardial infarction (NSTEMI). After the first experience with acute patients and an interim analysis, a decision was made to extend BVS utilization to the treatment of ST-elevation myocardial infarction (STEMI).

To assess the safety and procedural success of a BVS strategy in STEMI, optical coherence tomography (OCT) imaging was performed, according to clinical judgment, in patients with STEMI and BVS implantation, for a more comprehensive evaluation of the acute procedural outcome by the operator. OCT is a high-resolution intravascular imaging modality that enables visualization of the acute vascular response after stent implantation.<sup>8-11</sup> Specifically, OCT can accurately evaluate scaffold expansion and apposition, and can also assess vascular trauma and residual thrombotic burden.<sup>11-13</sup>

We previously reported on a systematic analysis of the OCT findings post BVS implantation in STEMI.<sup>6</sup> In the current report, we present patient-level angiographic and OCT findings from the first five patients of BVS-EXPAND presenting with NSTEMI and imaged by OCT, and the first five patients who underwent BVS implantation for STEMI followed by OCT imaging, in our institution, in an attempt to illustrate the main challenges of BVS implantation in thrombotic lesions.

## Methods

### *Study population*

The current series comprised 1) the first five patients of BVS-EXPAND presenting with NSTEMI and imaged by OCT, and 2) the first five patients who underwent BVS implantation for STEMI followed by OCT imaging, in our institution. The STEMI patients were not a part of BVS-EXPAND.

### *Procedure and OCT image acquisition*

Patients with NSTEMI typically underwent coronary angiography within 24-72 hours from symptom on-

set, according to the regional protocol, followed by urgent PCI after discussion in the HeartTeam, while patients with STEMI underwent primary PCI upon hospital arrival. Interventional management, including the use of thrombectomy, pre-dilation and post-dilation, was performed according to the operator's discretion. OCT was performed after BVS implantation using the C7™ imaging system and the Dragonfly™ catheter (both St. Jude Medical, St. Paul, Minnesota, USA), as previously described.<sup>11</sup> In several cases, OCT findings guided further procedural optimization (i.e. additional scaffold implantation and/or post-dilation). In these cases, a new OCT pullback was performed at the end of the procedure. The patients were contacted by telephone 6 months after the procedure, and adverse events (death, myocardial infarction, any unplanned revascularization), according to the Academic Research Consortium definitions, were recorded.<sup>14</sup>

### *Angiographic and OCT analysis*

Quantitative coronary angiography (QCA) analyses were performed offline by an experienced observer (TM) using CAAS 5.10 (Pie Medical Imaging, Maastricht, Netherlands) according to a previously reported methodology.<sup>13</sup> Intracoronary thrombus was identified angiographically and scored in five grades, as previously described.<sup>13</sup> Complications such as dissection, spasm, distal embolization and no-reflow were also recorded. OCT analysis was performed offline by an experienced observer in fixed 1-mm longitudinal intervals within the treated culprit segment, after exclusion of frames with <75% lumen contour visibility. Quantitative analysis included measurement of the minimal lumen and the minimal scaffold area, according to a previously described methodology.<sup>15</sup> Qualitative assessment included evaluation of in-scaffold and edge dissections, tissue prolapse and in-scaffold thrombus. Dissections were defined as the presence of intimal discontinuity, with or without flap formation, either within the scaffolded segment (intra-scaffold dissection), or within 5-mm-long proximal or distal edge segments (edge dissections).<sup>16</sup> Tissue prolapse was defined as the projection of tissue into the lumen between stent struts after implantation.<sup>16</sup> Incomplete strut apposition (ISA) was defined as a clear lack of contact between scaffold strut and vascular wall;<sup>15</sup> apposition was assessed at a scaffold-level basis, using a definition of malapposed scaffold as a scaffold with >5% malapposed struts.

## Ethics

This was an observational study, performed according to the privacy policy of Erasmus MC and the Erasmus MC regulations for the appropriate use of data in patient-oriented research. These are based on international regulations, including the declaration of Helsinki. A waiver from the Ethical Committee of Erasmus MC was obtained for written informed consent, as—according to Dutch law—written consent is not required if patients do not undergo procedures other than as part of their regular treatment. Invasive follow up in two of the patients was performed as part of an ethical committee-approved, single-center, investigator-driven, observational study (BVS-STEMI first) for which written informed consent was obtained from the patients.

## Results

The median patient age was 56 years (range 40-75 years). Baseline characteristics are presented in Table 1, while angiographic data are presented in Table 2. There were no cases with spasm, distal embolization or no-reflow. No in-hospital events were recorded. Table 3 summarizes the OCT findings. Clinical follow-up at 6 months was available for all patients, showing an absence of adverse clinical events. Specific illustrative cases demonstrating the challenges of BVS implantation in NSTEMI and STEMI are presented below.

## Patient 2 (Figure 1)

A 56-year-old man with no prior cardiovascular history, who presented with NSTEMI, had a total occlusion of the proximal left circumflex artery (LCx) with collateral filling from the left anterior descending artery (LAD), as documented by coronary angiography. OCT imaging performed after thrombus aspiration and predilation with a  $2.0 \times 20$  mm compliant Trek™ balloon (Abbott Vascular) revealed a thrombosed, severely stenotic lesion with plaque rupture and intimal tears, probably induced by balloon predilation (Panels A-D). After additional predilation with a  $3.0 \times 20$  mm Trek™ compliant balloon inflated at 14 atm (maximum diameter 3.11 mm; just below the maximum luminal diameter by QCA), a  $3.0 \times 18$  mm BVS was implanted in the culprit lesion (inflation pressure 16 atm). Following this strategy, post-implantation OCT showed no edge dissections or residual stenosis. There were, however, several sites with moderate tissue prolapse/thrombus within the scaffold (panels A'-C'), for which no additional treatment was applied.

## Patient 5 (Figures 2-3)

A 56-year-old man was admitted with NSTEMI and referred for PCI after HeartTeam consensus. Coronary angiography had demonstrated three-vessel disease: a lesion in the proximal LCx, a diffuse calcified lesion of the mid LAD, and a diffusely diseased right

**Table 1.** Baseline and procedural characteristics.

Patient	Age	Sex	Clinical syndrome	Lesions treated (n)	BVS implanted (n)	Thrombus aspiration	Balloon predilation	BVS size	Balloon post-dilation	Side-branch dilation
Patient 1	59	♀	NSTEMI	1	4	No	$3 \times 15$	$3 \times 28, 3 \times 28, 3 \times 18, 2.5 \times 28$	$3 \times 12, 3.5 \times 15$	No
Patient 2	56	♂	NSTEMI	1	1	Yes	$3 \times 20$	$3 \times 18$	No	No
Patient 3	75	♂	NSTEMI	1	3	No	$3 \times 15$	$3.5 \times 18, 3 \times 18, 2.5 \times 18$	No	$1.5 \times 8$
Patient 4	57	♀	NSTEMI	1	1	No	$2.5 \times 20$	$3 \times 28$	No	No
Patient 5	56	♂	NSTEMI	2	3	No	$3 \times 15$ (LCx) $3 \times 20$ (LAD)	$3.5 \times 18, 3.5 \times 12$ (LCx) $3.5 \times 28$ (LAD)	No (LCx) $3.75 \times 15$ (LAD)	No
Patient 6	56	♀	STEMI	1	1	Yes	$2.5 \times 20$	$3 \times 28$	$3.25 \times 15$	No
Patient 7	40	♂	STEMI	1	1	Yes	$2.5 \times 15$	$3.5 \times 18$	No	No
Patient 8	53	♂	STEMI	1	1	No	$2 \times 8$	$2.5 \times 18$	No	No
Patient 9	65	♂	STEMI	1	2	Yes	No	$3.5 \times 12, 3.5 \times 12$	$4 \times 8$	No
Patient 10	58	♂	STEMI	1	2	Yes	$3 \times 12$	$3.5 \times 18, 3.5 \times 18$	$3.5 \times 15$	$1.5 \times 15$

BVS – bioresorbable vascular scaffold; NSTEMI – non-ST-elevation myocardial infarction; STEMI – ST-elevation myocardial infarction; LCx – left circumflex artery; LAD – left anterior descending artery.

**Table 2.** Angiographic characteristics.

Patient	Culprit vessel	Pre procedure		Pre BVS implantation				Post implantation (in-scaffold)				
		Total Occlusion	Thrombus burden	Dmax (mm)	RVD (mm)	MLD (mm)	DS (%)	RVD (mm)	MLD (mm)	DS (%)	Final TIMI flow	Dissection
Patient 1	RCA	Yes	5	3.6	2.64	1.04	61	2.76	2.22	20	II	Yes
Patient 2	LCx	Yes	5	3.22	2.74	2.1	23	3.15	3	5	III	No
Patient 3	LAD	No	2	3.16	2.18	1.56	28	2.51	2.32	8	III	No
Patient 4	LAD	No	1	3.09	2.74	1.22	55	2.79	2.46	12	III	No
Patient 5, Lesion 1	LCx	No	0	3.44	2.96	1.39	53	2.71	2.36	13	III	No
Patient 5, Lesion 2	LAD	No	0	3.28	3.27	1.27	61	2.81	2.54	10	III	No
Patient 6	RCA	Yes	5	3.44	2.89	0.96	67	2.85	2.42	15	III	Yes
Patient 7	LAD	No	2	3.16	2.68	2.16	19	2.92	2.92	0	II	Yes
Patient 8	LD	Yes	5	2.55	2	0.51	74	2.47	2.05	17	III	No
Patient 9	RCA	Yes	5	3.97	3.52	1.4	60	3.17	2.39	25	III	No
Patient 10	LAD	No	3	3.63	2.29	0.9	61	2.58	1.93	25	III	No

Dmax – maximum diameter; RVD – reference vessel diameter; MLD – minimum lumen diameter; DS – diameter stenosis; RCA – right coronary artery; LD – diagonal branch. Other abbreviations as in Table 1.

coronary artery (RCA). It was decided to proceed with LCx and LAD revascularization, and staged revascularization of the RCA one month later.

The proximal LCx lesion (Panel 2I) was treated by  $3.5 \times 18$  mm BVS implantation and post-dilation with a  $3.0 \times 15$  mm compliant Trek™ balloon (Panel 2II). Subsequently, lumen narrowing with haziness was observed proximally, corresponding to an edge dissection by OCT (Panels 2A-B). The dissection was treated by implantation of an overlapping  $3.5 \times 12$  mm BVS with a good angiographic result (panel 2III). A final OCT pullback showed focal under-expansion due to calcification, as well as sites with mild tissue prolapse and in-stent thrombus (Panels 2A'-D').

The LAD lesion (Panel 3I) was treated by  $3.0 \times 20$  mm Trek™ balloon predilation,  $3.5 \times 28$  mm BVS implantation and post-dilation with a  $3.75 \times 15$  mm Trek™ non-compliant balloon (Panels 3II-III). OCT following predilation revealed a heavily calcified vessel without intracoronary thrombus. Post-implantation OCT demonstrated good scaffold apposition, moderate pinching of the ostium of the diagonal (Panel 3A'), focal under-expansion at sites with heavy calcification (Panel 3C'), lack of tissue prolapse, and a small distal edge dissection (Panel 3D').

#### Patient 7 (Figure 4)

A 40-year-old man with diabetes and no known cardiovascular history was admitted with anterior STEMI. Angiography demonstrated a stenotic LAD le-

sion with angiographic haziness (Panel I). The lesion was treated by thrombus aspiration,  $2.5 \times 15$  mm Trek™ compliant balloon pre-dilation and  $3.5 \times 18$  mm BVS implantation (Panels II-III). A small edge dissection was visible by angiography after implantation. OCT confirmed the diagnosis of distal edge dissection extending for  $\sim 5$  mm, which was left untreated (Panels D-E). The scaffold was well-expanded and apposed with moderate tissue prolapse and in-scaffold thrombus at the middle segment (Panels A-C). The patient underwent invasive follow up, including OCT imaging, 9 months post implantation for study purposes (Panel IV). The follow-up OCT showed a good healing response, without late ISA, high strut coverage (Panels A'-C') and complete healing of the dissection with integration of the dissection flap in the vessel wall (Panels D'-E').

#### Patient 8 (Figure 5)

A 52-year-old man with an unremarkable cardiovascular history was admitted with anterolateral STEMI. Angiography demonstrated total occlusion of the second diagonal branch (Panel I). The lesion was treated by  $2.0 \times 8$  mm Trek™ compliant balloon dilation and  $2.5 \times 18$  mm BVS implantation (Panels II-III). OCT showed a well-expanded and apposed scaffold with no vascular trauma at the middle and distal segments, and mild tissue prolapse and thrombus near the vessel ostium (Panels C-D). Scaffold struts were visible at the polygon of confluence of

**Table 3.** Optical coherence tomography (OCT) findings.

Patient	ISA	Minimal lumen area (mm <sup>2</sup> )	Minimal scaffold area (mm <sup>2</sup> )	Intraprocedural findings	Final OCT findings
Patient 1	Yes	Proximal BVS: 6.63	Proximal BVS: 7.85	Extensive intra-scaffold dissections with ISA in proximal scaffold, treated with post-dilation	<ul style="list-style-type: none"> <li>• Improvement of scaffold apposition after post-dilation.</li> <li>• Minimal tissue prolapse.</li> </ul>
Patient 2	No	7.60	8.34	-	<ul style="list-style-type: none"> <li>• Good expansion and apposition.</li> <li>• No edge dissections</li> <li>• Moderate tissue prolapse/thrombus.</li> </ul>
Patient 3	Yes	4.42	4.97	Side-branch compromise, treated with balloon dilation	<ul style="list-style-type: none"> <li>• Distal and middle scaffolds well-expanded without tissue prolapse or thrombus.</li> <li>• ISA in the proximal and middle scaffolds due to eccentric calcium and intra-scaffold dissections.</li> <li>• Mild tissue prolapse in the proximal scaffold.</li> <li>• No evident scaffold fracture at the level of the side-branch.</li> </ul>
Patient 4	No	6.05	6.57	-	<ul style="list-style-type: none"> <li>• Good expansion and apposition without edge dissections.</li> <li>• Short segment with moderate tissue prolapse/thrombus</li> </ul>
Patient 5	LCx: Yes LAD: No	LCx: 6.28 mm <sup>2</sup> LAD: 4.98 mm <sup>2</sup>	LCx: 6.28 mm <sup>2</sup> LAD: 5.36 mm <sup>2</sup>	Proximal dissection in LCx, treated with 2nd BVS	<ul style="list-style-type: none"> <li>• LCx: mild tissue prolapse/thrombus in both scaffolds.</li> <li>• Sub-optimal expansion and ISA focally.</li> <li>• LAD: good apposition with sub-optimal expansion focally due to calcium.</li> <li>• Small distal edge dissection.</li> </ul>
Patient 6	Yes	6.27	7.07	Extensive intra-scaffold dissection with ISA, treated with post-dilation.	<ul style="list-style-type: none"> <li>• Reduction of dissection cavity size and malapposition distance after post-dilation.</li> <li>• Mild tissue prolapse and in-scaffold thrombus ISA.</li> </ul>
Patient 7	No	7.55	8.33	-	<ul style="list-style-type: none"> <li>• Distal edge dissection ~5 mm long.</li> <li>• Sites with moderate tissue prolapse/in-scaffold thrombus proximally.</li> </ul>
Patient 8	No	4.21	4.76	-	<ul style="list-style-type: none"> <li>• Well-expanded and apposed scaffold with minimal tissue prolapse/thrombus.</li> <li>• Scaffold protrusion into the main branch for ~1 mm.</li> </ul>
Patient 9	Yes	5.72	7.6	Stenosis in distal RCA after BVS implantation in RPL, treated with 2nd BVS.	<ul style="list-style-type: none"> <li>• ISA proximally due to scaffold-lumen dimensions mismatch.</li> <li>• Minimal overlap at the crux with moderate tissue prolapse.</li> <li>• Presence of struts at the RPD ostium and residual red thrombus.</li> </ul>
Patient 10	No	6.77	7.15	Small edge dissection and residual lesion distally (MLA: 1.71 mm <sup>2</sup> ), treated with 2nd BVS - Side-branch compromise, treated with balloon dilation	<ul style="list-style-type: none"> <li>• Good expansion and apposition with minimal overlap.</li> <li>• Mild tissue prolapse/thrombus in both scaffolds.</li> <li>• No evident scaffold fracture at the level of the side-branch.</li> </ul>

ISA – incomplete scaffold apposition; RPL – right posterolateral branch; RPD – right posterior descending branch; MLA – minimal lumen area. Other abbreviations as in Tables 1 and 2.

the LAD-diagonal bifurcation, with minimal protrusion of the scaffold into the LAD (Panels A, B, G). Invasive follow up with OCT imaging was performed 1 year post implantation for study purposes (Panel IV). The follow-up OCT revealed a good healing re-

sponse without ISA and a low number of uncovered struts (Panels A'-D'). Dense tissue coverage was also observed at the side-branch-related struts located in the vessel ostium, resulting in the development of a neo-carina (Panel H).

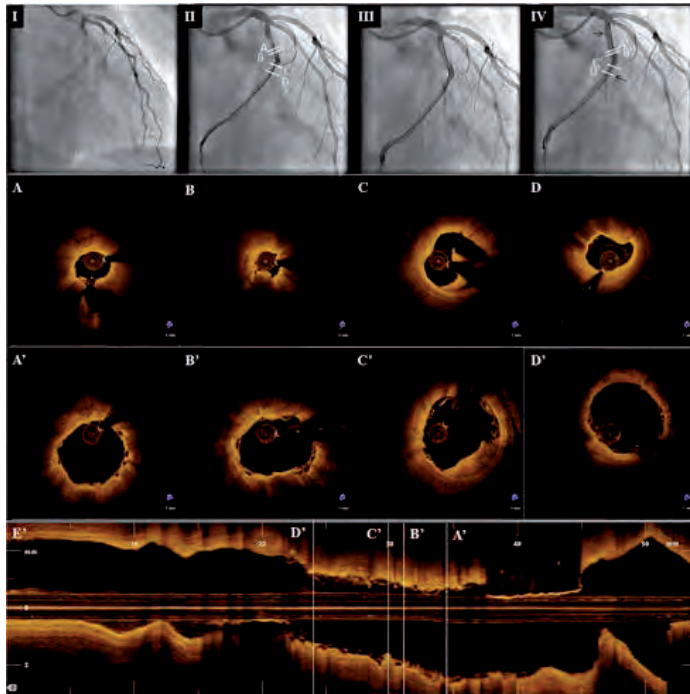


**Figure 1.** Top panels: Coronary angiography demonstrating the culprit lesion of the proximal left circumflex artery (I) pre-intervention, (II) after 2.0 mm balloon predilation, (III) after 3.0 mm balloon predilation, and (IV) after 3.0 × 18 mm bioresorbable vascular scaffold (BVS) implantation. Black arrows indicate scaffold markers, and white lines the sites corresponding to the bottom panels. Bottom panels: Culprit lesion optical coherence tomography images of matched sites (A-D) after 2.0 mm balloon dilation and (A'-D') after BVS implantation. Pre-implantation images demonstrate (A) plaque rupture with cavity, (B) minimal lumen area with red thrombus, (C) dissection flap, and (D) distal segment with macrophage infiltration. Findings after BVS implantation include (A') mild tissue prolapse at the cavity site, (B') residual compressed red thrombus, (C') tissue prolapse at the site of the flap, and (D') good expansion and apposition without tissue prolapse/thrombus.

## Discussion

The current series of patients provides real-life insights into the acute vascular response after BVS implantation in myocardial infarction. In order to assess the efficacy of BVS implantation, OCT imaging was employed. OCT-derived parameters can potentially be used as surrogate markers for assessing the acute outcome of BVS implantation in patients with myocardial infarction. In particular, in addition to the assessment of luminal dimensions and scaffold expansion, OCT allows a comprehensive assessment of the scaffold-vessel wall interaction, providing detailed information about scaffold apposition, vascular trauma

(intra-scaffold and edge dissections, tissue prolapse), and residual thrombotic burden. The clinical impact of such OCT parameters has not been established; however, their evaluation in studies of BVS implantation in myocardial infarction could be of significance, considering i) the increased incidence of incomplete apposition after metal stent implantation in myocardial infarction,<sup>17</sup> ii) the need for more aggressive lesion preparation with BVS, and iii) the association of increased residual thrombus with impaired reperfusion after metal stent implantation in myocardial infarction.<sup>18</sup>

In the ABSORB B study, in a relatively non-complex lesion subset of patients with stable and unstable

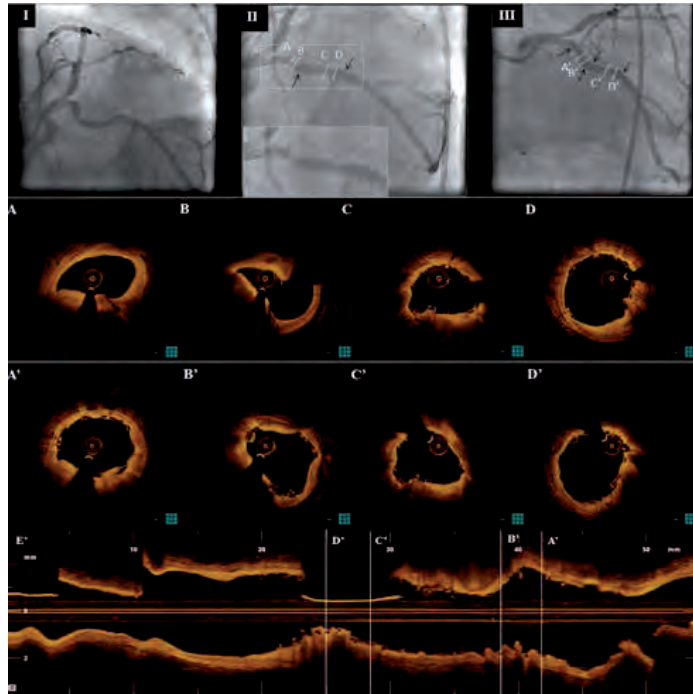


**Figure 2.** Top panels: Coronary angiography demonstrating the left circumflex artery lesion (I) pre-intervention, and (II) after  $3.5 \times 18$  mm bioresorbable vascular scaffold (BVS) implantation. Because of proximal dissection a  $3.5 \times 12$  mm scaffold was implanted (III). Black arrows indicate scaffold markers, and white lines the sites corresponding to the bottom panels. Bottom panels: Culprit lesion optical coherence tomography images of matched sites after (A-D) first and (A'-D') second BVS implantation. In the proximal scaffold, there is tissue prolapse at the sites of the dissection flaps with a small amount of intraluminal thrombus (A-A', B-B'). Mild under-expansion over a calcified plate (C-C') and mild tissue prolapse/in-stent thrombus (D-D') are observed at the distal scaffold.

angina, the BVS has shown adequate expansion, with a minimum scaffold area of  $6.31 \pm 1.25 \text{ mm}^2$ .<sup>15</sup> In our series of patients with myocardial infarction, good scaffold expansion was observed in all but one case, in which case the implanted scaffolds were focally under-expanded because of heavy calcification (Panels 2C' and 3C'). In all other patients the implanted scaffolds were well expanded, including a case with direct BVS implantation in STEMI (Patient 9).

Apposition was not optimal in all cases, with causes for incomplete apposition including extensive intra-scaffold dissections and in one case mismatch of lumen and scaffold dimensions after bail-out BVS implantation in a proximal segment (Patient 9). The selection of scaffold size during the acute phase of myocardial infarction can be challenging, as the increased

thrombus burden and the enhanced vascular tone can hamper evaluation of the true vessel size.<sup>12</sup> Post-dilation guided by OCT imaging—always in agreement with scaffold compliance and respecting the recommended maximum scaffold diameter—helped improve scaffold apposition in most cases. Still, the future course of scaffold apposition remains elusive. In the two patients in our series who underwent invasive follow up, no late incomplete scaffold apposition was observed. Although implantation of metal stents during primary PCI is associated with higher incomplete apposition at follow up compared to stable angina,<sup>8,17</sup> possibly due to resolution of vasoconstriction and thrombus,<sup>12</sup> no such data are currently available for the follow up of BVS implanted in myocardial infarction. Thus, longer-term follow up and prospective

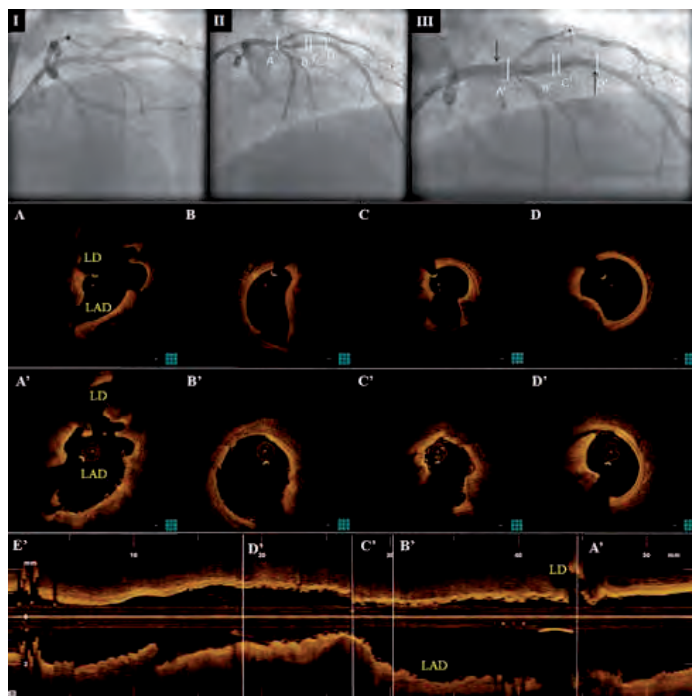


**Figure 3.** Top panels: Coronary angiography demonstrating the LAD lesion (I) pre-intervention, (II) after 3.0 mm balloon dilation, and (III) after 3.5 × 28 mm bioresorbable vascular scaffold (BVS) implantation and post-dilation with 3.75 mm non-compliant balloon. Black arrows demonstrate scaffold markers and white lines the sites corresponding to the bottom panels. Bottom panels: Culprit lesion optical coherence tomography images of matched sites after (A-D) pre-dilation and (A'-D') BVS implantation. (A-A') Small thrombus formation and pinching of the diagonal ostium post-implantation. (B-B') Good expansion and apposition at the site of a dissected eccentric calcified plaque. (C-C') Suboptimal scaffold expansion due to the presence of two protruding calcified plates at a site without dissection. (D-D') Small distal edge dissection at the site of a calcified nodule. LAD – left anterior descending branch; LD – diagonal branch.

studies are warranted to assess the true extent of incomplete scaffold apposition in myocardial infarction and its clinical implications at follow up.

Despite their similar pathophysiological mechanisms, NSTEMI and STEMI exhibit differences in lesion morphology and disease severity.<sup>19,20</sup> In our series, high disease heterogeneity was observed in NSTEMI. Two of the cases with NSTEMI (Patients 1 and 2) presented with total occlusion. Implantation was successful in both cases with a good final result, demonstrating the potential of BVS implantation in a highly thrombogenic setting, similar to STEMI. Indeed, the vascular response after BVS implantation in STEMI resembled these NSTEMI cases. The other end of the NSTEMI spectrum also includes patients with multiple lesions, increased calcification and min-

imal thrombus, as in Patient 5. Conversely, all STEMI cases in our series were associated with angiographic thrombus, dictating the use of thrombus aspiration in all but one case.

The different lesion substrate could have implications for the extent of vascular trauma and residual thrombotic burden. Both lesion morphology and unstable presentation have been associated with periprocedural vascular trauma.<sup>9</sup> In cases with heavy calcification, as in Patient 5, aggressive lesion preparation could help optimize scaffold expansion. However, lesion preparation should be performed with caution, as it may as well induce extensive vascular trauma, as in Patients 1 and 6.<sup>21</sup> Predilation has been associated with increased distal embolization in the setting of metal stent implantation for myocardial in-

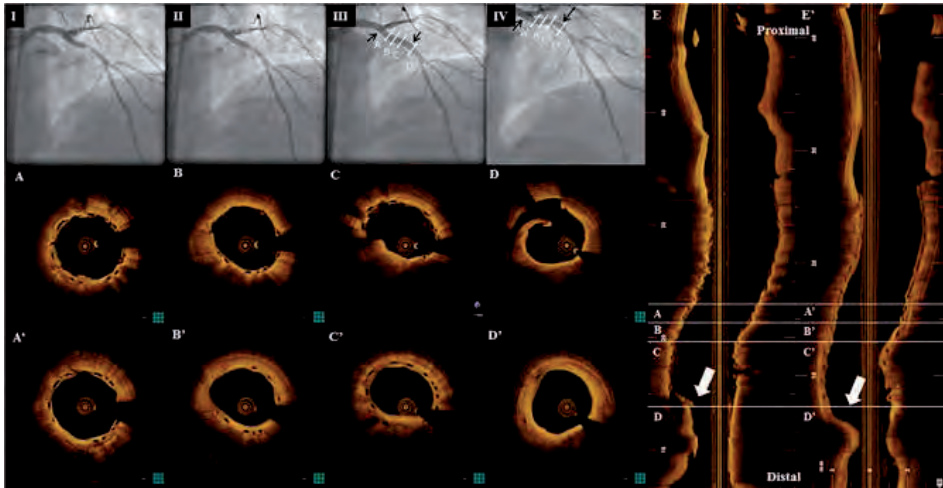


**Figure 4.** Top panels: Coronary angiography demonstrating the culprit left anterior descending artery lesion (I) pre-intervention, (II) post thrombus aspiration/2.5 mm balloon predilation, (III) post 3.5 × 18 mm BVS implantation, and (IV) at 9-month follow up. Black arrows indicate scaffold markers and white lines the sites corresponding to the bottom panels. Bottom panels: Optical coherence tomography of the treated lesion. Panels A-C disclose the presence of varying degrees of tissue prolapse/intra-scaffold thrombus, and Panel D an intra-scaffold dissection. Nine-month follow-up images show a favorable healing response with the absence of late incomplete apposition, symmetric coverage of the bioresorbable vascular scaffold (A'-C'), and the complete healing of the edge dissection (D'). L-mode images at baseline (E) and follow up (E') demonstrate the longitudinal morphology of the healed dissection (arrow).

faction,<sup>22</sup> however such data are not available for BVS. In our series, although distal embolization was not angiographically documented, OCT revealed varying degrees of tissue prolapse and/or residual thrombus in all cases. Importantly, increased tissue prolapse and/or residual thrombus have been associated with impaired reperfusion following stenting for STEMI.<sup>18</sup> Therefore, it is important to evaluate such findings systemically in BVS and to assess their significance and differences with metal platform stents.<sup>6</sup>

Another important aspect is the presence of culprit bifurcation lesions. In cases of ostial side-branch disease, as in Patients 8 and 9, BVS implantation constitutes an appealing option, given the favorable response observed in side-branch-related scaffold struts, with their gradual replacement by tissue bridges and development of a neo-carina.<sup>23</sup> Conversely, in metal stents, the permanent stent layer jailing side-branches is often characterized by impaired healing,<sup>24</sup> providing a potential substrate for thrombosis. In the case of culprit lesions with large side-branch involvement, however, a high thrombus burden can cause underestimation of the side-branch involvement, potentially resulting in side-branch compromise post-procedurally,

as in Patients 3 and 10. The good angiographic result after side-branch dilation and the absence of scaffold fracture by OCT suggest a potential role for this approach in the treatment of side-branch compromise.

It is important to note that the current series represents a preliminary report of a single-center experience with BVS implantation in myocardial infarction. The current report did not aim to conduct a systematic analysis of the OCT findings, but instead gives patient-specific descriptions of the acute vascular response, aiming to provide initial observations and demonstrate challenges and differences with stable disease. The impact of a thrombotic substrate on the vascular response following BVS implantation still needs to be systematically evaluated in larger patient cohorts with a longer follow up.

### Conclusions

In the current series, we presented angiographic and OCT findings following BVS implantation in myocardial infarction. Implantation was successful both in thrombotic culprit lesions of NSTEMI patients and in culprit lesions of STEMI patients, with a similar acute vascular response by OCT. The incidence of incom-

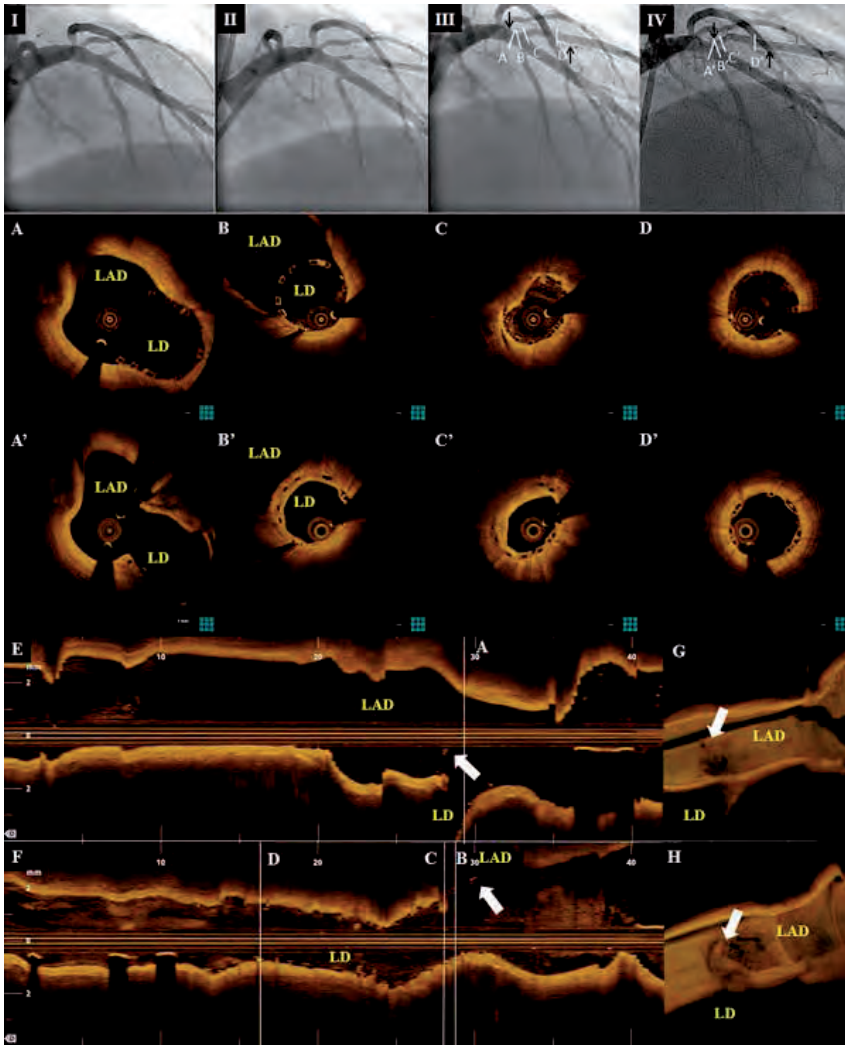


**Figure 5.** Top panels: Coronary angiography demonstrating (I) total occlusion of the LD, and the angiographic result after (II) 2.0 mm balloon predilation and (III) 2.5 × 18 mm bioresorbable vascular scaffold implantation. Panel IV shows the angiography at 12-month follow up. Black arrows indicate scaffold markers and white lines the sites corresponding to the bottom panels. Bottom panels: Optical coherence tomography (OCT) of the culprit diagonal branch lesion. Scaffold struts are protruding into the polygon of confluence of the LAD-diagonal bifurcation, as can be appreciated from both the LAD (A, E) and the diagonal pullback (B, F). There is mild tissue prolapse and thrombus near the vessel ostium (C), but minimal prolapse in the middle and distal scaffold segments, with good expansion and apposition (D). Follow-up OCT images at matched sites are presented in panels A'-D', showing coverage of the implanted scaffold, absence of incomplete apposition, and the development of tissue bridges in relation to side-branch-related struts. Three-dimensional renderings illustrate the development of a neo-carina at the site of scaffold protrusion into the LAD (E, E'). LAD – left anterior descending branch; LD – diagonal branch.

plete scaffold apposition at follow up, the role of the pathological substrate in the selection of lesion preparation strategy, and the impact of periprocedural trauma and residual thrombus post-intervention remain open questions regarding BVS implantation in myocardial infarction that warrant systematic evaluation in prospective studies.

## References

1. Stone GW, Lansky AJ, Pocock SJ, et al. Paclitaxel-eluting stents versus bare-metal stents in acute myocardial infarction. *N Engl J Med*. 2009; 360: 1946-1959.
2. Karanasos A, Simsek C, Serruys P, et al. Five-year optical coherence tomography follow-up of an everolimus-eluting bioresorbable vascular scaffold: changing the paradigm of coronary stenting? *Circulation*. 2012; 126: e89-91.
3. Ormiston JA, Serruys PW, Onuma Y, et al. First serial assessment at 6 months and 2 years of the second generation of absorb everolimus-eluting bioresorbable vascular scaffold: a multi-imaging modality study. *Circ Cardiovasc Interv*. 2012; 5: 620-632.
4. Serruys PW, Ormiston JA, Onuma Y, et al. A bioabsorbable everolimus-eluting coronary stent system (ABSORB): 2-year outcomes and results from multiple imaging methods. *Lancet*. 2009; 373: 897-910.
5. Gori T, Schulz E, Hink U, et al. Early outcome after implantation of Absorb bioresorbable drug-eluting scaffolds in patients with acute coronary syndromes. 2014; 9: 1036-1041.
6. Diletti R, Karanasos A, Muramatsu T, et al. Everolimus-eluting bioresorbable vascular scaffolds for treatment of patients presenting with ST-segment elevation myocardial infarction: BVS STEMI first study. *Eur Heart J*. 2014; 35: 777-786.
7. Kočka V, Malý M, Toušek P, et al. Bioresorbable vascular scaffolds in acute ST-segment elevation myocardial infarction: a prospective multicentre study "Prague 19". *Eur Heart J*. 2014; 35: 787-794.
8. Guagliumi G, Costa MA, Sirbu V, et al. Strut coverage and late malapposition with paclitaxel-eluting stents compared with bare metal stents in acute myocardial infarction: optical coherence tomography substudy of the Harmonizing Outcomes with Revascularization and Stents in Acute Myocardial Infarction (HORIZONS-AMI) Trial. *Circulation*. 2011; 123: 274-281.
9. Kubo T, Imanishi T, Kitabata H, et al. Comparison of vascular response after sirolimus-eluting stent implantation between patients with unstable and stable angina pectoris: a serial optical coherence tomography study. *JACC Cardiovasc Imaging*. 2008; 1: 475-484.
10. Karanasos A, Ligthart J, Witberg K, van Soest G, Bruining N, Regar E. Optical Coherence Tomography: Potential Clinical Applications. *Curr Cardiovasc Imaging Rep*. 2012; 5: 206-220.
11. Tearney GJ, Regar E, Akasaka T, et al. Consensus standards for acquisition, measurement, and reporting of intravascular optical coherence tomography studies: a report from the International Working Group for Intravascular Optical Coherence Tomography Standardization and Validation. *J Am Coll Cardiol*. 2012; 59: 1058-1072.
12. van Geuns RJ, Tamburino C, Fajadet J, et al. Self-expanding versus balloon-expandable stents in acute myocardial infarction: results from the APPOSITION II study: self-expanding stents in ST-segment elevation myocardial infarction. *JACC Cardiovasc Interv*. 2012; 5: 1209-1219.
13. Onuma Y, Thuesen L, van Geuns RJ, et al. Randomized study to assess the effect of thrombus aspiration on flow area in patients with ST-elevation myocardial infarction: an optical frequency domain imaging study—TROFI trial. *Eur Heart J*. 2013; 34: 1050-1060.
14. Cutlip DE, Windecker S, Mehran R, et al. Clinical end points in coronary stent trials: a case for standardized definitions. *Circulation*. 2007; 115: 2344-2351.
15. Serruys PW, Onuma Y, Ormiston JA, et al. Evaluation of the second generation of a bioresorbable everolimus drug-eluting vascular scaffold for treatment of de novo coronary artery stenosis: six-month clinical and imaging outcomes. *Circulation*. 2010; 122: 2301-2312.
16. Gonzalo N, Serruys PW, Okamura T, et al. Optical coherence tomography assessment of the acute effects of stent implantation on the vessel wall: a systematic quantitative approach. *Heart*. 2009; 95: 1913-1919.
17. Gonzalo N, Barlis P, Serruys PW, et al. Incomplete stent apposition and delayed tissue coverage are more frequent in drug-eluting stents implanted during primary percutaneous coronary intervention for ST-segment elevation myocardial infarction than in drug-eluting stents implanted for stable/unstable angina: insights from optical coherence tomography. *JACC Cardiovasc Interv*. 2009; 2: 445-452.
18. Magro M, Regar E, Gutiérrez-Chico JL, et al. Residual atherothrombotic material after stenting in acute myocardial infarction - An optical coherence tomographic evaluation. *Int J Cardiol*. 2013; 167: 656-663.
19. Toutouzas K, Karanasos A, Tsiamis E, et al. New insights by optical coherence tomography into the differences and similarities of culprit ruptured plaque morphology in non-ST-elevation myocardial infarction and ST-elevation myocardial infarction. *Am Heart J*. 2011; 161: 1192-1199.
20. Ferrara LA, Russo BF, Gente R, Esposito G, Rapacciuolo A, de Simone G. STEMI and NSTEMI: A mono versus a multi-vessel disease? *Int J Cardiol*. 2013; 168: 2905-2906.
21. Karanasos A, Regar E, Gecce P, van Mieghem NM. Bioresorbable scaffold in myocardial infarction: has the time come? *Int J Cardiol*. 2013; 167: e17-19.
22. Loubeyre C, Morice MC, Lefèvre T, Piéchaud JF, Louvard Y, Dumas P. A randomized comparison of direct stenting with conventional stent implantation in selected patients with acute myocardial infarction. *J Am Coll Cardiol*. 2002; 39: 15-21.
23. Okamura T, Onuma Y, García-García HM, et al. 3-Dimensional Optical Coherence Tomography Assessment of Jailed Side Branches by Bioresorbable Vascular Scaffolds: A Proposal for Classification. *JACC: Cardiovasc Interv*. 2010; 3: 836-844.
24. Gutiérrez-Chico JL, Regar E, Nüesch E, et al. Delayed coverage in malapposed and side-branch struts with respect to well-apposed struts in drug-eluting stents: in vivo assessment with optical coherence tomography. *Circulation*. 2011; 124: 612-623.



#### 4.5 Short-term outcomes of STEMI patients treated with the Absorb BVS

Everolimus-eluting bioresorbable vascular scaffolds for treatment of patients presenting with ST-segment elevation myocardial infarction: BVS STEMI first study.

*Eur Heart J.* 2014;35:777-86.

[Original research paper, Impact Factor (2013): 14.723]

Diletti R, Karanasos A, Muramatsu T, Nakatani S, van Mieghem NM, Onuma Y, Nauta ST, Ishibashi Y, Lenzen MJ, Ligthart J, Schultz C, Regar E, de Jaegere PP, Serruys PW, Zijlstra F, van Geuns RJ.





# Everolimus-eluting bioresorbable vascular scaffolds for treatment of patients presenting with ST-segment elevation myocardial infarction: BVS STEMI first study

Roberto Diletti, Antonios Karanasos, Takashi Muramatsu, Shimpei Nakatani, Nicolas M. Van Mieghem, Yoshinobu Onuma, Sjoerd T. Nauta, Yuki Ishibashi, Mattie J. Lenzen, Jurgen Ligthart, Carl Schultz, Evelyn Regar, Peter P. de Jaegere, Patrick W. Serruys, Felix Zijlstra, and Robert Jan van Geuns\*

Thoraxcenter, Erasmus MC, 's-Gravendijkwal 230, 3015 CE Rotterdam, the Netherlands

Received 11 September 2013; revised 6 November 2013; accepted 26 November 2013; online publish-ahead-of-print 6 January 2014

See page 753 for the editorial comment on this article (doi:10.1093/eurheartj/ehu005)

## Aims

We evaluated the feasibility and the acute performance of the everolimus-eluting bioresorbable vascular scaffolds (BVS) for the treatment of patients presenting with ST-segment elevation myocardial infarction (STEMI).

## Methods and results

The present investigation is a prospective, single-arm, single-centre study, reporting data after the BVS implantation in STEMI patients. Quantitative coronary angiography and optical coherence tomography (OCT) data were evaluated. Clinical outcomes are reported at the 30-day follow-up. The intent-to-treat population comprises a total of 49 patients. The procedural success was 97.9%. Pre-procedure TIMI-flow was 0 in 50.0% of the patients; after the BVS implantation, a TIMI-flow III was achieved in 91.7% of patients and the post-procedure percentage diameter stenosis was  $14.7 \pm 8.2\%$ . No patients had angiographically visible residual thrombus at the end of the procedure. Optical coherence tomography analysis performed in 31 patients showed that the post-procedure mean lumen area was  $8.02 \pm 1.92 \text{ mm}^2$ , minimum lumen area  $5.95 \pm 1.61 \text{ mm}^2$ , mean incomplete scaffold apposition area  $0.118 \pm 0.162 \text{ mm}^2$ , mean intraluminal defect area  $0.013 \pm 0.017 \text{ mm}^2$ , and mean percentage malapposed struts per patient  $2.80 \pm 3.90\%$ . Scaffolds with  $>5\%$  malapposed struts were 7. At the 30-day follow-up, target-lesion failure rate was 0%. Non-target-vessel revascularization and target-vessel myocardial infarction (MI) were reported. A non-target-vessel non-Q-wave MI occurred. No cases of cardiac death or scaffold thrombosis were observed.

## Conclusion

In the present series, the BVS implantation in patients presenting with acute MI appeared feasible, with high rate of final TIMI-flow III and good scaffold apposition. Larger studies are currently needed to confirm these preliminary data.

## Keywords

Bioresorbable vascular scaffolds • ST-segment elevation myocardial infarction • Optical coherence tomography

## Introduction

Primary percutaneous coronary intervention has been demonstrated to be superior to thrombolytic strategy and is currently the treatment of first choice for patients presenting with ST-segment elevation myocardial infarction (STEMI) in experienced centres with limited time delay.<sup>1</sup> First-generation drug-eluting stents (DES) have

been shown to reduce the need for repeat revascularization compared with bare-metal stents (BMS),<sup>2–4</sup> and the newer-generation DES with improved biocompatibility of polymers may lower the rate of clinical events also in acute patients.<sup>5,6</sup> However, the implantation of metal devices is not devoid of important limitations, such as permanent caging of the vessel with permanent impairment of coronary vasomotion, side branch jailing, impossibility of late lumen

\*Corresponding author. Tel: +31 10 4635260(33348), Fax: +31 10 4369154, Email: r.vangeuns@erasmusmc.nl

Published on behalf of the European Society of Cardiology. All rights reserved. © The Author 2014. For permissions please email: journals.permissions@oup.com

enlargement, non-invasive imaging and future surgical revascularization of stented segments.<sup>7</sup> Moreover, in spite of the beneficial effect of neointimal inhibition, the antiproliferative drug elution has been shown to interfere with the vascular healing processes providing the background for delayed strut coverage and persistent or acquired malapposition.<sup>8,9</sup> The above-mentioned limitations can be proposed for both stable and acute patients; however, primary stenting has additional specific characteristics that should be highlighted. Stent placement in acute thrombotic lesions has been reported to be an independent predictor of late stent malapposition after the BMS<sup>10</sup> or DES<sup>11</sup> implantation. Possible explanations for this phenomenon could be the thrombus sequestration behind the struts—which subsequently resolves—and the vasoconstriction during the acute phase. Both these factors may predispose to stent under-deployment, malapposition and finally to stent thrombosis. The everolimus-eluting bioresorbable vascular scaffold (BVS) has been designed to overcome the general limitations of the metallic stents and recently has been shown to provide excellent results for the treatment of stable patients.<sup>12,13</sup> However, so far very limited data are available on the use of this novel device in patients with acute coronary syndromes (ACS).<sup>14,15</sup> Given this background, a pilot study investigating the feasibility and acute performance of the BVS for the treatment of patients presenting with STEMI was initiated.

## Methods

### Rationale

As of 1 September 2012, the BVS (ABSORB; Abbott Vascular, Santa Clara, CA, USA) has been commercially available in the Netherlands. Based on previous experience and available evidence, reported in ABSORB Cohort A and B Trial<sup>13,16</sup> our institution initiated the use of BVS for the treatment of patients presenting for PCI in everyday clinical practice, with a preference for patients with a good life expectancy as demonstrated by the presence of limited co-morbidities. As these patients might have more complex lesions compared with the ABSORB study patients<sup>16,17</sup> the BVS-EXPAND registry was initiated. The BVS-EXPAND also included patients with ACS (unstable angina or non-STEMI). After the first experience with ACS patients and an interim analysis, a decision was made to extend BVS utilization to the treatment of STEMI.

As an additional measure for assessing the safety of a treatment approach with BVS in STEMI, optical coherence tomography (OCT) imaging was performed, according to clinical judgement, for a more comprehensive evaluation of the acute procedural outcome.

### Study design

The present report is an investigator initiated, prospective, single-arm, single-centre study to assess feasibility and performance of the second-generation everolimus-eluting BVS for the treatment of patients presenting with STEMI.

Subjects enrolled were patients of  $\geq 18$ -year-old admitted with STEMI, defined as at least 1 mm ST-segment elevation in two or more standard leads or at least 2 mm in two or more contiguous precordial leads or new left bundle branch block within 12 h after the onset of symptoms. Culprit lesions were located in vessels within the upper limit of 3.8 mm and the lower limit of 2.0 mm by online

quantitative coronary angiography (QCA). The absorb BVS was implanted according to the manufacturer's indication on target-vessel diameter ranges and absorb BVS diameters to be used. The absorb BVS with a nominal diameter of 2.5 mm was implanted in vessels  $\geq 2.0$  and  $\leq 3.0$  mm by online QCA; the 3.0 mm BVS was implanted in vessels  $\geq 2.5$  and  $\leq 3.3$  mm by online QCA; the 3.5 mm BVS was implanted in vessels  $\geq 3.0$  and  $\leq 3.8$  mm. Given the manufacturer's indication on maximum scaffold expansion, for each nominal diameter a further expansion of 0.5 mm was allowed. Enrolled subjects were willing to comply with specified follow-up evaluation and to be contacted by telephone. Exclusion criteria comprise pregnancy, known intolerance to contrast medium, uncertain neurological outcome after cardiopulmonary resuscitation, previous percutaneous coronary intervention with the implantation of a metal stent, left main (LM) disease previous coronary artery bypass grafting (CABG), age superior to 75 years, and participation to another investigational drug or device study before reaching the primary endpoints. The enrolment period started on 1 November 2012 and ended on 30 March 2013. Dual antiplatelet therapy after the BVS implantation was planned to have a duration of 12 months. Baseline and post-BVS implantation QCA analysis, OCT analyses at post-BVS implantation, and clinical outcomes at the 30-day follow-up were evaluated.

### Definitions

Success rates were defined as follows: device success was the attainment of  $< 30\%$  final residual stenosis of the segment of the culprit lesion covered by the BVS, by angiographic visual estimation. Procedure success was defined as device success and no major periprocedural complications (Emergent CABG, coronary perforation requiring pericardial drainage, residual dissection impairing vessel flow—TIMI-flow II or less). Clinical success was defined as procedural success and no in-hospital major adverse cardiac events (MACE). All deaths were considered cardiac unless an undisputed non-cardiac cause was identified. Myocardial infarction (MI) and scaffold thrombosis were defined according to the Academic Research Consortium definition.<sup>18</sup> Target-lesion revascularization (TLR) was defined as clinically driven if at repeat angiography the diameter stenosis was  $> 70\%$ , or if a diameter stenosis  $> 50\%$  was present in association with (i) presence of recurrent angina pectoris, related to the target vessel; (ii) objective signs of ischaemia at rest (ECG changes) or during exercise test, related to the target vessel; and (iii) abnormal results of any functional diagnostic test.

The device-oriented endpoint target-lesion failure was defined as the composite of cardiac death, target-vessel MI, or ischaemia-driven TLR. Major adverse cardiac events defined as the composite of cardiac death, any re-infarction (Q- or non-Q-wave), emergent bypass surgery (CABG), or clinically driven TLR. Target-vessel failure (TVF) was defined as cardiac death, target-vessel MI, or clinically driven TVR.

### Ethics

This is an observational study, performed according to the privacy policy of the Erasmus MC and to the Erasmus MC regulations for the appropriate use of data in patient-oriented research, which are based on international regulations, including the declaration of Helsinki. The BVS received the CE mark for clinical use, indicated for improving coronary lumen diameter in patients with ischaemic heart disease due to *de novo* native coronary artery lesions with no

restriction in terms of clinical presentation. Therefore, the BVS can be currently used routinely in Europe in different settings comprising the acute MI without a specific written informed consent in addition to the standard informed consent to the procedure. Given this background, a waiver from the hospital Ethical Committee was obtained for written informed consent, as according to Dutch law written consent is not required, if patients are not subject to acts other than as part of their regular treatment.

## Study device

The second-generation everolimus-eluting BVS is a balloon expandable device consisting of a polymer backbone of poly-L-lactide acid (PLLA) coated with a thin layer of amorphous matrix of poly-D and -L-lactide acid (PDLLA) polymer (strut thickness 157  $\mu\text{m}$ ). The PDLLA controls the release of the antiproliferative drug everolimus (100  $\mu\text{g}/\text{cm}^2$ ), 80% of which is eluted within the first 30 days. Both PLLA and PDLLA are fully bioresorbable. The polymers are degraded via hydrolysis of the ester bonds and the resulting lactate and its oligomers are metabolized by the Krebs cycles. Small particles ( $<2 \mu\text{m}$  in diameter) may be also phagocytized and degraded by macrophages.<sup>19</sup> According to preclinical studies, the time for complete bioresorption of the polymer backbone is  $\sim 2$ –3 years.<sup>20</sup> The BVS edges contain two platinum markers for accurate visualization during angiography or other imaging modalities.

## Quantitative coronary angiography analysis

Quantitative coronary angiography (QCA) analyses were performed using the Coronary Angiography Analysis System (Pie Medical Imaging, Maastricht, Netherlands).

Analyses were performed at pre-procedure, after thrombectomy, after balloon dilatation, and after the BVS implantation with a methodology already reported.<sup>21</sup>

In case of thrombotic total occlusion, pre-procedure QCA analysis was performed as proximally as possible from the occlusion (in case of a side branch distally to the most proximal take off of the side branch). Intracoronary thrombus was angiographically identified and scored in five grades as previously described.<sup>22</sup> Thrombus grade was assessed before procedure and after thrombectomy.

The QCA measurements included reference vessel diameter (RVD)—calculated with interpolate method—percentage diameter stenosis, minimal lumen diameter (MLD), and maximal lumen diameter ( $D_{\text{max}}$ ). Acute gain was defined as post-procedural MLD minus pre-procedural MLD (MLD value equal to zero was applied when culprit vessel was occluded pre-procedurally). Complications occurring any time during the procedure, such as dissection, spasm, distal embolization, and no-reflow were reported. As additional information, MI SYNTAX I and MI SYNTAX II scores providing long-term risk stratification for mortality and MACE in patients presenting with STEMI were assessed.<sup>23</sup>

## Optical coherence tomography image acquisition and analysis

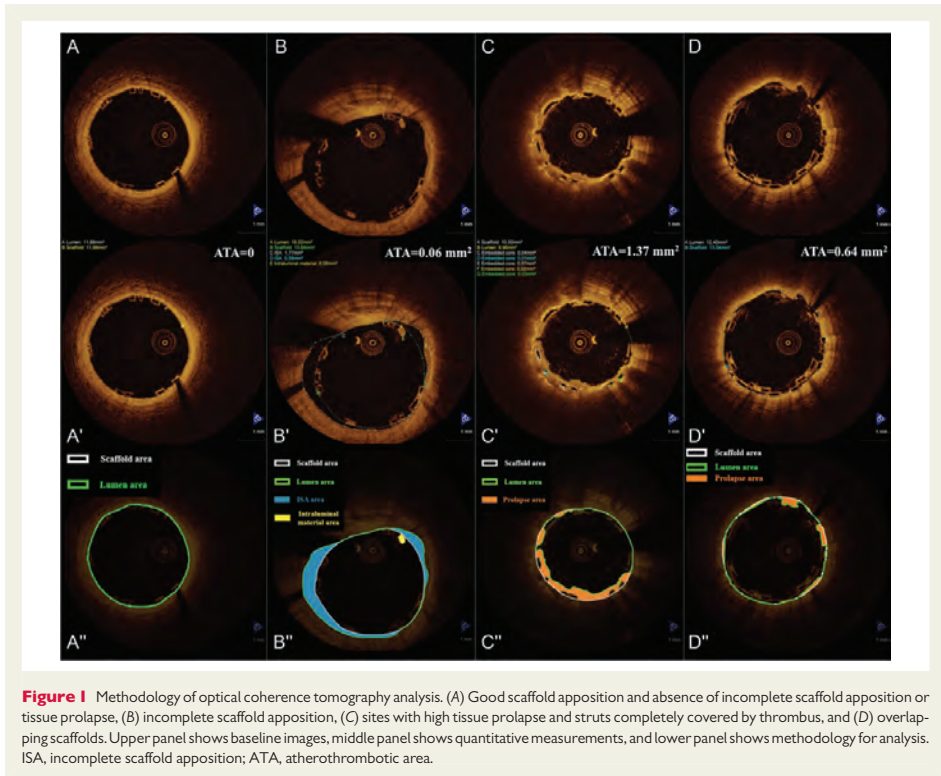
Optical coherence tomography imaging after the BVS implantation was encouraged in all patients but was not mandatory, subordinated to device availability and left at the operator's discretion.

Therefore, OCT imaging of the culprit lesion after treatment was performed in a subset of the population. The image acquisition was performed with C7XR imaging console and the Dragonfly intravascular imaging catheter (both St. Jude Medical, St. Paul, MN, USA). Image acquisition has been previously described.<sup>24</sup> Briefly, after positioning the OCT catheter distally to the most distal scaffold marker, the catheter is pulled back automatically at 20 mm/s with simultaneous contrast infusion by a power injector (flush rate 3–4 mL/s). In cases where the entire scaffold region was not imaged in one pullback, a second more proximal pullback was performed for complete visualization. Images were stored and analysed offline.

Analysis of the OCT images was performed with the St Jude/Lightlab offline analysis software (St. Jude Medical), using previously described methodology for BVS analysis.<sup>17</sup> Analysis was performed in 1-mm longitudinal intervals within the treated culprit segment, after exclusion of frames with  $<75\%$  lumen contour visibility. Lumen, scaffold, and incomplete scaffold apposition (ISA) area were calculated in accordance with standard methodology for analysis of bioresorbable scaffolds<sup>17</sup> (Figure 1A and B), while in sites with overlapping scaffolds, analysis was performed using previously suggested modifications<sup>25</sup> (Figure 1D). Specifically, the lumen contour is traced at the lumen border and in the abluminal (outer) side of apposed struts, while in the case of malapposed struts the contour is traced behind the malapposed struts. In cases where the scaffold struts are completely covered by tissue or thrombus, the lumen contour is traced above the prolapsing tissue (Figure 1C). The scaffold area is traced following interpolation of points located in the mid-point of the abluminal border of the black core in apposed struts and the mid-point of the abluminal strut frame border in malapposed or side branch-related struts, so that the scaffold area is identical to the lumen area in the absence of ISA and tissue prolapse. Incomplete scaffold apposition area is traced in the case of malapposed struts as the area delineated between the lumen and scaffold contours (Figure 1B).

A special consideration should be mentioned concerning BVS analysis in MI with the presence of increased tissue prolapse and residual thrombus post-implantation<sup>21,26</sup> (Figures 1C and 2). Tissue prolapse area can be quantified as the difference between the scaffold and the lumen area. For the calculation of prolapse area, in the case that one or more scaffold struts are completely covered by thrombus or tissue, the total black core area of these struts is also measured. Prolapse area is then calculated as [scaffold area + ISA area – lumen area – embedded black core area]. The area of non-attached intraluminal defects (e.g. thrombus) is also measured. Atherothrombotic area is then calculated as the sum of prolapse area and intraluminal defect area and normalized as a percent ratio of the scaffold area (atherothrombotic burden, ATB).<sup>21,26</sup> It should be noted that in the case of bioresorbable scaffolds where measurements of the scaffold area are performed using the abluminal side of the scaffold struts, ATB is overestimated compared with metal platform stents where measurements of the stent area are performed from the adluminal (inner) side of the struts. Additionally, flow area was assessed as [scaffold area + ISA area – atherothrombotic area – total strut area] and the minimal flow area was recorded.

A scaffold strut is defined as incompletely apposed when there is no contact between the abluminal border of the strut and the vessel wall. This does not include struts located in front of side branches or their ostium (polygon of confluence region), which are



defined as side branch-related struts. Intraluminal struts that are part of adjacent clusters of apposed struts in overlapping scaffolds are also not considered malapposed.<sup>25</sup> For illustrative purposes, OCT bi-dimensional images are reported by three-dimensional rendering by dedicated software (Intage Realia, KGT, Kyoto, Japan)<sup>17</sup> (Figures 2 and 3).

### Statistical analysis

Continuous variables are presented as mean and standard deviation, and categorical variables are reported as count and percentages. Descriptive statistics was provided for all variables. The present study is intended to be a 'first experience investigation' evaluating feasibility and acute performance of the everolimus-eluting BVS for the treatment of patients presenting with STEMI. A patient population of at least 30 patients was planned to be included in the present study. Comparisons among multiple means were performed with analysis of variance (one-way ANOVA). Score (Wilson) confidence intervals were reported for measures of success. Type A intraclass correlation coefficients (ICCs) for absolute agreement were used for assessing intra- and interobserver agreement, while measurement error and

95% limits of agreement were assessed by Bland–Altman analysis. The ICCs were computed with a two-way random effects model (single measures). All statistical tests were performed with SPSS, version 15.0 for windows (IL, USA).

### Results

From 1 November 2012 to 30 April 2013, a total of 267 patients presented with acute MI. Twenty-one of those patients were treated percutaneously without any stent implantation (thrombectomy or balloon dilatation alone). Seventy-four had a culprit lesion located in a coronary vessel with a vessel diameter out of the range availability of the BVS (i.e. RVD > 4.0 mm). Out of the remaining 172 patients, 125 were meeting the inclusion and none of the exclusion criteria of the present study (47 patients excluded for age, previous PCI or CABG, left main disease). Seventy-six of those patients were treated with metal stents and 49 cases (48 implanted with BVS) were enrolled in the present study (Figure 4, Table 1). Therefore, the patients implanted with BVS constitute the ~38% of the patients eligible for the present investigation.

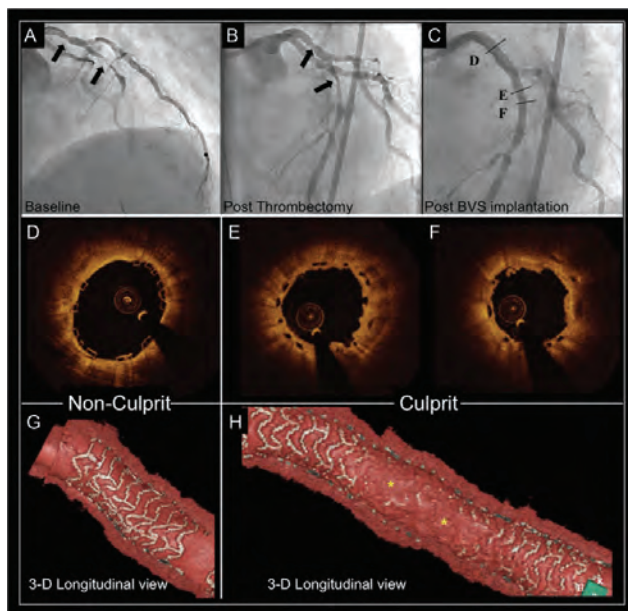


**Figure 2** Bioresorbable vascular scaffolds implantation in a culprit and a non-culprit lesion in myocardial infarction. (A) Coronary angiography demonstrating a stenotic lesion in proximal LAD (proximal non-culprit lesion) and a total occlusion of the mid-LAD (culprit lesion). (B) Angiography following thrombus aspiration. (C) Angiography following implantation of a  $3.5 \times 12$  mm bioresorbable vascular scaffolds at the proximal LAD lesion and a  $3.0 \times 28$  mm bioresorbable vascular scaffolds at the mid-LAD lesion. (D) Optical coherence tomography image from the proximal non-culprit lesion showing absence of tissue prolapse and thrombus in the  $3.5 \times 12$  mm scaffold. (E and F) Optical coherence tomography images from the culprit lesion showing complete coverage of the bioresorbable vascular scaffolds by tissue prolapse and presence of small amount of intraluminal defect. (G) Three-dimensional optical coherence tomography rendering in the proximal non-culprit lesion with complete scaffold visualization indicating the absence of prolapsing material. (H) Conversely, in the three-dimensional rendering of the culprit lesion, the morphology of the bioresorbable vascular scaffolds cannot be fully visualized due to high levels of tissue prolapse (\*).

Baseline clinical characteristics of the 172 patients (49 patients included in the intent-to-treat population and 123 patients implanted with metal stents) with vessels size in the range of the BVS availability are reported in Table 1. In the intent-to-treat population thirty-eight patients were male (77.6%), mean age was  $58.9 \pm 10.5$  years. Lesions were distributed as follows: left anterior descending 21 (42.9%), right coronary artery 22 (44.9%), and circumflex 6 (12.2%). Baseline clinical data of the enrolled patients were compared with the general population presenting with acute MI and implanted with a metal stent in vessels theoretically suitable for BVS implantation. Minimal differences were observed between the two groups. Namely, age  $58.9 \pm 10.5$  vs.  $66.4 \pm 12.2$ ,  $P < 0.001$  and previous PCI 0% vs. 12.2%,  $P = 0.007$ . All the other clinical characteristics of the two populations did not show any significant difference.

Mean door-to-balloon time was  $31.3 \pm 19.5$  min. All patients were treated with unfractionated heparin at the dose of 70–100 U/kg and dual antiplatelet therapy (aspirin plus, prasugrel in 45 patients or clopidogrel in 4 patients). Manual thrombectomy was performed in 38 patients. In 16 cases, direct stenting was performed; a total of 65 scaffolds were implanted (12 patients received overlapping scaffolds—overlap was systematically intended to be minimal). The scaffolds lengths used were 12, 18, and 28 mm, with scaffolds diameters 2.5, 3.0, and 3.5 mm. Mean scaffold length per-lesion was  $26.40 \pm 13.86$  mm, mean scaffold diameter per-lesion was  $3.2 \pm 34$  mm. A highly supportive wire was used in five cases and radial approach was performed in 26 patients (53.0%) (Table 2). The procedural success was 97.9% (48/49 patients); in one patient, the delivery of the BVS was unsuccessful (due to the remarkable vessel tortuosity was not

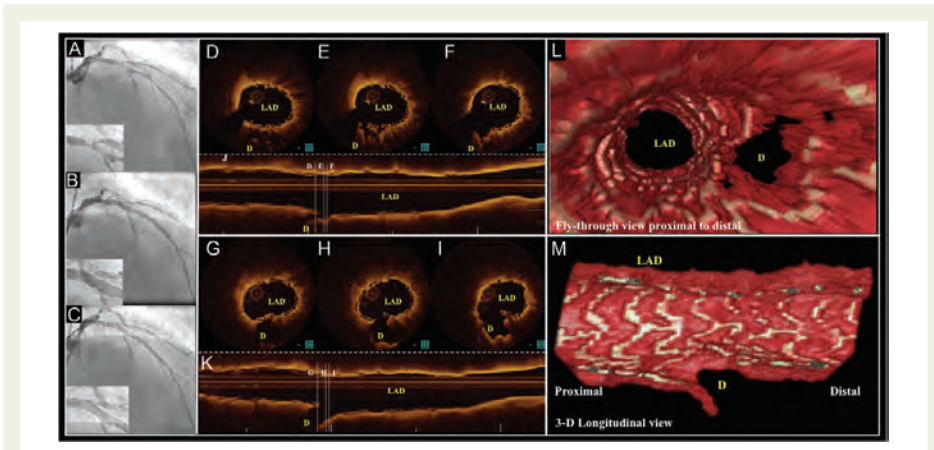


**Figure 3** Bioreabsorbable vascular scaffold implantation in a thrombotic bifurcation lesion treated with provisional approach. (A) Coronary angiography pre-intervention. (B) Angiography following bioreabsorbable vascular scaffold implantation in the LAD, showing pinching of the ostium of the diagonal (D). (C) Final angiographic result following side branch dilation with  $2.0 \times 15$  mm balloon. (D–F and J) Optical coherence tomography cross-sectional images and l-mode after bioreabsorbable vascular scaffolds implantation showing the compromise of the side branch after implantation and presence of thrombus at the side branch ostium. (G–I and K) Optical coherence tomography cross-sectional images and l-mode after side branch dilation, showing the opening of the carina of the side branch. (L and M) Three-dimensional reconstructions confirm the opening of the side branch ostium.

possible to advance the BVS at the site of the lesion) and a metallic DES was implanted. Clinical success was 97.9% (48/49 patients).

### Quantitative coronary angiography analysis

The QCA is reported only in patients implanted with BVS. In 50.0% of those patients, pre-procedure TIMI-flow was 0 and the RVD was  $2.94 \pm 0.77$  mm. In the non-totally occluded vessels, the RVD was  $2.62 \pm 0.63$  mm, with an MLD of  $0.75 \pm 0.44$  mm and a mean diameter stenosis of  $70.8 \pm 12.5\%$ . After thrombectomy and balloon dilatation, TIMI-flow grade 0 was present in 2.5 and 0.0% of patients, respectively, and TIMI-flow III in 52.5 and 59.3% of the cases, respectively. After the scaffold implantation, there were no cases of TIMI-flow 0, and a TIMI-flow III was achieved in 91.7% of patients, the mean post-procedure in-scaffold % diameter stenosis was  $14.7 \pm 8.2\%$ , in-scaffold MLD was  $2.44 \pm 0.49$  mm (Table 3). No angiographically visible residual thrombus was observed at post-procedure.

### Optical coherence tomography findings

Optical coherence tomography analysis was performed in a subgroup of 31 patients implanted with BVS. Mean lumen area was  $8.02 \pm 1.92$  mm<sup>2</sup>, minimum lumen area  $5.95 \pm 1.61$  mm<sup>2</sup>, and minimum flow area  $5.62 \pm 1.66$  mm<sup>2</sup>. Incomplete scaffold apposition (ISA) was observed in 20 patients with a mean ISA area of  $0.118 \pm 0.162$  mm<sup>2</sup> and a mean percentage of malapposed struts per patients equal to  $2.80 \pm 3.90\%$ . The mean prolapse area was  $0.60 \pm 0.26$  mm<sup>2</sup>, and the mean intraluminal defect area was

$0.013 \pm 0.017$  mm<sup>2</sup>. Scaffolds with >5% malapposed struts were 7 (Table 4). The OCT analysis stratified by scaffold size (5 BVS 2.5 mm, 13 BVS 3.0 mm, 24 BVS 3.5 mm) showed different lumen, scaffold, and flow areas, but similar amounts of incomplete stent apposition, plaque prolapse, and intraluminal mass areas (Table 5). In three cases, the observation of scaffold malapposition by OCT, guided an additional post-dilatation and in one patient the visualization of considerable intraluminal thrombus as assessed by OCT led to a repeated thrombus aspiration.

Intra-observer variability was excellent. Intraclass correlation coefficients were 0.999 for lumen area and 0.999 for scaffold area, and the corresponding measurement errors and limits of agreement were  $0.01$  mm<sup>2</sup> ( $-0.12$  to  $0.15$  mm<sup>2</sup>) for lumen area and  $-0.01$  mm<sup>2</sup> ( $-0.20$  to  $0.17$  mm<sup>2</sup>) for scaffold area. Similarly, inter-observer intraclass correlation coefficients were 0.997 for lumen area and 0.987 for scaffold area, and the corresponding measurement errors and limits of agreement were  $-0.01$  mm<sup>2</sup> ( $-0.30$  to  $0.28$  mm<sup>2</sup>) for lumen area and  $-0.22$  mm<sup>2</sup> ( $-0.68$  to  $0.24$  mm<sup>2</sup>) for scaffold area.

### Clinical outcomes

At the 30-day follow-up, the rate of the device-oriented endpoint, target-lesion failure, was 0%. None of the patients experienced target-vessel re-infarction, emergent bypass surgery, or clinically driven TLR. No cases of cardiac death or scaffold thrombosis were reported. The MACE rate was 2.6% as one patient, after discharge developed a non-Q-wave MI related to a non-target-vessel lesion and underwent a non-target-vessel revascularization within the

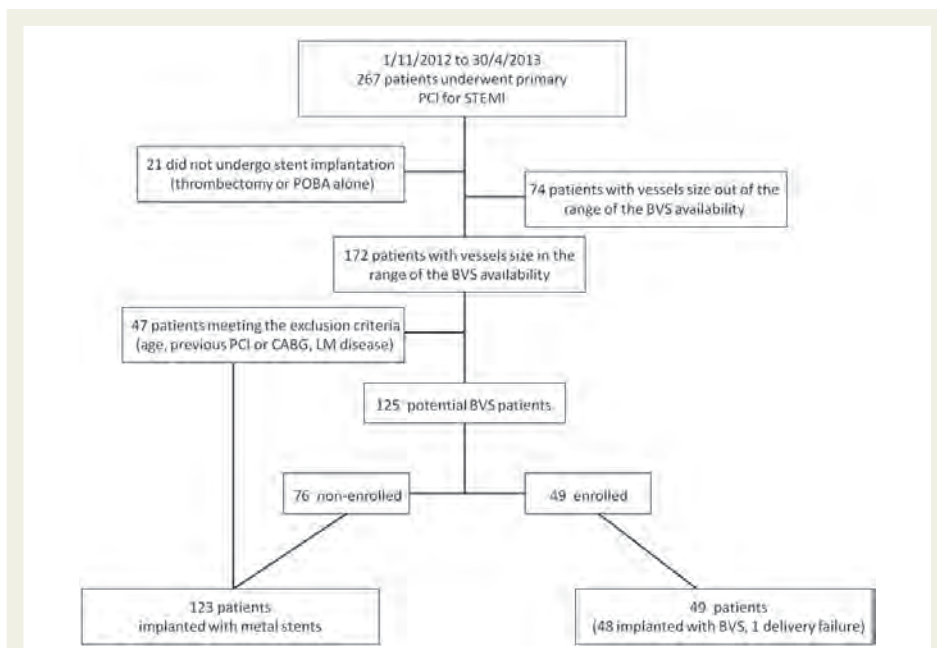


**Figure 4** Flow-chart of the study. From 1 November 2012 to 30 April 2013, a total of 267 patients presented with acute myocardial infarction. Twenty-one of those patients were treated percutaneously but without any stent implantation (thrombectomy or balloon dilatation alone). Seventy-four had a culprit lesion located in a coronary vessel with a vessel diameter out of the range availability of the bioresorbable vascular scaffolds (i.e. reference vessel diameter >4.0 mm). Out of the remaining 172 patients, 125 were meeting the inclusion and none of the exclusion criteria of the present study (47 patients excluded for age, previous PCI or CABG, left main disease). Seventy-six of those patients were treated with metal stents and 49 cases (48 implanted with BVS) were included in the present study.

30 days post-procedure. This was the only event reported in the studied population (Table 6).

## Discussion

The everolimus-eluting BVS has been tested so far only in elective patients with stable, unstable angina, or silent ischaemia;<sup>16,17,27–29</sup> showing promising results up to 4-year follow-up<sup>30</sup> for the first-generation and up to 2 years for the second-generation BVS.<sup>12,13,31</sup> The present study represents an early investigation reporting clinical and angiographic data on the use of the second-generation BVS for the treatment of patients presenting with STEMI and evaluating acute results with high-resolution intracoronary imaging (OCT).

A high device, procedural, and clinical success rates were observed with all the scaffolds achieving a residual stenosis <30% and no in-hospital MACE. Such data are supportive of feasibility and good acute performance of the BVS for the treatment of patients with acute MI.

## Angiographic data

The everolimus-eluting BVS was implanted in patients presenting with ST-segment elevation and a thrombus burden 4 or 5 in 63.0% of the cases. A theoretical concern related to the implantation of the BVS in such thrombotic lesions is the fact that scaffold positioning and placement may need a more aggressive lesion preparation (predilatation) compared with standard metal devices, due to its slightly higher profile. We hypothesized that this strategy might be prone to an increase in distal embolization following balloon inflations, favouring no-reflow and reducing the rate of final TIMI-flow III.

However, the analysis of the post-procedural angiographies revealed a TIMI-flow III in 91.7% of the cases; such results are in line with recently reported large trials evaluating the performance of metallic stents in patients presenting with acute MI.<sup>5,6</sup> Less thrombus embolization may result from a different pattern of thrombus dislodgment and compression to the arterial wall after deployment of a device with a larger strut width (157 μm) compared with currently available metallic stents. The percentage of vessel wall area

**Table 1** Baseline clinical characteristics intent-to-treat population and patients treated with metallic stent in the enrolment period

Clinical characteristics	BVS (N = 49)	Metal stents (N = 123)	P-value
Age (year)	58.9 ± 10.5	66.4 ± 12.2	<0.001
Male, n (%)	38 (77.6)	93 (75.6)	0.845
Hypertension, n (%)	19 (38.8)	53/105 (50.5)	0.225
Hypercholesterolemia, n (%)	11 (22.4)	30/100 (30.0)	0.435
Diabetes, n (%)	4 (8.2)	14/116 (12.1)	0.590
Smoke, n (%)	27 (69.2)	46/116 (39.7)	0.120
Family history of CAD, n (%)	12 (24.5)	31/95 (32.6)	0.343
Peripheral vascular disease, n (%)	1 (2.0)	8 (6.5)	0.449
Kidney disease, n (%)	1 (2.0)	7 (5.7)	0.442
Prior MI, n (%)	1 (2.0)	14 (11.4)	0.070
Prior PCI, n (%)	0 (0.0)	15 (12.2)	0.007
Prior CABG, n (%)	0 (0.0)	3 (2.4)	0.559
COPD, n (%)	2 (4.1)	5 (4.1)	1.000
Culprit vessel			0.624
LM, n (%)	0 (0)	2 (1.6)	
LAD, n (%)	21 (42.9)	52 (42.3)	
RCA, n (%)	22 (44.9)	46 (37.4)	
LCX, n (%)	6 (12.2)	21 (17.1)	
SVG, n (%)	0 (0)	2 (1.6)	

Patients with vessels diameters not feasible for BVS implantation (i.e. reference vessel diameter  $\geq 4.0$  mm) were excluded.

Data are expressed as mean  $\pm$  SD or number and proportion, n (%).

CAD, coronary artery disease; MI, myocardial infarction; PCI, percutaneous coronary intervention; CABG, coronary artery bypass graft; COPD, chronic obstructive pulmonary disease; LM, left main; LAD, left anterior descending; RCA, right coronary artery; LCX, circumflex; SVG, saphenous vein graft.

covered by the BVS polymer (scaffold/vessel ratio) has been previously evaluated to be 26%,<sup>32</sup> a value considerably higher compared with what observed for conventional metallic DES (i.e. EES provides a percentage stent/vessel ratio equal to 12%).<sup>32</sup> This characteristic of the BVS might be associated to an increased capacity of capturing debris and thrombotic material behind the struts before embolization to distal microcirculation. This so-called snow racket concept (entrapment of thrombotic material between the stent and the vessel) is currently the basis for the design of novel devices and clinical studies.<sup>33</sup>

### Optical coherence tomography findings

Given its high resolution, OCT allows the assessment of *in vivo* strut apposition and presence of thrombus.<sup>24,34–36</sup>

The present analysis was performed at 1 mm intervals in the OCT pullback. Although, the possibility for a more strict assessment of OCT analysis in thrombotic lesion may be considered,<sup>21</sup> this methodology is the current standard applied in our institution for clinical studies, and the most commonly used in the literature.

**Table 2** Procedural data intent-to-treat population

Procedural data	N = 49
Medications	
Aspirin, n (%)	49 (100)
Prasugrel, n (%)	45 (91.8)
Clopidogrel, n (%)	4 (8.2)
Glycoprotein IIb/IIIa antagonists, n (%)	17 (34.7)
Unfractionated heparin, n (%)	49 (100)
Mean door-to-balloon time (min)	31.3 ± 19.5
Manual thrombectomy, n (%)	38 (77.5)
Direct stenting, n (%)	16 (32.7)
Pre-dilatation, n (%)	33 (67.3)
Mean pre-dilatation balloon diameter per-lesion (mm)	2.6 ± 0.67
Post-dilatation, n (%)	10 (20.4)
Mean post-dilatation balloon diameter per-lesion (mm)	3.5 ± 0.47
Overlapping, n (%)	12 (24.5)
Overlap scaffolds diameters 3.5 mm–3.5 mm, n (%)	5 (10.2)
Overlap scaffolds diameters 3.5 mm – 3 mm n (%)	5 (10.2)
Overlap scaffolds diameters 3.5 mm–2.5 mm, n (%)	1 (2.0)
Overlap scaffolds diameters, 3 mm–2.5 mm, n (%)	1 (2.0)
Total number of scaffolds, n.	65
Mean scaffolds per-lesion, n.	1.35 ± 0.60
Mean scaffold length per-lesion (mm)	26.40 ± 13.86
Mean scaffold diameter per-lesion (mm)	3.2 ± 34
Supportive wire, n. (%)	5 (10.2)
Radial approach, n. (%)	26 (53.0)

Data are expressed as mean  $\pm$  SD or number and proportion, n (%).

Previous reports defined a stent malapposed if at least 5% of struts were observed to be malapposed,<sup>37,38</sup> in the present investigation, only seven scaffolds (22.6%) investigated with OCT showed a strut malapposition of  $>5\%$ , with an overall mean struts malapposition equal to  $2.8 \pm 3.90\%$ . A recently reported study using a similar methodology to investigate malapposition after metallic balloon expandable stent implantation in STEMI patients showed a total of 37.1% malapposed stents (stents with  $>5\%$  malapposition) with a mean percentage of strut malapposition equal to  $5.99 \pm 7.28\%$ .<sup>38</sup> In addition, the mean ISA area was  $0.118 \pm 0.162$  mm<sup>2</sup>, a value in line with data reported for metallic stent implantation in patients presenting with STEMI.<sup>21,38</sup> Similarly, the amount of intraluminal defect after scaffold implantation was minimal and comparable with what is observed in metallic stents.<sup>21</sup> Notably, these results were consistent among different scaffold sizes.

### Clinical outcomes

In the present series, none of patients treated with BVS experienced a clinical event related to the treated vessel at the 30-day follow-up. These observations support the feasibility of BVS implantation in patients presenting with acute STEMI.

**Table 3** Angiographic analysis in patients implanted with bioresorbable vascular scaffolds

Angiographic data	N = 48
Pre-procedure	
TIMI-flow, % (n)	
0	50.0% (23/46)
1	15.2% (7/46)
2	21.7% (10/46)
3	13.0% (6/46)
Thrombus burden, % (n)	
0	0.0% (0/46)
1	6.5% (3/46)
2	17.4% (8/46)
3	13.0% (6/46)
4	13.0% (6/46)
5	50.0% (23/46)
Total occlusion (N = 23)	
RVD (mm)	2.94 ± 0.77
Non-total occlusion (N = 23)	
RVD (mm)	2.62 ± 0.63
MLD (mm)	0.75 ± 0.44
Diameter stenosis (%)	70.8 ± 12.5
After thrombectomy	
TIMI-flow, % (n)	
0	2.5% (1/40)
1	7.5% (3/40)
2	37.5% (15/40)
3	52.5% (21/40)
Thrombus burden, % (n)	
0	0.0% (0/40)
1	30.0% (12/40)
2	35.0% (14/40)
3	22.5% (9/40)
4	10.0% (4/40)
5	2.5% (1/40)
After pre-dilatation	
TIMI-flow, % (n)	
0	0.0% (0/27)
1	7.4% (2/27)
2	33.3% (9/27)
3	59.3% (16/27)
Before BVS implantation	
RVD (mm)	2.63 ± 0.53
MLD (mm)	1.21 ± 0.46
Diameter stenosis (%)	53.2 ± 16.1
D <sub>max</sub> (mm)	3.01 ± 0.52
Post-procedure	
TIMI-flow, % (n)	
0	0.0% (0/48)
1	0.0% (0/48)

Continued

**Table 3** Continued

Angiographic data	N = 48
2	8.3% (4/48)
3	91.7% (44/48)
In-scaffold	
RVD (mm)	2.86 ± 0.52
MLD (mm)	2.44 ± 0.49
Diameter stenosis (%)	14.7 ± 8.2
In-segment	
RVD (mm)	2.74 ± 0.59
MLD (mm)	2.20 ± 0.53
Diameter stenosis (%)	21.8 ± 12.0
MI syntax score I <sup>a</sup>	10.0 (7.0–15.0)
MI syntax score II <sup>a</sup>	7.0 (4.25–10.0)
Dominant right coronary artery, % (n)	93.8% (45/48)
Scaffold-to-artery ratio	1.19 ± 0.24
Complications occurring any time during the procedure, % (n)	
Dissection	6.3% (3/48)
Spasm	4.2% (2/48)
Distal embolism	14.6% (7/48)
No-reflow	2.1% (1/48)

Data are expressed as mean ± SD or proportion (%).

<sup>a</sup>MI syntax scores I and II are expressed as median (interquartile range).

**Table 4** Optical coherence tomography findings post-implantation in patients implanted with bioresorbable vascular scaffolds

OCT variables	N = 31
Analysed length (mm)	28.16 ± 13.29
Analysed struts, n	245 ± 135
Minimum lumen area (mm <sup>2</sup> )	5.95 ± 1.61
Mean lumen area (mm <sup>2</sup> )	8.02 ± 1.92
Lumen volume (mm <sup>3</sup> )	225.78 ± 113.63
Minimum scaffold area (mm <sup>2</sup> )	6.69 ± 1.94
Mean scaffold area (mm <sup>2</sup> )	8.54 ± 1.97
Scaffold volume (mm <sup>3</sup> )	240.07 ± 118.48
Minimum flow area (mm <sup>2</sup> )	5.62 ± 1.66
ISA area (mm <sup>2</sup> ) (N = 20)	0.118 ± 0.162
Mean prolapse area (mm <sup>2</sup> )	0.60 ± 0.26
Mean intraluminal defect area (mm <sup>2</sup> )	0.013 ± 0.017
Maximum intraluminal defect area (mm <sup>2</sup> )	0.094 ± 0.077
Mean atherothrombotic area (mm <sup>2</sup> )	0.61 ± 0.27
Mean atherothrombotic burden (%)	7.29 ± 3.12
Malapposed struts per patient (%)	2.80 ± 3.90
Scaffolds with at least 1 malapposed strut, n (%)	20 (64.5)
Scaffolds with >5% malapposed struts, n (%)	7 (22.6)

ISA, incomplete scaffold apposition.

Data are expressed as mean ± SD or number and proportion, n (%).

**Table 5** Optical coherence tomography findings post-implantation stratified by scaffold size in patients implanted with bioresorbable vascular scaffolds

OCT variables	2.5 mm (N = 5)	3.0 mm (N = 13)	3.5 mm (N = 24)	P
Scaffold size				
Analysed length (mm)	18.80 ± 1.30	22.23 ± 6.46	21.33 ± 7.38	0.628
Minimum lumen area (mm <sup>2</sup> )	4.08 ± 0.24	5.60 ± 0.93	7.18 ± 1.58	0.001
Mean lumen area (mm <sup>2</sup> )	5.42 ± 0.75	7.18 ± 1.03	9.25 ± 1.72	0.001
Minimum scaffold area (mm <sup>2</sup> )	4.53 ± 0.51	6.13 ± 1.02	8.06 ± 1.82	0.001
Mean scaffold area (mm <sup>2</sup> )	5.62 ± 0.28	7.66 ± 0.88	9.82 ± 1.70	0.001
Minimum flow area (mm <sup>2</sup> )	3.84 ± 0.28	5.17 ± 0.86	6.77 ± 1.60	0.001
ISA area (mm <sup>2</sup> ) (N = 25)	0.190 ± 0.318 (N = 3)	0.063 ± 0.072 (N = 10)	0.133 ± 0.177 (N = 12)	0.429
Mean prolapse area (mm <sup>2</sup> )	0.40 ± 0.19	0.54 ± 0.27	0.62 ± 0.29	0.246
Mean intraluminal defect area (mm <sup>2</sup> )	0.007 ± 0.008	0.016 ± 0.021	0.012 ± 0.018	0.628
Maximum intraluminal defect area (mm <sup>2</sup> )	0.072 ± 0.081	0.102 ± 0.086	0.068 ± 0.065	0.096
Mean atherothrombotic area (mm <sup>2</sup> )	0.40 ± 0.19	0.56 ± 0.27	0.64 ± 0.30	0.237
Mean atherothrombotic burden (%)	6.00 ± 4.66	7.42 ± 3.79	6.20 ± 3.39	0.594

ISA, incomplete scaffold apposition.

Data are expressed as mean ± SD or number and proportion, n (%).

**Table 6** Clinical outcomes at the 30-day follow-up intent-to-treat population

Clinical events	N = 49	95% CI
Target-lesion failure	(0/49) 0%	(0–7.41)
TVF	(0/49) 0%	(0–7.41)
Cardiac death	(0/49) 0%	(0–7.41)
Target-vessel MI	(0/49) 0%	(0–7.41)
Q-wave MI	(0/49) 0%	(0–7.41)
Non Q-wave MI	(0/49) 0%	(0–7.41)
Clinically driven target-vessel revascularization	(0/49) 0%	(0–7.41)
Any MI	(1/49) 2.6%	(0–10.69)
Q-wave MI	(0/49) 0%	(0–7.41)
Non Q-wave MI	(1/49) 2.6%	(0–10.69)
Major adverse cardiac events	(1/49) 2.6%	(0–10.69)
Non-target-vessel revascularization	(1/49) 2.6%	(0–10.69)
Definite or probable scaffold thrombosis	(0/49) 0%	(0–7.41)

Data are expressed number and proportion, n (%). 95% CI, 95% confidence interval.

Data showed in the present report with optimal acute performance in terms of final TIMI-flow and scaffold apposition may suggest that everolimus-eluting BVS could be considered for the treatment of patients presenting with STEMI, however, due to the limited number of patients and events, caution should be made in reaching firm conclusions. Further larger studies are needed to fully evaluate the performance of the present device in STEMI patients.

## Limitations

The present study represents a feasibility study with a limited number of patients. The small sample size does not allow reaching conclusions in terms of clinical outcomes. The lack of a head-to-head comparison with the current standard of care is a major limitation of the present study. A longer follow-up is needed to fully evaluate the performance of this novel device in patients presenting with acute MI. During the enrolment period, the implantation of either metallic stent or BVS in STEMI patients was left to the operator's discretion; this methodology may be prone to selection bias. Therefore, these data should not stimulate at the current state of knowledge the use of BVS in patients presenting with acute MI. Larger randomized studies are needed to confirm these preliminary observations.

## Conclusion

In the present investigation, the implantation of the everolimus-eluting BVS was observed to be feasible in patients presenting with STEMI with optimal acute performance. These data are preliminary and need further confirmation in randomized controlled trials to define the true role of BVS for the treatment of patients presenting with acute myocardial infarction.

## Funding

**Conflict of interest:** Dr R.J. van Geuns received speakers fee from Abbott Vascular. Abbott Vascular is providing institution research grant for the Erasmus MC. Antonios Karanasos received funding support from the Hellenic Heart Foundation and St Jude Medical.

## References

1. Task Force on Myocardial Revascularization of the European Society of C, the European Association for Cardio-Thoracic S, European Association for Percutaneous

- Cardiovascular I, Wijns W, Kolh P, Danchin N, Di Mario C, Falk V, Folliguet T, Garg S, Huber K, James S, Knuuti J, Lopez-Sendon J, Marco J, Menicanti L, Ostojic M, Piepoli MF, Pirlir C, Pomar JL, Reifart N, Ribichini FL, Schali J, Serruys PW, Serruys PW, Silber S, Sousa Uva M, Taggart D. Guidelines on myocardial revascularization. *Eur Heart J* 2010;**31**:2501–2555.
2. Spaulding C, Henry P, Teiger E, Beatt K, Bramucci E, Carrie D, Slaama MS, Merkely B, Erglis A, Margheri M, Varenne O, Cebrian A, Stoll HP, Snead DB, Bode C, Investigators T. Sirolimus-eluting versus uncoated stents in acute myocardial infarction. *N Engl J Med* 2006;**355**:1093–1104.
  3. Stone GW, Lansky AJ, Pocock SJ, Gersh BJ, Dangas G, Wong SC, Witztzenbichler B, Guagliumi G, Peruga JZ, Brodie BR, Dudek D, Mocket M, Ochala A, Kellock A, Parise H, Mehran R, Investigators H-AT. Paclitaxel-eluting stents versus bare-metal stents in acute myocardial infarction. *N Engl J Med* 2009;**360**:1946–1959.
  4. Brar SS, Leon MB, Stone GW, Mehran R, Moses JW, Brar SK, Dangas G. Use of drug-eluting stents in acute myocardial infarction: a systematic review and meta-analysis. *J Am Coll Cardiol* 2009;**53**:1677–1689.
  5. Raber L, Kelbaek H, Ostojic M, Baumbach A, Heg D, Tuller D, von Birgelen C, Roffi M, Moschovitis A, Khattab AA, Wenaweser P, Bonvini R, Pedrazzini G, Kornowski R, Weber K, Trelle S, Luscher TF, Tanikawa M, Matter CM, Meier B, Juni P, Windecker S, Investigators CAT. Effect of biolimus-eluting stents with biodegradable polymer vs bare-metal stents on cardiovascular events among patients with acute myocardial infarction: the COMFORTABLE AMI randomized trial. *JAMA* 2012;**308**:777–787.
  6. Sabate M, Cequier A, Iniguez A, Serra A, Hernandez-Antolin R, Mainar V, Valgimigli M, Tespili M, den Heijer P, Bethencourt A, Vazquez N, Gomez-Hospital JA, Baz JA, Martin-Vuste V, van Geuns RJ, Alfonso F, Bordes P, Tebaldi M, Masotti M, Silvestro A, Backus B, Brugaletta S, van Es GA, Serruys PW. Everolimus-eluting stent versus bare-metal stent in ST-segment elevation myocardial infarction (EXAMINATION): 1 year results of a randomised controlled trial. *Lancet* 2012;**380**:1482–1490.
  7. Serruys PW, Garcia-Garcia HM, Onuma Y. From metallic cages to transient bioresorbable scaffolds: change in paradigm of coronary revascularization in the upcoming decade? *Eur Heart J* 2012;**33**:16–25b.
  8. Finn AV, Joner M, Nakazawa G, Kolodgie F, Newell J, John MC, Gold HK, Virmani R. Pathological correlates of late drug-eluting stent thrombosis: strut coverage as a marker of endothelialization. *Circulation* 2007;**115**:2435–2441.
  9. Joner M, Finn AV, Farb A, Mont EK, Kolodgie FD, Ladich E, Kutys R, Skorjia J, Gold HK, Virmani R. Pathology of drug-eluting stents in humans: delayed healing and late thrombotic risk. *J Am Coll Cardiol* 2006;**48**:193–202.
  10. Hong MK, Mintz GS, Lee CW, Kim YH, Lee SW, Song JM, Han KH, Kang DH, Song JK, Kim JJ, Park SW, Park SJ. Incidence, mechanism, predictors, and long-term prognosis of late stent malapposition after bare-metal stent implantation. *Circulation* 2004;**109**:881–886.
  11. Hong MK, Mintz GS, Lee CW, Park DW, Park KM, Lee BK, Kim YH, Song JM, Han KH, Kang DH, Cheong SS, Song JK, Kim JJ, Park SW, Park SJ. Late stent malapposition after drug-eluting stent implantation: an intravascular ultrasound analysis with long-term follow-up. *Circulation* 2006;**113**:414–419.
  12. Ormiston JA, Serruys PW, Onuma Y, van Geuns RJ, de Bruyne B, Dudek D, Thuesen L, Smits PC, Chevalier B, McClean D, Koolen J, Windecker S, Whitbourn R, Meredith I, Dorange C, Veldhof S, Hebert KM, Rapoza R, Garcia-Garcia HM. First serial assessment at 6 months and 2 years of the second generation of absorb everolimus-eluting bioresorbable vascular scaffold: a multi-imaging modality study. *Circ Cardiovasc Interv* 2012;**5**:620–632.
  13. Serruys PW, Onuma Y, Dudek D, Smits PC, Koolen J, Chevalier B, de Bruyne B, Thuesen L, McClean D, van Geuns RJ, Windecker S, Whitbourn R, Meredith I, Dorange C, Veldhof S, Hebert KM, Sudhir K, Garcia-Garcia HM, Ormiston JA. Evaluation of the second generation of a bioresorbable everolimus-eluting vascular scaffold for the treatment of de novo coronary artery stenosis: 12-month clinical and imaging outcomes. *J Am Coll Cardiol* 2011;**58**:1578–1588.
  14. Kajiyama T, Liang M, Sharma RK, Lee CH, Chan MY, Tay E, Chan KH, Tan HC, Low AF. Everolimus-eluting bioresorbable vascular scaffold (BVS) implantation in patients with ST-segment elevation myocardial infarction (STEMI). *EuroIntervention* 2013;**9**:501–504.
  15. Kocka V, Lisa L, Tousek P, Budesinsky T, Widimsky P. ST elevation myocardial infarction treated with bioresorbable vascular scaffold: rationale and first cases. *Eur Heart J* 2013;**34**:2073.
  16. Ormiston JA, Serruys PW, Regar E, Dudek D, Thuesen L, Webster MW, Onuma Y, Garcia-Garcia HM, McGreevy R, Veldhof S. A bioabsorbable everolimus-eluting coronary stent system for patients with single de novo coronary artery lesions (ABSORB): a prospective open-label trial. *Lancet* 2008;**371**:899–907.
  17. Serruys PW, Onuma Y, Ormiston JA, de Bruyne B, Regar E, Dudek D, Thuesen L, Smits PC, Chevalier B, McClean D, Koolen J, Windecker S, Whitbourn R, Meredith I, Dorange C, Veldhof S, Miquel-Hebert K, Rapoza R, Garcia-Garcia HM. Evaluation of the second generation of a bioresorbable everolimus drug-eluting vascular scaffold for treatment of de novo coronary artery stenosis: six-month clinical and imaging outcomes. *Circulation* 2010;**122**:2301–2312.
  18. Cutlip DE, Windecker S, Mehran R, Boam A, Cohen DJ, van Es GA, Steg PG, Morel MA, Mauri L, Vranckx P, McFadden E, Lansky A, Hamon M, Krucoff MW, Serruys PW, Academic Research C. Clinical end points in coronary stent trials: a case for standardized definitions. *Circulation* 2007;**115**:2344–2351.
  19. Onuma Y, Serruys PW. Bioresorbable scaffold: the advent of a new era in percutaneous coronary and peripheral revascularization? *Circulation* 2011;**123**:779–797.
  20. Onuma Y, Serruys PW, Perkins LE, Okamura T, Gonzalo N, Garcia-Garcia HM, Regar E, Kamberi M, Powers JC, Rapoza R, van Beusekom H, van der Giessen W, Virmani R. Intracoronary optical coherence tomography and histology at 1 month and 2, 3, and 4 years after implantation of everolimus-eluting bioresorbable vascular scaffolds in a porcine coronary artery model: an attempt to decipher the human optical coherence tomography images in the ABSORB trial. *Circulation* 2010;**122**:2288–2300.
  21. Onuma Y, Thuesen L, van Geuns RJ, van der Ent M, Desch S, Fajadet J, Christiansen E, Smits P, Ramsing Holm N, Regar E, van Mieghem N, Borovicin V, Pounovic D, Senshu K, van Es GA, Muramatsu T, Lee IS, Schuler G, Zijlstra F, Garcia-Garcia HM, Serruys PW, Investigators T. Randomized study to assess the effect of thrombus aspiration on flow area in patients with ST-elevation myocardial infarction: an optical frequency domain imaging study – TROFI trial. *Eur Heart J* 2013;**34**:1050–1060.
  22. Sianos G, Papafakis MI, Daemen J, Vaina S, van Mieghem CA, van Domburg RT, Michalis LK, Serruys PW. Angiographic stent thrombosis after routine use of drug-eluting stents in ST-segment elevation myocardial infarction: the importance of thrombus burden. *J Am Coll Cardiol* 2007;**50**:573–583.
  23. Magro M, Nauta S, Simsek C, Onuma Y, Garg S, van der Heide E, van der Giessen WJ, Boersma E, van Domburg RT, van Geuns RJ, Serruys PW. Value of the SYNTAX score in patients treated by primary percutaneous coronary intervention for acute ST-elevation myocardial infarction: The MI SYNTAX score study. *Am Heart J* 2011;**161**:771–781.
  24. Tearney GJ, Regar E, Akasaka T, Adriaenssens T, Barlis P, Bezerra HG, Bouma B, Bruining N, Cho JM, Chowdhary S, Costa MA, de Silva R, Dijkstra J, Di Mario C, Dudek D, Falk E, Feldman MD, Fitzgerald P, Garcia-Garcia HM, Gonzalo N, Granada JF, Guagliumi G, Holm NR, Honda Y, Ikeno F, Kawasaki M, Kochman J, Koltowski L, Kubo T, Kume T, Kyono H, Lam CC, Lamouche G, Lee DP, Leon MB, Maehara A, Manfrini O, Mintz GS, Mizuno K, Morel MA, Nadkarni S, Okura H, Otake H, Pietrasik A, Prati F, Raber L, Radu MD, Rieber J, Riga M, Rollins A, Rosenberg M, Sirbu V, Serruys PW, Shimada K, Shinke T, Shite J, Siegel E, Sonoda S, Suter M, Talarada S, Tanaka A, Terashima M, Thim T, Uemura S, Ughi GJ, van Beusekom HM, van der Steen AF, van Es GA, van Soest G, Virmani R, Waxman S, Weissman NJ, Weisz G, International Working Group for Intravascular Optical Coherence T. Consensus standards for acquisition, measurement, and reporting of intravascular optical coherence tomography studies: a report from the International Working Group for Intravascular Optical Coherence Tomography Standardization and Validation. *J Am Coll Cardiol* 2012;**59**:1058–1072.
  25. Farooq V, Onuma Y, Radu M, Okamura T, Gomez-Lara J, Brugaletta S, Gogas BD, van Geuns RJ, Regar E, Schultz C, Windecker S, Lefevre T, Brueren BR, Powers J, Perkins LL, Rapoza R, Virmani R, Garcia-Garcia HM, Serruys PW. Optical coherence tomography (OCT) of overlapping bioresorbable scaffolds: from benchwork to clinical application. *EuroIntervention* 2011;**7**:386–399.
  26. Magro M, Regar E, Gutierrez-Chico JL, Garcia-Garcia H, Simsek C, Schultz C, Zijlstra F, Serruys PW, van Geuns RJ. Residual atherothrombotic material after stenting in acute myocardial infarction – an optical coherence tomographic evaluation. *Int J Cardiol* 2013;**167**:656–663.
  27. Serruys PW, Ormiston JA, Onuma Y, Regar E, Gonzalo N, Garcia-Garcia HM, Nieman K, Bruining N, Dorange C, Miquel-Hebert K, Veldhof S, Webster M, Thuesen L, Dudek D. A bioabsorbable everolimus-eluting coronary stent system (ABSORB): 2-year outcomes and results from multiple imaging methods. *Lancet* 2009;**373**:897–910.
  28. Diletti R, Onuma Y, Farooq V, Gomez-Lara J, Brugaletta S, van Geuns RJ, Regar E, de Bruyne B, Dudek D, Thuesen L, Chevalier B, McClean D, Windecker S, Whitbourn R, Smits P, Koolen J, Meredith I, Li D, Veldhof S, Rapoza R, Garcia-Garcia HM, Ormiston JA, Serruys PW. 6-month clinical outcomes following implantation of the bioresorbable everolimus-eluting vascular scaffold in vessels smaller or larger than 2.5 mm. *J Am Coll Cardiol* 2011;**58**:258–264.
  29. Diletti R, Serruys PW, Farooq V, Sudhir K, Dorange C, Miquel-Hebert K, Veldhof S, Rapoza R, Onuma Y, Garcia-Garcia HM, Chevalier B, ABSORB II randomized controlled trial: a clinical evaluation to compare the safety, efficacy, and performance of the absorb everolimus-eluting bioresorbable vascular scaffold system against the XIENCE everolimus-eluting coronary stent system in the treatment of subjects with ischemic heart disease caused by de novo native coronary artery lesions: rationale and study design. *Am Heart J* 2012;**164**:654–663.
  30. Dudek D, Onuma Y, Ormiston JA, Thuesen L, Miquel-Hebert K, Serruys PW. Four-year clinical follow-up of the ABSORB everolimus-eluting bioresorbable vascular scaffold in patients with de novo coronary artery disease: the ABSORB trial. *EuroIntervention* 2012;**7**:1060–1061.

31. Diletti R, Farooq V, Girasis C, Bourantas C, Onuma Y, Heo JH, Gogas BD, van Geuns RJ, Regar E, de Bruyne B, Dudek D, Thuesen L, Chevalier B, McClean D, Windecker S, Whitbourn RJ, Smits P, Koolen J, Meredith I, Li X, Miquel-Hebert K, Veldhof S, Garcia-Garcia HM, Ormiston JA, Serruys PW. Clinical and intravascular imaging outcomes at 1 and 2 years after implantation of absorb everolimus eluting bioresorbable vascular scaffolds in small vessels. Late lumen enlargement: does bioresorption matter with small vessel size? Insight from the ABSORB cohort B trial. *Heart* 2013;**99**:98–105.
32. Muramatsu T, Onuma Y, Garcia-Garcia HM, Farooq V, Bourantas CV, Morel MA, Li X, Veldhof S, Bartorelli A, Whitbourn R, Abizaid A, Serruys PW, Investigators A-E. Incidence and short-term clinical outcomes of small side branch occlusion after implantation of an everolimus-eluting bioresorbable vascular scaffold: an interim report of 435 patients in the ABSORB-EXTEND single-arm trial in comparison with an everolimus-eluting metallic stent in the SPIRIT first and II trials. *JACC Cardiovasc Interv* 2013;**6**:247–257.
33. Stone GW, Abizaid A, Silber S, Dizon JM, Merkely B, Costa RA, Kornowski R, Abizaid A, Wojdyla R, Maehara A, Dressler O, Brener SJ, Bar E, Dudek D. Prospective, randomized, multicenter evaluation of a polyethylene terephthalate micronet mesh-covered stent (MGuard) in ST-segment elevation myocardial infarction: the MASTER trial. *J Am Coll Cardiol*. 2012;**60**:1975–1984.
34. Otake H, Shite J, Ako J, Shinke T, Tanino Y, Ogasawara D, Sawada T, Miyoshi N, Kato H, Koo BK, Honda Y, Fitzgerald PJ, Hirata K. Local determinants of thrombus formation following sirolimus-eluting stent implantation assessed by optical coherence tomography. *JACC Cardiovasc Interv* 2009;**2**:459–466.
35. Prati F, Guagliumi G, Mintz GS, Costa M, Regar E, Akasaka T, Barlis P, Tearney GJ, Jang IK, Arbustini E, Bezerra HG, Ozaki Y, Bruining N, Dudek D, Radu M, Erglis A, Motreff P, Alfonso F, Toutouzas K, Gonzalo N, Tamburino C, Adriaenssens T, Pinto F, Serruys PW, Di Mario C, Expert's OCTRD. Expert review document part 2: methodology, terminology and clinical applications of optical coherence tomography for the assessment of interventional procedures. *Eur Heart J* 2012;**33**:2513–2520.
36. Prati F, Regar E, Mintz GS, Arbustini E, Di Mario C, Jang IK, Akasaka T, Costa M, Guagliumi G, Grube E, Ozaki Y, Pinto F, Serruys PW, Expert's OCTRD. Expert review document on methodology, terminology, and clinical applications of optical coherence tomography: physical principles, methodology of image acquisition, and clinical application for assessment of coronary arteries and atherosclerosis. *Eur Heart J* 2010;**31**:401–415.
37. Barlis P, Regar E, Serruys PW, Dimopoulos K, van der Giessen WJ, van Geuns RJ, Ferrante G, Wandel S, Windecker S, van Es GA, Eerdmans P, Juni P, di Mario C. An optical coherence tomography study of a biodegradable vs. durable polymer-coated limus-eluting stent: a LEADERS trial sub-study. *Eur Heart J* 2010;**31**:165–176.
38. van Geuns RJ, Tamburino C, Fajadet J, Vrolix M, Witzenbichler B, Eekhout E, Spaulding C, Reczuch K, La Manna A, Spaargaren R, Garcia-Garcia HM, Regar E, Capodanno D, Van Langenhove G, Verhey S. Self-expanding versus balloon-expandable stents in acute myocardial infarction: results from the APPOSITION II study: self-expanding stents in ST-segment elevation myocardial infarction. *JACC Cardiovasc Interv* 2012;**5**:1209–1219.

# Chapter 5

## Lessons Learned from Early BVS Studies and Clinical Implications for Complex Subsets of Lesions or Patients

### 5.1 Scaffold thrombosis and scaffold dislodgement

Lessons learned from acute and late scaffold failures in the ABSORB EXTEND trial.

*Eurointervention*. 2014;10:449-57.

[Original research paper, Impact Factor (2013): 3.758]

Ishibashi Y, Onuma Y, Muramatsu T, Nakatani S, Iqbal J, Garcia-Garcia HM, Bartorelli AL, Whitbourn R, Abizaid A, Serruys PW.





# Lessons learned from acute and late scaffold failures in the ABSORB EXTEND trial

Yuki Ishibashi<sup>1</sup>, MD, PhD; Yoshinobu Onuma<sup>1</sup>, MD; Takashi Muramatsu<sup>1</sup>, MD, PhD; Shimpei Nakatani<sup>1</sup>, MD; Javaid Iqbal<sup>1</sup>, MRCP, PhD; Hector M. Garcia-Garcia<sup>1</sup>, MD, PhD; Antonio L. Bartorelli<sup>2</sup>, MD; Robert Whitbourn<sup>3</sup>, MD; Alexander Abizaid<sup>4</sup>, MD, PhD; Patrick W. Serruys<sup>1</sup>, MD, PhD; on behalf of the ABSORB EXTEND Investigators

1. Thoraxcenter, Erasmus University Medical Center, Rotterdam, The Netherlands; 2. Centro Cardiologico Monzino, IRCCS, University of Milan, Milan, Italy; 3. St Vincent's Hospital, Fitzroy, Victoria, Australia; 4. Instituto de Cardiologia Dante Pazzanese, Sao Paulo, Brazil

GUEST EDITOR: Antonio Colombo, MD; S. Raffaele Scientific Institute, Milan, Italy

## KEYWORDS

- bioresorbable scaffold
- scaffold dislodgement
- scaffold thrombosis

## Abstract

**Aims:** Bioresorbable scaffolds are increasingly used in patients with coronary artery disease undergoing percutaneous coronary interventions. ABSORB EXTEND is an ongoing study that will recruit 800 patients. This report evaluates acute and late scaffold failure in the first 450 patients enrolled in ABSORB EXTEND who have completed 12 months follow-up.

**Methods and results:** Clinical event data from the first 450 patients enrolled in ABSORB EXTEND have demonstrated low rates of ischaemia-driven MACE (4.2%) and target vessel failure (4.7%) at 12 months. There have been seven cases of device failure in this study: three cases of scaffold dislodgement (0.67%) and four cases of subacute or late scaffold thrombosis (0.89%). All scaffold dislodgements occurred in the left circumflex (LCX), and in two cases dislodgement was observed after reinsertion of the same device. Two cases of subacute scaffold thrombosis and two late scaffold thromboses were observed. Two out of four cases of scaffold thrombosis seemed to be related to either premature discontinuation of dual antiplatelet therapy (DAPT) or resistance to clopidogrel.

**Conclusions:** This is the first report specifically describing the incidence and the potential mechanisms of scaffold dislodgement and scaffold thrombosis as seen in the ABSORB EXTEND trial.

\*Corresponding author: Thoraxcenter, Ba-583, 's Gravendijkwal 230, 3015 CE Rotterdam, The Netherlands.  
E-mail: p.w.j.c.serruys@erasmusmc.nl

© Europa Digital & Publishing 2014. All rights reserved.

SUBMITTED ON 22/07/2013 - REVISION RECEIVED ON 24/09/2013 - ACCEPTED ON 19/11/2013

## Introduction

Acute vessel closure, due to dislodgement of a coronary stent during deployment or an early stent thrombosis, is a rare but potentially fatal complication of percutaneous coronary intervention (PCI)<sup>1</sup>. Late or very late thrombosis also remains a long-term concern with metallic drug-eluting stents, due to delayed healing potentially caused by the permanent presence of foreign bodies such as metals and coating materials<sup>1-4</sup>.

The Absorb everolimus-eluting poly-L-lactic acid (PLLA) bioresorbable vascular scaffold system (BVS; Abbott Vascular, Santa Clara, CA, USA) is a novel approach to treat coronary lesions<sup>5-8</sup>. After complete bioresorption of the polymeric struts<sup>8</sup>, the risk of very late scaffold thrombosis may theoretically be reduced due to the absence of foreign material<sup>9,10</sup>. On the other hand, the thick polymeric struts (total strut thickness=156 µm) crimped onto the delivery balloon contribute to the large profile of the device that may cause friction between the device and the diseased vessel wall or any daughter catheter, resulting in dislodgement of the scaffold<sup>10</sup>. Until now, however, there have been no specific reports of these acute and late complications with the Absorb BVS beyond anecdotal presentations of isolated cases.

ABSORB EXTEND (unique identifier NCT01023789) is an international prospective, single-arm study that will recruit 800 patients with long lesions (length up to 28 mm) or lesions in small vessels (2.0-3.8 mm diameter). Treatment of two *de novo* native coronary artery lesions is also permitted when each lesion is located in a different epicardial vessel. The details of the trial are described in the previous report<sup>11</sup>.

The first 450 patients enrolled in ABSORB EXTEND have completed 12 months follow-up and this interim report presents seven cases of device failure detected in this population. Three cases of scaffold dislodgement (0.67%) and four cases of subacute or late scaffold thrombosis (0.89%) are described in detail to evaluate the underlying mechanisms and to make some practical recommendations to avoid these serious complications.

## Case descriptions

### CASE 1. SCAFFOLD DISLODGE MENT SUBSEQUENTLY CRUSHED BY METALLIC STENTS

In a 74-year-old man coronary angiography showed a severe lesion with a percentage diameter stenosis (DS) of 83% (Table 1) in the mid segment of a calcified left circumflex (LCX) coronary artery (Figure 1A). After the first predilatation with a 2.5×15 mm balloon, a 3.0×18 mm Absorb BVS failed to cross the tortuous proximal LCX. After the second dilatation, the same Absorb scaffold was reinserted (time between the first and second insertion of the scaffold is unknown). However, the same Absorb scaffold still failed to cross and unexpectedly dislodged from the balloon at a site of fluoroscopic calcification proximal to the lesion when the device was pushed forward (Figure 1B, Figure 1C). Two 3.0×18 mm metallic everolimus-eluting metallic stents (EES) were deployed in an overlapping fashion to crush the dislodged scaffold against the vessel wall, and an additional 3.0×18 mm EES was deployed at the target lesion (Figure 1D). The follow-up was uneventful during 12 months.

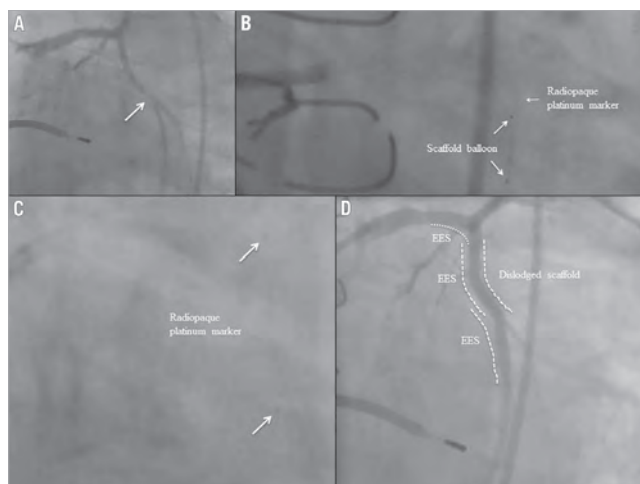


**Figure 1.** Case 1. A) Coronary angiography showing a severe lesion in the mid segment of a calcified left circumflex (LCX) coronary artery. B) & C) The same Absorb scaffold still failed to cross and unexpectedly dislodged. D) Two metallic everolimus-eluting metallic stents (EES) were deployed in an overlapping fashion to crush the dislodged scaffold against the vessel wall, and an additional EES was deployed at the target lesion.

**CASE 2. A DISLODGED SCAFFOLD LEFT INSIDE  
A PREVIOUSLY IMPLANTED METALLIC STENT**

In a 60-year-old man diagnostic coronary angiography showed a moderate stenosis (**Table 1**) in the mid segment of a highly tortuous LCX. Two metallic stents had previously been implanted in the left anterior descending coronary artery (LAD) and it seemed that the proximal stent had partially jailed the ostium of the LCX (**Figure 2A**). After predilatation using a 2.5×15 mm balloon, a 3.0×18 mm Absorb BVS was advanced beyond the ostium of the LCX, but it failed to progress into the proximal LCX despite the use of an extra support guidewire (**Figure 2B**). While the Absorb BVS delivery system and extra support guidewire were being withdrawn, the Absorb scaffold unexpectedly dislodged from the balloon and became positioned with its distal edge in the proximal LCX and its proximal edge in the LMS (**Figure 2C**). An attempt to retrieve the dislodged scaffold was made with a GooseNeck® snare (ev3 Inc., Plymouth, MN, USA). However, it failed as the dislodged scaffold was inadvertently pushed into the metallic stent located in the proximal LAD. Following this, another guidewire was inserted into the LAD and a second attempt was made to retrieve the dislodged scaffold using the GooseNeck snare, but it failed again. A balloon was

**Table 1. QCA analysis before and after the procedure in all cases.**

Case No.	MLD, mm	RVD, mm	DS, %	Obstruction length, mm	Curvature, cm <sup>-1</sup>	Angulation, degree
<b>before procedure</b>						
1	0.37	2.24	83	13.97	0.439	32.6
2	0.98	2.57	62	7.78	0.436	47.4
3	0.91	2.41	62	9.30	0.421	54.9
4	0.91	2.59	65	9.10	0.116	20.5
5	0.74	2.88	74	12.37	0.353	23.8
6	1.00	2.54	61	18.13	0.233	21.4
7	0.88	2.28	61	8.65	0.147	19.7
<b>after procedure</b>						
1	2.16	2.39	11	—	0.413	25.6
2	2.60	2.74	5	—	0.305	40.5
3	2.30	2.46	7	—	0.418	44.8
4	2.03	2.79	27	—	0.118	19.2
5	3.07	3.13	2	—	0.293	21.5
6	2.12	2.44	13	—	0.225	18.7
7	2.02	2.38	15	—	0.144	19.5

DS: diameter stenosis; MLD: minimal lumen diameter; QCA: quantitative coronary angiography; RVD: reference vessel diameter

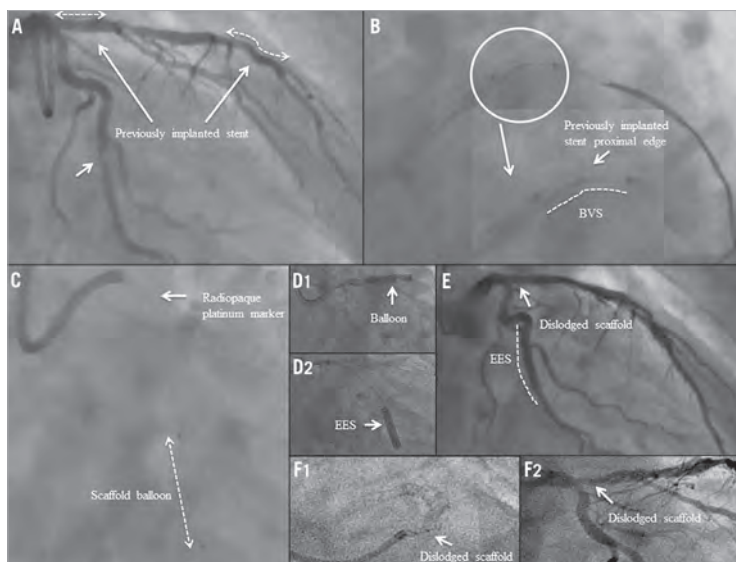


**Figure 2.** Case 2. A) Coronary angiography showing a moderate stenosis in the mid segment of a highly tortuous LCX. Two metallic stents had previously been implanted in the left anterior descending coronary artery (LAD) and it seemed that the proximal stent had partially jailed the ostium of the LCX. B) An Absorb BVS was advanced beyond the ostium of the LCX, but it failed to progress. C) The Absorb scaffold unexpectedly dislodged and became positioned with its distal edge in the proximal LCX and its proximal edge in the left main stem (LMS). D1) A balloon was then inflated to crush the dislodged scaffold in the proximal LAD. D2) An EES was successfully deployed at the target lesion. E) Final result. F1) & F2) Five months later, coronary angiography revealed a severe stenosis in the proximal LAD and LCX.

then inflated to crush the dislodged scaffold in the proximal LAD and finally an EES was successfully deployed at the target lesion (Figure 2D, Figure 2E). Five months later, coronary angiography revealed a severe stenosis in the proximal LAD and proximal LCX (Figure 2F), and the patient was referred for surgical treatment.

### CASE 3. SCAFFOLD DISLODGE MENT DUE TO A TORTUOUS VESSEL

A 61-year-old male underwent coronary angiography which showed a moderate stenosis (Table 1) in the mid segment of a calcified LCX (Figure 3A). After the first predilatation with a 2.5×15 mm balloon, a 3.0×18 mm Absorb BVS failed to cross the lesion. After two additional predilatations with a 3.0×15 mm balloon, the same Absorb BVS system was reinserted, but it was unable to pass a moderate bend in the LCX proximal to the predilated lesion. Another attempt was made to deliver the scaffold using a GuideLiner™ catheter (Vascular Solutions Inc., Minneapolis, MN, USA) and the scaffold delivery system was apparently positioned at the target lesion (Figure 3B1). However, after balloon inflation, the radiopaque markers at the edges of the scaffold were not visible on fluoroscopy (Figure 3B1, Figure 3B2). When the GuideLiner™, guidewire and the Absorb BVS delivery system were removed together as a single unit, the dislodged scaffold was found to be inside the GuideLiner™. Following this, a 2.75×18 mm EES was successfully deployed at the target lesion without any further procedural complications (Figure 3C). The patient had an uneventful clinical course and was discharged two days after the

procedure. Approximately three months after the procedure, the patient passed away at home (unwitnessed sudden death). This event was adjudicated as a possible stent thrombosis by the clinical events committee of the ABSORB EXTEND trial.

### CASE 4. SUBACUTE SCAFFOLD THROMBOSIS AT THE SITE OF OVERLAPPING SCAFFOLDS

In a 56-year-old man coronary angiography showed a moderate stenosis (Table 1) in the proximal segment of the LCX (Figure 4A1, Figure 4A2). After predilatation, a 3.0×28 mm Absorb scaffold failed to be delivered. Two additional predilatations were performed and the same Absorb BVS system was reinserted over an extra support guidewire (ASAHI GRAND SLAM™; Abbott Vascular, Santa Clara, CA, USA), but was unable to cross. A proximal scaffold deformation was observed (post-withdrawal observation) after having retracted the Absorb BVS system and the guidewire. Following this, two 3.0×18 mm Absorb BVS were successfully deployed (Figure 4B, Figure 4C). The distance between the scaffold radiopaque markers in the overlapping segment was 2.56 mm as measured by QCA.

Six days after the procedure the patient presented with a non-STEMI and was treated with thrombolytic therapy. Angiography on day seven revealed a thrombotic lesion at the site of the overlapping scaffolds in the mid segment of the LCX (Figure 4D1, Figure 4D2). The patient claimed to be fully compliant with dual antiplatelet therapy (DAPT). An EES was successfully implanted to cover the lesion and the overlapping segment of the scaffolds (Figure 4E, Figure 4F).

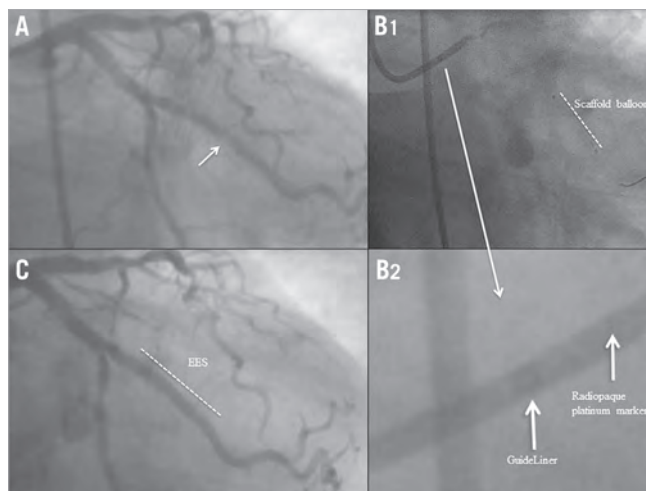


**Figure 3.** Case 3. A) Coronary angiography showing a moderate stenosis in the mid segment of a calcified LCX. B1) The scaffold delivery system was apparently positioned at the target lesion. B2) When the GuideLiner™ system was removed together as a single unit, the dislodged scaffold was found to be inside the GuideLiner™. C) An EES was successfully deployed at the target lesion.

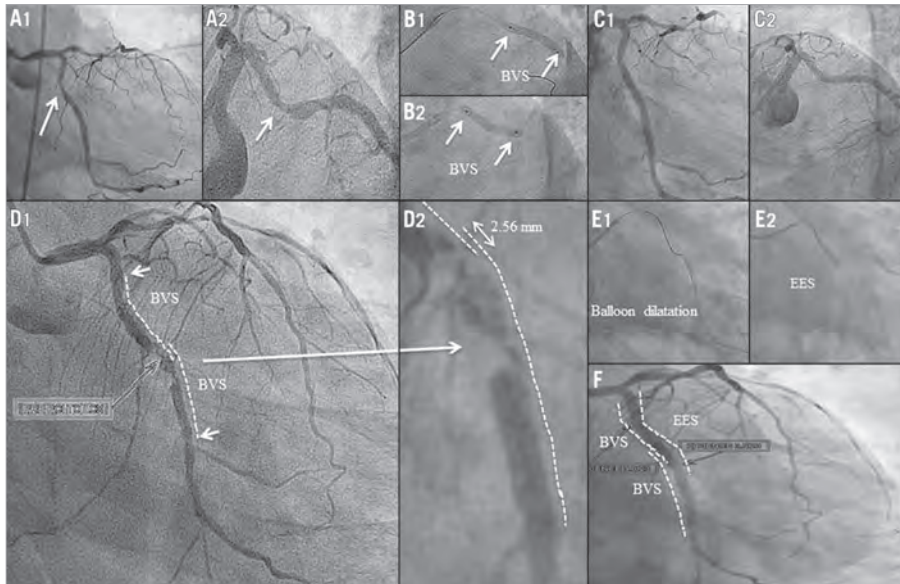


**Figure 4.** Case 4. A1) & A2) Coronary angiography showing a moderate stenosis in the proximal segment of the LCX. B1) & B2) Two Absorb BVS were successfully deployed. C1) & C2) Final results. D1) & D2) Angiography on day seven revealed a thrombotic lesion at the site of the overlapping scaffolds in the mid segment of the LCX. E1), E2) & F) An EES was successfully implanted to cover the lesion and the overlapping segment.

#### CASE 5. SUBACUTE SCAFFOLD THROMBOSIS OCCURRING TWO DAYS AFTER DISCONTINUATION OF DAPT

A 58-year-old woman underwent PCI with a 3.0×18 mm Absorb BVS in the mid segment of the LAD (Figure 5A, Figure 5B). On day 27, the patient stopped taking both aspirin and clopidogrel. Two days after DAPT discontinuation, she presented with a non-STEMI and was treated by thrombolysis. On day 32, coronary angiography showed a patent LAD with haziness (Figure 5C, Figure 5D). DAPT was restarted and follow-up was uneventful.

#### CASE 6. LATE SCAFFOLD THROMBOSIS IN A PATIENT WITH RESISTANCE TO CLOPIDOGREL

An 80-year-old woman underwent PCI with a 3.0×18 mm Absorb BVS for a moderate stenosis (Table 1) in the mid segment of the LAD (Figure 6A-Figure 6C).

Seventy-five days after the index procedure, she presented with an acute anterior STEMI. Coronary angiography showed complete thrombotic occlusion of the LAD proximal to the scaffold up to the take-off of a diagonal branch (Figure 6D). Primary PCI with a manual thrombectomy and a balloon dilatation was successfully performed (Figure 6E-Figure 6G). At the time of the emergency procedure, the patient reported that she was scrupulously taking her

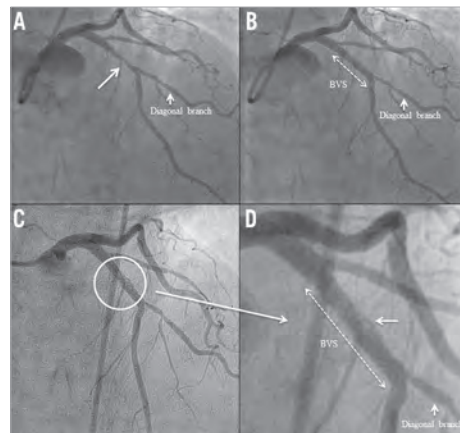


**Figure 5.** Case 5. A) Coronary angiography showing a moderate stenosis in the proximal segment of the LAD. B) An Absorb BVS was successfully deployed at the target lesion. C) & D) On day 32, coronary angiography showed a patent LAD with haziness.

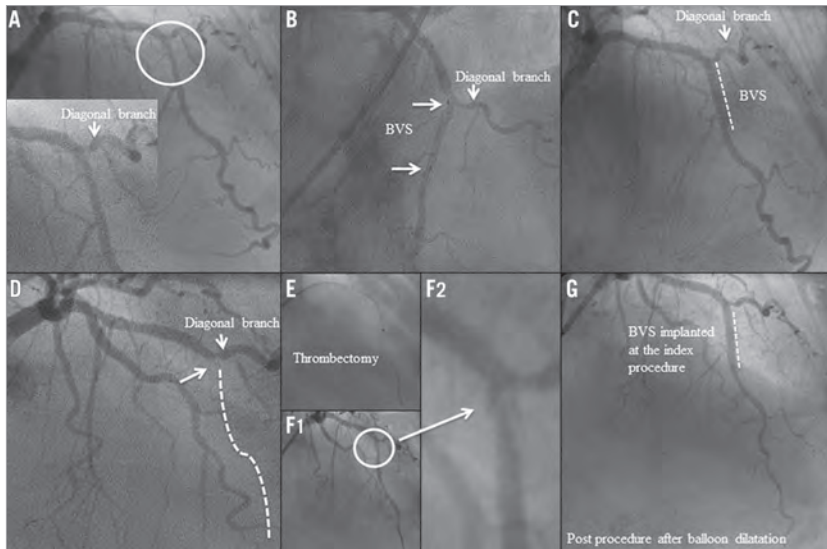


**Figure 6** Case 6. A) Coronary angiography showing a moderate stenosis in the mid segment of the LAD. B) & C) An Absorb BVS was successfully deployed at the target lesion. D) Coronary angiography showed complete thrombotic occlusion of the LAD. E) Primary PCI with a manual thrombectomy was performed. F1) & F2) Coronary angiography showed a patent LAD with haziness after thrombectomy. G) Coronary angiography showed a patent LAD without haziness after balloon dilatation.

DAPT. However, the platelet aggregation test indicated that she was either not on DAPT or resistant to clopidogrel, since her ADP-induced aggregation of platelets was normal. The patient claimed to be fully compliant with DAPT and hence a higher dose of clopidogrel (150 mg daily) was prescribed to prevent further scaffold thrombosis. The follow-up was uneventful.

#### CASE 7. LATE SCAFFOLD THROMBOSIS OF UNKNOWN CAUSE

A 56-year-old man with dyslipidaemia, a family history of coronary artery disease (CAD) and angina class II underwent PCI with a 3.0×18 mm Absorb BVS in the mid segment of the LAD (Figure 7A, Figure 7B). After Absorb BVS implantation, post-dilatation was performed with a 3.0×9.0 mm balloon (non-compliant balloon) at maximal pressure of 16 atm (rated balloon pressure: 18 atm).

At day 239, following a bee sting, he presented with an acute anterior STEMI. The patient was still on DAPT at that time. Urgent coronary angiography revealed total occlusion of the LAD, proximal to the previously implanted Absorb scaffold (Figure 7C). Following manual thrombectomy, an EES was successfully deployed (Figure 7D).

#### Discussion

The main findings of the current report are the following: 1) in the first 450 patients enrolled in the ABSORB EXTEND trial, scaffold dislodgement occurred in three cases; 2) all dislodgements occurred

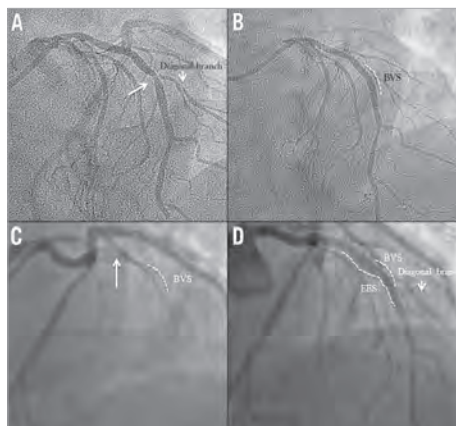


**Figure 7.** Case 7. A) Coronary angiography showing a moderate stenosis in the mid segment of the LAD. B) An Absorb BVS was successfully deployed at the target lesion. C) At day 239, coronary angiography revealed a total occlusion of the LAD, proximal to the previously implanted Absorb scaffold. D) Following manual thrombectomy, an EES was successfully deployed.

in the LCX, and in two cases dislodgement was observed after reinsertion of the same device; 3) two subacute scaffold thromboses and two late scaffold thromboses were observed; 4) two scaffold thromboses seemed to be related to either premature discontinuation of DAPT or resistance to clopidogrel.

### SCAFFOLD DISLODGEEMENT

Dislodgement of a metallic stent from the delivery balloon during deployment is a rare complication, reported in 0.32-1.2% of procedures in the early 2000s<sup>12</sup>. Metallic stent dislodgement from the delivery system occurs most often when the stent balloon device is pulled back into the guiding catheter, because the target lesion cannot be either reached or crossed despite a forceful pushing manoeuvre<sup>13-15</sup>. Risk factors for stent dislodgement include severe coronary angulations, coronary tortuosity, diffuse long lesions and calcified lesions. In addition, stent dislodgement has been reported to be the highest in the LMS or LAD<sup>16</sup>.

In the current series which included relatively simple lesions (mean lesion length: 11.6 mm, type B2/C lesions according to the American College of Cardiology/American Heart Association: 38.6%, calcification: 13.2%), scaffold dislodgement was observed in 0.67% (3/450). All cases of dislodgement occurred in the LCX (mean baseline vessel angulation: 45.0 degrees; mean baseline vessel curvature: 0.432 cm<sup>-1</sup>). One scaffold was dislodged when the crimped scaffold was retracted after the delivery failure of the device, one was dislodged from the balloon when the device was advanced through a 6 Fr daughter catheter, and one was observed after crossing the ostium of the LCX jailed by a metallic stent previously implanted in the LAD. Of these three cases, two scaffold dislodgements occurred when the same scaffolds were reinserted after failed delivery attempts.

The Absorb BVS has a crossing profile of 1.4 mm with a strut thickness of 156 µm, and consists of in-phase zigzag hoops linked by straight bridges<sup>17</sup>. Alternative processing techniques have been developed to enhance polymeric scaffold retention, and bench-top testing indicates retention forces equivalent to those observed with metallic stents. However, these thick polymeric struts with a large crossing profile may contribute to friction between the device and a tortuous/calcified vessel or a daughter catheter, resulting in device dislodgement when forcefully pushing the scaffold<sup>10</sup>. In case 3, a 6 Fr GuideLiner™ with a 6 Fr guiding catheter was used, which was not compatible with the current version of the Absorb scaffold. Usage of the 6 Fr GuideLiner™ system should be avoided.

The risk of scaffold dislodgement may increase with the combination of several factors, including tortuous and calcified vessels proximal to the target lesion, prolonged exposure to moisture during repeated removal and reinsertion of a scaffold, and friction against a tightly fitting delivery catheter (such as the GuideLiner™) where enough dimensional clearance for the scaffold is not assured. To prevent scaffold dislodgement, it is recommended to avoid prolonged contact with moisture in the setting of repeated removal and reinsertion of the same device after a failed delivery. It would be

advisable to use a new scaffold in such a situation. In the case of heavily calcified lesions, optimal lesion preparation using cutting/scoring balloons or rotational atherectomy should be considered before implantation of the Absorb BVS.

If dislodgement of a device occurs, prompt recognition and an attempt at percutaneous retrieval using a snare system or a multi-wire technique is advisable. If the retrieval manoeuvres are not technically feasible or fail, the dislodged scaffold could be crushed against the arterial wall by implantation of a metallic stent. In this case, however, the operator should be aware that the crushed polymeric scaffold will result in a circular and non-laminated structure as seen with crushed metallic stents.

### SCAFFOLD THROMBOSIS

Metallic stent thrombosis is multifactorial, including procedure-related factors such as underexpansion, multiple stent use, dissections, and late acquired stent malapposition due to resolution of thrombus on the vessel wall or abnormal vessel healing<sup>1-4,18</sup>.

In the current series, two subacute and two late scaffold thromboses were observed (0.89%). Acutely after implantation, PLLA polymer is, at least *in vitro*, somewhat less thrombogenic than a metal without a coating<sup>19</sup>. In the blood flow, however, the presence of thick struts creates alteration of shear stress, resulting in high shear stress on top of the strut and low shear stress behind the strut which may trigger platelet aggregation<sup>20</sup>. Preclinical reports have demonstrated that metallic stents with the thinner struts are less thrombogenic<sup>21,22</sup>. During the acute/subacute phase after implantation of an Absorb scaffold, efficient platelet inhibition is mandatory<sup>22</sup>. The optimal duration of DAPT after implantation of Absorb scaffolds has not been investigated. In a porcine coronary angioplasty model, the polymeric struts were associated with lesser granuloma formation than the first-generation sirolimus-eluting stents, suggesting that the bioresorption process does not provoke any significant inflammation. In the ABSORB Cohort B trial, tissue coverage as assessed by optical coherence tomography (OCT) was almost complete (97%) at six months<sup>5</sup>. The optimal duration of DAPT after implantation of Absorb scaffolds has not been investigated. The protocols of previous ABSORB trials mandated at least six months of DAPT. It is noteworthy that the mean duration of DAPT was 403 days in the ABSORB Cohort B trial<sup>5</sup>. Given the paucity of data, the optimal duration of DAPT should be prospectively assessed in future studies.

In the present series, late scaffold thrombosis occurred in one case with overlapping Absorb scaffolds. In a juvenile porcine model, the overlapping Absorb scaffolds showed delayed healing and slower tissue coverage than in non-overlapping scaffolds<sup>23</sup>: the coverage of the overlapping segment was 80.1% and 99.5% at 28 and 90 days after implantation, respectively, suggesting that complete coverage in humans may take up to 18 months<sup>4</sup>. In case of overlapping scaffolds, a relatively longer duration of DAPT with more potent agents (e.g., ticagrelor or prasugrel) could be considered.

One late scaffold thrombosis occurred following a bee sting. The mechanism responsible for STEMI in this patient could have been

coronary artery spasm (partly mediated by psychological stress related to the intensity of the anaphylactic reaction) with thrombosis secondary to cardiovascular collapse<sup>24</sup>. However, the precise mechanism of scaffold thrombosis in this case remains uncertain.

## Conclusion

This is the first report specifically describing the incidence and the potential mechanisms of scaffold dislodgement and scaffold thrombosis seen in the ABSORB EXTEND trial. To avoid scaffold dislodgement, appropriate lesion preparation is mandatory. In case of unsuccessful initial delivery, a second insertion of the same scaffold should be avoided. Adherence to antiplatelet therapy is of paramount importance to avoid acute or subacute scaffold thrombosis.

### Impact on daily practice

Bioresorbable scaffolds are increasingly used in patients with coronary artery disease undergoing percutaneous coronary interventions; however, the early clinical experiences in the ABSORB EXTEND trial (n=450) demonstrated scaffold dislodgement in 0.67% and scaffold thrombosis in 0.89% of cases. To avoid scaffold dislodgement, appropriate lesion preparation is mandatory and a second insertion of the same scaffold should be avoided. Adherence to the antiplatelet therapy is of paramount importance to avoid acute or subacute scaffold thrombosis.

## Guest Editor

This paper was guest edited by Antonio Colombo, MD, S. Raffaele Scientific Institute, Milan, Italy.

## Conflict of interest statement

The authors have no conflicts of interest to declare. The Guest Editor has no conflicts of interest to declare.

## References

1. Lüscher TF, Steffel J, Eberli FR, Joner M, Nakazawa G, Tanner FC, Virmani R. Drug-eluting stent and coronary thrombosis. Biological mechanisms and clinical implications. *Circulation*. 2007;115:1051-8.
2. Cook S, Wenaweser P, Togni M, Billinger M, Morger C, Seiler C, Vogel R, Hess O, Meier B, Windecker S. Incomplete stent apposition and very late stent thrombosis after drug-eluting stent implantation. *Circulation*. 2007;115:2426-34.
3. Farb A, Burke AP, Kolodgie FD, Virmani R. Pathological mechanisms of fatal late coronary stent thrombosis in humans. *Circulation*. 2003;108:1701-6.
4. Iakovou I, Schmidt T, Bonizzi E, Ge L, Sangiorgi GM, Stankovic G, Airoldi F, Chieffo A, Montorfano M, Carlino M, Michev I, Corvaja N, Brigatori C, Gerckens U, Grube E, Colombo A. Incidence, predictors and outcome of thrombosis after successful implantation of drug-eluting stents. *JAMA*. 2005;293:2126-30.
5. Onuma Y, Serruys PW, Ormiston JA, Regar E, Webster M, Thuesen L, Dudek D, Veldhof S, Rapoza R. Three-year results of clinical follow-up after a bioresorbable everolimus-eluting scaffold in patients with de novo coronary artery disease: the ABSORB trial. *EuroIntervention*. 2010;6:447-53.
6. Serruys PW, Onuma Y, Dudek D, Smits PC, Koolen J, Chevalier B, de Bruyne B, Thuesen L, McClean D, van Geuns RJ, Windecker S, Whitbourn R, Meredith I, Dorange C, Veldhof S, Hebert KM, Sudhir K, Garcia-Garcia HM, Ormiston JA. Evaluation of the second generation of a bioresorbable everolimus-eluting vascular scaffold for the treatment of de novo coronary artery stenosis: 12-month clinical and imaging outcomes. *J Am Coll Cardiol*. 2011;58:1578-88.
7. Dudek D, Onuma Y, Ormiston JA, Thuesen L, Miquel-Hebert K, Serruys PW. Four-year clinical follow-up of the ABSORB everolimus-eluting bioresorbable vascular scaffold in patients with de novo coronary artery disease: the ABSORB trial. *EuroIntervention*. 2012;7:1060-1.
8. Onuma Y, Serruys PW, Perkins LE, Okamura T, Gonzalo N, Garcia-Garcia HM, Regar E, Kamberi M, Powers JC, Rapoza R, van Beusekom H, van der Giessen W, Virmani R. Intracoronary optical coherence tomography and histology at 1 month and 2, 3, and 4 years after implantation of everolimus-eluting bioresorbable vascular scaffolds in a porcine coronary artery model: an attempt to decipher the human optical coherence tomography images in the ABSORB trial. *Circulation*. 2010;122:2288-300.
9. Serruys PW, Onuma Y, Ormiston JA, de Bruyne B, Regar E, Dudek D, Thuesen L, Smits PC, Chevalier B, McClean D, Koolen J, Windecker S, Whitbourn R, Meredith I, Dorange C, Veldhof S, Miquel-Hebert K, Rapoza R, Garcia-Garcia HM. Evaluation of the second generation of a bioresorbable everolimus drug-eluting vascular scaffold for treatment of de novo coronary artery stenosis: six-month clinical and imaging outcomes. *Circulation*. 2010;122:2301-12.
10. Oberhauser JP, Hossainy S, Rapoza R. Design principles and performance of bioresorbable polymeric vascular scaffolds. *EuroIntervention*. 2009;5:F15-22.
11. Muramatsu T, Onuma Y, Garcia-Garcia HM, Farooq V, Bourantas CV, Morel MA, Li X, Veldhof S, Bartorelli A, Whitbourn R, Abizaid A, Serruys PW; ABSORB-EXTEND Investigators. Incidence and short-term clinical outcomes of small side branch occlusion after implantation of an everolimus-eluting bioresorbable vascular scaffold: an interim report of 435 patients in the ABSORB-EXTEND single-arm trial in comparison with an everolimus-eluting metallic stent in the SPIRIT first and II trials. *JACC Cardiovasc Interv*. 2013;6:247-57.
12. Kwan TW, Chaudhry M, Huang Y, Liou M, Wong S, Zhou X, Pancholy S, Patel T. Approaches for dislodged stent retrieval during transradial percutaneous coronary interventions. *Catheter Cardiovasc Interv*. 2013;81:E245-9.
13. Curran PJ, Currier J, Tobis J. Percutaneous snare retrieval of a partially embedded Wallstent. *Catheter Cardiovasc Interv*. 2004; 61:400-2.
14. Eggebrecht H, Haude M, von Birgelen C, Oldenburg O, Baumgart D, Herrmann J, Welge D, Bartel T, Dages N, Erbel R. Nonsurgical retrieval of embolized coronary stents. *Catheter Cardiovasc Interv*. 2000;51:432-40.

15. Webb JG, Solankhi N, Carere RG. Facilitation of stent retention and retrieval with an emboli containment device. *Catheter Cardiovasc Interv*. 2000;50:215-7.
16. Laarman G, Muthusamy TS, Swart H, Westendorp I, Kiemeneij F, Slagboom T, van der Wieken R. Direct coronary stent implantation: safety, feasibility and predictors of success of the strategy of direct coronary stent implantation. *Catheter Cardiovasc Interv*. 2001;52:443-8.
17. Okamura T, Garg S, Gutiérrez-Chico JL, Shin ES, Onuma Y, García-García HM, Rapoza RJ, Sudhir K, Regar E, Serruys PW. In vivo evaluation of stent strut distribution patterns in the bioabsorbable everolimus-eluting device: an OCT ad hoc analysis of the revision 1.0 and revision 1.1 stent design in the ABSORB clinical trial. *EuroIntervention*. 2010;5:932-8.
18. Byrne RA, Kastrati A, Massberg S, Wiecek A, Laugwitz KL, Hadamitzky M, Schulz S, Pache J, Fusaro M, Hausleiter J, Schömig A, Mehilli J; ISAR-TEST 4 Investigators. Biodegradable polymer versus permanent polymer drug-eluting stents and everolimus- versus sirolimus-eluting stents in patients with coronary artery disease: 3-year outcomes from a randomized clinical trial. *J Am Coll Cardiol*. 2011;58:1325-31.
19. Seifert B, Romaniuk P, Groth TH. Bioresorbable, heparinized polymers for stent coating: in vitro studies on heparinization efficiency, maintenance of anticoagulant properties and improvement of stent haemocompatibility. *J Mater Sci Mater Med*. 1996;7:465-9.
20. Onuma Y, Serruys PW. The advent of a new era in percutaneous coronary and peripheral revascularization? *Circulation*. 2011;123:779-97.
21. Daemen J, Wenaweser P, Tsuchida K, Abrecht L, Vaina S, Morger C, Kukreja N, Juni P, Sianos G, Hellige G, van Domburg RT, Hess OM, Boersma E, Meier B, Windecker S, Serruys PW. Early and late coronary stent thrombosis of sirolimus-eluting and paclitaxel-eluting stents in routine clinical practice: data from a large two-institutional cohort study. *Lancet*. 2007;369:667-78.
22. Lüscher TF, Steffel J, Eberli FR, Joner M, Nakazawa G, Tanner FC, Virmani R. Drug-eluting stent and coronary thrombosis: biological mechanisms and clinical implications. *Circulation*. 2007;115:1051-8.
23. Farooq V, Serruys PW, Heo JH, Gogas BD, Onuma Y, Perkins LE, Diletti R, Radu MD, Räber L, Bourantas CV, Zhang Y, van Remortel E, Pawar R, Rapoza RJ, Powers JC, van Beusekom HM, García-García HM, Virmani R. Intracoronary optical coherence tomography and histology of overlapping everolimus-eluting bioreabsorbable vascular scaffolds in a porcine coronary artery model: the potential implications for clinical practice. *JACC Cardiovasc Interv*. 2013;6:523-32.
24. Kounis NG, Giannopoulos S, Tsigkas GG, Goudevenos J. Eosinophilic responses to stent implantation and the risk of Kounis hypersensitivity associated coronary syndrome. *Int J Cardiol*. 2012;156:125-32.



## 5.2 Scaffold restenosis

Early (before 6 months), late (6-12 months) and very late (after 12 months) angiographic scaffold restenosis in the ABSORB Cohort B trial.

*Eurointervention.* 2014 (Epub ahead of print)  
[Original research paper, Impact Factor (2013): 3.758]

Nakatani S, Onuma Y, Ishibashi Y, Muramatsu T, Iqbal J, Zhang YJ, van Geuns RJ, Ormiston JA, Serruys PW.





# Early (before 6 months), late (6-12 months) and very late (after 12 months) angiographic scaffold restenosis in the ABSORB Cohort B trial

Shimpei Nakatani<sup>1</sup>, MD; Yoshinobu Onuma<sup>1\*</sup>, MD; Yuki Ishibashi<sup>1</sup>, MD, PhD; Takashi Muramatsu<sup>1</sup>, MD, PhD; Javaid Iqbal<sup>1</sup>, MRCP, PhD; Yao-Jun Zhang<sup>1</sup>, MD, PhD; Robert-Jan van Geuns<sup>1</sup>, MD, PhD; John A. Ormiston<sup>2</sup>, MBChB, PhD; Patrick W. Serruys<sup>1</sup>, MD, PhD; on behalf of the ABSORB Cohort B investigators

1. Thoraxcenter, Erasmus Medical Center, Rotterdam, The Netherlands; 2. Auckland City Hospital, Auckland, New Zealand

GUEST EDITOR: Rafael Beyar, MD, DSc, MPH, Director, Rambam Health Care Campus, Women's Division/Dr Phillip and Sara Gottlieb Chair, Department of Medicine and Biomedical Engineering, Technion, Israel

## KEYWORDS

- bioresorbable scaffold
- everolimus
- intravascular imaging
- long-term follow-up
- restenosis

## Abstract

**Aims:** The long-term follow-up of the first-in-man ABSORB Cohort B trial showed that angiographic binary restenosis can occur early, late or very late after implantation of the Absorb everolimus-eluting bioresorbable vascular scaffold (Absorb BVS). Since the mechanical support of the scaffold decreases during bioresorption, the mechanism of in-segment restenosis (ISR) of the Absorb BVS might be different from that of metallic stents. The objective of the current analysis was to review the multimodality imaging of cases with binary restenosis to elucidate the mechanism of ISR after Absorb BVS implantation.

**Methods and results:** The ABSORB Cohort B trial enrolled 101 patients with a maximum of two *de novo* coronary lesions. At the three-year imaging and clinical follow-up, there were six cases of in-segment binary restenosis: two early ISR (<6 months), one late ISR (6-12 months) and three very late ISR (>12 months). Three of these ISR cases seemed to be induced by anatomical or procedural factors. In the other three cases, intravascular imaging (IVUS/OCT) demonstrated that the main mechanism of restenosis was significant intra-scaffold tissue growth, while the structural circularity and diameter of the scaffold were not affected.

**Conclusions:** Early and late restenosis after implantation of the Absorb bioresorbable scaffold could be related to anatomical or procedural factors. In this small cohort of patients late or very late restenosis seems to be attributed to pure intra-scaffold tissue growth without extrinsic encroachment of the scaffold.

---

\*Corresponding author: Thoraxcenter, Ba-583, 's Gravendijkwal 230, 3015 CE Rotterdam, The Netherlands.  
E-mail: yoshinobuonuma@gmail.com

© Europa Digital & Publishing 2014. All rights reserved.

## Introduction

The Absorb everolimus-eluting bioresorbable vascular scaffold (Absorb BVS; Abbott Vascular, Santa Clara, CA, USA) shows unique potential in vascular repair, such as late lumen enlargement, restoration of vasomotion and plaque media reduction<sup>1-4</sup>. However, in-scaffold restenosis may occur as frequently as with metallic drug-eluting stents (DES). Since the Absorb BVS loses its mechanical strength during bioresorption, unlike metallic stents, the mechanism of in-scaffold restenosis might be unique and different from DES and bare metal stents (BMS).

The process of lumen loss (LL) is a “time limited phenomenon” due to negative remodelling of the vessel and neointimal hyperplasia inside the stent, which occurs three to six months after implantation<sup>5,6</sup>. Beyond this critical period, the mechanical support of the scaffold and the active pharmacological inhibition of the neointima are no longer necessary. According to this concept, mechanical support of the scaffold could decrease approximately six months after implantation. Actually, it has been established in humans that the mechanical integrity is maintained over a period of six months but subsides afterwards<sup>7</sup>. However, one could speculate that the plaque behind the struts of the scaffold might progress and narrow the lumen once the scaffold has lost its mechanical strength.

Timing of restenosis and its potential mechanism after implantation of the Absorb BVS have not been investigated. We report six cases of ISR (quantitative coronary angiography [QCA] diameter stenosis  $\geq 50\%$  within the scaffolded segment and 5 mm proximal

and distal to the scaffolded segment) observed in the ABSORB Cohort B trial (101 patients, 102 lesions) according to the timing, and describe in detail the intravascular findings in an attempt to elucidate the mechanism of this complication. Two cases were early ISR (<6 months), one case was late ISR (6-12 months), and three cases were very late ISR (>12 months) (Table 1, Figure 1).

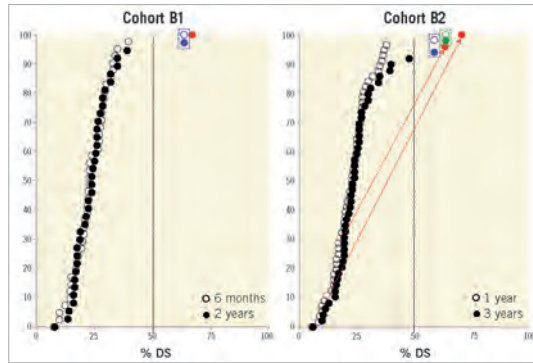
## Case histories

### CASE 1. EARLY ISR DUE TO MYOCARDIAL BRIDGE

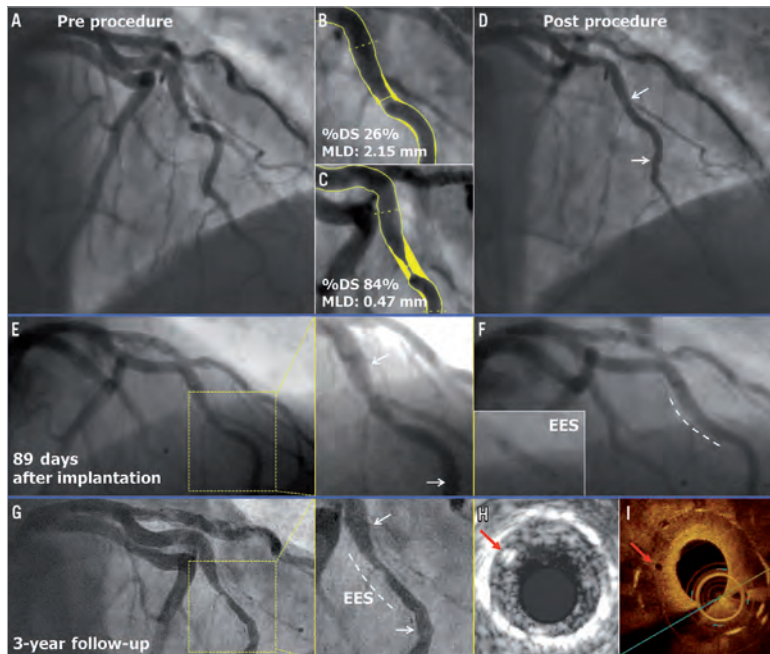
A 57-year-old man with a history of hypertension, dyslipidaemia, smoking and COPD presented with stable angina. The coronary angiography showed a type B2 lesion in the mid left anterior descending (LAD) artery with severe stenosis in systole (percentage diameter stenosis [%DS]: 84%), but without significant stenosis in diastole (%DS: 26%), thus with typical evidence of a myocardial bridge (Figure 2A-Figure 2C)<sup>8</sup>. After predilatation with a 2.75 mm semi-compliant balloon, a 3.0×18 mm Absorb BVS was deployed and post-dilated with a 3.5 mm non-compliant balloon at 16 atm (Figure 2D). On day 89, the patient experienced recurrent angina and underwent re-catheterisation. The angiography revealed a focal ISR at the site of the myocardial bridge (QCA minimum lumen diameter [MLD]: 1.20 mm, %DS: 59.0%, LL: 0.90 mm) (Figure 2E). This ISR was treated by implantation of a 3.5×15 mm XIENCE V stent (Abbott Vascular) inside the Absorb BVS (Figure 2F). At three years, angiography revealed a significant re-ISR of this XIENCE V stent (QCA MLD: 1.20 mm, %DS: 59.0%, LL: 0.90 mm) (Figure 2G).

Table 1. Case summary.

	Case 1	Case 2	Case 3	Case 4	Case 5	Case 6
Timing	Early	Early	Late	Very late	Very late	Very late
Day	89	168	354	383	567	833
Age	57	69	57	76	62	42
Sex	Male	Male	Male	Male	Male	Female
History of DM	no	no	no	no	no	no
<b>Pre procedure</b>						
RVD (mm)	2.51	2.05	2.64	2.82	2.97	2.24
Lesion length	10.3	5.9	12.0	8.1	15.4	10.2
%DS (%)	71.5	72.5	70.0	71.0	64.5	52.5
MLD (mm)	0.72	0.58	0.79	0.82	1.05	1.06
<b>Post procedure</b>						
%DS (%)	16.7	27.0	16.0	24.5	23.5	9.0
MLD (mm)	1.91	1.94	2.08	2.10	1.95	1.93
<b>At TLR</b>						
Clinical presentation	Stable angina	No angina	Stable angina	Unstable angina	Unstable angina	Stable angina
Examination for ischaemia	–	FFR: 0.72	Asynergy on echo.	–	–	Myocardial scintigram positive
%DS (%)	59.0	63.5	64.0	67.0	71.0	63.7
MLD (mm)	1.20	0.89	0.79	0.90	0.81	0.72
LL (mm)	0.90	0.50	1.58	1.20	1.47	1.38
DM: diabetes mellitus; RVD: reference vessel diameter; %DS: % diameter stenosis; MLD: minimum lumen diameter; LL: lumen loss; FFR: fractional flow reserve; TLR: target lesion revascularisation						



**Figure 1.** Cumulative frequency distribution curves of angiographic % diameter stenosis (%DS). A) %DS at 6 (circle) and 24 months (dot) of Cohort B1. B) %DS at 12 (circle) and 36 months (dot) of Cohort B2. If the patient had TLR before the planned angiography, %DS at the time of TLR (before repeat revascularisation) was used for the %DS at the later time point. Blue dots (●) and blue circles (○) represent %DS in TLR patients who experienced early ISR (<6 months). Green dots (●) and green circles (○) represent %DS in TLR patients who experienced late ISR (6-12 months). Red dots (●) and red circles (○) represent %DS in TLR patients who experienced very late ISR.



**Figure 2.** Early ISR due to myocardial bridge. The white arrows indicate the metallic markers of the implanted scaffold, while the white dotted line illustrates the implanted EES. The red arrows show the scaffold struts of the previously implanted Absorb BVS located inside the metal stent on IVUS (H) and OCT (I).

Optical coherence tomography (OCT) revealed intra-scaffold tissue growth with homogeneous light reflectivity. Of interest, OCT and intravascular ultrasound (IVUS) showed that some struts of the previously implanted Absorb BVS were located inside the metal stent (Figure 2H, Figure 2I). Finally, this re-ISR lesion was treated by a coronary artery bypass graft (CABG).

### CASE 2. EARLY ISR AT PROXIMAL EDGE

A 69-year-old male with a history of dyslipidaemia and previous coronary intervention of the left circumflex (LCX) artery presented with stable angina. Coronary angiography showed a type B1 severe stenosis in the mid right coronary artery (RCA) (Figure 3A). After predilatation with a 2.5 mm semi-compliant balloon, a 3.0×18 mm Absorb BVS was deployed and post-dilated with a 3.0 mm balloon at 15 atm (expected diameter according to the manufacturer was 3.3 mm) (Figure 3B). As the IVUS catheter failed to pass through the implanted scaffold, the guiding catheter was changed from JR4 to AL1. After repeated attempts to cross the IVUS catheter through the scaffold by seating the guiding catheter deeply up to the

proximal edge of the scaffold in order to perform the protocol-related imaging, the operator was unable to cross the scaffold and the procedure was ended (Figure 3C). On day 168, the patient underwent a planned repeat angiography, which showed a type 1B ISR at the proximal edge of the scaffold (QCA MLD: 0.89 mm, %DS: 63.5%, LL: 0.50 mm) without significant restenosis in the scaffold itself (Figure 3D). Greyscale IVUS (IVUS-GS) showed a high-echoic intra-scaffold tissue growth in the segment proximal to the scaffold, with maintained circularity of the scaffold (Figure 3E, Figure 3F). This ISR was treated by implantation of a 3×28 mm XIENCE V stent with full coverage of the previously implanted Absorb BVS.

### CASE 3. LATE ISR WITH HOMOGENEOUS INTRA-SCAFFOLD TISSUE ON OCT

In a 57-year-old man with a history of dyslipidaemia and smoking, and presenting with unstable angina, coronary angiography showed a severe type B1 stenosis in the proximal LAD with TIMI grade 2 flow (Figure 4A). After predilatation with a 2.5 mm semi-compliant

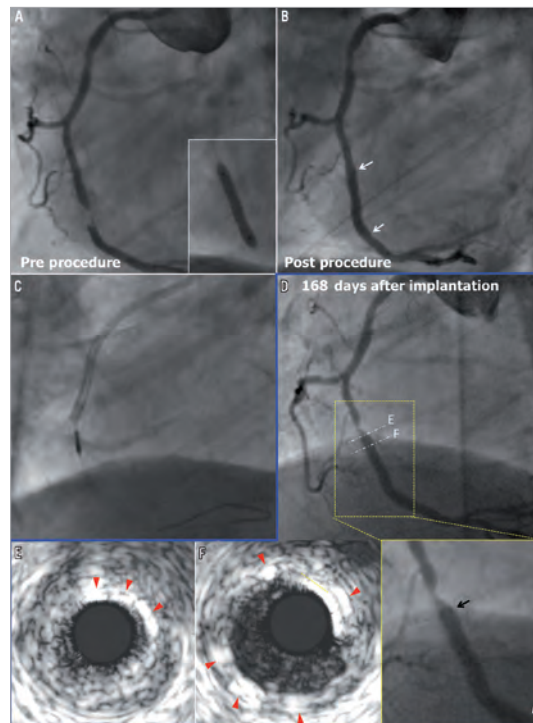
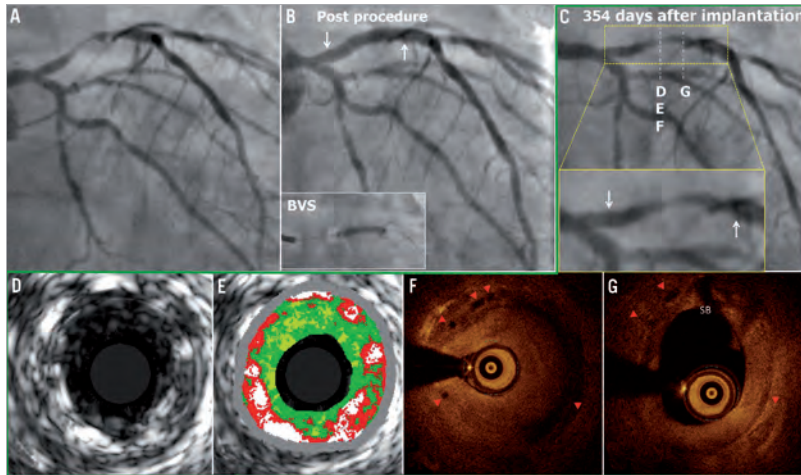


Figure 3. Early ISR at proximal edge. The white and black arrows indicate the metallic markers of the implanted scaffold. In panels E and F, the red arrows show the polymeric strut on IVUS.



**Figure 4.** Late ISR with homogeneous intra-scaffold tissue on OCT. The white arrows show the metallic marker of the implanted scaffold. In panels F and G, the red triangles show the scaffold struts on OCT (case 3).

balloon, a 3.0×18 mm Absorb BVS was deployed and post-dilated with a 3.0 mm non-compliant balloon at 20 atm (Figure 4B). On day 348, the patient had recurrence of angina pectoris. On day 354, the patient underwent a planned repeat angiography, which showed a significant type 1C ISR (QCA MLD: 0.79 mm, %DS: 64.0%, LL: 1.58 mm) in the body of the scaffold (Figure 4C)<sup>9</sup>. OCT showed that the circularity of the scaffold was maintained throughout the pull-back (the mean scaffold area was 5.67 mm<sup>2</sup> and the minimum scaffold area was 4.73 mm<sup>2</sup>) and all the struts were completely apposed and covered. At the site of the minimal lumen area (MLA), OCT revealed homogeneous signal-rich intra-scaffold tissue (Figure 4D-Figure 4G). On virtual histology IVUS (IVUS-VH), intra-scaffold tissue was documented as fibrous (Figure 4E). A XIENCE V stent was implanted to cover the previously implanted Absorb BVS.

#### CASE 4. VERY LATE ISR AT THE PROXIMAL EDGE

A 76-year-old gentleman with a history of dyslipidaemia, chronic kidney failure and coronary intervention to the mid LAD (non-target lesion) presented with stable angina. The coronary angiography showed a type B1 moderate stenosis in the mid LAD (Figure 5A). After predilatation with a 2.5 mm semi-compliant balloon, a 3.0×18 mm Absorb BVS was deployed. However, the Absorb BVS did not cover the proximal part of the predilated segment, resulting in a geographical miss (Figure 5B). After implantation of the scaffold, the jailed diagonal branch became occluded. Since this closure resulted in chest pain, bradycardia and hypotension, the side branch was dilated with a 1.5 mm balloon (Figure 5C). OCT post procedure revealed a small dissection in the proximal edge of

the scaffold, presumably due to the geographical miss during the procedure (Figure 5D, Figure 5E). The patient refused the scheduled follow-up angiography at six months. One year later, the patient presented with recurrence of angina pectoris, and repeat angiography showed a type 1B ISR in the segment proximal to the scaffold (QCA MLD: 0.90 mm, %DS: 67.0%, LL: 1.20 mm) (Figure 5F), while the scaffolded segment was free from significant restenosis<sup>9</sup>. A 3.0×15 mm XIENCE V stent was implanted to overlap the proximal part of the previously implanted Absorb BVS.

#### CASE 5. VERY LATE ISR WITH HOMOGENEOUS INTRA-SCAFFOLD TISSUE ON OCT

A 62-year-old man with a history of hypertension, smoking and COPD presented with stable angina. Coronary angiography showed a type B1 severe stenosis in the proximal LAD (Figure 6A). Although the proximal maximum luminal diameter (Dmax) on QCA was 3.90 mm, a 3.0 mm Absorb BVS was planned (Figure 6B, Figure 6C). After predilatation with a 2.5 mm semi-compliant balloon, this 3.0×18 mm Absorb BVS was implanted and post-dilated with a 3.5 mm non-compliant balloon at 12 atm (Figure 6F). Post-procedural OCT showed large incomplete stent apposition (ISA) (max ISA area: 11.89 mm<sup>2</sup>, max ISA distance 1.63 mm, the number of cross-sections with ISA: 25 frames) at the proximal edge of the scaffold, but additional dilatation was not performed (Figure 6D, Figure 6E). At one year, the planned follow-up coronary angiography showed patency of the scaffold (QCA MLD: 1.99 mm, %DS: 10.0%, LL: -0.04 mm) (Figure 6G). OCT showed persistent numerous malapposed struts with intraluminal mass attached to or free from the vessel wall at the proximal edge of the previously

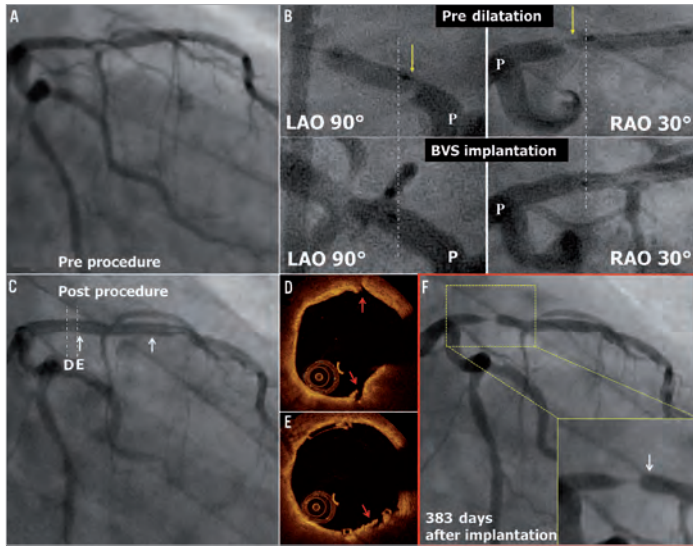


**Figure 5.** Very late ISR at the proximal edge. The white arrows show the metallic marker of the implanted scaffold. In panel B, the yellow arrows show the proximal edge of the predilatation balloon. The angiograms are matched anatomically between predilatation and scaffold implantation, and the white dotted lines show the proximal edge of the implanted scaffold. The red arrows show the small dissection observed post procedure on OCT in panels D and E.

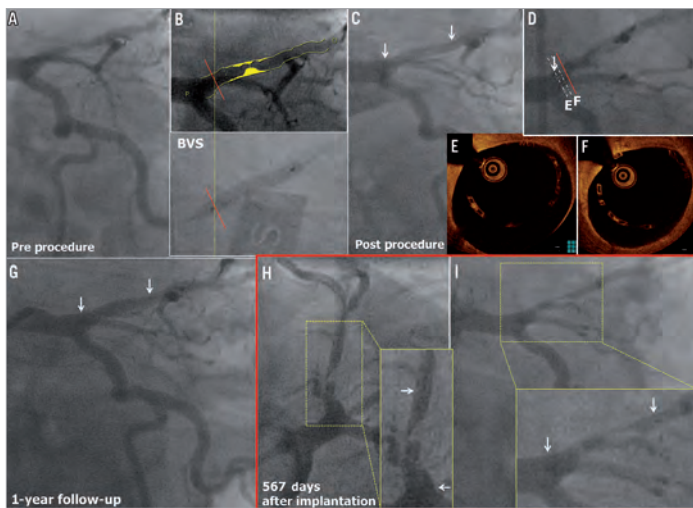


**Figure 6.** Very late ISR with homogeneous intra-scaffold tissue on OCT. The white arrows show the metallic marker of the implanted scaffold. The red line shows the point of Dmax on QCA, which is superimposed on the angiogram at scaffold implantation in panel B. The red line is superimposed on the angiogram at OCT study in panel D (case 5).

implanted scaffold (**Figure 7a**). On the three-dimensional OCT image, the intraluminal masses were interlinked to the malapposed struts and connected proximally to the vessel wall (**Figure 7a'**). On day 564 the patient was hospitalised with unstable angina and underwent a repeat angiography on day 567, which showed a type 1C ISR in the body of the scaffold (QCA MLD: 0.81 mm, %DS: 71.0% and LL: 1.47 mm)<sup>9</sup>. OCT showed homogeneous signal-rich intra-scaffold tissue in the middle of the scaffold segment with persistent malapposed struts at the proximal edge (**Figure 7B-E**)<sup>10</sup>. After predilatation, repeat OCT revealed an extensive tissue protrusion with maintained circularity of the scaffold (**Figure 7B'-E'**). On OCT analysis, the mean scaffold area was 8.32 mm<sup>2</sup>, and the minimum scaffold area was 6.23 mm<sup>2</sup> (**Figure 7A**). This ISR was treated by implantation of a 3.0×18 mm XIENCE V stent which overlapped the proximal part of the previously implanted Absorb BVS.

**CASE 6. VERY LATE ISR WITH ISO-ECHOIC INTRA-SCAFFOLD TISSUE ON IVUS-GS**

In a 42-year-old female with a history of smoking presenting with stable angina, coronary angiography demonstrated a type B1 moderate stenosis in the mid LAD (**Figure 8A**). After predilatation with a 2.5 mm semi-compliant balloon, a 3.0×18 mm Absorb BVS was implanted. After post-dilatation with a 3.0 mm non-compliant balloon at 20 atm, post-procedural angiography showed a residual stenosis of 9.0% (**Figure 8B**). At one year, a planned repeat angiography showed patency of the previously implanted scaffold (QCA MLD was 1.73 mm, %DS was 18.0% and LL was 0.35 mm) (**Figure 8C**). On day 833, the patient underwent a repeat angiography because of stable angina with ischaemia on a myocardial scintigraphy: the angiogram showed a type 1B ISR at the distal margin of the scaffold segment (QCA MLD: 0.72 mm, %DS: 63.7% and LL: 1.38 mm)

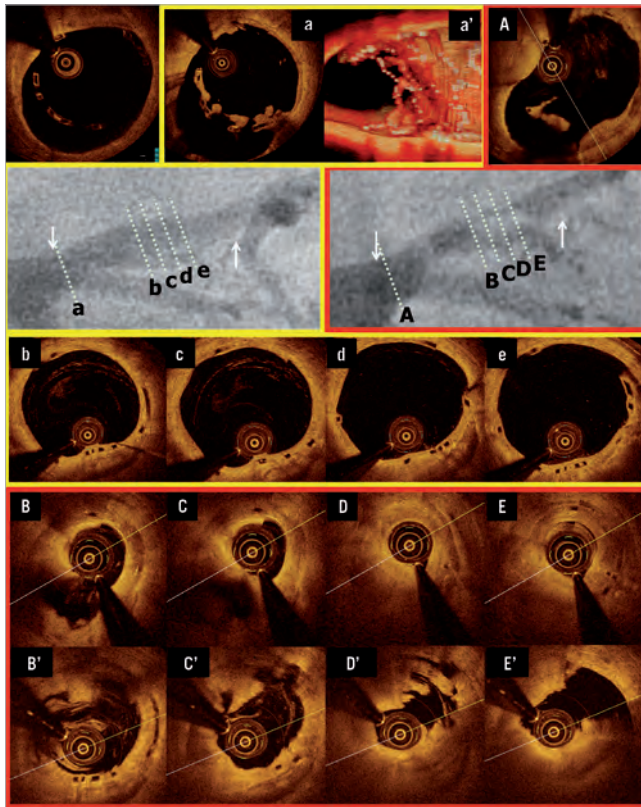


**Figure 7.** Very late ISR with homogeneous intra-scaffold tissue on OCT. The white arrows show the metallic marker of the implanted scaffold. OCT images pre TLR before ballooning are shown in panels B to E, and those after ballooning are shown in panels B' to E'. In panels b to e, the corresponding cross-sections to ISR site are shown at 12-month follow-up.

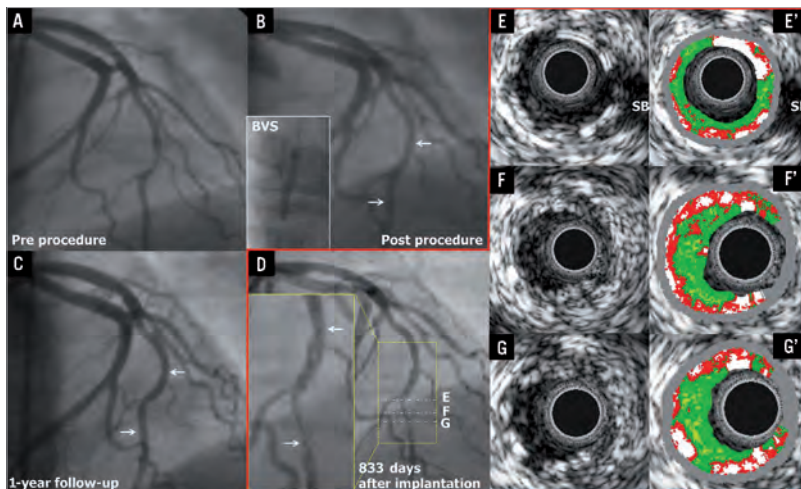


**Figure 8.** Very late ISR with iso-echoic intra-scaffold tissue on IVUS-GS. The white arrows show the metallic marker of the implanted scaffold.

(Figure 8D)<sup>9</sup>. IVUS-GS showed that the scaffold circularity was maintained and that the eccentric intra-scaffold tissue was iso-echoic (Figure 8E-G). On IVUS-VH, small necrotic core and dense calcium were detected in the intra-scaffold tissue (Figure 8E'-G'). In this case, the ISR lesion was treated by the implantation of a 3.0×23 mm XIENCE V which overlapped the distal part of the previously implanted Absorb BVS.

## Discussion

The main findings of the current report are the following: 1) out of 101 patients enrolled in the ABSORB trial, at three years early restenosis occurred in two cases (2.0%), late ISR in one case (1.0%), and very late ISR in three cases (3.0%); 2) the early ISR was associated with a myocardial bridge (case 1); 3) two of the three late ISR cases may have been caused by procedural edge injury at the index procedure (one case was due to the injury caused by deep insertion of the guiding catheter [case 2], while the other case could be attributed to proximal geographical miss [case 4]); 4) in three cases (one late ISR and two very late ISR), the mechanism of ISR could not be identified (case 3, case 5, and case 6), but in all cases the circularity of the scaffold was maintained.

It is noteworthy that ISR occurred in patients without diabetes, with relatively large vessels (reference vessel diameter 3 or more mm) and short lesion length (less than 10 mm).

### ISR ASSOCIATED WITH MYOCARDIAL BRIDGE

Myocardial bridging (MB) is a potential cause of myocardial ischaemia and in such cases medical therapy, with beta-blockers or calcium channel blockers, is recommended as a first-line strategy<sup>8,11</sup>.

Although intracoronary stent implantation is another therapeutic approach to prevent external systolic compression and ischaemia caused by the MB, this therapy is still controversial because of concerns regarding high restenosis rates, plaque prolapse and stent fracture<sup>12,13</sup>. In the current series, one early TLR occurred in a myocardial bridge at three months after implantation of an Absorb BVS, followed by a second failure occurring after implantation of a metallic drug-eluting stent. This case suggests that scaffold implantation for a myocardial bridge treatment should be discouraged. Myocardial bridges generate compressive pressure (up to 300 mmHg) capable of fully closing the vessel in systole. Although the initial radial strength of an Absorb BVS is approximately 900 mmHg and superior to this compressive pressure, this systolic external compression occurs at least 100,000 times/day, and in the course of bioresorption a bioresorbable transient scaffold might yield to such a mechanical stress<sup>5,14</sup>.

In this case, at three years, OCT and IVUS detected one scaffold strut inside the area of the metal stent, while post procedure no disrupted strut had been detected on IVUS. The location of a polymeric strut inside the metallic stent may suggest that the discontinued strut could protrude between the metallic mesh of the stent after TLR at three months.

### ISR PRESUMABLY TRIGGERED BY PROCEDURAL INJURY

It has been shown that procedural vessel injury might lead to late intra-scaffold tissue growth<sup>15</sup>. In one case in the current series, the deeply inserted AL1 guide catheter might have injured the edge of the scaffold at baseline and led to proximal edge ISR at six months.

Geographical miss is also a known cause of restenosis<sup>16,17</sup>. In one case, the predilatation might have caused “barotrauma” to the proximal plaque and the Absorb BVS did not cover the injured edge segment. Actually, a proximal edge dissection not scaffolded by the Absorb BVS was observed on OCT. The edge ISR could therefore be related to the proximal plaque injury associated with geographical miss<sup>18</sup>.

#### MAINTAINED CIRCULARITY OF SCAFFOLD AREA IN LATE/VERY LATE ISR

As previously described, the radial strength of the fully bioresorbable scaffold declines following polymer hydrolysis at six months, and this device becomes malleable without any supportive properties at 12 months. One could therefore speculate that the scaffold might become encroached by plaque growth behind the struts. In the balloon angioplasty era, Serruys et al demonstrated that the incidence of restenosis reaches a plateau at four months<sup>6</sup>. Ormiston et al demonstrated that the late loss in response to balloon injury reached a maximum before six months and then regressed, while some cases with an intermediate stenosis at six months showed very late lumen narrowing at five years<sup>19</sup>.

In this study, we observed three ISR cases without any possible causal relationship with procedural or anatomical factors: one case presented a late ISR and two cases a very late ISR. As shown in **Figure 9**, the circularity of the Absorb BVS, especially at MLA cross-section, was preserved post procedure in all cases. In addition, there were no changes in mean/minimum scaffold area.

This report suggests that the perceived relative weakness of the scaffold related to its polymeric nature does not seem to have any direct impact on the restenosis phenomenon, and late lumen loss seems to be the result of intra-scaffold tissue growth rather than late scaffold recoil.

Late and very late restenosis have also been reported with metallic drug-eluting stents. In the SPRIT II trial, the rate of ischaemia-driven TLR steadily increased from 1.8% at one year to 3.8% at two years and 4.6% at three years<sup>20-22</sup>. In the ABSORB Cohort B trial, the rate of ischaemia-driven TLR beyond one year increased similarly (4.0% at one year, 5.0% at two years, and 5.9% at three years). These data suggest that ISR with the Absorb BVS occurs as frequently as with metallic DES, and a reduced mechanical strength of the scaffold cannot be implicated in the occurrence of ISR.

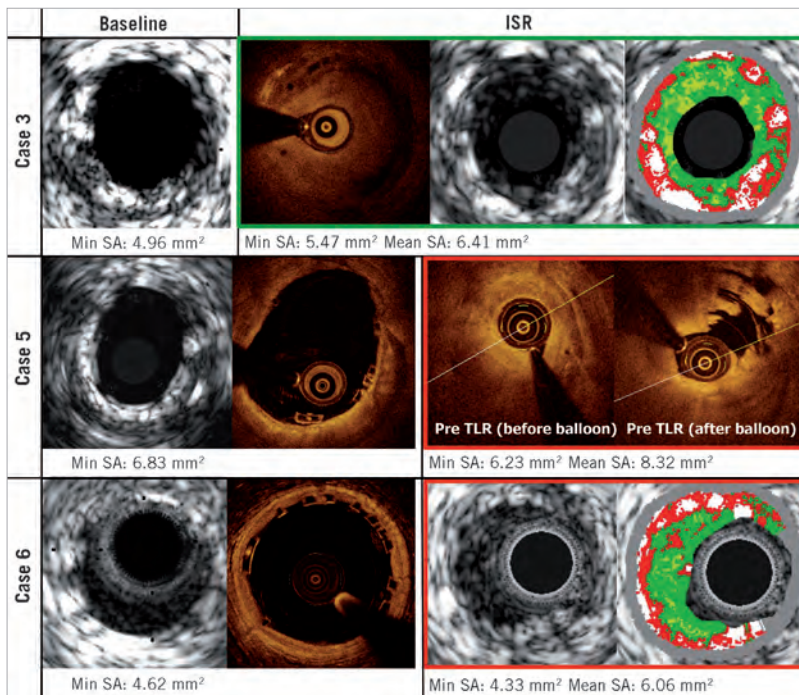


**Figure 9.** Intravascular imaging of the late and very late restenosis.

## MORPHOLOGICAL CHARACTERISTICS OF INTRA-SCAFFOLD TISSUE IN LATE/VERY LATE ISR

On IVUS-VH, a typical neointimal restenosis within one year after BMS implantation appears as fibrous or fibro-fatty tissue (green or green-yellow)<sup>23</sup>. Neointima after DES implantation or beyond one year after BMS implantation is sometimes detected as necrotic core tissue (red and red-white) on IVUS-VH<sup>23</sup>. It should be noted that intramural thrombus also has the appearance of fibrous or fibro-fatty tissue<sup>24</sup>. In the current series, two IVUS-VH images were available: one was a late ISR and the other was a very late ISR. In the late ISR case, the intra-scaffold tissue appeared as fibrous tissue, while, in the very late ISR case, the small necrotic core and dense calcium were interspersed in fibrous tissue (**Figure 9**).

OCT has been used to evaluate the efficacy of stenting by analysing tissue characteristics of in-stent intima<sup>25</sup>. Goto et al demonstrated that homogeneous high-signal band is a typical in-stent intima within one year after BMS implantation, while heterogeneous mixed-signal band is observed at all timing points after DES implantation<sup>24</sup>. In the current series, two OCT images were available: both of them were late ISR. In these cases, the intra-scaffold tissue appeared as a homogeneous tissue (**Figure 9**).

## Limitations

The sample size was small and the first-in-man trial had no control arm. The current findings therefore need to be confirmed in a large randomised trial.

## Conclusion

The current analysis suggests that early and late restenosis after implantation of the Absorb bioresorbable scaffold could be related to anatomical or procedural factors. Late or very late restenosis could be attributed to intra-scaffold tissue growth but not to the encroachment of the scaffold.

### Impact on daily practice

Since the Absorb everolimus-eluting bioresorbable vascular scaffold (BVS) loses its mechanical strength during bioresorption, the mechanism of in-scaffold restenosis (ISR) could be different from metallic stents. In the ABSORB Cohort B trial, at three years, ISR with the BVS occurs as frequently as with drug-eluting metallic stents. By investigating the ISR according to the time line of the mechanical change of the BVS, the perceived relative weakness of the scaffold does not seem to have any direct impact on the restenosis phenomenon, and seems to be the result of intra-scaffold tissue growth rather than late scaffold recoil and extrinsic encroachment of the scaffold. The disappearance of the device was not found to be a disadvantage in relation to ISR in the current study.

## Guest Editor

This paper was guest edited by Rafael Beyar, MD, DSc, MPH, Director, Rambam Health Care Campus, Women's Division/

Dr Phillip and Sara Gottlieb Chair, Department of Medicine and Biomedical Engineering, Technion, Israel.

## Funding

The ABSORB trial was sponsored by Abbott Vascular.

## Conflict of interest statement

The authors have no conflicts of interest to declare. The Guest Editor has no conflicts of interest to declare.

## References

1. Ormiston JA, Serruys PW, Onuma Y, van Geuns RJ, de Bruyne B, Dudek D, Thuesen L, Smits PC, Chevalier B, McClean D, Koolen J, Windecker S, Whitbourn R, Meredith I, Dorange C, Veldhof S, Hebert KM, Rapoza R, Garcia-Garcia HM. First serial assessment at 6 months and 2 years of the second generation of absorb everolimus-eluting bioresorbable vascular scaffold: a multi-imaging modality study. *Circ Cardiovasc Interv.* 2012;5:620-32.
2. Serruys PW, Ormiston JA, Onuma Y, Regar E, Gonzalo N, Garcia-Garcia HM, Nieman K, Bruining N, Dorange C, Miquel-Hebert K, Veldhof S, Webster M, Thuesen L, Dudek D. A bioabsorbable everolimus-eluting coronary stent system (ABSORB): 2-year outcomes and results from multiple imaging methods. *Lancet.* 2009;373:897-910.
3. Serruys PW, Onuma Y, Dudek D, Smits PC, Koolen J, Chevalier B, de Bruyne B, Thuesen L, McClean D, van Geuns RJ, Windecker S, Whitbourn R, Meredith I, Dorange C, Veldhof S, Hebert KM, Sudhir K, Garcia-Garcia HM, Ormiston JA. Evaluation of the second generation of a bioresorbable everolimus-eluting vascular scaffold for the treatment of de novo coronary artery stenosis: 12-month clinical and imaging outcomes. *J Am Coll Cardiol.* 2011;58:1578-88.
4. Onuma Y, Serruys PW, Ormiston JA, Regar E, Webster M, Thuesen L, Dudek D, Veldhof S, Rapoza R. Three-year results of clinical follow-up after a bioresorbable everolimus-eluting scaffold in patients with de novo coronary artery disease: the ABSORB trial. *EuroIntervention.* 2010;6:447-53.
5. Nobuyoshi M, Kimura T, Nosaka H, Mioka S, Ueno K, Yokoi H, Hamasaki N, Horiuchi H, Ohishi H. Restenosis after successful percutaneous transluminal coronary angioplasty: serial angiographic follow-up of 229 patients. *J Am Coll Cardiol.* 1988;12:616-23.
6. Serruys PW, Luijten HE, Beatt KJ, Geuskens R, de Feyter PJ, van den Brand M, Reiber JH, ten Katen HJ, van Es GA, Hugenholtz PG. Incidence of restenosis after successful coronary angioplasty: a time-related phenomenon. A quantitative angiographic study in 342 consecutive patients at 1, 2, 3, and 4 months. *Circulation.* 1988;77:361-71.
7. Onuma Y, Serruys PW, Gomez J, de Bruyne B, Dudek D, Thuesen L, Smits P, Chevalier B, McClean D, Koolen J, Windecker S, Whitbourn R, Meredith I, Garcia-Garcia H, Ormiston JA; ABSORB Cohort A and B investigators. Comparison of in vivo acute stent

recoil between the bioresorbable everolimus-eluting coronary scaffolds (revision 1.0 and 1.1) and the metallic everolimus-eluting stent. *Catheter Cardiovasc Interv*. 2011;78:3-12.

8. Ge J, Erbel R, Rupprecht HJ, Koch L, Kearney P, Gorge G, Haude M, Meyer J. Comparison of intravascular ultrasound and angiography in the assessment of myocardial bridging. *Circulation*. 1994;89:1725-32.

9. Mehran R, Dangas G, Abizaid AS, Mintz GS, Lansky AJ, Satler LF, Pichard AD, Kent KM, Stone GW, Leon MB. Angiographic patterns of in-stent restenosis: classification and implications for long-term outcome. *Circulation*. 1999;100:1872-8.

10. Tearney GJ, Regar E, Akasaka T, Adriaenssens T, Barlis P, Bezerra HG, Bouma B, Bruining N, Cho JM, Chowdhary S, Costa MA, de Silva R, Dijkstra J, Di Mario C, Dudek D, Falk E, Feldman MD, Fitzgerald P, Garcia-Garcia HM, Gonzalo N, Granada JF, Guagliumi G, Holm NR, Honda Y, Ikeno F, Kawasaki M, Kochman J, Koltowski L, Kubo T, Kume T, Kyono H, Lam CC, Lamouche G, Lee DP, Leon MB, Machara A, Manfrini O, Mintz GS, Mizuno K, Morel MA, Nadkarni S, Okura H, Otake H, Pietrasik A, Prati F, Raber L, Radu MD, Rieber J, Riga M, Rollins A, Rosenberg M, Sirbu V, Serruys PW, Shimada K, Shinke T, Shite J, Siegel E, Sonoda S, Suter M, Takarada S, Tanaka A, Terashima M, Thim T, Uemura S, Ughi GJ, van Beusekom HM, van der Steen AF, van Es GA, van Soest G, Virmani R, Waxman S, Weissman NJ, Weisz G; International Working Group for Intravascular Optical Coherence Tomography (IWG-IVOCT). Consensus standards for acquisition, measurement, and reporting of intravascular optical coherence tomography studies: a report from the International Working Group for Intravascular Optical Coherence Tomography Standardization and Validation. *J Am Coll Cardiol*. 2012;59:1058-72.

11. Schwarz ER, Klues HG, vom Dahl J, Klein I, Krebs W, Hanrath P. Functional, angiographic and intracoronary Doppler flow characteristics in symptomatic patients with myocardial bridging: effect of short-term intravenous beta-blocker medication. *J Am Coll Cardiol*. 1996;27:1637-45.

12. Tandar A, Whisenant BK, Michaels AD. Stent fracture following stenting of a myocardial bridge: report of two cases. *Catheter Cardiovasc Interv*. 2008;71:191-6.

13. Arora P, Bhatia V, Parida AK, Kaul U. Myocardial bridge in association with fixed atherosclerotic lesions treated with drug-eluting stents: a follow-up report with quantitative coronary analysis. *Indian Heart J*. 2008;60:594-6.

14. Oberhauser JP, Hossainy S, Rapoza RJ. Design principles and performance of bioresorbable polymeric vascular scaffolds. *EuroIntervention*. 2009;5:F15-22.

15. Lee JH, Kim EM, Ahn KT, Kim MS, Kim KS, Jung IS, Park JH, Choi SW, Seong IW, Jeong JO. Significant left main coronary artery disease from iatrogenic dissection during coronary angiography. *Int J Cardiol*. 2010;138:e35-7.

16. Costa MA, Angiolillo DJ, Tannenbaum M, Driesman M, Chu A, Patterson J, Kuehl W, Battaglia J, Dabbons S, Shamoon F,

Fliesman B, Niederman A, Bass TA; STLLR Investigators. Impact of stent deployment procedural factors on long-term effectiveness and safety of sirolimus-eluting stents (final results of the multicenter prospective STLLR trial). *Am J Cardiol*. 2008;101:1704-11.

17. Sabate M, Costa MA, Kozuma K, Kay IP, van der Giessen WJ, Coen VL, Ligthart JM, Serrano P, Levendag PC, Serruys PW. Geographic miss: a cause of treatment failure in radio-oncology applied to intracoronary radiation therapy. *Circulation*. 2000;101:2467-71.

18. Gogas BD, Onuma Y, van Geuns RJ, Serruys PW. The edge vascular response following implantation of a fully bioresorbable device: 'a miss always counts'. *Int J Cardiol*. 2012;158:455-7.

19. Ormiston JA, Stewart FM, Roche AH, Webber BJ, Whitlock RM, Webster MW. Late regression of the dilated site after coronary angioplasty: a 5-year quantitative angiographic study. *Circulation*. 1997;96:468-74.

20. Claessen BE, Beijk MA, Legrand V, Ruzyllo W, Manari A, Varenne O, Suttorp MJ, Tijssen JG, Miquel-Hebert K, Veldhof S, Henriques JP, Serruys PW, Piek JJ. Two-year clinical, angiographic, and intravascular ultrasound follow-up of the XIENCE V everolimus-eluting stent in the treatment of patients with de novo native coronary artery lesions: the SPIRIT II trial. *Circ Cardiovasc Interv*. 2009;2:339-47.

21. Garg S, Serruys P, Onuma Y, Dorange C, Veldhof S, Miquel-Hebert K, Sudhir K, Boland J, Huber K, Garcia E, te Riele JA; SPIRIT II Investigators. 3-year clinical follow-up of the XIENCE V everolimus-eluting coronary stent system in the treatment of patients with de novo coronary artery lesions: the SPIRIT II trial (Clinical Evaluation of the Xience V Everolimus Eluting Coronary Stent System in the Treatment of Patients with de novo Native Coronary Artery Lesions). *JACC Cardiovasc Interv*. 2009;2:1190-8.

22. Ruygrok PN, Desaga M, Van Den Branden F, Rasmussen K, Suryapranata H, Dorange C, Veldhof S, Serruys PW. One year clinical follow-up of the XIENCE V Everolimus-eluting stent system in the treatment of patients with de novo native coronary artery lesions: the SPIRIT II study. *EuroIntervention*. 2007;3:315-20.

23. Wakabayashi K, Mintz G, Delhaye C, Choi YJ, Doh JH, Bendor I, Gaglia M Jr, Pakala R, Suddath W, Satler L, Kent K, Pichard A, Weissman N, Waksman R. In vivo virtual histology intravascular ultrasound comparison of neointimal hyperplasia within drug-eluting versus bare metal stents. *J Invasive Cardiol*. 2011;23:262-8.

24. Nasu K, Tsuchikane E, Katoh O, Vince DG, Margolis PM, Virmani R, Surmely JF, Ehara M, Kinoshita Y, Fujita H, Kimura M, Asakura K, Asakura Y, Matsubara T, Terashima M, Suzuki T. Impact of intramural thrombus in coronary arteries on the accuracy of tissue characterization by in vivo intravascular ultrasound radiofrequency data analysis. *Am J Cardiol*. 2008;101:1079-83.

25. Gonzalo N, Serruys PW, Okamura T, van Beusekom HM, Garcia-Garcia HM, van Soest G, van der Giessen W, Regar E. Optical coherence tomography patterns of stent restenosis. *Am Heart J*. 2009;158:284-93.



### 5.3 Acute disruption and late discontinuities

Incidence and imaging outcomes of acute scaffold disruption and late structural discontinuity after implantation of the Absorb everolimus-eluting fully bioresorbable scaffolds:

Optical coherence tomography assessment in the ABSORB Cohort B trial.

*JACC Cardiovasc Interv.* 2014;7:1400-11.

[Original research paper, Impact Factor (2013): 7.440]

Onuma Y, Serruys PW, Muramatsu T, Nakatani S, van Geuns RJ, de Bruyne B, Dudek D, Thuesen L, Smits PC, Chevalier B, McClean D, Koolen J, Windecker S, Whitbourn R, Meredith IT, Garcia-Garcia HM, Veldhof S, Rapoza R, Ormiston JA.





# Incidence and Imaging Outcomes of Acute Scaffold Disruption and Late Structural Discontinuity After Implantation of the Absorb Everolimus-Eluting Fully Bioresorbable Vascular Scaffold



## Optical Coherence Tomography Assessment in the ABSORB Cohort B Trial (A Clinical Evaluation of the Bioabsorbable Everolimus Eluting Coronary Stent System in the Treatment of Patients With De Novo Native Coronary Artery Lesions)

Yoshinobu Onuma, MD,\* Patrick W. Serruys, MD, PhD,\* Takashi Muramatsu, MD, PhD,\* Shimpei Nakatani, MD,\* Robert-Jan van Geuns, MD, PhD,\* Bernard de Bruyne, MD, PhD,† Dariusz Dudek, MD,‡ Evald Christiansen, MD,§ Pieter C. Smits, MD, PhD,|| Bernard Chevalier, MD,¶ Dougal McClean, MD,# Jacques Koolen, MD, PhD,\*\* Stephan Windecker, MD,†† Robert Whitbourn, MD,‡‡ Ian Meredith, MD, PhD,§§ Hector M. Garcia-Garcia, MD, PhD,|||| Susan Veldhof, RN,¶¶ Richard Rapoza, PhD,## John A. Ormiston, MChB, PhD\*\*\*

### ABSTRACT

**OBJECTIVES** This study sought to describe the frequency and clinical impact of acute scaffold disruption and late strut discontinuity of the second-generation Absorb bioresorbable polymeric vascular scaffolds (Absorb BVS, Abbott Vascular, Santa Clara, California) in the ABSORB (A Clinical Evaluation of the Bioabsorbable Everolimus Eluting Coronary Stent System in the Treatment of Patients With De Novo Native Coronary Artery Lesions) cohort B study by optical coherence tomography (OCT) post-procedure and at 6, 12, 24, and 36 months.

**BACKGROUND** Fully bioresorbable scaffolds are a novel approach to treatment for coronary narrowing that provides transient vessel support with drug delivery capability without the long-term limitations of metallic drug-eluting stents. However, a potential drawback of the bioresorbable scaffold is the potential for disruption of the strut network when over-expanded. Conversely, the structural discontinuity of the polymeric struts at a late stage is a biologically programmed fate of the scaffold during the course of bioresorption.

**METHODS** The ABSORB cohort B trial is a multicenter single-arm trial assessing the safety and performance of the Absorb BVS in the treatment of 101 patients with de novo native coronary artery lesions. The current analysis included 51 patients with 143 OCT pullbacks who underwent OCT at baseline and follow-up. The presence of acute disruption or late discontinuities was diagnosed by the presence on OCT of stacked, overhung struts or isolated intraluminal struts disconnected from the expected circularity of the device.

**RESULTS** Of 51 patients with OCT imaging post-procedure, acute scaffold disruption was observed in 2 patients (3.9%), which could be related to overexpansion of the scaffold at the time of implantation. One patient had a target lesion revascularization that was presumably related to the disruption. Of 49 patients without acute disruption, late discontinuities were observed in 21 patients. There were no major adverse cardiac events associated with this finding except for 1 patient who had a non-ischemia-driven target lesion revascularization.

**CONCLUSIONS** Acute scaffold disruption is a rare iatrogenic phenomenon that has been anecdotally associated with anginal symptoms, whereas late strut discontinuity is observed in approximately 40% of patients and could be viewed as a serendipitous OCT finding of a normal bioresorption process without clinical implications. (ABSORB Clinical Investigation, Cohort B [ABSORB B]; NCT00856856) (*J Am Coll Cardiol Intv* 2014;7:1400-11) © 2014 by the American College of Cardiology Foundation.

Fully bioresorbable scaffolds are a novel approach for treatment of coronary narrowing that provides transient vessel support with drug delivery capability without the long-term limitations of metallic drug-eluting stents, such as permanent caging with either outward bulging (evagination) of the luminal wall outside of the “cage,” or intracage neoatherosclerosis (1,2). By freeing the coronary artery from metallic caging, the vessel thereby recovers its pulsatility, and vasomotion becomes again responsive without any constraint to the biochemical milieu, the endothelial shear stress, and the physiological cyclic strain (3,4). The technology has the potential to overcome many of the safety concerns associated with metallic drug-eluting stents and could possibly even provide further clinical benefit (5).

In the ABSORB (A Clinical Evaluation of the Bioabsorbable Everolimus Eluting Coronary Stent System in the Treatment of Patients With De Novo Native Coronary Artery Lesions) cohort A trial, the first generation of the Absorb everolimus-eluting fully bioresorbable polymeric vascular scaffolds (Absorb BVS, Abbott Vascular, Santa Clara, California) showed a low event rate with a late lumen enlargement from 6 months to 2 years. At 5 years, the absence of metallic material allowed the noninvasive anatomical as well as functional assessment by multislice computed tomography of arteries previously treated with a bioresorbable scaffold (4,6,7). In the subsequent ABSORB cohort B trial, the second generation of the Absorb BVS showed a low late loss of 0.19 mm

without any reduction of the scaffold area at 6 months by intravascular ultrasound (IVUS) and optical coherence tomography (OCT) (8,9). At 12-month follow-up, the angiographic late loss was  $0.27 \pm 0.32$  mm, with an unchanged scaffold area. In addition, vasomotion induced by ergonovine and acetylcholine followed by intracoronary nitrate became detectable again, suggesting that the scaffolds mechanical integrity had subsided. At 24-month follow-up, the angiographic late loss remained stable ( $0.27 \pm 0.20$  mm) with a late enlargement of the scaffold that compensated for the neointimal growth as detected by OCT (10–12).

However, a potential drawback of this new technology is the risk for disruption of the strut network when it is overexpanded. Historically, the phenomenon was documented for the first time in an anecdotal case from the ABSORB cohort A trial. A 3.0-mm scaffold was overexpanded with a 3.5-mm balloon, resulting in scaffold disruption as documented by OCT (7). Due to the recurrence of anginal symptoms at 40 days, this patient underwent repeat revascularization despite an angiographically nonsignificant stenosis by quantitative coronary angiography (QCA) (diameter stenosis of 42%) (13). It is important that this acute mechanical disruption, is distinguished from the structural discontinuity of the polymeric struts at a later stage, a biologically programmed process during the course of bioresorption (13–15).

#### ABBREVIATIONS AND ACRONYMS

**BVS** = bioresorbable polymeric vascular scaffolds  
**Dmax** = maximum diameter  
**IVUS** = intravascular ultrasound  
**OCT** = optical coherence tomography  
**QCA** = quantitative coronary angiography  
**TLR** = target lesion revascularization

From the \*Department of Interventional Cardiology, ThoraxCenter, Erasmus Medical Center, Rotterdam, the Netherlands; †Department of Interventional Cardiology, Cardiovascular Center, Aalst, Belgium; ‡Department of Cardiology and Cardiovascular Interventions, Jagiellonian University, Krakow, Poland; §Department of Cardiology, Skejby Sygehus University Hospital, Aarhus, Denmark; ¶Department of Interventional Cardiology, Maastad Hospital, Rotterdam, the Netherlands; ¶¶Institut Cardiovasculaire Paris Sud, Institut Jacques Cartier, Massy, France; #Department of Interventional Cardiology, Christchurch Hospital, Christchurch, New Zealand; \*\*Department of Interventional Cardiology, Catharina Hospital, Eindhoven, the Netherlands; ††Department of Interventional Cardiology, Bern University Hospital, Bern, Switzerland; †††Cardiac Investigation Unit, St. Vincents Hospital, Fitzroy, Australia; §§Department of Medicine, Cardiology, Monash Cardiovascular Research Centre, Melbourne, Australia; |||Department of Interventional Cardiology, Cardialysis, Rotterdam, the Netherlands; ¶¶Department of Clinical Research, Abbott Vascular, Diegem, Belgium; ##Research and Development, Abbott Vascular, Santa Clara, California; and the \*\*\*Department of Interventional Cardiology, Auckland City Hospital, Auckland, New Zealand. This study was sponsored by Abbott Vascular. Dr. van Geuns has consulted for Abbott Vascular. Dr. Dudek has received consulting and lecture fees from Abbott, Adamed, Adyton Medical Polska, Abiomed Europe, AstraZeneca, Biotronik, Balton, Bayer, BBraun, BioMatrix, Boston Scientific, Boehringer Ingelheim, Bracco, Bristol-Myers Squibb, Comesa Polska, Cordis, Cook, Covidien Polska Sp. z o. o., DRG MedTek, Eli Lilly, EuroCor, Hammermed, GE Healthcare, GlaxoSmithKline, Inspire-MD, Iroko Cardio International, Medianet Sp. z o. o., Medtronic, Medicines Company, Meril Life Sciences, MSD, Orbus-Neich, Pfizer Inc., Possis, ProCardia Medical, Promed, REVA Medical, Sano-Aventis, Siemens, Solvay, Stentys, St. Jude Medical, Terumo, Tyco, and Volcano. Dr. Smits has received speaking and travel fees from Abbott Vascular; and research grants from Abbott Vascular, St. Jude Medical, and Terumo. Dr. Chevalier has consulted for Abbott Vascular. Dr. Whitbourn has been awarded institutional grants from Abbott Vascular. Ms. Veldhof and Dr. Rapoza are full-time employees of Abbott Vascular. Dr. Ormiston has served on the advisory boards of Abbott Vascular and Boston Scientific; and has received honoraria from Abbott Vascular and Boston Scientific. All other authors have reported that they have no relationships relevant to the contents of this paper to disclose. Drs. Ormiston and Serruys are coprincipal and principal investigators. The other investigators are listed as coauthors according to the recruitment of their respective centers.

Manuscript received January 21, 2014; revised manuscript received May 20, 2014, accepted June 2, 2014.

The purpose of the present report therefore is to describe the frequency and clinical impact of acute scaffold disruption and late strut discontinuity of the second-generation Absorb BVS in the ABSORB cohort B study. The frequency and impact are documented in a serial or nonserial manner by OCT post-procedure and at 6, 12, 24, and 36 months.

## METHODS

**STUDY POPULATION.** The ABSORB cohort B trial is a multicenter single-arm trial assessing the safety and performance of the second-generation Absorb BVS in the treatment of 101 patients with a maximum of 2 de novo native coronary artery lesions. The inclusion and exclusion criteria have been described previously (8,12). The first 45 patients (B1) had an invasive imaging follow-up at 6 and 24 months, whereas the latter 56 patients (B2) had an imaging follow-up at 12 months and at 36 months.

The current analysis included 51 patients who underwent OCT at baseline as an optional investigation. The details of the follow-up are presented in Online Figure 1. In total, the analysis included 143 OCT pullbacks performed at baseline and follow-up. The details of the study device and study procedure are described in the Online Appendix.

**OPTICAL COHERENCE TOMOGRAPHY.** As an optional investigation, intravascular OCT imaging using either time-domain OCT (M3 system, LightLab Imaging, Westford, Massachusetts) or frequency-domain OCT (C7XR system, LightLab Imaging) was performed at baseline and at follow-up (15-19). The OCT measurements were performed with proprietary software for offline analysis (LightLab Imaging). To search for the presence of scaffold disruption, the analysis of continuous cross sections was performed in all frames within the treated segment. The main quantitative measurements (strut core area, strut area, lumen area, scaffold area, incomplete scaffold apposition area, and neointimal area) required different analysis rules than metallic stents (8,9,12,20). The thickness of the neointimal coverage was measured for every strut between the abluminal side of the strut core and the lumen. Because the strut thickness is approximately 150  $\mu\text{m}$ , the strut was considered as covered whenever the thickness of the coverage was above this threshold value (8,12).

**DEFINITION OF ACUTE SCAFFOLD DISRUPTION OR LATE DISCONTINUITY ON OCT.** Ex vivo experiments were performed to identify OCT findings of disrupted struts. In a silicon phantom with a diameter of 3.5 mm, a 3.0-mm Absorb BVS (maximal labeled

diameter expansion of 3.5 mm) was deployed and expanded with a 4.0-mm compliant balloon (21). After disrupting the scaffold, OCT pullback was performed and analyzed (Figure 1). Acute (periprocedural) structural scaffold disruption or late strut discontinuities were diagnosed by at least 1 of the following: 1) if 2 struts overhung each other in the same angular sector of the lumen perimeter, without close contact (overhung strut) or with contact (stacked strut) in at least 1 cross section; or 2) if there was isolated (malapposed) struts that could not be integrated in the expected circularity of the device in at least 1 cross section. "Isolated strut" was defined as a strut located at a distance from the vessel wall ( $>1/3$  of span between the center of gravity and the luminal border) (8,12,21).

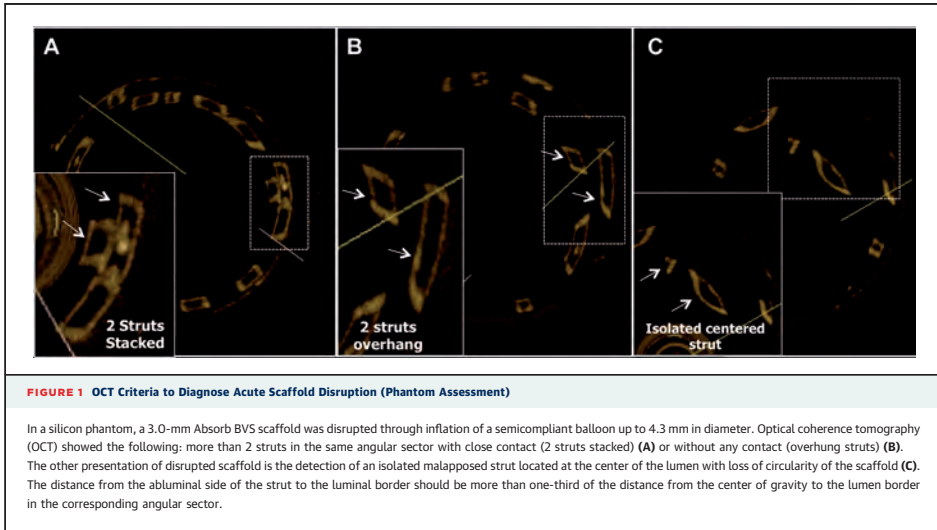
If acute scaffold disruption was persistently observed at follow-up, the case was classified as persistent scaffold disruption. Late discontinuity at follow-up was diagnosed when no initial procedural scaffold disruption could be documented post-procedure. In the case of iterative follow-up, late discontinuities could be classified as resolved or persistent (Table 1). Using the new criteria, the OCT image was reanalyzed for the presence of acute disruption or late discontinuities. The details of 3-dimensional OCT analysis, IVUS grayscale analysis, and definition of clinical events are described in the Online Appendix.

**STATISTICAL ANALYSIS.** Continuous variables are presented as mean  $\pm$  SD, whereas categorical variables are expressed as percent. Categorical variables were compared using Pearson chi-square test or Fisher exact test and continuous variables were compared using *F* test for analysis of variance. As no formal hypothesis testing was planned for assessing the success of the study, no statistical adjustment was applied. The p values presented are exploratory analyses only and therefore should be interpreted cautiously. Statistical analysis was performed with SPSS (version 20 for Macintosh, SPSS Inc., Chicago, Illinois).

## RESULTS

Baseline characteristics are presented in Online Table 1. All patients received 1 Absorb scaffold except for 1 patient who received 2. Post-dilation was performed in 57% of lesions.

**ACUTE PROCEDURAL SCAFFOLD DISRUPTION AT BASELINE.** Of 51 patients with OCT imaging post-procedure (52 scaffolded lesions), acute scaffold disruption was observed in 2 patients (3.9%). Table 2



tabulates the details of the procedures and imaging by OCT, IVUS, and QCA. Scaffold disruption at baseline was detectable on IVUS in 1 of these 2 cases.

Notably, 1 patient had a target lesion revascularization (TLR) presumably associated with the acute disruption and its worsening at 1 month. In this case (Figure 2), an Absorb BVS 3.0 mm × 18 mm scaffold was implanted in an obtuse marginal branch with a reference diameter of 3.26 mm (13). After post-dilation with a 3.25-mm noncompliant balloon at

24 atm, malapposition remained at the proximal part of the scaffold on OCT. To correct the malapposition, an additional post-dilation was performed with a compliant 3.5-mm balloon at 16 atm (expected diameter, approximately 4.0 mm). The repeat OCT and IVUS demonstrated acute scaffold disruption in the scaffolded segment. At 1 month, the patient experienced 5 episodes of recurrent angina at rest. Despite the fact that the exercise tolerance test was negative, the patient underwent recatheterization because of

**TABLE 1** Classification of OCT Findings

	Etiology	Time of OCT Observation	
		Post-Procedure	Late
Scaffold disruption	Procedure-related	<ul style="list-style-type: none"> <li>Stacked struts</li> <li>Overhung struts</li> <li>Isolated intraluminal strut(s)</li> </ul>	Late persistent*/Late procedural† <ul style="list-style-type: none"> <li>Stacked struts with/without coverage, with/without malapposition</li> <li>Overhung struts with/without coverage, with/without malapposition</li> <li>Isolated malapposed struts with/without coverage</li> </ul>
Scaffold discontinuities	Resorption-related	NA	Late acquired* <ul style="list-style-type: none"> <li>Stacked/overhung/isolated or intraluminal strut(s) with or without coverage or malapposition</li> </ul>

Artifacts such as nonuniform rotational deformation and noncoaxial positioning of the catheter should be excluded with caution (21). \*Late persistent or late acquired can be only diagnosed when serial OCT is available (baseline/follow-up). If serial imaging cannot determine the etiology, the absence of a circular strut configuration at a late imaging time point may support a procedural disruption etiology, whereas the presence of a circular strut configuration may support the etiology of a resorption-related discontinuity. †Late procedural is related to the diagnostic procedure at follow-up, which either aggravates or creates the disruption. ‡Isolated malapposed struts can be detected as neointimal bridge where the struts are thickly covered with homogeneous tissue.

NA = not applicable; OCT = optical coherence tomography.

	Case #1	Case #2
Sex	Male	Male
Age, yrs	78	83
Pre-procedural QCA		
Minimal lumen diameter, mm	1.61	0.87
Reference vessel diameter, mm	3.26	2.24
Angulation, °	35.54	2.97
Curvature, cm <sup>-1</sup>	0.04	0.005
Procedural details		
Size of implanted BVS, mm	3.0 × 18	3.0 × 18
Post-dilation	Performed	Performed
Size of post-dilation balloon, mm	3.5 × 9 mm (compliant)	3.0 × 10 (noncompliant)
Maximal pressure at post-dilation, atm	16	24
Expected diameter of balloon at maximal pressure according to the chart,* mm	>3.96	>3.22
Maximal balloon diameter by QCA, mm	3.87	2.98
OCT findings at baselines		
Total CS with strut disruption	6	5
CS with isolated struts	1	1
CS with overhang struts	5	4
CS with stacked struts	0	0
Minimal lumen area, mm <sup>2</sup>	5.82	3.59
Minimal scaffold area, mm <sup>2</sup>	7.83	5.23
IVUS at baselines		
Visibility of strut disruption on IVUS	Yes	No
Minimal lumen area, mm <sup>2</sup>	6.04	4.68
Minimal scaffold area, mm <sup>2</sup>	6.04	4.68
QCA at baselines		
Percent of diameter stenosis, %	20	1.3
Minimal lumen diameter, mm	2.7	1.94
Timing of 1st follow-up	1 months	6 months
OCT findings at 1st follow-up		
Total CS with strut disruptions	22	8
CS with isolated struts	2	4
CS with overhang struts	20	6
CS with stacked struts	1	0
Minimal lumen area, mm <sup>2</sup>	NA†	4.82
Minimal scaffold area, mm <sup>2</sup>	NA†	6.01

Continued in the next column

persisting symptoms. The angiography revealed a patent scaffold segment with a TIMI (Thrombolysis In Myocardial Infarction) flow grade 3; however, OCT, compared with baseline images, showed a deterioration of scaffold disruption. There was no tissue

	Case #1	Case #2
IVUS at 1st follow-up		
Visibility of strut disruption on IVUS	Yes	No
Minimal lumen area, mm <sup>2</sup>	5.23	4.21
Minimal scaffold area, mm <sup>2</sup>	5.23	4.21
QCA at 1st follow-up		
Percent of diameter stenosis, %	23	23
Minimal lumen diameter, mm	2.47	1.84
Late loss, mm	0.23	0.1
OCT findings at 2 yrs		
Total CS with strut disruptions	0	25
CS with isolated struts	0	14
CS with overhang struts	0	12
CS with stacked struts	0	0
Minimal lumen area, mm <sup>2</sup>	NA‡	5.15
Minimal scaffold area, mm <sup>2</sup>	NA‡	7.46
Findings in 3-dimensional reconstruction	NA‡	Tissue arch
IVUS at 2 yrs		
Visibility of strut disruption on IVUS	No	Yes
Minimal lumen area, mm <sup>2</sup>	NA	5.87
Minimal scaffold area, mm <sup>2</sup>	NA	6.15
QCA at 2 yrs		
Percent of diameter stenosis, %	14.5	25.5
Minimal lumen diameter, mm <sup>2</sup>	2.74	1.8
Late loss, mm	-0.4	0.11
Clinical events up to 2 yrs	Non-ischemia-driven target lesion revascularization	None

Values are n unless otherwise indicated. \*The balloon diameter at maximal pressure is in a chart provided by the balloon manufacturer. †The quantitative assessment was not performed because in many cross sections, the complete luminal border was not visualized. ‡The quantitative assessment was not performed because the segment was covered by a metallic stent after non-ischemia-driven revascularization.  
CS = cross section(s); IVUS = intravascular ultrasound; NA = not available; QCA = quantitative coronary angiography.

observed around the struts. A metallic Xience V stent (Abbott Vascular) was placed inside the Absorb scaffold, which eliminated the symptoms. After this nonischemic TLR, there was a rise in troponin (0.09 µl/g with an upper limit of normal of 0.03 µl/g), which would be adjudicated as a non-Q-wave myocardial infarction according to the Academic Research Consortium definition.

In the second case, a 3.0-mm scaffold was implanted in a small vessel with a reference vessel diameter

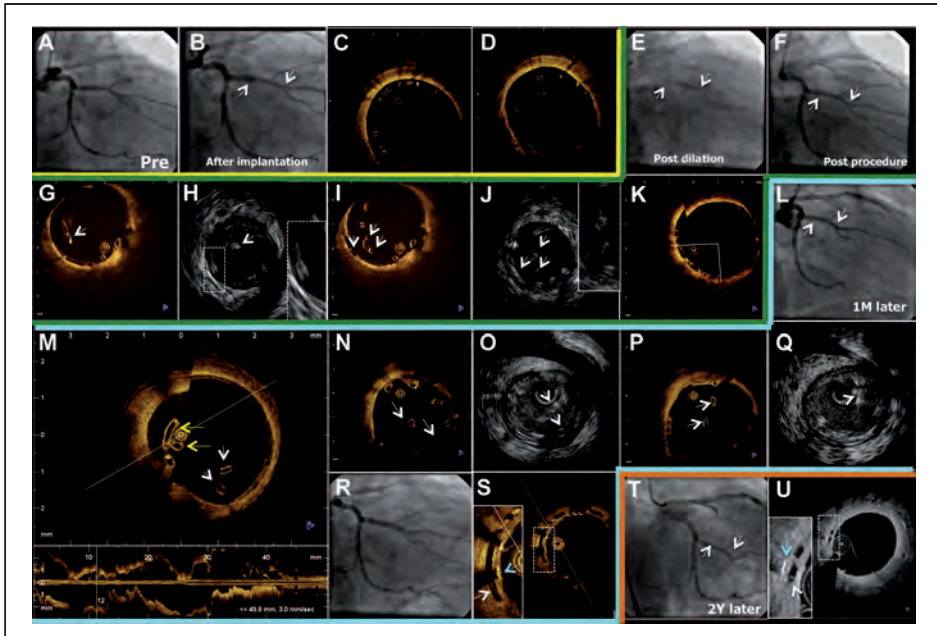


**FIGURE 2** A Case of Acute Disruption

Each series of framed illustrations (**yellow, green, blue, and orange**) represents the observation at different time points (before post-dilation, after post-dilation, at 1 month [M] and at 2 years [Y]). An Absorb BVS 3.0 mm × 18 mm scaffold was implanted in an obtuse marginal branch (A) (pre-procedural angiography) with a reference diameter of 3.26 mm. After the first post-dilation by a 3.25-mm noncompliant balloon at 24 atm (B), malapposition remained at the proximal part of the scaffold on optical coherence tomography (OCT) (C, D). To correct the malapposition, an additional post-dilation was performed with a compliant 3.5-mm balloon at 16 atm (expected diameter, approximately 4.0 mm) (E). The angiographic result was successful (F) but the post-procedural OCT (G and I) and intravascular ultrasound (IVUS) demonstrated acute strut disruption (H and J) in the scaffolded segment. Presence of a long strut extending greater than 90 degree suggests overexpansion of scaffold (K). On both OCT and IVUS, isolated intraluminal struts (**white arrow**: OCT in G and IVUS in H) and overhung struts (**white arrow**: OCT in I and IVUS in J) were observed. At 1 month, the patient had 5 episodes of recurrent angina at rest. The angiography (L) revealed a patent scaffold segment with a TIMI (Thrombolysis In Myocardial Infarction) flow grade 3; however, OCT (M, N, P) showed a deterioration of strut discontinuity (**white arrows**: isolated intraluminal or overhung struts). In the corresponding IVUS frames (O and Q), the disrupted struts were also visible. A metallic Xience V stent was placed inside the Absorb BVS scaffold (R). Post-target lesion revascularization OCT (S) showed the metallic struts, with shadows behind (**blue arrows**), are located inside of a polymeric strut (**white arrow**). At 2 years, the planned repeat angiography showed a patent stented segment (T), whereas OCT (U) showed in some cross sections the presence of covered polymeric struts (**white arrow**) inside the metallic struts (**light blue arrow**).

of 2.24 mm followed by a post-dilation with a 3.0-mm noncompliant balloon at 24 atm. Immediately after procedure, overhung struts were observed on OCT at baseline in 5 cross sections (Figure 3). According to the protocol, this asymptomatic patient underwent repeat angiography at 6 months with IVUS and OCT imaging. After the IVUS acquisition, the operator experienced difficulty recrossing the scaffolded vessel, OCT was successfully acquired,

which demonstrated extremely malapposed struts close to the OCT catheter (see the noncircularity of struts). The irregularity of the strut structure might have been caused by advancing the wire outside of the scaffold and pushing the OCT catheter under the abluminal side of the struts. At 2-year imaging follow-up, OCT revealed detached struts densely encapsulated with homogeneous tissue, forming an arch attached proximally and distally to the vessel wall. On IVUS, it was documented as a

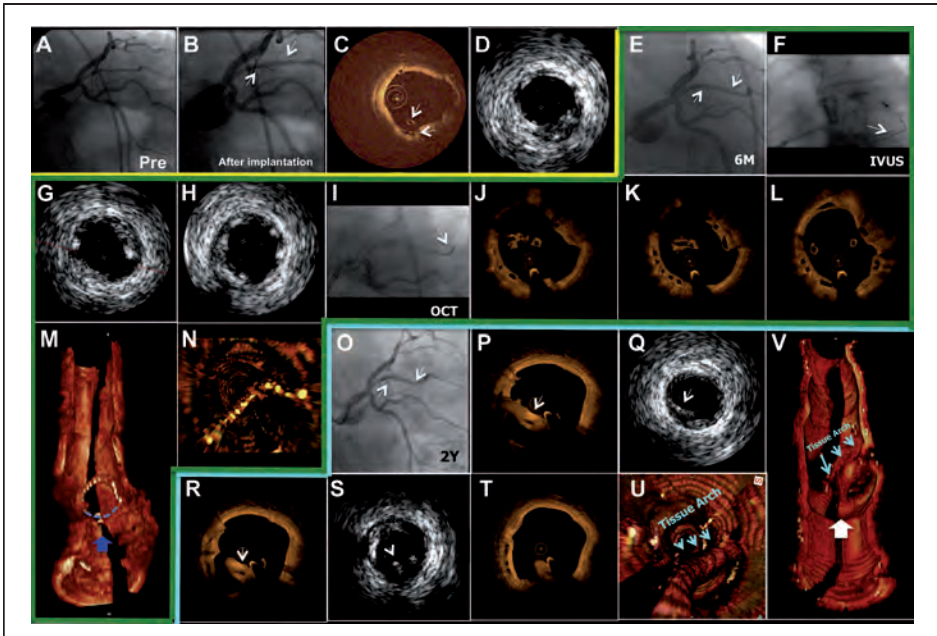


**FIGURE 3** An Example of Acute Disruption

Each series of framed illustrations (yellow, green, and blue) represents the observation at different time points (post-procedure, at 6 months, and at 2 years). An Absorb BVS scaffold was implanted in a small circumflex (reference vessel diameter 2.42 mm) (A) followed by post-dilation with a 3.0-mm noncompliant balloon at a maximal pressure of 24 atm (B). Post-procedural OCT detected overhung struts or isolated struts in 5 cross sections (C), which were not detected by IVUS (D). At 6-month follow-up, the patient underwent repeat angiography that revealed low angiographic late loss of 0.10 mm (E). According to the protocol, IVUS (F) and OCT were performed. IVUS did not detect any abnormality (G, H). After IVUS, the operator experienced difficulty crossing the scaffolded segment with the OCT catheter (I). After rewiring the scaffolded segment, OCT was successfully acquired and showed isolated struts close to the OCT catheter with loss of circularity of the scaffold (J, K, L: corresponding frames with G and H). On 3-dimensional OCT, it was evident that 1 ring of the scaffold was detached from the vessel wall (M) and divided the coronary flow (N) (endoscopic view). The late disruption of the scaffold might have been induced by advancing the wire outside of the scaffold, pushing the OCT catheter under the abluminal side of the struts during the first crossing attempt. Despite the abnormal OCT findings, the patient remained asymptomatic up to 2 years. At 2-year angiographic follow-up (O), OCT revealed detached struts (P, R, T), which were fully covered by thick homogeneous tissue extending as an endoluminal arch connected proximally and distally to the vessel wall (3-dimensional) (U, V). On IVUS, it was documented as a “dissection” in a scaffold segment (Q, S). P, R, and Q, S are the corresponding frames on OCT and IVUS, respectively. Abbreviations as in Figure 2.

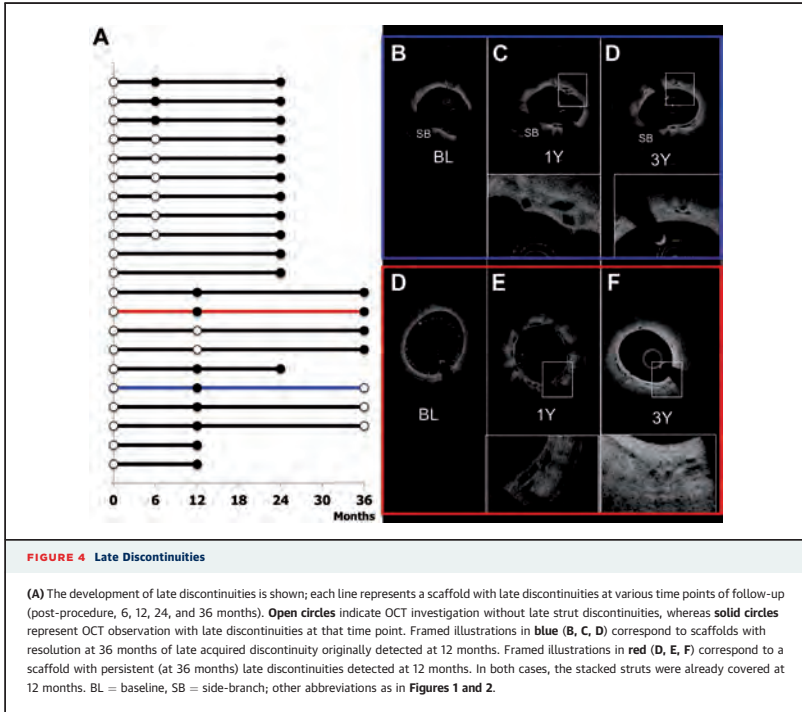
dissection in the scaffold segment. Despite the abnormal imaging findings, the patient remains asymptomatic to date.

**LATE STRUT DISCONTINUITIES AT FOLLOW-UP.**

Follow-up OCT images were obtained in all but 2 patients (at 6 months, 1 year, 2 years, or 3 years) (Online Figure 1). Of 50 scaffolded lesions (49 patients) without acute scaffold disruption, late acquired structural discontinuity was observed in 21 scaffolds (n = 21, 42%). The cases are detailed in Online Table 2

and Figure 4. There were no differences in baseline characteristics between patients with or without late discontinuities except for the pre-procedural minimal lumen diameter and diameter stenosis, which could be a play of chance. On IVUS, late discontinuities were detected only in 3 cases.

In the series with 6- and 24-month follow-up, late discontinuities were observed in 3 cases at 6 months and were persistently observed at the second follow-up at 24 months (Online Figure 2). In 8 cases, late discontinuities were observed only at 2 years.



In the series with 1- and 3-year follow-up, late structural discontinuities were observed at 1 year in 8 cases. Two discontinuities were persistently observed in serial OCT images at 3 years, whereas in 3 cases, discontinuities were resolved at 3 years. In 2 cases, no follow-up was performed after 1 year, so the outcomes of these discontinuities remained unknown. One patient underwent unscheduled OCT at 2 years, revealing persistent discontinuities. Two scaffolds had late structural discontinuities only at 3 years. **Figure 4** illustrates the complex timing and outcome of these serial or nonserial investigations.

There were no events associated with these late discontinuities observed on OCT at follow-up except for 1 patient who underwent a non-ischemia-driven repeat TLR (Online Figure 3). The 45-year-old man received a 3.0 mm × 18 mm Absorb BVS scaffold in the mid-left anterior descending artery. Post-procedural OCT did not show malapposition. At 1 year, the patient underwent a planned repeat

angiography, which showed an enlargement of the lumen. OCT showed late discontinuity with malapposed overhanging struts over a length of 4 mm. Due to the pronounced malapposition, clopidogrel treatment was continued after 1 year. The patient had stable angina of Canadian Cardiovascular Society class 2 to 3 and underwent a repeat angiography on day 722. On angiography, the lumen was found to become ectatic (QCA maximal diameter: 3.6 mm) without any significant stenosis in the scaffolded segment, whereas on OCT, 1 ring of scaffold showed persistent discontinuity with malapposition. Despite the absence of evidence of ischemia, it was thought that the anginal symptoms were somewhat related to the malapposition. A 3.0 mm × 28 mm metallic Xience Prime stent was placed in the scaffolded segment. After post-dilation with a 3.5-mm balloon, retention of angiographic contrast medium was observed along the new stent and diagnosed as malapposed struts on OCT. The segment was further dilated with a 4.5-mm

balloon. Following the dilation, contrast retention was resolved.

## DISCUSSION

The main findings of the current analysis are the following: 1) acute disruption induced by the procedure was observed in 2 of 51 patients (52 pull-backs, 3.9%), with 1 patient, it was presumably related to the TLR; 2) late resorption-related discontinuity was observed in 21 patients with 1, presumably nonrelated, non-ischemia-driven TLR; 3) QCA was unable to detect these structural changes, whereas IVUS was able to detect some of the major acute disruptions/late discontinuities (4 of 23 cases).

### ACUTE SCAFFOLD DISRUPTION AND SIZING.

Although both acute scaffold disruption and late discontinuity can be diagnosed as stacked/overhung struts or isolated struts on OCT, the 2 phenomena should be categorized differently: 1 as an accidental occurrence; and 1 as a programmed biological process. At the time of implantation, the bioresorption process does not influence the mechanical integrity of the scaffold at all, so that any disrupted struts observed immediately after the procedure are the result of a mechanical disruption caused by extreme overexpansion of the scaffold. The radial force of the polymeric device is comparable with a metallic scaffold as long as the device is expanded within certain restricted limits; however, the mechanical force yields quickly if expanded over the pre-determined boundary of expansion.

The tensile strength of the poly-L-lactide is 50 to 70 MPa, whereas that of cobalt-chrome alloy or stainless steel is in the range of 668 to 1,449 MPa. Percent of elongation at break is 2% to 10% for poly-L-lactide, whereas it is more than 40% for cobalt chromium or stainless steel. The expansion range of the polymeric device is therefore inherently limited (12).

The relationship between the diameter of expansion and likelihood of device disruption was investigated ex vivo in 30,000 scaffolds. After inflating a 3.0-mm balloon in a phantom, the presence of acute scaffold disruption was examined. Up to a size of 3.65 mm, no scaffold disruption was observed. However, when a 3.0-mm scaffold was expanded to 3.70, 3.76, 3.83, and 3.92 mm in diameter, the likelihood of acute disruption increased by 3%, 24%, 58%, and 80%. The expansion capability is, however, one of multiple attributes related to the performance of the scaffold, such as radial strength, vessel support time, flexibility, fatigue, and acute recoil. To ensure an

optimal performance of the drug-eluting scaffold, the scaffold should be expanded within its indicated range, so that the scaffold will not become disrupted and will still perform as expected. This expansion capacity should also be maintained during the entire shelf life of the device. The manufacturer accordingly recommends the maximal limits of expansion of the 3.0-mm device examined in this study as 3.5 mm.

To prevent overexpansion, it is important to implant the scaffold in a properly sized vessel using angiography or intravascular imaging in order to avoid severe mismatch between the device and vessel size. In a previously published study, QCA was used to detect the maximal diameter (Dmax) of the vessel in the landing zone proximal or distal to the stenosis. Three vessel-size groups according to Dmax (small: <2.5 mm, middle: 2.5 to 3.3 mm, large: >3.3 mm) were investigated by OCT post-procedure. The small vessel group presented with a higher percent of lesions with any degree of edge dissections visually detected on OCT (small: 61.5% vs. middle: 33.3% vs. large: 11.1%;  $p = 0.05$ ). Lesions with >5% of incomplete scaffold apposition were significantly higher in the large vessel group with a Dmax >3.3 mm (7.7% vs. 36.7% vs. 66.7%;  $p = 0.02$ ). Thus, sizing according to Dmax seems to be useful in optimizing the acute OCT outcomes (22).

Although the incidence of acute scaffold disruption is low (2 cases, 3.9%), 1 of these 2 cases was associated with a clinical event of non-ischemia-driven TLR at 1 month, followed by a rise of troponin after repeat intervention. On OCT, from baseline to 1 month, more struts became malapposed and isolated toward the lumen center, suggesting that the degree of scaffold disruption may have become worse over time. Although the presence of ischemia was not proven, the fact that chest pain vanished after repeat intervention suggests a relationship between the acute disruption and the symptoms. This could be due to the vasomotion disturbance triggered by the intraluminal presence of struts, or due to small thrombus formation around the malapposed struts with subsequent embolization. Both explanations are hypothetical as objective proof was not observed. Although ex vivo analysis showed that the thrombogenicity of polymeric struts is less than that of bare-metal struts, the possibility exists that a small thrombus could form around the isolated and malapposed struts. This is also suggested by 1 of the cases of acute disruption in cohort A of the ABSORB trial. The patient presented with chest pain at rest with OCT showing intraluminal masses with irregular contour around the disrupted strut (7).

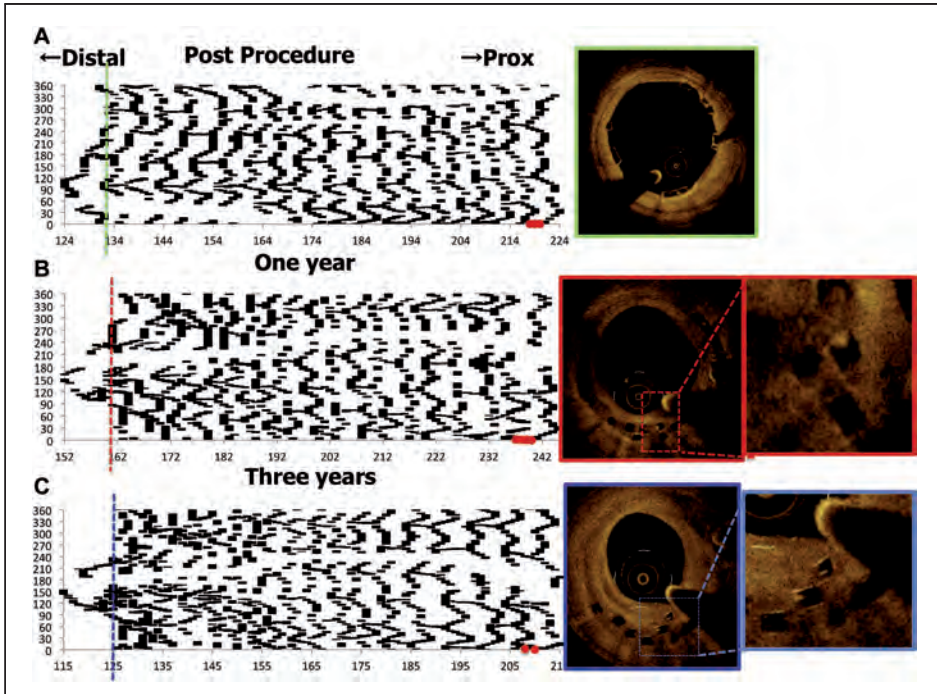


**FIGURE 5** Serial Assessment of Late Discontinuities Using Spread-Out-Vessel Graphics

(A to C) The foldout views represent spread-out-vessel graphics created by correlating the longitudinal distance from the distal scaffold edge to the individual struts detected in a single cross section (abscissa) with on the ordinate the angle where the individual strut was located in the circular cross section with respect to the center of gravity of the vessel (ordinates). In each cross section (axial resolution of 200  $\mu\text{m}$ ), the circumferential length of each individual strut was depicted in an angular fashion. The resultant graphic represented the scaffolded vessel, as if it had been cut longitudinally along the reference angle and spread out on a flat surface. The spread-out view post-procedure (A) showed that the scaffold consisted of 19 rings interconnected by 3 links. At 1 year (B) and 3 years (C), mechanical integrity has gradually subsided and the distal part of the scaffold was starting to show signs of dismantling, along which late discontinuities were observed. At baseline, in the distal edge of the scaffold (green dotted line in the foldout view), 2-dimensional optical coherence tomography (OCT) (green frame) revealed well apposed struts. At 1 year, in the distal edge (red dotted line in the foldout view), 2-dimensional OCT (red frame) showed overhung and apposed struts. At 3 years, these struts remained overhung (blue line in the foldout view, corresponding to 2-dimensional OCT with a blue frame). The phenomenon is considered benign because the struts are mostly covered at 1 and 3 years. Red dots represent the proximal metallic markers.

**LATE, RESORPTION-RELATED STRUCTURAL DISCONTINUITIES.** The hydrolysis of polymeric strut starts immediately after the device comes in contact with water, whereas the decrease in mechanical support of the scaffold starts approximately 6 months after implantation. The process of restenosis is a time-limited phenomenon due to negative remodeling of the vessel and neointimal hyperplasia inside of the stent, which occurs 3 to 6 months after

implantation in the coronary artery. During this time, the maintenance of the mechanical structure as well as the elution of everolimus is critical to prevent restenosis. Beyond this critical period, however, the mechanical support of the scaffold, as well as the active neointimal inhibition are no longer necessary, because the restenosis process is no longer ongoing. In fact, after 6 months, the polymeric scaffold starts losing its mechanical integrity and that can lead to

expected late discontinuity. **Figure 5** shows the progression of structural disintegration over time due to bioresorption. The spread-out view showed that post-procedure, the scaffold consisted of 19 rings connected to each other with 3 links, as manufactured. As shown in **Figure 5**, at 1 year, mechanical integrity had partially subsided and the distal part of the scaffold has started to dismantle, which corresponds to late discontinuities of individual struts. This phenomenon is considered benign because the struts are mostly covered at 1 and 3 years.

Among the 21 cases with late strut discontinuity, 20 cases had no clinical consequences during the entire follow-up. In 1 case, non-ischemia-driven TLR with a metallic stent was performed at 2 years to remediate an abnormal outward bulging of the vessel wall, resulting in major malapposition and late strut discontinuities already detected by OCT at 1-year follow-up. Although a huge malapposition could increase a risk of scaffold thrombosis, the microscopic resolution of OCT imaging may have triggered a new kind of “occulo-OCT” reflex because, on angiography, this was inconspicuous.

**SINGLE OR SERIAL OBSERVATION.** In the current analysis, post-procedural OCT was available in all cases, which enabled us to distinguish the persistent acute disruption from late discontinuities. Whenever OCT was not available post-procedure, differentiation of persistent acute disruption from late discontinuities was speculative (**Table 1**). Stacked, overhung, or isolated malapposed struts with circular structure that were observed later than 6 months, especially when covered and apposed, could likely be attributed to late resorption-related discontinuities.

**OCT AND IVUS.** The current analysis showed that IVUS is less sensitive than OCT in the detection of acute strut disruption or late strut discontinuity. IVUS was able to detect major disruptions or discontinuities, but overlooked some disruptions or could not differentiate them from malapposition (23). Because acute scaffold disruption could be associated with anginal symptoms, OCT might be recommended as an additional diagnostic technique when the scaffolded vessel angiographically appears patent, and oversizing and/or overexpansion is suspected.

**IMAGING PROCEDURE AT FOLLOW-UP.** The anecdotal cases presented in this report highlight the fact that imaging procedures at follow-up can worsen pre-existing scaffold disruptions at late follow-up. The mechanical strength of the device starts to subside 6 months after implantation so that intravascular

imaging follow-up occurring later than 6 months post-implantation has to be performed cautiously. Introducing a guidewire into the scaffolded segment should be carried out carefully in cases of known malapposition post-procedure. The operator should not reinvestigate the vessel if any resistance in advancing the imaging device into the scaffolded segment is experienced.

**STUDY LIMITATIONS.** The current study has a limited number of patients who underwent OCT at the different time points. However, it is the largest series of patients investigated with serial OCT over a follow-up period of 3 years. The “snapshot” nature of the OCT investigations precludes any dynamic interpretation of the ongoing and intended mechanical dismantling of the scaffold. For instance, the longitudinal polymeric links rather than the rings may be the first structures to degrade and the longitudinal mechanical stress might be more intense along the outer epicardial border of the vessel rather than at the inner myocardial side. These speculations should be the focus of further preclinical investigations involving other techniques such as a permanently implanted sono-micrometer. The OCT criteria used in this analysis (stacked struts or overhung struts) will not be applicable to the overlapped segment, because these strut dispositions are normally seen in such segments.

## CONCLUSIONS

Acute scaffold disruptions are rare procedural phenomena that have been anecdotally associated with angina symptoms, although pathological correlation between disrupted struts and angina remain elusive. They can be generally avoided by respecting the stated expansion limits for each scaffold diameter. In case of recurrent angina without angiographic stenosis, OCT might be recommended as an additional diagnostic technique, whereas the imaging follow-up later than 6 months needs a careful advance of the imaging device. Late discontinuities as a result of the expected resorption process are observed in approximately 40% of patients who experienced, at the time of follow-up, the struts fully covered or embedded in tissue and should be viewed as a serendipitous OCT finding of a normal bioresorption process without clinical implication.

**REPRINT REQUESTS AND CORRESPONDENCE:** Prof. Patrick W. Serruys, ThoraxCenter, Ba-583, 's Gravenhijkwal 230, 3015 CE Rotterdam, the Netherlands. E-mail: patrick.w.j.c.serruys@gmail.com.

## REFERENCES

1. Nakazawa G, Otsuka F, Nakano M, et al. The pathology of neointimal hyperplasia in human coronary implants bare-metal and drug-eluting stents. *J Am Coll Cardiol* 2011;57:1314-22.
2. Räber L, Baumgartner S, Garcia HM, et al. Long-term vascular healing in response to sirolimus- and paclitaxel-eluting stents: an optical coherence tomography study. *J Am Coll Cardiol Intv* 2012;5:946-57.
3. Farooq V, Vergouwe Y, Räber L, et al. Combined anatomical and clinical factors for the long-term risk stratification of patients undergoing percutaneous coronary intervention: the Logistic Clinical SYNTAX score. *Eur Heart J* 2012;33:3098-104.
4. Gonzalo N, Serruys PW, Garcia-Garcia HM, et al. Quantitative ex vivo and in vivo comparison of lumen dimensions measured by optical coherence tomography and intravascular ultrasound in human coronary arteries. *Rev Esp Cardiol* 2009;62:615-24.
5. Serruys PW, Garcia-Garcia HM, Onuma Y. From metallic cages to transient bioresorbable scaffolds: change in paradigm of coronary revascularization in the upcoming decade? *Eur Heart J* 2012;33:16-25b.
6. Ormiston JA, Serruys PW, Regar E, et al. A bioabsorbable everolimus-eluting coronary stent system for patients with single de-novo coronary artery lesions (ABSORB): a prospective open-label trial. *Lancet* 2008;371:899-907.
7. Onuma Y, Serruys PW, Ormiston JA, et al. Three-year results of clinical follow-up after a bioresorbable everolimus-eluting scaffold in patients with de novo coronary artery disease: the ABSORB trial. *EuroIntervention* 2010;6:447-53.
8. Serruys PW, Onuma Y, Ormiston JA, et al. Evaluation of the second generation of a bioresorbable everolimus drug-eluting vascular scaffold for treatment of de novo coronary artery stenosis: six-month clinical and imaging outcomes. *Circulation* 2010;122:2301-12.
9. Gomez-Lara J, Brugaletta S, Diletti R, et al. A comparative assessment by optical coherence tomography of the performance of the first and second generation of the everolimus-eluting bioresorbable vascular scaffolds. *Eur Heart J* 2011;32:294-304.
10. Serruys PW, Luitjen HE, Beatt KJ, et al. Incidence of restenosis after successful coronary angioplasty: a time-related phenomenon. A quantitative angiographic study in 342 consecutive patients at 1, 2, 3, and 4 months. *Circulation* 1988;77:361-71.
11. Nobuyoshi M, Kimura T, Nosaka H, et al. Restenosis after successful percutaneous transluminal coronary angioplasty: serial angiographic follow-up of 229 patients. *J Am Coll Cardiol* 1988;12:616-23.
12. Onuma Y, Serruys PW. Bioresorbable scaffold: the advent of a new era in percutaneous coronary and peripheral revascularization? *Circulation* 2011;123:779-97.
13. Ormiston JA, De Vroey F, Serruys PW, Webster MW. Bioresorbable polymeric vascular scaffolds: a cautionary tale. *Circ Cardiovasc Interv* 2011;4:535-8.
14. Serruys PW, Onuma Y, Dudek D, et al. Evaluation of the second generation of a bioresorbable everolimus-eluting vascular scaffold for the treatment of de novo coronary artery stenosis: 12-month clinical and imaging outcomes. *J Am Coll Cardiol* 2011;58:1578-88.
15. Okamura T, Garg S, Gutiérrez-Chico J, et al. In vivo evaluation of stent strut distribution patterns in the bioabsorbable everolimus-eluting device: an OCT ad hoc analysis of the revision 1.0 and revision 1.1 stent design in the ABSORB clinical trial. *EuroIntervention* 2010;5:932-8.
16. Sihan K, Botha C, Post F, et al. Fully automatic three-dimensional quantitative analysis of intracoronary optical coherence tomography: method and validation. *Catheter Cardiovasc Interv* 2009;74:1058-65.
17. Prati F, Regar E, Mintz GS, et al. Expert review document on methodology, terminology, and clinical applications of optical coherence tomography: physical principles, methodology of image acquisition, and clinical application for assessment of coronary arteries and atherosclerosis. *Eur Heart J* 2010;31:401-15.
18. Gonzalo N, Serruys PW, Okamura T, et al. Optical coherence tomography assessment of the acute effects of stent implantation on the vessel wall: a systematic quantitative approach. *Heart* 2009;95:1913-9.
19. Regar E, van Leeuwen AMGJ, Serruys PW. *Optical Coherence Tomography in Cardiovascular Research*. London: Informa Healthcare, 2007.
20. Gomez-Lara J, Radu M, Brugaletta S, et al. Serial analysis of the malapposed and uncovered struts of the new generation of everolimus-eluting bioresorbable scaffold with optical coherence tomography. *J Am Coll Cardiol Intv* 2011;4:992-1001.
21. Radu MD. The Clinical Atlas of Intravascular Optical Coherence Tomography for iPad. *Eur Heart J* 2012;33:1174-5.
22. Gomez-Lara J, Diletti R, Brugaletta S, et al. Angiographic maximal luminal diameter and appropriate deployment of the everolimus-eluting bioresorbable vascular scaffold as assessed by optical coherence tomography: an ABSORB cohort B trial sub-study. *EuroIntervention* 2012;8:214-24.
23. Gomez-Lara J, Brugaletta S, Diletti R, et al. Agreement and reproducibility of gray-scale intravascular ultrasound and optical coherence tomography for the analysis of the bioresorbable vascular scaffold. *Catheter Cardiovasc Interv* 2012;79:890-902.

**KEY WORDS** atherosclerosis, biodegradable polymer, bioresorbable scaffold, everolimus, stent

**APPENDIX** For supplemental methods, figures, and tables, please see the online version of this article.

#### 5.4 Absorb BVS in diabetic patients

One-year clinical outcomes of diabetic patients treated with the everolimus-eluting bioresorbable vascular scaffolds:  
A pooled analysis from the ABSORB Cohort B and the ABSORB EXTEND trials.

*JACC Cardiovasc Interv.* 2014;7:482-93.

[Original research paper, Impact Factor (2013): 7.440]

Muramatsu T, Onuma Y, van Geuns RJ, Chevalier B, Patel T, Seth A, Diletti R, García-García HM, Dorange C, Veldhof S, Cheong WF, Ozaki Y, Whitbourn R, Bartorelli A, Stone GW, Abizaid A, Serruys PW.





# 1-Year Clinical Outcomes of Diabetic Patients Treated With Everolimus-Eluting Bioresorbable Vascular Scaffolds

## A Pooled Analysis of the ABSORB and the SPIRIT Trials

Takashi Muramatsu, MD, PhD,\*† Yoshinobu Onuma, MD,\* Robert-Jan van Geuns, MD, PhD,\* Bernard Chevalier, MD,‡ Tejas M. Patel, MD,§ Ashok Seth, MD,|| Roberto Diletti, MD,\* Hector M. García-García, MD, PhD,\* Cécile C. Dorange, MSc,¶ Susan Veldhof, RN,¶ Wai-Fung Cheong, PhD,# Yukio Ozaki, MD, PhD,† Robert Whitbourn, MD,\*\* Antonio Bartorelli, MD,†† Gregg W. Stone, MD,‡‡ Alexandre Abizaid, MD, PhD,§§ Patrick W. Serruys, MD, PhD,\* on behalf of the ABSORB Cohort B, the ABSORB EXTEND, and the SPIRIT FIRST, II, III, and IV Investigators

*Rotterdam, the Netherlands; Toyoko, Japan; Massy, France; Ahmedabad and New Delhi, India; Diegem, Belgium; Santa Clara, California; Melbourne, Victoria, Australia; Milan, Italy; New York, New York; and São Paulo, Brazil*

**Objectives** The aim of this study was to evaluate 1-year clinical outcomes of diabetic patients treated with the Absorb bioresorbable vascular scaffold (BVS).

**Background** Clinical outcomes of diabetic patients after BVS implantation have been unreported.

**Methods** This study included 101 patients in the ABSORB Cohort B trial and the first consecutive 450 patients with 1 year of follow-up in the ABSORB EXTEND trial. A total of 136 diabetic patients were compared with 415 nondiabetic patients. In addition, 882 diabetic patients treated with everolimus-eluting metal stents (EES) in pooled data from the SPIRIT trials (SPIRIT FIRST [Clinical Trial of the Abbott Vascular XIENCE V Everolimus Eluting Coronary Stent System], SPIRIT II [A Clinical Evaluation of the XIENCE V Everolimus Eluting Coronary Stent System], SPIRIT III [Clinical Trial of the XIENCE V Everolimus Eluting Coronary Stent System (EECSS)], SPIRIT IV Clinical Trial [Clinical Evaluation of the XIENCE V Everolimus Eluting Coronary Stent System]) were used for the comparison by applying propensity score matching. The primary endpoint was a device-oriented composite endpoint (DoCE), including cardiac death, target vessel myocardial infarction, and target lesion revascularization at 1-year follow-up.

**Results** The cumulative incidence of DoCE did not differ between diabetic and nondiabetic patients treated with the BVS (3.7% vs. 5.1%,  $p = 0.64$ ). Diabetic patients treated with the BVS had a similar incidence of the DoCE compared with diabetic patients treated with EES in the matched study group (3.9% for the BVS vs. 6.4% for EES,  $p = 0.38$ ). There were no differences in the incidence of definite or probable scaffold/stent thrombosis (0.7% for both diabetic and nondiabetic patients with the BVS; 1.0% for diabetic patients with the BVS vs. 1.7% for diabetic patients with EES in the matched study group).

**Conclusions** In the present analyses, diabetic patients treated with the BVS showed similar rates of DoCEs compared with nondiabetic patients treated with the BVS and diabetic patients treated with EES at 1-year follow-up. (ABSORB Clinical Investigation, Cohort B; NCT00856856; ABSORB EXTEND Clinical Investigation; NCT01023789; Clinical Trial of the Abbott Vascular XIENCE V Everolimus Eluting Coronary Stent System [SPIRIT FIRST]; NCT00180453; A Clinical Evaluation of the XIENCE V Everolimus Eluting Coronary Stent System [SPIRIT II]; NCT00180310; Clinical Trial of the XIENCE V Everolimus Eluting Coronary Stent System [EECSS] [SPIRIT III]; NCT00180479; Clinical Evaluation of the XIENCE V Everolimus Eluting Coronary Stent System [SPIRIT IV Clinical Trial]; NCT00307047). (J Am Coll Cardiol Intv 2014;7:482–93) © 2014 by the American College of Cardiology Foundation

A dramatic increase in the incidence of diabetes mellitus has been recognized as a serious worldwide issue (1). Diabetes causes systemic microvascular and macrovascular complications including coronary artery disease (CAD) that ultimately contributes to cardiovascular mortality (2,3).

See page 494

Drug-eluting stents (DES) considerably reduce the need for repeat revascularization in diabetic patients compared with bare-metal stents (BMS) (4). The presence of diabetes, however, has still been associated with an increased risk of adverse clinical events after percutaneous coronary intervention (PCI) with DES (5,6). Although newer generation DES have generally shown better long-term outcomes compared with first-generation DES (7–9), a pooled analysis of 4 randomized trials using newer generation everolimus-eluting metal stents (EES) showed a marked attenuation of beneficial effects compared with first-generation paclitaxel-eluting stents in a subset of diabetic patients (10). The best type of DES for the treatment of diabetic patients remains unclear.

Bioresorbable vascular scaffolds (BVSs) are a novel approach to the treatment of CAD in that they provide transient vessel support and drug delivery to the vessel wall (11). The ABSORB Cohort B trial investigating the current generation of the everolimus-eluting BVS system (Absorb BVS, Abbott Vascular, Santa Clara, California) has shown an acceptable incidence rate of major adverse cardiac events (10.0%) without any scaffold thrombosis up to 3 years of follow-up (12).

To date, clinical outcomes of diabetic patients treated with the Absorb BVS have not been specifically described. Thus, the aim of this study was: 1) to assess the 1-year clinical outcomes of diabetic patients treated with the Absorb BVS compared with nondiabetic patients, using pooled individual data of the ABSORB Cohort B and the ABSORB EXTEND trials; and 2) to compare the 1-year clinical outcomes of diabetic patients treated with the Absorb BVS with that of diabetic patients treated with EES, using propensity-score (PS) matching of pooled data from the SPIRIT trials (SPIRIT FIRST [A Clinical Trial of the Abbott Vascular XIENCE V Everolimus Eluting Coronary Stent System], SPIRIT II [A Clinical Evaluation of the

XIENCE V Everolimus Eluting Coronary Stent System], SPIRIT III [Clinical Trial of the XIENCE V Everolimus Eluting Coronary Stent System (EECSS)], SPIRIT IV Clinical Trial [Clinical Evaluation of the XIENCE V Everolimus Eluting Coronary Stent System]).

## Methods

**Study population.** We included all patients enrolled in the ABSORB Cohort B trial and the first consecutive 450 patients with 1 year of follow-up in the ABSORB EXTEND trial. As enrollment in the ABSORB EXTEND trial was completed on October 2, 2013, clinical follow-up is currently ongoing, and the data for this analysis were obtained from an interim data cutoff date of December 3, 2012. The details of these 2 trials have been described elsewhere (13,14). In brief, both trials were prospective, multicenter, single-arm studies assessing the safety and feasibility of the Absorb BVS. Patients older than 18 years of age who have 1 or 2 de novo lesions located in a different major epicardial vessel were enrolled. Target lesions must have a visually estimated stenosis of  $\geq 50\%$  and  $< 100\%$  and a Thrombolysis In Myocardial Infarction flow grade of  $\geq 1$ . Major exclusion criteria were patients presenting with an acute myocardial infarction (MI), left ventricular ejection fraction  $< 30\%$ , renal insufficiency, aorto-ostial lesions, left main coronary artery lesions, total occlusions, heavily calcified lesions, and lesions with visible thrombus.

For the current analysis, diabetic patients treated with the XIENCE V EES (Abbott Vascular) were pooled from the SPIRIT FIRST, the SPIRIT II, the SPIRIT III and the SPIRIT IV trials as

### Abbreviations and Acronyms

<b>ARC</b>	= Academic Research Consortium
<b>BMS</b>	= bare-metal stent(s)
<b>BVS</b>	= bioresorbable vascular scaffold
<b>CAD</b>	= coronary artery disease
<b>DES</b>	= drug-eluting stent(s)
<b>DOCE</b>	= device-oriented composite endpoint
<b>EES</b>	= everolimus-eluting metal stent(s)
<b>MI</b>	= myocardial infarction
<b>PCI</b>	= percutaneous coronary intervention
<b>PoCE</b>	= patient-oriented composite endpoint
<b>PS</b>	= propensity score
<b>ST</b>	= scaffold/stent thrombosis
<b>TLR</b>	= target lesion revascularization

From the \*Thoraxcenter, Erasmus Medical Center, Rotterdam, the Netherlands; †Department of Cardiology, Fujita Health University Hospital, Toyoake, Japan; ‡Institut Cardiovasculaire Paris Sud, Massy, France; §Krishna Heart Institute, Ahmedabad, India; ||Fortis Escorts Heart Institute, New Delhi, India; ¶Abbott Vascular, Diegem, Belgium; #Abbott Vascular, Santa Clara, California; \*\*Cardiovascular Research Center, St. Vincent's Hospital, Melbourne, Victoria, Australia; ††Centro Cardiologico Monzino, IRCCS, University of Milan, Milan, Italy; ‡‡Columbia University Medical Center/New York-Presbyterian Hospital and Cardiovascular Research Foundation, New York, New York; and §§Istituto Dante Pazzanese de Cardiologia, São Paulo, Brazil. The ABSORB Cohort B, the ABSORB EXTEND, the SPIRIT FIRST, the SPIRIT II, the SPIRIT III, and the SPIRIT IV

trials have been sponsored and funded by Abbott Vascular. Dr. Cheong, Ms. Veldhof, and Ms. Dorange are full-time employees of Abbott Vascular. Dr. Bartorelli has served on the advisory board, as a consultant for, and received minor honoraria from Abbott Vascular. Dr. Stone has served as a consultant for Boston Scientific and Reva Medical. Dr. van Geuns has received speaker fees from Abbott Vascular. Dr. Chevalier has served as a consultant for Abbott Vascular. Dr. Patel is the Chairman of Apex Heart Institute. Dr. Seth is the Chairman of Fortis Heart Institute. All other authors have reported that they have no relationships relevant to the contents of this paper to disclose.

Manuscript received October 21, 2013; revised manuscript received December 30, 2013, accepted January 4, 2014.

historical controls. The details of all these SPIRIT trials were also described previously (7,8,15,16). Of note, major inclusion and exclusion criteria of these trials were similar to those of the ABSORB Cohort B and the ABSORB EXTEND trials, whereas inclusion criteria of the SPIRIT IV trial were more liberal than the other trials by permitting enrollment of patients with complex lesions that were defined as a maximum of 3 target lesions in 3 separate major epicardial coronary arteries, a maximum of 2 target lesions in a single coronary artery, an ostial right coronary artery lesion, or bifurcation lesions in which the side branch was  $\geq 2$  mm in diameter or the ostium of the side branch was  $>50\%$  stenosed (8). The features of the aforementioned trials are summarized in Online Table 1.

All of these trials were sponsored and funded by Abbott Vascular. The research ethics committee of each participating institution approved the protocol, and all enrolled patients provided written informed consent before inclusion.

**Study devices and treatment procedure.** The details of study devices and diabetic treatment are presented in the Online Appendix. Lesions were treated using standard interventional techniques, with mandatory pre-dilation and scaffold/stent implantation at a pressure not exceeding the burst pressure rate. Post-dilation was left to the discretion of the operator and only permitted with balloons sized to fit within the boundaries of the scaffold/stent. Patients were treated with aspirin  $\geq 80$  mg pre-procedurally. A  $\geq 300$ -mg loading dose of clopidogrel between 6 and 24 h before the procedure was required. After the index procedure, aspirin  $\geq 75$  or 80 mg daily throughout the duration of the trial and clopidogrel 75 mg daily for a minimum of 6 months should be administered except for the SPIRIT First trial (a minimum of 3 months for clopidogrel).

**Definition of clinical outcomes.** In the present analysis, the primary clinical outcome was assessed by a device-oriented composite endpoint (DoCE), which is also known as target lesion failure at 1 year after the index procedure. This was defined as a composite of cardiac death, target vessel MI, or ischemia-driven target lesion revascularization (TLR). Secondary clinical outcome was a patient-oriented composite endpoint (PoCE) that was defined as a composite of all-cause death, all MIs, or any repeat revascularization. These classifications of outcome measures were on the basis of the Academic Research Consortium (ARC) definitions (17). In the event of a death that could not be attributed to another cause, it was considered as a cardiac death. The incidence of scaffold/stent thrombosis (ST) according to the ARC criteria is also reported up to 1 year of follow-up. Per-protocol MI was defined either as the development of new Q waves or as an increase in the creatine kinase level to greater than twice the upper limit of normal, accompanied by an increased level of creatine kinase-myocardial band (18). Notably, this definition of per-protocol MI was

consistently applied in all trials used for the present analysis. All clinical outcomes were adjudicated by an independent clinical events committee.

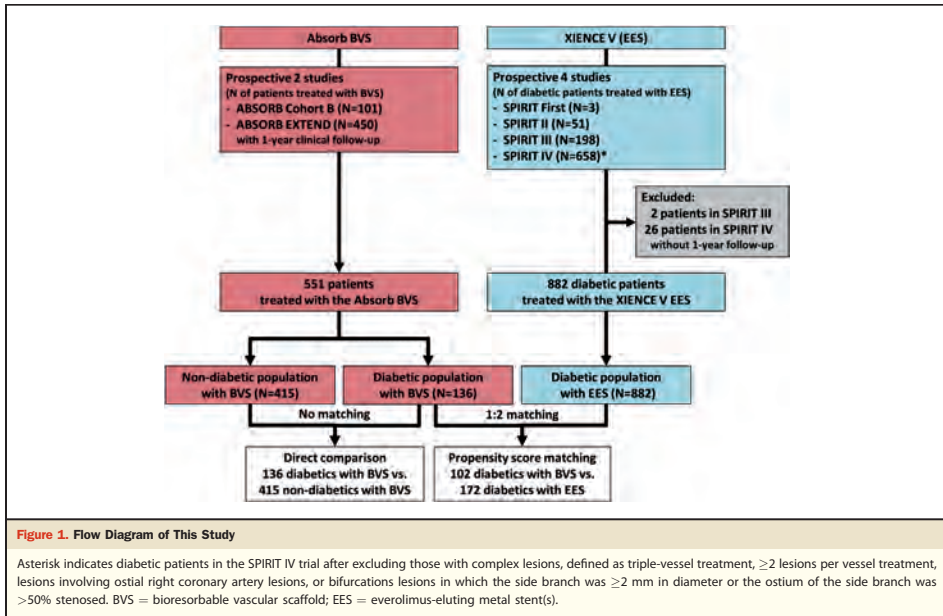
**Clinical follow-up and source document verification.** Except for the studies with planned angiographic follow-up at 1 year, patients were clinically followed by their visits to the outpatient clinic or by telephone calls. In the ABSORB Cohort B, the SPIRIT First, the SPIRIT II, the SPIRIT III, and the SPIRIT IV trials, source document verification was performed in 100% of patients through 1-year follow-up. In the ABSORB EXTEND trial, source document verification was routinely performed in 100% of patients through 30-day follow-up, subsequently in a random 20% of patients, and in 100% of all reported events for the remaining follow-up period.

**Statistical analysis.** For the present analyses, individual data were pooled on a patient-level basis. Continuous variables are expressed as mean  $\pm$  SD and categorical variables are presented as proportion (%). Comparisons were performed by the *t* test for continuous variables and by chi-square or Fisher exact test when the Cochran rule is not met for categorical variables. Time-to-event variables are presented as Kaplan-Meier curves. Subjects were counted only once for a composite endpoint in hierarchical order, whereas the incidence of the components and ST events are shown in nonhierarchical order. PS matching was applied to compare 1-year clinical outcomes of diabetic patients treated with the BVS and those treated with EES. The details of PS matching are presented in the Online Appendix. Considering the larger number of diabetic patients treated with EES ( $N = 882$ ) compared with that of diabetic patients treated with the BVS ( $N = 136$ ), a 1:2 matching (BVS:EES) was performed in this study. A 2-sided *p* value  $<0.05$  was considered statistically significant.

## Results

**Study population.** A flow diagram of this study is shown in Figure 1. We included 101 patients in the ABSORB Cohort B trial and 450 patients in the ABSORB EXTEND trial. All patients were treated with the Absorb BVS and were classified as either diabetic ( $n = 136$ ) or nondiabetic ( $n = 415$ ). For diabetic patients treated with EES as a control group, we first excluded the patients with complex lesions in the SPIRIT IV trial ( $n = 128$ ). In addition, 2 patients in the SPIRIT III trial and 26 patients in the SPIRIT IV trial were excluded because of the lack of 1-year follow-up data. A total of 882 diabetic patients treated with EES in a pooled study group from the SPIRIT trials was used for the comparisons between the BVS and EES.

Of these diabetic patients, the PS was not assessable for 11 of 136 patients in the BVS group and 221 of 882 patients in the EES group because of missing baseline characteristics



necessary to compute the PS. By applying the aforementioned methodology of PS matching, 23 patients in the BVS group and 489 patients in the EES group were excluded during the matching process. Consequently, there were 102 diabetic patients in the BVS group matched with 172 diabetic patients in the EES group for the comparative analyses. **Comparisons between diabetic and nondiabetic patients treated with the BVS.** Patient demographics were comparable between diabetic and nondiabetic patients treated with the BVS, except for a history of hypertension requiring medication that was more prevalent in diabetic patients (Table 1). Lesion characteristics were also comparable between the 2 groups, except for the left anterior descending artery target lesion location being less prevalent in diabetic patients. Use of dual antiplatelet therapy did not differ between the 2 groups at each time point (at discharge, 6 months, and 1 year after the index procedure).

Time-to-event curves showing the cumulative incidence of DoCE and the components up to 1 year after the index procedure appear in Figure 2. DoCE at 1 year occurred in 3.7% of diabetic patients and 5.1% of nondiabetic patients ( $p = 0.64$ ). There were no significant differences in the incidence of the components up to 1 year of follow-up between the 2 groups (Table 2). Similarly, PoCE was observed in 7.4% of diabetic patients and 8.2% of nondiabetic patients

( $p = 0.86$ ). One patient with diabetes experienced definite late ST (0.7%), whereas 1 definite and 1 probable subacute ST and 1 definite late ST (0.7%) were observed in the nondiabetes group ( $p = 1.0$ ).

**Comparisons between the BVS and EES in diabetic patients.** In the entire study groups with diabetes, the mean age, rates of hypertension requiring medication, hypercholesterolemia requiring medication, diabetes requiring insulin treatment, family history of CAD, previous coronary intervention, multivessel disease, type B2/C lesion, lesion length, reference vessel diameter, and percent of diameter stenosis were significantly greater in the EES group than in the BVS group. Conversely, male sex, rates of diabetes requiring oral hypoglycemic agents, unstable angina, and minimal luminal diameter were significantly less in the EES group (Table 3). After PS matching, all variables became comparable between the BVS group (102 patients) and the EES group (172 patients), except for left anterior descending artery target lesion location being less prevalent in the BVS group. Use of dual antiplatelet therapy was also comparable between the 2 treatment groups.

In the matched study group, DoCE at 1 year occurred in 3.9% of patients in the BVS group and in 6.4% of patients in the EES group ( $p = 0.38$ ) (Fig. 3). There were no significant differences in the incidence of each component and

**Table 1. Baseline Characteristics of Diabetic and Nondiabetic Patients Treated With the Absorb BVS**

	Absorb BVS Diabetics (n = 136)	Absorb BVS Nondiabetics (n = 415)	p Value
<b>Demographic characteristics</b>			
Age, yrs	61.6 ± 10.0 (136)	61.9 ± 10.5 (415)	0.81
Male	73.5 (100/136)	73.7 (306/415)	1.00
Current smoker	19.9 (27/136)	21.0 (87/414)	0.81
Hypertension requiring medication	75.0 (102/136)	61.4 (254/414)	0.004
Hypercholesterolemia requiring medication	67.6 (92/136)	63.6 (264/415)	0.41
<b>Diabetes treatment</b>			
Insulin	16.9 (23/136)	0.0 (0/415)	<0.001
Oral hypoglycemic drugs	74.3 (101/136)	0.0 (0/415)	<0.001
Physical exercise and/or diet modification only	4.4 (6/136)	0.0 (0/415)	<0.001
No treatment	4.4 (6/136)	100.0 (415/415)	<0.001
<b>Family history of coronary artery disease</b>			
Unstable angina	33.8 (46/136)	27.7 (115/415)	0.19
Previous coronary intervention	23.5 (32/136)	24.6 (102/415)	0.80
Previous myocardial infarction	26.5 (36/136)	28.8 (119/413)	0.66
Multivessel disease	23.5 (32/136)	17.6 (73/415)	0.13
<b>Target vessel</b>			
Right coronary artery	36.8 (53/144)	28.2 (124/439)	0.06
Left anterior descending artery	36.1 (52/144)	45.8 (201/439)	0.043
Left circumflex artery or ramus	27.1 (39/144)	26.0 (114/439)	0.83
Left main coronary artery	0.0 (0/144)	0.0 (0/439)	NA
<b>ACC/AHA lesion class</b>			
A/B1	62.9 (90/143)	59.7 (259/434)	0.49
B2/C	37.1 (53/143)	40.3 (175/434)	0.49
<b>Target lesion characteristics</b>			
Lesion length, mm	11.7 ± 5.1 (143)	11.2 ± 4.6 (429)	0.25
<b>Pre-procedure</b>			
Reference vessel diameter, mm	2.60 ± 0.33 (143)	2.62 ± 0.37 (429)	0.69
Minimal luminal diameter, mm	1.07 ± 0.33 (144)	1.08 ± 0.30 (434)	0.79
% Diameter stenosis	58.8 ± 10.8 (144)	58.4 ± 10.3 (433)	0.70
<b>Dual antiplatelet therapy*</b>			
At discharge	100.0 (136/136)	99.5 (413/415)	1.00
At 6 mo	96.3 (131/136)	97.1 (403/405)	0.58
At 1 yr	82.4 (112/136)	82.9 (344/415)	0.90

Values are mean ± SD (N) and % (n/N). \*Patients taking both aspirin and thienopyridine. NA = not available; ACC/AHA = American College of Cardiology/American Heart Association; BVS = bioresorbable vascular scaffold.

definite/probable ST at 1-year follow-up between the 2 treatment groups (Table 4). Similarly, PoCE was observed in 7.8% of the BVS group and in 11.0% of the EES group, where the difference was not statistically significant ( $p = 0.39$ ).

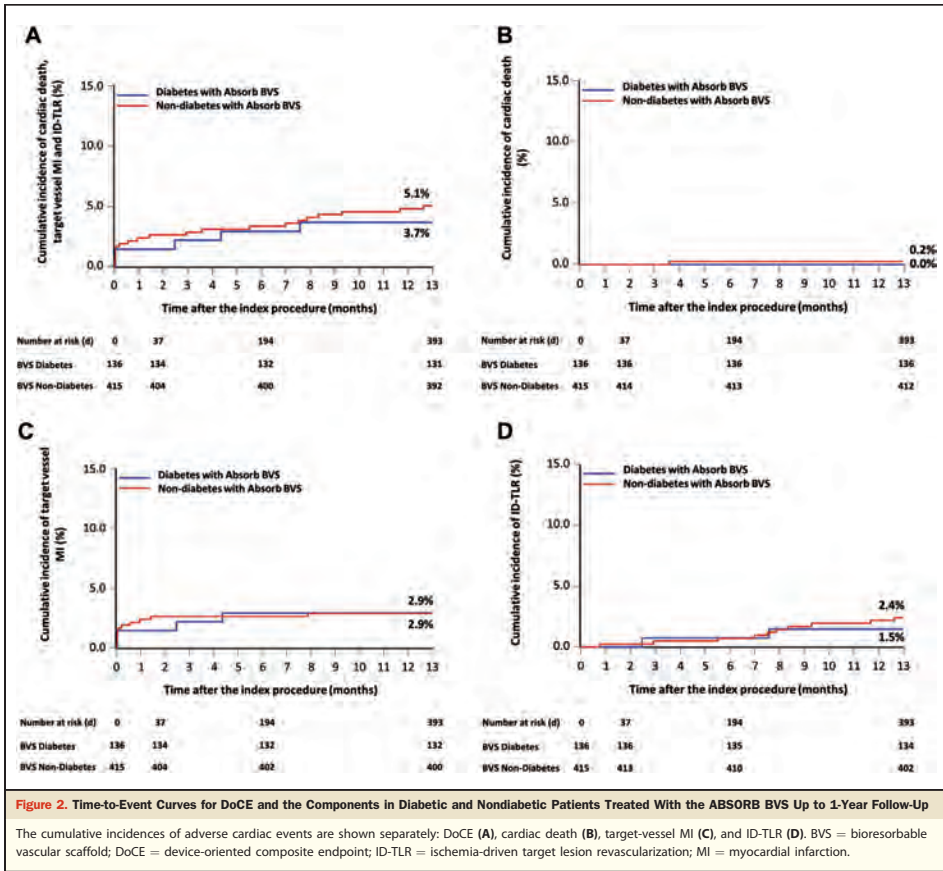
**Incidence of adverse events according to diabetes status in patients treated with the BVS.** In the present analysis, the BVS cohort included 415 nondiabetic patients, and 113 noninsulin-treated and 23 insulin-treated patients with diabetes. The incidences of DoCE, PoCE, and their components at 1 year according to diabetes status are shown in Figure 4. Insulin-treated diabetic patients tended to have a higher rate of adverse events compared with nondiabetic and noninsulin-treated diabetic patients, whereas these differences did not reach statistical significance (5.1% in no diabetes, 2.7% in noninsulin-treated diabetes, and 8.7% in insulin-treated diabetes for DoCE [ $p = 0.37$ ]; 8.2% in no diabetes, 7.1% in noninsulin-treated diabetes, and 8.7% in insulin-treated diabetes for PoCE [ $p = 0.92$ ]).

## Discussion

This is the first study addressing the clinical outcomes of diabetic patients treated with the Absorb BVS. The main findings of the present study can be summarized as follows: 1) there were no significant differences in 1-year rates of DoCE, PoCE, or ST between diabetic and nondiabetic patients treated with the Absorb BVS; 2) diabetic patients treated with the Absorb BVS showed 1-year rates of DoCE, PoCE, and ST similar to the matched diabetic patients treated with EES.

In general, diabetic patients undergoing PCI have an increased risk of restenosis and ST (10,19,20). Anatomic complexity of CAD, a phenotype expression of severity and duration of diabetic syndrome, may show a differential effect on the clinical outcomes in diabetic patients (21,22). In the present study, patient demographics and lesion characteristics were nearly identical between diabetic and nondiabetic patients treated with the BVS, and similar clinical outcomes were observed up to 1 year of follow-up. Specifically, the incidence rates of DoCE (3.7%) and definite/probable ST (0.7%) in diabetic patients treated with the BVS were favorable, although it should be emphasized that the present study included patients with relatively low risk profiles and noncomplex lesions. In addition, the potential under-reporting of events related to the specific monitoring of the ABSORB EXTEND trial should be noted.

Current therapeutic guidelines recommend DES rather than BMS for diabetic patients undergoing PCI for obstructive CAD (23,24). These guidelines, however, rely on the data derived from first-generation DES, showing considerable risk reduction of restenosis and TLR compared with BMS (4). Conversely, first-generation DES raised safety concerns regarding an increased risk of very late ST (25–27). Five-year follow-up data of the LEADERS (Limus Eluted From A Durable Versus ERodable Stent Coating) trial indicated that the newer generation biolimus-eluting stent with biodegradable polymer was associated with significantly lower incidence of PoCE and very late ST compared with the first-generation sirolimus-eluting stent in



the entire study group (9). Although the ESSENCE-DIABETES (Randomized Comparison of Everolimus-Eluting Stent Versus Sirolimus-Eluting Stent Implantation for De Novo Coronary Artery Disease in Patients With Diabetes Mellitus) trial and the diabetic subgroup analysis of the RESET (Randomized Evaluation of Sirolimus-eluting Versus Everolimus-Eluting Stent) trial showed the favorable trends toward the EES compared with the sirolimus-eluting stent, no data have supported the superiority of newer generation DES over first-generation DES in diabetic patients with respect to clinical outcomes (28,29). In the present analysis, a large number of diabetic patients from the SPIRIT trials facilitated fair comparisons between 2 different technologies eluting the same antiproliferative

drug everolimus by means of PS matching. One-year DoCE was observed in 3.9% and 6.4% in the BVS and EES groups, respectively ( $p = 0.38$ ). Although this result should be interpreted with caution due to the limited sample size and post-hoc analysis nature, our data suggest that the Absorb BVS is feasible, safe, and effective for the treatment of diabetic patients with noncomplex lesions.

Insulin and insulin-like growth factors promote stimulatory action on vascular smooth muscle cells, which might result in accelerated smooth muscle cell proliferation after coronary stenting (30). Everolimus reduces excessive neointimal hyperplasia by inhibiting the mammalian target of rapamycin that subsequently interferes with cellular mitosis. This process is tightly regulated by glycosylation-dependent

**Table 2. Clinical Outcomes of Diabetic and Nondiabetic Patients Treated With the Absorb BVS at 1-Year Follow-Up**

Outcomes	Absorb BVS: Diabetic Patients (N = 136)		Absorb BVS: Nondiabetic Patients (N = 415)		p Value
	% (n/N)	95% CI	% (n/N)	95% CI	
Device-oriented composite endpoint	3.7 (5/136)	1.2–8.4	5.1 (21/415)	3.2–7.6	0.64
Components (nonhierarchical)					
Cardiac death	0.0 (0/136)	0.0–2.7	0.2 (1/415)	0.0–1.3	1.00
Target vessel MI	2.9 (4/136)	0.8–7.4	2.9 (12/415)	1.5–5.0	1.00
Q-wave MI	0.0 (0/136)	0.0–2.7	1.0 (4/415)	0.3–2.5	0.58
Non-Q-wave MI	2.9 (4/136)	0.8–7.4	1.9 (8/415)	0.8–3.8	0.50
ID-TLR	1.5 (2/136)	0.2–5.2	2.4 (10/415)	1.2–4.4	0.74
CABG	0.0 (0/136)	0.0–2.7	0.2 (1/415)	0.0–1.3	1.00
PCI	1.5 (2/136)	0.2–5.2	2.2 (9/415)	1.0–4.1	1.00
Patient-oriented composite endpoint	7.4 (10/136)	3.6–13.1	8.2 (34/415)	5.7–1.3	0.86
Components (nonhierarchical)					
All-cause death	0.0 (0/136)	0.0–2.7	0.7 (3/415)	0.2–2.1	1.00
All MI	2.9 (4/136)	0.8–7.4	2.9 (12/415)	1.5–5.0	1.00
Q-wave MI	0.0 (0/136)	0.0–2.7	1.0 (4/415)	0.3–2.5	0.58
Non-Q-wave MI	2.9 (4/136)	0.8–7.4	1.9 (8/415)	0.8–3.8	0.50
Any repeat revascularization	5.1 (7/136)	2.1–10.3	5.1 (21/415)	3.2–7.6	1.00
CABG	0.0 (0/136)	0.0–2.7	0.7 (3/415)	0.2–2.1	1.00
PCI	5.1 (7/136)	2.1–10.3	4.6 (19/415)	2.8–7.1	0.82
Scaffold thrombosis per ARC definition					
Acute, <1 day					
Definite	0.0% (0/136)	0.0–2.7	0.0% (0/415)	0.0–0.9	NA
Probable	0.0% (0/136)	0.0–2.7	0.0% (0/415)	0.0–0.9	NA
Possible	0.0% (0/136)	0.0–2.7	0.0% (0/415)	0.0–0.9	NA
Definite + probable	0.0% (0/136)	0.0–2.7	0.0% (0/415)	0.0–0.9	NA
Subacute, 1–30 days					
Definite	0.0 (0/136)	0.0–2.7	0.2 (1/415)	0.0–1.3	1.00
Probable	0.0 (0/136)	0.0–2.7	0.2 (1/415)	0.0–1.3	1.00
Possible	0.0 (0/136)	0.0–2.7	0.0 (0/415)	0.0–0.9	NA
Definite + probable	0.0 (0/136)	0.0–2.7	0.5 (2/415)	0.1–1.7	1.00
Late, 31–365 days					
Definite	0.7 (1/136)	0.0–4.0	0.2 (1/414)	0.0–1.3	0.43
Probable	0.0 (0/136)	0.0–2.7	0.0 (0/414)	0.0–0.9	NA
Possible	0.0 (0/136)	0.0–2.7	0.2 (1/414)	0.0–1.3	1.00
Definite + probable	0.7 (1/136)	0.0–4.0	0.2 (1/414)	0.0–1.3	0.43
Overall up to 1 yr (0–365 days)					
Definite	0.7 (1/136)	0.0–4.0	0.5 (2/414)	0.1–1.7	0.57
Probable	0.0 (0/136)	0.0–2.7	0.2 (1/414)	0.0–1.3	1.00
Possible	0.0 (0/136)	0.0–2.7	0.2 (1/414)	0.0–1.3	1.00
Definite + probable	0.7 (1/136)	0.0–4.0	0.7 (3/414)	0.2–2.1	1.00

ARC = Academic Research Consortium; CABG = coronary artery bypass graft; CI = confidence interval; ID-TLR = ischemia-driven target lesion revascularization; MI = myocardial infarction; PCI = percutaneous coronary intervention; other abbreviations as in Table 1.

enzymes in contrast to paclitaxel, which interferes with multiple cellular processes (31). Indeed, a previous pooled analysis suggested an interaction between insulin use and drug type for the incidence of ischemia-driven TLR (10). In the present study, there were no significant differences in the incidence of DoCE among patients with insulin-treated diabetes, noninsulin-treated diabetes, and no diabetes treated

with the BVS. In addition, 1-year rates of DoCE in insulin-treated diabetic patients were similar between the BVS and EES (8.7% vs. 8.8%,  $p = 1.0$ ), although the present study might be underpowered to elicit small differences due to the sample size and relatively short follow-up period.

The ARC recommended 2 methodological approaches to report composite clinical outcomes: DoCE and PoCE. In

Table 3. Baseline Characteristics of Diabetic Patients Before and After Propensity-Score Matching						
	Before PS Matching			After PS Matching		
	Absorb BVS Diabetes (n = 136)	EES Diabetes (n = 882)	p Value	Absorb BVS Diabetes (n = 102)	EES Diabetes (n = 172)	p Value
Demographic characteristics						
Age, yrs	61.6 ± 10.0 (136)	63.6 ± 9.9 (882)	0.032	62.2 ± 9.8 (102)	62.2 ± 9.7 (172)	0.97
Male sex	73.5 (100/136)	64.3 (567/882)	0.035	71.6 (73/102)	66.9 (115/172)	0.42
Current smoker	19.9 (27/136)	18.5 (159/859)	0.71	19.6 (20/102)	20.3 (35/172)	0.88
Hypertension requiring medication	75.0 (102/136)	85.6 (754/881)	0.002	84.3 (86/102)	80.2 (138/172)	0.40
Hypercholesterolemia requiring medication	67.6 (92/136)	82.3 (718/872)	<0.001	73.5 (75/102)	76.7 (132/172)	0.55
Diabetes treatment						
Insulin	16.9 (23/136)	25.7 (227/882)	0.025	18.6 (19/102)	20.9 (36/172)	0.76
Oral hypoglycemic drugs	74.3 (101/136)	59.8 (527/882)	0.001	73.5 (75/102)	65.7 (113/172)	0.23
Physical exercise and/or diet modification only	4.4 (6/136)	9.8 (86/882)	0.052	3.9 (4/102)	9.3 (16/172)	0.15
No treatment	4.4 (6/136)	4.8 (42/882)	1.00	3.9 (4/102)	4.1 (7/172)	1.00
Family history of coronary artery disease	41.4 (53/128)	51.1 (377/738)	0.043	45.1 (46/102)	48.8 (84/172)	0.55
Unstable angina	33.8 (46/136)	26.5 (229/864)	0.08	31.4 (32/102)	31.4 (54/172)	1.00
Previous coronary intervention	23.5 (32/136)	34.7 (305/880)	0.010	21.6 (22/102)	31.4 (54/172)	0.08
Previous myocardial infarction	26.5 (36/136)	22.0 (187/849)	0.25	25.5 (26/102)	26.2 (45/172)	0.90
No. of diseased vessels						
Multivessel disease	23.5 (32/136)	41.7 (368/882)	<0.001	25.5 (26/102)	22.7 (39/172)	0.60
Target vessel						
	144 lesions	1,035 lesions		108 lesions	183 lesions	
Right coronary artery	36.8 (53/144)	28.8 (298/1,035)	0.049	37.0 (40/108)	24.0 (44/183)	0.018
Left anterior descending artery	36.1 (52/144)	41.4 (429/1,035)	0.22	35.2 (38/108)	49.7 (91/183)	0.016
Left circumflex artery or ramus	27.1 (39/144)	29.7 (307/1,035)	0.52	27.8 (30/108)	26.2 (48/183)	0.77
Left main coronary artery	0.0 (0/144)	0.1 (1/1,035)	1.00	0.0 (0/108)	0.0 (0/183)	NA
ACC/AHA lesion class						
	143 lesions	1,026 lesions		108 lesions	183 lesions	
A/B1	62.9 (90/143)	44.5 (457/1,026)	<0.001	60.2 (65/108)	55.2 (101/183)	0.41
B2/C	37.1 (53/143)	55.5 (569/1,026)	<0.001	39.8 (43/108)	44.8 (82/183)	0.41
Target lesion characteristics						
	144 lesions	1,035 lesions		108 lesions	183 lesions	
Lesion length, mm						
	11.7 ± 5.1 (143)	15.3 ± 6.6 (1,026)	<0.001	12.2 ± 5.2 (108)	12.6 ± 5.2 (183)	0.56
Pre-procedure						
Reference vessel diameter, mm	2.60 ± 0.33 (143)	2.74 ± 0.47 (1,029)	<0.001	2.62 ± 0.32 (108)	2.64 ± 0.41 (183)	0.62
Minimal luminal diameter, mm	1.07 ± 0.33 (144)	0.77 ± 0.39 (1,033)	<0.001	1.04 ± 0.30 (108)	0.99 ± 0.36 (183)	0.28
% diameter stenosis	58.8 ± 10.8 (144)	71.2 ± 12.6 (1,033)	<0.001	60.5 ± 9.5 (108)	62.4 ± 10.3 (183)	0.11
Dual antiplatelet therapy*						
At discharge	100.0 (136/136)	98.1 (862/879)	0.15	100.0 (102/102)	97.1 (167/172)	0.16
At 6 months	96.3 (131/136)	95.2 (837/879)	0.57	96.1 (98/102)	96.5 (166/172)	1.00
At 1 yr	82.4 (112/136)	81.2 (714/879)	0.75	83.3 (85/102)	79.7 (137/172)	0.45

Values are mean ± SD (N) and % (n/N).

EES = everolimus-eluting metal stent; PS = propensity score; other abbreviations as in Table 1.

the present analyses, we applied a DoCE as a primary endpoint because this represents the efficiency and efficacy of a new device. We also reported a PoCE because it represents the most critical clinical approach and may reflect the systemic risk and benefit for patients related to a new treatment. In the matched diabetic study group, the 1-year rate of PoCE was approximately twice as high as that of DoCE in both the BVS group and the EES group (3.9% for DoCE vs. 7.8% for PoCE in the BVS group and 6.4% for DoCE vs. 11.0% for PoCE in the EES group), driven by non-target lesion revascularizations. This finding is similar to those of previous DES studies (32) and highlights the

importance of optimal medical therapies and life-style modification for glycemic control as well as the frequently accompanying comorbidities such as hypertension, dyslipidemia, and obesity if clinical outcomes of diabetic patients with obstructive CAD are to be improved (33).

In the most recent report on serial angiographic assessment from the ABSORB Cohort B trial, the in-scaffold late loss of the BVS increased between 6 months and 1 year, whereas it remained stable after 1 year (0.16, 0.27, 0.27, and 0.29 mm at 6 months, 1 year, 2 years, and 3 years, respectively) (12,13,34). Conversely, in the SPIRIT II trial, the in-stent late loss of EES increased from 0.17 mm at

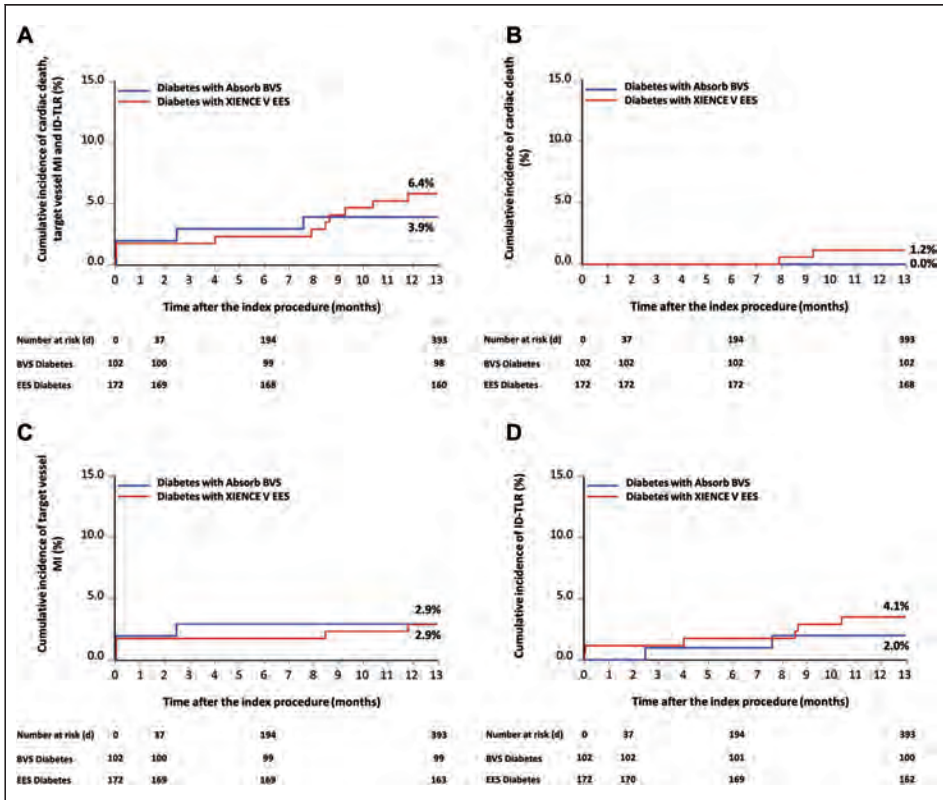


**Figure 3.** Time-to-Event Curves for DoCE and the Components in the Matched Diabetic Patients Treated With the BVS and in Those Treated With EES Up to 1-Year Follow-up

The cumulative incidences of adverse cardiac events are shown separately: DoCE (A), cardiac death (B), target-vessel MI (C), and ID-TLR (D). Abbreviations as in Figures 1 and 2.

6 months to 0.33 mm at 2 years (35). In this indirect comparison, the absolute change in late loss between 6 months and 2 years tended to be smaller with the BVS ( $\Delta 0.11$  mm) than EES ( $\Delta 0.16$  mm). More interestingly, intravascular ultrasound data demonstrated that the EES lumen volume slightly decreased between 6 months and 2 years in the SPIRIT II trial ( $159 \text{ mm}^3$  at 6 months and  $153 \text{ mm}^3$  at 2 years), whereas the BVS mean lumen area significantly increased from 1 to 3 years ( $6.35 \text{ mm}^2$  at 1 year and  $6.81 \text{ mm}^2$  at 3 years,  $p < 0.001$ ) in the serial observation of the ABSORB Cohort B trial (12). This phenomenon can be explained by the fact that mean and minimal scaffold

areas significantly increased and thereby compensated for neointimal hyperplasia. Therefore, the favorable trend toward BVS observed in 1-year clinical outcomes in the present study might become more pronounced with longer follow-up.

From a physiological perspective, the absence of permanent vessel caging facilitates the restoration of vasomotor function, adaptive shear stress, cyclic strain, and late luminal enlargement (11,36). In addition, fewer material triggers for very late ST such as uncovered struts and durable polymers would theoretically be present after bioresorption with the BVS compared with the DES (37). These beneficial effects

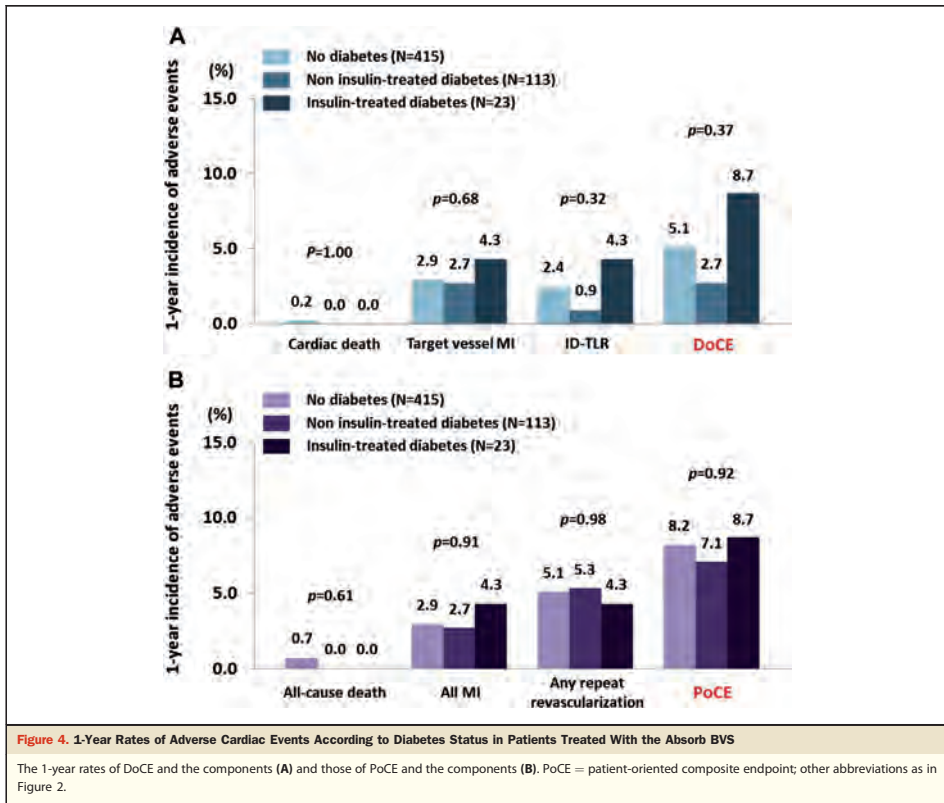
Table 4. Clinical Outcomes of Diabetic Patients Treated With BVS and EES at 1-Year Follow-Up										
Outcomes	Entire Population					Matched Population				
	Absorb BVS Diabetes (N = 136)		EES Diabetes (N = 882)		p Value	Absorb BVS Diabetes (N = 102)		EES Diabetes (N = 172)		p Value
	% (n/N)	95% CI	% (n/N)	95% CI		% (n/N)	95% CI	% (n/N)	95% CI	
Device-oriented composite endpoint	3.7 (5/136)	1.2–8.4	6.3 (56/882)	4.9–8.3	0.22	3.9 (4/102)	1.1–9.7	6.4 (11/172)	3.2–11.2	0.38
Components (nonhierarchical)										
Cardiac death	0.0 (0/136)	0.0–2.7	1.0 (9/882)	0.5–1.9	0.62	0.0 (0/102)	0.0–3.6	1.2 (2/172)	0.1–4.1	0.53
Target vessel MI	2.9 (4/136)	0.8–7.4	2.7 (24/882)	1.8–4.0	0.78	2.9 (3/102)	0.6–8.4	2.9 (5/172)	1.0–6.7	1.00
Q-wave MI	0.0 (0/136)	0.0–2.7	0.2 (2/882)	0.0–0.8	1.00	0.0 (0/102)	0.0–3.6	1.2 (2/172)	0.1–4.1	0.53
Non-Q-wave MI	2.9 (4/136)	0.8–7.4	2.5 (22/882)	1.6–3.8	0.77	2.9 (3/102)	0.6–8.4	1.7 (3/172)	0.4–5.0	0.67
ID-TLR	1.5 (2/136)	0.2–5.2	3.9 (34/882)	2.7–5.4	0.21	2.0 (2/102)	0.2–6.9	4.1 (7/172)	1.7–8.2	0.49
CABG	0.0 (0/136)	0.0–2.7	0.7 (6/882)	0.3–1.5	1.00	0.0 (0/102)	0.0–3.6	1.2 (2/172)	0.1–4.1	0.53
PCI	1.5 (2/136)	0.2–5.2	3.3 (29/882)	2.2–4.7	0.42	2.0 (2/102)	0.2–6.9	3.5 (6/172)	1.3–7.4	0.71
Patient-oriented composite endpoint	7.4 (10/136)	3.6–13.1	12.4 (109/882)	10.3–14.7	0.09	7.8 (8/102)	3.5–14.9	11.0 (19/172)	6.8–16.7	0.39
Components (nonhierarchical)										
All-cause death	0.0 (0/136)	0.0–2.7	1.8 (16/882)	1.0–2.9	0.15	0.0 (0/102)	0.0–3.6	1.2 (2/172)	0.1–4.1	0.53
All MI	2.9 (4/136)	0.8–7.4	2.8 (25/882)	1.8–4.2	1.00	2.9 (3/102)	0.6–8.4	2.9 (5/172)	1.0–6.7	1.00
Q-wave MI	0.0 (0/136)	0.0–2.7	0.2 (2/882)	0.0–0.8	1.00	0.0 (0/102)	0.0–3.6	1.2 (2/172)	0.1–4.1	0.53
Non-Q-wave MI	2.9 (4/136)	0.8–7.4	2.6 (23/882)	1.7–3.9	0.77	2.9 (3/102)	0.6–8.4	1.7 (3/172)	0.4–5.0	0.67
Any repeat revascularization	5.1 (7/136)	2.1–10.3	9.3 (82/882)	7.5–11.4	0.11	5.9 (6/102)	2.2–12.4	9.3 (16/172)	5.4–14.7	0.31
CABG	0.0 (0/136)	0.0–2.7	1.8 (16/882)	1.0–2.9	0.15	0.0 (0/102)	0.0–3.6	2.9 (5/172)	1.0–6.7	0.16
PCI	5.1 (7/136)	2.1–10.3	7.7 (68/882)	6.0–9.7	0.29	5.9 (6/102)	2.2–12.4	7.0 (12/172)	3.7–11.9	0.72
SST per ARC definition										
Acute, <1 day										
Definite	0.0 (0/136)	0.0–2.7	0.2 (2/882)	0.0–0.8	1.00	0.0 (0/102)	0.0–3.6	0.6 (1/172)	0.0–3.2	1.00
Probable	0.0 (0/136)	0.0–2.7	0.0 (0/882)	0.0–0.4	NA	0.0 (0/102)	0.0–3.6	0.0 (0/172)	0.0–2.1	NA
Possible	0.0 (0/136)	0.0–2.7	0.0 (0/882)	0.0–0.4	NA	0.0 (0/102)	0.0–3.6	0.0 (0/172)	0.0–2.1	NA
Definite + probable	0.0 (0/136)	0.0–2.7	0.2 (2/882)	0.0–0.8	1.00	0.0 (0/102)	0.0–3.6	0.6 (1/172)	0.0–3.2	1.00
Subacute, 1–30 days										
Definite	0.0 (0/136)	0.0–2.7	0.1 (1/882)	0.0–0.6	1.00	0.0 (0/102)	0.0–3.6	0.0 (0/172)	0.0–2.1	NA
Probable	0.0 (0/136)	0.0–2.7	0.0 (0/882)	0.0–0.4	NA	0.0 (0/102)	0.0–3.6	0.0 (0/172)	0.0–2.1	NA
Possible	0.0 (0/136)	0.0–2.7	0.0 (0/882)	0.0–0.4	NA	0.0 (0/102)	0.0–3.6	0.0 (0/172)	0.0–2.1	NA
Definite + probable	0.0 (0/136)	0.0–2.7	0.1 (1/882)	0.0–0.6	1.00	0.0 (0/102)	0.0–3.6	0.0 (0/172)	0.0–2.1	NA
Late, 31–365 days										
Definite	0.7 (1/136)	0.0–4.0	0.5 (4/874)	0.1–1.2	0.52	1.0 (1/102)	0.0–5.3	1.2 (2/172)	0.1–4.1	1.00
Probable	0.0 (0/136)	0.0–2.7	0.2 (2/874)	0.0–0.8	1.00	0.0 (0/102)	0.0–3.6	0.0 (0/172)	0.0–2.1	NA
Possible	0.0 (0/136)	0.0–2.7	0.7 (6/874)	0.3–1.5	1.00	0.0 (0/102)	0.0–3.6	1.2 (2/172)	0.1–4.1	0.53
Definite + probable	0.7 (1/136)	0.0–4.0	0.7 (6/874)	0.3–1.5	1.00	1.0 (1/102)	0.0–5.3	1.2 (2/172)	0.1–4.1	1.00
Overall up to 1 yr (0–365 days)										
Definite	0.7 (1/136)	0.0–4.0	0.8 (7/874)	0.3–1.6	1.00	1.0 (1/102)	0.0–5.3	1.7 (3/172)	0.4–5.0	1.00
Probable	0.0 (0/136)	0.0–2.7	0.2 (2/874)	0.0–0.8	1.00	0.0 (0/102)	0.0–3.6	0.0 (0/172)	0.0–2.1	NA
Possible	0.0 (0/136)	0.0–2.7	0.7 (6/874)	0.3–1.5	1.00	0.0 (0/102)	0.0–3.6	1.2 (2/172)	0.1–4.1	0.53
Definite + probable	0.7 (1/136)	0.0–4.0	1.0 (9/874)	0.5–2.0	1.00	1.0 (1/102)	0.0–5.3	1.7 (3/172)	0.4–5.0	1.00

ST = scaffold/stent thrombosis; other abbreviations as in Tables 1 to 3.

of the BVS, however, are not expected to be evident until after 1 year. Therefore, longer clinical follow-up is needed to elucidate the differential consequences of the Absorb BVS from a permanent metal prosthesis, in particular, for the diabetic patients.

**Study limitations.** First, the present analysis included noncomplex lesions according to pre-specified trial protocols.

Therefore, the clinical performance of the BVS in diabetic patients with complex lesions (e.g., diffuse lesion and calcified lesion) is still unknown. Second, despite the PS matching to allow fair comparisons between the BVS and the EES, the possibility of results being affected by unknown confounding factors cannot be excluded. Third, our results should be considered hypothesis generating due to the



nonrandomized, post-hoc nature of the analyses. In addition, the present analyses might be underpowered to demonstrate the differences of clinical efficacy between the devices. Further investigation is thus required in large-scale, randomized, controlled trials for a pre-specified diabetic study group.

### Conclusions

In this first report of the Absorb BVS in diabetic patients, the 1-year incidence rate of DoCE was 3.7%, similar to that in nondiabetic patients. In addition, no differences in the rates of 1-year DoCE, PoCE, or ST were observed in diabetic patients treated with the Absorb BVS and the XIENCE V EES in the matched study group from pooled prospective trials. These promising results should stimulate future trials of the Absorb BVS in larger cohorts of diabetic

patients with both complex and noncomplex lesions with long-term follow-up to demonstrate whether clinical advantages are present with this novel technology.

### Acknowledgments

The authors express their sincere appreciation to the participants and investigators of the ABSORB Cohort B, the ABSORB EXTEND, the SPIRIT First, the SPIRIT II, the SPIRIT III, and the SPIRIT IV trials. They are also grateful to Drs. Richard J. Rapoza, Krishna Sudhir, and Peter Staehr for their critical review of the manuscript and Sherry Cao for statistical assistance.

**Reprint requests and correspondence:** Dr. Patrick W. Serruys, Department of Interventional Cardiology, Thoraxcenter, Erasmus Medical Center, Ba 583, Dr Molewaterplein 40, 3015 GD, Rotterdam, the Netherlands. E-mail: p.w.j.c.serruys@erasmusmc.nl

## REFERENCES

- Zimmet P, Alberti KG, Shaw J. Global and societal implications of the diabetes epidemic. *Nature* 2001;414:782–7.
- Stamler J, Vaccaro O, Neaton JD, Wentworth D. Diabetes, other risk factors, and 12-yr cardiovascular mortality for men screened in the Multiple Risk Factor Intervention Trial. *Diabetes Care* 1993;16:434–44.
- Haffner SM, Lehto S, Ronnemaa T, Pyörälä K, Laakso M. Mortality from coronary heart disease in subjects with type 2 diabetes and in nondiabetic subjects with and without prior myocardial infarction. *N Engl J Med* 1998;339:229–34.
- Stettler C, Allemann S, Wandel S, et al. Drug eluting and bare metal stents in people with and without diabetes: collaborative network meta-analysis. *BMJ* 2008;337:a1331.
- Van Belle E, Perie M, Braune D, et al. Effects of coronary stenting on vessel patency and long-term clinical outcome after percutaneous coronary revascularization in diabetic patients. *J Am Coll Cardiol* 2002;40:410–7.
- Mathew V, Holmes DR. Outcomes in diabetics undergoing revascularization: the long and the short of it. *J Am Coll Cardiol* 2002;40:424–7.
- Stone GW, Midei M, Newman W, et al. Comparison of an everolimus-eluting stent and a paclitaxel-eluting stent in patients with coronary artery disease: a randomized trial. *JAMA* 2008;299:1903–13.
- Stone GW, Rizvi A, Newman W, et al. Everolimus-eluting versus paclitaxel-eluting stents in coronary artery disease. *N Engl J Med* 2010;362:1663–74.
- Serruys PW, Farooq V, Kalesan B, et al. Improved safety and reduction in stent thrombosis associated with biodegradable polymer-based biolimus-eluting stents versus durable polymer-based sirolimus-eluting stents in patients with coronary artery disease: final 5-year report of the LEADERS (Limus Eluted From A Durable Versus ERodable Stent Coating) randomized, noninferiority trial. *J Am Coll Cardiol Intv* 2013;6:777–89.
- Stone GW, Kedhi E, Kereiakes DJ, et al. Differential clinical responses to everolimus-eluting and paclitaxel-eluting coronary stents in patients with and without diabetes mellitus. *Circulation* 2011;124:893–900.
- Onuma Y, Serruys PW. Bioresorbable scaffold: the advent of a new era in percutaneous coronary and peripheral revascularization? *Circulation* 2011;123:779–97.
- Serruys PW, Onuma Y, Garcia-Garcia HM, et al. Dynamics of vessel wall changes following the implantation of the Absorb everolimus-eluting bioresorbable vascular scaffold: a multi-imaging modality study at 6, 12, 24 and 36 months. *EuroIntervention* 2013 Dec 3 [E-pub ahead of print].
- Serruys PW, Onuma Y, Dudek D, et al. Evaluation of the second generation of a bioresorbable everolimus-eluting vascular scaffold for the treatment of de novo coronary artery stenosis: 12-month clinical and imaging outcomes. *J Am Coll Cardiol* 2011;58:1578–88.
- Muramatsu T, Onuma Y, Garcia-Garcia HM, et al. Incidence and short-term clinical outcomes of small side branch occlusion after implantation of an everolimus-eluting bioresorbable vascular scaffold: an interim report of 435 patients in the ABSORB-EXTEND single-arm trial in comparison with an everolimus-eluting metallic stent in the SPIRIT First and II trials. *J Am Coll Cardiol Intv* 2013;6:247–57.
- Serruys PW, Ong AT, Piek JJ, et al. A randomized comparison of a durable polymer Everolimus-eluting stent with a bare metal coronary stent: the SPIRIT first trial. *EuroIntervention* 2005;1:58–65.
- Serruys PW, Ruysgrok P, Neuzner J, et al. A randomised comparison of an everolimus-eluting coronary stent with a paclitaxel-eluting coronary stent: the SPIRIT II trial. *EuroIntervention* 2006;2:286–94.
- Cutlip DE, Windecker S, Mehran R, et al. Clinical end points in coronary stent trials: a case for standardized definitions. *Circulation* 2007;115:2344–51.
- Vranckx P, Cutlip DE, Mehran R, et al. Myocardial infarction adjudication in contemporary all-comer stent trials: balancing sensitivity and specificity. Addendum to the historical MI definitions used in stent studies. *EuroIntervention* 2010;5:871–4.
- Kornowski R, Mintz GS, Kent KM, et al. Increased restenosis in diabetes mellitus after coronary interventions is due to exaggerated intimal hyperplasia. A serial intravascular ultrasound study. *Circulation* 1997;95:1366–9.
- Iakovou I, Schmidt T, Bonizzoni E, et al. Incidence, predictors, and outcome of thrombosis after successful implantation of drug-eluting stents. *JAMA* 2005;293:2126–30.
- Farkouh ME, Domanski M, Sleeper LA, et al. Strategies for multivessel revascularization in patients with diabetes. *N Engl J Med* 2012;367:2375–84.
- Serruys PW, Farooq V. Revascularization strategies in patients with diabetes. *N Engl J Med* 2013;368:1454–5.
- Wijns W, Kolh P, Danchin N, et al. Guidelines on myocardial revascularization. *Eur Heart J* 2010;31:2501–55.
- Levine GN, Bates ER, Blankenship JC, et al. American College of Cardiology Foundation; American Heart Association Task Force on Practice Guidelines; Society for Cardiovascular Angiography and Interventions. 2011 ACCF/AHA/SCAI guideline for percutaneous coronary intervention. A report of the American College of Cardiology Foundation/American Heart Association Task Force on Practice Guidelines and the Society for Cardiovascular Angiography and Interventions. *J Am Coll Cardiol* 2011;58:e44–122.
- Camenzind E, Steg PG, Wijns W. Stent thrombosis late after implantation of first-generation drug-eluting stents: a cause for concern. *Circulation* 2007;115:1440–55, discussion 1455.
- Maisel WH. Unanswered questions—drug-eluting stents and the risk of late thrombosis. *N Engl J Med* 2007;356:981–4.
- Spaulding C, Daemen J, Boersma E, Cutlip DE, Serruys PW. A pooled analysis of data comparing sirolimus-eluting stents with bare-metal stents. *N Engl J Med* 2007;356:989–97.
- Kim WJ, Lee SW, Park SW, et al. Randomized comparison of everolimus-eluting stent versus sirolimus-eluting stent implantation for de novo coronary artery disease in patients with diabetes mellitus (ESSENCE-DIABETES): results from the ESSENCE-DIABETES trial. *Circulation* 2011;124:886–92.
- Kimura T, Morimoto T, Natsuaki M, et al. Comparison of everolimus-eluting and sirolimus-eluting coronary stents: 1-year outcomes from the Randomized Evaluation of Sirolimus-eluting Versus Everolimus-eluting stent Trial (RESET). *Circulation* 2012;126:1225–36.
- Bornfeldt KE, Raines EW, Nakano T, Graves LM, Krebs EG, Ross R. Insulin-like growth factor-I and platelet-derived growth factor-BB induce directed migration of human arterial smooth muscle cells via signaling pathways that are distinct from those of proliferation. *J Clin Invest* 1994;93:1266–74.
- Rocic P. Differential phosphoinositide 3-kinase signaling: implications for PTCA? *Am J Physiol Heart Circ Physiol* 2009;297:H1970–1.
- Silber S, Windecker S, Vranckx P, Serruys PW. Unrestricted randomised use of two new generation drug-eluting coronary stents: 2-year patient-related versus stent-related outcomes from the RESOLUTE All Comers trial. *Lancet* 2011;377:1241–7.
- Ryden L, Standl E, Bartnik M, et al. Guidelines on diabetes, pre-diabetes, and cardiovascular diseases: executive summary. The Task Force on Diabetes and Cardiovascular Diseases of the European Society of Cardiology (ESC) and of the European Association for the Study of Diabetes (EASD). *Eur Heart J* 2007;28:88–136.
- Ormiston JA, Serruys PW, Onuma Y, et al. First serial assessment at 6 months and 2 years of the second generation of absorb everolimus-eluting bioresorbable vascular scaffold: a multi-imaging modality study. *Circ Cardiovasc Interv* 2012;5:620–32.
- Claessen BE, Beijk MA, Legrand V, et al. Two-year clinical, angiographic, and intravascular ultrasound follow-up of the XIENCE V everolimus-eluting stent in the treatment of patients with de novo native coronary artery lesions: the SPIRIT II trial. *Circ Cardiovasc Interv* 2009;2:339–47.
- Serruys PW, Garcia-Garcia HM, Onuma Y. From metallic cages to transient bioresorbable scaffolds: change in paradigm of coronary revascularization in the upcoming decade? *Eur Heart J* 2012;33:16–25b.
- Muramatsu T, Onuma Y, Zhang YJ, et al. Progress in treatment by percutaneous coronary intervention: the stent of the future. *Rev Esp Cardiol* 2013;66:483–96.

**Key Words:** bioresorbable scaffold ■ coronary artery disease ■ diabetes mellitus ■ drug-eluting stent.

## APPENDIX

For supplemental material including a table, please see the online version of this article.

## 5.5 Clinical use of the Absorb BVS in true bifurcation lesion

Complex bifurcation percutaneous coronary intervention with the Absorb bioresorbable vascular scaffold.

*Eurointervention.* 2013;9:888.

[Case report, Impact Factor (2013): 3.758]

Džavík V, Muramatsu T, Crooks N, Nakatani S, Onuma Y.





# Complex bifurcation percutaneous coronary intervention with the Absorb bioresorbable vascular scaffold

Vladimír Džavík<sup>1\*</sup>, MD; Takashi Muramatsu<sup>2</sup>, MD; Noel Crooks<sup>1</sup>, MD; Shimpei Nakatani<sup>2</sup>, MD; Yoshinubu Onuma<sup>2</sup>, MD

1. Peter Munk Cardiac Centre, University Health Network, Toronto, Ontario, Canada; 2. Thoraxcenter, Erasmus Medical Center, Rotterdam, The Netherlands

GUEST EDITOR: Carlo Di Mario, MD, PhD; NHLI Cardiovascular Biomedical Research Unit, Royal Brompton Hospital, London, United Kingdom

The accompanying supplementary data are published online at: [http://www.pronline.com/eurointervention/66th\\_issue/145](http://www.pronline.com/eurointervention/66th_issue/145)

A 50-year-old diabetic man underwent percutaneous coronary intervention of an LAD/diagonal bifurcation lesion with deployment of a 3.0×28 mm Absorb bioresorbable vascular scaffold (Abbott Vascular, Santa Clara, CA, USA) in the LAD (**Online Figure 1A, Moving image 1**). After through-the-strut dilation, a 2.5×38 mm XIENCE PRIME™ stent (Abbott Vascular) was deployed in the side branch with a 3.0×15 mm non-compliant balloon positioned in the LAD. A final kissing balloon inflation (FKB) was then performed at 4 atmospheres (**Online Figure 1B, Moving image 2**). Optical coherence tomography 3-D reconstruction revealed preserved integrity of the bioresorbable vascular scaffold (BVS) rings and complete opening of the side branch ostium (**Figure 1, Online Figures 2-5, Moving image 3-5**). Inflation through the struts of the BVS is feasible but must be performed slowly. Aggressive inflation can result in ring fracture, instability of the scaffold, and potentially thrombosis. BVS disruption has been observed clinically, and in bench testing after FKB at or just

above the maximal recommended diameter for the BVS, using Finet's principle. If FKB is necessary, inflation must be performed slowly and to low pressures only, maintaining the combined inflated balloon diameter below the recommended limit of the device. Intravascular imaging of the final result is mandatory.

Editorial, see page 777

## Guest Editor

This paper was Guest Edited by Carlo Di Mario, MD, PhD; NHLI Cardiovascular Biomedical Research Unit, Royal Brompton Hospital, London, United Kingdom.

## Conflict of interest statement

V. Džavík has received educational and travel grants, and speaker honoraria from Abbott Vascular, and educational grants from St. Jude Medical. The other authors have no conflicts of interest to declare.

## Online data supplement

**Online Figure 1.** LAD diagonal bifurcation before (A) and after (B) T-stenting.

**Online Figure 2.** 2-D OCT images through the side branch showing BVS/EES overlap at the carina (A), the carina (B) and proximal to the carina (C).

**Online Figure 3.** 3-D OCT reconstruction of the side branch ostium.

**Online Figure 4.** 3-D OCT details of the BVS/EES interface at the side branch ostium.

**Online Figure 5.** Fly-through views from the distal main vessel and from the side-branch.

**Moving image 1.** Pre-PCI angiogram of a Medina 0,1,1 LAD/D1 bifurcation lesion.

**Moving image 2.** Final post-PCI angiogram.

**Moving image 3.** An OCT pullback from the diagonal branch to the proximal LAD.

**Moving image 4.** An OCT pullback from the mid LAD to the proximal LAD.

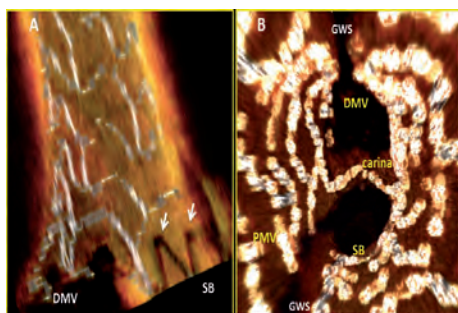


**Figure 1.** A) 3-D OCT of the BVS/EES interface at the side branch ostium. B) fly-through view from the side branch. DMV: distal main vessel; GWS: guidewire shadow; PMV: proximal main vessel; SB: side branch. Arrows indicate XIENCE V stent struts

\*Corresponding author: Peter Munk Cardiac Centre, University Health Network, 6-246 EN, Toronto General Hospital, 200 Elizabeth Street, Toronto, Ontario, M5G 2C4, Canada. E-mail: [vlad.dzavik@uhn.ca](mailto:vlad.dzavik@uhn.ca)

© Europa Digital & Publishing 2013. All rights reserved.



## 5.6 Side branch occlusion and peri-procedural myocardial infarction

Incidence and short-term clinical outcomes of small side branch occlusion after implantation of an everolimus-eluting bioresorbable vascular scaffold: An interim report of 435 patients in the ABSORB-EXTEND single-arm trial in comparison with an everolimus-eluting metallic stent in the SPIRIT first and II trials.

*JACC Cardiovasc Interv.* 2013;6:247-57.

[Original research paper, Impact Factor (2013): 7.440]

Muramatsu T, Onuma Y, García-García HM, Farooq V, Bourantas CV, Morel MA, Li X, Veldhof S, Bartorelli A, Whitbourn R, Abizaid A, Serruys PW.





# Incidence and Short-Term Clinical Outcomes of Small Side Branch Occlusion After Implantation of an Everolimus-Eluting Bioresorbable Vascular Scaffold

An Interim Report of 435 Patients in the ABSORB-EXTEND Single-Arm Trial in Comparison With an Everolimus-Eluting Metallic Stent in the SPIRIT First and II Trials

Takashi Muramatsu, MD, PhD,\* Yoshinobu Onuma, MD,\*  
Hector M. García-García, MD, PhD,\*† Vasim Farooq, MBChB,\*  
Christos V. Bourantas, MD, PhD,\* Marie-Angèle Morel, BSc,† Xiaolin Li, MSc,‡  
Susan Veldhof, RN,§ Antonio Bartorelli, MD,|| Robert Whitbourn, MD,¶  
Alexandre Abizaid, MD, PhD,# Patrick W. Serruys, MD, PhD,\* on behalf of the  
ABSORB-EXTEND Investigators

*Rotterdam, the Netherlands; Diegem, Belgium; Melbourne, Australia; and São Paulo, Brazil*

**Objectives** The aim of this study was to investigate the incidence and clinical sequelae of small side branch occlusion (SBO) after Absorb (Abbott Vascular, Santa Clara, California) bioresorbable vascular scaffold (BVS) implantation.

**Background** The thicker strut of metallic stents potentially contributes to a higher incidence of SBO.

**Methods** We performed a post-hoc angiographic assessment of 1,209 side branches in 435 patients enrolled in the ABSORB-EXTEND single-arm trial (ABSORB EXTEND Clinical Investigation: A Continuation in the Clinical Evaluation of the ABSORB Bioresorbable Vascular Scaffold [BVS] System in the Treatment of Subjects With de Novo Native Coronary Artery Lesions), in comparison with 682 side branches in 237 patients treated with the everolimus-eluting metallic stent (EES) in the SPIRIT (A Clinical Evaluation of an Investigational Device. The Abbott XIENCE V Everolimus Eluting Coronary Stent System in the Treatment of Patients With de Novo Native Coronary Artery Lesions) first and II trials. Any visible side branches originating within the device implantation site or the 5-mm proximal and distal margins were included in the angiographic assessment. The SBO was defined as a reduction in Thrombolysis In Myocardial Infarction flow grade 0 or 1.

**Results** Post-procedural SBO was observed in 73 side branches (6.0%) in BVS group and 28 side branches (4.1%) in EES group ( $p = 0.09$ ). Patients with post-procedural SBO were significantly associated with an increased incidence of in-hospital myocardial infarction (6.5% in SBO group vs. 0.5% in non-SBO group,  $p < 0.01$ ). Multivariable analysis revealed that BVS was an independent predictor of post-procedural SBO (odds ratio: 2.09; 95% confidence interval: 1.18 to 3.68). By stratified analysis, BVS demonstrated a higher incidence of post-procedural SBO compared with EES only in small side branches with a reference vessel diameter  $\leq 0.5$  mm (10.5% vs. 3.9%,  $p = 0.03$  between the groups,  $p$  for interaction = 0.08).

**Conclusions** Bioresorbable vascular scaffold was associated with a higher incidence of post-procedural SBO compared with EES. This effect was more pronounced with small side branches with a reference vessel diameter  $\leq 0.5$  mm. (ABSORB EXTEND Clinical Investigation: A Continuation in the Clinical Evaluation of the ABSORB Bioresorbable Vascular Scaffold [BVS] System in the Treatment of Subjects With de Novo Native Coronary Artery Lesions: NCT01023789) (J Am Coll Cardiol Intv 2013;6:247–57) © 2013 by the American College of Cardiology Foundation

Side branch occlusion (SBO) has been implicated as a contributing factor to the development of periprocedural myocardial infarction (MI) after percutaneous coronary intervention (1–3). Periprocedural MI has been associated with unfavorable late clinical outcomes, including an increased risk of cardiac mortality (4–6). Mechanisms to explain the incidence of SBO after the metallic platform stent implantation have included mechanical vessel straightening and enlargement of the stented vessel, bifurcation carina shift, and/or coronary plaque shift into the orifice of side branch (7–9). In addition, the increased strut thicknesses of the first-generation drug-eluting stents (DES) has been implicated in contributing to a higher incidence of SBO compared with the thinner strut second-generation DES (10,11).

### Abbreviations and Acronyms

- BVS** = bioresorbable vascular scaffold(s)
- CK** = creatine kinase
- CK-MB** = creatine kinase myocardial band
- DES** = drug-eluting stent(s)
- DS** = diameter stenosis
- EES** = everolimus-eluting metallic stent(s)
- MI** = myocardial infarction
- NQMI** = non-Q-wave myocardial infarction
- PES** = paclitaxel-eluting stent(s)
- QCA** = quantitative coronary angiography
- ROI** = region of interest
- RVD** = reference vessel diameter
- SBO** = side branch occlusion
- TIMI** = Thrombolysis In Myocardial Infarction
- ZES** = zotarolimus-eluting stent(s)

Fully bioresorbable vascular scaffolds (BVS) are a novel approach to the treatment of coronary lesions, in that they provide transient vessel support and drug delivery to the vessel wall, without the potential long-term limitations of conventional metallic DES, such as stent thrombosis and prevention of future surgical revascularization (12–14). In addition, the BVS has the potential to restore a more normal vascular physiology of the treated vessel (13,14). Early studies investigating the current generation of the everolimus-eluting BVS system (Absorb, Abbott Vascular, Santa Clara, California) have been shown to have excellent angiographic and clinical outcomes (12,15–17). The strut thickness of Absorb BVS is 157  $\mu\text{m}$ , which is comparable to the first-generation

DES (e.g., Cypher [Cordis Corporation, Johnson & Johnson, Warren, New Jersey], 153  $\mu\text{m}$ ; Taxus Express2 [Bos-

ton Scientific, Natick, Massachusetts], 148  $\mu\text{m}$ ) and thicker than newer-generation DES (e.g., Xience V [Abbott Vascular, Santa Clara, California], 89  $\mu\text{m}$ ) (18). The increased strut thickness of the Absorb BVS is to allow for sufficient radial strength and prevent acute vessel recoil (19,20). Given the increased strut thickness of the Absorb BVS, a potential concern exists that it might be associated with a higher incidence of SBO compared with newer-generation DES. The aim of this study is to assess the incidence and clinical impact of SBO after Absorb BVS implantation in a prospective, multicenter, single-arm trial. To allow for comparisons between the Absorb BVS and newer-generation DES, the SPIRIT (A Clinical Evaluation of an Investigational Device. The Abbott XIENCE V Everolimus Eluting Coronary Stent System in the Treatment of Patients With de Novo Native Coronary Artery Lesions) first and II trials investigating the everolimus-eluting metallic stent (EES) will act as a historical control (21,22).

### Methods

**Study population.** We studied patients enrolled in the ABSORB-EXTEND single-arm trial (ABSORB EXTEND Clinical Investigation: A Continuation in the Clinical Evaluation of the ABSORB Bioresorbable Vascular Scaffold [BVS] System in the Treatment of Subjects With de Novo Native Coronary Artery Lesions). This trial is prospectively assessing the safety and feasibility of the Absorb BVS (see trial registry information after abstract). In brief, patients older than 18 years who have 1 or 2 de novo lesions located in different native coronary arteries were enrolled. Target lesions must have been located in a major epicardial vessel or side branch with a visually estimated stenosis of  $\geq 50\%$  and  $< 100\%$  and a Thrombolysis In Myocardial Infarction (TIMI) flow grade of  $\geq 1$ . The target lesions must have a diameter of 2.0 to 3.3 mm and a lesion length of  $\leq 28$  mm, both assessed by online quantitative coronary angiography (QCA). Exclusion criteria included aorto-ostial lesions, left main coronary artery lesions, total occlusions, lesions with visible thrombus, heavily calcified lesions, and bifurcation lesions involving a side branch  $\geq 2$  mm in diameter and ostial lesions  $> 40\%$  stenosed by visual estimation or a side branch requiring pre-dilation.

For the current analysis, patients treated with EES (Xience V) in the SPIRIT first and II trials were used as a historical control. The SPIRIT first and II trials compared the EES with either the bare-metal stent (SPIRIT first trial, NCT00180453) or with the paclitaxel-eluting stent (SPIRIT II trial, NCT00180310). The details of the SPIRIT first and II trials have previously been described (21,22). The SPIRIT first trial included patients with single de novo lesion that was 3.0 mm in diameter and that could be covered by an 18-mm stent. The SPIRIT II trial allowed for the inclusion of patients with 1 or 2 lesions in different

From the \*Thoraxcenter, Erasmus Medical Center, Rotterdam, the Netherlands; †Cardialysis B.V., Rotterdam, the Netherlands; ‡Abbott Vascular, Santa Clara, California; §Abbott Vascular, Diegem, Belgium; ||Department of Cardiovascular Sciences, University of Milan, Centro Cardiologico Monzino, IRCCS, Milan, Italy; ¶Department of Cardiology, St. Vincent's Hospital, Fitzroy, Victoria, Melbourne, Australia; and the #Instituto Dante Pazzanese de Cardiologia, São Paulo, Brazil. The ABSORB-EXTEND trial has been sponsored and funded by Abbott Vascular. Ms. Li and Ms. Veldhof are full employees of Abbott Vascular. Dr. Bartorelli has served on the advisory board and received minor honoraria for Abbott Vascular. All other authors have reported that they have no relationships relevant to the contents of this paper to disclose.

Manuscript received October 18, 2012; accepted October 26, 2012.

	Macroscopic appearance	Material	Cross-section	Strut thickness
Absorb BVS		PLLA + PDLLA		157 $\mu\text{m}$
Xience V		Co-Cr + durable fluoropolymer		89 $\mu\text{m}$

**Figure 1.** Features of Absorb BVS and Xience V

Absorb BVS (Abbott Vascular, Santa Clara, California) and Xience V (Abbott Vascular, Santa Clara, California). Co-Cr = cobalt–chromium; PLLA = poly-L-lactide; PDLLA = poly-D,L-lactide.

major epicardial vessels that were 2.5 to 4.25 mm in diameter and  $\leq 28$  mm in lesion length. Exclusion criteria were similar to that in the ABSORB-EXTEND trial. All trials were approved by the institutional review board, and

written informed consent was obtained from each patient before inclusion.

**Study devices.** The backbone of the Absorb BVS is made of semi-crystalline poly-L-lactide (12). The coating consists of

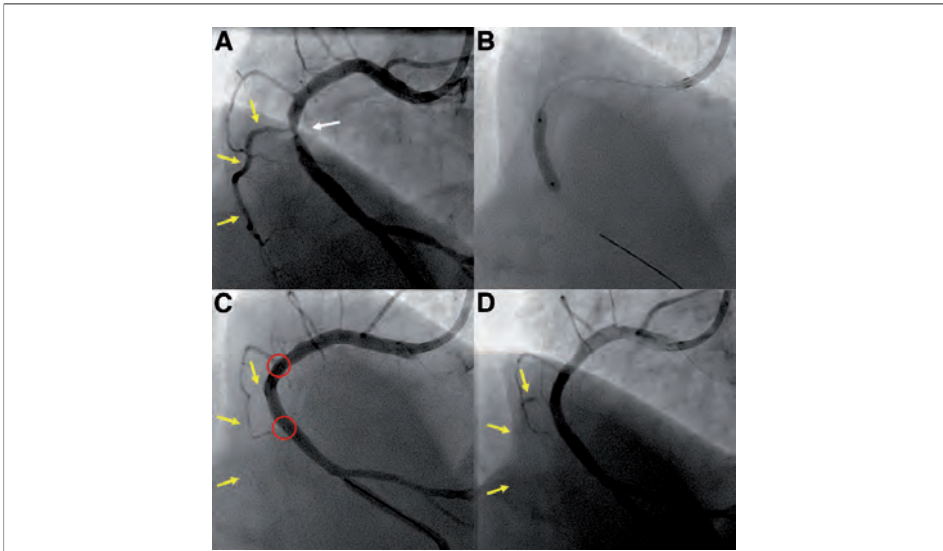


**Figure 2.** Representative Case of Side Branch Occlusion

Pre-procedure angiography showed a focal stenosis (A, white arrow) and a side branch in the mid-segment of the right coronary artery (A, yellow arrows). Immediately after Absorb bioresorbable vascular scaffold (BVS) implantation (B), a jailed side branch was occluded at the ostium (C, yellow arrows; red circles indicate the proximal and distal markers of the Absorb BVS). This side branch continued to be occluded at the post-procedural angiography (D, yellow arrows).

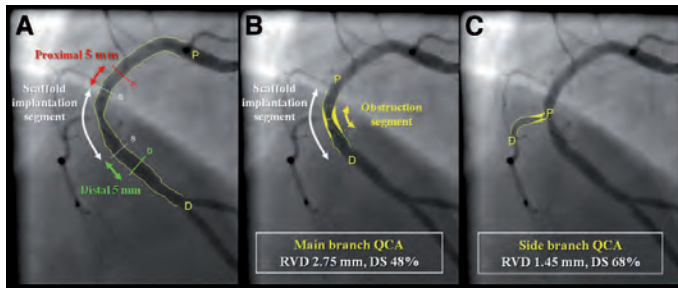


**Figure 3. Assessment of QCA**

Pre-procedural quantitative coronary angiography (QCA) analyses are shown. The QCA analysis delineates 5-mm proximal (A, red double arrow) and distal segment (A, green double arrow) to the intended device implantation site (A, white double arrow). Any visible side branches originating from this region of interest were analyzed. The conventional QCA analysis automatically delineates an obstruction segment in the main branch (yellow double arrow). An example of side branch analysis is shown in C. The results of QCA analysis are shown in the white-outlined box. DS = diameter stenosis; RVD = reference vessel diameter.

poly-D,L-lactide which controls the release of the antiproliferative drug everolimus. Both poly-L-lactide and poly-D,L-lactide are fully bioresorbable and degrade to lactic acid, which is metabolized via the Krebs cycle. The Absorb BVS has struts with a thickness of 157  $\mu\text{m}$  and zigzag hoops connected by 3 links, similar to the Xience V design. The

Xience V is an everolimus-eluting metallic stent with a platform of cobalt-chromium alloy and the durable fluoropolymer coating (23). The overall strut thickness of the Xience V is 89  $\mu\text{m}$  (Fig. 1).

**Treatment procedure.** Lesions were treated with standard interventional techniques, with mandatory pre-dilation and

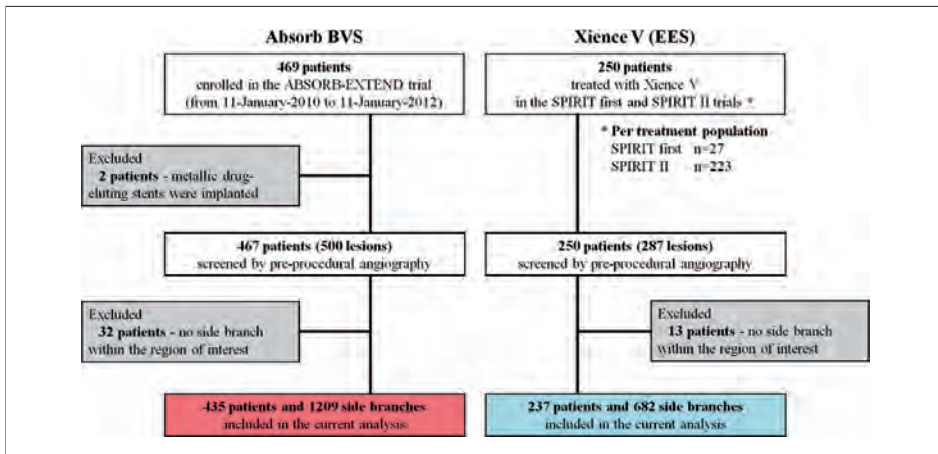


**Figure 4. Flow Diagram of Study**

Absorb BVS (Abbott Vascular, Santa Clara, California); ABSORB-EXTEND single-arm trial (ABSORB EXTEND Clinical Investigation: A Continuation in the Clinical Evaluation of the ABSORB Bioresorbable Vascular Scaffold [BVS] System in the Treatment of Subjects With de Novo Native Coronary Artery Lesions); SPIRIT (A Clinical Evaluation of an Investigational Device: The Abbott XIENCE V Everolimus Eluting Coronary Stent System in the Treatment of Patients With de Novo Native Coronary Artery Lesions) first and II trials; Xience V (Abbott Vascular, Santa Clara, California).

scaffold/stent implantation at a pressure not exceeding the burst pressure rate. Post-dilation was left to the discretion of the operator and only permitted with balloons sized to fit within the boundaries of the scaffold/stent. The Absorb BVS was available in diameters of 2.5 and 3.0 mm and lengths of 18 and 28 mm, in the ABSORB-EXTEND trial. A single 3.0 × 18 mm EES was used in the SPIRIT first trial, whereas the EES in diameters of 2.5, 3.0, 3.5, and 4.0 mm and lengths of 8, 18, and 28 mm were used in the SPIRIT II trial.

**Definition of SBO and clinical outcomes.** Side branch occlusion was defined as a reduction in TIMI flow to grade 0 or 1. Accordingly, side branches with pre-procedural TIMI flow grade 0 or 1 were excluded. In the current analysis, the primary clinical outcome was evaluated by in-hospital Q-wave MI or non-Q-wave myocardial infarction (NQMI). In-hospital events were defined as those occurring during hospital stay ≤7 days post-procedure. Per protocol definition of MI was an increase in the creatine kinase (CK) level to more than twice the upper limit of the normal, accompanied by an increased level of creatine kinase myocardial band (CK-MB) (24). Per protocol CK-MB assessment was a mandatory requirement if the CK was greater than upper limit of the normal. Within study sites where troponin is routinely used in the clinical practice, CK, and CK-MB assessments were obligatory if the troponin level was elevated. All clinical outcomes were adjudicated by an independent Clinical Events Committee.

**Angiographic assessment and QCA.** The region of interest (ROI) was defined as the study device implantation site and the 5-mm proximal and distal margins in the main branch. All pre-procedural visible small side branches originating within ROI were included in the angiographic assessment. All side branches were assessed in at least 2 different projections, with angiographic assessment for each side branch performed at 5 time points during the procedure (i.e., pre-procedure, after pre-dilation, after study device implantation, after post-dilation and post-procedure). A case example of SBO in the ABSORB-EXTEND trial is shown in Figure 2.

The main branch and side branch were evaluated separately by conventional 2-dimensional, single-vessel, off-line QCA analysis (25). The obstruction segment was automatically delineated by main branch QCA analysis within the scaffold/stent implantation segment, as defined by radio-opaque markers for the Absorb BVS, or by the stent borders identified on the positioning/implantation cine-runs for the EES (26). The ostial side branch location was classified into 3 subsegments: 1) obstruction segment, 2) the scaffold/stent implantation segment outside obstruction, and 3) the 5-mm proximal and distal margins of the scaffold/stent implantation site (Fig. 3). A QCA analyses of small side branches, with a reference vessel diameter (RVD) of ≤0.5 mm, could not be undertaken because the angiographic analysis system

was not validated for the vessels with this size (CAAS 5.10, Pie Medical, Maastricht, the Netherlands) (27,28). Therefore, such small side branches were assessed only for TIMI flow grade during the procedure.

**Statistical analysis.** Data were analyzed on a patient-level basis. Continuous variables are expressed as means ± SD and were compared by *t* test. Categorical variables are presented as proportions (percentage) and compared by Fisher exact test. Univariable and multivariable logistic regression models were applied to determine the predictors of post-procedural SBO. The logistic regression model was performed on a patient-level basis, including the following variables; age, male sex, current smoking, hypertension requiring treatment, dyslipidemia requiring treatment, any diabetes, unstable angina, family history of coronary artery disease, prior MI, number of diseased vessels (single or

**Table 1. Baseline Demographic Data and Angiographic Characteristics in Patients With Side Branches**

Variables	Absorb BVS (n = 435)	EES (n = 237)	p Value
Age (yrs)	61.4 ± 10.6	62.2 ± 10.4	0.35
Male (%)	75.2	70.0	0.17
Hypertension	65.5	68.4	0.49
Diabetes mellitus	26.2	22.4	0.30
Dyslipidemia	62.3	68.8	0.11
Current smoker	21.8	32.6	<0.01
Unstable angina	31.3	26.2	0.18
Family history of coronary artery disease	34.1	45.0	0.01
Prior history of myocardial infarction	28.7	33.9	0.19
Number of diseased vessels			
1-vessel disease	80.0	69.2	<0.01
2-vessel disease	16.3	26.2	<0.01
3-vessel disease	3.7	4.6	0.54
Number of lesions/patient	1.07 ± 0.26	1.13 ± 0.34	0.02
Lesion location			
Right coronary artery	28.5	28.7	1.00
Left anterior descending artery	45.8	42.9	0.49
Left circumflex artery	25.7	28.4	0.44
ACC/AHA lesion complexity			
A	2.6	0.8	0.10
B1	59.2	23.5	<0.01
B2	34.8	63.8	<0.01
C	3.5	11.9	<0.01
Angulation ≥45°	3.2	7.3	0.02
Calcification (moderate/severe)	12.6	29.5	<0.01
Eccentric lesion	96.3	98.9	0.06
Thrombus	2.2	0.8	0.23
Reference vessel diameter (mm)	2.62 ± 0.35	2.69 ± 0.52	0.04
Percentage diameter stenosis	58.6 ± 10.6	60.9 ± 11.0	0.01
Lesion length (mm)	11.7 ± 4.9	12.8 ± 5.6	0.01

Values are mean ± SD or %.  
ACC/AHA = American College of Cardiology/American Heart Association; BVS = bioresorbable vascular scaffold(s); EES = everolimus-eluting metallic stent(s).

multivessel disease), angulation ( $\geq 45^\circ$ ), calcification (moderate/severe), eccentric lesion, pre-procedural visible thrombus, lesion classification (type B2/C), main branch lesion length, main branch pre-procedural RVD, main branch pre-procedural percentage diameter stenosis (DS), number of side branches within ROI, location of side branch (obstruction segment), size of side branch (RVD  $> 1.0$  mm), ostial stenosis of side branch (DS  $> 50\%$ ), post-dilation, number of study devices implanted, 2.5-mm scaffold/stent implanted, and device type (Absorb BVS or EES). In patients with 2 lesions treated with the study device (6.7% in total population), we took the patients who had at least 1 lesion that met the condition described in the preceding text, and the greater main branch DS and lesion length and smaller main branch RVD were applied in such cases. In patients with multiple side branches within ROI, we took the patients who had at least 1 side branch that met the condition. The multivariable model was created with a stepwise elimination procedure, where the independent variables were entered into the model at the 0.20 significance level and removed at the 0.05 level. If some variables were highly correlated with each other ( $r > 0.5$  and  $p < 0.05$ ), the variables that had a higher level of significance were eligible for inclusion in the multivariable model. A

2-sided  $p$  value  $< 0.05$  was considered statistically significant.

## Results

**Study population.** A total of 469 consecutive patients were enrolled in the ABSORB-EXTEND trial from January 11, 2010 to January 11, 2012. Two patients treated with DES implantation were excluded. In the first patient, the Absorb BVS failed to be delivered to the lesion. In the second patient, the appropriate size of the Absorb BVS for the lesion was not available. In addition, 32 patients without any visible side branches within ROI and 4 side branches with pre-procedural TIMI flow grade 0 or 1 were excluded. Conversely, 27 patients in the SPIRIT first and 223 patients in the SPIRIT-II trial were treated with EES at the baseline procedure. Among the total 250 patients in both trials, 13 patients were without any visible side branches within ROI, and 6 side branches with pre-procedural TIMI flow grade 0 or 1 were excluded. In total, 435 patients and 1,209 side branches in the Absorb BVS group and 237 patients and 682 side branches in the EES group were included in the current analysis (Fig. 4).

Variables	Absorb BVS	EES	p Value
Total number of analyzed side branches	1,209	682	
Mean number/patient	2.8 $\pm$ 1.5	2.9 $\pm$ 1.5	0.37
Mean number/lesion	2.6 $\pm$ 1.2	2.6 $\pm$ 1.2	0.69
Location of the side branch			
Obstruction segment	36.3% (439/1,209)	36.2% (247/682)	0.97
Device implantation segment outside obstruction	49.1% (594/1,209)	47.9% (327/682)	0.63
Outside device implantation segment (5-mm proximal or distal)	14.6% (176/1,209)	15.8% (108/682)	0.46
Pre-procedure QCA analysis			
RVD (mm)	1.18 $\pm$ 0.39	1.19 $\pm$ 0.39	0.81
Percentage diameter stenosis (%)	20.1 $\pm$ 13.5	19.8 $\pm$ 12.2	0.74
Pre-procedure TIMI flow grade			
Grade 2	0.7% (8/1,209)	0.9% (6/682)	0.59
Grade 3	99.3% (1,201/1,209)	99.1% (676/682)	0.59
Non-hierarchical incidence of SBO*			
After pre-dilation	0.3% (4/1,204)	0.7% (5/672)	0.30
After scaffold/stent implantation	6.0% (73/1,209)	5.3% (36/682)	0.54
After post-dilation	6.7% (53/787)	5.1% (15/293)	0.40
Hierarchical incidence of SBO			
After pre-dilation	0.3% (4/1,209)	0.7% (5/682)	0.30
After scaffold/stent implantation	5.8% (70/1,209)	4.7% (32/682)	0.34
After post-dilation	0.3% (4/1,209)	0.3% (2/682)	1.00
Post-procedural SBO	6.0% (73/1,209)	4.1% (28/682)	0.09

Values are n, mean  $\pm$  SD, or % (n/N). \*Side branch occlusion (SBO) is defined as a reduction in Thrombolysis in Myocardial Infarction (TIMI) flow to grade 0 or 1.  
QCA = quantitative coronary angiography; RVD = reference vessel diameter.  
Other abbreviations as in Table 1.

**Patient demographic data and lesion characteristics.** Patient demographic data in patients with side branches were comparable in both groups, except for current smoker and family history of coronary artery disease, which were significantly higher in the EES group (Table 1). In addition, single vessel disease was more prevalent in the Absorb BVS group. With regard to the lesion characteristics, the EES group demonstrated a significantly higher prevalence of type B2/C lesions, angulation  $\geq 45^\circ$ , and moderate/severe calcification, compared with the Absorb BVS group. Comparisons of QCA measurements in the main branch indicated that the RVD was significantly greater in the EES group compared with the Absorb BVS group ( $2.62 \pm 0.35$  mm vs.  $2.69 \pm 0.52$  mm,  $p = 0.04$ ). In addition, percentage DS was greater and the lesion length was longer in the EES group compared with the Absorb BVS group ( $58.6 \pm 10.6\%$  vs.  $60.9 \pm 11.0\%$ ,  $p = 0.01$ ;  $11.7 \pm 4.9$  mm vs.  $12.8 \pm 5.6$  mm,  $p = 0.01$ ; respectively).

**Angiographic findings of side branches.** Pre-procedural angiographic characteristics of the side branches were comparable between both study groups (Table 2). The mean number of analyzed side branches/patient was  $2.8 \pm 1.5$  in the Absorb BVS group and  $2.9 \pm 1.5$  in the EES group ( $p = 0.37$ ). Side branch occlusion occurred predominantly after the implantation of the study device in both groups. The incidence of post-procedural SBO demonstrated a trend toward being higher in the Absorb BVS group compared with the EES group (6.0% vs. 4.1%,  $p = 0.09$ ).

**Cardiac enzymes and incidence of periprocedural MI.** Post-procedurally any cardiac enzymes were obtained from 424 patients (98%) in the Absorb BVS group and from 219 patients (92%) in the EES group (Online Fig. S1). There was no significant difference in the incidence of post-procedural CK-MB elevation between the 2 treatment groups (Fig. 5A). A significantly higher incidence of post-procedural CK-MB elevation was observed in patients with angiographic evidence of SBO (SBO group) compared with those without SBO (non-SBO group) in each cutoff level (Fig. 5B). Cardiac troponin was assessed in 360 patients post-procedurally. Similarly to CK-MB, there was no significant difference in the peak level between the 2 treatment groups (Fig. 6A), whereas the SBO group had a significantly greater release of cardiac troponin compared with the non-SBO group (Fig. 6B).

In-hospital and 30-days clinical outcomes after the procedure are shown in Table 3. Of 92 patients in the SBO group, 6 (6.5%) were adjudicated to have experienced in-hospital NQMI, whereas 3 of 580 patients in the non-SBO group (0.5%) developed an in-hospital NQMI ( $p < 0.01$ ).

**Predictors of SBO.** Multivariable analyses indicated several factors to be significantly associated with post-procedural SBO, including the main branch lesion length, main branch pre-procedural percentage DS, location of side branch

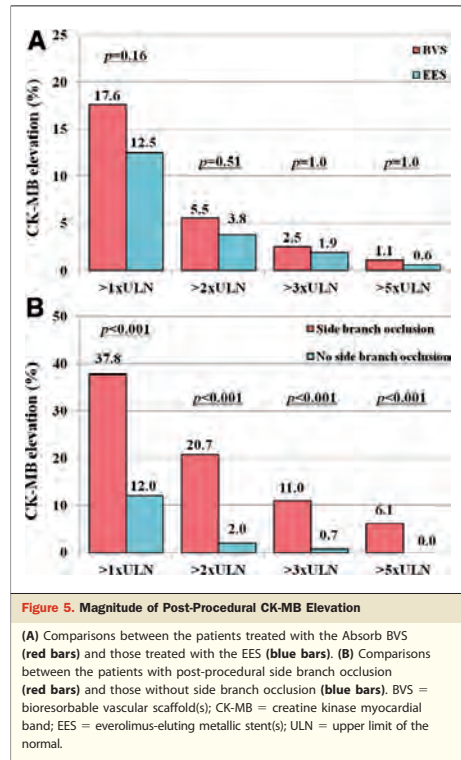


**Figure 5. Magnitude of Post-Procedural CK-MB Elevation**

(A) Comparisons between the patients treated with the Absorb BVS (red bars) and those treated with the EES (blue bars). (B) Comparisons between the patients with post-procedural side branch occlusion (red bars) and those without side branch occlusion (blue bars). BVS = bioresorbable vascular scaffold(s); CK-MB = creatine kinase myocardial band; EES = everolimus-eluting metallic stent(s); ULN = upper limit of the normal.

(obstruction segment), ostial stenosis of side branch (DS  $>50\%$ ), and device type (Absorb BVS vs. EES; odds ratio: 2.09, 95% confidence interval: 1.18 to 3.68,  $p = 0.01$ ) (Table 4). By stratified analysis, the Absorb BVS demonstrated a higher incidence of post-procedural SBO compared with the EES, only in side branches with an RVD of  $\leq 0.5$  mm (10.5% vs. 3.9%,  $p = 0.03$  between the groups,  $p$  for interaction = 0.08) (Fig. 7).

## Discussion

The present study is the first demonstrating the angiographic incidence of small SBO after Absorb BVS implantation and the impact of post-procedural SBO on short-term clinical outcomes. The main findings of this study are: 1) post-procedural SBO after Absorb BVS implantation was observed in 6.0% of all visible side branches; 2) patients with post-procedural SBO were significantly associated with a higher incidence of in-hospital MI compared with

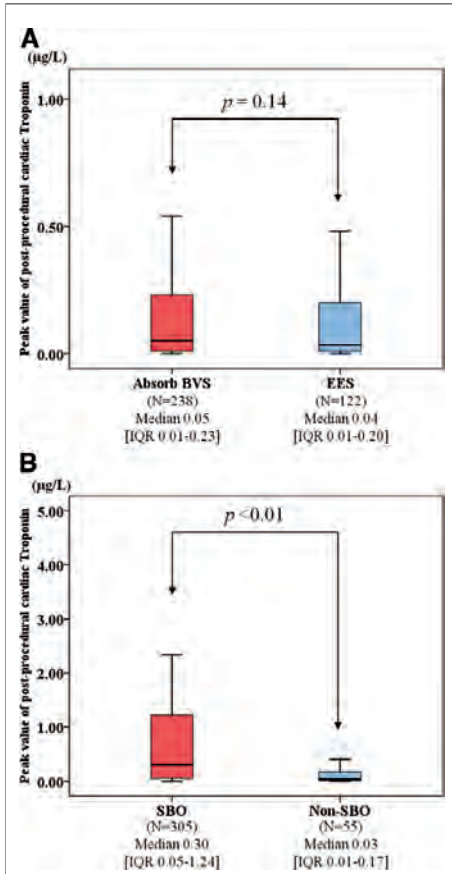


**Figure 6. Peak Value of Post-Procedural Cardiac Troponin**

(A) Comparisons between the patients treated with the Absorb bioresorbable vascular scaffold(s) (BVS) (red bar) and those treated with the everolimus-eluting metallic stent (EES) (blue bar). (B) Comparisons between the patients with post-procedural side branch occlusion (SBO) (red bar) and those without SBO (blue bar). IQR = interquartile range.

those without SBO; 3) lesion length and pre-procedural percentage DS in the main branch and location and ostial stenosis of side branch were all independent predictors of post-procedural SBO; and 4) the treatment with the Absorb BVS was a significant independent predictor of post-procedural SBO compared with EES in the study population.

Side branch occlusion is well recognized as a contributing factor toward periprocedural MI and resultant clinical out-

comes (4–6). Previous studies have suggested several potential mechanisms for SBO after metallic stent implantation, including the presence of coronary spasm, coronary dissection, thrombus formation, embolization of plaque debris, and the bifurcation carina shift and/or plaque shift into the orifice of side branch (7–9,29,30). Notably, intracoronary nitroglycerin was administered before angiography, and the patients principally had stable and noncomplex lesion characteristics in keeping with the protocol of the ABSORB-EXTEND and SPIRIT trials. Although unplanned bailout stenting was performed in 7 patients in the Absorb BVS group and 6 patients in the EES group because of edge dissection, it did not affect the consequences of side branches originating within the ROI. In addition, post-procedural intraluminal defects, suggestive of plaque prolapse or thrombus, could not be detected. In the present study, multivariable analyses demonstrated both the location (i.e., obstruction segment) and ostial stenosis (DS >50%) of side branch to be independent predictors of post-procedural SBO. This finding is consistent with a previous study suggesting the lesion morphology at the origin of side branch to be an angiographic predictor of SBO (31). Although we cannot clearly ascertain the exact mechanism of SBO after Absorb BVS implantation because of the lack of intracoronary imaging data, the generally accepted view is that small side branch compromise and occlusion is secondary to plaque shift from the main branch into the orifice of small side branch, although carina shift might play a further role, potentially dependent on the bifurcation angle (9,32,33).

There have been 2 publications addressing the incidence of SBO with 2 different metallic platform DES. Lansky et al. (11) performed a post hoc angiographic analysis of side branches in 606 patients treated with the EES (strut thickness 89 µm) and 304 patients treated with

**Table 3. Short-Term Clinical Outcomes for Patients With or Without Post-Procedural SBO**

Clinical Events	SBO (n = 92)	Non-SBO (n = 580)	p Value
<b>In-hospital events*</b>			
Myocardial infarction	6.5% (6/92)	0.5% (3/580)	<0.01
Q-wave	0.0% (0/92)	0.0% (0/580)	N/A
Non-Q-wave	6.5% (6/92)	0.5% (3/580)	<0.01
Ischemia driven TLR	0.0% (0/92)	0.2% (1/580)	1.0
Cardiac death	0.0% (0/92)	0.0% (0/580)	N/A
<b>30-days events</b>			
Myocardial infarction	6.5% (6/92)	1.2% (7/580)	<0.01
Q-wave	0.0% (0/92)	0.7% (4/580)	1.0
Non-Q-wave	6.5% (6/92)	0.5% (3/580)	<0.01
Ischemia-driven TLR	0.0% (0/92)	0.2% (1/580)	1.0
Cardiac death	0.0% (0/92)	0.0% (0/580)	N/A

\*In-hospital is defined as hospital stay ≤7 days post-procedure.

N/A = not available; SBO = side branch occlusion; TLR = target lesion revascularization.

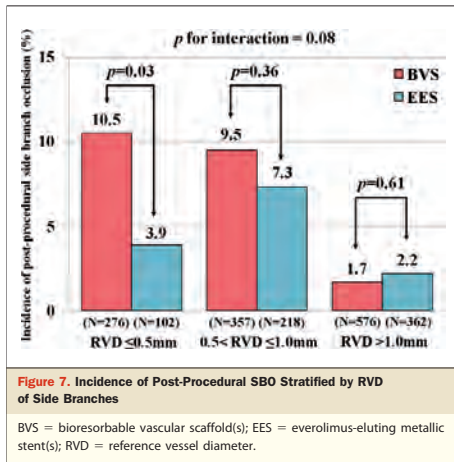
**Table 4. Univariable and Multivariable Analyses for Predictors of Post-Procedural Side Branch Occlusion**

Covariates	Univariable p Value	Odds Ratio (95%)	Multivariable p Value	Odds Ratio (95%)
<b>Patient-related factors</b>				
Age (yrs)	0.46	1.01 (0.99–1.03)	—	—
Male	0.16	0.71 (0.44–1.15)	—	—
Current smoker	0.25	0.72 (0.42–1.25)	—	—
Hypertension requiring treatment	0.09	0.68 (0.43–1.06)	—	—
Dyslipidemia requiring treatment	0.86	0.96 (0.61–1.52)	—	—
Any diabetes mellitus	0.07	1.56 (0.97–2.52)	—	—
Unstable angina	0.15	1.41 (0.89–2.23)	—	—
Family history of coronary artery disease	0.86	1.04 (0.65–1.68)	—	—
Prior myocardial infarction	0.64	1.12 (0.70–1.79)	—	—
Number of diseased vessels (single vessel disease vs. multivessel disease)	0.42	0.81 (0.49–1.34)	—	—
<b>Lesion-related factors</b>				
Angulation $\geq 45^\circ$	0.19	0.38 (0.09–1.61)	—	—
Moderate/severe calcification	0.91	0.97 (0.55–1.71)	—	—
Eccentric lesion	CS	CS	—	—
Pre-procedural visible thrombus	0.59	0.57 (0.07–4.43)	—	—
Type B2/C lesion	0.47	1.18 (0.76–1.84)	—	—
Main branch lesion length (mm)	<0.01	1.07 (1.03–1.12)	0.02	1.05 (1.01–1.11)
Main branch pre-procedural RVD (mm)	0.24	0.72 (0.41–1.26)	—	—
Main branch pre-procedural DS (%)	<0.01	1.03 (1.01–1.05)	0.02	1.03 (1.00–1.06)
Number of side branches	<0.01	1.30 (1.13–1.48)	—	—
Location of side branch (obstruction segment)	<0.01	28.91 (7.05–118)	<0.01	22.40 (5.41–92.73)
Size of side branch (RVD $\geq 1.0$ mm)	0.43	0.81 (0.48–1.37)	—	—
Ostial stenosis of side branch (DS $>50\%$ )	<0.01	7.08 (3.50–14.3)	<0.01	4.30 (1.95–9.47)
<b>Treatment-related factors</b>				
Treatment with $\geq 2$ study devices	0.64	1.17 (0.60–2.26)	—	—
2.5mm device implanted	0.32	0.66 (0.29–1.50)	—	—
Post-dilation	0.15	1.41 (0.88–2.24)	—	—
Device type (BVS vs. EES)	0.09	1.54 (0.94–2.52)	0.01	2.09 (1.18–3.68)

The multivariable model was created with a stepwise elimination procedure, where the independent variables were entered into the model at the 0.20 significance level and removed at the 0.05 level.  
 BVS = bioresorbable vascular scaffold(s); CS = complete separation; CI = confidence interval; DS = diameter stenosis; EES = everolimus-eluting metallic stent; RVD = reference vessel diameter.

the paclitaxel-eluting stent (PES) (Taxus Express2) (strut thickness 148  $\mu\text{m}$ ) in the SPIRIT-III substudy. Post-procedural SBO was observed in 2.7% of analyzed side branches in the EES group and 4.3% in the PES group ( $p = 0.06$ ). Similarly, Popma et al. (10) assessed side branches with an RVD of  $>1.0$  mm in 597 patients treated with the zotarolimus-eluting stent (ZES) (Endeavor; Medtronic Cardio Vascular, Santa Rosa, California) (strut thickness 96  $\mu\text{m}$ ) and 619 patients treated with the PES in the ENDEAVOR-IV (Randomized Comparison of Zotarolimus- and Paclitaxel-Eluting Stents in Patients With Coronary Artery Disease) substudy. Post-procedural SBO was observed in 2.0% of the analyzed side branches in the ZES group and 3.4% in the PES group ( $p = 0.07$ ). Both studies suggested that strut thickness was a potential contributing factor toward SBO, on the basis of the findings of PES to be an independent predictor of SBO in both studies (10,11). In the present study, the Absorb BVS (strut thickness 157  $\mu\text{m}$ ) showed a trend toward higher incidence of post-procedural SBO compared with the EES (6.0% vs.

4.1%,  $p = 0.09$ ). By multivariable analysis, the Absorb BVS seemed to be an independent predictor of post-procedural SBO. These results are in line with the previous studies, despite the differences between the polymeric and metallic platform devices. It is, however, noteworthy that a smaller RVD and larger number of analyzed side branches/lesion (mean 1.18 mm and 2.6, respectively) were evident in the present study when compared with those in the SPIRIT-III (mean 1.61 mm and 2.0, respectively) and in the ENDEAVOR-IV substudies (mean 1.52 mm and 1.6, respectively) and that this might partially contribute to the higher incidence rates of SBO reported in the present study. When only side branches with an RVD of  $>1.0$  mm were considered, according to the methodology used in the ENDEAVOR-IV substudy, the incidence rates of post-procedural SBO were 1.7% in the Absorb BVS group and 2.2% in the EES group and comparable to the ZES (2.0%). This result prompts the question of how small side branches were more likely to be affected by the devices with different strut thickness. By stratified analysis, the incidence of



post-procedural SBO was higher in the Absorb BVS group compared with the EES group, only in small side branches with an RVD  $\leq 0.5$  mm, despite the borderline significant interaction. Furthermore, when taking only side branches with an RVD  $> 1.0$  mm into account, multivariable analyses indicated that the Absorb BVS was no longer an independent predictor of post-procedural SBO (data not shown). Considering the greater vessel wall area covered by the Absorb BVS strut (26%) compared with the EES (12%), there is a greater probability of covering the orifice of side branches with the Absorb BVS. Thus, these findings might suggest that such small side branches are more likely to be compromised by the thicker strut of the Absorb BVS.

In the current analysis, patients with post-procedural SBO had a significantly greater release of CK-MB and cardiac troponin and also a higher risk of in-hospital MI, compared with those without SBO. There were, however, no significant differences between the 2 treatment groups with respects to the incidence of post-procedural CK-MB elevation and the peak level of cardiac troponin. A potential explanation is that the Absorb BVS was associated with a higher risk of SBO compared with the EES only in small side branches with an RVD of  $\leq 0.5$  mm, resulting in minimal impact on periprocedural myocardial necrosis. Because bioresorbable scaffolds are programmed to be completely resorbed between 2 and 3 years after implantation, the impact of SBO on long-term clinical outcomes might differ from that caused by permanent metallic endoluminal prosthesis (34). Further investigations are required to elucidate this issue.

**Study limitations.** The present study relies on a nonrandomized comparison of different study populations. Conse-

quently, there were significant differences in several baseline characteristics, and the possibility of results being affected by unknown confounding factors cannot be excluded. Second, these trials principally included patients with stable coronary artery disease and excluded patients with complex lesion characteristics, such as total occlusions, thrombotic lesions, and bifurcation lesions with side branch  $\geq 2$  mm in diameter. The incidence of SBO would be expected to be higher in more complex lesions.

## Conclusions

Absorb BVS implantation was associated with a 6.0% incidence of post-procedural SBO in 435 patients with 1,209 side branches. Absorb BVS was related to a higher incidence of post-procedural SBO compared with the EES, and this effect was more pronounced with small side branches with an RVD  $\leq 0.5$  mm. Further investigation is required in a pivotal randomized controlled trial.

## Acknowledgments

The authors wish to express their sincere appreciation to Dr. Richard J. Rapoza for the critical review of manuscript and Ms. Cécile Dorange and Mr. Ken Wu for the statistical assistance.

**Reprint requests and correspondence:** Dr. Patrick W. Serruys, Department of Interventional Cardiology, Thoraxcenter, Erasmus Medical Center, and Ba 583, Drive Molewaterplein 40, 3015 GD, Rotterdam, the Netherlands. E-mail: p.w.j.c.serruys@erasmusmc.nl.

## REFERENCES

- Meier B, Gruentzig AR, King SB III, et al. Risk of side branch occlusion during coronary angioplasty. *Am J Cardiol* 1984;53:10–4.
- Holmes DR Jr., Holubkov R, Vlietstra RE, et al. Comparison of complications during percutaneous transluminal coronary angioplasty from 1977 to 1981 and from 1985 to 1986: the National Heart, Lung, and Blood Institute percutaneous transluminal coronary angioplasty registry. *J Am Coll Cardiol* 1988;12:1149–55.
- Porto I, Selvanayagam JB, Van Gaal WJ, et al. Plaque volume and occurrence and location of periprocedural myocardial necrosis after percutaneous coronary intervention: insights from delayed-enhancement magnetic resonance imaging, thrombolysis in myocardial infarction myocardial perfusion grade analysis, and intravascular ultrasound. *Circulation* 2006;114:662–9.
- Califf RM, Abdelmeguid AE, Kuntz RE, et al. Myonecrosis after revascularization procedures. *J Am Coll Cardiol* 1998;31:241–51.
- Prasad A, Singh M, Lerman A, Lennon RJ, Holmes DR Jr., Rihal CS. Isolated elevation in troponin T after percutaneous coronary intervention is associated with higher long-term mortality. *J Am Coll Cardiol* 2006;48:1765–70.
- Jensen LO, Maeng M, Kaltoft A, et al. Stent thrombosis, myocardial infarction, and death after drug-eluting and bare-metal stent coronary interventions. *J Am Coll Cardiol* 2007;50:463–70.
- Fischman DL, Savage MP, Leon MB, et al. Fate of lesion-related side branches after coronary artery stenting. *J Am Coll Cardiol* 1993;22:1641–6.
- Mazur W, Grinstead WC, Hakim AH, et al. Fate of side branches after intracoronary implantation of the Gianturco-Roubin flex-stent for

- acute or threatened closure after percutaneous transluminal coronary angioplasty. *Am J Cardiol* 1994;74:1207–10.
9. Farooq V, Serruys PW, Heo JH, et al. New insights into the coronary artery bifurcation hypothesis-generating concepts utilizing 3-dimensional optical frequency domain imaging. *J Am Coll Cardiol Intv* 2011;4:921–31.
  10. Popma JJ, Mauri L, O'Shaughnessy C, et al. Frequency and clinical consequences associated with sidebranch occlusion during stent implantation using zotarolimus-eluting and paclitaxel-eluting coronary stents. *Circ Cardiovasc Interv* 2009;2:133–9.
  11. Lansky AJ, Yaqub M, Hermiller JB, et al. Side branch occlusion with everolimus-eluting and paclitaxel-eluting stents: three-year results from the SPIRIT III randomised trial. *EuroIntervention* 2010;6:J44–52.
  12. Ormiston JA, Serruys PW, Regar E, et al. A bioabsorbable everolimus-eluting coronary stent system for patients with single de-novo coronary artery lesions (ABSORB): a prospective open-label trial. *Lancet* 2008; 371:899–907.
  13. Serruys PW, Garcia-Garcia HM, Onuma Y. From metallic cages to transient bioresorbable scaffolds: change in paradigm of coronary revascularization in the upcoming decade? *Eur Heart J* 2012;33:16–25b.
  14. Onuma Y, Serruys PW. Bioresorbable scaffold: the advent of a new era in percutaneous coronary and peripheral revascularization? *Circulation* 2011;123:779–97.
  15. Serruys PW, Ormiston JA, Onuma Y, et al. A bioabsorbable everolimus-eluting coronary stent system (ABSORB): 2-year outcomes and results from multiple imaging methods. *Lancet* 2009;373:897–910.
  16. Onuma Y, Serruys PW, Ormiston JA, et al. Three-year results of clinical follow-up after a bioresorbable everolimus-eluting scaffold in patients with de novo coronary artery disease: the ABSORB trial. *EuroIntervention* 2010;6:447–53.
  17. Dudek D, Onuma Y, Ormiston JA, Thuesen L, Miquel-Hebert K, Serruys PW. Four-year clinical follow-up of the ABSORB everolimus-eluting bioresorbable vascular scaffold in patients with de novo coronary artery disease: the ABSORB trial. *EuroIntervention* 2012;7:1060–1.
  18. Oberhauser JP, Hossainy S, Rapoza RJ. Design principles and performance of bioresorbable polymeric coronary scaffolds. *EuroIntervention* 2009;5:F15–22.
  19. Onuma Y, Serruys PW, Gomez J, et al. Comparison of in vivo acute stent recoil between the bioresorbable everolimus-eluting coronary scaffolds (revision 1.0 and 1.1) and the metallic everolimus-eluting stent. *Catheter Cardiovasc Interv* 2011;78:3–12.
  20. Farooq V, Gomez-Lara J, Brugaletta S, et al. Proximal and distal maximal luminal diameters as a guide to appropriate deployment of the ABSORB everolimus-eluting bioresorbable vascular scaffold: a sub-study of the ABSORB cohort B and the on-going ABSORB EXTEND single arm study. *Catheter Cardiovasc Interv* 2012;79:880–8.
  21. Serruys PW, Ong AT, Piek JJ, et al. A randomized comparison of a durable polymer everolimus-eluting stent with a bare metal coronary stent: the SPIRIT first trial. *EuroIntervention* 2005;1:58–65.
  22. Serruys PW, Ruygrok P, Neuzner J, et al. A randomised comparison of an everolimus-eluting coronary stent with a paclitaxel-eluting coronary stent: the SPIRIT II trial. *EuroIntervention* 2006;2:286–94.
  23. Garg S, Serruys PW. Coronary stents: current status. *J Am Coll Cardiol* 2010;56:S1–42.
  24. Vranckx P, Cutlip DE, Mehran R, et al. Myocardial infarction adjudication in contemporary all-comer stent trials: balancing sensitivity and specificity. Addendum to the historical MI definitions used in stent studies. *EuroIntervention* 2010;5:871–4.
  25. Foley DP, Escaned J, Strauss BH, et al. Quantitative coronary angiography (QCA) in interventional cardiology: clinical application of QCA measurements. *Prog Cardiovasc Dis* 1994;36:363–84.
  26. Gronenschild E, Janssen J, Tjeldens F. CAAS. II: A second generation system for off-line and on-line quantitative coronary angiography. *Cathet Cardiovasc Diagn* 1994;33:61–75.
  27. Haase J, Escaned J, van Swijndregt EM, et al. Experimental validation of geometric and densitometric coronary measurements on the new generation cardiovascular angiography analysis system (CAAS II). *Cathet Cardiovasc Diagn* 1993;30:104–14.
  28. Tsuchida K, van der Giessen WJ, Patterson M, et al. In vivo validation of a novel three-dimensional quantitative coronary angiography system (CardiOp-B): comparison with a conventional two-dimensional system (CAAS II) and with special reference to optical coherence tomography. *EuroIntervention* 2007;3:100–8.
  29. Aliabadi D, Tilli FV, Bowers TR, et al. Incidence and angiographic predictors of side branch occlusion following high-pressure intracoronary stenting. *Am J Cardiol* 1997;80:994–7.
  30. Morimoto S, Hiramitsu S, Yamada K, Uemura A, Kubo N, Mizuno Y. Lesions in side branches of arteries having undergone percutaneous transluminal coronary angioplasty: a histopathologic study. *Am Heart J* 1990;120:864–72.
  31. Tanabe K, Serruys PW, Degertekin M, et al. Fate of side branches after coronary arterial sirolimus-eluting stent implantation. *Am J Cardiol* 2002;90:937–41.
  32. Farooq V, Okamura T, Onuma Y, Gogas BD, Serruys PW. Unraveling the complexities of the coronary bifurcation: is this raising a few eyebrows? *EuroIntervention* 2012;7:1133–41.
  33. Diletti R, Farooq V, Muramatsu T, et al. Serial 2- and 3-dimensional visualization of side branch jailing after metallic stent implantation. *J Am Coll Cardiol Intv* 2012;5:1089–90.
  34. Okamura T, Serruys PW, Regar E. The fate of bioresorbable struts located at a side branch ostium: serial three-dimensional optical coherence tomography assessment. *Eur Heart J* 2010;31:2179.

**Key Words:** bioresorbable vascular scaffold ■ complications ■ drug-eluting stent(s) ■ myocardial infarction ■ side branch occlusion

 **APPENDIX**

For a supplementary figure, please see the online version of this article.



## 5.7 Peri-procedural myocardial infarction in a randomized controlled trial

Incidence and potential mechanism(s) of post-procedural rise of cardiac enzyme in patients with coronary artery narrowing after implantation of an everolimus eluting bioresorbable vascular scaffold or everolimus eluting metallic stent.

(Submitted)

[Original research paper]

Ishibashi Y, Muramatsu T, Cho YK, Nakatani S, Grundeken MJ, Garcia-Garcia HM, van Boven AJ, Piek JJ, Sabaté M, Kelbæk H, Baumbach A, McClean D, de Sousa Almeida M, Wasungu L, Miquel-Hebert K, Chevalier B, Onuma Y, Serruys PW.





## **Incidence and Potential Mechanism(s) of Post-procedural Rise of Cardiac Enzyme in Patients with Coronary Artery Narrowing after Implantation of an Everolimus Eluting Bioresorbable Vascular Scaffold or Everolimus Eluting Metallic Stent**

Yuki Ishibashi<sup>1</sup>, M.D., Ph.D., Takashi Muramatsu<sup>1,2</sup>, M.D., Ph.D., Yun-kyeong Cho<sup>1</sup>, M.D., Ph.D., Shimpei Nakatani<sup>1</sup>, M.D., Maik J. Grundeken<sup>3</sup>, M.D., Hector M. Garcia-Garcia<sup>1</sup> M.D., Ph.D., A. J. van Boven<sup>4</sup>, M.D., Ph.D., Jan J. Piek<sup>3</sup>, M.D., Ph.D., Manel Sabaté<sup>5</sup>, M.D., Ph.D., Henning Kelbæk<sup>6</sup>, M.D., Ph.D., Andreas Baumbach<sup>7</sup>, M.D., Ph.D., Dougal McClean<sup>8</sup>, M.D., Ph.D., Manuel de Sousa Almeida<sup>9</sup>, M.D., Ph.D., Luc Wasungu<sup>10</sup> Ph.D., Karine Miquel-Hebert<sup>10</sup> Ph.D., Bernard Chevalier<sup>11</sup> M.D., Yoshinobu Onuma<sup>1</sup>, M.D., Ph.D., Patrick W. Serruys<sup>12</sup>, M.D., Ph.D.

<sup>1</sup>Thoraxcenter, Erasmus University Medical Center, Rotterdam, The Netherlands

<sup>2</sup>Department of Cardiology, Fujita Health University Hospital, Toyoake, Japan

<sup>3</sup>The Heart Center, Academic Medical Center, Amsterdam, The Netherlands

<sup>4</sup>Medical Center Leeuwarden, the Netherlands

<sup>5</sup>Thorax Institute, Hospital Clinic, University of Barcelona, IDIBAPS

<sup>6</sup>Rigshospitalet, University of Copenhagen, Denmark

<sup>7</sup>Bristol Heart Institute, Bristol, United Kingdom

<sup>8</sup>Christchurch Hospital, Christchurch, New Zealand

<sup>9</sup>Hospital Santa Cruz, Carnaxide, Portugal

<sup>10</sup>Abbott Vascular, Diegem, Belgium

<sup>11</sup>CA Institut Jacques Cartier, Massy, France,

<sup>12</sup>International Centre for Cardiovascular Health, Imperial College, London, UK.

**Short title:** *peri-procedural cardiac biomarker rise in ABSORB II*

**Key words:** *bioresorbable scaffold, cardiac biomarker, peri-procedural MI*

Correspondence: Prof. P.W. Serruys, MD, PhD  
Emeritus Professor of Medicine, Erasmus MC, Rotterdam, the Netherlands  
Professor in Cardiology  
International Centre for Circulatory Health, NHLI, Imperial College  
London, London, United Kingdom  
E-mail: patrick.w.j.c.serruys@gmail.com

Author Disclosures:

- 1) Luc Wasungu is a contractor employed by Abbott Vascular.
- 2) Karine Miquel-Hebert is an employee of Abbott Vascular.
- 3) The other authors have no conflicts of interest to declare regarding the manuscript

Study Sponsor and Funding: Abbott Cardiovascular Systems, Inc, A subsidiary of Abbott Vascular, 3200 Lakeside Drive, Santa Clara, CA 95045 USA

**ABSTRACT** (word count: 299 words)

**Background:** According to a non-randomized comparison using historical data, Absorb BVS might be associated with a higher incidence of peri-procedural myocardial injury compared with everolimus-eluting metallic stents (EES).

**Methods:** We assessed 501 patients with stable or unstable coronary artery disease treated with either Absorb BVS (335 patients) or EES (166 patients) in the ABSORB II randomized controlled trial. Three types of biomarkers (CK, CKMB and troponin) were obtained within 48 hours after implantation of the device. Peri-procedural cardiac biomarker rise (CBR) and myocardial infarction (PMI) by protocol according to the WHO definition (CK rise  $>2$  x upper limit of normal accompanied by CKMB rise) was categorized as: type 1) side-branch occlusion (SBO): type 2) other anatomic complications detected by angiography and: type 3) without anatomic complications.

**Results:** A total of 3,813 blood samples comprising of 1,257 CK, 1,253 CKMB and 1,303 troponin were available. The rise of these three cardiac enzymes subcategorized in five different ranges was comparable between the two treatment arms. An incidence rate of any anatomic complications was similar between the two treatment arms (BVS; 16.4% vs. EES; 19.9%,  $p=0.39$ ) with the incidence of SBO (per side branch analysis) being more frequently observed in the EES than in the BVS arm (5.3% vs. 7.6%,  $p =$

0.07). Per protocol PMI was adjudicated in 13/335 (3.9%) in the BVS arm and 2/166 (1.2%) in the EES arm ( $p=0.16$ ). Out of 15 patients who experienced PMI, 10(66.7%) were angiographically classified as type 1 while three (20.0%) were type 2. Treatment with overlapping devices was the only independent determinant of per protocol PMI (OR: 4.36, 95% CI:1.48-12.61,  $p < 0.01$ ).

**Conclusion:** There were no differences in the incidence and correlates of CMR and PMI between the BVS and the EES. Overlapping of scaffolds or stents might be a precipitating factor of peri-procedural myocardial injury.

## **ABBREVIATIONS AND ACRONYMS**

BVS = Bioresorbable Vascular Scaffold

DES = Drug- Eluting Stent

PLLA = Poly-L-Lactide

SBO = Side Branch Occlusion

TIMI = Thrombolysis In Myocardial Infarction

NHLBI = National Heart, Lung and Blood Institute

CEC = Clinical Events Committee

WHO = World Health Organization

ULN = Upper Limit of the Normal

PMI = Peri-procedural Myocardial Infarction

ITT = Intention to Treat

MACE = Major Adverse Cardiac Events

PCI = Percutaneous Coronary Intervention

QCA = Quantitative Coronary Angiography

CBR = Cardiac Biomarker Rise

## **Introduction**

The everolimus-eluting bioresorbable vascular scaffold (Absorb BVS; Abbott Vascular, Santa Clara, CA, USA) was developed to provide a novel approach to treat coronary artery stenosis with transient vessel support and drug delivery<sup>1-4</sup>. The performance of the second generation Absorb BVS was investigated in the ABSORB Cohort B Trial which reported excellent clinical results<sup>5-7</sup>. However, the clinical relevance of this technology in comparison with metallic drug eluting stents still remains a matter of debate due to the absence of randomized comparative data between the Absorb BVS and conventional metallic drug-eluting stents. The ABSORB II randomized controlled trial<sup>8</sup>(Clinical trials. gov. NCT01425281) is the first randomized clinical trial assessing the clinical outcomes in 501 patients treated with either the Absorb BVS or the everolimus-eluting metallic stent (XIENCE ; Abbott Vascular, Santa Clara, CA, USA).

In the non-randomized comparison using historical data, Absorb BVS was associated with a higher incidence of post-procedural side branch occlusion (SBO) compared with the EES<sup>9</sup>. Given the increased strut thickness of the Absorb BVS, a potential concern exists that it might be associated with a higher incidence of peri-procedural myocardial injury and myocardial infarction (MI) compared to newer-generations of DES<sup>9</sup>.

Therefore, the aim of this study is to investigate the incidence and correlates of post procedural cardiac biomarker rise following Absorb BVS implantation compared to metallic EES.

## **Methods**

### ***Study design***

The ABSORB II randomized controlled trial design has been described in detail previously<sup>8</sup>. In brief, the ABSORB II trial was a prospective, multicenter, single blinded, randomized controlled trial that compared the safety and efficacy of the Absorb BVS vs. the EES in patients with stable or unstable angina due to up to two de novo coronary artery lesions, each located in different major epicardial vessels, all with an angiographic maximal luminal diameter between 2.25 and 3.8mm as estimated by online quantitative coronary angiography (QCA) and a lesion length of  $\leq$  48mm. A total of 501 patients were randomized 2:1 into either the Absorb BVS arm or the EES arm in Europe and New Zealand.

### ***Study devices***

The second generation Absorb BVS is a balloon-expandable device consisting of a polymer backbone of poly-L-lactide (PLLA) coated with a thin layer of a 1:1 mixture of

an amorphous matrix of poly-D, L-lactide (PDLLA) polymer and  $100 \mu\text{g}/\text{cm}^2$  of the antiproliferative drug everolimus<sup>2, 10</sup>. The PDLLA controls the release of everolimus, 80% of which is eluted within 30 days. Both PLLA and PDLLA are fully bioresorbable and degrade into lactic acid, which is metabolized via the Krebs cycle. The second generation Absorb BVS has struts with  $157 \mu\text{m}$  and zigzag hoops connected by 3 links<sup>10</sup>.

The XIENCE stent is formulated from L-605 cobalt chromium alloy with a stent strut thickness of  $81 \mu\text{m}$  and with a thin ( $7.8 \mu\text{m}$ ), non-adhesive, durable, biocompatible fluorinated copolymer coat consisting of two layers, a primer layer and a drug matrix layer containing everolimus at a concentration of  $100 \mu\text{g}/\text{cm}^2$ , which is eluted over the same period as the Absorb BVS<sup>11</sup>.

### ***Qualitative and Quantitative Angiographic Assessment***

Side branch occlusions, occurrence of no reflow, abrupt closure, dissection and distal embolization in main and side branches were assessed qualitatively at pre-procedure, after balloon pre-dilatation, after device deployment and after final balloon inflation. Coronary dissections were assessed using the National Heart, Lung and Blood Institute criteria (NHLBI)<sup>12, 13</sup>. A previous study categorized the source of cardiac biomarker rise (CBR) into two types: Type 1 (proximal type), which is related specifically to the target

lesion and most likely due to SBO, and Type 2 (distal type) with CBR related to the perfusion territory of the treated coronary arteries.<sup>14,15</sup> In the present study, according to the underlying “anatomic complications” detected by angiography, CBR and PMI were classified into three types: Type 1, CBR and PMI due to side branch occlusion ; Type 2, CBR and PMI due to other anatomic complications (e.g.; slow flow or no-reflow, distal embolization, thrombus during procedure, flow-limiting dissection, coronary dissection of NHLBI type D or E, or disruption of collateral flow); Type 3, CBR and PMI without angiographic identifiable causes for the rise of cardiac enzyme (**Figure 1**).

The quantitative angiographic analysis by the 2D single-vessel QCA (CAAS 5.10, Pie Medical BV, Maastricht, the Netherlands) included the reference size of the side branch and the percent diameter stenosis of any side branch lesion as well as the side branch TIMI flow pre-procedure, after pre-dilatation, after post-dilatation and post-procedure<sup>9</sup>. Region of interest (ROI) was defined as the study device implantation site and the 5-mm proximal and distal margins in the main branch (**Figure 2**). A detailed side branch analysis was performed of all side branches identified within the ROI pre-procedurally, during the course of the intervention to capture any transient complications, and post-procedure. SBO was defined as a reduction in the Thrombolysis In Myocardial Infarction (TIMI) flow grade to 0 or 1. Accordingly, side branches with

pre-procedural TIMI flow grade 0 or 1 were excluded. Transient or final side branch occlusion was defined as SBO that occurred during the procedure and either disappeared or persisted at the end of the procedure. Angiographic assessment of side branch was based on the consensus of three experienced cardiologists (Y.I, T.M, and Y.C) and assessed in at least two different projections, with angiographic assessment for each side branch.

### ***Blood Sampling***

The protocol mandated that blood sampling for cardiac enzymes was to be collected within 6 hours before the index-PCI procedure, and at 6, 12 and 18 hours after the procedure or at hospital discharge, whichever came first. These blood samples were sent to not only local hospital laboratories but also the central core laboratory (ICON, Dublin, Ireland) for analysis. Whenever clinically indicated additional sampling could be taken and analyzed by the local hospital laboratories.

This yielded a mixture of local and central biomarker results with different upper limits of normal. When both local and central laboratories cardiac enzyme data were available at the same time, the Clinical Events Committee (CEC) used central laboratories results for the adjudication of MI.

### ***Definitions of peri-procedural myocardial infarction***

In this study, MI was defined according to two definitions<sup>16-18</sup>; 1) per protocol (modified World Health Organization [WHO]) definition, 2) extended historical definition<sup>16</sup>. In the protocol, MI without distinction of being spontaneous or peri-procedural MI (PMI) is defined by elevation of total creatine kinase (CK) to  $>2$  x normal along with elevated or “positive” creatine kinase myocardial band (CKMB). A hierarchical approach was used for the adjudication of PMI based upon cardiac biomarker availability when an analyzable cardiac biomarker was missing (extended historical definition: CK-MB mass when CK was not available, cTn when CK and CK-MB mass were not available). In the present study, another definition (elevation of total CKMB to  $>5$  x normal with or without symptom or ECG change) was also used for post hoc analysis. Whenever at least one pre-procedure and one post-procedure CK-MB measure was available, adjudication of MI was based solely on these biomarker values. If the patient has stable ischemic heart disease and pre-procedural CK-MB measure was not available, the cardiac enzymes were assumed to be within normal limits and MI was adjudicated by the CEC solely according to the post-procedural CK-MB measures. All protocol defined clinical outcomes were adjudicated by an independent CEC.

### ***Statistical analysis***

All analyses were performed on the intention-to-treat (ITT) basis, utilizing all patients randomized in the study, regardless of the treatment actually received. The counts of PMI are summarized and tabulated according to the frequency. Categorical variables were compared by Fisher's exact test. Continuous variables are presented as mean  $\pm$  standard deviation and were compared by t-test. The logistic regression model was performed on a patient-level basis, including the following variables; age, male sex, body-mass index, current smoking, hypertension requiring treatment, dyslipidemia requiring treatment, any diabetes, unstable angina, pre-procedural diameter stenosis, pre-procedural minimum lumen diameter, pre-procedural reference diameter, obstruction length, pre-procedural curvature, treatment with overlapping devices, device type (Absorb BVS or EES), post-dilatation and bail-out. The multivariable model was created with a stepwise elimination procedure, where the independent variables were entered into the model at the 0.20 significance level and removed at the 0.10 level. If some variables were highly correlated with each other ( $r > 0.5$  and  $p < 0.05$ ), the variables that had a higher level of significance were eligible for inclusion in the multivariable model.

All statistical tests were performed with SPSS, version 22.0 for windows (IL, USA). A two-sided  $p$  value  $< 0.05$  was considered to indicate statistical significance.

## **Results**

### ***Patient and procedural characteristics***

Patient demographics were comparable in both arms (**Table 1**). The lesion characteristics such as type B2/C lesions, bifurcation lesions, eccentricity, moderate/severe tortuosity, thrombus and moderate/severe calcification were similar between the 2-treatment arms.

### ***Availability of cardiac biomarkers of myocardial injury***

At least one of the three cardiac enzymes was available in 490 patients (97.8%) within 48 hours after the index procedure. In the serial sample analysis, a total of 1,446 blood time points for the assessment of cardiac enzyme biomarkers were available with 572 central and 874 local biomarker data (**Figure 3**). A total of 3,813 blood samples with 1,257 CK, 1,253 CKMB and 1,303 troponin values were available. For the peak-level assessment of each cardiac enzyme, the central biomarker data was used in 56.9% for CK (271/476), 69.2% for CKMB (337/487), and 43.9% for troponin (213/485). The availability of paired biomarkers (CK and CKMB) for per protocol PMI adjudication at post-procedure was available in 93.4% (313/335) of the BVS arm and 96.4% (160/166) of the EES arm. Troponin was available in 98.8% (325/335) of the BVS arm and 97.6%

(160/166) of the EES arm.

### ***Qualitative and quantitative angiographic assessment***

The frequencies of “angiographic complications” are shown in **Table 2**. In the present analysis, a total of 335 patients with 988 side branches in the BVS arm and 166 patients with 503 side branches in the EES arm were assessed. An incidence rate of any “angiographic complications” was comparable between the two treatment arms (BVS; 16.4% vs. EES; 19.9%,  $p=0.39$ ) with the incidence of SBO (per side branch analysis) being more frequently observed in the EES arm than in the BVS arm (5.3% vs. 7.6%,  $p = 0.07$ ). The incidence of post-procedural SBO in the obstruction segment was significantly lower in the BVS arm compared with the EES arm (4.3% vs. 6.8%,  $p=0.046$ ) although there were no significant differences in the incidence of SBO according to the RVD size ( $RVD \leq 0.5\text{mm}$ ,  $0.5 < RVD \leq 1.0$ ,  $1.0 < RVD$ ). Each type (Type 1, Type 2, and Type 3) of “anatomic complications” after revascularization was similarly observed between the two treatment groups. However, two abrupt occlusions were documented after EES implantation (**Table 2**).

### ***Incidence of cardiac enzyme rise***

As recently described, we compared the peak value of the three cardiac enzyme (CE) values post-procedure according to five threshold ranges (CE:  $>1 \times \text{ULN}$ ,  $>2 \times \text{ULN}$ ,  $>3$

x ULN, >5 x ULN and >10 x ULN) after scaffold or stent implantation. In the present study, the rise of three cardiac enzymes subcategorized in five different ranges was comparable between the two treatment arms (**Table 3**).

#### ***Incidence of peri-procedural MI***

Based on cardiac biomarkers, per protocol PMI was adjudicated in 12/315 (3.8%) in the BVS arm and 2/161 (1.2%) in the EES arm; with the extended historical CK-based definition of MI, the PMI rate was 3.9% (13/335) in the BVS arm and 1.2 % (2/166) in the EES arm (**Table 4**). An incidence rate of PMI according to “anatomic complications” assessed by angiography was similar between the two treatment arms.

#### ***Cardiac biomarker rise and angiographic assessment***

**Figure 4** shows magnitude of post-procedural CBR in patients with “anatomic complications” (Type 1 and Type 2) assessed by angiography. Distributions of post-procedural CBR subcategorized in five different ranges was similar between the two treatment arms in the patients with “anatomic complications”. (**Figure 4**).

#### ***Predictors of peri-procedural myocardial infarction***

In the multivariable analyses, treatment with overlapping devices appeared to be the only independent determinant of protocol (odds ratio: 4.36, 95% confidence interval: 1.48-12.61,  $p < 0.01$ ) and post hoc definition of PMI (odds ratio: 2.91, 95% confidence

interval: 1.06-7.44,  $p=0.04$ ) (**Table 5**).

***Impact on short-term clinical outcomes***

Clinical outcomes in terms of a composite of cardiac death, target-vessel myocardial infarction or ischemia driven target lesion revascularization after the procedure for patients with or without “anatomic complications” assessed by angiography were assessed at 30 days and 12 months. At 12 months, of 89 patients with “anatomic complications” assessed by angiography, 15 (16.9%) were adjudicated to have experienced NQMI or QMI, whereas 2 of 412 patients without identifiable mechanism developed a NQMI or QMI ( $p < 0.01$ ).

## **Discussion**

The present study is the first randomized clinical trial to assess the difference in frequencies of PMI and CBR after implantation of the Absorb BVS or the EES. The main findings of this study are: 1) rise of three cardiac enzymes subcategorized in five different ranges was comparable between the two treatment arms: 2) per protocol PMI was adjudicated in 13/335 (3.9%) in the Absorb BVS arm and 2/166 (1.2%) in the EES arm (p=0.16): 3) an incidence rate of “anatomic complications” was similar between the two treatment arms (16.4% vs. 19.9%, p=0.39) although the incidence of SBO (per side branch analysis) tended to be more frequently observed in the EES arm than in the Absorb BVS arm (5.2% vs. 7.7%, p = 0.07): 4) treatment with overlapping devices was the only independent determinant of per protocol PMI (odds ratio: 4.36, 95% confidence interval: 1.48-12.61, p <0.01).

### ***Availability of cardiac enzyme and peri-procedural cardiac biomarker rise***

This is the first scaffold or metallic stent study in which three different cardiac enzyme values were simultaneously available at a central core laboratory, the compliance of enzyme collection was notably high (CK: 95%, CKMB: 97.2 %, troponin: 96.8%). Of note, in the Resolute-all comers trial, an analyzable dataset for cardiac troponin (cTn) was available in 55.3% (1173/2121) patients.<sup>16</sup> In addition, 44.1% (935/2121) of

patients had an analyzable dataset for both cTn and CK-MB<sup>16</sup>. When CBR is subcategorized according to contemporary PMI criteria such as the third universal definition and the SCAI definition, PMI rates were 5.2% vs. 2.5% (CKMB >5x ULN), or 32.0% vs. 26.9% (troponin >5x ULN), 0.6% vs. 0.6% (CKMB >10xULN) and 4.6 % vs. 1.9 % (troponin >70x ULN) in the Absorb BVS and the Xience arms, respectively. The Venn diagrams (**Figure 5 panel a**) illustrate the concordance of CMR using two different enzymes and SCAI definitions of PMI (CK-MB >10 or cTn >70), cardiac enzymes simultaneously increased in only one patient. The Venn diagrams (**Figure 5 panel b**) illustrate the concordance of CBR using three different enzymes and three different definitions of PMI (CK >2 or CK-MB >5 or cTn >5). In 10 patients, three cardiac enzymes simultaneously increased while discordance in CBR was documented in 128 patients, suggesting that the sensitivity of cardiac enzymes to detect myocardial damage varies according to the criteria and the type of cardiac enzymes measured.

The prognostic relevance of CBR is shown by Park and colleagues, in a large cohort of 23,604 patients, the prognostic implication of a CKMB rise three to five times above the upper limit of normal.<sup>19</sup> Myint, et al reported that prognostic significance of troponin in acute coronary syndrome attenuates with increased age and that older age is associated with a worse prognosis compared with younger counterparts given the same level of

troponin rise, even at very low levels of troponin.<sup>20</sup>

Numerous definitions have been proposed for the diagnosis of PMI after coronary revascularization<sup>16, 21-23</sup>. In the present study, when the CBR using only the threshold level of cardiac enzyme is subcategorized according to contemporary PMI criteria such as the third universal definition and the SCAI definition, PMI rates were 5.2% vs. 2.5% (CKMB >5x ULN), or 32.0% vs. 26.9% (troponin >5x ULN), 0.6% vs. 0.6% (CKMB >10xULN) and 4.6 % vs. 1.9 % (troponin  $\geq$  70x ULN) in the BVS and the EES arms, respectively. There were no statistical differences between the two arms, however, it is notable that the PMI rate in overall incidence according to different definitions varied from 1.9% to 29.5%. These results strongly emphasize the arbitrary character of any definition of PMI.

***Anatomic complications assessed by angiography and peri-procedural cardiac biomarker rise with BVS or EES***

At variance with a previous report<sup>9</sup>, the Absorb BVS showed a trend toward lower incidence of post-procedural SBO compared with the EES. Although the nominal sizes of devices used ( $3.01 \pm 0.31$  mm vs.  $3.05 \pm 0.28$  mm,  $p=0.10$ ) and frequency of post device dilatation were comparable (61.8% vs. 57.7%,  $p=0.36$ ), the nominal balloon size and the pressure used during either implantation or post dilatation was larger and higher

in the EES arm, so that the expected balloon diameter tended to be larger accordingly ( $3.30 \pm 0.35$  mm vs.  $3.35 \pm 0.37$  mm,  $p=0.15$ ), the acute gain in minimal lumen diameter (QCA measurement by Core Lab) was significantly larger in the EES arm ( $1.15 \pm 0.38$  mm vs.  $1.46 \pm 0.38$  mm,  $p<0.001$ ). Whether the aggressive (post)dilatation may have resulted in a higher incidence of post-procedural SBO in the EES arm - due to presence of the bifurcation carina shift and/or plaque shift into the orifice of side branch<sup>18, 24</sup> remains speculative. Among the patients with post-dilatation, the peak ratio of CKMB post procedure was significantly higher in the Absorb BVS arm than in the EES arm ( $1.43 \pm 2.41$  vs.  $1.00 \pm 1.89$ ,  $p=0.016$ ) (**Table 6**). The current protocol did not recommend post-dilatation of the Absorb device with a balloon larger than 0.25mm with respect to the nominal size of the device. The post procedural CBR with the patients who underwent post-dilatation seems to justify retrospectively this conservative recommendation.

***Anatomic complications assessed by angiography and peri-procedural MI with Absorb BVS or EES***

Previous studies revealed that side-branch occlusion was the most common cause of peri-procedural MI<sup>24, 25</sup>. In the present study, out of 15 patients with per protocol PMI, 10 (66.7%) were angiographically classified as Type 1 (SBO) while three (20.0%) were

Type 2 (other anatomic complication). In two patients (13.3%), no angiographic complications could be identified. Thus, our results are in concordance with previous studies<sup>14, 15, 18</sup>.

### ***Predictors for peri-procedural rise of cardiac biomarker for injury***

The predictors of peri-procedural myocardial infarction can be broadly categorized as patient-, lesion-, and procedure-related risk factors<sup>18, 24</sup>. In the Spirit IV trial which randomized 3687 patients in a 2:1 fashion to receive either everolimus eluting stents or paclitaxel eluting stents, the total stent length was a strong predictor of PMI by criteria using CK or troponin<sup>18</sup>. In the present study, by multivariable analysis, treatment with overlapping devices was the only independent determinant of per protocol PMI and the post hoc definition of MI (CKMB >5), while there was overall no significant difference in PMI between the two device types (Absorb BVS vs. EES). One MI (non-Q-wave) was attributed to definite scaffold thrombosis involving overlapping scaffolds. Of note, in a juvenile porcine model<sup>26</sup>, overlapping Absorb scaffolds showed delayed healing on histology and OCT and slower tissue coverage than in non-overlapping scaffolds: the coverage of the overlapping segment was 80.1% and 99.5% at 28 and 90 days after implantation respectively, suggesting that complete coverage in humans may take up to 18 months. Similar findings<sup>27, 28</sup> - delayed healing and promotion of inflammation at

sites of overlap- have been reported in the atherosclerotic rabbit model implanted with EES, suggesting the general detrimental effect and potential biohazard of overlapping devices.

Adjacent implantation of scaffolds instead of true overlapping may circumvent this problem.

## **Limitations**

The results of the current sub-study are a post-hoc analysis. The study was not powered to detect difference in clinical events such as peri-procedural myocardial infarction and per protocol definition of PMI does not include clinical symptoms or ECG changes.

## **Conclusions**

There were no statistically significant differences in the incidence of cardiac enzyme rise and peri-procedural MI between Absorb BVS and EES. Overlapping of scaffolds or stents might be a precipitating factor of myocardial injury. Larger randomized trials are currently ongoing to confirm these findings.

As demonstrated in the present study that collected all three cardiac enzymes, binary definition of peri-procedural MI is not only dependent on the selection of cardiac enzymes but also on the thresholds of the CMR which is arbitrarily chosen.

## **Acknowledgments**

The authors wish to express their sincere appreciation to Dr. Charles Simonton and Ms. Veldhof Susan for the critical review of manuscript and Dr. Jan G. P. Tijssen and Ms.

Lei Peng for the statistical assistance.

## **References**

1. Serruys PW, Ormiston JA, Onuma Y, Regar E, Gonzalo N, Garcia-Garcia HM, Nieman K, Bruining N, Dorange C, Miquel-Hebert K, Veldhof S, Webster M, Thuesen L, Dudek D. A bioabsorbable everolimus-eluting coronary stent system (absorb): 2-year outcomes and results from multiple imaging methods. *Lancet*. 2009;373:897-910
2. Ormiston JA, Serruys PW, Regar E, Dudek D, Thuesen L, Webster MW, Onuma Y, Garcia-Garcia HM, McGreevy R, Veldhof S. A bioabsorbable everolimus-eluting coronary stent system for patients with single de-novo coronary artery lesions (absorb): A prospective open-label trial. *Lancet*. 2008;371:899-907
3. Ormiston JA, Webster MW, Armstrong G. First-in-human implantation of a fully bioabsorbable drug-eluting stent: The bvs poly-l-lactic acid everolimus-eluting coronary stent. *Catheterization and cardiovascular interventions : official journal of the Society for Cardiac Angiography & Interventions*. 2007;69:128-131
4. Onuma Y, Serruys PW, Ormiston JA, Regar E, Webster M, Thuesen L, Dudek D, Veldhof S, Rapoza R. Three-year results of clinical follow-up after a bioresorbable everolimus-eluting scaffold in patients with de novo coronary artery disease: The absorb trial. *EuroIntervention : journal of EuroPCR in collaboration with the Working Group on Interventional Cardiology of the European Society of Cardiology*. 2010;6:447-453
5. Serruys PW, Onuma Y, Dudek D, Smits PC, Koolen J, Chevalier B, de Bruyne B, Thuesen L, McClean D, van Geuns RJ, Windecker S, Whitbourn R, Meredith I, Dorange C, Veldhof S, Hebert KM, Sudhir K, Garcia-Garcia HM, Ormiston JA. Evaluation of the second generation of a bioresorbable everolimus-eluting vascular scaffold for the treatment of de novo coronary artery stenosis: 12-month clinical and imaging outcomes. *Journal of the American College of Cardiology*. 2011;58:1578-1588
6. Serruys PW, Onuma Y, Ormiston JA, de Bruyne B, Regar E, Dudek D, Thuesen L, Smits PC, Chevalier B, McClean D, Koolen J, Windecker S, Whitbourn R, Meredith I, Dorange C, Veldhof S, Miquel-Hebert K, Rapoza R, Garcia-Garcia HM. Evaluation of the second generation of a bioresorbable everolimus drug-eluting vascular scaffold for treatment of de novo coronary artery stenosis: Six-month clinical and imaging outcomes. *Circulation*. 2010;122:2301-2312
7. Serruys PW, Onuma Y, Garcia-Garcia HM, Muramatsu T, van Geuns RJ, de Bruyne B, Dudek D, Thuesen L, Smits PC, Chevalier B, McClean D, Koolen J, Windecker S, Whitbourn R, Meredith I, Dorange C, Veldhof S, Hebert KM, Rapoza R, Ormiston JA.

- Dynamics of vessel wall changes following the implantation of the absorb everolimus-eluting bioresorbable vascular scaffold: A multi-imaging modality study at 6, 12, 24 and 36 months. *EuroIntervention : journal of EuroPCR in collaboration with the Working Group on Interventional Cardiology of the European Society of Cardiology*. 2014;9:1271-1284
8. Diletti R, Serruys PW, Farooq V, Sudhir K, Dorange C, Miquel-Hebert K, Veldhof S, Rapoza R, Onuma Y, Garcia-Garcia HM, Chevalier B. Absorb ii randomized controlled trial: A clinical evaluation to compare the safety, efficacy, and performance of the absorb everolimus-eluting bioresorbable vascular scaffold system against the xience everolimus-eluting coronary stent system in the treatment of subjects with ischemic heart disease caused by de novo native coronary artery lesions: Rationale and study design. *American heart journal*. 2012;164:654-663
  9. Muramatsu T, Onuma Y, Garcia-Garcia HM, Farooq V, Bourantas CV, Morel MA, Li X, Veldhof S, Bartorelli A, Whitbourn R, Abizaid A, Serruys PW, Investigators A-E. Incidence and short-term clinical outcomes of small side branch occlusion after implantation of an everolimus-eluting bioresorbable vascular scaffold: An interim report of 435 patients in the absorb-extend single-arm trial in comparison with an everolimus-eluting metallic stent in the spirit first and ii trials. *JACC. Cardiovascular interventions*. 2013;6:247-257
  10. Garg S, Serruys PW. Coronary stents: Current status. *Journal of the American College of Cardiology*. 2010;56:S1-42
  11. Onuma Y, Ormiston J, Serruys PW. Bioresorbable scaffold technologies. *Circulation journal : official journal of the Japanese Circulation Society*. 2011;75:509-520
  12. Roubin GS, Cannon AD, Agrawal SK, Macander PJ, Dean LS, Baxley WA, Breland J. Intracoronary stenting for acute and threatened closure complicating percutaneous transluminal coronary angioplasty. *Circulation*. 1992;85:916-927
  13. Bell MR, Reeder GS, Garratt KN, Berger PB, Bailey KR, Holmes DR, Jr. Predictors of major ischemic complications after coronary dissection following angioplasty. *The American journal of cardiology*. 1993;71:1402-1407
  14. Herrmann J. Peri-procedural myocardial injury: 2005 update. *European heart journal*. 2005;26:2493-2519
  15. Park DW, Kim YH, Yun SC, Ahn JM, Lee JY, Kim WJ, Kang SJ, Lee SW, Lee CW, Park SW, Park SJ. Impact of the angiographic mechanisms underlying periprocedural myocardial infarction after drug-eluting stent implantation. *The American journal of cardiology*. 2014;113:1105-1110
  16. Vranckx P, Farooq V, Garg S, Van Es GA, Silber S, Windecker S, Stone GW, Serruys

- PW. Different cardiac biomarkers to detect peri-procedural myocardial infarction in contemporary coronary stent trials: Impact on outcome reporting. *Heart*. 2012;98:1424-1430
17. Thygesen K, Alpert JS, Jaffe AS, Simoons ML, Chaitman BR, White HD, Joint ESCAAHAWHFTFFUDoMI, Authors/Task Force Members C, Thygesen K, Alpert JS, White HD, Biomarker S, Jaffe AS, Katus HA, Apple FS, Lindahl B, Morrow DA, Subcommittee ECG, Chaitman BR, Clemmensen PM, Johanson P, Hod H, Imaging S, Underwood R, Bax JJ, Bonow JJ, Pinto F, Gibbons RJ, Classification S, Fox KA, Atar D, Newby LK, Galvani M, Hamm CW, Intervention S, Uretsky BF, Steg PG, Wijns W, Bassand JP, Menasche P, Ravkilde J, Trials, Registries S, Ohman EM, Antman EM, Wallentin LC, Armstrong PW, Simoons ML, Trials, Registries S, Januzzi JL, Nieminen MS, Gheorghide M, Filippatos G, Trials, Registries S, Luepker RV, Fortmann SP, Rosamond WD, Levy D, Wood D, Trials, Registries S, Smith SC, Hu D, Lopez-Sendon JL, Robertson RM, Weaver D, Tendera M, Bove AA, Parkhomenko AN, Vasilieva EJ, Mendis S, Guidelines ESCCfP, Bax JJ, Baumgartner H, Ceconi C, Dean V, Deaton C, Fagard R, Funck-Brentano C, Hasdai D, Hoes A, Kirchhof P, Knuuti J, Kolh P, McDonagh T, Moulin C, Popescu BA, Reiner Z, Sechtem U, Sirnes PA, Tendera M, Torbicki A, Vahanian A, Windecker S, Document R, Morais J, Aguiar C, Almahmeed W, Arnar DO, Barili F, Bloch KD, Bolger AF, Botker HE, Bozkurt B, Bugiardini R, Cannon C, de Lemos J, Eberli FR, Escobar E, Hlatky M, James S, Kern KB, Moliterno DJ, Mueller C, Neskovic AN, Pieske BM, Schulman SP, Storey RF, Taubert KA, Vranckx P, Wagner DR. Third universal definition of myocardial infarction. *Journal of the American College of Cardiology*. 2012;60:1581-1598
  18. Pervaiz MH, Sood P, Sudhir K, Hermiller JB, Hou L, Hattori K, Su X, Cao S, Wang J, Applegate RJ, Kereiakes DJ, Yaqub M, Stone GW, Cutlip DE. Periprocedural myocardial infarction in a randomized trial of everolimus-eluting and paclitaxel-eluting coronary stents: Frequency and impact on mortality according to historic versus universal definitions. *Circulation. Cardiovascular interventions*. 2012;5:150-156
  19. Park DW, Kim YH, Yun SC, Ahn JM, Lee JY, Kim WJ, Kang SJ, Lee SW, Lee CW, Park SW, Park SJ. Frequency, causes, predictors, and clinical significance of peri-procedural myocardial infarction following percutaneous coronary intervention. *European heart journal*. 2013;34:1662-1669
  20. Myint PK, Kwok CS, Bachmann MO, Stirling S, Shepstone L, Zaman MJ. Prognostic value of troponins in acute coronary syndrome depends upon patient age. *Heart*.

2014

21. Moussa ID, Klein LW, Shah B, Mehran R, Mack MJ, Brilakis ES, Reilly JP, Zoghbi G, Holper E, Stone GW. Consideration of a new definition of clinically relevant myocardial infarction after coronary revascularization: An expert consensus document from the society for cardiovascular angiography and interventions (scai). *Journal of the American College of Cardiology*. 2013;62:1563-1570
22. Thygesen K, Alpert JS, White HD, Joint ESCAAHAWHFTFFtRoMI. Universal definition of myocardial infarction. *Journal of the American College of Cardiology*. 2007;50:2173-2195
23. Moussa ID, Klein LW, Shah B, Mehran R, Mack MJ, Brilakis ES, Reilly JP, Zoghbi G, Holper E, Stone GW. Consideration of a new definition of clinically relevant myocardial infarction after coronary revascularization: An expert consensus document from the society for cardiovascular angiography and interventions (scai). *Catheterization and cardiovascular interventions : official journal of the Society for Cardiac Angiography & Interventions*. 2014;83:27-36
24. Lansky AJ, Stone GW. Periprocedural myocardial infarction: Prevalence, prognosis, and prevention. *Circulation. Cardiovascular interventions*. 2010;3:602-610
25. Farooq V, Serruys PW, Vranckx P, Bourantas CV, Girasis C, Holmes DR, Kappetein AP, Mack M, Feldman T, Morice MC, Colombo A, Morel MA, de Vries T, Dawkins KD, Mohr FW, James S, Stahle E. Incidence, correlates, and significance of abnormal cardiac enzyme rises in patients treated with surgical or percutaneous based revascularisation: A substudy from the synergy between percutaneous coronary interventions with taxus and cardiac surgery (syntax) trial. *International journal of cardiology*. 2013;168:5287-5292
26. Farooq V, Serruys PW, Heo JH, Gogas BD, Onuma Y, Perkins LE, Diletti R, Radu MD, Raber L, Bourantas CV, Zhang Y, van Remortel E, Pawar R, Rapoza RJ, Powers JC, van Beusekom HM, Garcia-Garcia HM, Virmani R. Intracoronary optical coherence tomography and histology of overlapping everolimus-eluting bioresorbable vascular scaffolds in a porcine coronary artery model: The potential implications for clinical practice. *JACC. Cardiovascular interventions*. 2013;6:523-532
27. Nakazawa G, Nakano M, Otsuka F, Wilcox JN, Melder R, Pruitt S, Kolodgie FD, Virmani R. Evaluation of polymer-based comparator drug-eluting stents using a rabbit model of iliac artery atherosclerosis. *Circulation. Cardiovascular interventions*. 2011;4:38-46
28. Palmerini T, Biondi-Zoccai G, Della Riva D, Mariani A, Genereux P, Branzi A, Stone

GW. Stent thrombosis with drug-eluting stents: Is the paradigm shifting? *Journal of the American College of Cardiology*. 2013;62:1915-1921

## **Figure legends**

### **Figure 1**

According to the underlying angiographic mechanisms, the peri-procedural MI after revascularization was classified into three types: Type 1 denotes cardiac biomarker rise due to side-branch occlusion, Type 2 denotes cardiac biomarker rise due to other anatomic complications, and Type 3 denotes cardiac biomarker rise without any identifiable anatomic causes in the coronary artery.

Pre-procedure angiography showed a focal stenosis (**white arrows**), side branches in the target lesion (**yellow arrows**) and distal embolization was observed after device implantation (**B, red arrow**).

### **Figure 2**

Pre-procedural quantitative coronary angiography (QCA) analyses are shown. The QCA analysis delineates 5-mm proximal (**A, red double arrow**) and distal segment (**A, green double arrow**) to the intended device implantation site (**B, white double arrow**). Any visible side branches originating from this region of interest were analyzed. The conventional QCA analysis automatically delineates an obstruction segment in the main branch (**B, yellow double arrow**). An example of side branch analysis is shown in **C** and **D**.

DS, diameter stenosis; RVD, reference vessel diameter

### **Figure 3**

In the serial sample analysis, a total of 1446 blood time points for the assessment of cardiac enzyme biomarkers were available with 572 central and 874 local biomarker values.

### **Figure 4**

The figure shows magnitude of post-procedural cardiac enzyme rise for the patients with side branch occlusion after PCI (**blue bars**) and those with the other anatomical complications (**red bars**). Incidence of three cardiac enzymes rise subcategorized in five different ranges was similar between the two treatment groups (CK>1xULN: 0.28, CK>2xULN: 0.24, CK>3xULN: 1.0, CK>5xULN: 0.34, CK>10xULN: 1.0, CKMB>1xULN: 1.0, CKMB>2xULN: 0.49, CKMB>3xULN: 0.17, CKMB>5xULN: 0.60, CKMB>10xULN: 1.0, cTn>1xULN: 0.61, cTn>2xULN: 1.0, cTn>3xULN: 1.0, cTn>5xULN: 0.23, cTn>10xULN: 0.49).

CPK, creatine kinase; CK-MB, creatine kinase-myoband; cTn, cardiac troponin;

**Figure 5**

- (a) The Venn diagrams illustrate the concordance of cardiac enzyme rise using two different enzymes and SCAI definitions of PMI (CK-MB > 10 or cTn >70) , cardiac enzymes simultaneously increased in only one patient.
- (b) The Venn diagrams illustrate the concordance of cardiac enzyme rise using three different enzymes and three different definitions of PMI (CK >2 or CK-MB > 5 or cTn >5). In 9 patients, three cardiac enzymes simultaneously increased while in 107 patients, discordance in cardiac enzyme rise was documented, suggesting that the sensitivity of cardiac enzymes to detect myocardial damage varies according to criteria and types of enzymes.

**Table1.** Baseline demographic data and angiographic characteristics

	<b>Absorb BVS (N=335*, L=364*)</b>	<b>EES (N=166*, L=182*)</b>	<i>p</i> value
Age in years, mean± SD	61.5 ± 10.0	60.9 ± 10.0	0.51
Male, n (%)	253 (75.5)	132 (79.5)	0.37
Body-mass index in kg/m <sup>2</sup> , mean± SD	27.92 ± 4.09	28.14 ± 3.69	0.56
Current smoker, n (%)	79 (23.6)	36 (21.7)	0.65
Hypertension requiring treatment, n (%)	220 (65.7)	112 (67.5)	0.76
Dyslipidemia requiring treatment, n (%)	238 (71.0)	123 (74.1)	0.53
Any diabetes mellitus, n (%)	80 (23.9)	40 (24.1)	1.00
Unstable Angina, n (%)	68 (20.3)	37 (22.3)	0.64
Family history of coronary artery disease, n (%)	112 (36.6)	64 (41.3)	0.36
Prior history of myocardial infarction, n (%)	93 (28.0)	48 (28.9)	0.83
Number of lesions/patient, mean± SD	1.09 ± 0.28	1.10 ± 0.30	0.72
Lesion location			
Right coronary artery, n (%)	95 (26.1)	56 (30.8)	0.27
Left anterior descending artery, n (%)	163 (44.8)	84 (46.2)	0.78
Left circumflex artery or Ramus, n (%)	106 (29.1)	42 (23.1)	0.15
ACC/AHA lesion complexity			
A, n (%)	5 (1.4)	1 (0.6)	0.67
B1, n (%)	193 (53.2)	90 (50.0)	0.52
B2, n (%)	159 (43.8)	87 (48.3)	0.36
C, n (%)	6 (1.7)	2 (1.1)	1.00

TIMI Flow 0 or 1 , n (%)	1 (0.3)	2 (1.1)	0.26
Calcification (moderate or severe) , n (%)	46 (12.7)	28 (15.5)	0.43
Tortuosity (moderate or severe) , n (%)	34 (9.4)	13 (7.2)	0.42
Eccentric , n (%)	357 (98.3)	178 (99.4)	0.43
Thrombus, n (%)	5 (1.4)	4 (2.2)	0.49
Bifurcation, n (%)	13 (3.6)	5 (2.8)	0.80
Reference vessel diameter in mm, mean± SD	2.59 ± 0.38	2.63 ± 0.40	0.29
Percentage diameter stenosis in %, mean± SD	58.6 ± 11.1	59.7 ± 11.6	0.30
Obstruction Lesion length in mm, mean± SD	13.8 ± 6.5	13.8 ± 6.6	0.92

---

BVS bioresorbable vascular scaffold(s); EES everolimus-eluting metallic stent(s); ACC/AHA American College of Cardiology/American Heart Association; SD standard deviation; \* N=number of patients, L=number of lesions

Table 2. Anatomic complications assessed by angiography

Per patient analysis	Absorb BVS (N=335 pts)	EES (N=166 pts)	p value
<i>Any anatomic complications assessed by angiography, % (N)</i>	16.4 (56/335)	19.9 (33/166)	0.39
<i>Type1 anatomic complication assessed by angiography, % (N)</i>	-	-	-
<b>Side Branch Occlusion</b>			
Side branch occlusion after pre dilatation	12.5 (43/335)	15.7 (26/166)	0.41
Side branch occlusion after device implantation	0 (0/335)	0 (0/166)	1.00
Side branch occlusion improvement after NTG	12.5 (43/335)	15.7 (26/166)	0.41
Side branch occlusion after procedure	0.9 (3/335)	0 (0/166)	0.55
	11.6 (40/335)	15.7 (26/166)	0.26
<i>Type2 anatomic complication assessed by angiography, % (N)</i>	-	-	-
Abrupt closure	0 (0/335)	1.8 (2/166)	0.11
Distal embolization	0.3 (1/335)	0 (0/166)	1.00
Coronary perforation	0.6 (2/335)	0 (0/166)	1.00
Flow limiting dissection (NHLBI type F)	0.3 (1/335)	0 (0/166)	1.00
Coronary dissection after pre dilatation (NHLBI D or E)	1.8 (6/335)	1.2 (2/166)	1.00
Coronary dissection after device implantation	0.3 (1/335)	0.6 (1/166)	1.00
Thrombus during procedure	0.3 (1/335)	0 (0/166)	1.00
Disruption of collateral flow	0.3 (1/335)	1.2 (2/166)	0.26
<b>Per side branch analysis</b>	<b>N=998 side-branches</b>	<b>N=503 side-branches</b>	
<b>Incidence of side branch occlusion after procedure, % (N)</b>	5.3 (52/988)	7.6 (39/503)	0.07
<b>Location of occluded side branch</b>	-	-	-
Outside Scaffold Segment	0 (0 / 988)	0 (0 / 503)	1.00

To-be-scaffold segment outside obstruction	0.9 (9 / 988)	1.0 (5 / 503)	1.00
Obstruction segment	4.3 (42 / 988)	6.8 (34 / 503)	0.046
<b>Reference vessel diameter of occluded side branch, % (N)</b>	-	-	-
reference vessel diameter > 1.0mm	0.9% (9 / 988)	1.2 % (6 / 503)	0.59
0.5 <reference vessel diameter ≤ 1.0mm	2.9% (29 / 988)	4.2 % (21 / 503)	0.22
reference vessel diameter ≤ 0.5mm	1.3% (13 / 988)	2.4 % (12 / 503)	0.14

BVS bioresorbable vascular scaffold(s); EES everolimus-eluting metallic stent(s)

**Table 3. Comparison of the peak value of cardiac enzyme rise post-procedure using either central lab and/or local lab results.**

	CK 476/501 (95.0%)		CKMB 487/501 (97.2%)		cTn 485/501 (96.8%)		
	BVS (n=315)	Xience (n=161)	BVS (n=324)	Xience (n=163)	BVS (n=325)	Xience (n=160)	
	P value	P value	P value	P value	P value	P value	
Mean ± SD	0.69±0.61	0.63±0.63	1.27±1.99	1.06±1.64	13.38±30.64	9.08±21.01	0.121
>1×ULN	16.2% (51/315)	8.7% (14/161)	32.1% (104/324)	25.8% (42/163)	62.8% (204/325)	61.9% (99/160)	0.848
>2×ULN	5.1% (16/315)	1.9% (3/161)	13.3% (43/324)	9.8% (16/163)	48.6% (158/325)	45.6% (73/160)	0.535
>3×ULN	1.3% (4/315)	1.9% (3/161)	7.1% (23/324)	6.1% (10/163)	38.2% (124/325)	36.9% (59/160)	0.785
>5×ULN	0% (0/315)	0.6% (1/161)	4.9% (16/324)	2.5% (4/163)	29.8% (97/325)	25.6% (41/160)	0.333
>10×ULN	0% (0/315)	0% (0/161)	0.6% (2/324)	0.6% (1/163)	19.1% (62/325)	15.0% (24/160)	0.269

CPK, creatine kinase; CK-MB, creatine kinase-myoband; cTn, cardiac troponin; ULN, upper limit of normal

Table 4. Incidence of per protocol peri-procedural myocardial infarction according to anatomic complications assessed by angiography

	Absorb BVS (N=335 pts)	EES (N=166 pts)	p value
<b>Per protocol peri-procedural MI, % (N)</b>	3.9 (13/335)	1.2 (2/166)	0.16
<b>Type 1: Side Branch Occlusion, % (N)</b>	2.7 (9/335)	0.6 (1/166)	0.18
Side branch occlusion after pre dilatation	0 (0/335)	0 (0/166)	1.00
Side branch occlusion after device implantation	2.7 (9/335)	0.6 (1/166)	0.18
Side branch occlusion improvement after NTG	0 (0/335)	0 (0/166)	1.00
Side branch occlusion after procedure	2.7 (9/335)	0.6 (1/166)	0.18
<b>Type 2: Angiographic Other Complication, % (N)</b>	0.6 (2/335)	0.6 (1/166)	1.00
Abrupt closure	0 (0/335)	0.6 (1/166)	0.33
Distal embolization	0.3 (1/335)	0 (0/166)	1.00
coronary perforation	0 (0/335)	0 (0/166)	1.00
Flow limiting dissection (NHLBI type F)	0 (0/335)	0 (0/166)	1.00
coronary dissection after pre dilatation (NHLBI D or E)	0.3 (1/335)	0 (0/166)	1.00
coronary dissection after device implantation	0 (0/335)	0 (0/166)	1.00
Thrombus during procedure	0 (0/335)	0 (0/166)	1.00
Disruption of collateral flow	0 (0/335)	0 (0/166)	1.00
<b>Non-identifiable mechanism causes, % (N)</b>	0.6 (2/335)	0 (0/166)	1.00

Per protocol PMI: elevation of total creatine kinase (CK) to >2 x normal along with elevated or “positive” creatine kinase myocardial band (CKMB) without clinical symptom and electrocardiogram (ECG) change

BVS bioresorbablevascular scaffold(s); EES everolimus-eluting metallic stent(s)

Table 5. Predictors of periprocedural myocardial infarction

	Per Protocol (CK rise of > 2 times of ULN accompanied by CKMB rise)				CKMB rise of >5 x ULN			
	Univariable p Value	Odds Ratio (95%)	Multivariable p Value	Odds Ratio (95%)	Univariable p Value	Odds Ratio (95%)	Multivariable p Value	Odds Ratio (95%)
<b>Covariates</b>								
<b>Patient-related factors</b>								
Age (yrs)	0.56	1.02 (0.96-1.07)	-	-	0.84	0.78 (0.07-9.07)	-	-
Male	0.77	1.21 (0.38-5.38)	-	-	0.09	0.44 (0.18-1.14)	0.07	0.41 (0.16-1.07)
Body-mass index (kg/m <sup>2</sup> )	0.35	0.94 (0.80-1.07)	-	-	0.99	0.99 (0.88-1.11)	-	-
Current smoker	0.36	1.82 (0.50-6.67)	-	-	0.81	1.14 (0.36-3.01)	-	-
Hypertension requiring treatment	0.11	2.31 (0.81-6.69)	-	-	0.69	1.22 (0.48-3.49)	-	-
Dyslipidemia requiring treatment	0.33	0.57 (0.19-1.88)	-	-	0.49	0.72 (0.29-1.94)	-	-
Any diabetes mellitus	0.30	0.48 (0.07-1.77)	-	-	0.92	1.06 (0.34-2.80)	-	-
Unstable Angina	0.93	0.94 (0.21-3.03)	-	-	0.92	0.94 (0.27-2.64)	-	-
<b>Lesion-related factors</b>								
Pre-procedural Diameter Stenosis (%)	0.98	1.00 (0.93-1.02)	-	-	0.94	0.99 (0.96-1.04)	-	-
Pre-procedural Minimum Lumen Diameter (mm)	0.69	1.38 (0.27-6.49)	-	-	0.88	1.28 (0.27-4.35)	-	-
Pre-procedural Reference Diameter	0.29	0.48 (0.11-1.84)	-	-	0.68	0.79 (0.24-2.44)	-	-

(mm)								
Obstruction length (mm)	0.84	0.99 (0.91-1.07)	-	-		0.75	1.01 (0.94-1.07)	-
Pre-procedural curvature (cm <sup>-1</sup> )	0.14	0.20 (0.01-1.59)	-	-		0.72	1.31 (0.27-4.74)	-
<b>Treatment-related factors</b>								
Treatment with ≥ overlapping devices	0.01	4.07 (1.39-11.6)	<0.01	4.36 (1.48-12.61)		0.05	2.73 (1.00-6.89)	0.04
Scaffold or stent length	0.04	1.05 (1.00-1.09)	0.51	1.04 (0.95-1.12)		0.11	1.04 (0.90-1.08)	-
Device type (Absorb BVS vs. EES)	0.07	3.31 (0.90-21.30)	0.10	2.83 (0.72-18.9)		0.17	2.06 (0.74-7.30)	-
Scaffold or stent lumen acute gain	0.84	0.72 (0.03-16.18)	-	-		0.80	1.00 (0.97-1.04)	-
Post-dilatation	0.77	1.18 (0.41-3.83)	-	-		0.79	1.13 (0.46-3.07)	-
Bail-out	0.24	1.32 (0.43-11.02)	-	-		0.42	1.96 (0.30-7.34)	-

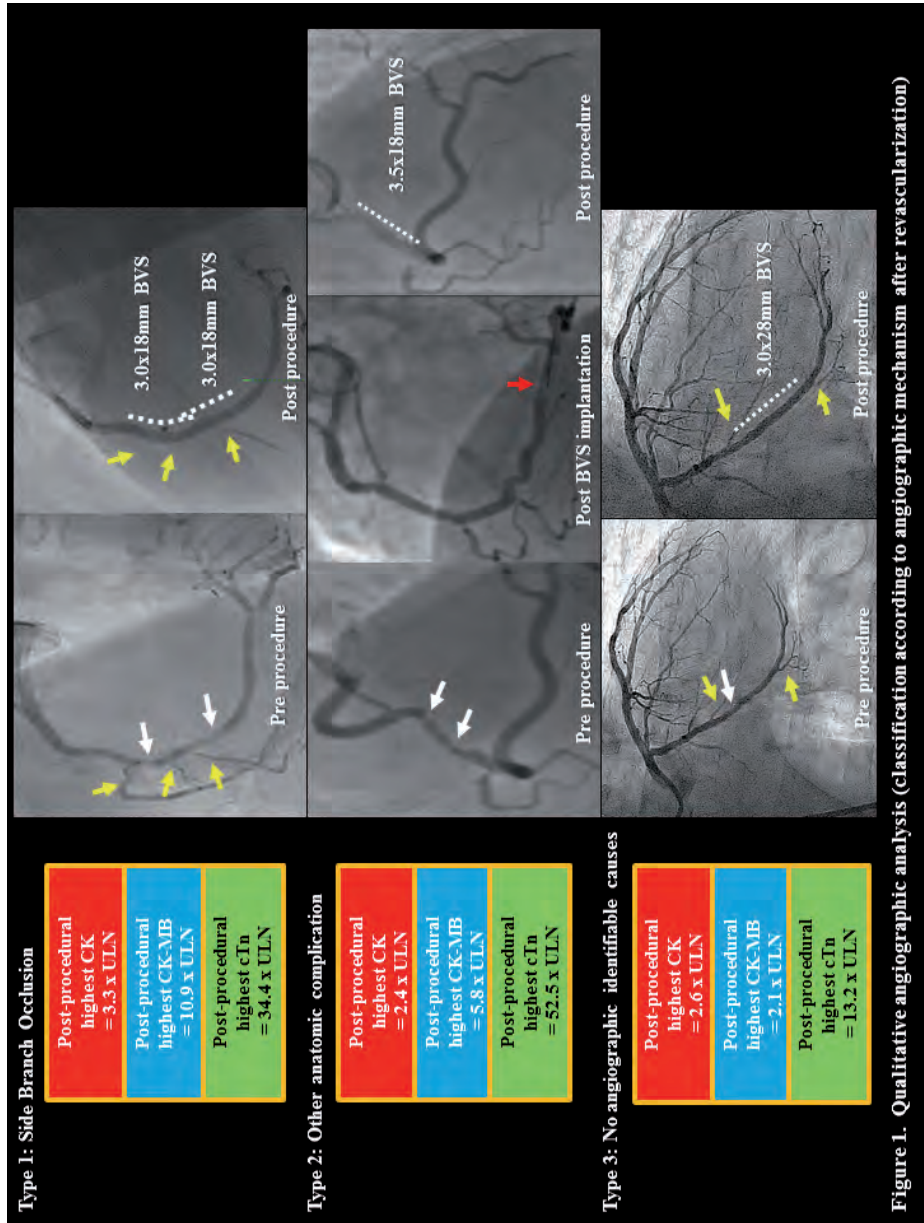
Univariable and multivariable stepwise logistic regression analyses were used to determine the predictors of peri-procedural MI. The multivariable model was created with a stepwise elimination procedure, where the independent variables were entered into the model at the 0.20 significance level and removed at the 0.10 level.

BVS = bioresorbable vascular scaffold(s); EES = everolimus eluting metallic stent(s); ULN = upper limit of normal

**Table 6. The correlation between post-dilatation and cardiac enzymes**

	Absorb BVS		EES		P value
	Number	Mean±SD	Number	Mean±SD	
<b>CK ratio</b>					
Without post-dilatation	114	0.63±0.54	64	0.68±0.69	0.268
With post-dilatation	201	0.75±0.66	97	0.63±0.61	0.303
<i>p</i> value between without post-dilatation and post -dilatation		0.029		0.855	-
<b>CKMB ratio</b>					
Without post-dilatation	118	1.10±1.36	65	1.19±1.21	0.402
With post-dilatation	204	1.43±2.41	96	1.00±1.89	0.016
<i>p</i> value between without post-dilatation and post -dilatation		0.304		0.044	-
<b>cTn ratio</b>					
Without post-dilatation	106	12.37±35.42	54	12.77±28.91	0.119
With post-dilatation	168	11.59±25.79	78	5.10±9.21	0.054
<i>p</i> value between without post-dilatation and post -dilatation		0.123		0.056	-

Ratio is the value after procedure / upper limit of normal



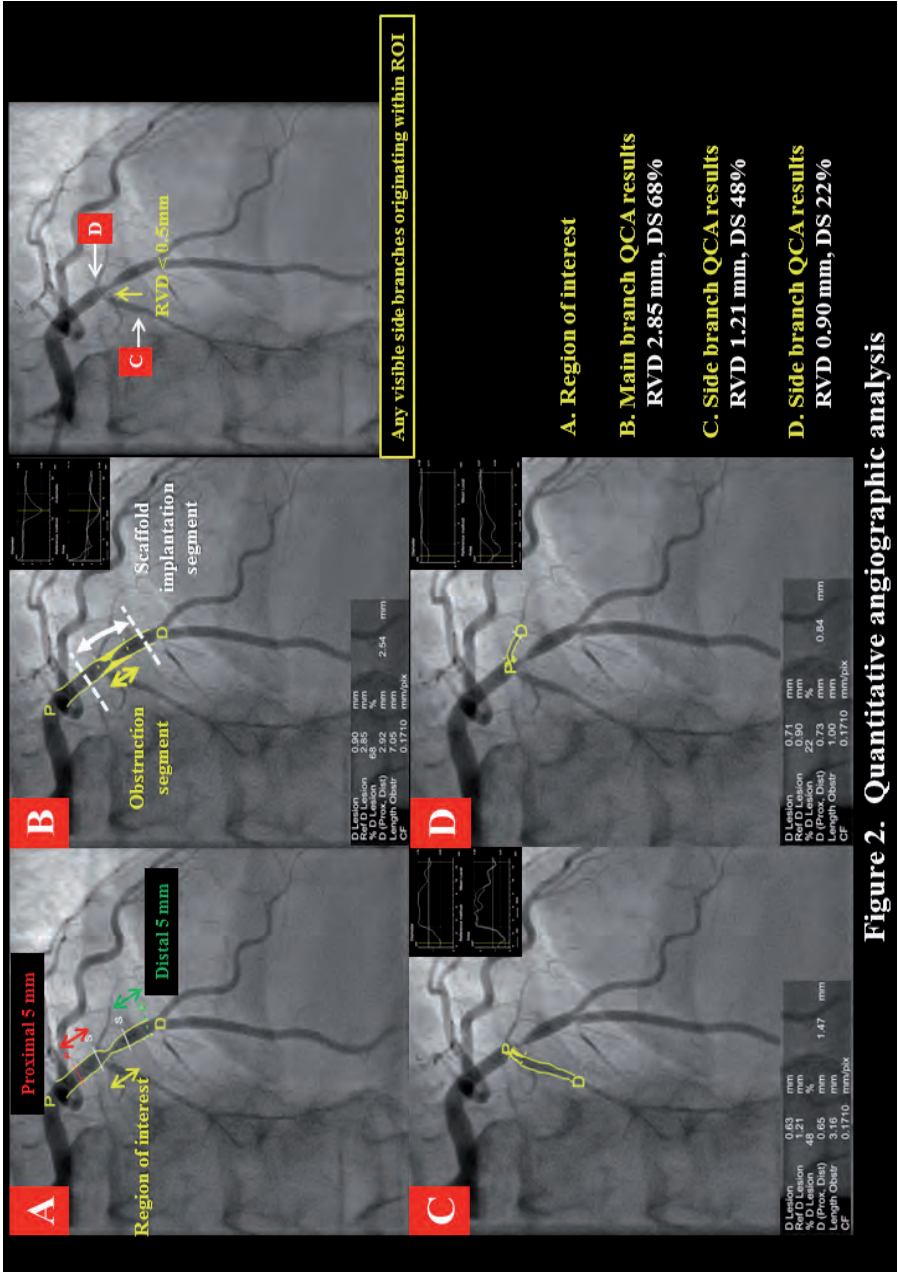


**Figure 2. Quantitative angiographic analysis**

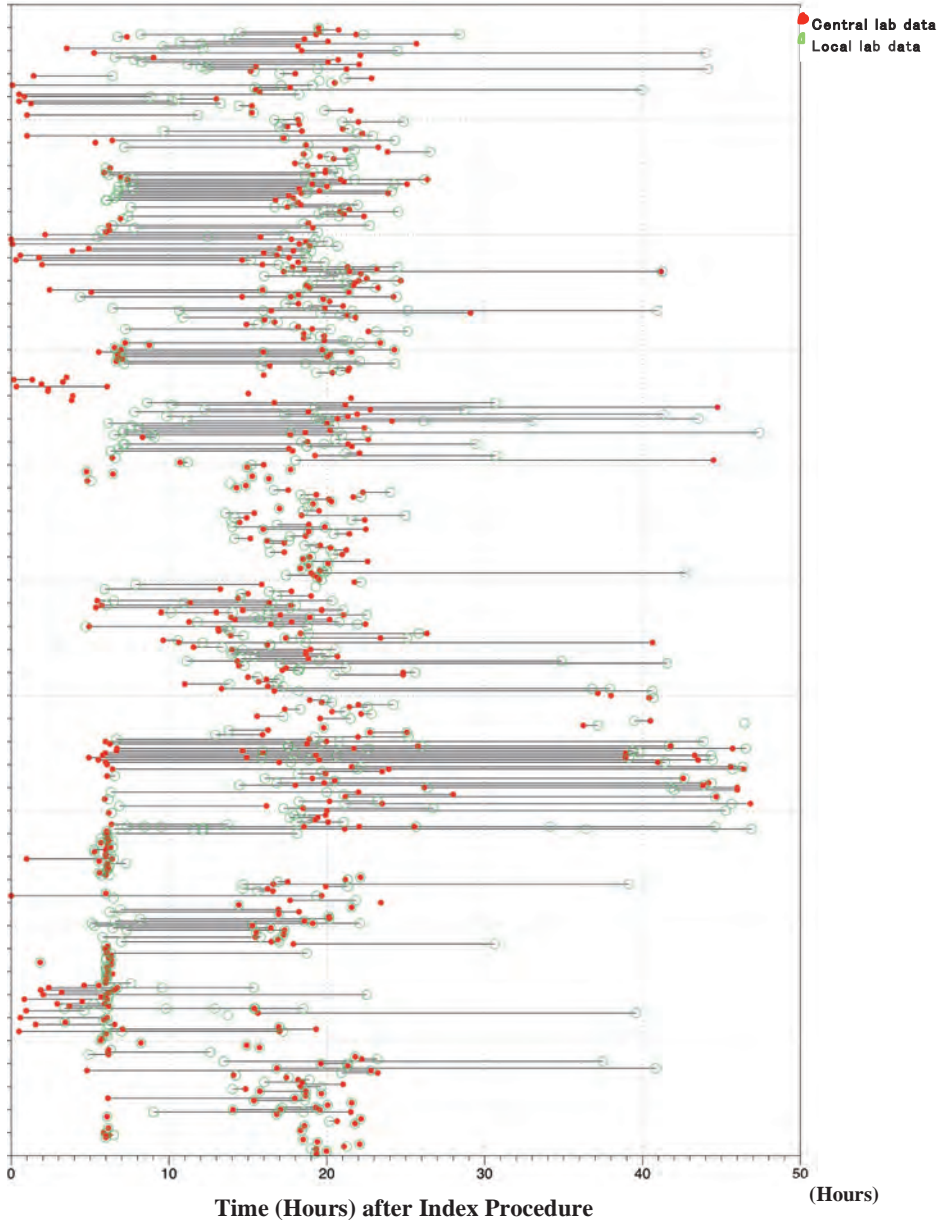
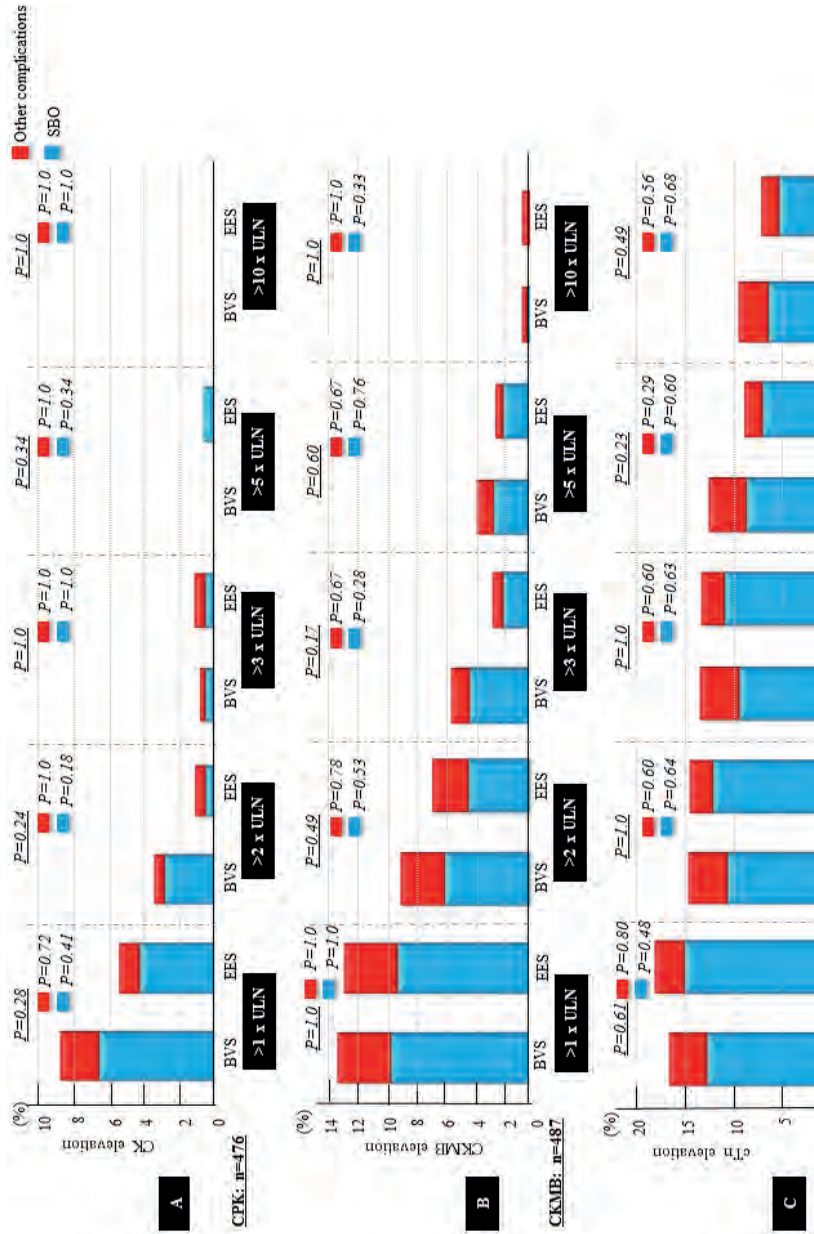
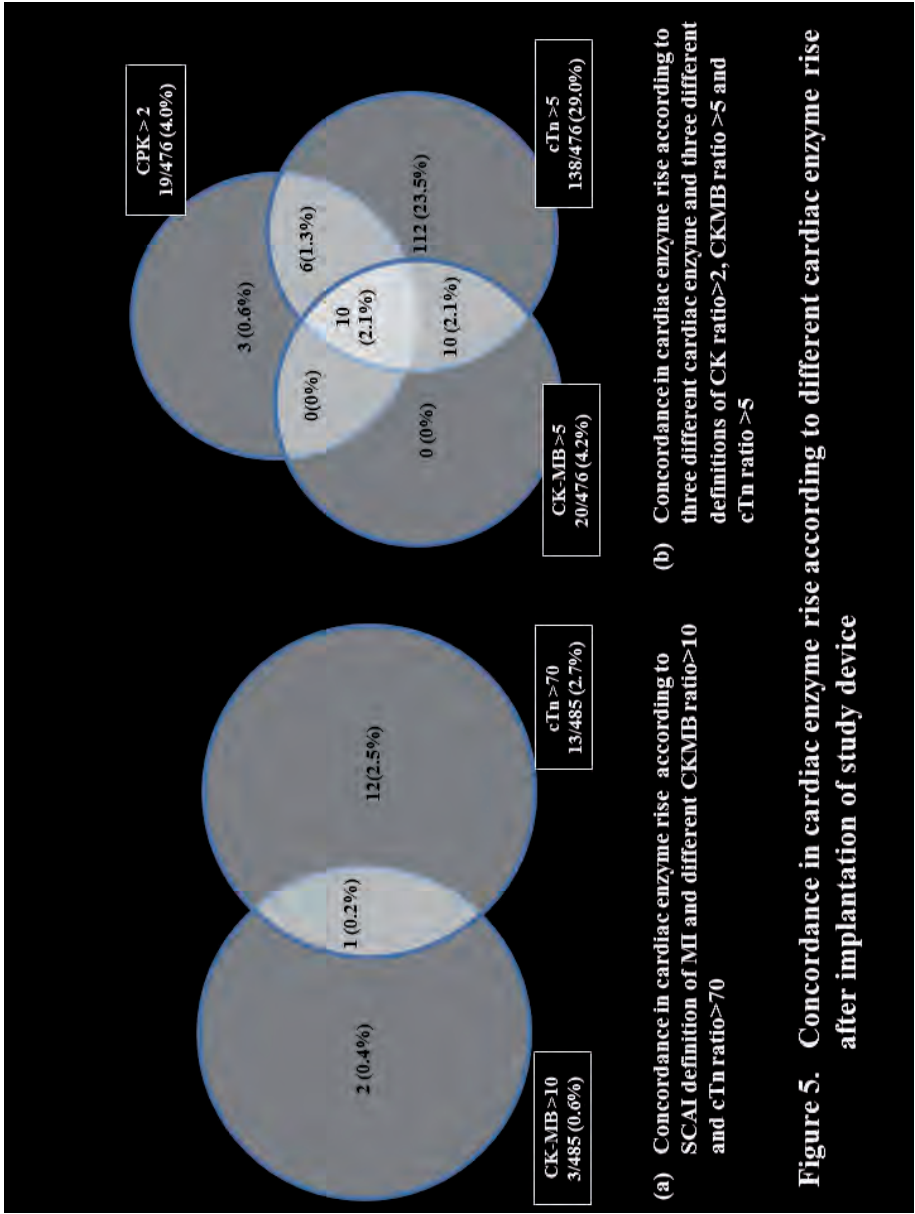


Figure 3. Time-point for the assessment of cardiac biomarker rise post procedure using either central lab or local lab





**Figure 5. Concordance in cardiac enzyme rise according to different cardiac enzyme rise after implantation of study device**

## 5.8 Preventive passivation of high-risk plaques by BRS technologies

Early detection and invasive passivation of future culprit lesions:  
A future potential or an unrealistic pursuit of Chimeras?

*Am Heart J.* 2013;165:869-81.

[Review, Impact Factor (2013): 4.696]

Bourantas CV, Garcia-Garcia CV, Diletti R, Muramatsu T, Serruys PW.





# Early detection and invasive passivation of future culprit lesions: A future potential or an unrealistic pursuit of Chimeras?

Christos V. Bourantas, MD, PhD, Hector M. Garcia-Garcia, MD, PhD, Roberto Diletti, MD, Takashi Muramatsu, MD, PhD, and Patrick W. Serruys, MD, PhD *Rotterdam, The Netherlands*

New advances in image and signal processing have allowed the development of numerous invasive and noninvasive imaging modalities that have revealed details of plaque pathology and allowed us to study *in vivo* the atherosclerotic evolution. Recent natural history of atherosclerosis studies permitted us to evaluate changes in the compositional and morphological characteristics of the plaque and identify predictors of future events. The idea of being able to identify future culprit lesions and passivate these plaques has gradually matured, and small scale studies have provided proofs about the feasibility of this concept. This review article summarizes the recent advances in the study of atherosclerosis, cites the current evidence, highlights our limitations in understanding the evolution of the plaque and in predicting plaque destabilization, and discusses the potentiality of an early invasive sealing of future culprit lesions. (*Am Heart J* 2013;165:869-881.e4.)

The miniaturization of medical devices, technological innovations, new developments in image and signal processing, and advances in biological and molecular imaging have provided us with a variety of imaging modalities that permit detection of local inflammation and detailed evaluation of changes in atheroma burden and its composition. These techniques demonstrated that coronary atherosclerosis has focal and eccentric manifestations that evolve in an independent manner, which is affected by the composition of the plaque, the presence of inflammation, and the local hemodynamic environment. Prospective natural history of atherosclerosis studies shed light into the mechanisms involved in this process and allowed us to identify predictors of future culprit lesions.<sup>1,3</sup> The idea of being able to predict plaque development has gradually evolved and recently the Shield Evaluated at Cardiac Hospital in Rotterdam for Investigation and Treatment of TCFA study has been reported, which examined the feasibility of sealing non-flow-limiting lesions that have features associated with increased vulnerability (Figure 1).<sup>4</sup>

The aim of this review article is to summarize the technological advances in the study of atherosclerosis, cite the current evidence, and discuss the potentiality of an invasive passivation of future culprit lesions.

## Effect of the composition of the plaque on the natural course of atherosclerosis

Even before the development of intravascular imaging, it was apparent that the composition of the atheroma has significant prognostic implications and affects its natural course. Pathology-based studies have shown that the type of the plaque is associated with the final act of atherosclerosis and allowed identification of plaque characteristics associated with acute coronary events.<sup>5</sup> Today, it is known that most of the acute myocardial infarctions (MIs) are due to plaque rupture, which occurs in lesions referred as thin-capped fibroatheromas (TCFAs). These plaques exhibit positive remodeling, have a large lipid core that is covered by a thin fibrous cap, and are rich in macrophages.<sup>6,7</sup> Other features associated with increased vulnerability are the presence of microcalcifications and neoangiogenesis.<sup>8,9</sup> The introduction of intravascular imaging permitted *in vivo* visualization of these characteristics and opened new horizons in the study of plaque growth.

### Invasive imaging modalities

**Intravascular ultrasound.** Intravascular ultrasound (IVUS) was the first invasive modality that allowed imaging of the lumen and vessel wall, quantification of plaque burden, and characterization of its composition. The

From the Thoraxcenter, Erasmus Medical Center, Rotterdam, The Netherlands.

Submitted December 18, 2012; accepted February 18, 2013.

Reprint requests: Patrick W. S. Serruys, MD, PhD, Department of Interventional Cardiology, Erasmus MC, 's-Gravendijkwal 230, 3015 CE Rotterdam, The Netherlands. Hector M. Garcia-Garcia, MD, PhD, Thoraxcenter, Erasmus MC, z120 Dr Molewaterplein 403015 GD Rotterdam, The Netherlands.

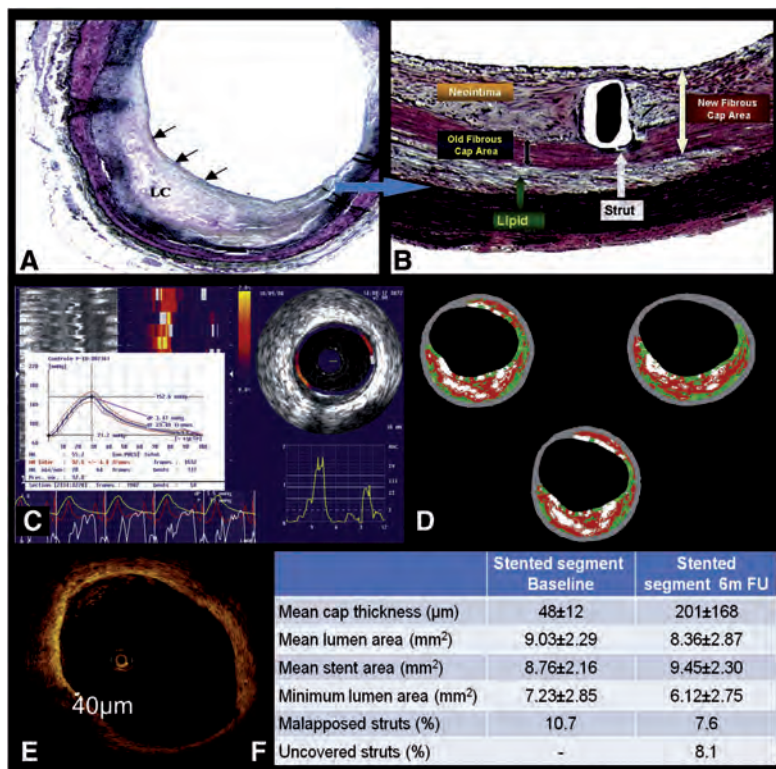
E-mails: h.garciagarcia@erasmusmc.nl, p.w.j.c.serruys@erasmusmc.nl

0002-8703/\$ - see front matter

© 2013, Mosby, Inc. All rights reserved.

<http://dx.doi.org/10.1016/j.ahj.2013.02.015>

Figure 1



Stent implantation in a high-risk plaque leads to neointimal formation and increases the thickness of the tissue that covers a lipid core (LC) (A) resulting in the potential passivation of the plaque (B). Imaging data acquired at baseline from a patient recruited in the SECRIT study: palpography demonstrated high strain (C), radiofrequency analysis of the backscattered intravascular ultrasound signal showed a lipid-rich plaque, which, however, did not cause luminal obstruction (D), whereas optical coherence tomography demonstrated a TCFA (cap thickness 40  $\mu\text{m}$ ) (E). The results of the study are summarized in panel (F): at 6-month follow-up, the thickness of the fibrous cap was increased by 170  $\mu\text{m}$ , there was a minor reduction in the mean lumen area, minimal malapposition, and most of the struts were fully covered. Panel A and B were obtained with permission from Moreno.<sup>73</sup>

analysis of the radiofrequency backscatter IVUS signal (RF-IVUS) permitted more reliable detection of the type of the plaque and has been extensively implemented to quantify and assess changes in the composition of the atheroma.<sup>10-12</sup> Numerous studies used RF-IVUS at 1 time point to assess the distribution of the atheroma and evaluate differences in the composition of the plaque in patients with different clinical presentations, whereas others implemented serial RF-IVUS to evaluate atherosclerotic process and the effect of medical treatment on plaque

growth.<sup>11-13</sup> The most recent study with serial assessment was reported by Kubo et al<sup>13</sup> and included 99 patients who had RF-IVUS examination at baseline and at 12-month follow-up. Two hundred sixteen lesions were examined at these 2 time points. At baseline, 20 TCFA were identified, 5 of which were unchanged at follow-up, whereas 15 regressed to more stable forms. On the other hand, 12 new TCFA appeared at the follow-up examination. These findings demonstrated the dynamic nature of atherosclerosis and the value of RF-IVUS in assessing this process.<sup>13</sup>

The PROSPECT trial was the largest natural history of atherosclerosis study and used RF-IVUS to detect anatomical and compositional features associated with an increased risk for a plaque to evolve to a culprit lesion.<sup>1</sup> Six hundred ninety-seven patients treated for an acute coronary syndrome underwent RF-IVUS post intervention at the 3 epicardial coronary arteries. At 3-year follow-up, 104 new symptomatic lesions became manifest in the nontreated segments. Multivariable analysis demonstrated that the presence of TCFA, a minimum lumen area  $\leq 4 \text{ mm}^2$ , and a plaque burden  $\geq 70\%$  were associated with future events. Similar results were reported by the VH-IVUS in Vulnerable Atherosclerosis Study study that had a similar design.<sup>3</sup> The PROSPECT trial not only showed the potential predictive value of intravascular imaging but also highlighted its limited prognostic accuracy as only 4% of the detected TCFA evolved to culprit lesions. This should be attributed to the fact that the included patients were on optimal treatment and to the inherited limitations of IVUS imaging.<sup>14</sup>

**Optical coherence tomography.** Optical coherence tomography (OCT) is the light-based analogous of IVUS. It provides high-resolution cross-sectional images and permits visualization of details, which cannot be imaged by other intravascular techniques such as evaluation of the thickness of the fibrous cap, detection of macrophages, and neovascularization and identification of plaque erosion.<sup>15</sup> Optical coherence tomography is the method of choice for characterizing the superficial plaque and detecting culprit lesions, and it has been used to assess the distribution of different plaque types in patients with different clinical presentations.<sup>16-18</sup> A limitation of OCT is its poor penetration, which often does not allow complete visualization of the vessel wall and assessment of vessel remodeling. In addition, OCT signal cannot penetrate lipid tissue, and thus, it is unable to quantify the lipid component. To overcome these pitfalls, multimodality imaging has been proposed, and currently, the Integrated Biomarkers and Imaging Study (IBIS) 4 is underway that implements serial IVUS and OCT examination to investigate the effect of pharmaceutical treatment on plaque burden and characteristics in patients who have sustained an acute coronary event.<sup>18,19</sup>

**Other invasive imaging techniques—Upcoming hybrid imaging modalities.** Angioscopy and intravascular magnetic spectroscopy have been used in the past in the study of atherosclerosis, but today, they have limited use. On the other hand, near-infrared spectroscopy (NIRS) is a relatively new modality, introduced to provide more accurate identification of lipid component, and has already applications in research arena. Furthermore, intravascular magnetic imaging, photoacoustic imaging, Raman spectroscopy, and time-resolved fluorescence spectroscopy are emerging techniques, which are

currently under evaluation and are expected to provide additional information about plaque evolution (online Appendix Supplementary Table D).

In parallel, an effort is being made to overcome the limitations of the prominent intravascular imaging modalities either by developing new methodologies that would allow better processing of the acquired data (eg, focused acoustic computed tomography, micro-OCT, polarized OCT) or by creating hybrid catheters that would permit multimodality intravascular imaging, provide complete visualization of coronary pathology, and more accurate detection of future culprit lesions.<sup>20,21</sup> A hybrid catheter that combines an IVUS and a NIRS probe (TVC, MC 7 system; InfraRedx, Burlington, MA) is currently available and being used in research arena, whereas catheters that permit fusion of IVUS with OCT, photoacoustic imaging, or time resolved fluorescence spectroscopy are under evaluation.<sup>22</sup> Initial experimental studies have shown promising results.<sup>23-25</sup> However, the large dimensions of the available catheters, the concerns regarding the safety of the new techniques, and the low image acquisition rate as well as the moderate image quality that they provide have not allowed their implementation in humans yet.

### Noninvasive imaging modalities

Advances in computed tomographic imaging (eg, the use of dual x-ray sources, the increased number of detectors, the decreased slice thickness, and the faster rotation gantry) have permitted imaging of coronary anatomy and pathology and reduced the radiation dose. Several studies used intravascular imaging techniques as criterion standard to validate computed tomographic coronary angiography (CTCA) and demonstrated that it can accurately measure the luminal and vessel wall dimensions, identify the presence of vessel wall remodeling, and discriminate calcified from noncalcified plaques.<sup>26,27</sup> On the other hand, CTCA has limited capability in differentiating lipid-rich from fibrotic plaques and has low resolution, which does not permit visualization of plaque characteristics associated with increased vulnerability.<sup>28</sup>

Although CTCA has considerable limitations, it seems that it provides useful prognostic information. A study conducted by Motayama et al<sup>29</sup> that included >1,000 patients who underwent CTCA because of suspected coronary artery disease (CAD) demonstrated that the detected by CTCA vessel wall remodeling and the low-attenuated plaques were independent predictors of cardiac morbidity. Moreover, the Coronary CT Angiography Evaluation for Clinical Outcomes: An International Multicenter registry showed that in symptomatic patients the combination of the Morise risk score and the CTCA derived data—in particular, the number of the epicardial vessels with obstructive ( $\geq 50\%$ ) stenoses—allowed more

accurate prediction of the 2-year major adverse cardiac events (all-cause mortality, nonfatal myocardial infarction, and revascularization) than the Morise score (accuracy 0.83 vs 0.68, respectively).<sup>30</sup> In view of these findings, an ambitious prospective study commenced, the BioImage trial that aims to include >6,000 asymptomatic subjects who will undergo noninvasive imaging (including CTCA if they have a high-risk cardiovascular profile) to identify new imaging-based predictors of future cardiovascular events.<sup>31</sup>

Magnetic resonance imaging (MRI) appears to be able to detect the composition of the plaque and has been used to study the atherosclerotic process in the aorta and the carotids, but it has a limited value in assessing coronary pathology, as it requires prolonged acquisition time and has poor spatial resolution.<sup>32</sup> Further improvements in external coils as well as the development of contrast agents that will allow more accurate plaque characterization are required so as this modality to be useful in this setting.

### Role of inflammation on plaque development and destabilization

Cumulative evidence has demonstrated that inflammation plays an important role in atherogenesis as it regulates the expression of mediators associated with plaque development. Several metabolic pathways triggered by increased inflammation appear to contribute to plaque destabilization and promote thrombus formation and collagen breakdown, which increase the fragility of the fibrous cap.<sup>33,34</sup> Appreciating the prominent role of inflammation on plaque rupture research focused on developing methodologies to detect and quantify its presence on vessel wall.

Invasive techniques for the detection of inflammation

**Thermography.** Thermography is the first invasive imaging technique developed to identify vessel wall inflammation and relies on the measurement of plaque heat. High temperatures indicate increased inflammatory activity and vulnerability of the plaque. Initial reports demonstrated the efficacy of thermography in detecting high-risk plaques, but recent studies have raised concerns about its effectiveness in patent coronaries suggesting that blood flow obstruction is necessary to obtain accurate estimations, fact that has limited its current applications.<sup>35,36</sup>

**Near-infrared fluorescence molecular imaging.** Near-infrared fluorescence (NIRF) imaging is a novel technique introduced to detect vascular activity. It involves injection of agents that bind molecules related to plaque's inflammation and have the ability to fluoresce after being irradiated with near-infrared light emitted by a specially designed catheter. Experimental studies demonstrated the feasibility and the potential of this

technology.<sup>37</sup> Recently, a hybrid NIRF-OCT catheter (diameter 2.4F) has been designed that allows simultaneous molecular functional imaging (provided by NIRF) and visualization of vessel pathology (given by OCT).<sup>38</sup> The feasibility of this approach has been tested *ex vivo* and *in vivo* in animal models and the first results appear promising. However, the safety of this technique has to be proven before being implemented in humans.<sup>39</sup>

Noninvasive imaging of vessel wall inflammation

**Nuclear imaging.** Nuclear imaging constitutes the leading noninvasive modality for the evaluation of vascular activity. Initial positron emission tomography (PET) studies, conducted to detect malignant tumors, demonstrated an increased 18F-fluorodeoxyglucose (<sup>18</sup>F-FDG) uptake in large arteries and later reports confirmed a correlation between <sup>18</sup>F-FDG and vessel wall inflammation.<sup>40</sup> Recent reports demonstrated the feasibility of the combined CTCA-<sup>18</sup>F-FDG imaging for the identification of inflamed plaques on the coronary tree.<sup>41,42</sup> The concept of fusing 2 noninvasive modalities that provide anatomical (derived from CTCA) and biological (given by PET) information constitutes a breakthrough in the study of atherosclerosis as it will allow detailed imaging of plaque pathology in larger populations and it is expected to provide additional information about the distribution of plaque inflammation and its association with different plaque components.

Apart from <sup>18</sup>F-FDG, several other tracers have been developed to assess vascular activity, such as the <sup>99m</sup>Tc-AA5, which binds phosphatidylserine produced by apoptotic cells; the <sup>99m</sup>Tc matrix metalloproteinase inhibitor that binds active metalloproteinases; and the IK17 tracer, which is labeled with <sup>125</sup>I and is able to detect the presence of oxidized low density lipoprotein, without however being used in clinical setting yet.<sup>43-45</sup>

**Other noninvasive techniques.** A significant limitation of nuclear imaging is the increased radiation dose required, which restricts its research applications. Therefore, an effort has been made toward the development of alternative imaging techniques, which would be able to evaluate vessel wall inflammation. Injection of iodinate nanoparticles has been recently proposed to detect the presence of macrophages with CTCA.<sup>46</sup> Initial validation of this methodology in rabbit models using histology as criterion standard showed that it is accurate and that it compares favorably to the estimations of PET.<sup>47</sup>

The current value of MRI in assessing vascular activity is limited as most of the paramagnetic contrast agents are not able to deliver the necessary amount of gadolinium ions that would permit MRI detection. Moreover, most of the MRI contrast agents have large dimensions, which do not allow them to access to biochemical epitopes within the vessel wall.<sup>52</sup>

## Role of blood flow on the atherosclerotic evolution and plaque destabilization

The implications of blood flow on plaque development have been observed several years ago by Caro et al<sup>48</sup> who speculated the athero-promoting effect of low endothelial shear stress (ESS). This observation was supported later by studies conducted in cadaver specimens and experimental models. Recent advances in invasive and noninvasive imaging permitted in vivo reconstruction of coronary anatomy and allowed detailed assessment of the role of the hemodynamic forces on atherosclerotic evolution.

### Blood flow simulation in models derived from invasive and noninvasive imaging modalities

Several small scale studies fused IVUS and coronary angiographic data to reconstruct coronary anatomy and showed that low or oscillating ESS promotes plaque growth and neointimal formation and alters the composition of the plaque.<sup>49,51</sup> Recently, the PREDICTION study examined prospectively in a large number of patients the implications of ESS on plaque development.<sup>2</sup> This trial included 506 patients who were admitted for an acute coronary event and underwent 3-vessel IVUS examination at baseline and at 6- to 10-month follow-up. The baseline IVUS and angiographic data were used to reconstruct coronary anatomy and evaluate the ESS distribution. It was found that low ESS promoted plaque growth and was independent predictor of future revascularizations.

Although today there are robust data to support the effect of the hemodynamic environment on plaque progression, there is little evidence about its role on plaque destabilization.<sup>52,53</sup> It has been speculated that high ESS and increased axial tensile stress may cause plaque deformation and disruption of the fibrous cap leading to rupture.<sup>54</sup> However, further research is required toward this direction to test the validity of this hypothesis.

Computed tomographic coronary angiography and MRI have limited resolution and cannot provide meticulous visualization of luminal morphology. This limitation has raised concerns about the value of CTCA- and MRI-derived models in the assessment of ESS distribution. However, recent experimental studies demonstrated that noninvasive imaging reconstructions allow reliable blood flow simulation supporting their applications in research.<sup>55</sup> Initial reports have confirmed the potential use of CTCA patient-derived models for the evaluation of ESS distribution and provided the substrate for the conduction of large scale prospective trials, which will examine the impact of the hemodynamic milieu on plaque growth.<sup>56</sup>

## Future trends in the study of atherosclerosis

Today, our ability to predict plaque rupture is limited. In the PROSPECT study, the quantitative and qualitative

information provided by RF-IVUS predicted future culprit lesions with a positive predictive value of 18%, whereas in the PREDICTION study, the positive predictive value of the ESS and IVUS-derived measurements for identifying future significant stenoses was 42%.<sup>1,2</sup> It worth to be mentioned that, in both studies, only few of the reported events/revascularizations were related to acute coronary syndromes.

The aforementioned results highlight the potential value of multimodality imaging in the identification of future culprit lesions among high-risk plaques. Today, it is impossible to perform a complete study of the coronary tree using multiple intravascular imaging catheters that would permit evaluation of vessel morphology (given by IVUS or OCT), composition (obtained by RF-IVUS, OCT, or NIRS), and inflammation (derived by OCT or NIRF) and provide reliable reconstruction of coronary anatomy for blood flow simulation. This, however, is likely to become feasible in the near future with the development of hybrid catheters that will allow simultaneous data acquisition (eg, a combined IVUS—intravascular photoacoustic catheter would permit assessment of the plaque burden, characterization of the type of the plaque, and detection of vessel wall inflammation) and a thorough assessment of coronary pathology (Figure 2).

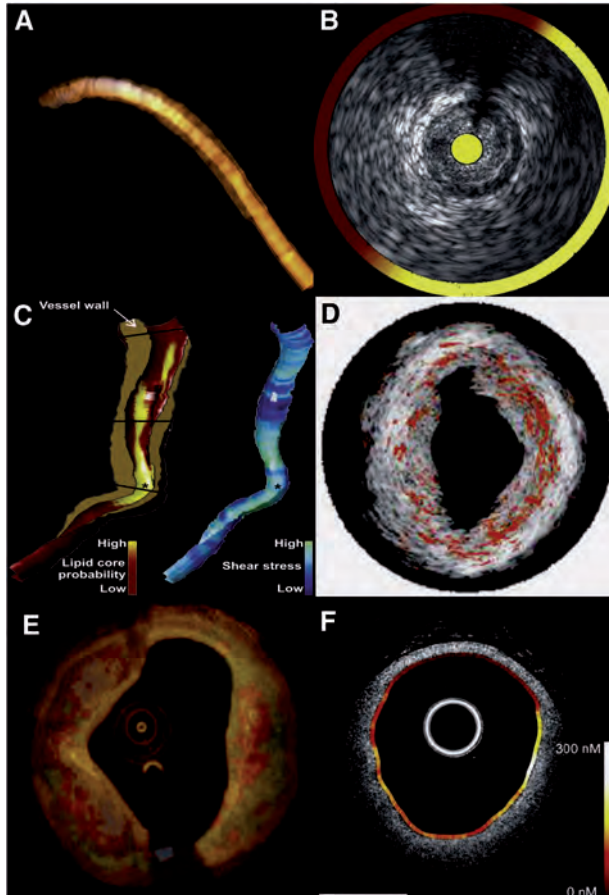
Similarly, the integration of CTCA, nuclear imaging, and computational fluid dynamics is expected to provide a holistic noninvasive evaluation of the plaque, whereas the introduction of nanoparticles for the detection of inflammation is anticipated to reduce the radiation dose and allow the conduction of large scale studies that will enhance our understanding about atherosclerotic evolution (Figure 3).

## Considerations that need to be addressed before advocating an invasive treatment of vulnerable plaques

How accurate can we predict an upcoming event in patients with known coronary artery disease?

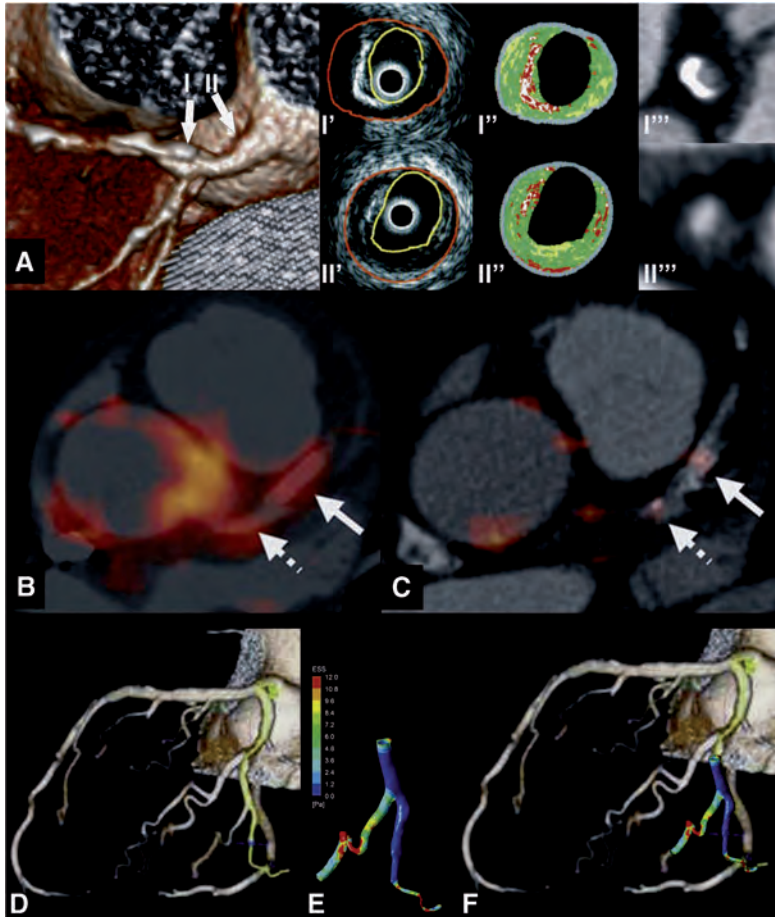
Although our knowledge about plaque vulnerability has increased over the last few years, our ability to predict the time of a future event remains low. The traditional risk models appear to predict with a moderate accuracy the short-term cardiovascular morbidity and mortality (cardiac death, MI, and repeat revascularization) in patients who have sustained an acute coronary syndrome (range 0.26-0.84) (online Appendix Supplementary Table ID). To improve the performance of these scores, several new variables have been added such as the SYNergy between PCI with TAXUS and Cardiac Surgery (SYNTAX) score or biomarkers related with worse outcomes (eg, activated protein C, N-terminal pro-brain natriuretic peptide, glucose, cardiac troponin T). However, the information regarding coronary anatomy, given by the SYNTAX score,

Figure 2



Output of hybrid imaging techniques. **A**, Fusion of coronary angiography and IVUS imaging. In the obtained model, the outer vessel wall is portrayed in a semitransparent fashion. **B**, Output of a dual-modality IVUS-NIRS catheter. Intravascular ultrasound permits visualization of the lumen, plaque, and outer vessel wall, whereas NIRS allows detection of the lipid tissue. **C**, Fusion of computed tomography, IVUS, and NIRS. The obtained models provide information about vessel geometry, and the distribution of the lipid tissue on the plaque and can be used to simulate blood flow and evaluate the endothelial shear stress. **D**, Combination of IVUS and intravascular photoacoustic imaging. Intravascular photoacoustic imaging allows detection of the lipid tissue (portrayed in an orange color), whereas IVUS provides visualization of the luminal morphology and the plaque. **E**, Fusion of OCT and IVUS radiofrequency backscatter images. The integration of different information acquired by these techniques permits more accurate characterization of the plaque. **F**, Output of a dual-modality catheter that allows simultaneous acquisition and coregistration of OCT and near-infrared fluorescence data. Optical coherence tomography provides information about the luminal morphology and the composition of the plaque, whereas near-infrared fluorescence allows identification of vessel wall inflammation portrayed in a color-coded map with the white-yellow color corresponding to increased inflammation. Images were obtained with permission from Bourantas et al, Wentzel et al, Wang et al, Raber et al, and Yoo et al.<sup>38,74-77</sup>

Figure 3



Implications of CTCA in the study of atherosclerosis. **A**, Ability of CTCA to detect the composition of the plaque. The arrows indicate the location of the IVUS and CTCA cross-sectional images. Panels (I'-I''') portray IVUS, IVUS radiofrequency backscatter analysis, and CTCA cross-sections for the distal calcified plaque, whereas the panels (II'-II'''), the corresponding cross-sections for the proximal plaque. The luminal morphology and the distribution of the plaque are similar in the CTCA and IVUS images. CTCA appears to allow accurate differentiation between calcified from noncalcified plaques. **B**, Fusion of CTCA and positron emission computed tomography. Increased  $^{18}\text{F}$ -FDG uptake was noted in the aorta, left main stem, and left anterior descending artery (arrows) of a patient admitted with an acute coronary syndrome. **C**, On the other hand, minor inflammation was detected in the aorta and coronary tree of a patient with stable angina. **D**, Reconstruction of coronary tree from CTCA. **E**, These data were used to model the distal circumflex, simulate blood flow, and evaluate the shear stress distribution (portrayed in a color-coded map). **F**, Superimposition of the reconstructed model onto the coronary tree provided by CTCA. Panels **B** and **C** were obtained with permission from Rogers et al, whereas panels D to F were provided by Sakellarios AI and Fotiadis DI.<sup>41</sup>

has only slightly increased the accuracy of these models, whereas the scores that included biomarkers were designed to predict all-cause mortality and not to estimate the risk of future cardiac events (online Appendix Supplementary Table II).

How accurately can we predict a future event in an asymptomatic population?

Most of the conventional models, designed for asymptomatic populations, focus on the prediction of the long-term cardiac outcomes (death, MI, coronary revascularization), and have low predictive accuracy. The new risk models that include biomarkers or genetic information have a slightly better predictive accuracy, whereas the ones that include CTCA data appear to allow accurate prediction of major adverse cardiovascular events but focus on the long-term outcomes (range 3.9-10 years) (online Appendix Supplementary Table III).

Over the last few years, several new markers associated with increased vulnerability have been identified (eg, patient genotype, myeloperoxidase, A2 phospholipase, blood monocytes subsets count, pregnancy associated plasma protein A, etc), and in a recent report, Brennan et al<sup>57</sup> combined the traditional with new risk factors, provided by patients' hematology profile (including leukocyte peroxidase, erythrocyte- and platelet-related parameters), into a model that permitted prediction of 1-year MI and death with an accuracy of almost 80%.<sup>57-60</sup> Further research is required toward this direction to find new predictors and construct novel models that would give precise short-term risk stratification and potentially reliable estimation of upcoming coronary events.

Should we always treat a ruptured plaque?

Even if we were able to foresee which plaque and when this will rupture, it would be still debatable whether we should seal it. Several intravascular imaging studies have demonstrated the presence of ruptured plaque in the coronary tree of asymptomatic patients and of patients with CAD indicating that plaque rupture does not always cause an acute coronary event (Figure 4).<sup>61,62</sup> Furthermore, chronically ruptured plaques appear clinically silent and do not require an interventional treatment.<sup>63</sup> Which of the ruptured plaques will cause MI and which will heal are still unclear. A small study that compared culprit and nonculprit ruptured plaques demonstrated that the culprit lesions had increased length, plaque burden, and remodeling index and exhibited a smaller luminal area comparing with the asymptomatic ulcerated plaques.<sup>64</sup> Apart from the morphological characteristics of the plaque, systemic factors and more specifically blood viscosity, platelet activity, fibrinogen levels, von Willebrand factor, and the interplay between coagulation and fibrinolytic system

seem also to determine the final clinical consequences of plaque rupture.<sup>65-67</sup> Therefore, further effort should be made to identify predictors associated with extensive thrombus formation, blood flow obstruction, and the clinical manifestation of an acute coronary syndrome.

Should we focus only on thin capped fibroatheromas?

Histology-based studies have demonstrated that one-third of the acute coronary syndromes are due to plaque erosion occurring in plaques, which do not have the typical characteristics of a high-risk lesion. These plaques have the histologic appearance of pathologic intimal thickening or fibroatheroma and are rich in proteoglycan and smooth muscle cells.<sup>68</sup> The underlying mechanism of plaque erosion is poorly understood, and it has been speculated that it can be due to coronary vasospasm. Today, it is impossible to predict which of these stable-looking plaques will erode and cause MI.

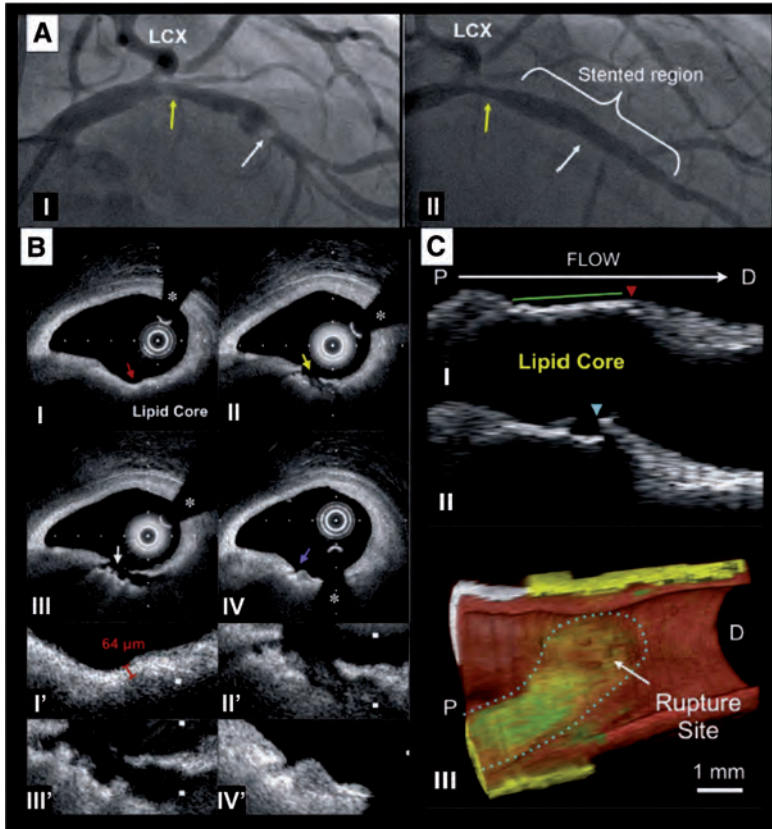
Is there an ideal device to seal future culprit lesions?

The invasive treatment of a potential culprit lesion in asymptomatic patients can be justified only if stent implantation is safe. Initial reports demonstrated an unacceptable high risk of complications in non-flow-limiting lesions treated with balloon angioplasty or bare metal stents, whereas the new developments in stent design may have reduced the risk of complications, but they have not eradicated them.<sup>69</sup> The distortion of vessel wall physiology as well as the risk of neoatherosclerosis and of an inflammatory reaction to a permanent foreign body remains considerable pitfalls of metallic stents. Bioresorbable scaffold is a recent technology introduced to address the abovementioned drawbacks. These devices have the ability to dissolve after restoring the patency of the vessel allowing the coronary artery to maintain its physiologic integrity.<sup>70</sup> Recent reports demonstrated that the neointimal tissue developed postimplantation of a bioresorbable scaffold can seal the underlying plaques, whereas studies in animal models showed that the neotissue has features associated with plaque stability.<sup>71,72</sup> These initial reports may support the use of bioresorbable scaffolds for paving diseased coronary segments with vulnerable plaques, but long-term follow-up data are required to elucidate this prospective (Figure 5).

## Summary

New developments in invasive and noninvasive imaging have allowed detailed visualization of coronary pathology and have considerably increased our knowledge about plaque growth and rupture. Prospective natural history of atherosclerosis studies permitted evaluation of changes in plaque composition and assessment of the complexity of plaque evolution. Our inability to accurately predict which of the detected vulnerable plaques will rupture, when this will occur, and whether this event will have

Figure 4



In vivo OCT imaging of an asymptomatic plaque rupture. Angiographic images showing 2 lesions, a distal (white arrow), which was stented successfully and a proximal (yellow arrow) that was left untreated (A1-A11). Optical coherence tomographic examination revealed a TCFA at the proximal lesion (red arrow) (B1, B1'). Repeat imaging few minutes later demonstrated plaque disruption (yellow arrow) (BII, BII') and an intimal flap (BIII, BIII'). Thrombus was gradually formed, which covered the created crater (BIV, BIV'). Longitudinal images (C1, CII) and 3-dimensional reconstruction of the OCT data (CIII) showed increased macrophages accumulation (indicated with a green color) at the ruptured plaque (arrow), which was located at the distal site of the lipid core.

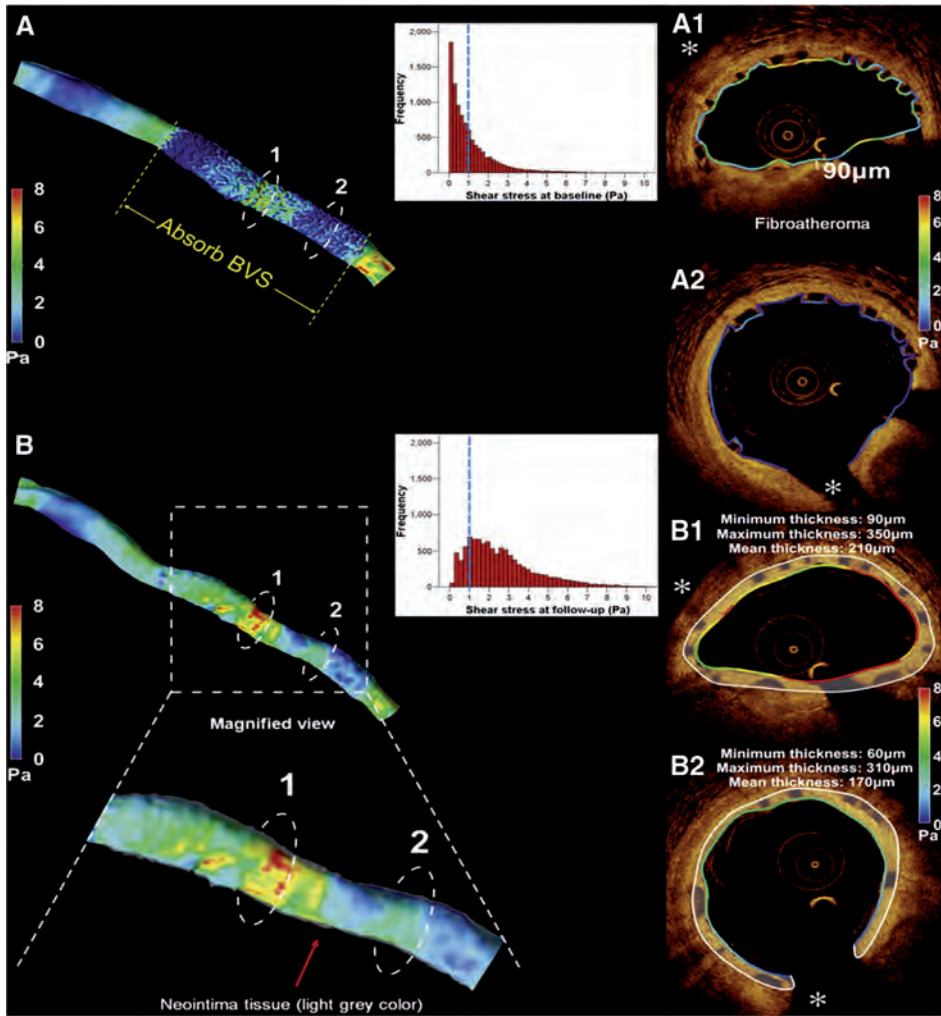
clinical implications cannot justify an invasive sealing of potential culprit lesions. However, this is likely to change in the future. The revolution occurring in invasive and noninvasive imaging and the advances in molecular biology are expected to provide additional information about atherosclerotic disease progression/regression, allow us to study this process in larger populations, and probably predict with a higher accuracy events and plaque ruptures. Although, few years ago, the early

detection and invasive passivation of future culprit lesions appeared as an unrealistic dream, nowadays, it is regarded as a future potentiality.

### Disclosures

Christos Bourantas wishes to acknowledge the funding support of the Hellenic Heart Foundation (ELIKAR), Athens, Greece. The authors are solely responsible for

Figure 5



**A**, Three-dimensional reconstruction of a left anterior descending coronary artery from coronary angiographic and OCT data acquired immediately after an Absorb bioresorbable vascular scaffold implantation. The ESS is portrayed in the reconstructed surface with the use of a color-coded map. Low ESS is noted in the scaffolded segment with 61% of the ESS being  $<1$  Pa. Panels A1 and A2 illustrate 2 OCT cross-sectional images and the estimated ESS along the luminal circumference. The asterisk indicates a side branch. A fibroatheroma is shown at panel A1 with a cap thickness of  $90\ \mu\text{m}$ . Panel **B** portrays the reconstructed vessel at 2-year follow-up. The ESS in the scaffolded segment (B, B2) is normalized (only 17% of the ESS estimations are  $<17\%$ ) at follow-up creating an atheroprotective for the vessel environment. In addition, as it is shown in the magnified view, a thin layer of neointimal tissue is developed with a mean thickness of  $160\ \mu\text{m}$  that covers the vessel wall and the fibroatheroma detected at baseline (B1). Image was obtained modified and used with permission from Bourantas et al.<sup>78</sup>

the design and conduct of this study, all study analyses, the drafting and editing of the manuscript, and its final contents. None of the authors have any conflict of interest to declare.

## References

- Stone GW, Maehara A, Lansky AJ, et al. A prospective natural-history study of coronary atherosclerosis. *N Engl J Med* 2011;364(3):226-35.
- Stone PH, Saito S, Takahashi S, et al. Prediction of progression of coronary artery disease and clinical outcomes using vascular profiling of endothelial shear stress and arterial plaque characteristics: The PREDICTION Study. *Circulation* 2012;126(2):172-81.
- Calvert PA, Obaid DR, O'Sullivan M, et al. Association between IVUS findings and adverse outcomes in patients with coronary artery disease: the VIVA (VH-IVUS in Vulnerable Atherosclerosis) Study. *JACC Cardiovasc Imaging* 2011;4(8):894-901.
- Wykrzykowska JJ, Diletti R, Gutierrez-Chico JL, et al. Plaque sealing and passivation with a mechanical self-expanding low outward force nitinol vShield device for the treatment of IVUS and OCT-derived thin cap fibroatheromas (TCFAs) in native coronary arteries: report of the pilot study vShield Evaluated at Cardiac hospital in Rotterdam for Investigation and Treatment of TCFa (SECRIT). *EuroIntervention* 2012;8:945-54.
- Kragel AH, Reddy SG, Wittes JT, et al. Morphometric analysis of the composition of atherosclerotic plaques in the four major epicardial coronary arteries in acute myocardial infarction and in sudden coronary death. *Circulation* 1989;80(6):1747-56.
- Moreno PR, Bernardi VH, Lopez-Cuellar J, et al. Macrophages, smooth muscle cells, and tissue factor in unstable angina. Implications for cell-mediated thrombogenicity in acute coronary syndromes. *Circulation* 1996;94(12):3090-7.
- Burke AP, Farb A, Malcom GT, et al. Coronary risk factors and plaque morphology in men with coronary disease who died suddenly. *N Engl J Med* 1997;336(18):1276-82.
- Ehara S, Kobayashi Y, Yoshiyama M, et al. Coronary artery calcification revisited. *J Atheroscler Thromb* 2006;13(1):31-7.
- Virmani R, Kolodgie FD, Burke AP, et al. Atherosclerotic plaque progression and vulnerability to rupture: angiogenesis as a source of intraplaque hemorrhage. *Arterioscler Thromb Vasc Biol* 2005;25(10):2054-61.
- Garcia-Garcia HM, Mintz GS, Lerman A, et al. Tissue characterisation using intravascular radiofrequency data analysis: recommendations for acquisition, analysis, interpretation and reporting. *EuroIntervention* 2009;5(2):177-89.
- Marso SP, Frutkin AD, Mehta SK, et al. Intravascular ultrasound measures of coronary atherosclerosis are associated with the Framingham risk score: an analysis from a global IVUS registry. *EuroIntervention* 2009;5(2):212-8.
- Serruys PW, Garcia-Garcia HM, Buzszman P, et al. Effects of the direct lipoprotein-associated phospholipase A(2) inhibitor darapladib on human coronary atherosclerotic plaque. *Circulation* 2008;118(11):1172-82.
- Kubo T, Maehara A, Mintz GS, et al. The dynamic nature of coronary artery lesion morphology assessed by serial virtual histology intravascular ultrasound tissue characterization. *J Am Coll Cardiol* 2010;55(15):1590-7.
- Thim T, Hagensen MK, Wallace-Bradley D, et al. Unreliable assessment of necrotic core by virtual histology intravascular ultrasound in porcine coronary artery disease. *Circ Cardiovasc Imaging* 2010;3(4):384-91.
- Tearney GJ, Regar E, Akasaka T, et al. Consensus standards for acquisition, measurement, and reporting of intravascular optical coherence tomography studies: a report from the International Working Group for Intravascular Optical Coherence Tomography Standardization and Validation. *J Am Coll Cardiol* 2012;59(12):1058-72.
- Kang SJ, Mintz GS, Akasaka T, et al. Optical coherence tomographic analysis of in-stent neoatherosclerosis after drug-eluting stent implantation. *Circulation* 2011;123(25):2954-63.
- Fujii K, Kawasaki D, Masutani M, et al. OCT assessment of thin-cap fibroatheroma distribution in native coronary arteries. *JACC Cardiovasc Imaging* 2010;3(2):168-75.
- Gonzalo N, Garcia-Garcia HM, Regar E, et al. In vivo assessment of high-risk coronary plaques at bifurcations with combined intravascular ultrasound and optical coherence tomography. *JACC Cardiovasc Imaging* 2009;2(4):473-82.
- Sawada T, Shite J, Garcia-Garcia HM, et al. Feasibility of combined use of intravascular ultrasound radiofrequency data analysis and optical coherence tomography for detecting thin-cap fibroatheroma. *Eur Heart J* 2008;29(9):1136-46.
- Gialtina SD, Courtney BK, Herz PR, et al. Assessment of coronary plaque collagen with polarization sensitive optical coherence tomography (PS-OCT). *Int J Cardiol* 2006;107(3):400-9.
- Liu L, Gardecki JA, Nadkarni SK, et al. Imaging the subcellular structure of human coronary atherosclerosis using micro-optical coherence tomography. *Nat Med* 2011;17(8):1010-4.
- Simek C, Garcia-Garcia HM, van Geuns RJ, et al. The ability of high dosage rosuvastatin to improve plaque composition and decrease necrotic core in non-intervened coronary arteries: rationale and design of the integrated biomarker and imaging study-3 (IBIS-3). *EuroIntervention* 2012;8:235-41.
- Karpiouk AB, Wang B, Emelianov SY. Development of a catheter for combined intravascular ultrasound and photoacoustic imaging. *Rev Sci Instrum* 2010;81(1):014901.
- Li BH, Leung AS, Soong A, et al. Hybrid intravascular ultrasound and optical coherence tomography catheter for imaging of coronary atherosclerosis. *Catheter Cardiovasc Interv* 2013;81:494-507.
- Stephens DN, Park J, Sun Y, et al. Intraluminal fluorescence spectroscopy catheter with ultrasound guidance. *J Biomed Opt* 2009;14(3):030505.
- Papadopoulos SL, Neefjes LA, Schaap M, et al. Detection and quantification of coronary atherosclerotic plaque by 64-slice multidetector CT: a systematic head-to-head comparison with intravascular ultrasound. *Atherosclerosis* 2011;219(1):163-70.
- Gauss S, Achenbach S, Pfleiderer T, et al. Assessment of coronary artery remodelling by dual-source CT: a head-to-head comparison with intravascular ultrasound. *Heart* 2011;97(12):991-7.
- Voros S, Rinehart S, Qian Z, et al. Prospective validation of standardized, 3-dimensional, quantitative coronary computed tomographic plaque measurements using radiofrequency backscatter intravascular ultrasound as reference standard in intermediate coronary arterial lesions: results from the ATLANTA (assessment of tissue characteristics, lesion morphology, and hemodynamics by angiography with fractional flow reserve, intravascular ultrasound and virtual histology, and noninvasive computed tomography in atherosclerotic plaques) I study. *JACC Cardiovasc Interv* 2011;4(2):198-208.
- Motoyama S, Sarai M, Harigaya H, et al. Computed tomographic angiography characteristics of atherosclerotic plaques subsequently resulting in acute coronary syndrome. *J Am Coll Cardiol* 2009;54(1):49-57.

30. Villines TC, Hulten EA, Shaw LJ, et al. Prevalence and severity of coronary artery disease and adverse events among symptomatic patients with coronary artery calcification scores of zero undergoing coronary computed tomography angiography: results from the CONFIRM (Coronary CT Angiography Evaluation for Clinical Outcomes: An International Multicenter) registry. *J Am Coll Cardiol* 2011;58(24):2533-40.
31. Muntendam P, McCall C, Sanz J, et al. The Biomag Study: novel approaches to risk assessment in the primary prevention of atherosclerotic cardiovascular disease—study design and objectives. *Am Heart J* 2010;160(1):49 e1-57 e1.
32. Corti R, Fuster V. Imaging of atherosclerosis: magnetic resonance imaging. *Eur Heart J* 2011;32(14):1709-1719b.
33. Mach F, Schonbeck U, Bonnefoy JY, et al. Activation of monocyte/macrophage functions related to acute atheroma complication by ligation of CD40: induction of collagenase, stromelysin, and tissue factor. *Circulation* 1997;96(2):396-9.
34. Amento EP, Ehsani N, Palmer H, et al. Cytokines and growth factors positively and negatively regulate interstitial collagen gene expression in human vascular smooth muscle cells. *Arterioscler Thromb* 1991;11(5):1223-30.
35. Rzeszutko L, Legutko J, Kaluza GL, et al. Assessment of culprit plaque temperature by intracoronary thermography appears inconclusive in patients with acute coronary syndromes. *Arterioscler Thromb Vasc Biol* 2006;26(8):1889-94.
36. Stefanadis C, Diamantopoulos L, Vlachopoulos C, et al. Thermal heterogeneity within human atherosclerotic coronary arteries detected in vivo: A new method of detection by application of a special thermography catheter. *Circulation* 1999;99(15):1965-71.
37. Jaffer FA, Calton MA, Rosenthal A, et al. Two-dimensional intravascular near-infrared fluorescence molecular imaging of inflammation in atherosclerosis and stent-induced vascular injury. *J Am Coll Cardiol* 2011;57(25):2516-26.
38. Yoo H, Kim JW, Shishkov M, et al. Intra-arterial catheter for simultaneous microstructural and molecular imaging in vivo. *Nat Med* 2011;17(12):1680-4.
39. Tearney GJ, Yabushita H, Houser SL, et al. Quantification of macrophage content in atherosclerotic plaques by optical coherence tomography. *Circulation* 2003;107(11):113-9.
40. Tawakol A, Migrino RQ, Bashian GG, et al. In vivo 18F-fluorodeoxyglucose positron emission tomography imaging provides a noninvasive measure of carotid plaque inflammation in patients. *J Am Coll Cardiol* 2006;48(9):1818-24.
41. Rogers IS, Nasir K, Figueroa AL, et al. Feasibility of FDG imaging of the coronary arteries: comparison between acute coronary syndrome and stable angina. *JACC Cardiovasc Imaging* 2010;3(4):388-97.
42. Wykrzykowska J, Lehman S, Williams G, et al. Imaging of inflamed and vulnerable plaque in coronary arteries with 18F-FDG PET/CT in patients with suppression of myocardial uptake using a low-carbohydrate, high-fat preparation. *J Nucl Med* 2009;50(4):563-8.
43. Fujimoto S, Hartung D, Ohshima S, et al. Molecular imaging of matrix metalloproteinase in atherosclerotic lesions: resolution with dietary modification and statin therapy. *J Am Coll Cardiol* 2008;52(23):1847-57.
44. Kietselaer BL, Reutelingsperger CP, Heidendal GA, et al. Noninvasive detection of plaque instability with use of radiolabeled annexin A5 in patients with carotid-artery atherosclerosis. *N Engl J Med* 2004;350(14):1472-3.
45. Tsimikas S. Noninvasive imaging of oxidized low-density lipoprotein in atherosclerotic plaques with tagged oxidation-specific antibodies. *Am J Cardiol* 2002;90(10C):22L-7L.
46. Hyafil F, Cornily JC, Feig JE, et al. Noninvasive detection of macrophages using a nanoparticulate contrast agent for computed tomography. *Nat Med* 2007;13(5):636-41.
47. Hyafil F, Cornily JC, Rudd JH, et al. Quantification of inflammation within rabbit atherosclerotic plaques using the macrophage-specific CT contrast agent N1177: a comparison with 18F-FDG PET/CT and histology. *J Nucl Med* 2009;50(6):959-65.
48. Caro CG, Fitz-Gerald JM, Schroter RC. Arterial wall shear and distribution of early atheroma in man. *Nature* 1969;223(5211):1159-60.
49. Samady H, Eshtehardi P, McDaniel MC, et al. Coronary artery wall shear stress is associated with progression and transformation of atherosclerotic plaque and arterial remodeling in patients with coronary artery disease. *Circulation* 2011;124(7):779-88.
50. Wentzel JJ, Krams R, Schurbiers JC, et al. Relationship between neointimal thickness and shear stress after Wallstent implantation in human coronary arteries. *Circulation* 2001;103(13):1740-5.
51. Stone PH, Coskun AU, Kinlay S, et al. Regions of low endothelial shear stress are the sites where coronary plaque progresses and vascular remodeling occurs in humans: an in vivo serial study. *Eur Heart J* 2007;28(6):705-10.
52. Bourantas CV, Papafalakis MI, Naka KK, et al. Fusion of optical coherence tomography and coronary angiography—in vivo assessment of shear stress in plaque rupture. *Int J Cardiol* 2012;155(2):e24-6.
53. Fukumoto Y, Hiro T, Fujii T, et al. Localized elevation of shear stress is related to coronary plaque rupture: a 3-dimensional intravascular ultrasound study with in-vivo color mapping of shear stress distribution. *J Am Coll Cardiol* 2008;51(6):645-50.
54. Slager CJ, Wentzel JJ, Gijsen FJ, et al. The role of shear stress in the destabilization of vulnerable plaques and related therapeutic implications. *Nat Clin Pract Cardiovasc Med* 2005;2(9):456-64.
55. Goubergrits L, Kertzschner U, Schoneberg B, et al. CFD analysis in an anatomically realistic coronary artery model based on non-invasive 3D imaging: comparison of magnetic resonance imaging with computed tomography. *Int J Cardiovasc Imaging* 2008;24(4):411-21.
56. van der Giessen AG, Wentzel JJ, Meijboom WB, et al. Plaque and shear stress distribution in human coronary bifurcations: a multislice computed tomography study. *EuroIntervention* 2009;4(5):654-61.
57. Brennan ML, Reddy A, Tang WH, et al. Comprehensive peroxidase-based hematologic profiling for the prediction of 1-year myocardial infarction and death. *Circulation* 2010;122(1):70-9.
58. Elesber AA, Conover CA, Denktas AE, et al. Prognostic value of circulating pregnancy-associated plasma protein levels in patients with chronic stable angina. *Eur Heart J* 2006;27(14):1678-84.
59. Prins BP, Lagou V, Asselbergs FW, Snieder H, Fu J. Genetics of coronary artery disease: genome-wide association studies and beyond. *Atherosclerosis* 2012;225:1-10.
60. Thompson A, Gao P, Orfei L, et al. Lipoprotein-associated phospholipase A(2) and risk of coronary disease, stroke, and mortality: collaborative analysis of 32 prospective studies. *Lancet* 2010;375(9725):1536-44.
61. Maehara A, Mintz GS, Bui AB, et al. Morphologic and angiographic features of coronary plaque rupture detected by intravascular ultrasound. *J Am Coll Cardiol* 2002;40(5):904-10.
62. Tanaka A, Imanishi T, Kitabata H, et al. Distribution and frequency of thin-capped fibroatheromas and ruptured plaques in the entire culprit coronary artery in patients with acute coronary syndrome as determined by optical coherence tomography. *Am J Cardiol* 2008;102(8):975-9.

63. Rioufol G, Gilard M, Finet G, et al. Evolution of spontaneous atherosclerotic plaque rupture with medical therapy: long-term follow-up with intravascular ultrasound. *Circulation* 2004;110(18):2875-80.
64. Fujii K, Kobayashi Y, Mintz GS, et al. Intravascular ultrasound assessment of ulcerated ruptured plaques: a comparison of culprit and nonculprit lesions of patients with acute coronary syndromes and lesions in patients without acute coronary syndromes. *Circulation* 2003;108(20):2473-8.
65. Cecchi E, Liotta AA, Gori AM, et al. Comparison of hemorheological variables in ST-elevation myocardial infarction versus those in non-ST-elevation myocardial infarction or unstable angina pectoris. *Am J Cardiol* 2008;102(2):125-8.
66. Smyth SS, Monroe III DM, Wysokinski WE, et al. Platelet activation and its patient-specific consequences. *Thromb Res* 2008;122(4):435-41.
67. Spiel AO, Gilbert JC, Jilma B. von Willebrand factor in cardiovascular disease: focus on acute coronary syndromes. *Circulation* 2008;117(11):1449-59.
68. Farb A, Burke AP, Tang AL, et al. Coronary plaque erosion without rupture into a lipid core. A frequent cause of coronary thrombosis in sudden coronary death. *Circulation* 1996;93(7):1354-63.
69. Mercado N, Maier W, Boersma E, et al. Clinical and angiographic outcome of patients with mild coronary lesions treated with balloon angioplasty or coronary stenting. Implications for mechanical plaque sealing. *Eur Heart J* 2003;24(6):541-51.
70. Serruys PW, Garcia-Garcia HM, Onuma Y. From metallic cages to transient bioresorbable scaffolds: change in paradigm of coronary revascularization in the upcoming decade? *Eur Heart J* 2012;33(1):16-25b.
71. Onuma Y, Serruys PW, Perkins LE, et al. Intracoronary optical coherence tomography and histology at 1 month and 2, 3, and 4 years after implantation of everolimus-eluting bioresorbable vascular scaffolds in a porcine coronary artery model: an attempt to decipher the human optical coherence tomography images in the ABSORB trial. *Circulation* 2010;122(22):2288-300.
72. Brugaletta S, Radu MD, Garcia-Garcia HM, et al. Circumferential evaluation of the neointima by optical coherence tomography after ABSORB bioresorbable vascular scaffold implantation: can the scaffold cap the plaque? *Atherosclerosis* 2012;221(1):106-12.
73. Moreno PR. Vulnerable plaque: definition, diagnosis, and treatment. *Cardiol Clin* 2010;28(1):1-30.
74. Raber L, Heo JH, Radu MD, et al. Offline fusion of co-registered intravascular ultrasound and frequency domain optical coherence tomography images for the analysis of human atherosclerotic plaques. *EuroIntervention* 2012;8(1):98-108.
75. Wang B, Su JL, Amiran J, et al. Detection of lipid in atherosclerotic vessels using ultrasound-guided spectroscopic intravascular photoacoustic imaging. *Opt Express* 2010;18(5):4889-97.
76. Bourantas CV, Kalatzis FG, Papafaklis MI, et al. ANGIOCARE: an automated system for fast three-dimensional coronary reconstruction by integrating angiographic and intracoronary ultrasound data. *Catheter Cardiovasc Interv* 2008;72(2):166-75.
77. Wentzel JJ, van der Giessen AG, Garg S, et al. In vivo 3D distribution of lipid-core plaque in human coronary artery as assessed by fusion of near infrared spectroscopy-intravascular ultrasound and multislice computed tomography scan. *Circ Cardiovasc Imaging* 2010;3(6):e6-7.
78. Bourantas CV, Papafaklis MI, Garcia-Garcia HM, et al. Short- and long-term implications of a bioresorbable vascular scaffold implantation on the local endothelial shear stress patterns. *JACC Cardiovasc Interv* 2013 In press.

## Appendix

**Supplementary Table I.** Ability of the available imaging modalities to detect plaque features associated with increased vulnerability

Plaque characteristics associated with increased vulnerability	Thin fibrous cap	Necrotic core	Assessment of plaque burden	Positive remodeling	Neo-angiogenesis	Active inflammation
IVUS/IVUS-RF	++ <sup>79</sup>	++ <sup>80</sup>	+++ <sup>81</sup>	+++ <sup>61</sup>	–	–
OCT	+++ <sup>15</sup>	+++ <sup>80</sup>	++ <sup>15</sup>	+ <sup>15</sup>	++ <sup>15</sup>	+ <sup>39</sup>
Angioscopy	–	++ <sup>82</sup>	–	–	–	–
IV-MRI spectroscopy*	–	++ <sup>83</sup>	–	–	–	–
NIRS	–	+++ <sup>84</sup>	–	–	–	–
IV-MRI*	–	+ <sup>85</sup>	+ <sup>85</sup>	+ <sup>85</sup>	–	–
Photoacoustic imaging*	–	++ <sup>86</sup>	–	–	+ <sup>87</sup>	+ <sup>87</sup>
TRFS*	+	++ <sup>88</sup>	–	–	–	–
CTCA	–	+ <sup>28</sup>	++ <sup>28</sup>	++ <sup>27</sup>	–	–
Thermography	–	–	–	–	–	+ <sup>35,36</sup>
NIRF*	–	–	–	–	+	+++ <sup>89</sup>
PET*	–	–	–	–	–	+++ <sup>42</sup>

Abbreviations: IV-MRI, Intravascular MRI; TRFS, time-resolved fluorescence imaging.

The ability of the presented modalities to detect plaque characteristics associated with increased instability is graded as: unable (–), low (+), moderate (++), and high (+++).

\*The modalities marked with an asterisk are in their infancy, and therefore, the data provided for these techniques derive from small scale in vivo or histology-based in vitro studies.

**Supplementary Table II.** Risk scores proposed to predict cardiovascular events in patients who have sustained an acute coronary event

Risk model	Included variables	Studied population	No. of patients	Studied period	Type of events	C statistics
TIMI score <sup>90</sup>	Clinical variables	Patient suffered a STEMI	855	30 d	Cardiac death, MI, coronary revascularization	0.64
GRACE score <sup>90</sup>	Clinical variables	Patient suffered a STEMI	855	30 d	Cardiac death, MI, coronary revascularization	0.54
Mini Grace score <sup>91</sup>	Clinical variables	Patients sustained a STEMI and NSTEMI	495263	6 m	All-cause mortality	0.84
PAMI score <sup>90</sup>	Clinical variables	Patient suffered a STEMI	855	30 d	Cardiac death, MI, coronary revascularization	0.65
CADILLAC score <sup>90</sup>	Clinical variables	Patient suffered a STEMI	855	30 d	Cardiac death, MI, coronary revascularization	0.71
ACEF score <sup>92</sup>	Clinical variables	Patients who had NSTEMI	2094	1 y	• Cardiac death • MI • Cardiac death MI, coronary revascularization	• 0.49 for cardiac death • 0.23 for MI • 0.26 for the combined end point
Garg et al. <sup>93</sup>	Clinical variables and the SYNTAX score	Patients sustained a STEMI	807	1 y	Death, MI, coronary revascularization	0.69
Clinical SYNTAX score <sup>92</sup>	Clinical and angiographic variables	Patients who had NSTEMI	2094	1 y	• Cardiac death • MI • Cardiac death MI, coronary revascularization	• 0.77 for cardiac death • 0.62 for MI • 0.59 for the combined end point
NERS score <sup>92</sup>	Clinical and angiographic variables	Patients who had NSTEMI	2094	1 y	• Cardiac death • MI • Cardiac death, MI, coronary revascularization	• 0.76 for cardiac death • 0.60 for MI • 0.60 for the combined end point

**Supplementary Table II** (continued)

Risk model	Included variables	Studied population	No. of patients	Studied period	Type of events	C statistics
Residual SYNTAX score <sup>94</sup>	Angiographic variables	Patients sustained a STEMI	2686	1 y	<ul style="list-style-type: none"> <li>• Cardiac death</li> <li>• MI</li> <li>• All-cause mortality, MI, coronary revascularization</li> </ul>	<ul style="list-style-type: none"> <li>• 0.63 for cardiac death</li> <li>• 0.57 for MI</li> <li>• 0.55 for the combined end point</li> </ul>
Clinical SYNTAX score <sup>95</sup>	Clinical and angiographic variables	Patients with stable angina or an acute coronary syndrome	848	5 y	<ul style="list-style-type: none"> <li>• All-cause mortality</li> <li>• Cardiac death</li> <li>• All-cause mortality, MI, coronary revascularization</li> </ul>	<ul style="list-style-type: none"> <li>• 0.63 for all-cause mortality</li> <li>• 0.66 for cardiac death</li> <li>• 0.62 for the combined end point</li> </ul>
Clinical SYNTAX score <sup>96</sup>	Clinical and angiographic variables	Patients with stable angina or an acute coronary syndrome	2033	1 y	<ul style="list-style-type: none"> <li>• Cardiac death</li> <li>• MI</li> <li>• All-cause mortality, MI, coronary revascularization</li> </ul>	<ul style="list-style-type: none"> <li>• 0.71 for cardiac death</li> <li>• 0.65 for MI</li> <li>• 0.68 for the combined end point</li> </ul>
Chiba et al <sup>97</sup>	Activated protein C	Patients suffered a STEMI	335	Hospital stay	In-hospital all-cause mortality	0.78
Damman et al <sup>98</sup>	Clinical variables and biomarkers	Patients suffered a STEMI	1034	901 d	All-cause mortality	Harrell's C index: 0.81

Abbreviations: ACEF, Age creatinine ejection fraction; CADILLAC, Controlled Abciximab and Device Investigation to Lower Late Angioplasty Complications; GRACE, Global Registry for Acute Coronary Events; NERS, new risk stratification; NSTEMI, non-ST-elevation myocardial infarction; PAMI, primary angioplasty in myocardial infarction; STEMI, ST-elevation myocardial infarction; TIMI, thrombolysis in myocardial infarction.

**Supplementary Table III.** Available risk score models suggested for the prediction of future cardiovascular events in asymptomatic subjects

Risk model	Included variables	Studied population	No. of patients	Studied period	Type of events	C-statistics
FRS <sup>99</sup>	Clinical variables	Asymptomatic population with different ethnicity (6 different cohorts)	23424	5 y	Cardiac death and MI	Range in different cohorts from 0.64-0.84
McNeil et al <sup>100</sup>	FRS and the presence of metabolic syndrome	Black and white asymptomatic subjects	12089	10 y	Cardiac death, MI and coronary revascularization	0.73 for women and 0.63 for men
SCORE <sup>101</sup>	Clinical variables	Asymptomatic European population	205178	10 y	Cardiovascular mortality	Range varied in different ages from 0.71-0.84
ASSIGN <sup>102</sup>	Clinical and socioeconomic variables	Asymptomatic Scottish population	13297	10 y	Cardiovascular mortality, newly diagnosed CAD, or CVD	0.77 for women and 0.73 for men
QRISK <sup>103</sup>	Clinical variables	Asymptomatic British population	1072800	10 y	Newly diagnosed CAD, MI or CVD	0.79 for women and 0.76 for men
Wang et al <sup>104</sup>	Clinical variables and biomarkers	Patients with and without CAD	3209	5 y	<ul style="list-style-type: none"> <li>• All cause mortality</li> <li>• MI, HF, newly diagnosed CAD and stroke</li> </ul>	<ul style="list-style-type: none"> <li>• 0.82 for death</li> <li>• 0.77 for MI, HF, newly diagnosed CAD and stroke</li> </ul>
Melander et al <sup>105</sup>	Clinical variables and biomarkers	Asymptomatic Swedish population	5067	10 y	<ul style="list-style-type: none"> <li>• Cardiac death and MI</li> <li>• Cardiac death, MI and stroke</li> </ul>	<ul style="list-style-type: none"> <li>• 0.76 for cardiac death and MI</li> <li>• 0.76 cardiac death, MI and stroke</li> </ul>
Zethelius et al <sup>106</sup>	Clinical variables and biomarkers	Swedish patients with and without CAD	1135	10 y	<ul style="list-style-type: none"> <li>• All -cause mortality</li> <li>• Cardiovascular mortality</li> </ul>	<ul style="list-style-type: none"> <li>• 0.68 for all cause mortality</li> <li>• 0.76 for cardiovascular mortality</li> </ul>
Fowkes et al <sup>107</sup>	FRS and the ankle brachial index	Asymptomatic subjects	47334	10 y	Cardiac death, MI	0.66 for both women and men
St Francis Heart Study <sup>108</sup>	FRS and CRP and the Calcium risk score	Asymptomatic subjects	1293	10 y	Cardiac death, MI, coronary revascularization, stroke, and peripheral vascular surgery	0.85

**Supplementary Table III** (continued)

Risk model	Included variables	Studied population	No. of patients	Studied period	Type of events	C-statistics
Detrano et al <sup>109</sup>	Clinical variables and the calcium risk score	Asymptomatic subjects from 4 racial or ethnic group	6722	3.9 y	• Cardiac death and MI • Cardiac death, MI and angina	• Range in different populations from 0.79-0.88 • Range in different populations from 0.79-0.87
Morrison et al <sup>110</sup>	Clinical and genetic risk factors	Asymptomatic black and white populations	13907	13 y	Cardiac death, MI and coronary revascularization	0.77 for both blacks and whites
Brautbar et al <sup>111</sup>	Clinical and genetic risk factor	Analyzed data from the Atherosclerosis risk communities study, Framingham and Rotterdam studies	8542, 2068, and 2339, respectively	10 y	Cardiac death, MI, and coronary revascularization	0.75 for the atherosclerosis risk communities study, 0.78 for the Framingham and 0.74 for the Rotterdam study
Talmud et al <sup>112</sup>	FRS and genetic risk factors	Asymptomatic middle aged men	2742	14 y	Cardiac death, MI and coronary revascularization	0.76

Abbreviations: ASSIGN, ASsessing cardiovascular risk using sICG; CRP, C-reactive protein; CVD, cerebrovascular disease; FRS, Framingham Risk Score; HF, heart failure; SCORE, Systematic Coronary Risk Evaluation.

## Supplementary References

79. Kubo T, Nakamura N, Matsuo Y, et al. Virtual histology intravascular ultrasound compared with optical coherence tomography for identification of thin-cap fibroatheroma. *Int Heart J* 2011;52:175-9.
80. Kawasaki M, Bouma BE, Bressner J, et al. Diagnostic accuracy of optical coherence tomography and integrated backscatter intravascular ultrasound images for tissue characterization of human coronary plaques. *J Am Coll Cardiol* 2006;48:81-8.
81. Garcia-Garcia HM, Costa MA, Serruys PW. Imaging of coronary atherosclerosis: intravascular ultrasound. *Eur Heart J* 2010;31:2456-69.
82. Ohtani T, Ueda Y, Mizote I, et al. Number of yellow plaques detected in a coronary artery is associated with future risk of acute coronary syndrome: detection of vulnerable patients by angiography. *J Am Coll Cardiol* 2006;47:2194-200.
83. Schneiderman J, Wilensky RL, Weiss A, et al. Diagnosis of thin-cap fibroatheromas by a self-contained intravascular magnetic resonance imaging probe in ex vivo human aortas and in situ coronary arteries. *J Am Coll Cardiol* 2005;45:1961-9.
84. Gardner CM, Tan H, Hull EL, et al. Detection of lipid core coronary plaques in autopsy specimens with a novel catheter-based near-infrared spectroscopy system. *JACC Cardiovasc Imaging* 2008;1:638-48.
85. Sathyanarayana S, Schar M, Kraitchman DL, et al. Towards real-time intravascular endoscopic magnetic resonance imaging. *JACC Cardiovasc Imaging* 2010;3:1158-65.
86. Wang B, Karpiouk A, Yeager D, Amirian J, et al. In vivo intravascular ultrasound-guided photoacoustic imaging of lipid in plaques using an animal model of atherosclerosis. *Ultrasound Med Biol* 2012;38:2098-103.
87. Wang B, Su JL, Karpiouk AB, et al. Intravascular photoacoustic imaging. *IEEE J Quantum Electron* 2010;16:588-99.
88. Marcu L. Fluorescence lifetime in cardiovascular diagnostics. *J Biomed Opt* 2010;15:011106.
89. Jaffer FA, Vinegoni C, John MC, et al. Real-time catheter molecular sensing of inflammation in proteolytically active atherosclerosis. *Circulation* 2008;118:1802-9.
90. Lev EI, Kornowski R, Vaknin-Assa H, et al. Comparison of the predictive value of four different risk scores for outcomes of patients with ST-elevation acute myocardial infarction undergoing primary percutaneous coronary intervention. *Am J Cardiol* 2008;102:6-11.
91. Simms AD, Reynolds S, Pieper K, et al. Evaluation of the NICE mini-GRACE risk scores for acute myocardial infarction using the Myocardial Ischaemia National Audit Project (MINAP) 2003-2009: National Institute for Cardiovascular Outcomes Research (NICOR). *Heart* 2013;99:35-40.
92. Palmerini T, Caixeta A, Genereux P, et al. Comparison of clinical and angiographic prognostic risk scores in patients with acute coronary syndromes: Analysis from the Acute Catheterization and Urgent Intervention Triage Strategy (ACUITY) trial. *Am Heart J* 2012;163:383-91.
93. Garg S, Samo G, Serruys PW, et al. Prediction of 1-year clinical outcomes using the SYNTAX score in patients with acute ST-segment elevation myocardial infarction undergoing primary percutaneous coronary intervention: a substudy of the STRATEGY (Single High-Dose Bolus Tirofiban and Sirolimus-Eluting Stent Versus Abciximab and Bare-Metal Stent in Acute Myocardial Infarction) and MULTISTRATEGY (Multicenter Evaluation of Single High-Dose Bolus Tirofiban Versus Abciximab With Sirolimus-Eluting Stent or Bare-Metal Stent in Acute Myocardial Infarction Study) trials. *JACC Cardiovasc Interv* 2011;4:66-75.
94. Genereux P, Palmerini T, Caixeta A, et al. Quantification and impact of untreated coronary artery disease after percutaneous coronary intervention: the residual SYNTAX (Synergy Between PCI with Taxus and Cardiac Surgery) score. *J Am Coll Cardiol* 2012;59:2165-74.
95. Girasis C, Garg S, Raber L, et al. SYNTAX score and Clinical SYNTAX score as predictors of very long-term clinical outcomes in patients undergoing percutaneous coronary interventions: a substudy of

- SIRolimus-eluting stent compared with pacliTAXel-eluting stent for coronary revascularization (SIRTAX) trial. *Eur Heart J* 2011;32:3115-27.
96. Garg S, Serruys PW, Silber S, et al. The prognostic utility of the SYNTAX score on 1-year outcomes after revascularization with zotarolimus- and everolimus-eluting stents: a substudy of the RESOLUTE All Comers Trial. *JACC Cardiovasc Interv* 2011;4:432-41.
  97. Chiba N, Nagao K, Mukoyama T, et al. Decreased activated protein C levels as a clinical predictor in patients with ST-elevation myocardial infarction. *Am Heart J* 2008;156:931-8.
  98. Damman P, Beijk MA, Kuijij WJ, et al. Multiple biomarkers at admission significantly improve the prediction of mortality in patients undergoing primary percutaneous coronary intervention for acute ST-segment elevation myocardial infarction. *J Am Coll Cardiol* 2011;57:29-36.
  99. D'Agostino Sr RB, Grundy S, Sullivan LM, et al. Validation of the Framingham coronary heart disease prediction scores: results of a multiple ethnic groups investigation. *JAMA* 2001;286:180-7.
  100. McNeill AM, Rosamond WD, Girman CJ, et al. The metabolic syndrome and 11-year risk of incident cardiovascular disease in the atherosclerosis risk in communities study. *Diabetes Care* 2005;28:385-90.
  101. Conroy RM, Pyörälä K, Fitzgerald AP, et al. Estimation of ten-year risk of fatal cardiovascular disease in Europe: the SCORE project. *Eur Heart J* 2003;24:987-1003.
  102. Woodward M, Brindle P, Tunstall-Pedoe H. Adding social deprivation and family history to cardiovascular risk assessment: the ASSIGN score from the Scottish Heart Health Extended Cohort (SHHEC). *Heart* 2007;93:172-6.
  103. Collins GS, Altman DG. An independent external validation and evaluation of QRISK cardiovascular risk prediction: a prospective open cohort study. *BMJ* 2009;339:b2584.
  104. Wang TJ, Gona P, Larson MG, et al. Multiple biomarkers for the prediction of first major cardiovascular events and death. *N Engl J Med* 2006;355:2631-9.
  105. Melander O, Newton-Cheh C, Almgren P, et al. Novel and conventional biomarkers for prediction of incident cardiovascular events in the community. *JAMA* 2009;302:49-57.
  106. Zethelius B, Berglund L, Sundstrom J, et al. Use of multiple biomarkers to improve the prediction of death from cardiovascular causes. *N Engl J Med* 2008;358:2107-16.
  107. Fowkes FG, Murray GD, Butcher I, et al. Ankle brachial index combined with Framingham Risk Score to predict cardiovascular events and mortality: a meta-analysis. *JAMA* 2008;300:197-208.
  108. Arad Y, Goodman KJ, Roth M, et al. Coronary calcification, coronary disease risk factors, C-reactive protein, and atherosclerotic cardiovascular disease events: the St. Francis Heart Study. *J Am Coll Cardiol* 2005;46:158-65.
  109. Detrano R, Guerci AD, Carr JJ, et al. Coronary calcium as a predictor of coronary events in four racial or ethnic groups. *N Engl J Med* 2008;358:1336-45.
  110. Morrison AC, Bare LA, Chambless LE, et al. Prediction of coronary heart disease risk using a genetic risk score: the Atherosclerosis Risk in Communities Study. *Am J Epidemiol* 2007;166:28-35.
  111. Brautbar A, Pompeii LA, Dehghan A, et al. A genetic risk score based on direct associations with coronary heart disease improves coronary heart disease risk prediction in the Atherosclerosis Risk in Communities (ARIC), but not in the Rotterdam and Framingham Offspring, Studies. *Atherosclerosis* 2012;223:421-6.
  112. Talmud PJ, Cooper JA, Palmen J, et al. Chromosome 9p21.3 coronary heart disease locus genotype and prospective risk of CHD in healthy middle-aged men. *Clin Chem* 2008;54:467-74.



# Chapter 6

## Future Perspectives

Freeing the vessel from metallic cage:  
what can we achieve with bioresorbable vascular scaffolds?

*Cardiovasc Interv and Ther.* 2012;27:141-54.  
[Review]

Onuma Y, Muramatsu T, Kharlamov A, Serruys PW.





# Freeing the vessel from metallic cage: what can we achieve with bioresorbable vascular scaffolds?

Yoshinobu Onuma · Takashi Muramatsu ·  
Alexander Kharlamov · Patrick W. Serruys

Published online: 9 May 2012  
© Japanese Association of Cardiovascular Intervention and Therapeutics 2012

**Keywords** Biodegradable polymers · Coronary artery disease · Bioresorbable scaffold · Coronary stent

## Introduction

After the era of balloon angioplasty and bare-metal stents, drug eluting stents were introduced to solve the problem of in-stent restenosis [1]. The follow-up of the first 45 patients implanted with the sirolimus eluting Bx velocity stent (Cordis, Johnson & Johnson, Warren, NJ, USA) was found to have negligible neointimal hyperplasia [2, 3]. This was confirmed in the randomized RAVEL study [4, 5]. The introduction of drug eluting stents was thus dubbed the third revolution in interventional cardiology. Both large scale randomised trials and all-comer registries showed excellent results in terms of the need for repeat revascularisation.

However, these new devices created again a new enemy: by interfering profoundly with the healing process, lack of endothelialization and late persistent or acquired malapposition of the permanent metallic implant became the nidus of late and very late stent thrombosis, without mentioning the hypersensitive reaction mediated by eosinophils which sometimes triggered these catastrophic events [6–8]. Vasomotion testing demonstrated abnormal vasoconstriction responses to acetylcholine distal to the deployed stent, suggesting that the structure and function of the endothelium remained abnormal [9, 10].

Fully bioresorbable scaffolds (BRS) are a novel approach that provides transient vessel support with drug delivery capability without the long-term limitations of metallic drug-eluting stents, such as permanent caging with or without malapposition. By liberating the coronary artery from the metallic caging, the vessel recovers pulsatility and becomes responsive to the shear stress and physiological cyclic strain. The technology has a potential to overcome many of the safety concerns associated with metallic drug-eluting stents, and possibly even convey more clinical benefits.

## Fully bioresorbable scaffold: what are the advantages over metallic stents?

Fully bioresorbable vascular scaffolds have potential advantages over current metallic drug-eluting stent technology; these include:

1. A reduction in adverse events such as very late stent thrombosis (ST). As drug elution and scaffolding are temporary and are only provided by the device until the vessel has healed, no foreign material, such as non-endothelialised struts and drug polymers (potential triggers for ST) can persist long-term.
2. The removal, through bioresorption, of the stented vessel's rigid caging. This can facilitate the return of the vessel's vasomotion, adaptive shear stress, late luminal enlargement and late expansive remodeling. Furthermore, this might also reduce the problems of jailing the ostium of side branches as seen with permanent metallic stent struts.
3. An improvement in future treatment options. The treatment of complex multi-vessel disease frequently results in the use of multiple long DES; for example in

---

Y. Onuma · T. Muramatsu · A. Kharlamov · P. W. Serruys (✉)  
Thoraxcenter, Erasmus Medical Center, 's Gravendijkwal 230,  
3015 CE Rotterdam, The Netherlands  
e-mail: p.w.j.c.serruys@erasmusmc.nl

the SYNTAX trial the average number of stents was four, and one third of patients had greater than 100 mm of stent implanted [11]. In such cases, repeat revascularization—either by means of percutaneous or surgical revascularisation, is potentially challenging because of the metallic cages formed by previously implanted DES. The use of a BRS would mean that there would potentially be no restriction on any future percutaneous or surgical revascularisation should they be needed.

4. The use of non-invasive imaging such as computed tomography (CT) angiography or magnetic resonance imaging (MRI) at follow-up. Presently, metallic stents can cause a blooming effect with these imaging modalities making interpretation more difficult [12]. The PLLA scaffold should not restrict the use of CT or MRI as it is radio-lucent; once bioabsorption has been completed with a metallic BRS then this should also not restrict the use of CT or MRI. Non-invasive imaging follow-up could therefore become an alternative to invasive imaging follow-up. When compared to angiographic follow-up (routinely performed in Japan), follow-up by MSCT might be more cost effective and less invasive.
5. Reservoir for the local delivery of drugs and genes. Since the duration of bioresorption is modifiable, according to the type of polymers/co-polymers, a tuned elution of multiple drugs can potentially be achievable (e.g. early elution of antiproliferative agent from a coated polymer and chronic elution of anti-inflammatory or other agent from the backbone polymer).
6. The elimination of the concern that some patients have at the thought of having an implant in their bodies for the rest of their lives [13]. This would be relevant to Asian population such as Japanese: traditionally people respect their natural bodies that were given by their parents, and for respect to their parents people they do not appreciate receiving surgical incisions and foreign bodies—even small carbon particles of tattoo. This tendency is evident in the following facts: (a) Proportion of PCI and CABG in Japan is as high as 10, 5 and 1 in the single, two and three vessel diseases respectively [14]; (b) Only few cases of organ transplantation from brain dead cadaver have been performed. For example, the number of heart transplantation throughout Japan is limited to 119 in 14 years since the organ transplantation law was established [15]. Considering these cultural backgrounds, the concept of bioresorbable scaffold—temporary scaffolding without leaving any material behind—is likely to be accepted well in Japan.

## Bioabsorption and Bioresorption

After the first commercially medical devices made of artificial polymers degradable *in vivo* (surgical sutures made from lactic acid and/or glycolic acid) were referred to as “absorbable sutures” [14], such devices were frequently dubbed as “bioabsorbable”, which in general reflects the disappearance of a compound into another substance. However, the term “bioabsorbable” is not appropriate, because “bioabsorption” does not necessarily mean “degradation”, and even less, “elimination of the polymer from the body”. Indeed, even if a “bioabsorbable” polymeric device was no longer visible as a result of degradation (“bioabsorption”), high molecular mass molecules can be still be trapped between skin and mucosa without passing physiological barriers. Therefore, bioabsorption does not necessarily mean complete cleavage of macromolecules up to small molecules that can be eliminated from the body through natural pathways, namely kidney or lungs. To indicate the total elimination of polymers by excretion and assimilation, the concept of “bioresorption” was introduced [15, 16].

## What are the biological implications of metallic caging?

There are complex biological interferences resulting from metallic caging. In the bare metal stent era, our group as well as others have shown that stiff metallic stents can alter vessel geometry and biomechanics, and that long-term flow disturbances and chronic irritation contribute to adverse events, without mentioning late strut fractures, that could lead to restenosis and clinical events [16–19]. In these studies, after metallic stent implantation, the curvature increased by 121% at the entrance and by 100% at the exit of the stent, resulting in local changes in shear stress correlated with the local curvature. Stent implantation changed 3-D vessel geometry in such a way that regions with decreased and increased shear stress emerged close to the stent edges (Fig. 1). These changes were related to the asymmetric patterns of in-stent restenosis [16]. From that point of view, the initial superior conformability and flexibility of the ABSORB with respect to metallic stents (Multilink Vision) can, at an early stage, contribute to less change in vessel geometry and biomechanics [19]. Late strut fracture should not be an issue, since at late time points the struts have disappeared.

Not only change in curvature but also mismatch in area/diameter (step-up, proximal edge of the stent; step down, distal edge of the stent) may generate oscillatory shear stress, which gives rise to the expression of several growth factors [20].

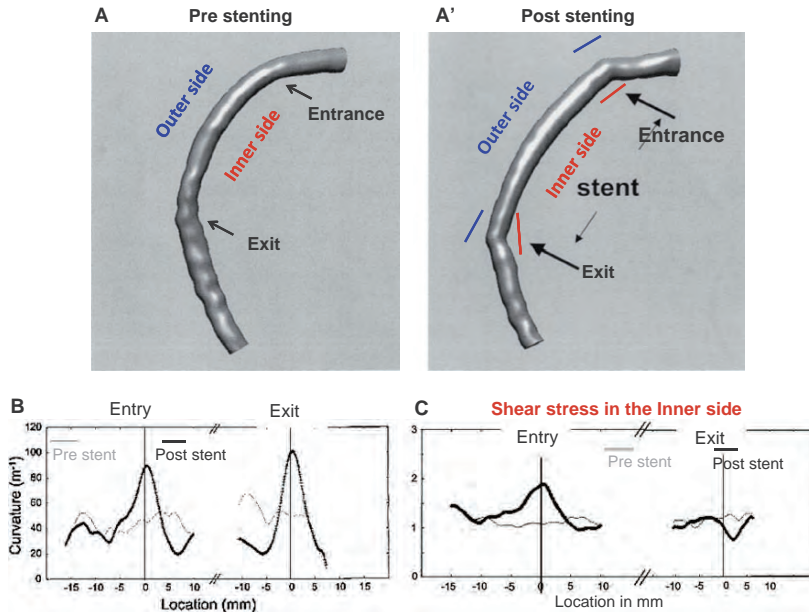


**Fig. 1** Three-dimensional reconstruction of a right coronary artery in a porcine model pre- (a) and after (a') metallic stent implantation. Average curvature of the arteries relative to the location of the entrance and exit of the stent before (grey) and after (black) stent

implantation (b). Average normalized shear stress relative to the location of the entrance (0 mm) and exit of the stent (0 mm) before (grey) and after (black) stent implantation in the inner curve (c). Location sign: distal is positive. Modified from Wentzel et al. [16]

With bare-metal stents, we demonstrated that neointimal thickness was at 6 months inversely related to the relative shear stress distribution. Subsequently, we studied the impact of shear stress pattern (obtained from computational fluid dynamic calculations) on the true 3-dimensional neointimal thickness distribution in sirolimus-eluting stents in coronary arteries. Small pits were observed between the stent struts; deeper pits were present on the outside curvature of the stented segments. In regions of low or even oscillatory shear stress, distal to the endoluminal protrusion of the strut, it is hypothesized that prolonged tissue contact and retention of the cytostatic drugs within the vessel wall could affect the metabolism of the vessel wall tissue resulting in the crenated appearance of the vessel wall between the struts [21].

**What is the biological advantage of disappearing device? Mechanical conditioning, renewed compliance, dynamic vasomotion and mechanotransduction**

Using palpography, we have demonstrated after implantation of everolimus-eluting PLLA bioresorbable scaffold

that the scaffolding properties of the bioresorbable polymer offer the advantages of gradual load transfer of mechanical strain to the healing tissue (mechanical conditioning) (Strain values post procedure:  $0.16 \pm 0.10$ , 6 months:  $0.28 \pm 0.12$ , 2 years:  $0.31 \pm 0.17\%$ ) [22] so that the healthy compliance of the vessel can be progressively restored long term (renewed compliance). Gradual exposure of cellular structures within the vessel wall to normal physiologic stress conditions has a positive effect on cellular organization and function. In the field of orthopedic biodegradable implants, mechanical conditioning via progressive dynamic loading improves proteoglycan and collagen deposition [23]. A similar scenario has been deciphered with vascular bioresorbable implants. After bioresorption of the polylactide, the void previously occupied by the struts is filled progressively by proteoglycan and collagen. The full disappearance of the struts—that has been documented by ultrasound, optical coherence tomography, histology, and pharmacologically induced dynamic vasomotion—suggested that the vessel wall will ultimately sense again the mechanical strains of pulsatile blood flow (pulsatility), which is an important stimulus for the cell biology of the vessel wall [22].

Pulsatility is the fluctuation of blood pressure and blood flow velocity during systole and diastole. As blood is pumped through the coronary vessels, the vessel wall is exposed to two sets of forces, both of which are critically important: (a) Shear stress is the frictional force on the vessel lining as blood flows through it, (b) Cyclic strain is the force generated by the stretching of the vessel wall during systole and is affected by vessel distensibility (stretchability), (c) The interplay of shear stress and cyclic strain controls cell signaling—the chemical signals sent from one cell to another, which can lead to atheroprotective/thromboresistant changes, or disease progression and instability (Fig. 2). For instance, cyclic strain stimulates e-NOS gene regulation and steady state levels of prostacyclin are significantly increased if the shear stress force is applied in a pulsatile fashion compared with steady laminar flow [24, 25]. Cell signaling may be altered in stented segments, where the vessel distensibility is eliminated by metallic caging of the vessel segment. The translation of mechanical forces into chemical signals by cells is referred to as 'mechanotransduction' (Fig. 2).

Applied mechanical strain preferentially preserves collagen fibrils, stretch of the vascular wall stimulates increased actin polymerization, activating synthesis of smooth muscle-specific proteins (Table 1). Under such conditions smooth muscle cells preferentially maintain their contractile phenotype, while such differentiation is lost in sites of vascular injury (i.e., atherosclerosis or restenosis). From that point of view, the transmission microscopy of neointima and media, at 1 and 36 months in pigs having received ABSORB, is very illustrative of the changes in phenotype observed short and the long-term in these vessels.

In summary, with the progressive disappearance of the polymeric scaffold, physiological stimuli can again have an active impact on the vessel wall, and the return of pulsatility may be of paramount importance in effecting optimal repair of the vessel wall.

In our patients treated with BRS, vasomotion of the scaffolded segment following intraluminal administration of acetylcholine [26, 27] suggests that: (a) the scaffolding function of the polymeric struts has completely disappeared and the so-called scaffolded segment can now exhibit vasomotion, (b) the endothelial lining (coverage) is coalescent; (c) the ciliary function of the endothelial cell is functional; (d) the biochemical process through which nitric oxide is released, works properly. A positive acetylcholine test with vasodilatation of the scaffold is the indirect proof that the endothelium is anatomically and functionally normal and healthy. In a porcine model transmission electron microscopy shows sign of maturation of endothelial junctions between 1 and 36 months with robust and dense intercellular desmosome at 3 years. Of

note, a healthy endothelium releases chemical signals that promote vasodilation (NO), inhibit thrombosis (prostacyclin, tissue plasminogen activator, thrombomodulin), inhibit smooth muscle cell proliferation, and inhibit inflammation. Conversely, an unhealthy endothelium releases chemical signals that promote vasoconstriction (endothelin, angiotensin II, thromboxane A<sub>2</sub>), thrombosis (von Willebrand factor, fibrinogen, tissue factor, plasminogen activator inhibitor, thromboxane A<sub>2</sub>), disease progression (vascular endothelial growth factor, platelet derived growth factor), and inflammation (vascular cell adhesion molecules, inter-cellular adhesion molecule) [28].

As mentioned above, late lumen enlargement was not associated with vessel enlargement, and thus was obtained through a reduction in plaque area [22]. A few hypothetical mechanisms can be put forward to explain this phenomenon. First, everolimus may significantly lower monocyte chemotaxis, without inducing monocyte cell death by affecting chemotactic factors such as monocyte chemoattractant protein1, fractalkine, interleukin-8, and *N*-formyl-methionyl-leucyl-phenylalanine (fMLP) [29]. Second, the drug itself has been shown to reduce advanced and intermediate lesions in mice knock out for LDL receptor (−/−) [30]. Third, everolimus has been shown to selectively clear macrophages in plaque by inducing autophagy in animal models (see above). This could result in a reduction in plaque volume. Fourth, pulsatile laminar flow may trigger plaque regression, through stimulation of matrix metalloproteinases [31].

### Clinically tested BRS

Details of BRS devices are presented in Table 2.

#### Igaki–Tamai stent

The Igaki–Tamai PLLA coronary stent was the first fully bioresorbable stent to be implanted in humans with complete degradation taking 18–24 months. The stent had a helical zigzag design, which differed from previous knitted patterns. This resulted in less vessel wall injury during implantation and therefore less initial thrombus formation and reduced intimal hyperplasia [32]. The stent was mounted on a standard angioplasty balloon and was both thermal self-expanding and balloon expandable. Self-expansion occurred in response to heating the PLLA, which was achieved by using heated contrast (up to 70°C) to inflate the delivery balloon. Stent expansion was further optimised by inflating the delivery balloon to 6–14 atm for 30 s, and the stent's nominal size was ultimately achieved by continued self-expansion at 37°C in the 20–30 min after

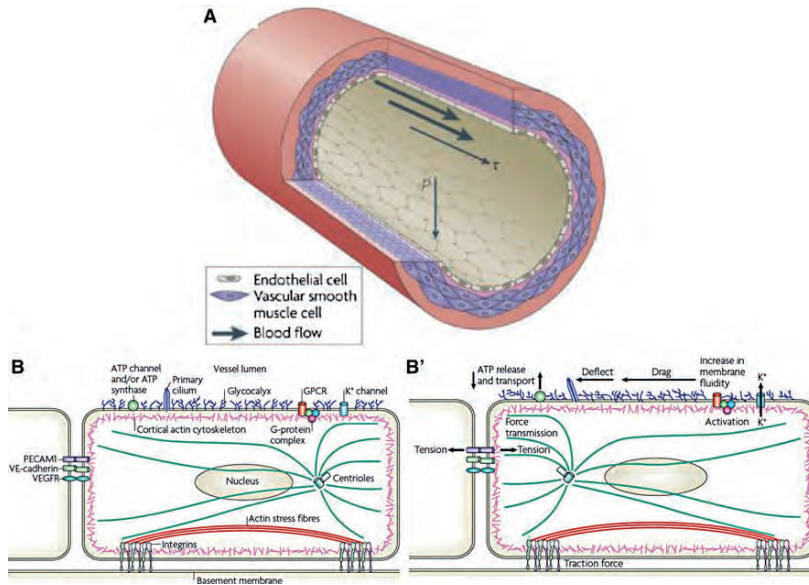


**Fig. 2** a A section of an artery wall shows the endothelial cells that form the inner lining and align longitudinally, and vascular smooth muscle cells that for the outer layers and align circumferentially. Pressure ( $p$ ) is normal to the vessel wall, which results in circumferential stretching of the vessel wall. Shear stress ( $\tau$ ) is parallel to the vessel wall and is exerted longitudinally in the direction of blood flow. b The upper surface of the endothelium has a carbohydrate-rich glycocalyx that extends 0.4–0.5 micrometres into the vessel lumen. A fraction of cells in regions of low shear also have a luminal primary cilium that is several micrometres long. G-protein-coupled receptors (GPCRs), heterotrimeric G proteins and ion channels might also reside in the upper plasma membrane. Cells also have ATP channels and/or cell surface ATP synthase. The lateral cell membrane contains the homophilic adhesion receptors platelet/endothelial cell-adhesion molecule 1 (PECAM1) and vascular endothelial (VE)-cadherin,

which bind to their counterparts on adjacent cells. Vascular endothelial growth factor receptor (VEGFR) associates laterally with VE-cadherin in these domains. The cortical actin cytoskeleton, actin stress fibres, microtubules and intermediate filaments (not shown) mechanically connect different regions of the cell. Integrin-dependent complexes anchor the cell to the basement membrane. b' Under fluid shear stress, the glycocalyx experiences drag that is transmitted to the cortical cytoskeleton. The cilium is deflected by flow and bends relative to the apical membrane or cytoskeleton. Both ATP release and its transport near the cell surface are modified by flow. Tension is transmitted to the lateral borders and basal membrane, where adhesion receptors, such as PECAM1 or integrins, experience changes in tension. Changes in fluidity of the apical membrane have been observed and might activate  $K^+$  channels, GPCRs or G proteins. Figures were reused from Hahn et al. [71] with permission

stent deployment. The stent had a standard length of 12 mm, and was available in diameters of 3, 3.5 and 4 mm; the stent strut thickness was 0.17 mm. An 8F guiding catheter was required because the stent was initially constrained by a sheath that was removed once it was across the lesion. At either end of the stent to aid visualisation were two radio-opaque cylindrical gold markers (0.6 mm high by 0.18 mm in diameter). The first in man (FIM) study of the Igaki–Tamai stent (15 patients, 19 lesions, 25 stents), demonstrated no major adverse cardiovascular events (MACE) or ST within 30 days, and one repeat PCI at 6 months follow-up. Encouragingly, the loss index (late loss/acute gain) was 0.48 mm, which was comparable to BMS, and demonstrated for the first time that BRS did not

induce an excess of intimal hyperplasia. Furthermore, intravascular ultrasound (IVUS) imaging demonstrated no significant stent recoil at day one, and continued stent expansion was observed in the first 3 months of follow-up. The mean stent cross sectional area increased from  $7.42 \pm 1.51 \text{ mm}^2$  at baseline to  $8.18 \pm 2.42 \text{ mm}^2$  ( $p = 0.086$ ) at 3 months, and  $8.13 \pm 2.52 \text{ mm}^2$  at 6 months [32]. A second larger study of 50 elective patients (63 lesions, 84 stents) also showed promising results. IVUS performed at 3 years follow-up demonstrated the complete absence of stent struts, whilst angiographic analysis demonstrated a mean diameter stenosis of 25%, compared to 38, 29 and 26% at 6, 12, and 24 months respectively. Clinical outcomes at 4-year follow-up showed rates of

**Table 1** Overview of extra-cellular matrix modulation studies for cardiovascular cell types

Cell type	ECM protein changes with strain	
	Static	Cyclic
Cardiac	↑Collagen	↑↑Collagen
Fibroblasts	↑↓Others	↑↑Others
Cardiomyocytes	↑↑Others	↑↑MMPs
Endothelial cells	↑GAGs and PGs	↓↓Collagen
	↑↑Others	↑↓GAGs and PGs
Smooth muscle cells		↑↑MMPs
		↑↓Others
	↓Collagen	↑Collagen
	↑↑Elastin	↑↑Elastin
	↑↑GAGs and PGs	↑↓GAGs and PGs
	↓MMPs	↑MMPs
		↑↑Others

“Others” include total protein, growth factors and signaling molecules. Double arrow = 100%, single arrow = 60–99%, combined arrow = 40–60%, contradictory studies, or different responses to various strain magnitudes. Reproduced from Gupta et al. [72] with permission

overall and MACE-free survival rates of 97.7 and 82.0%, respectively [33].

At 10-year clinical follow-up, freedom from cardiac death, non-cardiac death and MACE were 98, 87, and 48% respectively [34]. In the limited cases with serial angiographic follow-up, the MLD was stable: the mean MLD was 2.01 mm at 1 year and 2.06 mm at 10 years. There were two ST events: 1 subacute event occurring at day 5 possibly due to inadequate heparinisation at the time of PCI, and one very late ST event occurring in the sirolimus-eluting metallic stent which was later implanted proximal to the previously placed Igaki–Tamai stent. Serial angiographic and OCT images of the stent struts out to 10-year follow-up in one anecdotal case are shown.

Despite these impressive results, the failure of the stent to progress was primarily related to the use of heat to induce self-expansion. There were concerns that this could cause necrosis of the arterial wall leading to excessive intimal hyperplasia or increased platelet adhesion leading to ST [35]. None of these concerns were substantiated in the initial studies, however only low-risk patients were enrolled. After completion of the PERSEUS study [36], the stent became available in Europe for peripheral use, however there are plans to review its use in coronary arteries. At present the stent has no drug elution, although preclinical studies of the polymeric stent eluting the tyrosine kinase antagonist ST 638 showed promising results [37].

## Magnesium alloy

Magnesium (Mg) is the fourth commonest cation within the human body; the total body content is ~20 g, with 350 mg required daily. It is essential for the synthesis of over 300 enzymes and is a co-factor for ATPase. A high dose infusion of Mg can cause vasodilatation; the promotion and recruitment of collaterals during ischaemia; and can function as a direct inhibitor stent thrombosis.

The absorbable metallic stent (AMS-1) (Biotronik, Berlin, Germany) is the first metallic biodegradable stent, composed of 93% magnesium (approximate weight of  $3.0 \times 10$  mm is 3 mg) and 7% rare earth metals. The first generation AMS-1 stent, which is balloon-expandable, is available in diameters of 3.0–3.5 and lengths of 10–15 mm (Fig. 3). It has a high mechanical strength; and has comparable properties to stainless steel stents in view of its low elastic recoil (<8%), high collapse pressure (0.8 bar) and minimal shortening after inflation (<5%) [38]. The degradation of Mg produces an electronegative charge that results in the stent being hypo-thrombogenic [39]. In the porcine model, the AMS-1 has been shown to be rapidly endothelialised, and within 60 days is largely degraded into inorganic salts, with little associated inflammatory response [40]. After promising initial preclinical trials, and successful deployment in 20 patients with critical limb ischaemia [41], the PROGRESS AMS trial was performed. This was a multicenter, non-randomized, prospective study, which assessed the efficacy and safety of the stent in 63 patients (71 stents) with single de novo lesions.

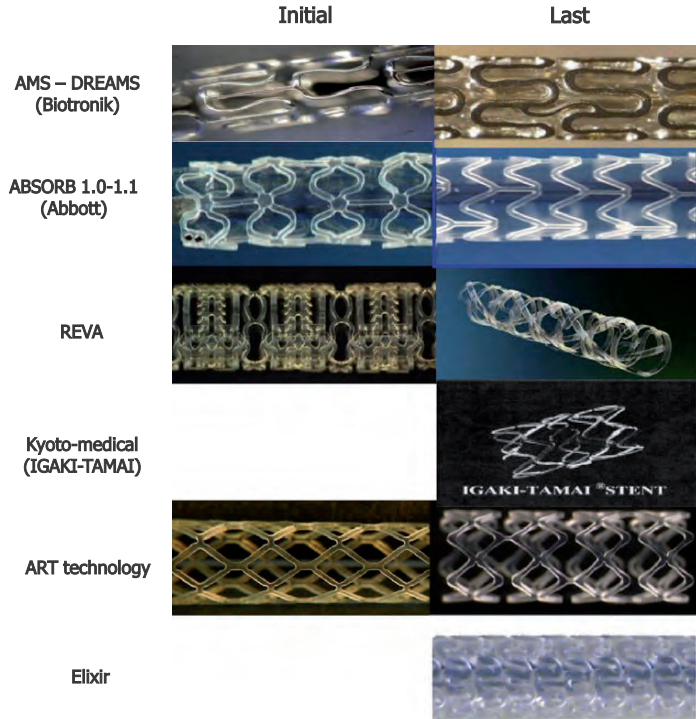
The study reached the primary endpoint, a composite of cardiac death, non-fatal MI, and clinically driven TLR (=MACE) at 4 months, by achieving a rate of MACE of 23.8%; the rate of MACE at 12 months was 26.7%. The study demonstrated the safety of the AMS-1 with no reported death, MI or ST during 12 months follow-up; in addition, there was a return of vessel vaso-reactivity. Unfortunately, the rate of any TLR was a disappointing 23.8% at 4 months, and 45% at 12 months [38]. QCA and IVUS have both provided important information regarding the mechanism of this restenosis, all of which have had important implications on future stent designs. QCA showed an acute gain post stenting of 1.41 mm (SD 0.46 mm), and a reduction in the mean diameter stenosis from 61.5% pre-stenting (SD 13.1%), to 12.7% (SD 5.6%) post-stenting. At 4 months follow-up the mean diameter stenosis was 48.4% (SD 17.0%) and the in-stent late loss was 1.08 mm (SD 0.49 mm). Immediately after post-stenting balloon dilatation, which was required in 42 patients, IVUS demonstrated that the mean stent cross sectional area ( $6.2 \pm 1.5$  mm<sup>2</sup>), and mean stent volume ( $116.5 \pm 40.2$  mm<sup>3</sup>) were both lower than that seen with standard metallic stents deployed in similar sized vessels.

**Table 2** Summary of clinically tested bioresorbable vascular scaffolds

Scaffold	Stent material	Coating material	Design	Absorption products	Drug elution	Stent radio-opacity	Total strut thickness (strut + coating), micron	Crossing profile (mm)	Stent-to-artery coverage (%)	Duration radial support	Absorption time	Angiographic late loss	TLR rate
Igaki-Tamai	Poly-L-lactic acid	Nil	Zigzag helical coils with straight bridges	Lactic acid, CO <sub>2</sub> , and H <sub>2</sub> O	Nil	Gold markers	170	-	24	6 months	2 years	late loss index at 6 months: 0.48 mm	At 6 months: 6.7%
AMS-I	Metal-magnesium alloy	Nil	Sinusoidal in-phase hoops linked by straight bridges	Not applicable	Nil	Nil	165	1.2	10	Days or weeks	<4 months	At 4 months: 1.08 mm	At 1 year: 4.5%
AMS-II	Metal-magnesium alloy	Nil	Not applicable	Not applicable	Nil	Nil	125	-	-	Weeks	>4 months	-	-
AMS-III	Metal-magnesium alloy	Nil	Not applicable	Not applicable	Paclitaxel	Nil	125	-	-	Weeks	>4 months	At 6 months: 0.68 mm	At 6 months: 9.1%#
REVA	Poly-tyrosine-derived polycarbonate polymer	Nil	Side and lock	Amino acid, ethanol, CO <sub>2</sub>	Nil	Iodine impregnated	200	1.7	55	3-6 months	2 years	At 6 months: 1.81 mm	At 1 year: 67%
BTI	Polymer salicylate + linker	Salicylate + different linker	Tube with laser-cut voids	Salicylate, CO <sub>2</sub> and H <sub>2</sub> O	Sirolimus salicylate	Nil	200	2	65	3 months	6 months	-	-
ABSORB 1.0	Poly-L-lactide	Poly-D,L-lactide	Out-of-phase sinusoidal hoops with straight and direct links	Lactic acid, CO <sub>2</sub> , and H <sub>2</sub> O	Everolimus	Platinum markers	156	1.4	25	2 years	2 years	At 6 months: 0.44 mm	At 4 years: 0%
ABSORB 1.1	Poly-L-lactide	Poly-D,L-lactide	In-phase hoops with straight links	Lactic acid, CO <sub>2</sub> , and H <sub>2</sub> O	Everolimus	Platinum markers	156	1.4	25	6 months	2 years	At 6 months: 0.19 mm at 12 months: 0.27 mm	At 1 year: 3.6%
Elixir	Poly-L-lactide	?	Sinusoidal in phase hoops with straight connectors	Lactic acid, CO <sub>2</sub> , and H <sub>2</sub> O	Myofolimus	Metallic markers	Approximately 150	1.47	-	-	1-2 years	Not available	Not available

# in the Cohort 1 population (Haude et al. at EuroPCR 2011)  
TLR target lesion revascularization

**Fig. 3** Device designs of the initial and last iteration of fully bioresorbable vascular scaffolds from different developers



These results were consistent with QCA results, and were probably related to both the lower radial force of the Mg alloy compared to stainless steel, and by immediate vessel recoil after stent implantation. At 4 months follow-up IVUS demonstrated that only small remnants of the original struts were visible, which were all well embedded into the intima. IVUS also showed a 42% reduction in the area delineated by the external elastic membrane, suggesting that early vessel recoil was indeed the primary cause of the high late loss, and restenosis. This vessel recoil was attributable to the loss of radial force from the early, rapid AMS-1 stent degradation, such that no stent support was available to oppose constrictive remodeling; a natural response of the vessel to injury. Exacerbating the problem was evidence to suggest that stent degradation was possibly faster than previously anticipated. A repeat IVUS in one patient only 3 weeks post AMS-1 implantation showed 50% of struts were already degraded [42]. Other factors besides constrictive recoil contributing to the luminal loss seen at follow-up were intra-stent tissue growth (intra-stent neointima) (41%) and tissue growth behind the stent struts

(extra-stent neointima) (13.5%). Reassuringly long-term data from angiographic and IVUS performed in the eight patients who did not experience an event at 4 months have shown that there was no evidence of either later recoil or late development of neointima. In fact, in some patients evidence was seen of neointimal regression, and/or an increase in vessel and lumen volume [42]. Of note, the AMS stent is proven to be MRI compatible [43] and furthermore, the vasodilator function after nitroglycerin injection was restored in the treated segment at follow-up [44].

The results from the patients enrolled in studies of the AMS-1 stent demonstrated it was safe for use in both coronary and peripheral vessels [38, 41, 45]. The stent was resorbed as intended, with no undue safety concerns. The disappointingly high TLR rate compared to standard BMS and DES has led to modifications in the future stent's design. These aim to prolong degradation and enable drug elution, and thereby reduce restenosis that was partly due to negative remodeling, and partly due to an excessive healing response. Two new stents have been developed: AMS-2 and AMS-3. The AMS-2 stent is designed to

overcome some of the problems of excessive vessel recoil seen with AMS-1. It provides prolonged mechanical stability, which has been achieved by using a different magnesium alloy, which has not only a higher collapse pressure of 1.5 bar, compared to 0.8 bar with AMS-1, but also a slower degradation time. In addition, the stent surface has been modified; the stent strut thickness has been reduced from 165 to 125  $\mu\text{m}$  and the shape of the strut in cross-section has been altered from rectangular to square (improving radial strength). These changes have in animal models prolonged scaffolding and stent integrity, improved radial strength and reduced neointima proliferation.

The AMS-3 stent (DREAMS: Drug Eluting AMS) is designed to reduce neointimal hyperplasia by incorporating a bioresorbable matrix for controlled release of an anti-proliferative drug onto the AMS-2 stent. Research is currently focused on establishing the ideal drug kinetics; initial animal trials have demonstrated a sustained anti-proliferative effect at 1 month. A new clinical programme resumed in July 2010. The preliminary results of follow-up were presented at EuroPCR 2011. At 6 months in cohort 1 of Biosolve-1 FIM study, MLD was 1.88 mm resulting in late lumen loss of 0.68 mm (compared to 1.08 mm at 4 months in PROGRESS study with earlier bare version of device), a reduction of 37%. In the same cohort, there was 100% device and procedural success; TLF rate at 6 months was 9.1%, due to 2 clinically driven TLRs.

#### **Tyrosine polycarbonate: the REVA stent**

The REVA stent (REVA Medical, San Diego, CA USA) is a tyrosine derived poly carbonate (specifically poly(iodinated desaminotyrosyl-tyrosine ethyl ester) carbonate) stent that is both resorbable, and radio-opaque following the chemical modification of desaminotyrosine to incorporate iodine molecules. The polymer degrades into water, carbon dioxide and ethanol; in addition the monomers are rapidly excreted from the body with no accumulation in the organs. The stent's resorption time is dependent on the polymer formulation with reported times of over 18 months, or under 12 months for the high and low molecular-weight polymers respectively. In addition to its radio-opacity, the REVA stent also has a distinctive Slide & Lock design that provides both flexibility, and strength (Fig. 3). During the deployment of a standard deformable stent, significant strain is concentrated at hinge points; the consequence of straining a polymer beyond its yield point is a significant loss of mechanical strength. The slide and lock design eliminates hinge points, and therefore minimises polymer strain over a wide range of deployment diameters, thereby preventing deformation and weakening of the polymer during stent deployment. The locking mechanism maintains the acute lumen gain following stent deployment, and

provides additional support to the stent during vessel remodelling. Company data report negligible recoil, and a radial force that is superior to the MULTI-LINK VISION bare metal stent (ABBOTT Vascular, Santa Clara, USA) [46]. Preclinical data from 600 stents in 300 animals showed encouraging results. Histological samples taken at day 5 demonstrated minimal injury, a non-thrombogenic response, and low inflammation. Electron microscopy at 30 days confirmed complete endothelialisation with histology at 6 months confirming complete encapsulation. Inflammation was noted to be higher with the REVA stent as compared to BMS at 1 month, but comparable by 12 months; a similar trend was noted for area stenosis. Notably IVUS data demonstrated an increase in the luminal area with the REVA stent from 3.65 mm<sup>2</sup> at 1 month to 8.28 mm<sup>2</sup> at 12 months respectively, whilst only a minimal rise was observed over the same period in the BMS control (5.84–6.28 mm<sup>2</sup>) [47]. The 30 patient multicentre FIM clinical study of the REVA stent, the RESORB (REVA Endovascular Study Of a BioResorbable Coronary Stent) study commenced enrollment in June 2007. The study was designed to evaluate the stent's safety in de novo lesions  $\leq 12$  mm in length, and between 3.0 and 3.4 mm in diameter. The primary endpoint was MACE at 30 days, and the secondary endpoint was IVUS and QCA derived parameters at 6 months follow-up. The stent's strength was demonstrated by pre- and post-stenting mean minimum lumen diameters of  $0.88 \pm 0.39$  and  $2.76 \pm 0.36$  mm respectively, whilst the respective mean diameter stenosis pre- and post-stenting was 70 and 5.9%. Follow-up at 6 months showed the absence of any significant vessel recoil as indicated by the external elastic lamina which went from  $15.5 \pm 4.0$  to  $15.3 \pm 3.1$  mm<sup>2</sup>. Unfortunately, focal mechanical failures driven by polymer embrittlement led to a higher than anticipated rate of TLR (66.7%) between 4 and 6 months follow-up. Interestingly, the degree of neointimal hyperplasia was similar to a BMS [48]. A redesign of the stent has ensued resulting in the second generation ReZolve™ stent. This stent has a more robust polymer, a spiral 'Slide & Lock' mechanism to improve clinical performance, and a coating of sirolimus. The sirolimus elution is such that 70% is eluted by 30 days, and 85% by 90 days. Successful pre-clinical trials have been performed, and clinical trials are anticipated in 2011. REVA plans to start the RESTORE study with the ReZolve drug-eluting stent in August 2011; final data collection date for primary endpoint is now May 2012; study end date is November 2016.

#### **Everolimus-eluting PLLA stent: ABSORB scaffold**

The ABSORB scaffold design is characterized by a crossing profile of 1.4 mm with circumferential hoops of PLLA. The struts are 150 microns thick and are either

directly joined or linked by straight bridges. Both ends of the stent have two adjacent radio-opaque platinum markers. The radial strength, measured in a water bath at 37°C using IVUS and by flat plate compression of 10, 15 and 25% is  $0.048 \pm 0.007$ ,  $0.070 \pm 0.008$  and  $0.106 \pm 0.009$  N/mm<sup>2</sup>, while comparative values for a contemporary bare-metal stent (Vision coronary stent, Abbott Vascular, Santa Clara, CA, USA) is  $0.073 \pm 0.011$ ,  $0.114 \pm 0.012$  and  $0.155 \pm 0.012$  N/mm<sup>2</sup>, respectively [26].

The backbone of ABSORB device is made of semi-crystalline polymer called poly-L-lactic acid [26]. The coating consists of poly D,L-lactide, which is a random copolymer of D- and L-lactic acid with lower crystallinity than the ABSORB backbone. The coating contains and controls the release of the anti-proliferative drug, everolimus. Both PLLA and PDLA are fully bioresorbable. During bioresorption, the long chains of PLLA and PDLA are progressively shortened as ester bonds between lactide repeat units are hydrolyzed, and small particles less than 2 µm in diameter are phagocytosed by macrophages. Ultimately, PLLA and PDLA degrade to lactic acid, which is metabolized via the Krebs cycle. In a porcine coronary artery model, mass decreased with time; 30% at 12 months increasing to 60% at 18 months and to 100% at 24 months post implantation.

The Absorb Cohort A trial was a single-arm, prospective, open label first-in-man study with safety and imaging endpoints. Between March and July 2006, 30 patients were enrolled at 4 participating sites. Briefly speaking, the 2-year follow-up of the trial with multiple modality imaging can be summarized as follows: (1) bioresorption of polymeric struts [documented with intravascular ultrasonography (IVUS) and optical coherence tomography (OCT)]; (2) Late enlargement of lumen from 6 months to 2 years (IVUS and OCT); (3) Restoration of vasomotion and endothelial function in some patients; (4) Sustained scaffolding of plaque deformability (palpography); (5) Feasibility of non-invasive imaging with MSCT [22, 49–53]. At 5 years, clinical follow-up was obtained from 29 out of 30 enrolled patients [54]. There was only one non-Q wave myocardial infarction (peak troponin 2.21 ng/ml) related to the treatment of a non-flow-limiting stenosis (QCA DS 42%) in a patient implanted with the ABSORB scaffold 46 days earlier. Furthermore, this patient experienced a single episode of angina at rest without any electrocardiographic evidence of ischemia. Otherwise, there were no new MACE events between 6 months and 3 years, and no instances of stent thrombosis as defined by the protocol or ARC definitions. In total, the MACE rate at 5 years was 3.4% [55].

In the ABSORB A trial, the late scaffold shrinkage at 6 months was the primary reason of late loss: at 6 months, the lumen area was reduced by 16.6%, while the late recoil

was 11.7%. This suggested that approximately two-thirds of the luminal area reduction was caused by late recoil [52]. To enhance the mechanical strength of the struts and to reduce acute and late recoil [42], the strut design and the manufacturing process of the polymer were modified in the revised version: ABSORB 1.1. Firstly, the new design has in-phase zigzag hoops linked by bridges that allow a more uniform strut distribution, reduce maximum circular unsupported surface area (MCUSA) and provide more uniform vessel wall support and drug transfer [56]. Secondly, a modified manufacturing process has resulted in a slower hydrolysis (in vivo degradation) rate of the polymer, thus preserving its mechanical integrity for a longer period of time [57].

The ABSORB revision 1.1 was tested in 101 patients of the ABSORB Cohort B study (Fig. 3). This cohort was subdivided in two subgroups of patients: the first group (B1) had to undergo invasive imaging with QCA, IVUS, IVUS-VH and OCT at 6 and 24 months whereas the second group (B2) underwent invasive imaging at 12 and will repeat at 36 months. In Cohort B2 population, the 12-month clinical and imaging results are now available. Fifty-six patients successfully received 57 ABSORB scaffolds. One patient had a post procedural non Q-wave myocardial infarction; a second patient sustained an iatrogenic non Q-wave MI during an unplanned diagnostic angiography for atypical chest pain. At follow-up, paired analyses were available for QCA in all patients, for Q-IVUS in 52 patients, and for OCT in 22 patients. QCA demonstrated intra-scaffold and in-segment binary restenosis in two patients (3.5%), one resulting from myocardial bridging, one due to neointimal hyperplasia. Both underwent repeat intervention, so that the Major Adverse Cardiac Event (MACE) rate at 1 year was 7.1% (4/56). Overall the scaffold area remained unchanged with IVUS as well as with OCT, whereas the radiofrequency backscattering and the echogenicity of the struts decreased by 16.8% ( $p < 0.001$ ) and 20%, ( $p < 0.001$ ) respectively; more specifically the strut core area on OCT decreased by 11.4% ( $p = 0.003$ ). Despite the absence of scaffold area loss, pharmacological vasomotion was restored. On an intention-to-treat basis, the angiographic late lumen loss amounted to  $0.27 \pm 0.32$  mm with an IVUS relative decrease in minimal lumen area of 1.94% ( $p = 0.12$ ), without significant changes in mean lumen area. OCT at follow-up showed that 96.69% of the struts were covered and that malapposition of at least one strut, initially observed in 18 scaffolds was only detected at follow-up in 4 scaffolds. Mean neointimal growth measured by OCT between and on top of the polymeric struts amounted to  $1.34 \pm 0.67$  mm<sup>2</sup> with a mean and minimum flow area reduction of  $18.1 \pm 14.9\%$ ,  $23.4 \pm 18.8\%$ , respectively. Modified manufacturing processes of the polymer and

geometric changes in the polymeric platform have substantially improved the medium-term performance of this new generation of drug-eluting scaffold so that it has become comparable to current generation drug eluting stents.

The promising results at 6 and 12 months of this second-generation bioresorbable drug-eluting scaffold (ABSORB 1.1) constitute the proof of concept that this device can adequately revascularize coronary vessels and prevent restenosis. In the meantime, the ABSORB 1.1 is being tested in the extended registry of ABSORB EXTEND, which will enroll approximately 1,000 patients. The randomized trials comparing a metallic everolimus eluting stents with drug-eluting bioresorbable scaffolds was initiated in Europe in 2011, which will be followed in 2012 by the pivotal trials in Japan and the United states.

### Elixir

Elixir has multiple pharmaceutical agents in its drug product portfolio. Elixir developed Novolimus, a novel mTOR inhibitor macrocyclic lactone, with antiproliferative and anti-inflammatory properties, for drug eluting stent applications. Elixir has an exclusive worldwide license for use of Myolimus in fully biodegradable stents. Myolimus is a novel mTOR inhibitor macrocyclic lactone with a broad therapeutic index and an excellent stability profile that makes it desirable for BDES applications (Fig. 3). Pre-clinical studies were performed to evaluate the biological response, pharmacokinetics and bioresorption profile of the BRS in a porcine coronary artery model. Upon successful completion of these studies, Elixir started to evaluate the BRS in a FIM trial [58]. So far, 15 patients have been enrolled from Europe and New Zealand in the DESsolve trial and the 6-month angiographic follow-up is expected to be complete in the first half of 2012.

### Future perspectives

Clinical advantages of BRS technology over the currently available drug eluting stents need to be investigated further. ABSORB and Mg stents showed the recovery of responsiveness of the treated vessel to vasoactive agents such as nitroglycerin. The restoration of vasomotion can indirectly stand for the completeness of vessel healing, however, it is still unclear what the real impact of this phenomenon on clinical outcomes is. A number of studies using metallic DES have reported the abnormal vasomotion in the distal segment to the DES. Some consider that this abnormality might restrict the distal flow and therefore predispose to the occurrence of late stent thrombosis,

however, the clinical consequences of these findings are still not clear [59]. In patients with early atherosclerosis, the presence of abnormal endothelial function was associated with poor outcomes or more frequent angina [60–63].

To elucidate these issues further, larger studies with specific endpoints such as anginal status, functional exercise testing or flow reserve (FFR) [64–66], radioisotopic investigation flow and myocardial metabolism may be necessary. Similarly, the feasibility that MSCT/MRI has shown in the initial clinical trials, in terms of comparability with other modalities, needs to be further investigated [67].

Another point of discussion that could be raised is to whether the metallic stents with thin struts covered by a thin biodegradable polymer or metallic drug-eluting stents without polymer can succeed in minimizing stent thrombosis. So far the evidence shows that late stent thrombosis can occur with BMS [68, 69]. Considering the deadly consequence of stent thrombosis, we should aim at eradicating this complication, and BRS technology theoretically seems closer in achieving this goal, in addition to the elimination of the deleterious caging effect of the permanent metallic endoluminal prosthesis.

One of expectations with the bioresorbable scaffold might be shortening of dual antiplatelet therapy with eventual reduction of bleeding. After complete resorption of the biodegradable material, there is no need for dual platelet therapy to prevent thrombosis. Short dual antiplatelet therapy less than 6 months therefore might be theoretically feasible for the biodegradable scaffolds with short degradation time, such as magnesium stent. On the other hands, PLLA—the most frequently used polymer to make bioresorbable scaffold—has a long duration of biodegradation of approximately 2 years. For bioresorbable scaffolds made of PLLA, tissue coverage according to optical coherence tomography can be used to judge the cessation of the dual antiplatelet therapy, since the coverage of polymeric strut should be easier with polymeric struts than metallic struts due to absence of high intensity artifact resulting from the reflection of light by metal.

A potential drawback or “new enemy” of this new technology is strut fracture. Unlike metallic stents, the polymeric devices have inherent limit of expansion and can break as a result of over-dilatation. In an anecdotal case from the ABSORB cohort A, a 3.0 mm scaffold was over-expanded with 3.5 mm balloon, which resulted in strut fracture as documented with OCT [54]. Due to the recurrence of limited anginal symptoms, this patient underwent TLR despite an angiographically non-significant stenosis by QCA (%DS of 42%). The clinical significance of such a case, only evidenced by OCT, needs to be further elucidated, although initial studies suggests that actual clinical events related to this phenomenon are rare [57, 70].

## Conclusion

The currently available metallic drug eluting stents have demonstrated their ability to provide a permanent scaffolding and to prevent restenosis; however, legitimate safety concerns have emerged. These concerns have also provided the impetus for the development of stents which only provide a temporary scaffold—bioresorbable scaffolds. Freeing the vessel wall from rigid caging has certain physiological advantages. Currently this technology is still in its infancy, however, the initial clinical results are promising. This therapy is an exciting development, and certainly worthy of the accolade of being the revolution in interventional cardiology.

## References

1. Serruys PW, Daemen J. Are drug-eluting stents associated with a higher rate of late thrombosis than bare metal stents? Late stent thrombosis: a nuisance in both bare metal and drug-eluting stents. *Circulation*. 2007;115:1433–9. discussion 1439.
2. Sousa JE, Costa MA, Abizaid A, Abizaid AS, Feres F, Pinto IM, Seixas AC, Staico R, Mattos LA, Sousa AG, Falotico R, Jaeger J, Popma JJ, Serruys PW. Lack of neointimal proliferation after implantation of sirolimus-coated stents in human coronary arteries: a quantitative coronary angiography and three-dimensional intravascular ultrasound study. *Circulation*. 2001;103:192–5.
3. Rensing BJ, Vos J, Smits PC, Foley DP, van den Brand MJ, van der Giessen WJ, de Feijter PJ, Serruys PW. Coronary restenosis elimination with a sirolimus eluting stent: first European human experience with 6-month angiographic and intravascular ultrasound follow-up. *Eur Heart J*. 2001;22:2125–30.
4. Sousa JE, Costa MA, Abizaid AC, Rensing BJ, Abizaid AS, Tanajura LF, Kozuma K, Van Langenhove G, Sousa AG, Falotico R, Jaeger J, Popma JJ, Serruys PW. Sustained suppression of neointimal proliferation by sirolimus-eluting stents: one-year angiographic and intravascular ultrasound follow-up. *Circulation*. 2001;104:2007–11.
5. Morice MC, Serruys PW, Sousa JE, Fajadet J, Ban Hayashi E, Perin M, Colombo A, Schuler G, Barragan P, Guagliumi G, Molnar F, Falotico R. A randomized comparison of a sirolimus-eluting stent with a standard stent for coronary revascularization. *N Engl J Med*. 2002;346:1773–80.
6. Finn AV, Joner M, Nakazawa G, Kolodgie F, Newell J, John MC, Gold HK, Virmani R. Pathological correlates of late drug-eluting stent thrombosis: strut coverage as a marker of endothelialization. *Circulation*. 2007;115:2435–41.
7. Joner M, Finn AV, Farb A, Mont EK, Kolodgie FD, Ladich E, Kutys R, Skorija K, Gold HK, Virmani R. Pathology of drug-eluting stents in humans: delayed healing and late thrombotic risk. *J Am Coll Cardiol*. 2006;48:193–202.
8. Cook S, Ladich E, Nakazawa G, Eshetehardi P, Neidhart M, Vogel R, Togni M, Wenaweser P, Billinger M, Seiler C, Gay S, Meier B, Pichler WJ, Juni P, Virmani R, Windecker S. Correlation of intravascular ultrasound findings with histopathological analysis of thrombus aspirates in patients with very late drug-eluting stent thrombosis. *Circulation*. 2009;120:391–9.
9. Hofma SH, van der Giessen WJ, van Dalen BM, Lemos PA, McFadden EP, Sianos G, Ligthart JM, van Essen D, de Feyter PJ, Serruys PW. Indication of long-term endothelial dysfunction after sirolimus-eluting stent implantation. *Eur Heart J*. 2006;27:166–70.
10. Togni M, Windecker S, Cocchia R, Wenaweser P, Cook S, Billinger M, Meier B, Hess OM. Sirolimus-eluting stents associated with paradoxical coronary vasoconstriction. *J Am Coll Cardiol*. 2005;46:231–6.
11. Serruys PW, Morice MC, Kappetein AP, Colombo A, Holmes DR, Mack MJ, Stahle E, Feldman TE, van den Brand M, Bass EJ, Van Dyck N, Leadley K, Dawkins KD, Mohr FW. Percutaneous coronary intervention versus coronary-artery bypass grafting for severe coronary artery disease. *N Engl J Med*. 2009;360:961–72.
12. Spuentrup E, Ruebben A, Mahnken A, Stuber M, Kolker C, Nguyen TH, Gunther RW, Buecker A. Artifact-free coronary magnetic resonance angiography and coronary vessel wall imaging in the presence of a new, metallic, coronary magnetic resonance imaging stent. *Circulation*. 2005;111:1019–26.
13. Ormiston JA, Serruys PW. Bioabsorbable coronary stents. *Circ Cardiovasc Interv*. 2009;2:255–60.
14. Kohsaka S, Kimura T, Goto M, Lee VV, Elayda M, Furukawa Y, Fukushima M, Komeda M, Sakata R, Willerson JT, Wilson JM, Kita T. Difference in patient profiles and outcomes in Japanese versus American patients undergoing coronary revascularization (collaborative study by credo-kyoto and the texas heart institute research database). *Am J Cardiol*. 2010;105:1698–704.
15. Network Jot. Number of organ transplantation after brain death; 2011. [http://www.jotnw.or.jp/datafile/offer\\_brain.html](http://www.jotnw.or.jp/datafile/offer_brain.html).
16. Wentzel JJ, Whelan DM, van der Giessen WJ, van Beusekom HM, Andhyiswara I, Serruys PW, Slager CJ, Krams R. Coronary stent implantation changes 3-d vessel geometry and 3-d shear stress distribution. *J Biomech*. 2000;33:1287–95.
17. Gyongyosi M, Yang P, Khorsand A, Glogar D. Longitudinal straightening effect of stents is an additional predictor for major adverse cardiac events. Austrian wiktör stent study group and European paragon stent investigators. *J Am Coll Cardiol*. 2000;35:1580–9.
18. Gomez-Lara J, Brugaletta S, Diletti R, Garg S, Onuma Y, Gogas BD, van Geuns RJ, Dorange C, Veldhof S, Rapoza R, Whitbourn R, Windecker S, Garcia-Garcia HM, Regar E, Serruys PW. A comparative assessment by optical coherence tomography of the performance of the first and second generation of the everolimus-eluting bioresorbable vascular scaffolds. *Eur Heart J*. 2011;32:294–304.
19. Gomez-Lara J, Garcia-Garcia HM, Onuma Y, Garg S, Regar E, De Bruyne B, Windecker S, McClean D, Thuesen L, Dudek D, Koolen J, Whitbourn R, Smits PC, Chevalier B, Dorange C, Veldhof S, Morel MA, de Vries T, Ormiston JA, Serruys PW. A comparison of the conformability of everolimus-eluting bioresorbable vascular scaffolds to metal platform coronary stents. *JACC Cardiovasc Interv*. 2010;3:1190–8.
20. Thury A, Wentzel JJ, Vinke RV, Gijssen FJ, Schuurbiens JC, Krams R, de Feyter PJ, Serruys PW, Slager CJ. Images in cardiovascular medicine. Focal in-stent restenosis near step-up: roles of low and oscillating shear stress? *Circulation*. 2002;105:e185–7.
21. Cheng C, Tempel D, Oostlander A, Helderman F, Gijssen F, Wentzel J, van Haperen R, Huitsma DB, Serruys PW, van der Steen AF, de Crom R, Krams R. Rapamycin modulates the enos vs. Shear stress relationship. *Cardiovasc Res*. 2008;78:123–9.
22. Serruys PW, Ormiston JA, Onuma Y, Regar E, Gonzalo N, Garcia-Garcia HM, Nieman K, Bruining N, Dorange C, Miquel-Hebert K, Veldhof S, Webster M, Thuesen L, Dudek D. A bioabsorbable everolimus-eluting coronary stent system (absorb): 2-year outcomes and results from multiple imaging methods. *Lancet*. 2009;373:897–910.
23. Ciccone WJ 2nd, Motz C, Bentley C, Tasto JP. Bioabsorbable implants in orthopaedics: new developments and clinical applications. *J Am Acad Orthop Surg*. 2001;9:280–8.

24. Resnick N, Yahav H, Shay-Salit A, Shushy M, Schubert S, Zilberman LC, Wofowitz E. Fluid shear stress and the vascular endothelium: for better and for worse. *Prog Biophys Mol Biol.* 2003;81:177–99.
25. Slager CJ, Wentzel JJ, Gijzen FJ, Schuurbers JC, van der Wal AC, van der Steen AF, Serruys PW. The role of shear stress in the generation of rupture-prone vulnerable plaques. *Nat Clin Pract Cardiovasc Med.* 2005;2:401–7.
26. Ormiston JA, Serruys PW, Regar E, Dudek D, Thuesen L, Webster MW, Onuma Y, Garcia-Garcia HM, McGreevy R, Veldhof S. A bioabsorbable everolimus-eluting coronary stent system for patients with single de novo coronary artery lesions (absorb): a prospective open-label trial. *Lancet.* 2008;371:899–907.
27. Serruys PW, Onuma Y, Dudek D, Smits PC, Koolen J, Chevalier B, Bruyne Bd, Thuesen L, McClean D, Geuns R-Jv, Windecker S, Whitbourn R, Meredith I, Dorange C, Veldhof S, Hebert KM, Sudhir K, Garcia-Garcia HM, Ormiston JA. Evaluation of the second generation of a bioresorbable everolimus-eluting vascular scaffold for the treatment of de novo coronary artery stenosis: 12-month clinical and imaging outcomes. *J Am Coll Cardiol.* 2011;58(15):1578–88.
28. Alberts B, Johnson A, Lewis J, Raff M, Roberts K, Walter P. Molecular biology of the cell. Garland Science, New York; 2002.
29. Cheng C, Noordeloos AM, Jeney V, Soares MP, Moll F, Pasterkamp G, Serruys PW, Duckers HJ. Heme oxygenase 1 determines atherosclerotic lesion progression into a vulnerable plaque. *Circulation.* 2009;119:3017–27.
30. Mueller MA, Beutner F, Teupser D, Ceglarek U, Thiery J. Prevention of atherosclerosis by the mtor inhibitor everolimus in ldlr<sup>-/-</sup> mice despite severe hypercholesterolemia. *Atherosclerosis.* 2008;198:39–48.
31. Lehoux S, Tedgui A. Cellular mechanics and gene expression in blood vessels. *J Biomech.* 2003;36:631–43.
32. Tamai H, Igaki K, Kyo E, Kosuga K, Kawashima A, Matsui S, Komori H, Tsuji T, Motohara S, Uehata H. Initial and 6-month results of biodegradable poly-L-lactic acid coronary stents in humans. *Circulation.* 2000;102:399–404.
33. Tsuji T, Tamai H, Igaki K, Hsu Y-S, Kosuga K, Hata T, OKada M, Nakamura T, Fujita S. Four-year follow-up of the biodegradable stent (Igaki-Tamai stent). *Circ J.* 2004;68:135.
34. Nishio S. Long-term (>10 years) clinical outcomes of first-in-man biodegradable poly-L-lactic acid coronary stents. In: *Euro-PCR; 2010.*
35. Post MJ, de Graaf-Bos AN, van Zanten HG, de Groot PG, Sixma JJ, Borst C. Thrombogenicity of the human arterial wall after interventional thermal injury. *J Vasc Res.* 1996;33:156–63.
36. Biamino G, Schmidt A, Scheinert D. Treatment of sfa lesions with plla biodegradable stents: results of the perseus study. *J Endovasc Ther.* 2005;12:5.
37. Yamawaki T, Shimokawa H, Kozai T, Miyata K, Higo T, Tanaka E, Egashira K, Shiraishi T, Tamai H, Igaki K, Takeshita A. Intramural delivery of a specific tyrosine kinase inhibitor with biodegradable stent suppresses the restenotic changes of the coronary artery in pigs in vivo. *J Am Coll Cardiol.* 1998;32:780–6.
38. Erbel R, Di Mario C, Bartunek J, Bonnier J, de Bruyne B, Eberli FR, Erne P, Haude M, Heublein B, Horrigan M, Ilesley C, Bose D, Koolen J, Luscher TF, Weissman N, Waksman R. Temporary scaffolding of coronary arteries with bioabsorbable magnesium stents: a prospective, non-randomised multicentre trial. *Lancet.* 2007;369:1869–75.
39. Heublein B, Rohde R, Kaese V, Niemeyer M, Hartung W, Haverich A. Biocorrosion of magnesium alloys: a new principle in cardiovascular implant technology? *Heart.* 2003;89:651–6.
40. Waksman R, Pakala R, Kuchulakanti PK, Baffour R, Hellinga D, Seabron R, Tio FO, Wittchow E, Hartwig S, Harder C, Rohde R, Heublein B, Andrae A, Waldmann KH, Haverich A. Safety and efficacy of bioabsorbable magnesium alloy stents in porcine coronary arteries. *Catheter Cardiovasc Interv.* 2006;68:607–17. discussion 618–9.
41. Peeters P, Bosiers M, Verbiest J, Deloese K, Heublein B. Preliminary results after application of absorbable metal stents in patients with critical limb ischemia. *J Endovasc Ther.* 2005;12:1–5.
42. Waksman R, Erbel R, Di Mario C, Bartunek J, de Bruyne B, Eberli FR, Erne P, Haude M, Horrigan M, Ilesley C, Bose D, Bonnier H, Koolen J, Luscher TF, Weissman NJ. Early- and long-term intravascular ultrasound and angiographic findings after bioabsorbable magnesium stent implantation in human coronary arteries. *JACC Cardiovasc Interv.* 2009;2:312–20.
43. Eggebrecht H, Rodermann J, Hunold P, Schmermund A, Bose D, Haude M, Erbel R. Images in cardiovascular medicine. Novel magnetic resonance-compatible coronary stent: the absorbable magnesium-alloy stent. *Circulation.* 2005;112:e303–4.
44. Ghimire G, Spiro J, Kharbada R, Roughton M, Barlis P, Mason M, Ilesley C, Di Mario C, Erbel R, Waksman R, Dalby M. Initial evidence for the return of coronary vasoreactivity following the absorption of bioabsorbable magnesium alloy coronary stents. *EuroIntervention.* 2009;4:481–4.
45. Bosiers M, Peeters P, D'Archambeau O, Hendriks J, Pilger E, Duber C, Zeller T, Gussmann A, Lohle PN, Minar E, Scheinert D, Hausegger K, Schulte KL, Verbiest J, Deloese K, Lammer J. Ams insight-absorbable metal stent implantation for treatment of below-the-knee critical limb ischemia: 6-month analysis. *Cardiovasc Intervent Radiol.* 2009;32:424–35.
46. Schulze R. Reva medical, inc. Bioresorbable stent. *Cardiovascular Revascularization Therapies* 2007. 2007.
47. Schultz R. Reva medical, inc. Bioresorbable technology. CRT; 2006.
48. Grube E. Bioabsorbable stent. The Boston scientific and reva technology. In: *EuroPCR 2009.* 2009.
49. Ormiston JA, Webster MW, Armstrong G. First-in-human implantation of a fully bioabsorbable drug-eluting stent: The ABSORB poly-L-lactic acid everolimus-eluting coronary stent. *Catheter Cardiovasc Interv.* 2007;69:128–31.
50. Bruining N, Tanimoto S, Otsuka M, Weustink A, Lighthart J, Winter Sd, Miegheem Cv, Nieman K, Feijter PJD, Domburg RTv, Serruys PW. Quantitative multi-modality imaging analysis of a bioabsorbable poly-L-lactic acid stent design in the acute phase: a comparison between 2- and 3D-QCA, QCU and QMSCT-CA. *EuroInterv.* 2008;4:1–7.
51. Garcia-Garcia HM, Gonzalo N, Pawar R, Kukreja N, Dudek D, Thuesen L, Ormiston JA, Regar E, Serruys PW. Assessment of the absorption process following bioabsorbable everolimus-eluting stent implantation: temporal changes in strain values and tissue composition using intravascular ultrasound radiofrequency data analysis. A substudy of the absorb clinical trial. *EuroIntervention.* 2008;4:443–8.
52. Tanimoto S, Bruining N, van Domburg RT, Rotger D, Radeva P, Lighthart JM, Serruys PW. Late stent recoil of the bioabsorbable everolimus-eluting coronary stent and its relationship with plaque morphology. *J Am Coll Cardiol.* 2008;52:1616–20.
53. Tanimoto S, Serruys PW, Thuesen L, Dudek D, de Bruyne B, Chevalier B, Ormiston JA. Comparison of in vivo acute stent recoil between the bioabsorbable everolimus-eluting coronary stent and the everolimus-eluting cobalt chromium coronary stent: insights from the absorb and spirit trials. *Cathet Cardiovasc Interv.* 2007;70(4):515–23.
54. Onuma Y, Serruys P, Ormiston J, Regar E, Webster M, Thuesen L, Dudek D, Veldhof S, Rapozo R. Three-year results of clinical follow-up after a bioresorbable everolimus-eluting scaffold in patients with de novo coronary artery disease: The absorb trial. *EuroIntervention.* 2010;6(4):447–53.

55. Cutlip DE, Windecker S, Mehran R, Boam A, Cohen DJ, van Es GA, Steg PG, Morel MA, Mauri L, Vranckx P, McFadden E, Lansky A, Hamon M, Krucoff MW, Serruys PW. Clinical end points in coronary stent trials: a case for standardized definitions. *Circulation*. 2007;115:2344–51.
56. Okamura T, Garg S, Gutiérrez-Chico J, Shin E, Onuma Y, García-García H, Rapoza R, Sudhir K, Regar E, Serruys P. In vivo evaluation of stent strut distribution patterns in the bio-absorbable everolimus-eluting device: an oct ad hoc analysis of the revision 1.0 and revision 1.1 stent design in the absorb clinical trial. *EuroIntervention*. 2010;5:932–38.
57. Serruys PW, Onuma Y, Ormiston JA, Bruyne Bd, Regar E, Dudek D, Thuesen L, Smits PC, Chevalier B, McClean D, Koolen J, Windecker S, Whitbourn R, Meredith I, Dorange C, Veldhof S, Hebert KM, Rapoza R, García-García HM. Evaluation of the second generation of a bioresorbable everolimus drug-eluting vascular scaffold for treatment of de novo coronary artery stenosis: 6-month clinical and imaging outcomes. *Circulation*. 2010;122(22):2301–12.
58. Yan J, Bhat VD. Elixir medical's bioresorbable drug eluting stent (bdes) programme: an overview. *EuroIntervention*. 2009;5:F80–2.
59. Pendyala LK, Yin X, Li J, Chen JP, Chronos N, Hou D. The first-generation drug-eluting stents and coronary endothelial dysfunction. *JACC Cardiovasc Interv*. 2009;2:1169–77.
60. Halcox JP, Schenke WH, Zalos G, Mincemoyer R, Prasad A, Waclawiw MA, Nour KR, Quyyumi AA. Prognostic value of coronary vascular endothelial dysfunction. *Circulation*. 2002;106:653–8.
61. Suwaidi JA, Hamasaki S, Higano ST, Nishimura RA, Holmes DR Jr, Lerman A. Long-term follow-up of patients with mild coronary artery disease and endothelial dysfunction. *Circulation*. 2000;101:948–54.
62. Beltrame JF, Sasayama S, Maseri A. Racial heterogeneity in coronary artery vasomotor reactivity: differences between Japanese and Caucasian patients. *J Am Coll Cardiol*. 1999;33:1442–52.
63. Shimokawa H. Cellular and molecular mechanisms of coronary artery spasm: lessons from animal models. *Jpn Circ J*. 2000;64:1–12.
64. Egashira K, Inou T, Hirooka Y, Yamada A, Urabe Y, Takeshita A. Evidence of impaired endothelium-dependent coronary vasodilatation in patients with angina pectoris and normal coronary angiograms. *N Engl J Med*. 1993;328:1659–64.
65. Doucette JW, Corl PD, Payne HM, Flynn AE, Goto M, Nassi M, Segal J. Validation of a doppler guide wire for intravascular measurement of coronary artery flow velocity. *Circulation*. 1992;85:1899–911.
66. Serruys PW, Zijlstra F, Laarman GJ, Reiber HH, Beatt K, Roelandt J. A comparison of two methods to measure coronary flow reserve in the setting of coronary angioplasty: intracoronary blood flow velocity measurements with a doppler catheter, and digital subtraction cineangiography. *Eur Heart J*. 1989;10:725–36.
67. Bruining N, Tanimoto S, Otsuka M, Weustink A, Ligthart J, de Winter S, van Mieghem C, Nieman K, de Feyter PJ, van Domburg RT, Serruys PW. Quantitative multi-modality imaging analysis of a bioabsorbable poly-L-lactic acid stent design in the acute phase: a comparison between 2- and 3D-QCA, QCU and QMSCT-CA. *EuroIntervention*. 2008;4:285–91.
68. Daemen J, Wenaweser P, Tsuchida K, Abrecht L, Vaina S, Morger C, Kukreja N, Juni P, Sianos G, Hellige G, van Domburg RT, Hess OM, Boersma E, Meier B, Windecker S, Serruys PW. Early and late coronary stent thrombosis of sirolimus-eluting and paclitaxel-eluting stents in routine clinical practice: data from a large two-institutional cohort study. *Lancet*. 2007;369:667–78.
69. Stettler C, Wandel S, Allemann S, Kastrati A, Morice MC, Schomig A, Pfisterer ME, Stone GW, Leon MB, de Lezo JS, Goy JJ, Park SJ, Sabate M, Suttrop MJ, Kelbaek H, Spaulding C, Menichelli M, Vermeersch P, Dirksen MT, Cervinka P, Petronio AS, Nordmann AJ, Diem P, Meier B, Zwahlen M, Reichenbach S, Trelle S, Windecker S, Juni P. Outcomes associated with drug-eluting and bare-metal stents: a collaborative network meta-analysis. *Lancet*. 2007;370:937–48.
70. Serruys PW, Onuma Y, Dudek D, Smits PC, Koolen J, Chevalier B, de Bruyne B, Thuesen L, McClean D, van Geuns RJ, Windecker S, Whitbourn R, Meredith I, Dorange C, Veldhof S, Hebert KM, Sudhir K, Garcia-Garcia HM, Ormiston JA. Evaluation of the second generation of a bioresorbable everolimus-eluting vascular scaffold for the treatment of de novo coronary artery stenosis: 12-month clinical and imaging outcomes. *J Am Coll Cardiol*. 2011;58:1578–88.
71. Hahn C, Schwartz MA. Mechanotransduction in vascular physiology and atherogenesis. *Natl Rev Mol Cell Biol*. 2009;10:53–62.
72. Gupta V, Grande-Allen KJ. Effects of static and cyclic loading in regulating extracellular matrix synthesis by cardiovascular cells. *Cardiovasc Res*. 2006;72:375–83.

# Summary and Conclusions





## SUMMARY AND CONCLUSIONS

The new enemy in the drug-eluting stent (DES) era - stent thrombosis (ST) - has accelerated a technological evolution in interventional cardiology. There is a fundamental difference in concept between the DES and the bioresorbable scaffold (BRS) technologies, with the latter having a capability of liberating the vessel from a permanent metallic cage. Therefore, the BRS technology has a theoretical advantage in reducing ST by means of endoluminal prosthesis elimination. BRS also facilitates the restoration of vasomotor function, which indirectly results in the completeness of vessel healing. The entire process of this treatment has been hence named as vascular reparative therapy (VRT).

One possible fate of coronary artery narrowing treated with the metallic stents is the development of in-stent neointimal tissue (even seen with DES), in which the antiproliferative drugs could slow down or postpone this phenomenon. Neointimal tissue may in turn become atherosclerotic, degenerate to vulnerable plaques, and finally rupture inside the cage of the stent (i.e. neoatherosclerosis). A metallic stent can also alter vessel geometry and biomechanics, which may also result in long-term flow disturbances and chronic irritation, in addition to the risk of late strut fractures, which potentially contribute to restenosis and adverse clinical events. From a physiological perspective, the absence of a rigid metallic cage facilitates the restoration of vasomotor function, adaptive shear stress, and late luminal enlargement. After bioresorption, there would be no triggers for thrombosis, such as uncovered struts or durable polymers. The absence of foreign materials may also reduce our concerns about future treatment options, such as precluding bypass-graft surgery, and the requirements for long-term dual antiplatelet therapy with a potential reduction in associated bleeding complications. In addition, it should be emphasized that this technology could be relevant to East Asian population (e.g. Japanese) who have different cultures from Western countries, in that they would not like to mutilate their natural bodies by medical devices or even surgical incisions that will remain in their lifetime. These are the main reasons why emergence of the BRS technology has been so-called “the 4<sup>th</sup> revolution in coronary interventions” that may have potential clinical advantages over the metallic stent technologies (chapter 1).

## METHOD TO ASSESS CORONARY ARTERY DISEASE AND BIORESORBABLE SCAFFOLDS

This chapter highlights the multimodality imaging assessment for the BRS, mainly focusing on the ABSORB everolimus-eluting bioresorbable vascular scaffold (BVS). A global overview of multimodality imaging assessment for the BRS is described in the chapter 2.1. As an exploratory investigation prior to the upcoming randomized controlled trial, we compared angiographic acute gain and late luminal loss as surrogates of device performance between the BVS and the XIENCE everolimus-eluting metallic stents (EES) in the matched population with a historical control (the ABSORB Cohort B trial and the SPIRIT II trial). This study showed a similar acute gain and in-scaffold/in-stent late luminal loss as well as clinical outcomes at 2 years between the two device groups, while the BVS group revealed a significantly lower minimal lumen diameter following the index procedure (2.02 vs. 2.22 mm,  $p=0.01$ ). These results should be confirmed in a European pivotal randomized controlled trial, namely the ABSORB II (chapter 2.2). We also reported high reproducibility of IVUS grey-scale and virtual histology (IVUS-VH) analyses in *ex-vivo* human coronary arteries with a new generation 45-MHz rotational catheter used in the ABSORB II trial (chapter 2.3). Palpography, which is also based on the IVUS technique, provides important information with respect to differential vessel wall strain after implantation of bioresorbable scaffolds. In addition to the IVUS-based differential echogenicity and OCT, this technique could also be used for monitoring of bioresorption process (chapter 2.4). It is clear that the advantages of light-based intracoronary imaging devices (i.e. OCT/OFDI) will be more pronounced when using the PLLA-based BRS (e.g. BVS) rather than the metallic prosthesis because light can penetrate through the PLLA scaffold and thus the light-based imaging techniques provide more detail depictions of whole scaffold structures as compared to IVUS. Using the OCT, we introduced an OCT-based definition of coronary “evaginations” that are frequently observed specifically in the first generation sirolimus-eluting metallic stents (chapter 2.5). Another promising imaging modality for the BVS is multislice computed tomography (MSCT). The PLLA scaffold has a unique feature with its radiolucency, so that non-invasive luminal assessment within the scaffolded segment is technically feasible. Using a dedicated software that automatically traces not only lumen but also vessel borders, we compared the coronary plaque evolution between the scaffolded segments and the non-intervened segments in the ABSORB Cohort A population. This study showed a significant benefit of the BVS in terms of change in percentage plaque volume that may reflect the possibility of coronary plaque stabilization

after the BVS implantation (-1.2% in the scaffolded segments vs. 2.7% in the non-intervened segments,  $p=0.03$ ) (chapter 2.6). Finally in this chapter, we demonstrated the longitudinal follow-up data after BVS implantation using aforementioned multimodality imaging approaches, confirming for the first time the significant reduction of plaque media over 3 years in the serial Cohort B study population (chapter 2.7).

### **ADVANCED IMAGING TECHNIQUES FOR THE ANATOMICAL AND FUNCTIONAL LESION ASSESSMENT**

Angiographic assessment of bifurcation lesion still remains to be a challenging field of research. We validated a dedicated three-dimensional quantitative coronary angiography (QCA) analysis algorithm using bifurcation phantom models (chapter 3.1) We also explored functional assessment of intermediate coronary lesions by applying computational fluid dynamics (CFD) algorithm with three-dimensional angiography in comparison with pressure wire-derived FFR as a gold standard method (chapter 3.2). As a next step for the future trials, comparisons between two-dimensional (2D) and three-dimensional (3D) bifurcation analyses in bifurcation lesions are described (chapter 3.3). In this study, minimal lumen diameter within bifurcation segment was similar between the two approaches, while percentage diameter stenosis was in general larger and lesion length was consistently shorter with 2D-QCA than 3D-QCA. Although 3D approach theoretically provides more accurate measurements by minimising potential foreshortening and vessel overlap as compared to 2D approach, further studies are needed to demonstrate clinical benefits in using 3D-QCA over 2D-QCA for the assessment of bifurcation lesions. Dynamic change in overhanging struts of the BRS in bifurcation would also be of great scientific interest. We demonstrated the changes in appearance by 3D-OCT, suggesting a potential benefit in terms of disappearance of jailed struts at the ostium of side branch by means of bioresorption of the metallic BRS, namely the DREAMS (chapter 3.4).

### **LIGHT-BASED IMAGING ASSESSMENT FOR STEMI PATIENTS**

STEMI patients have been a major target subset for PCI. Ultra high-resolution images obtained with light-based coronary imaging modalities (i.e. OCT/OFDI) have provided new insights into not only coronary atherosclerosis and stent apposition but also intracoronary thrombus observed in STEMI patients. A previous literature from the Thoraxcenter clearly indicated an impact of angiographic thrombus burden on late clinical outcomes of STEMI

patients. Methodology of volumetric assessment of thrombus by OCT/OFDI, however, has not been described. We thus demonstrated the methodology to assess the post-procedural in-stent thrombotic materials, what we called in-stent structure (ISS), and investigated the impact of sampling rates (i.e. minimal longitudinal distance between analyzed frames) on volumetric assessment of the ISS. Larger sampling rate may lead to overestimation of the ISS volume, we thus concluded that more detailed evaluation with smaller sampling rate should be considered when addressing the volume of thrombotic materials by OCT/OFDI as compared to the standard sampling rate of 1.0-mm (chapter 4.1). In addition, we demonstrated the feasibility of morphological assessment of thrombotic materials using 3D reconstruction of OFDI images (chapter 4.2). This may help our better understanding of distributions and extents of protruding thrombotic materials after stenting. The TROFI trial was a prospective, multicentre, randomised controlled trial assessing the efficacy of manual aspiration thrombectomy prior to stent implantation in STEMI patients. In the TROFI trial, we proposed a new surrogate endpoint - minimal flow area - assessed by OFDI. Thrombus aspiration group showed trend towards larger minimal flow area post-procedure despite the lack of statistical significance when compared to non-thrombus aspiration group. We also reported the results of serial OFDI follow-up at 6 months, showing a moderate positive association between the post-procedural ISS volume and neointima volume at the follow-up ( $r=0.41$ ,  $p=0.004$ ) (chapter 4.3). After we tested the safety of the Absorb BVS for acute myocardial infarction (STEMI and NSTEMI) patients in our preliminary data (chapter 4.4), clinical application of the Absorb BVS has been extended to STEMI patients. Finally in this chapter, we demonstrated for the first time an excellent short-term (30 days) clinical outcome of STEMI patients treated with the BVS in a real-world clinical setting. This BVS STEMI first study may support to justify the use of the BVS for STEMI patients by the fact that neither target lesion failure or scaffold thrombosis was observed (chapter 4.5).

#### **LESSONS LEARNED FROM EARLY BVS STUDIES AND CLINICAL IMPLICATIONS FOR COMPLEX SUBSETS**

In the early BVS studies, several technical failure and adverse events were documented. We had to learn the potential reasons and then share such cases with the other interventional communities specifically in the early phase of the BRS technology. We thus summarised the cases who experienced subacute/late scaffold thrombosis or scaffold dislodgement (chapter 5.1), and restenosis (chapter 5.2) following BVS implantation. Based

on a different mechanical property of polylactide from that of metal, specific technical considerations should also be given for BVS implantation in order to avoid acute scaffold disruption and the potential risk of periprocedural adverse events. We also highlighted late structural discontinuities observed in serial OCT investigations (chapter 5.3). These findings seemed to be interesting and very unique to the BRS technology as the former is considered as malignant and the latter as a benign phenomenon related to the bioresorption process.

Even in the DES era, diabetic patients still remain to be a high-risk subset for PCI. Using the historical controls from the SPIRIT trials (the first, II, III and IV), we reported similar 1-year clinical outcomes in diabetic patients treated with the BVS compared to those with metallic EES after matching with their propensity scores from different populations (chapter 5.4). Given thicker struts of the BVS than that of the metallic EES, the BVS might be associated with a higher risk of side branch occlusion (SBO) and subsequent periprocedural MI. We thus reported a significantly higher risk of SBO in the BVS group than in the EES group, while there were no significant differences in the incidence of periprocedural MI because in this study only small side branches with a vessel size of <0.5 mm were associated with significantly higher incidence of post-procedural occlusion in the BVS group, suggesting minimal impact of SBO after BVS implantation on short-term clinical outcomes (chapter 5.6). Using cardiac enzymes analysed by a central laboratory in the randomized Absorb II trial, we confirmed that there were no statistically significant differences in either the incidence of cardiac enzyme rise or peri-procedural MI between the BVS and the EES. Overlapping scaffolds or stents were shown to be a precipitating factor of myocardial injury (chapter 5.7). In this study, we also emphasized that binary definition of peri-procedural MI is not only dependent on the selection of cardiac enzymes (i.e. CK, CK-MB, or cardiac troponin) but also on their thresholds that have been arbitrarily chosen even in the universal definitions. Another fascinating potential of BRS technology would be passivation and ultimately stabilisation of high-risk plaques. Possibilities of early detection of high-risk plaques by multimodality imaging techniques and subsequent invasive passivation by BRS technologies were extensively reviewed (chapter 5.8).

## **CONCLUSIONS**

Since the BRS technologies have only been evaluated in limited patients mainly with non-complex lesions, the feasibility of these devices in complex lesions requires further clinical evaluations. In addition, the optimal design of scaffolds, polymers, antiproliferative drugs and their degradation/release kinetics are still under investigation. Although future investigations are required to establish if the BRS technology is superior to permanent metallic DES, we hope that this thesis has given some implications for on-going or future studies to prove the efficacy of the BRS technologies and to improve clinical outcomes of our patients.

*March 2015,  
Takashi Muramatsu*

# Samenvatting en Conclusies





## SAMENVATTING EN CONCLUSIES

De nieuwe vijand in het tijdperk van de medicijn-afgeevende stent (DES) - stent trombose (ST) - heeft de technologische evolutie in interventionele cardiologie versneld. Er is een fundamenteel verschil in concept tussen de DES en de bioresorbabele scaffold (BRS)-technologieën, waarbij de laatstgenoemde het mogelijk maken om het bloedvat van een permanente metalen kooi te bevrijden. Daarom heeft de BRS-technologie een theoretisch voordeel bij de vermindering van ST door de endoluminale prothese te elimineren. BRS bevordert ook het herstel van een vasomotorische functie, die indirect tot de volledige genezing van een bloedvat leidt. Vandaar dat het hele proces van deze behandeling vasculaire herstelbehandeling genoemd wordt.

Een mogelijke consequentie bij het behandelen van vernauwde kransslagaders met metalen stents is de groei van neointima-weefsel in de stent (zelfs met DES waargenomen), dat het antiproliferatieve geneesmiddel kan vertragen of uitstellen. Dit neointima-weefsel kan vervolgens atherosclerotisch worden, tot een kwetsbare plaque degenereren, en op den duur binnen de kooi van de stent breuken veroorzaken (i.e. neoatherosclerosis). Een stijve metalen stent kan ook de geometrie en biomechanica van een bloedvat veranderen, wat op lange termijn bloedstroom-verstoringen en chronische irritatie kan veroorzaken, naast het risico van late strut-discontinuïteit, die mogelijk kunnen bijdragen aan restenose en klinische bijwerkingen. Vanuit fysiologisch oogpunt bevordert de afwezigheid van een stijve metalen kooi het herstel van de vasomotorische functie, adaptieve shear stress, en late lumen-uitbreiding. Na de bioresorptie zouden er geen triggers zijn voor trombose, zoals ongedekte struts of duurzame polymeren. De afwezigheid van de lichaamsvreemde materialen kunnen tevens de zorgen over toekomstige behandelingsopties verminderen, bijvoorbeeld een anders onmogelijke bypassoperatie. Ook kunnen de vereisten voor langdurige duale antiplaatjetherapie daardoor verminderen met als neveneffect een potentiële vermindering van de hiermee geassocieerde bloedingscomplicaties. Bovendien moet er benadrukt worden dat deze technologie mogelijk relevant is voor Oost-Aziaten (e.g. Japanners) met een andere cultuur dan Westerlingen, in die zin dat ze geneigd zijn om hun lichaam een chirurgische operatie te besparen, laat staan chirurgische incisies te ondergaan die permanente, levenslange littekens achterlaten. Dit zijn de hoofdredenen

waarom de opkomst van de BRS “the 4<sup>th</sup> revolution in coronary interventions” is genoemd, die potentiële voordelen kan hebben boven de metalen stent-technologieën (hoofdstuk 1).

## **ONDERZOEKSMETHODE VAN CORONAIRE HARTZIEKTE EN BIORESORBEERBARE SCAFFOLDS**

Dit hoofdstuk legt de nadruk op het multimodale beeldvormende onderzoek van de BRS, dat vooral gericht is op de ABSORB everolimus-afgeevende bioresorbeerbare vasculaire scaffold (BVS). Een globaal overzicht van het multimodale beeldvormende onderzoek van de BRS wordt gegeven in hoofdstuk 2.1. In een verkennend onderzoek voorafgaand aan de gerandomiseerde gecontroleerde trial, hebben wij angiografische acute winst en laat lumen-verlies vergeleken als surrogate eindpunten van de prestatie tussen de BVS en de XIENCE everolimus-afgeevende metalen stents (EES) in de gematchte populatie met een historische controlegroep (ABSORB Cohort B en SPIRIT II trials). Deze studie toonde een vergelijkbare acute winst en in-scaffold/stent laat lumen-verlies alsmede klinische resultaten na 2 jaar in de BVS- en EES groep, maar tegelijkertijd heeft de BVS-groep een significant kleinere minimale lumen-diameter aangetoond volgens de index-procedure (2.02 vs. 2.22 mm,  $p=0.01$ ). Deze resultaten moeten in een Europese gerandomiseerde gecontroleerde pivotal trial bevestigd worden, te weten de ABSORB II (hoofdstuk 2.2). We hebben tevens hoge reproduceerbaarheid gerapporteerd van “IVUS grayscale” en virtuele histologie (IVUS-VH) analyses in ex-vivo menselijke kransslagaders met een nieuwe generatie 45-MHz roterende katheter die in de ABSORB II trial gebruikt werd (hoofdstuk 2.3). Palpografie, dat ook gebaseerd is op IVUS-techniek, levert belangrijke informatie met betrekking tot het verschil in spanning van de bloedvatwanden na implantatie van bioresorbeerbare scaffolds. In aanvulling op de op IVUS-gebaseerde differentiële echogeniciteit en OCT, kan deze techniek ook voor het monitoren van het bioresorptieproces toegepast worden (hoofdstuk 2.4). Het is duidelijk dat de op licht gebaseerde intracoronaire beeldvormingsapparaten (i.e. OCT/OFDI) meer uitgesproken voordelen zullen hebben bij het gebruiken van de PLLA BRS (e.g. BVS) dan van de metalen stents, omdat de op licht gebaseerde beeldvorming meer gedetailleerde afbeeldingen biedt van hele scaffold-structuur wegens lichtdoorlatendheid door de PLLA scaffold ten opzichte van IVUS. Met behulp van OCT, hebben we de op OCT-gebaseerde definities van coronaire evaginaties vastgesteld, die vooral vaak voorkomen in de eerste generatie sirolimus-afgeevende metalen stents (hoofdstuk 2.5). Een andere veelbelovende

beeldvormingsmodaliteit voor de BVS is multislice computer tomografie (MSCT). Een unieke eigenschap van de PLLA-scaffold is zijn radiolucentie, zodat het technisch haalbaar is om lumen binnen het gescaffolde segment niet-invasief te beoordelen. Door middel van een speciale software die niet alleen lumen automatisch opspoorde maar ook vaatgrenzen, hebben we de coronaire plaque-ontwikkeling vergeleken tussen de gescaffolde segmenten en niet-behandelde segmenten in de ABSORB Cohort A populatie. Deze studie heeft een significant voordeel van de BVS aangetoond in termen van verandering in “plaque burden”, dat een coronaire plaque-stabilisatie na de BVS-implantatie kan betekenen (hoofdstuk 2.6). Ten slotte presenteren we in dit hoofdstuk de longitudinale follow-up data na BVS-implantatie met behulp van de bovengenoemde multimodale beeldvorming, die voor het eerst de significante vermindering van plaque media bevestigden na 3 jaar in de first-in-man studie cohort (hoofdstuk 2.7).

## **GEAVANCEERDE BEELDFORMINGSTECHNIEKEN VOOR DE ANATOMISCHE EN FUNCTIONELE BEOORDELING VAN LAESIES**

Angiografische beoordeling van bifurcatie-laesie blijft nog steeds een uitdagend onderzoeksgebied. We hebben een speciaal algoritme gevalideerd om driedimensionale kwantitatieve coronaire angiografie (QCA) te analyseren met bifurcatie-fantoommodellen (hoofdstuk 3.1). Tevens verkenden we de functionele beoordeling van middelmatige coronaire laesies door het toepassen van een computational fluid dynamics algoritme met driedimensionale angiografie in vergelijking met een pressure wire-derived FFR (hoofdstuk 3.2). Als een volgende stap voor toekomstige trials, zijn vergelijkingen tussen twee- en driedimensionale bifurcatie-analyses in bifurcatie-laesies beschreven (hoofdstuk 3.3). Bij deze studie, waren twee- en driedimensionale bifurcatie-analyses vergelijkbaar in de minimale lumen-diameter binnen het bifurcatiesegment, terwijl 2D-QCA met het percentage diameter stenose in het algemeen groter was en met de laesie lengte consistent korter was. Alhoewel de driedimensionale aanpak theoretisch tot meer nauwkeurige metingen leidt door het minimaliseren van de potentiële perspectivische verkorting en bloedvatoverlapping ten opzichte van de tweedimensionale aanpak, zijn er meer studies nodig om het klinische voordeel van het gebruik van 3D-QCA ten opzichte van 2D-QCA te bestuderen voor de beoordeling van bifurcatie-laesies. Dynamische verandering van overhangende BVS-struts bij bifurcatie zou ook van groot wetenschappelijk belang zijn. We bewezen de uiterlijke veranderingen met behulp van OCT, die wijst op een potentiële

voordeel van het verdwijnen van struts die gevangen zitten in het ostium van de zijtak, dankzij de bioresorptie van metalen en polylactide BRS (hoofdstuk 3.4).

### **OP LICHT GEBASEERD BEELDVORMEND ONDERZOEK VAN STEMI-PATIËNTEN**

STEMI-patiënten zijn een belangrijke doelsubgroep van de PCI-behandeling. De hoge-resolutiebeelden die worden verkregen met op licht gebaseerde coronaire beeldvorming (i.e. OCT/OFDI), hebben nieuwe inzichten opgeleverd, niet alleen in coronaire atherosclerose en stent appositie maar ook in intracoronaire trombus die waargenomen is bij STEMI-patiënten. Een eerder verschenen literair werk van het Thoraxcenter heeft de impact van angiografische trombus last op late klinische resultaten bij STEMI-patiënten duidelijk aangegeven. De methodologie van volumetrisch onderzoek naar trombus met OCT/OFDI is echter niet beschreven. We hebben daarom de methodologie bewezen voor het beoordelen van de postprocedurele in-stent trombotische materialen, wat we in-stent structure (ISS) hebben genoemd, en ook hebben we de impact van bemonsteringsfrequenties onderzocht (i.e. longitudinale afstand tussen geanalyseerde frames) op het volumetrische onderzoek van ISS. Een hogere bemonsteringsfrequentie kan leiden tot overschatting van het ISS-volume, dus hebben we geconcludeerd dat een meer gedetailleerde evaluatie met een lagere bemonsteringsfrequentie nodig zijn bij de aanpak van trombotische materialen in STEMI-patiënten met OCT/OFDI ten opzichte van de standaard bemonsteringsfrequentie van 1.0-mm (hoofdstuk 4.1). Daarnaast hebben we de haalbaarheid van het morfologische onderzoek van trombotische materialen bewezen met behulp van de driedimensionale reconstructie met OFDI-beelden (hoofdstuk 4.2). Dit kan bijdragen tot een beter begrip van de distributie en omvang van een uitstekende trombus na de stentimplantatie. De TROFI-trial was een prospectieve, gerandomiseerde gecontroleerde, multicentre trial die de effectiviteit van trombectomie onderzocht door middel van manuele aspiratie, voorafgaand aan een stentimplantatie bij STEMI-patiënten. In de TROFI-trial hebben we een nieuw surrogaat eindpunt - minimale doorstroomoppervlakte - voorgesteld die beoordeeld wordt met OFDI. De trombus aspiratiegroep vertoonde na de implantatie een neiging naar grotere minimale doorstroomoppervlakte in vergelijking met de non-trombus aspiratiegroep ondanks het gebrek aan statistische significantie. We hebben tevens de resultaten gerapporteerd van een serie OFDI-follow-up na 6 maanden onder meer met betrekking tot postprocedurele distributies van trombotische materialen en neointimaformatie bij de follow-up (hoofdstuk 4.3). Ten slotte bewezen we in dit

hoofdstuk voor het eerst uitstekende klinische resultaten op korte termijn bij MI-patiënten die behandeld zijn met de BVS in een reële klinische omgeving (hoofdstuk 4.4 en 4.5).

## **GELEERDE LESSEN VAN VROEGE BVS-STUDIES EN KLINISCHE IMPLICATIES VOOR COMPLEXE SUBGROEPEN**

In de vroege BVS-studies was er een aantal keer sprake van technische falen en bijwerkingen. Het was belangrijk om de potentiële redenen hiervoor te weten en dergelijke gevallen met de andere “interventional communities” delen. We hebben derhalve de gevallen samengevat en gerapporteerd, waarin patiënten subacute of late scaffold-trombose, het losraken van scaffold (hoofdstuk 5.1) en scaffold-restenose (hoofdstuk 5.2) hebben ervaren. Aangezien een mechanische eigenschap van polylactide anders is dan die van metaal, moet er ook speciale technische aandacht besteed worden aan BVS-implantatie ter voorkoming van het acute losscheuren van scaffolds en het potentiële risico van periprocedurele bijwerkingen. We zijn ook op late structurele discontinuïteiten ingegaan aan de hand van bioresorptie die waargenomen is in een serie OCT-onderzoeken. Deze bevindingen zijn zeer specifiek voor de BRS-technologie, en het eerste fenomeen wordt als kwaadaardig beschouwd en het laatste als goedaardig (hoofdstuk 5.3). Zelfs in het tijdperk van DES zijn diabetespatiënten nog steeds een hoog-risico subgroep bij het uitvoeren van PCI. Met behulp van de historische controlegroep van de SPIRIT-trials, rapporteerden we vergelijkbare klinische resultaten na 1 jaar bij diabetespatiënten, die behandeld zijn met de BVS in vergelijking met de patiënten met metalen EES, nadat de propensity scores van twee verschillende populaties gematcht zijn (hoofdstuk 5.4). Wegens de dikkere struts van BVS ten opzichte van metalen EES, kan de BVS in verband gebracht worden met een hoger risico van zijtak-occlusie en de daaropvolgende periprocedurele MI. Zo hebben we een risico op zijtak-occlusie bevestigd dat significant hoger is in de BVS-groep dan in de EES-groep. Er is echter geen significant verschil gevonden tussen twee groepen in de incidentie van periprocedurele MI, omdat alleen kleine zijtakken met een diameter van <0.5 mm geassocieerd waren met een significant hogere incidentie van postprocedurele occlusie, dat een minimale impact van zijtak-occlusie na BVS-implantatie suggereert op klinische resultaten op korte termijn (hoofdstuk 5.6). Aan de hand van hartenzymen die intensief geanalyseerd zijn bij het centraal laboratorium in de gerandomiseerde Absorb II trial, hebben we bevestigd dat er geen statistiek significante verschillen waren in de incidentie van hartenzymstijging noch

van periprocedurele MI tussen de BVS en de EES. Overlapping van scaffolds of stents kan een precipiterende factor zijn van myocardletsel (hoofdstuk 5.7). In deze studie hebben we ook benadrukt dat de binaire definitie van periprocedurele MI niet alleen afhankelijk is van de selectie van hartenzymen, maar ook van de drempels die willekeurig gekozen werden. Een andere fascinerende potentie van de BRS-technologie zou de passivering en uiteindelijke stabilisatie van hoog-risico plaques zijn. Er werd opnieuw gekeken of hoog-risico plaques vroegtijdig te detecteren zijn door multimodale beeldvormingstechnieken en of invasieve passivering mogelijk is door BRS-technologieën (hoofdstuk 5.8).

## **CONCLUSIES**

Aangezien BRS alleen geëvalueerd is bij een beperkt aantal patiënten, voornamelijk met niet-complexe laesies zijn verdere klinische evaluaties noodzakelijk om de haalbaarheid van deze apparaten in complexe laesies vast te stellen. Bovendien worden het optimale ontwerp van scaffolds, polymeren, antiproliferatieve geneesmiddelen en hun afbraak-/afgiftekinetics nog onderzocht. Hoewel toekomstige onderzoeken noodzakelijk zijn om vast te stellen of de BRS-technologie superieur is aan de permanente metalen DES, hopen we dat dit proefschrift een aantal implicaties voor lopende of toekomstige studies heeft om de effectiviteit van de BRS-technologieën te bewijzen en om klinische resultaten bij onze patiënten te verbeteren.

*Maart 2015,  
Takashi Muramatsu*

# Acknowledgement





## ACKNOWLEDGEMENTS

First of all, this thesis would not have been possible without kind support of all my mentors, colleagues and friends. Herein I would love to express my sincere appreciation to the person who reached this section. Those who are reading here may have read more in detail my thesis and are mostly perhaps those dearest to me.

Telling my personal career followed by the research fellowship in Rotterdam, I started my cardiology training in 2002. At that time, my scientific interest was focused on medical therapy by statins or renin-angiotensin system inhibitors for the prevention of cardiovascular diseases. Eventually I was fascinated by a scientific paper describing the “LIPS” study published in JAMA, however, I did not know the first author “Patrick W. Serruys” at the moment. During the clinical fellowship in general cardiology, my interest had gradually been shifted to the sub-speciality in terms of invasive diagnostics and therapeutics, namely “interventional cardiology.” In 2004, the Japanese PMDA finally approved the Sirolimus-eluting CYPHER stent that reinforced the 3<sup>rd</sup> revolution of coronary interventions. After introduction of this device, I became more aggressive to treat my patients with coronary artery disease and implanted numerous CYPHER stents without either enough knowledge or cautions. In 2007, I saw the sensational news highlighting a potential risk in increasing cardiovascular mortality of patients treated with the 1<sup>st</sup> generation drug-eluting stents including CYPHER. This news was really shocking and painful for me because I had already experienced several patients suffering very late stent thrombosis or even sudden cardiac death. This issue naturally drove me to a more scientific way of thinking in medicine. In December 2008, I joined the local Japanese meeting in Tokyo and listened to a striking lecture introducing novel technologies in interventional cardiology. The speaker was Dr. Yoshi Onuma, and soon I noticed that he is a fellow of the “big name” previously seen in the “LIPS” paper! I was so fascinated by the future potential of bioresorbable scaffold technology that could minimize or even eradicate the risk of our new enemy “very late stent thrombosis.” But at that moment, nobody (even myself) could imagine that I will join their team in the near future. During my Ph.D. course at Nagoya University since 2007 until 2011 (mentored by Prof. Toyooki Murohara), I mainly worked on clinical epidemiology and was involved in a clinical investigation comparing the efficacy of two major antihypertensive medications (ARB vs. CCB) for diabetic hypertensive patients in

a multi-centre, randomised controlled trial. Even during my great experience to manage such a big trial, I did never lose my passion for interventional cardiology. Then I started considering the possibility of working as a fellow with aforementioned scientists in Rotterdam. In a meantime, my colleagues kindly proposed several places mainly in US for my scientific fellowship, but my answer was always “NO” because I believed the Thoraxcenter is the only place for me to deserve working on what I was most interested in. It was really lucky to meet Prof. Yukio Ozaki (my current boss!) who was the pioneer of Japanese fellows in the Thoraxcenter and worked in the same city Nagoya in Japan. According to his suggestions, I immediately started to learn English conversation and decided to meet Prof. Serruys at my earliest convenience. In November 2010, I flew to Chicago for the AHA Scientific Sessions just to see Prof. Serruys without any appointment. After arriving at the congress, I soon checked his agenda through the programme. OMG, I realized that there might be only one chance to see him after his presentation regarding 4-year follow-up of the ABSORB Cohort A study. Immediately after the session, I got closed to him and handed several documents with my CV. Honestly I did not remember what I said, but certainly he said “Ok, you are gentle” with a slight smile. This was my first contact to him and his only a few words really made me relief. In March 2011, I visited Rotterdam for the first time to receive an interview with Prof. Serruys. It was very fruitful for my preparation since that was not only for an interview but also for discussions about future projects in Rotterdam. After the interview, he gave me a compendium of the ABSORB (we called it bible) with his signature, then took my wife Yuko and me around many departments in CARDIALYSIS, and kindly introduced lots of staffs and fellows. That was unforgettable moment to recognize that my dream will come true... but afterward somebody said that professor accepted myself as a fellow since he liked Yuko very much! I still believe that was no more than joke.

I belonged to the Thoraxcenter and the team of Prof. Serruys as a research fellow since 12-July-2011 until 15-Sep-2013. I will never forget a total of 797 days shared with friends and colleagues worldwide. Even in the weekend, we always shared the time by working, chatting, traveling and sometimes fighting. Now everything has become unforgettable memory, and I would like to thank all of you for kind support and friendship. I owe you the vast majority of Rotterdam experiences.

Dearest my promotor Professor Serruys, I deeply appreciate for everything you gave me in Rotterdam: self-confidence, passion for truly scientific research and “never-compromise” attitude. My great honour and really proud of myself being a member of the Thoraxcenter in which you have created legends and revolutions in interventional cardiology. Your endless energy towards scientific research made me drive to become a hard-worker. In addition, your intensive mentorship and guidance shaped me as a researcher and a person in many positive ways in my life.

Dear my co-promotor Yoshi-san, many thanks for your powerful support and close friendship. You are definitely more than my friend. You always stayed by my side and kindly supported not only research but also my life in Rotterdam. This thesis would not be possible without your tremendous help and great navigations of research. We often enjoyed our Rotterdam life together... meeting, travelling, parties, movies, BBQs and mostly drinking. I am grateful that you saved my life when I extremely got drunk at the Belgian beer cafe “Boudewijn.” Now everything shared with you became my beautiful memory. Wish our further collaborations and do hope to enjoy sake together whenever flying back to our country. I promise to prepare your favorite sake label “Uragasumi.”

Dear the members of doctoral committee: Prof. Yukio Ozaki, Prof. Robert-Jan van Geuns, Dr. Koen Nieman (the inner committee), Prof. Pim de Feyter, Prof. Ken Kozuma, and Dr. Hector Garcia-Garcia (the plenary committee). Sincerely I would like to thank all of you for critical evaluation of my thesis.

Dear Hector-san, muy bien mi amigos. Definitely you are the “God Father” of fellows and of course it’s not an exception for me either. You willingly gave me countless advices and always tried to keep us fellows working as a team. I am also grateful that you were so kind to take care of health issues of Yuko. My dream is to make a nice family like you did. We will never forget your big smile. Look forward to watching a baseball game together with your family when Andreas becomes a professional baseball player in Japan!

Dear Marie-Angèle, I would say you are not only a great sister of fellows but also a master of connecting people (e.g. Nieuwe Haring Party and Pleinbioscoop etc.). When I was irritated to see >30 boxes of useless data sent from the company, your innocent laughing voice always made my emotions soften and positive. I believe that you have also been a part of Rotterdam “Legend”.

Dear Hanny-san, many thanks for everything you kindly supported to me. Even after I returned to Japan, you always took care of my leg injury and helped me a lot about this thesis. You must be the only person who can sufficiently manage the deadly busy Prof's agenda. You are so active and so good at speaking many foreign languages (including Japanese!) that all fellows worldwide can enjoy working with you in CARDIALYSIS. Hope to keep working with Prof. and his fellows by taking care of yourself.

Dear Osama, thank you for your lecture about cultures and politics in Arabic countries. Someday I would love to visit Egypt since I know there are many nice places. Look forward to your invitation when you buy a nice room with beautiful scenery besides the Maas river.

Dear Paul, I cannot imagine how hard you worked to improve the quality and consequent impact factor of the EIJ. A new journal "*Asiaintervention*" in collaboration with the EIJ is also of my great interest. I like your humorous talk despite very difficult English. Very nice to see you in Nanjing but someday you should visit Japan as well.

Dear Sylvie, many thanks for your help of the EIJ issues and a nice friendship with Yuko. You were definitely her best English (and French) teacher ever and made her European life absolutely happier! Please keep in touch with us through the Skype and so.

I must thank many staffs working in the CARDIALYSIS: Gerrit-Anne van Es, Monique Schuijjer, Bianca Backx, Anne Marie Bruinsma, Jeannette Fong-Pien-Joe, Eliane Lopes, Ana Guimaraes, Ton de Vries, Michael Swart, Joost de Vries, Coby Bouwman, Ravindra Pawar, Jamal Khachabi, Marije Hoogen, Glenda Bochove, and Hans Jonker for their kind friendship and technical assistance.

Dear Maria-san, you are a great friend of mine and I really respect your personality. It was my great pleasure to work with you even for a short time in Rotterdam and many thanks for inviting us to your excellent thesis defense and ceremony in Rigshospitalet. We shared a fantastic moment with your family and I do believe our friendship is everlasting. Someday I am willing to invite you to Japan as one of the leading OCT specialist and hope you enjoy our culture together.

Dear Lorenz, you are the most intelligent and the smartest colleague I have ever seen. It was my great pleasure to work with you and hope to see you in Switzerland. Your wine (Weißwein) is one of the best I ever drank!

Dear Yao-jun, many thanks for your great friendship with me. I cannot imagine how long we talked together day and night in the fellows' room. Your kind invitation to the CBS

meeting in 2014 is greatly appreciated. It was my first time visit to China and all the hospitality was really amazing. You are a serious and sensitive guy, but I know you have a great mind. Hope to keep our friendship closely and see you more in China/Japan.

Dear Christos and Thekla, your beautiful wedding ceremony is definitely a big part of my memories. It was our great privilege to be invited to Athens. Thank you for your kind proposal to collaborate with your colleagues in Ioannina (Greece) and Boston (US). You convinced me an importance of scientific collaboration. Looking forward to seeing you both and your beautiful baby in the near future.

Dear Vas, thank you for many advices and suggestions as a senior fellow although it was hard to understand what you said mostly in the beginning of my fellowship. Please do not sneak into my room at night, otherwise you may cause me a heart attack.

Dear Roberto, I worked with you during a whole period of my fellowship. Thank you for teaching me nice Italian phrases, but I understand that it should not be a good idea to say in your country. Hope you to become a great senior interventional cardiologist and let's collaborate in the future studies.

Dear Shimpei and Dear Yuki, many thanks for your support and friendship. Had hourly meetings at the backyard of CARDIALYSIS. Indeed we might sacrifice something but I enjoyed a lot with you both. Our task would be to restart our collaborations of academic work together in Japan.

Dear Carlos, thank you for nice friendship despite a short period shared with you in Rotterdam. I love your personality and great passions for football (Flamengo and Zico). Do not open a Brazilian restaurant in Netherlands since I believe you will become a good interventional cardiologist. I will be happy to keep our friendship and have nice churrasco together in the future.

I would also love to thank all my colleagues: Bill D. Gogas, Salvatore Brugaletta, Josep Gomez-Lara, Chrysafios Girasis, Antonis Karanasos, Javaid Iqbal, Jung Ho Heo, Il Soo Lee, and Yun Kyeong Cho, for their kind friendship.

Dear Nicolas, I respect your personality and “never surrender” style in complex PCI procedures. My only regret would be that I didn't have so many chances to see TAVI procedures in the Thoraxcenter since I rather focused on BRS research. Anyway it was good to introduce Dr. Yusuke Watanabe for your collaborative work with the Massy team, and now I am pretty sure that TAVI also deserves a revolution in interventional cardiology. As

we started TAVI in Japan, I hope to keep our friendship and someday look forward to talking about PCI/TAVI together with a glass of beer.

Dear Nico, thank you for your kind instructions and collaborations about echogenicity analysis. It was a very nice moment to work with you and beautiful European ladies filled in your room. Please let me consult with you when considering a development of new analysis algorithms.

Dear Jurgen and Karen, probably you are the persons I met the first at the Thoraxcenter. Thank you both very much for your kind supports from the very beginning of my fellowship. I have never met such great imaging technicians like you. Really enjoyed talking many things with you having a cup of coffee in the database room.

I would also like to express my gratitude to the senior interventional cardiologists in the Thoraxcenter: Prof. Felix Zijlstra, Prof. Peter de Jaegere, Dr. Evelyn Regar, and Dr. Carl Schultz for their intellectual guidance.

Herewith I would also like to highlight special recognition of Prof. Toyooki Murohara (Nagoya University, Nagoya, Japan) who is the leading scientist in the field of angiogenesis and cell therapy for ischemic heart and peripheral diseases. You kindly joined and celebrated our wedding ceremony in 2003, and I was happy to work with you under your supervisions. I must thank you for giving me a chance to move to Europe from Nagoya. My life and career might become completely different ones without your understanding and kind support for my fellowship. Deeply appreciate for your continuous support and close relationship.

Dear Prof. Yukio Ozaki-sensei, everybody here knows that you are the great pioneer of Japanese fellows in Rotterdam. As I worked in Rotterdam, I realized that your achievements in interventional cardiology are absolutely great and you are still working very actively. You gave me a lot of chances that will certainly enrich my career, and now I feel somewhat a destiny to work with you. My next goal is to further improve three important components of our cardiology department (i.e. clinical work, academic research, and education) under your outstanding supervisions.

Finally, my special thanks to my family: my mother Yoshika, my sister Kaori and my beloved wife Yuko. I lost my father because of hepatic cancer when I was 14 years old. Then my family experienced really hard time, but always they encouraged and supported me. I believe that my dad would also be happy to read this thesis if he is still alive.

Dearest Yuko, there are no words to thank you for everything enough. Since I was a medical student, you enormously supported not only to build up my career but also to enrich my life. You are not only a great wife but also the best friend of mine as I truly respect your personality. Certainly this thesis would not exist without your devoted support to me. More importantly, we were very lucky to have many good friends worldwide and priceless experiences in Rotterdam that will bring us in a good way of our future.

*April 2015,*  
*With my best regards,*  
*Taka*



# Curriculum Vitae





## CURRICULUM VITAE

Name Takashi Muramatsu  
Date of Birth April 1, 1975  
Place of Birth Nagoya, Japan  
Nationality Japan  
Professional Address Department of Cardiology  
Fujita Health University Hospital  
Room 310a, 1-98 Dengaku, Kutsukake, Toyoake 470-1192, Japan  
E-mail takam@fujita-hu.ac.jp

### Education:

1990-1993 Tokai High School, Nagoya, Japan  
1994-2000 Nagoya University School of Medicine, Nagoya, Japan  
(Awarded the degree of M.D.)  
2007-2011 Nagoya University Graduate School of Medicine, Nagoya,  
Japan (Awarded the degree of Ph.D.)

### Professional Training and Employment:

2000-2002 Residency in Internal Medicine  
Nagoya Daini Red Cross Hospital, Nagoya, Japan  
2002-2007 Clinical Fellowship in Cardiology  
Cardiovascular Center  
Nagoya Daini Red Cross Hospital, Nagoya, Japan  
2007-2011 Clinical Scientist / Ph.D. Candidate  
Department of Cardiology  
Nagoya University Graduate School of Medicine, Nagoya,  
Japan  
2011-2013 Research Fellowship in Interventional Cardiology  
Thoraxcenter  
Erasmus Medical Center, Rotterdam, the Netherlands  
2013- Lecturer / Senior Assistant Professor  
Department of Cardiology  
Fujita Health University Hospital, Toyoake, Japan

### License and Certification:

2000	Japanese Full Medical License (#413927)
2004	Board Certified Member of the Japanese Society of Internal Medicine (#26708)
2006	Fellow of the Japanese Association of Cardiovascular Intervention and Therapeutics (#7445)
2006	Fellow of the Japanese Society of Internal Medicine (FJSIM, #11194)
2009	Board Certified Member of the Japanese Circulation Society (#17764)
2013	Fellow of the European Society of Cardiology (FESC)

# List of Publications





## LIST OF PUBLICATIONS

### Bioresorbable scaffolds

- 1. Early and late optical coherence tomography findings following everolimus-eluting bioresorbable vascular scaffold implantation in myocardial infarction: a preliminary report.**  
Karanasos A, **Muramatsu T**, Diletti R, Nauta S, Onuma Y, Lenzen M, Nakatani S, van Mieghem NM, Schultz C, de Jaegere PP, Serruys PW, Zijlstra F, Regar E, van Geuns RJ. *Hellenic J Cardiol.* 2015;56:125-35.
- 2. Incidence and imaging outcomes of acute scaffold disruption and late structural discontinuity after implantation of the Absorb everolimus-eluting fully bioresorbable vascular scaffold: optical coherence tomography assessment in the ABSORB Cohort B trial.**  
Onuma Y, Serruys PW, **Muramatsu T**, Nakatani S, van Geuns RJ, de Bruyne B, Dudek D, Christiansen E, Smits PC, Chevalier B, McClean D, Koolen J, Windecker S, Whitbourn R, Meredith I, García-García HM, Veldhof S, Rapoza R, Ormiston JA. *JACC Cardiovasc Interv.* 2014;7:1400-11.
- 3. Assessing bioresorbable coronary devices. Methods and parameters.**  
García-García HM, Serruys PW, Campos CM, **Muramatsu T**, Nakatani S, Zhang YJ, Onuma Y, Stone GW. *JACC Cardiovasc Imaging.* 2014;7:1130-48.
- 4. One-year clinical outcomes of diabetic patients treated with everolimus-eluting bioresorbable vascular scaffolds: A pooled analysis of the ABSORB and the SPIRIT trials.**  
**Muramatsu T**, Onuma Y, van Geuns RJ, Chevalier B, Patel T, Seth A, Diletti R, García-García HM, Dorange C, Veldhof S, Cheong WF, Ozaki Y, Whitbourn R, Bartorelli A, Stone GW, Abizaid A, Serruys PW. *JACC Cardiovasc Interv.* 2014;7:482-93.
- 5. Serial 2-dimensional and 3-dimensional optical coherence tomography assessment of overhanging struts of drug-eluting absorbable metal scaffold. “DREAMS” for jailed side branch?**  
**Muramatsu T**, García-García HM, Serruys PW, Waksman R, Verheye S. *JACC Cardiovasc Interv.* 2014;7:575-6.

6. **Circumferential distribution of the neointima at six-month and two-year follow-up after a bioresorbable vascular scaffold implantation: a substudy of the ABSORB Cohort B Clinical Trial.**  
 Bourantas CV, Farooq V, Zhang Y, **Muramatsu T**, Gogas BD, Thuesen L, McClean D, Chevalier B, Windecker S, Koolen J, Ormiston J, Whitbourn R, Dorange C, Rapoza R, Onuma Y, Garcia-Garcia HM, Serruys PW.  
*Eurointervention.* (Epub ahead of print)
7. **Early (before 6 months), late (6-12 months) and very late (after 12 months) angiographic scaffold restenosis in the ABSORB Cohort B trial.**  
 Nakatani S, Onuma Y, Ishibashi Y, **Muramatsu T**, Iqbal J, Zhang YJ, van Geuns RJ, Ormiston JA, Serruys PW; on behalf of the ABSORB Cohort B investigators.  
*Eurointervention.* (Epub ahead of print)
8. **Comparison of acute gain and late lumen loss after PCI with bioresorbable vascular scaffolds versus everolimus-eluting stents: an exploratory observational study prior to a randomised trial.**  
 Zhang YJ, Bourantas CV, **Muramatsu T**, Iqbal J, Farooq V, Diletti R, Campos CA, Onuma Y, Garcia-Garcia HM, Serruys PW.  
*Eurointervention.* 2014;10:672-80.
9. **Lessons learned from acute and late scaffold failures in the ABSORB EXTEND trial.**  
 Ishibashi Y, Onuma Y, **Muramatsu T**, Nakatani S, Iqbal J, Garcia-Garcia HM, Bartorelli AL, Whitbourn R, Abizaid A, Serruys PW.  
*Eurointervention.* 2014;10:449-57.
10. **Fusion of optical coherence tomographic and angiographic data for more accurate evaluation of the endothelial shear stress patterns and neointimal distribution after bioresorbable scaffold implantation: comparison with intravascular ultrasound-derived reconstructions.**  
 Bourantas CV, Papafaklis MI, Lakkas L, Sakellarios A, Onuma Y, Zhang YJ, **Muramatsu T**, Diletti R, Bizopoulos P, Kalatzis F, Naka KK, Fotiadis DI, Wang J, Garcia Garcia HM, Kimura T, Michalis LK, Serruys PW.  
*Int J Cardiovasc Imaging.* 2014;30:485-94.
11. **Dynamics of vessel wall changes following the implantation of the Absorb everolimus-eluting bioresorbable vascular scaffold: a multi-imaging modality study at 6, 12, 24 and 36 months.**

Serruys PW, Onuma Y, Garcia-Garcia HM, **Muramatsu T**, van Geuns RJ, de Bruyne B, Dudek D, Thuesen L, Smits PC, Chevalier B, McClean D, Koolen J, Windecker S, Whitbourn R, Meredith I, Dorange C, Veldhof S, Hebert KM, Rapoza R, Ormiston JA.

*Eurointervention*. 2014;9:1271-84.

12. **Implications of a bioresorbable vascular scaffold implantation on vessel wall strain of the treated and the adjacent segments.**

Bourantas CV, Garcia-Garcia HM, Campos CA, Zhang YJ, **Muramatsu T**, Morel MA, Nakatani S, Gao X, Cho YK, Isibashi Y, Gijsen FJ, Onuma Y, Serruys PW.

*Int J Cardiovasc Imaging*. 2014;30:477-84.

13. **Everolimus-eluting bioresorbable vascular scaffolds for treatment of patients presenting with ST-segment elevation myocardial infarction: BVS STEMI first study.**

Diletti R, Karanasos A, **Muramatsu T**, Nakatani S, Van Mieghem NM, Onuma Y, Nauta ST, Ishibashi Y, Lenzen MJ, Ligthart J, Schultz C, Regar E, de Jaegere PP, Serruys PW, Zijlstra F, van Geuns RJ.

*Eur Heart J*. 2014;35:777-86.

14. **Effect of the endothelial shear stress patterns on neointimal proliferation following drug-eluting bioresorbable vascular scaffold implantation: An optical coherence tomography study.**

Bourantas CV, Papafaklis MI, Kotsia A, Farooq V, **Muramatsu T**, Gomez-Lara J, Zhang Y, Iqbal J, Kalatzis F, Naka K, Fotiadis D, Dorange C, Wang J, Rapoza R, Garcia-Garcia HM, Onuma Y, Michalis L, Serruys PW.

*JACC Cardiovasc Interv*. 2014;7:315-24.

15. **Short- and long-term implications of a bioresorbable vascular scaffold implantation on the local endothelial shear stress patterns.**

Bourantas CV, Papafaklis MI, Garcia-Garcia HM, Farooq V, Diletti R, **Muramatsu T**, Zhang Y, Kalatzis F, Naka K, Fotiadis D, Onuma Y, Michalis L, Serruys PW.

*JACC Cardiovasc Interv*. 2014;7:100-1.

16. **Bioresorbable vascular scaffolds in the clinical setting.**

Campos CM, Zhang YJ, Bourantas CV, **Muramatsu T**, Garcia-Garcia HM, Lemos PA, Iqbal J, Onuma Y, Serruys PW.

*Interventional Cardiology*. 2013;5:639-46.

17. **Incidence and short-term clinical outcomes of small side branch occlusion after implantation of an everolimus-eluting bioresorbable vascular scaffold: An interim report**

- of 435 patients in the ABSORB-EXTEND single-arm trial in comparison with an everolimus-eluting metallic stent in the SPIRIT first and II trials.**  
Muramatsu T, Onuma Y, García-García HM, Farooq V, Bourantas CV, Morel MA, Li X, Veldhof S, Bartorelli A, Whitbourn R, Abizaid A, Serruys PW.  
*JACC Cardiovasc Interv.* 2013;6:247-57.
18. **Edge vascular response after percutaneous coronary intervention. An intracoronary ultrasound and optical coherence tomography appraisal: from radioactive platforms to first- and second-generation drug-eluting stents and bioresorbable scaffolds.**  
Gogas BD, Garcia-Garcia HM, Onuma Y, Muramatsu T, Farooq V, Bourantas CV, Serruys PW.  
*JACC Cardiovasc Interv.* 2013;6:211-21.
19. **Progress in treatment by percutaneous coronary intervention: the stent of the future.**  
Muramatsu T, Onuma Y, Zhang Y, Bourantas CV, Kharlamov A, Diletti R, Farooq V, Gogas BD, Garg S, García-García HM, Ozaki Y, Serruys PW.  
*Rev Esp Cardiol.* 2013;66:483-96.
20. **Bioresorbable drug-eluting magnesium-alloy scaffold for treatment of coronary artery disease.**  
Campos CM, Muramatsu T, Iqbal J, Zhang YJ, Onuma Y, Garcia-Garcia HM, Haude M, Lemos PA, Warnack B, Serruys PW.  
*Int J Mol Sci.* 2013;14:24492-500.
21. **Complex bifurcation percutaneous coronary intervention with the Absorb bioresorbable vascular scaffold.**  
Dzavík V, Muramatsu T, Crooks N, Nakatani S, Onuma Y.  
*Eurointervention.* 2013;9:888.
22. **In vivo assessment of the three-dimensional haemodynamic micro-environment following drug-eluting bioresorbable vascular scaffold implantation in a human coronary artery: fusion of frequency domain optical coherence tomography and angiography.**  
Papafaklis MI, Bourantas CV, Farooq V, Diletti R, Muramatsu T, Zhang Y, Fotiadis DI, Onuma Y, Garcia Garcia HM, Michalis LK, Serruys PW.  
*Eurointervention.* 2013;9:890.
23. **Early detection and invasive passivation of future culprit lesions. A future potential or an unrealistic pursuit of Chimeras?**  
Bourantas CV, Garcia-Garcia HM, Diletti R, Muramatsu T, Serruys PW.  
*Am Heart J.* 2013;165:869-81.

24. **The edge vascular response following implantation of the Absorb everolimus-eluting bioresorbable vascular scaffold and the XIENCE V metallic everolimus-eluting stent. First serial follow-up assessment at six months and two years: insights from the first-in-man ABSORB Cohort B and SPIRIT II trials.**  
Gogas BD, Bourantas CV, Garcia-Garcia HM, Onuma Y, **Muramatsu T**, Farooq V, Diletti R, van Geuns RJ, De Bruyne B, Chevalier B, Thuesen L, Smits PC, Dudek D, Koolen J, Windecker S, Whitbourn R, McClean D, Dorange C, Miquel-Hebert K, Veldhof S, Rapoza R, Ormiston JA, Serruys PW.  
*Eurointervention*. 2013;22:709-20.
25. **Bioresorbable scaffolds in the treatment of coronary artery disease.**  
Zhang Y, Bourantas CV, Farooq V, **Muramatsu T**, Diletti R, Onuma Y, García-García HM, Serruys PW.  
*Medical Devices: Evidence and Research*. 2013;6:37-48.
26. **Long-term (>10 Years) clinical outcomes of first-in-man biodegradable poly-L-lactic acid coronary stents: Igaki-Tamai stents.**  
Nishio S, Kosuga K, Igaki K, Okada M, Kyo E, Tsuji T, Takeuchi E, Inuzuka Y, Takeda S, Hata T, Takeuchi Y, Kawada Y, Harita T, Seki J, Akamatsu S, Hasegawa S, Bruining N, Brugaletta S, de Winter S, **Muramatsu T**, Onuma Y, Serruys PW, Ikeguchi S.  
*Circulation*. 2012;125:2343-53.
27. **Freeing the vessel from metallic cage: what can we achieve with bioresorbable vascular scaffolds?**  
Onuma Y, **Muramatsu T**, Kharlamov A, Serruys PW.  
*Cardiovasc Interv and Ther*. 2012;27:151-54.

## Drug-eluting stents

28. **Impact of body mass index on long-term clinical outcomes after second-generation drug eluting stent implantation: Insights from the international global RESOLUTE program.**  
Diletti R, Garcia-Garcia HM, Bourantas C, Van Mieghem NM, van Geuns RJ, **Muramatsu T**, Zhang YJ, Mauri L, Belardi J, Silber S, Widimsky P, Leon M, Windecker S, Meredith I, Neumann FJ, Yeung AC, Saito S, Liu M, van Leeuwen F, Serruys PW.  
*Catheter Cardiovasc Interv*. (Epub ahead of print)

29. **Nine-month angiographic and two-year clinical follow-up of polymer-free sirolimus-eluting stent versus durable-polymer sirolimus-eluting stent for coronary artery disease: the Nano randomized trial.**  
Zhang Y, Chen F, Muramatsu T, Xu B, Li Z, Ge J, He Q, Yang Z, Li S, Wang L, Wang H, He B, Li K, Qi G, Li T, Zeng H, Peng J, Jiang T, Zeng Q, Zhu J, Fu G, Bourantas CV, Serruys PW, Huo Y.  
*Chin Med J.* 2014;127:2153-8.
30. **Impact of biodegradable versus durable polymer drug-eluting stents on clinical outcomes in patients with coronary artery disease: a meta-analysis of 15 randomized trials.**  
Zhang Y, Tian N, Dong S, Ye F, Li M, Bourantas CV, Iqbal J, Onuma Y, Muramatsu T, Diletti R, Garcia-Garcia HM, Xu B, Serruys PW, Chen S.  
*Chin Med J.* 2014;127:2159-66.
31. **Simultaneous occlusion of left anterior descending and left circumflex arteries by very late stent thrombosis: vascular response to drug-eluting stents assessed by intravascular ultrasound.**  
Yamawaki M, Onuma Y, Nakano M, Muramatsu T, Nakatani S, Ishibashi Y, Ishimori H, Hirano K, Ito Y, Tsukahara R, Muramatsu T.  
*Heart and Vessels.* (Epub ahead of print)
32. **Single-vessel or multivessel PCI in patients with multivessel disease presenting with non-ST-elevation acute coronary syndromes.**  
Onuma Y, Muramatsu T, Girisic C, Kukreja N, Garcia-Garcia HM, Daemen J, Gonzalo N, Piazza N, Einthoven J, van Domburg R, Serruys PW.  
*Eurointervention.* 2013;9:916-22.
33. **Clinical and angiographic outcomes following first-in-man implantation of a novel thin-strut low-profile fixed-wire stent: the Svelte Coronary Stent Integrated Delivery System first-in-man trial.**  
Diletti R, Garcia-Garcia HM, Bourantas CV, van Geuns RJ, Van Mieghem NM, Agostoni P, Muramatsu T, Farooq V, Spencer R, De Schepper J, Pomeranz M, Stella P, Serruys PW.  
*Eurointervention.* 2013;9:125-34.

## Angiography and SYNTAX score

34. **Fast virtual functional assessment of intermediate coronary lesions using routine angiographic data and blood flow simulation in humans: comparison with pressure wire-fractional flow reserve.**  
Papafaklis MI, **Muramatsu T\***, Ishibashi Y, Lakkas LS, Nakatani S, Bourantas CV, Ligthart J, Onuma Y, Echavarria-Pinto M, Tsirka G, Kotsia A, Nikas DN, Mogabgab O, van Geuns RJ, Naka KK, Fotiadis DI, Brilakis ES, Garcia-Garcia HM, Escaned J, Zijlstra F, Michalis LK, Serruys PW.  
**\*Equally contributed to the first author.**  
*Eurointervention.* 2014;10:574-83.
35. **Impact of 3-dimensional bifurcation angle on 5-year outcome of patients after percutaneous coronary intervention for left main coronary artery disease: A substudy of the SYNTAX trial (Synergy Between Percutaneous Coronary Intervention With Taxus and Cardiac Surgery).**  
Girasis C, Farooq V, Diletti R, **Muramatsu T**, Bourantas CV, Onuma Y, Holmes DR, Feldman TE, Morel MA, van Es GA, Dawkins KD, Morice MC, Serruys PW.  
*JACC Cardiovasc Interv.* 2013;6:1250-1260.
36. **Clinical and angiographic characteristics of patients likely to have vulnerable plaques. Analysis from the PROSPECT study.**  
Bourantas CV, Garcia-Garcia HM, Farooq V, Maehara A, Xu K, Génereux P, Diletti R, **Muramatsu T**, Fahy M, Weisz G, Stone GW, Serruys PW.  
*JACC Cardiovasc Imaging.* 2013;6:1263-72.
37. **Quantification of incomplete revascularisation and its association with five-year mortality in the synergy between percutaneous coronary intervention with taxus and cardiac surgery (SYNTAX) trial. Validation of the residual SYNTAX score.**  
Farooq V, Serruys PW, Bourantas CV, Zhang YJ, Feldman T, Holmes DR, Mack M, Morice MC, Ståhle E, Colombo A, **Muramatsu T**, de Vries T, Morel MA, Dawkins KD, Kappetein AP, Mohr FW.  
*Circulation.* 2013;128:141-51.
38. **Advanced three-dimensional quantitative coronary angiographic assessment of bifurcation lesions: methodology and phantom validation.**

Girasis C, Schuurbiens JC, **Muramatsu T**, Aben JP, Onuma Y, Soekhradj S, Morel MA, van Geuns RJ, Wentzel JJ, Serruys PW.  
*Eurointervention*. 2013;8:1451-60.

## Intracoronary imaging

39. **Reproducibility of intravascular ultrasound radiofrequency data analysis (Virtual Histology) with a 45 MHz rotational imaging catheter in ex vivo human coronary arteries.**  
**Muramatsu T**, García-García HM, Brugaletta S, Heo JH, Onuma Y, Fedewa RJ, Nair A, Ozaki Y, Serruys PW.  
*J Cardiol*. 2015;65:134-42.
40. **Serial optical frequency domain imaging in STEMI patients: the follow-up report of TROFI study.**  
García-García HM, **Muramatsu T**, Nakatani S, Lee IS, Holm NR, Thuesen L, van Geuns RJ, van der Ent M, Borovicainin V, Paunovic D, Onuma Y, Serruys PW.  
*Eur Heart J Cardiovasc Imaging*. 2014;15:987-95.
41. **Coronary evaginations are associated with positive vessel remodeling and are nearly absent following implantation of newer-generation drug-eluting stents: An optical coherence tomography and intravascular ultrasound study.**  
Radu MD, Råber L, Kalesan B, **Muramatsu T**, Kelbæk H, Heo JH, Jørgensen E, Helqvist S, Farooq V, Brugaletta S, Garcia-Garcia HM, Jüni P, Saunamäki K, Windecker S, Serruys PW.  
*Eur Heart J*. 2014;35:795-807.
42. **Natural history of optical coherence tomography-detected non-flow-limiting edge dissections following drug-eluting stent implantation.**  
Radu MD, Råber L, Heo JH, Gogas BD, Jørgensen E, Kelbæk H, **Muramatsu T**, Farooq V, Helqvist S, Garcia-Garcia HM, Windecker S, Saunamäki K, Serruys PW.  
*Eurointervention*. 2014;9:1085-94.
43. **How clinically effective is intravascular ultrasound in interventional cardiology? Present and future perspectives.**  
Nakatani S, Proniewska K, Pociask E, Paoletti G, de Winter S, **Muramatsu T**, Bruining N.  
*Expert Rev Med Devices*. 2013;10:735-49.
44. **Assessment of plaque evolution in coronary bifurcations located beyond everolimus eluting scaffolds: serial intravascular ultrasound virtual histology study.**

- Lee IS, Bourantas CV, Muramatsu T, Gogas BD, Heo JH, Diletti R, Farooq V, Zhang Y, Onuma Y, Serruys PW, Garcia-Garcia HM.  
*Cardiovasc Ultrasound*. 2013;11:25.
45. **Intimal flaps detected by optical frequency domain imaging in the proximal segments of native coronary arteries - an innocent bystander? Insights from the TROFI trial.**  
Muramatsu T, García-García HM, Onuma Y, Zhang YJ, Bourantas CV, Diletti R, Iqbal J, Radu MD, Ozaki Y, Serruys PW; on behalf of the TROFI investigators.  
*Circ J*. 2013;77:2327-33.
46. **Randomized study to assess the effect of thrombus aspiration on flow area in patients with ST-elevation myocardial infarction: an optical frequency domain imaging study-TROFI trial.**  
Onuma Y, Thuesen L, van Geuns RJ, van der Ent M, Desch S, Fajadet J, Christiansen E, Smits P, Holm NR, Regar E, van Mieghem NM, Borovicinanin V, Paunovic D, Senshu K, van Es GA, Muramatsu T, Lee IS, Schuler G, Zijlstra F, Garcia-Garcia HM, Serruys PW.  
*Eur Heart J*. 2013;34:1050-60.
47. **In vivo three dimensional optical coherence tomography. A novel imaging modality to visualize the edge vascular response.**  
Gogas BD, Muramatsu T, Garcia-Garcia HM, Bourantas CV, Holm NR, Thuesen L, Farooq V, Onuma Y, Serruys PW.  
*Int J Cardiol*. 2013;164:e35-7.
48. **Quantitative optical frequency domain imaging assessment of in-stent structures in patients with ST-segment elevation myocardial infarction: impact of imaging sampling rate.**  
Muramatsu T, Garcia-Garcia HM, Lee IS, Bruining N, Onuma Y, Serruys PW.  
*Circ J*. 2012;76:2822-31.
49. **Serial two- and three-dimensional visualization of side branch jailing after metallic stent implantation.**  
Diletti R, Farooq V, Muramatsu T, Gogas BD, Garcia-Garcia HM, van Geuns RJ, Serruys PW.  
*JACC Cardiovasc Interv*. 2012;5:1089-90.
50. **Thrombotic arch in ST-segment elevation myocardial infarction: comparison between 2-dimensional and 3-dimensional optical frequency domain imaging.**  
Muramatsu T, Serruys PW, Onuma Y.  
*Eur Heart J*. 2012;33:1510

## Others

51. **Thin cap fibroatheroma defined as lipid core abutting lumen (LCAL) on integrated backscatter intravascular ultrasound: comparison with optical coherence tomography and correlation with peri-procedural myocardial infarction.**  
Ozaki Y, Ohota M, Ismail TF, Okumura M, Ishikawa M, Muramatsu T.  
*Circ J*. 2015;79:808-17.
52. **Fate and clinical significance of angiographically visible stent malapposition (peri-stent contrast staining) after drug-eluting stent implantation: a long-term clinical follow-up study.**  
Ozaki Y, Kawai T, Ismail TF, Ohota M, Okumura M, Takahashi H, Muramatsu T, Umeda H, Murohara T.  
*Asiaintervention*. 2015;1:48-56.
53. **Multimarker approach to risk stratification for long-term mortality in patients on chronic hemodialysis.**  
Ishii J, Takahashi H, Kitagawa F, Kuno A, Okuyama R, Kawai H, Muramatsu T, Naruse H, Motoyama S, Matsui S, Hasegawa M, Aoyama T, Kamoi D, Kasuga H, Izawa H, Ozaki Y, Yuzawa Y.  
*Circ J*. 2015;79:656-63.
54. **European Society of Cardiology (ESC) congress report from Barcelona 2014.**  
Muramatsu T, Ozaki Y.  
*Circ J*. 2014;78:2610-8.
55. **Major bleeding complications related to combined antithrombotic therapy in atrial fibrillation patients 12 months after coronary artery stenting.**  
Kawai H, Watanabe E, Yamamoto M, Harigaya H, Sano K, Takatsu H, Muramatsu T, Naruse H, Sobue Y, Motoyama S, Sarai M, Takahashi H, Arakawa T, Kan S, Sugiura A, Murohara T, Ozaki Y.  
*J Cardiol*. (Epub ahead of print)
56. **Independent association of liver fat accumulation with insulin resistance.**  
Yatsuya H, Nihashi T, Li Y, Hotta Y, Matsushita K, Muramatsu T, Otsuka R, Matsunaga M, Yamashita K, Wang C, Uemura M, Harada A, Fukatsu H, Toyoshima H, Aoyama A, Tamakoshi K.  
*Obes Res Clin Pract*. 2014;8:e350-e355.

57. **The ginsenoside Rg1 prevents transverse aortic constriction-induced left ventricular hypertrophy and cardiac dysfunction by inhibiting fibrosis and enhancing angiogenesis.**  
Zhang YJ, Zhang XL, Li MH, Iqbal J, Bourantas CV, Li JJ, Su XY, Muramatsu T, Tian NL, Chen SL.  
*J Cardiovasc Pharmacol.* 2013;62:50-7.
58. **Radial approach for patients with ST-segment elevation acute coronary syndrome: it is definitely the best access site.**  
Zhang Y, Xu B, Serruys PW, Bourantas CV, Iqbal J, Muramatsu T, Li MH, Ye F, Tian NL, Garcia-Garcia HM, Chen SL.  
*Int J Cardiol.* 2013;168:3140-2.
59. **Effects of valsartan versus amlodipine in diabetic hypertensive patients with or without previous cardiovascular disease.**  
Yamashita K, Kondo T, Muramatsu T, Matsushita K, Nagahiro T, Maeda K, Shintani S, Murohara T.  
*Am J Cardiol.* 2013;112:1750-6.
60. **Cardiovascular events increased at normal and high-normal blood pressure in young and middle-aged Japanese male smokers but not in nonsmokers.**  
Kondo T, Osugi S, Shimokata K, Honjo H, Okumura N, Matsudaira K, Yamashita K, Maeda K, Muramatsu T, Shintani S, Matsushita K, Murohara T.  
*J Hypertens.* 2013;31:263-70.
61. **Comparison between valsartan and amlodipine regarding cardiovascular morbidity and mortality in hypertensive patients with glucose intolerance: NAGOYA HEART Study.**  
Muramatsu T, Matsushita K, Yamashita K, Kondo T, Maeda K, Shintani S, Ichimiya S, Ohno M, Sone T, Ikeda N, Watarai M, Murohara T; for the NAGOYA HEART Study Investigators.  
*Hypertension.* 2012;59:580-6.
62. **The significance of measuring body fat percentage determined by bioelectrical impedance analysis for detecting subjects with cardiovascular disease risk factors.**  
Yamashita K, Kondo T, Osugi S, Shimokata K, Maeda K, Okumura N, Matsudaira K, Shintani S, Muramatsu T, Matsushita K, Murohara T.  
*Circ J.* 2012;76:2435-42.
63. **Association of coffee consumption with serum adiponectin, leptin, inflammation and metabolic markers in Japanese workers: a cross-sectional study.**  
Yamashita K, Yatsuya H, Muramatsu T, Toyoshima H, Murohara T, Tamakoshi K.

*Nutrition and diabetes.* 2012;2:e33.

64. **Smoking and smoking cessation in relation to all-cause mortality and cardiovascular events in 25,464 healthy male Japanese workers.**  
Kondo T, Osugi S, Shimokata K, Honjo H, Morita Y, Maeda K, Yamashita K, Muramatsu T, Shintani S, Matsushita K, Murohara T.  
*Circ J.* 2011;75:2885-92.
65. **Metabolic syndrome and all-cause mortality, cardiac events, and cardiovascular events: a follow-up study in 25,471 young- and middle-aged Japanese men.**  
Kondo T, Osugi S, Shimokata K, Honjo H, Morita Y, Yamashita K, Maeda K, Muramatsu T, Shintani S, Matsushita K, Murohara T.  
*Eur J Cardiovasc Prev Rehabil.* 2011;18:574-80.
66. **Higher dietary intake of alpha-linolenic acid is associated with lower insulin resistance in middle-aged Japanese.**  
Muramatsu T, Yatsuya H, Toyoshima H, Sasaki S, Li Y, Otsuka R, Wada K, Hotta Y, Mitsuhashi H, Matsushita K, Murohara T, Tamakoshi K.  
*Prev Med.* 2010;50:272-6.
67. **Rationale and design of the NAGOYA HEART Study: comparison between valsartan and amlodipine regarding morbidity and mortality in patients with hypertension and glucose intolerance.**  
Matsushita K, Muramatsu T, Kondo T, Maeda K, Shintani S, Murohara T; NAGOYA HEART Study Group.  
*J Cardiol.* 2010;56:111-7.
68. **Maximum derivative of left ventricular pressure predicts cardiac mortality after cardiac resynchronization therapy.**  
Suzuki H, Shimano M, Yoshida Y, Inden Y, Muramatsu T, Tsuji Y, Tsuboi N, Hirayama H, Shibata R, Murohara T.  
*Clin Cardiol.* 2010;33:E18-23.
69. **Changes in activities of daily living, physical fitness, and depressive symptoms after six-month periodic well-rounded exercise programs for older adults living in nursing homes or special nursing facilities.**  
Ouyang P, Yatsuya H, Toyoshima H, Otsuka R, Wada K, Matsushita K, Ishikawa M, Yuanying L, Hotta Y, Mitsuhashi H, Muramatsu T, Kasuga N, Tamakoshi K.  
*Nagoya J Med Sci.* 2009;71:115-26.

70. **Uric acid and left ventricular hypertrophy in Japanese men.**  
Mitsuhashi H, Yatsuya H, Matsushita K, Zhang H, Otsuka R, Muramatsu T, Takefuji S, Hotta Y, Kondo T, Murohara T, Toyoshima H, Tamakoshi K.  
*Circ J.* 2009;73:667-72.
71. **Acute and chronic effects of cardiac resynchronization in patients developing heart failure with long-term pacemaker therapy for acquired complete atrioventricular block.**  
Shimano M, Tsuji Y, Yoshida Y, Inden Y, Tsuboi N, Itoh T, Suzuki H, Muramatsu T, Okada T, Harata S, Yamada T, Hirayama H, Nattel S, Murohara T.  
*Europace.* 2007;9:869-74.

*“Nothing is impossible. It’s just a matter of time.”*

*“If the future is realistic, it will be soon the past.  
If the future is unrealistic, it will become the future.”*

*Professor Patrick W.J.C. Serruys*



ESC Congress in Amsterdam, September-2013.

**Photo: MY MENTORS**

Professors Toyoaki Murohara (left), Patrick W. Serruys (centre right),  
and Yukio Ozaki (right) met at the ESC-JCS joint session.

